CYPRUS CRUSTAL STUDY PROJECT: INITIAL REPORT, HOLES CY-2 and 2a

Editors:

P.T. ROBINSON I.L. GIBSON A. PANAYIOTOU

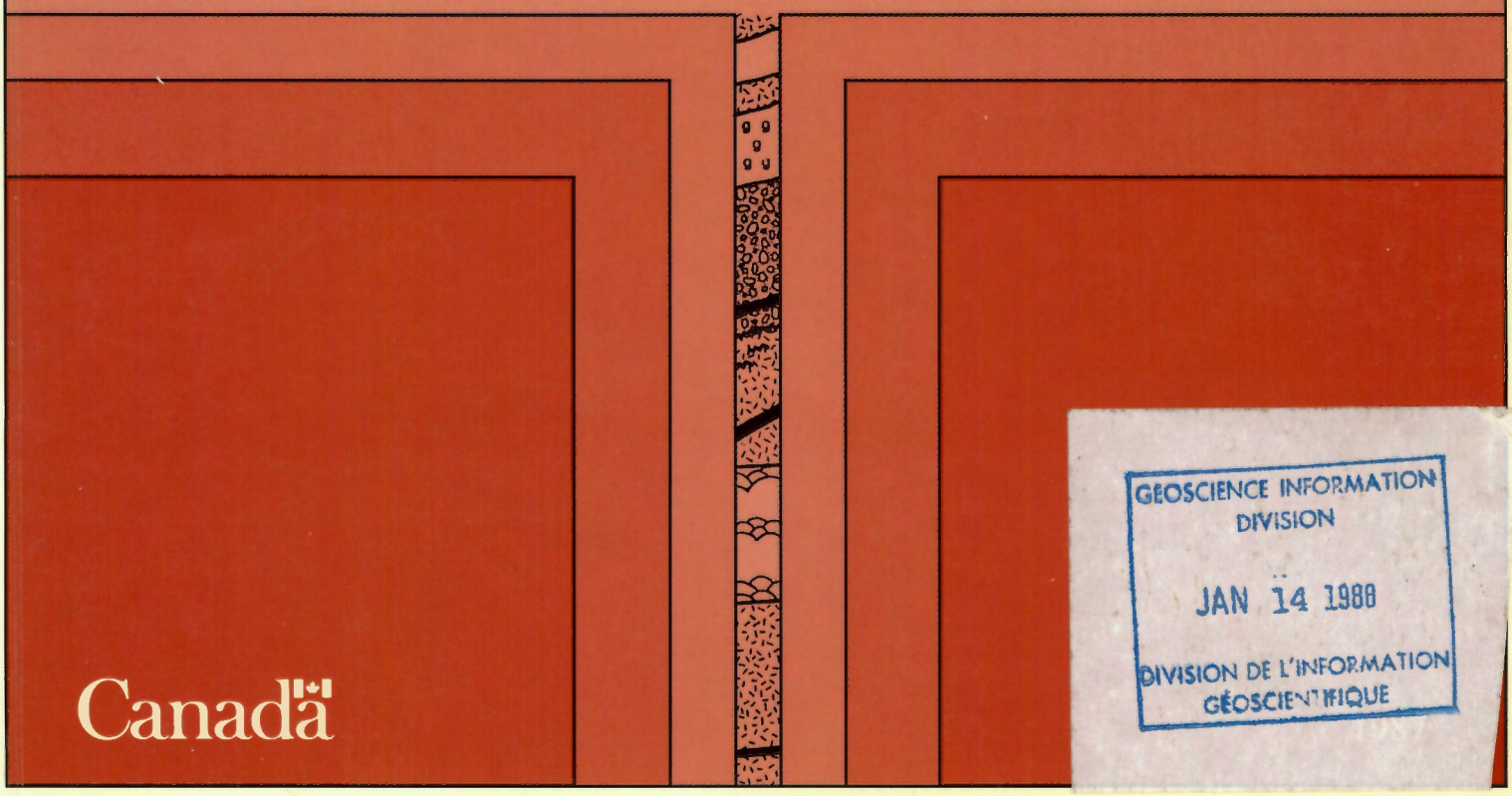

Canada

GEOLOGICAL SURVEY OF CANADA

Paper 85-29

Cyprus Crustal Study Project: Initial Report, Holes CY-2 and 2a

edited by
P.T. Robinson, I.L. Gibson and A. Panayiotou

1987

Energy, Mines and Resources Canada

Énergie, Mines et Ressources Canada

Available in Canada through

authorized bookstore agents and other bookstores

or by mail from

Canadian Government Publishing Centre
Supply and Services Canada
Ottawa, Canada K1A 0S9

and from

Geological Survey of Canada offices:

601 Booth Street
Ottawa, Canada K1A 0E8

3303-33rd Street N.W.,
Calgary, Alberta T2L 2A7

A deposit copy of this publication is also available for reference in public libraries across Canada

Cat. No. M44-85/29E Canada: $20.00
ISBN 0-660-12672-9 Other countries: $24.00

Price subject to change without notice

This volume has been printed by the Geological Survey of Canada on behalf of the Cyprus Crustal Study Project from camera-ready copy prepared, under the direction of the volume editors, by Louise Wallace in the Department of Earth Sciences, University of Waterloo. The material is set in 10 pt Times and was printed using the APS-Micro 5 Phototypesetter, and Waterloo SCRIPT computer software in the Department of Graphic Services, University of Waterloo.

Foreword

In 1978, an international consortium of scientists from Canada, Denmark, the United Kingdom, Iceland, the United States and West Germany successfully completed a deep drilling project in Iceland for research purposes. This group, subsequently formed into the International Crustal Research Drilling Group (ICRDG) proposed to use the results of such deep drilling projects for comparison with results from the Deep Sea Drilling Project in order to better understand the structure and composition of the ocean crust. The projects undertaken by the group are selected and organized by a Management Panel and each project is overseen by a Project Director. The members of the Management Panel during the period of 1980 to 1986 are listed below. Those marked with an asterisk are current members. Dr. Abdul Razzak Bakor*, King Abdul Aziz University, Saudi Arabia; Dr. Robert Baragar*, Geological Survey of Canada, Canada; Dr. Tom Calon*, Memorial University, Canada; Dr. George Constantinou*, Geological Survey Department, Cyprus; Dr. Martin F.J. Flower*, University of Illinois, U.S.A.; Dr. Ingvar Birgir Fridleifsson*, Orkustofnun, Iceland; Dr. Ian Gass, The Open University, U.K.; Dr. Ian Gibson*, University of Waterloo, Canada; Dr. James Hall*, Dalhousie University, Canada; Dr. James Hawkins*, Scripps Institution of Oceanography, U.S.A.; Dr. H.P. Johnson, University of Washington, U.S.A.; Dr. John Malpas*, Memorial University, Canada; Dr. Eldridge Moores*, University of California, U.S.A.; Dr. John Orcutt, Scripps Institution of Oceanography, U.S.A.; Dr. Andreas Panayiotou*, Geological Survey Department, Cyprus; Dr. Paul T. Robinson, Chairman*, Dalhousie University, Canada; Dr. Fritz Rummel*, Ruhr-Universität Bochum, West Germany; Dr. Matthew Salisbury*, Dalhousie University, Canada; Dr. Andrew Saunders*, University of Leicester, U.K.; Dr. Hans-Ulrich Schmincke*, Ruhr-Universität Bochum, West Germany; Dr. Gunther Schoenharting*, University of Copenhagen, Denmark; Dr. M. Treuil, Université Pierre et Marie Curie, France; Dr. Fred Vine*, University of East Anglia, U.K.

Ophiolites have long been recognized as portions of ancient oceanic lithosphere emplaced onto continental margins during periods of orogenesis. As such, complete ophiolites present a full stratigraphy of the oceanic crust and portion of the upper mantle. The Cyprus Crustal Study Project to investigate the Troodos ophiolite was proposed by P.T. Robinson and formally approved by the Management Panel in May, 1980. At this time Robinson was appointed Project Director with overall responsibility for the drilling operations and organization of the scientific investigations. The project was conceived as an integrated petrological, structural and geophysical study of the Troodos ophiolite, involving both field mapping and diamond drilling. The Troodos ophiolite was chosen for this study because it is one of the best studied and least deformed ophiolites available for

Avant-propos

En 1978, un groupe international de scientifiques du Canada, du Danemark, du Royaume-Uni, de l'Islande, des États-Unis et de l'Allemagne de l'Ouest a complété avec succès, en Islande, un projet expérimental de forage à grande profondeur. Ce groupe, qui par la suite a constitué le Groupe international pour le forage expérimental de la croûte terrestre (International Crustal Research Drilling Group, ICRDG), a proposé d'utiliser les résultats de projets de forage profond pour les comparer aux résultats obtenus dans le cadre du Projet de forage des fonds marins, de façon à permettre une meilleure compréhension de la structure et de la composition de la croûte océanique. Les projets entrepris par le groupe sont sélectionnés et organisés par un comité de gestion, et chaque projet est supervisé par un directeur de projet. Les membres nommés au comité de gestion durant la période allant de 1980 à 1986 sont énumérés ci-dessous. Les noms indiqués par un astérisque sont les membres actuels. M. Abdul Razzak Bakor*, université King Abdul Aziz, Arabie Saoudite; M. Robert Baragar*, Commission géologique du Canada, Canada; M. Tom Calon*, université Memorial, Canada; M. George Constantinou*, Commission géologique de Chypre, Chypre; M. Martin F.J. Flower*, université de l'Illinois, É.-U.; M. Ingvar Birgir Fridlefsson*, Orkustofnun, Islande; M. Ian Gass, The Open University, R.-U.; M. Ian Gibson*, université de Waterloo, Canada; M. James Hall*, université Dalhousie, Canada; M. James Hawkins*, Scripps Institution of Oceanography, É.-U.; M. H.P. Johnson, université de Washington, É.-U.; M. John Malpas*, université Memorial, Canada; M. Eldridge Moores*, université de Californie, É-.U.; M. John Orcutt, Scripps Institution of Oceanography, É.-U.; M. Andreas Panayiotou*, Commission géologique de Chypre, Chypre; M. Paul T. Robinson, Président*, université Dalhousie, Canada; M. Fritz Rummel*, Ruhr-Universität Bochum, Allemagne de l'Ouest; M. Matthew Salisbury*, université Dalhousie, Canada; M. Andrew Saunders*, université de Leicester, R.-U.; M. Hans-Ulrich Schmincke*, Ruhr-Universität Bochum, Allemagne de l'Ouest; M. Gunther Schoenharting*, université de Copenhague, Danemark; M. M. Treuil, université Pierre et Marie Curie, France; M. Fred Vine*, université de East Anglia, R.-U.

On admet depuis longtemps que les ophiolites sont des portions de l'ancienne lithosphère océanique dont la mise en place a eu lieu sur les marges continentales durant des périodes d'orogénèse. De ce fait, les ophiolites complètes représentent la stratigraphie intégrale de la croûte océanique et d'une partie du manteau supérieur. Le Projet d'étude de la croûte terrestre à Chypre, qui permettra d'étudier l'ophiolite du Troodos, a été proposé par M. P.T. Robinson, et officiellement approuvé par le comité de gestion en mai 1980. À cette époque, M. Robinson a été nommé directeur du projet, et assume la responsabilité globale des opérations de forage et de l'organisation des études scientifiques. Le projet a été conçu comme une étude intégrée, à la fois pétrologique, structurale et géophysique, de l'ophiolite du Troodos; cette étude comprend à la fois des travaux de cartographie

investigation, and because its unique domal structure permitted sampling of the complete stratigraphy in a series of relatively shallow holes.

During the period 1980 to 1982 field studies were started, research proposals were written and approval of the Cyprus Government for the project was obtained. A drilling contract with Bradley Bros., Noranda, Quebec, Canada was approved by the Management Panel in October, 1981 and drilling began in April, 1982. The drilling continued intermittently until March, 1985 by which time five holes had been drilled at three sites. Total penetration was approximately 4563 metres with an average core recovery of over 95%.

Funding for the project came from a number of agencies: the National Science and Engineering Research Council, the International Development Research Centre, Dalhousie University, Memorial University and the University of Western Ontario (Canada); the Natural Science Research Council (Denmark); the National Environmental Research Council and the Royal Society (UK); the National Science Foundation (USA); the Volkswagen Foundation (West Germany); King Abdul Aziz University (Saudi Arabia); and the Government of Cyprus. In all, a total of approximately Can. $1,575,000 was spent on drilling and related work and a roughly equal amount on field studies, geophysical logging and laboratory studies.

The core recovered from the drill holes is stored in a facility provided by the Government of Cyprus in Nicosia and can be accessed with the permission of the Management Panel of ICRDG through the Geological Survey Department of Cyprus. Lithological core logs were produced on site immediately after recovery of core and are available from ICRDG at the Centre for Marine Geology, Dalhousie University, Nova Scotia, Canada.

The ICRDG Management Panel acknowledges with thanks the support provided by the Geological Survey of Canada in publishing the Initial Report volumes in their Paper Series and the assistance of the Geological Survey Department of Cyprus in providing pocket material. The Natural Sciences and Engineering Research Council of Canada provided financial assistance in the form of a production grant. The volumes aim to present descriptions of the cores along with other geological, geophysical and geochemical data, so that the original information is widely available. No attempt has been made to reconcile all the differences in interpretation between authors of papers in the volume. The papers were reviewed by the editors who are grateful to colleagues who provided external reviews. The editors gratefully acknowledge the assistance of Louisa Horne in supervising the editing and compilation of this volume.

sur le terrain et des forages au diamant. On a choisi d'étudier l'ophiolite du Troodos, parce qu'elle est l'une des ophiolites le mieux étudiées et le moins déformées que l'on puisse examiner; en raison de sa structure exceptionnelle en forme de dôme, on a pu échantillonner la colonne stratigraphique toute entière au moyen d'une série de sondages relativement peu profonds.

Durant la période 1980 à 1982, on a commencé des études de terrain, rédigé des propositions concernant la recherche et obtenu l'approbation du gouvernement de Chypre pour ce projet. Le comité de gestion a approuvé en octobre 1981 un contrat de forage conclu avec la société Bradley Bros. à Noranda (Québec) au Canada, et les sondages ont commencé en avril 1982. Les forages ont continué de façon intermittente jusqu'en mars 1985, époque à laquelle cinq sondages avaient déjà été effectués à trois endroits. La profondeur totale de pénétration était d'environ 4563 m, et le taux moyen de récupération des carottes dépassait 95 %.

Le financement du projet a été assuré par un certain nombre d'organismes: le Conseil national de recherches scientifiques et technologiques, l'International Development Research Centre (Centre de recherches sur le développement international), l'université Dalhousie, l'université Memorial et l'université de Western Ontario (Canada); le Conseil de recherches des sciences naturelles (Danemark); le National Environmental Research Council et la Royal Society (R.-U.); la National Science Foundation (É.-U); la fondation Volkswagen (Allemagne de l'Ouest); l'université King Abdul Aziz (Arabie Saoudite); et le gouvernement de Chypre. En tout, a été consacré un total d'environ 1 575 000 $ CAN aux forages et aux travaux connexes, et une quantité approximativement égale aux études de terrain, aux diagraphies géophysiques et aux études en laboratoire.

Les carottes extraites des trous de sondage sont entreposées dans une installation fournie par le gouvernement de Chypre à Nicosie, et il est possible d'avoir accès à ces échantillons avec la permission du comité de gestion de l'ICRDG par l'entremise de la Commission géologique de Chypre. Des diagraphies lithologiques des sondages ont été produites à l'endroit du forage, immédiatement après l'extraction des carottes, et peuvent être obtenues auprès de l'ICRDG au Centre de géologie marine (Centre for Marine Geology) de l'université Dalhousie (Nouvelle-Écosse) au Canada.

Le Comité de gestion de l'ICRDG remercie la Commission géologique du Canada qui l'a aidé à publier les volumes du Rapport initial de sa série d'articles, de même qu'elle remercie la Commission géologique de Chypre qui l'a aidé à se procurer les documents en pochette. Le Conseil de recherches en sciences naturelles et en génie apporte son appui financier sous forme d'une subvention destinée au règlement des frais de publication. Ces volumes donnent des descriptions des carottes de sondage, de même que d'autres données géologiques, géophysiques et géochimiques, de sorte que l'information originale est facile à obtenir. On n'a pas cherché à accommoder toutes les différences d'interprétation que l'on peut noter entre articles rédigés par divers auteurs et regroupés dans ce volume. Les articles ont été examinés par les rédacteurs, qui remercient leurs collègues d'avoir présenté leurs critiques. Les rédacteurs expriment leur reconnaissance à Mme Louisa Horne pour l'aide qu'elle leur a prodiguée au moment des étapes de révision et de compilation du présent volume.

ICRDG acknowledges with gratitude those agencies which have supported its research drilling programmes. Special thanks are due to Drs. G. Constantinou, A. Panayiotou and C. Xenophontos of the Geological Survey Department, Cyprus. This project is a clear indication of the successful cooperation between a number of national governments, the industrial sector and the academic community.

L'ICRDG exprime sa reconnaissance aux organismes qui ont appuyé ces programmes de forage expérimental. Les membres du comité de gestion remercient en particulier MM. G. Constantinou, A. Panayiotou et C. Xenophontos de la Commission géologique de Chypre. Ce projet est un clair témoignage de succès de la coopération entre un certain nombre de gouvernements nationaux, le secteur industriel et la collectivité académique.

ICRDG Management Panel
August, 1987

Comité de gestion de l'ICRDG
Août 1987

Table of Contents

Holes CY-2 and CY-2a of the Cyprus Crustal Study Project: an Outline of Objectives and Operations

PAUL T. ROBINSON

Centre for Marine Geology, Dalhousie University, Halifax, Nova Scotia, Canada, B3H 3J5

Robinson, P.T., Holes CY-2 and CY-2a of the Cyprus Crustal Study Project: an outline of objectives and operations; in *Cyprus Crustal Study Project: Initial Report, Holes CY-2 and 2a, ed. P.T. Robinson, I.L. Gibson and A. Panayiotou; Geological Survey of Canada, Paper 85-29, p. 1-17, 1987.*

Abstract

Two holes were drilled in the Agrokipia ore deposits of the Troodos ophiolite in order to investigate the nature of hydrothermal circulation and ore formation in oceanic crust. Hole CY-2 penetrated 226 m beneath the Agrokipia 'A' deposit with 92% recovery. It sampled 100 m of hydrothermally altered lavas before passing into relatively fresh, glassy rocks. Hole CY-2a, located directly above the Agrokipia 'B' deposit, penetrated 154 m of weakly altered lavas, 143 m of hydrothermally altered and mineralized rock, and 392 m of highly altered dykes and pillow screens. Recovery in CY-2a averaged about 93%, being lowest in the hydrothermally altered section. Of the 97 days spent at these two sites, only 60 were actually used in drilling operations, giving an average penetration rate of just over 15 m per day. The recovered core was washed, fitted together and described on site. Units were defined on the basis of cooling breaks and changes in grain size, lithology, mineralogy or degree of alteration. One hundred and nine units were recognized in hole CY-2 and 373 in hole CY-2a. These units were grouped into larger scale lithologic units for comparison with exposed sequences. The core is stored in Nicosia, Cyprus and may be sampled upon application to the Chairman of the International Crustal Research Drilling Group. Use of the core for further study is encouraged.

Résumé

Deux forages ont été réalisés dans les dépôts de minerai d'Agrokipia de l'ophiolite Troodos pour étudier la nature de la circulation hydrothermale et la formation de minerai dans la croûte océanique. Le forage CY-2 a pénétré 226 m sous le dépôt Agrokipia 'A' avec une recupération de 92%. Il échantillonna 100 m de laves altérées hydrothermalement avant de passer dans le roc vitreux relativement frais. Le forage CY-2a, situé directement au-dessus du dépôt Agrokipia 'B', a pénétré 154 m de laves faiblement altérées, 143 m de roc avec altération hydrothermale et minéralisé, et 392 m de dykes et écrans de coussins hautement altérés. La récupération de CY-2a était en moyenne de 93%, étant plus faible dans la partie avec altération hydrothermale. Des 97 jours passés à ces deux sites, seulement 60 furent utilisés pour les opération de forage, donnant un taux de pénétration moyen de 15 m par jour. La carotte récupérée fut lavée, assemblée et décrite sur le site. Les unités furent définies sur la base des pauses de refroidissement et des changements de granulométrie, lithologie, minéralogie ou degré d'altération. Cent neuf unités furent reconnues dans le forage CY-2 et 373 dans le forage CY-2a. Ces unités furent groupées en unités lithologiques de plus grande échelle pour comparaison avec les séquences exposées. La carotte de forage est storée à Nicosia, Cyprus et peut être échantillonée sur demande au Président du Groupe International de Forage pour la Recherche sur la Croûte. L'usage de la carotte pour poursuivre l'étude est encouragé.

INTRODUCTION

One of the principal goals of the Cyprus Crustal Study Project was to investigate the processes of hydrothermal circulation and ore formation in the oceanic crust. Numerous copper sulphide ore bodies occur in the lavas of the Troodos ophiolite and previous studies of these had suggested that they formed around hydrothermal vents similar to the black smokers on the East Pacific Rise (Oudin and Constantinou, 1984). Fluid inclusion and strontium isotope studies of the Cyprus deposits had confirmed that sea water was the main ore-bearing fluid (Spooner and Bray, 1977; Spooner et al., 1977), and textural and mineralogical comparisons with black smoker deposits suggested a similar mode of formation.

The massive sulphide ore bodies in the Troodos ophiolite are restricted to the pillow lavas where they occur in clusters of four or more bodies which define five major mining districts (Figure 1). They range in size from about 50,000 to over 20,000,000 tonnes and have an average copper content that varies from less than 0.5 to 4.5 percent (Constantinou, 1980). In addition, many small gossans and zones of hydrothermal alteration occur within the extrusive sequence.

The massive ores typically have a conglomeratic structure consisting of variously shaped blocks of sulphide material in a matrix of sandy sulphide (Constantinou, 1980). Pyrite, chalcopyrite, marcasite, and sphalerite are the principal ore minerals, and most bodies consist chiefly of sulphur, iron, and copper with minor amounts of zinc and nickel.

Directly overlying some of the ore bodies is a thin layer of ochre, a manganese-poor, iron-rich sediment which contains abundant sulphide material, either disseminated or in thin bands and layers.

Beneath each massive orebody lies a stockwork zone which consists of mineralized and hydrothermally altered breccias and pillow lavas. The mineralization in this zone is chiefly in the form of quartz-sulphide veins and the sulphur content ranges from about 30 percent at the top to 10 percent in the deeper parts. The veins consist largely of pyrite and quartz or chalcedony with lesser amounts of chalcopyrite and sphalerite. The host rock is also impregnated with disseminated pyrite.

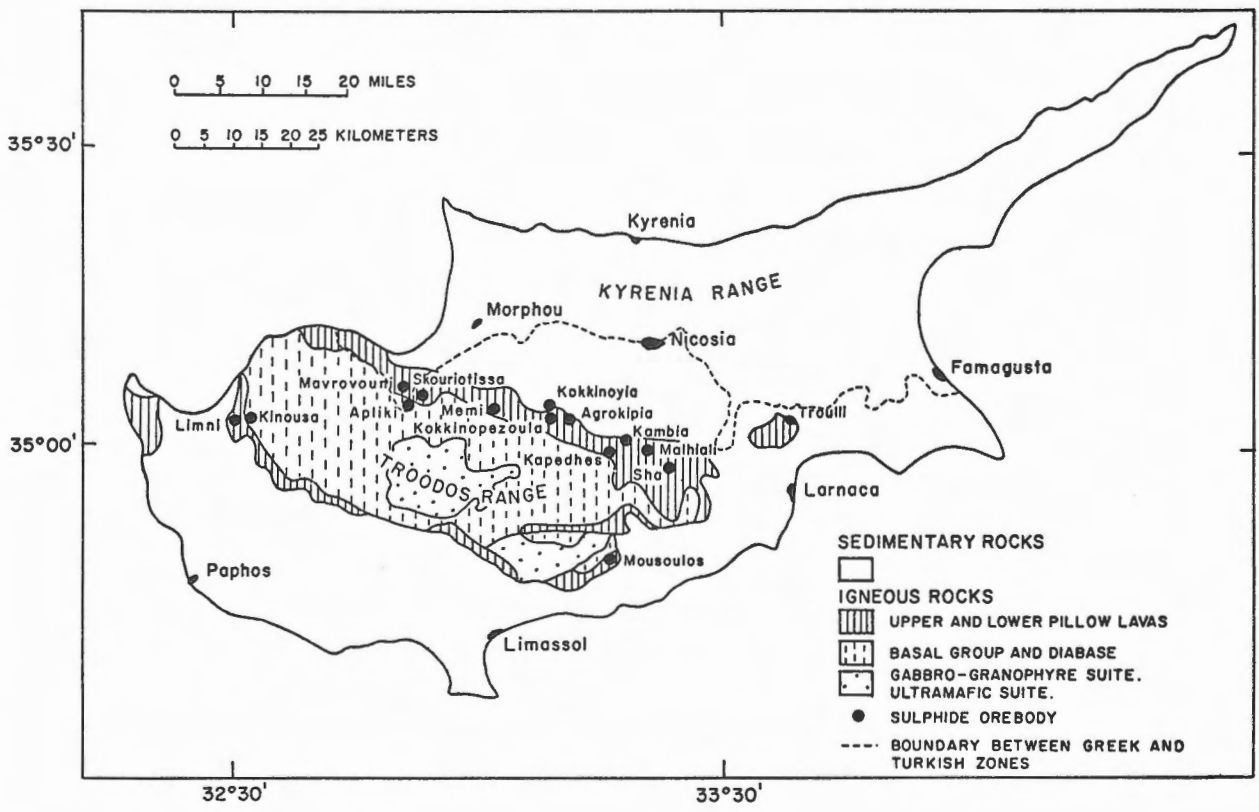

Figure 1: Simplified geological map of the Troodos ophiolite showing the position of the major lithological units and the sulphide ore bodies.

Because many of the ore deposits are overlain by unmineralized lavas or cut by later dykes, they were thought originally to lie at the boundary between the Upper and Lower Pillow Lavas as previously defined in Cyprus. Gass and Smewing (1973) considered this boundary to be a transition from a lower axis sequence formed during spreading to an upper off-axis sequence that post-dated spreading.

By 1980 it was generally accepted that the Troodos orebodies formed as exhalative deposits on the seafloor. Spooner (1977) suggested a model involving deep circulation of sea water in an active spreading zone to levels at which the temperature exceeded 300°C. The hot fluids then returned to the surface along narrow channelways, causing hydrothermal alteration in the stockwork zones and precipitation of massive sulphide ores on the sea floor. Some of the sulphur and the metallic ore elements were believed to have been leached from the rocks through which the brines had passed. The remainder of the sulphur was thought to be of seawater origin. Based on the spacing of the ore bodies, Spooner (1977) postulated that they formed from a series of axially symmetrical convection cells, from 3 to 5 km deep, extending to the level of the gabbros and plagiogranites. Individual cells were thought to have half widths approximately equal to the thickness of the permeable layer.

It was anticipated that a combined field and drilling investigation of these deposits would help to define the lateral and vertical extent of convecting systems, the general paths of fluid flow, paleo-temperature variations within single systems, and changes in fluid composition in space and time. Detailed studies of compositional variations in altered rocks were also planned in order to determine the original lava compositions and how these had been affected by alteration (Miyashiro, 1973; Hynes, 1975; Moores, 1975; Smewing et al., 1975).

Two holes were planned originally for this part of the project; one directly beneath an orebody to sample the underlying stockwork zone and deeper altered rocks, the other located 1 to 2 km away to sample lavas in the associated downwelling zone. The latter hole was also intended to sample a complete section of relatively fresh lavas.

SITE SELECTION

After consultation with geologists of the Cyprus Geological Survey Department, it was decided to carry out the drilling investigations of the Troodos ophiolite within a rectangular corridor on the northern flank of the massif, roughly between the villages of Malounda and Palekhori. Based on field studies in this area during 1981, the hole through relatively fresh lavas (CY-1) was sited in the Akaki River canyon at the contact between the lavas and the overlying sediments (Figure 2). In addition to sampling the extrusive section, this hole was intended to investigate the downwelling portion of a hydrothermal cell. When this hole had to be abandoned at 485 m, Hole CY-1a was drilled to sample the lower part of the extrusive section (Figure 2). The Agrokipia ore deposits, located 1 km west of Agrokipia village, were selected as representing an associated upwelling zone, although the age relationships between the two sections were not completely clear.

The Agrokipia ore deposits form part of the Tamassos Mining District in which four major groups of deposits and a large number of prospects and gossans occur. In the Agrokipia area, northward-dipping, Upper Cretaceous and Tertiary sediments overlie a sequence of dominantly pillowed olivine basalts containing few intrusions, which in turn overlies a sequence of aphyric, locally glassy lavas. The principal structure in the area is the Agrokipia fault, which strikes about N30°W. The structure passes through the Agrokipia 'B' ore deposit and appears to offset it.

Two distinct ore bodies are known in the Agrokipia area. Agrokipia 'A' consists of two massive lenses near the top of the aphyric lavas which were exploited by open pit mining during the 1950's. Reserves were estimated at about 7×10^5 tonnes. Agrokipia 'B' is centred about 300 m east of Agrokipia 'A' and is located within the aphyric lavas, about 150 m stratigraphically deeper in the section. No indication of Agrokipia 'B' is seen at the surface - discovery was made by the Hellenic Mining Company through percussion drilling on a gravity anomaly. The main body is roughly pyramidal in form with a vertical extent of about 150 m; other smaller bodies appear to be downthrown segments north of the Agrokipia fault zone. Ore reserves are estimated at about 5.7×10^6 tonnes of which about 5×10^5 tonnes are of high grade Cu-Zn ore. A small amount of the highest grade ore was removed by underground mining during the 1950's and 1960's.

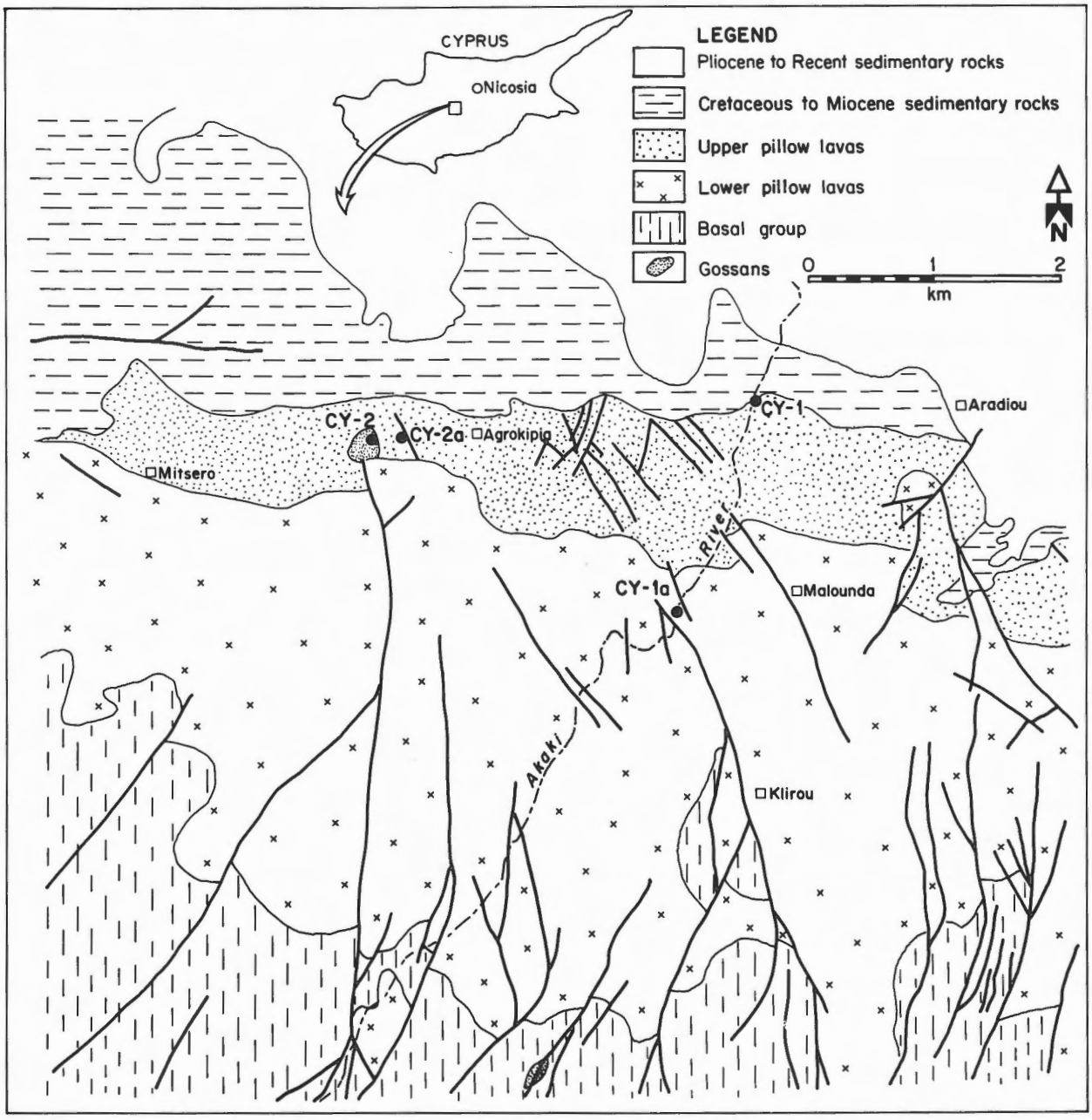

Figure 2: Simplified geological map of part of the northern flank of the Troodos ophiolite showing the position of the bore holes CY-1, CY-1a, CY-2, and CY-2a in relation to the lava stratigraphy.

Specific site selection was based on existing geologic maps, interpretations of percussion drilling logs by the Hellenic Mining Company and detailed magnetic and gravity surveying (Johnson et al., 1982). Hole CY-2 was located at 35°02′43″N, 33°08′48″E on the eastern edge of the pit from which the Agrokipia 'A' ore body had been removed. The hole was spudded at the minimum of a 6,000 gamma peak to peak magnetic low on the assumption that the low magnetization reflected the destruction of magnetic minerals by high-temperature hydrothermal fluids in the underlying stockwork zone. It was hoped that this hole would penetrate the stockwork zone to a depth of approximately 1,000 m. However, the hole was terminated at a depth of 226 m when it became apparent that it had passed out of the hydrothermally altered zone into relatively fresh lavas.

Hole CY-2a was then sited 270 m east of CY-2 at 35°02′40″N, 33°08′55″E, directly above the Agrokipia 'B' ore body. Selection of the site was based largely on interpretations of percussion drilling records and the geology of underground workings. The hole was intended to extend from the surface of the lavas through the Agrokipia 'B' orebody and into the stockwork zone beneath. These objectives were achieved before the hole was voluntarily terminated at a depth of 689 m.

OPERATIONS

Drill Hole CY-2

Site preparation for Hole CY-2, which involved bulldozing a road to the edge of the Agrokipia 'A' pit and leveling a space for the drill rig, began on June 11 and was completed by June 14, 1982. Set up of the rig was completed by June 18 but another two days were required to locate and collect HW casing needed to start the hole. Drilling began on June 22 with HQ rod, followed by reaming in of HW casing. Because of the soft and broken nature of the rock it was necessary to case the upper portions of the hole to a depth of 31 m.

Drilling then continued routinely in HQ size to a depth of 68 m where a two-day delay occurred because of insufficient rod. At 77 and 90 m the bit became blocked and could only be cleaned by pulling the rod. During re-entry several blockages were encountered in the uncased portion of the hole and these had to be reamed out.

On June 30, the drill rods broke in the hole about 9 m above the bit. After two fishing attempts the broken rod was removed from the hole. Drilling then continued to a depth of 102 m at which point it was considered necessary to ream the HW casing to this level in order to prevent further sticking and breaking of the rod. However, all available HW casing had been used and it was necessary to airfreight additional rod from London. Consequently, the rig was shut down from July 1-13 while waiting for the casing to be delivered.

Upon delivery of the new casing, the drillers attempted to pull the existing casing from the hole only to discover that it had unscrewed at the first joint below the surface. No HW tap was available with which to fish the casing and one had to be hand carried from Canada by the drilling supervisor.

On July 17, the HW casing was successfully removed and the hole reamed and cased to a depth of 91 m. Drilling with HQ rod resumed on July 19 and continued uneventfully until July 26 at which time a depth of 226 m had been reached. It was apparent at this point that the hole had passed from the stockwork zone into a sequence of relatively fresh lavas, some of which still contained fresh glass. Because it appeared that the initial drilling objectives could not be achieved in this hole, the decision was made to move the rig to a location above the Agrokipia 'B' orebody and to start a new hole.

The HQ rod and HW casing were removed from Hole CY-2 on July 27, and by July 30 the drill rig had been dismantled and transferred to the location of Hole CY-2a.

Two hundred and twenty six metres were drilled in Hole CY-2 in 37 days for an overall average of 6.1 m/day. However, if the time during which the rig was shutdown is excluded, the average penetration rate was 15.1 m/day. Once the crew had the proper equipment, drilling proceeded with relatively few problems, particularly considering the broken and altered nature of the rock. Overall, the core recovery averaged 91.8 percent, being lowest in the highly altered zones.

Drill Hole CY-2a

The specific site of CY-2a was selected and prepared on July 28, 1982. By July 31, the move from Hole CY-2 was completed and drilling was started on August 2. The hole was spudded with HQ rod and then reamed with HQ casing to a depth of 6 m. Easy drilling and rapid penetration prevailed to a depth of 32 m at which point a soft layer was encountered which caused torqueing of the drill string. The HW casing was then reamed down to this depth to prevent collapse of the hole walls.

Drilling and casing continued routinely to a depth of 154 m where the first hydrothermally altered rocks were encountered. Below this level drilling became more difficult due to torqueing of the rod. During reaming of the HW casing it broke 9 m below the surface but the string was easily fished and replaced. Between 215 and 230 m serious torqueing was encountered again and an attempt was made to ream the casing to this level. However, the casing

became stuck at 195 m and could not be freed. Thus, the hole was cleaned and drilling continued with HQ rod. At a depth of 266 m the bit became blocked and the drill string was pulled. Upon re-entering the hole it was found that considerable collapse had occurred between 222 and 256 m. However, the hole was finally cleaned and drilling continued to 283 m. At this point drilling became so difficult that the drillers decided to case the hole with the HQ rod and continue drilling in NQ size. Consequently, the HQ rods were pulled, a casing shoe attached, and the string reamed to 283 m. When drilling was resumed with NQ rod, soft and broken rock was encountered and penetration was very slow. The drilling foreman recommended reaming the HQ rod down to the first solid rock with a loss of core but when this was attempted the HQ rod broke 30 m above the bottom. After several unsuccessful fishing attempts it was decided to wedge the rod laterally and bypass the closed hole. Thus, starting at 283 m the hole was diverted and drilling continued with NQ rod. At about 288 m the rock became much more coherent and few problems were encountered until, at a depth of 332, the NQ rod broke in the hole and had to be fished. On September 6, the rod broke at 343 m and was again fished successfully from the hole.

Drilling then proceeded rapidly to 438 m by September 11, although the hole had to be flushed periodically. Because some torqueing developed at this depth it was decided to switch to BQ rod at 438 m, leaving the NQ rod in the hole as casing. The NQ rod was then cemented in place and the cement plug drilled out. Drilling continued with BQ rod with no further interruptions to 689 m on September 18, at which time the hole was terminated voluntarily.

Once drilling finished, the BQ rods were pulled and an attempt was made to pull the NQ rods after blasting just above the point at which they were cemented in the hole. However, the rods were stuck in the hole and had to be severed at 283 m where the HQ casing ended. The HQ rod was also stuck in the hole and was blasted free at a depth of 85 m. The rig was then dismantled and the site abandoned on September 25.

Sixty days were spent at this location of which 12 were used to set up and dismantle the rig. Forty one of the remaining forty eight days were actually spent in drilling, yielding an average penetration rate of 16.8 m/day, a very reasonable figure considering the nature of the rock being drilled. Most of the drilling difficulties were encountered in the interval from about 154 to 297 m where soft, argillic material alternated with hard, siliceous layers. In the more coherent rocks above and below this interval the average penetration rate was over 20 m/day.

Core recovery was also very high considering the nature of the rocks. Recovery averaged 93.4 percent for the entire hole but was significantly higher outside of the hydrothermally altered zone between 154 and 297 m. Even in this section, however, the recovery was in excess of 85 percent, thus providing a representative sample of the stockwork zone.

Acid tests for hole inclination were taken at 122 and 564 m. The maximum deviation was less than 2 degrees.

CORE DESCRIPTION

Upon receipt in the lab, the core was washed, reassembled and marked with an orientation line indicating the up direction. A continuous orientation line indicates pieces that could be fitted together and aligned relative to one another. The depth was marked on the core in centimeters, extrapolated between drilling markers, which were usually placed in the core at 15-foot intervals.

A visual representation of each 1.5-m-long core section was then drawn on a core sheet and units identified and described. Units were recognized by distinct cooling breaks, marked changes in grain size, lithology and mineralogy, or by changes in the degree or type of alteration. During description of the core, units were numbered sequentially down the hole. The unit numbers designate the core box in which unit first appears.

After checking and editing, the core descriptions were bound and distributed to interested parties. Copies of these are available from the International Crustal Research Drilling Group, Centre for Marine Geology, Dalhousie University, Halifax, Nova Scotia. In Hole CY-2, 109 units were recognized (Table 1) and these were grouped into 14 larger lithologic units (see Lithologic Description of CY-2). In Hole CY-2a, 373 units were described (Table 2) and these comprise 22 lithologic units (see Lithologic Description of CY-2a).

TABLE 1. Unit Summary Table: Hole CY-2

CY-2 Unit	Upper Contact Depth(m)	Nat	G	Lower Contact Depth(m)	Nat	G	Lithology Ut	Rt	Cl	Vesicles (%)	Veins (%)	Gma (%)
				Core Lost 0.00 - 4.40 m								
1.01	4.40	A	N	6.72	A	N	UK	UK	YW	0	2	99
1.02	6.72	A	N	7.40	A	N	UK	UK	GW	0	2	80
				Core Lost 7.40 - 9.70 m								
1.03	9.70	A	N	11.00	A	N	UK	BA	DD	1	2	50
				Core Lost 11.00 - 12.80 m								
1.04	12.80	A	N	16.50	A	N	UK	UK	GD	1	3	12
2.01	16.50	A	N	16.90	A	N	UK	UK	DG	1	0	20
2.02	16.90	A	N	17.40	A	N	UK	UK	DG	1	0	20
2.03	17.40	A	N	18.15	A	N	UK	BA	DD	0	0	85
				Core Lost 18.15 - 19.50 m								
2.04	19.50	A	N	20.05	A	A	PI	BA	-	1	0	15
2.05	20.05	D	A	21.10	D	A	PI	BA	DD	1	0	15
3.01	21.10	D	A	21.65	D	A	PI	BA	DD	1	1	20
				Core Lost 21.65 - 21.90 m								
3.02	21.90	A	A	22.35	A	A	PI	BA	DD	1	1	15
3.03	22.35	A	A	22.90	D	A	PI	BA	DD	1	2	25
3.04	22.90	A	A	23.40	A	A	PI	BA	DG	1	1	10
3.05	23.40	A	N	24.40	A	N	PI	BA	DD	1	2	12
				Core Lost 24.40 - 25.00 m								
3.06	25.00	A	N	27.70	A	N	PI	BA	DD	1	1	20
4.01	27.70	A	N	36.20	A	N	UK	UK	YW	1	2	85
				Core Lost 36.20 - 37.20 m								
4.02	37.20	A	N	48.60	A	N	UK	BA	DD	1	1	90
6.01	48.60	A	N	48.74	A	N	UK	UK	RR	3	0	99
6.02	48.74	A	N	50.90	A	N	UK	UK	DG	1	2	60
6.03	50.90	A	N	53.60	A	N	UK	UK	DG	1	1	75
				Core Lost 53.60 - 54.25 m								
6.04	54.25	A	N	57.50	A	A	MF	BA	DD	1	0	20
7.01	57.50	A	A	63.40	A	N	MF	BA	DD	4	1	12
				Core Lost 63.40 - 64.62 m								
8.01	64.62	A	N	65.10	A	N	UK	BA	DD	3	1	25
				Core Lost 65.10 - 66.45 m								
8.02	66.45	A	N	66.60	A	N	UK	-	DD	3	0	0
				Core Lost 66.60 - 67.67 m								
8.03	67.67	A	N	67.95	A	N	UK	BA	DD	8	1	15
				Core Lost 67.95 - 69.50 m								
8.04	69.50	A	N	69.85	A	N	UK	BA	DD	10	1	40
				Core Lost 69.85 - 70.50 m								
8.05	70.50	A	N	85.80	A	N	MF	BA	DD	3	1	4
11.01	85.80	A	A	86.75	D	A	UK	BA	DD	5	1	0
12.01	86.75	D	A	90.00	A	N	MF	BA	DD	12	1	5
12.02	90.00	A	N	91.00	D	A	UK	BA	DD	2	1	5
12.03	91.00	A	N	91.90	A	N	UK	UK	DW	2	1	0
13.01	91.90	A	N	92.50	A	N	PI	BA	DG	1	1	0
13.02	92.50	A	N	93.30	A	A	PI	BA	DG	1	0	0
13.03	93.30	A	N	96.45	A	N	MF	BA	DD	2	1	0
14.01	96.45	A	N	97.45	A	N	UK	BA	DD	2	0	99
14.02	97.45	D	N	99.60	A	N	UK	BA	DG	3	1	0
				Core Lost 99.60 - 100.30 m								
14.03	100.30	A	N	101.40	A	N	UK	BA	DD	1	1	0
15.01	101.40	A	A	102.10	D	Y	UK	BA	DD	2	1	0
15.02	102.10	A	N	103.15	A	Y	UK	BA	DD	10	1	0

CY-2 Unit	Upper Contact Depth(m)	Nat	G	Lower Contact Depth(m)	Nat	G	Lithology Ut	Rt	Cl	Vesicles (%)	Veins (%)	Gma (%)
				Core Lost 103.15 - 103.33 m								
15.03	103.33	A	N	103.60	A	Y	UK	BA	DD	3	0	10
15.04	103.60	A	N	103.70	A	N	UK	UK	RB	0	0	99
15.05	103.70	A	N	105.30	A	Y	MF	BA	DD	2	1	0
16.01	105.30	A	Y	106.00	A	A	UK	BA	DD	8	1	0
16.02	106.00	A	A	107.35	A	N	UK	BA	DD	2	1	0
16.03	107.35	A	N	107.45	A	N	UK	UK	RR	0	1	99
16.04	107.45	A	N	109.70	A	N	UK	BA	DD	10	0	15
16.05	109.70	A	N	110.35	A	N	UK	UK	RR	0	1	99
17.01	110.35	A	N	112.30	A	Y	MF	BA	DD	2	1	0
17.02	112.30	A	Y	114.55	A	N	MF	BA	DD	4	3	5
18.01	114.55	D	Y	117.35	A	N	MF	BA	GG	1	1	10
18.02	117.35	A	Y	118.30	A	N	MF	BA	DD	0	0	0
19.01	118.30	A	N	120.10	A	N	MF	BA	DD	1	5	5
19.02	120.10	A	Y	120.50	A	Y	UK	BA	DD	5	1	0
19.03	120.50	A	Y	123.55	D	Y	MF	BA	DD	2	7	5
20.01	123.55	D	N	125.85	A	N	MF	BA	DD	10	13	10
21.01	125.85	D	Y	126.72	A	Y	MF	BA	DD	2	3	5
21.02	126.72	D	Y	129.40	D	Y	MF	BA	GD	2	7	0
22.01	129.40	D	A	131.20	D	Y	MF	BA	DD	1	2	0
22.02	131.20	D	Y	132.20	D	Y	MF	BA	DD	3	1	0
22.03	132.20	D	Y	133.00	D	N	MF	BA	DD	15	2	0
23.01	133.00	D	Y	134.60	A	Y	MF	BA	GD	1	0	20
23.02	134.60	A	Y	134.85	A	Y	MF	BA	GD	1	0	20
23.03	134.85	A	N	136.90	D	Y	MF	BA	GD	2	1	10
23.04	136.90	A	N	138.15	D	Y	MF	BA	DD	3	8	0
24.01	138.15	D	Y	139.29	A	A	MF	BA	DD	2	2	15
24.02	139.29	A	Y	142.34	A	N	MF	BA	GD	1	1	10
25.01	142.34	A	Y	146.45	A	Y	MF	BA	DD	2	2	12
26.01	146.45	A	Y	152.65	A	N	MF	BA	DD	1	1	12
28.01	152.65	D	Y	153.01	A	Y	MF	BA	DD	7	1	25
28.02	153.01	A	Y	154.40	D	Y	MF	BA	DD	3	2	12
28.03	154.40	D	Y	155.07	D	Y	MF	BA	DD	10	1	5
28.04	155.07	D	Y	157.40	A	Y	MF	BA	GD	6	1	12
29.01	157.40	D	Y	158.40	D	Y	MF	BA	GD	1	0	40
29.02	158.40	D	Y	158.80	D	N	MF	BA	DD	20	0	10
29.03	158.80	D	Y	159.00	D	Y	MF	BA	BG	2	0	80
29.04	159.00	D	N	159.60	D	Y	MF	BA	DD	10	1	7
29.05	159.60	D	Y	160.90	D	Y	MF	BA	DD	8	0	12
30.01	160.90	A	Y	165.35	D	Y	MF	BA	GD	7	1	10
31.01	165.35	D	Y	170.20	D	Y	MF	BA	DD	1	3	10
32.01	170.20	D	Y	171.30	D	Y	MF	BA	DD	1	1	5
33.01	171.30	D	Y	172.10	D	Y	MF	BA	DD	1	1	5
33.02	172.10	D	Y	173.00	D	Y	MF	BA	DD	15	1	15
33.03	173.00	D	N	175.82	D	Y	MF	BA	DD	2	1	5
34.01	175.82	D	A	176.40	A	Y	MF	BA	GD	1	0	40
34.02	176.40	A	Y	181.60	A	N	MF	BA	DD	8	1	5
35.01	181.60	A	N	182.20	A	N	MF	BA	DD	10	0	0
35.02	182.20	A	Y	188.70	A	Y	MF	BA	DD	3	1	3
37.01	188.70	D	Y	190.50	D	Y	MF	BA	GD	12	0	15
37.02	190.50	D	Y	191.55	A	Y	MF	BA	GD	5	0	10
38.01	191.55	D	Y	192.90	D	Y	MF	BA	GD	2	1	20
38.02	192.90	D	Y	194.00	D	Y	MF	BA	DD	3	1	15
38.03	194.00	D	Y	198.20	D	Y	MF	BA	GD	3	2	20

CY-2 Unit	Upper Contact Depth(m)	Nat	G	Lower Contact Depth(m)	Nat	G	Lithology Ut	Rt	Cl	Vesicles (%)	Veins (%)	Gma (%)
39.01	198.20	D	Y	198.90	D	Y	MF	BA	GD	8	0	5
39.02	198.90	D	Y	200.40	D	Y	MF	BA	DD	2	2	5
40.01	200.40	D	Y	200.55	T	N	MF	BA	DD	1	1	3
40.02	200.55	I	A	200.60	A	N	DY	BA	DD	1	0	0
40.03	200.60	A	N	201.90	A	Y	MF	BA	DD	1	4	3
40.04	201.90	A	Y	203.90	D	Y	MF	BA	GD	2	3	5
41.01	203.90	D	Y	205.13	A	N	MF	BA	GD	1	0	20
41.02	205.13	D	Y	206.25	D	Y	MF	BA	DD	5	1	15
41.03	206.25	D	Y	210.60	A	Y	MF	BA	DD	5	2	20
42.01	210.60	A	Y	211.75	A	Y	MF	BA	DD	2	1	10
43.01	211.75	A	Y	212.33	A	Y	MF	BA	GD	10	1	8
43.02	212.33	A	Y	213.20	A	Y	MF	BA	GD	12	1	15
43.03	213.20	A	N	216.50	D	Y	MF	BA	DD	15	1	5
44.01	216.50	D	Y	221.95	D	Y	MF	BA	DD	7	3	15
45.01	221.95	D	Y	223.10	D	Y	MF	BA	DD	5	1	18
46.01	223.10	D	Y	224.00	D	Y	MF	BA	DD	2	1	0
46.02	224.00	D	Y	226.16	-	-	MF	BA	DD	4	1	0

Explanations for abbreviations used in Tables 1 and 2:

Upper Contact/ Lower Contact

- Nat: nature of the contact
  - A: altered
  - D: depositional
  - F: faulted
  - G: gradational
  - I: intrusive
  - T: truncated by intrusion
- G: glass, is it present?
  - A: altered
  - N: no
  - Y: yes

Lithology

- Ut: lithology of the unit
  - BR: breccia
  - DY: dyke
  - SI: sill
  - MF: massive flow
  - MG: massive glass
  - PB: pillow breccia
  - PI: pillow lava
  - VB: vesicular basalt
  - UK: unknown
- Rt: rock type
  - BA: basalt
  - DI: diabase
  - GL: glass
  - JA: jasper
  - OR: ore
  - UK: unknown
- Cl: colour
  - BB: brown
  - DD: grey
  - GG: green
  - RR: red
  - WW: white
  - YY: yellow
  - BR: brownish red, etc.

Gma: Groundmass alteration

TABLE 2. Unit Summary Table: Hole CY-2a

CY-2a Unit	Upper Contact Depth(m)	Nat	G	Dip(°)	Lower Contact Depth(m)	Nat	G	Dip(°)	Lithology Ut	Rt	Cl	Vesicles (%)	Veins (%)	Gma (%)
1.01	3.35	A	N	-	30.72	G	N	-	MF	BA	DD	1	1	5
7.01	30.72	A	N	5	31.15	D	N	3	SI	BA	GG	0	0	99
7.03	31.15	A	N	-	32.37	A	N	-	UK	BA	DD	7	1	10
8.01	32.37	A	N	-	32.44	A	N	-	UK	-	GG	0	0	99
8.02	32.44	A	N	-	38.10	A	A	-	MF	BA	DD	0	0	0
9.01	38.10	A	A	-	41.55	D	A	-	MF	BA	DD	5	0	10
9.02	41.55	D	N	-	46.09	D	A	2	MF	BA	DD	7	1	10
10.01	46.09	A	N	-	67.50	A	N	-	MF	BA	DD	3	1	50
15.01	67.50	A	N	-	89.90	A	N	-	MF	BA	GD	3	1	60
21.01	89.90	A	N	-	90.20	A	A	-	MF	BA	DD	10	3	15
21.02	90.20	A	N	-	92.05	A	A	-	UK	BA	DD	1	0	0
21.03	92.05	A	A	-	92.61	A	A	-	UK	GL	GB	2	0	99
21.04	92.61	A	N	-	96.45	A	A	50	MF	BA	DD	5	1	10
22.01	96.45	A	A	-	98.10	A	N	-	MF	BA	DD	3	1	8
23.01	98.10	D	A	30	102.00	A	A	-	MF	BA	DD	2	1	10
24.01	102.00	A	A	-	109.00	A	N	-	MF	BA	DD	1	1	10
25.01	109.00	A	A	-	110.95	A	A	-	MF	GL	DG	2	0	98
25.02	110.95	A	A	-	112.58	A	N	-	MF	BA	DG	1	0	25
25.03	112.58	A	A	-	114.30	A	A	-	MF	GL	DG	1	1	90
26.01	114.30	A	N	-	116.23	A	N	-	MF	BA	GD	1	0	70
26.02	116.23	A	A	-	116.35	A	A	-	MF	GL	GD	1	1	99
26.03	116.35	A	N	-	116.45	A	N	-	MF	BA	GD	1	0	80
26.04	116.45	A	A	-	116.83	A	A	-	MF	GL	BD	1	0	99
26.05	116.83	A	N	-	118.33	D	A	-	MF	BA	BD	1	0	60
27.01	118.33	D	A	30	118.78	A	A	-	MF	GL	BD	1	1	95
27.02	118.78	A	N	-	118.91	A	N	-	MF	BA	DG	5	1	70
27.03	118.91	A	A	-	119.87	A	A	-	MF	GL	BD	1	1	60
27.04	119.87	A	N	-	120.10	A	N	-	MF	BA	GD	6	0	40
27.05	120.10	A	A	-	125.17	A	A	-	MF	GL	BD	1	1	50
28.01	125.17	A	N	-	125.94	A	N	-	MF	BA	BD	1	0	40
28.02	125.94	A	A	-	126.85	A	A	-	UK	GL	BG	1	0	98
29.01	126.85	A	N	-	133.17	A	N	-	MF	BA	GD	1	0	50
29.02	133.17	A	Y	-	133.30	A	N	-	MF	GL	DD	1	0	99
30.01	133.30	A	N	-	134.65	A	N	-	MF	BA	BD	5	0	40
30.02	134.65	A	A	-	137.65	A	A	-	MF	GL	GD	2	1	60
31.01	137.65	A	N	-	141.50	A	N	-	MF	BA	GD	2	1	20
32.01	141.50	A	Y	-	141.74	G	Y	65	MF	GL	DD	1	0	70
32.02	141.74	G	A	65	142.40	A	N	-	MF	BA	GD	7	0	50
32.03	142.40	A	A	-	142.61	A	A	-	MF	GL	DD	2	0	75
32.04	142.61	A	N	-	148.45	D	N	45	MF	BA	GD	2	0	45
33.01	148.45	G	A	-	149.22	A	Y	-	MF	GL	DG	1	0	95
33.02	149.22	A	N	-	154.24	A	N	-	MF	BA	BD	1	1	40
35.01	154.24	A	N	-	156.55	A	N	-	MF	UK	BD	10	0	99
35.02	156.55	A	N	-	158.20	A	N	-	UK	UK	DB	1	1	99
36.01	158.20	A	N	-	159.33	A	N	-	MG	UK	DD	15	1	9
36.02	159.33	A	N	-	160.11	A	N	-	MG	UK	DD	1	10	99
36.03	160.11	A	N	-	164.56	A	N	-	MF	UK	DD	2	2	99
37.01	164.56	A	N	-	167.03	A	N	-	MG	UK	DD	8	1	99
38.01	167.03	A	N	-	167.74	A	N	-	MF	UK	DD	1	1	99
38.02	167.74	A	N	-	168.29	A	N	-	MF	UK	DD	2	1	99
38.03	168.29	A	N	-	168.86	G	N	-	MF	UK	DD	1	1	99
38.04	168.86	G	N	-	170.90	A	N	-	MG	UK	DD	1	1	99
39.01	170.90	A	N	-	175.25	A	N	-	MF	UK	DD	1	1	99

CY-2a Unit	Upper Contact Depth(m)	Nat	G	Dip(°)	Lower Contact Depth(m)	Nat	G	Dip(°)	Lithology Ut	Rt	Cl	Vesicles (%)	Veins (%)	Gma (%)
40.01	175.25	A	N	-	179.63	A	N	-	MG	UK	DD	3	1	99
40.02	179.63	A	N	-	182.33	A	N	-	MF	UK	DD	2	1	99
41.01	182.33	A	N	-	184.82	G	N	-	MF	GL	DD	10	0	99
42.01	184.82	G	N	-	185.50	A	N	-	MF	UK	DD	2	10	99
42.02	185.50	A	N	-	186.29	A	N	-	UK	OR	DD	0	0	99
42.03	186.29	A	N	-	186.80	G	N	-	MG	UK	DD	0	0	99
42.04	186.80	G	N	-	187.96	G	N	-	MF	UK	DD	1	4	99
42.05	187.96	G	N	-	189.02	G	N	-	MF	UK	DD	1	0	99
42.06	189.02	A	N	-	189.45	A	N	-	MF	UK	DD	2	0	99
43.01	189.45	G	N	-	191.82	A	N	-	MG	UK	DD	1	0	99
43.02	191.82	A	N	-	191.99	G	N	50	UK	OR	DD	0	0	99
43.03	191.99	D	N	-	192.69	A	N	-	MF	UK	DD	7	0	99
43.04	192.69	A	N	-	193.25	A	N	-	UK	OR	DD	0	0	99
43.05	193.25	A	N	-	196.75	A	N	-	MG	UK	DD	1	1	99
44.01	196.75	A	N	-	197.97	A	N	-	MF	UK	DD	1	1	99
44.02	197.97	A	N	-	205.55	A	N	-	MG	UK	DD	3	1	99
46.01	205.55	A	N	-	209.50	A	N	-	MG	UK	DD	1	2	99
46.02	209.50	A	N	-	213.06	A	N	-	UK	UK	DD	0	2	99
					Core Lost 213.06 - 214.58 m									
46.03	214.58	A	N	-	215.21	G	N	-	MG	UK	DD	0	0	99
47.01	215.21	G	N	-	219.01	G	N	-	MF	UK	DD	2	1	99
48.01	219.01	G	N	-	219.80	A	N	-	MG	UK	DD	3	1	99
48.02	219.80	A	N	-	222.35	A	N	-	MF	UK	DD	1	1	99
48.03	222.35	A	N	-	229.30	G	N	-	MG	UK	-	1	1	0
49.01	229.30	A	N	-	229.85	A	N	-	UK	OR	DD	0	0	99
49.02	229.85	A	N	-	230.30	A	N	-	MG	UK	DD	0	0	99
50.01	230.30	A	N	-	230.61	A	N	-	MF	UK	DD	4	1	99
50.02	230.61	A	N	-	232.90	A	N	-	MG	UK	DD	0	0	99
50.03	232.90	A	N	-	233.30	A	N	-	MG	UK	DD	0	0	99
50.04	233.30	A	N	-	233.60	A	N	-	MF	UK	DD	2	1	99
50.05	233.60	G	N	-	234.89	G	N	-	MG	UK	DD	5	0	99
51.01	234.89	A	N	-	235.30	A	N	-	MF	UK	DD	1	0	99
51.02	235.30	A	N	-	236.20	A	N	-	MG	UK	DD	0	0	99
51.03	236.20	A	N	-	237.01	A	N	-	UK	JA	RR	1	0	99
51.04	237.01	A	N	-	238.59	G	N	-	MF	UK	DD	2	0	99
51.05	238.59	A	N	-	240.50	G	N	-	MG	UK	DD	1	0	99
52.01	240.50	A	N	-	242.16	A	N	-	MF	UK	DD	3	2	99
52.02	242.16	D	N	-	243.20	D	N	-	MG	UK	DD	1	0	99
52.03	243.20	D	N	30	244.01	A	N	-	MF	UK	DD	1	0	99
53.01	244.01	A	N	-	244.52	A	N	-	MG	UK	DD	0	0	99
53.02	244.52	A	N	-	245.57	A	N	-	MF	UK	DD	1	2	99
53.03	245.57	A	N	-	246.18	A	N	-	MG	UK	DD	0	0	99
53.04	246.18	D	N	60	246.48	G	N	-	MF	UK	DD	4	0	99
53.05	246.48	G	N	-	247.46	D	N	75	MG	UK	DD	0	0	99
53.06	247.46	D	N	70	248.40	A	N	-	MF	UK	DD	0	0	0
54.01	248.40	A	N	-	249.53	A	N	-	MG	UK	DD	3	0	99
54.02	249.53	A	N	-	249.96	A	N	-	UK	UK	RR	0	0	99
54.03	249.96	A	N	-	252.69	D	N	-	MF	UK	DD	2	1	99
54.04	252.69	D	N	-	253.22	D	N	-	MG	UK	DD	0	0	99
54.05	253.22	D	N	-	253.40	D	N	-	MF	UK	DD	0	0	99
54.06	253.40	D	N	-	255.42	A	N	-	MG	UK	DD	1	0	99
55.01	255.42	A	N	-	256.49	G	N	-	MG	UK	DD	1	0	99
55.02	256.49	G	N	-	257.89	D	N	55	MF	UK	DD	1	0	99
56.01	257.89	D	N	50	258.50	G	N	-	MG	UK	DD	0	2	99

CY-2a Unit	Upper Contact Depth(m)	Nat	G	Dip(°)	Lower Contact Depth(m)	Nat	G	Dip(°)	Lithology Ut	Rt	Cl	Vesicles (%)	Veins (%)	Gma (%)
56.02	258.50	A	N	-	260.69	A	N	-	MF	UK	DD	3	1	99
56.03	260.69	A	N	-	261.04	A	N	-	MG	UK	DD	0	0	99
56.04	261.04	A	N	-	261.69	A	N	-	MF	UK	DD	4	1	99
56.05	261.69	A	N	-	262.08	A	N	-	MG	UK	DD	1	0	99
57.01	262.08	A	N	-	262.91	A	N	-	MF	UK	DD	1	1	99
57.02	262.91	A	N	-	263.02	A	N	-	MG	UK	DD	1	0	99
					Core Lost 263.04 - 264.87 m									
57.03	264.87	A	N	-	266.18	A	N	-	MF	UK	DD	2	0	99
57.04	266.18	A	N	-	272.08	A	N	-	MG	UK	DD	1	0	99
58.01	272.08	A	N	-	272.71	A	N	-	UK	UK	RD	0	0	99
59.01	272.71	A	N	-	272.91	A	N	-	MG	UK	DD	0	0	99
59.02	272.91	A	N	-	274.70	A	N	-	MF	UK	DD	1	2	99
59.03	274.70	A	N	-	275.55	A	N	-	MG	UK	DD	0	0	99
59.04	275.55	A	N	-	278.69	A	N	-	MF	UK	DD	4	1	99
60.01	278.69	A	N	-	280.60	A	N	-	MG	UK	DD	0	0	99
60.02	280.60	A	N	-	281.05	A	N	-	UK	UK	RD	0	0	99
60.03	281.05	A	N	-	282.85	A	N	-	DY	BA	DD	0	1	25
61.01	258.20	A	N	-	260.59	A	N	-	MF	UK	DD	6	1	99
62.01	260.59	A	N	-	261.40	A	N	-	MG	UK	DD	1	0	99
62.02	261.40	A	N	-	263.04	A	N	-	MF	UK	DD	2	1	99
62.03	263.04	A	N	-	264.26	A	N	-	UK	UK	DD	0	0	99
62.04	264.26	A	N	-	264.92	D	N	20	MF	UK	DD	2	1	99
62.05	264.92	D	N	20	265.05	D	N	0	MG	UK	DD	0	0	99
62.06	265.05	G	N	-	265.60	A	N	-	MF	BA	DD	1	0	99
63.01	265.60	A	N	-	267.62	A	N	-	MG	UK	DD	0	0	99
63.02	267.62	A	N	-	268.69	A	N	-	MF	UK	DD	3	0	99
63.03	268.69	A	N	-	271.93	A	N	-	UK	UK	RD	2	1	99
64.01	271.93	A	N	-	272.80	A	N	-	UK	UK	RD	0	0	99
64.02	272.80	A	N	-	273.09	G	N	-	MG	UK	DD	0	0	99
64.03	273.09	G	N	-	275.40	A	N	-	MF	UK	DD	5	1	99
65.01	275.40	A	N	-	275.86	A	N	-	MG	UK	DD	0	0	99
65.02	275.86	A	N	-	277.72	A	N	-	MF	UK	DD	5	1	99
65.03	277.72	A	N	-	278.19	A	N	-	MG	UK	DD	5	0	99
65.04	278.19	A	N	-	278.78	A	N	-	MF	UK	DD	11	1	99
65.05	278.78	A	N	-	280.70	A	N	-	MG	UK	DD	0	0	99
66.01	280.70	A	N	-	280.86	A	N	-	UK	UK	RD	0	0	99
66.02	280.86	A	N	-	282.56	A	N	-	MF	UK	DD	0	1	25
66.03	282.56	A	N	-	283.32	A	N	-	MG	UK	DD	0	0	99
67.01	283.32	A	N	-	284.12	A	N	-	UK	UK	DD	0	0	99
67.02	284.12	A	N	-	285.19	A	N	-	UK	UK	RD	1	1	99
67.03	285.19	A	N	-	285.58	A	N	-	MG	UK	DD	1	0	99
67.04	285.58	A	N	-	286.19	G	N	-	MF	UK	DD	1	0	99
67.05	286.19	G	N	-	287.75	A	N	65	MG	UK	DD	1	1	99
67.06	287.75	A	N	65	289.40	A	N	-	UK	UK	RD	0	1	99
68.01	289.40	A	N	-	292.45	A	N	-	MG	UK	DD	1	1	99
68.02	292.45	A	N	-	296.46	A	N	-	MF	UK	DD	0	0	45
68.03	296.46	A	N	-	297.14	A	N	-	MG	UK	DD	0	0	99
69.01	297.14	A	N	-	297.49	A	N	-	BR	UK	GD	0	0	99
69.02	297.49	A	N	-	297.99	A	N	-	UK	UK	GD	0	0	99
69.03	297.99	A	N	-	298.29	A	N	-	DY	BA	GD	0	0	99
69.04	298.29	A	N	-	299.26	A	N	-	UK	UK	DD	0	0	99
69.05	299.26	A	N	-	299.35	A	N	-	DY	BA	GD	0	0	0
69.06	299.35	A	N	-	299.40	A	N	-	UK	BA	GD	2	1	99
69.07	299.40	A	N	-	299.49	G	N	-	UK	BA	DD	2	0	99

CY-2a Unit	Upper Contact Depth(m)	Nat	G	Dip(°)	Lower Contact Depth(m)	Nat	G	Dip(°)	Lithology Ut	Rt	Cl	Vesicles (%)	Veins (%)	Gma (%)
69.08	299.49	G	N	-	303.03	A	N	-	UK	BA	DD	5	1	99
70.01	303.03	A	N	-	303.34	A	N	-	BR	BA	DD	0	0	99
70.02	303.34	A	N	-	304.86	A	N	-	DY	BA	DD	1	1	99
71.01	304.86	A	N	-	306.43	T	N	-	UK	BA	DD	2	1	99
71.02	306.43	I	N	-	306.47	A	N	-	DY	BA	DD	0	0	99
71.03	306.47	A	N	-	308.00	A	N	-	UK	BA	DD	3	0	99
71.04	308.00	A	N	-	312.41	A	N	-	DY	BA	GD	0	10	0
72.01	312.41	A	N	-	312.82	A	N	30	DY	BA	DD	1	0	99
72.02	312.82	A	N	-	313.67	A	N	-	DY	BA	DD	0	0	99
73.01	313.67	A	N	-	313.92	F	N	-	-	-	DD	1	0	99
73.02	313.92	F	N	-	314.19	A	N	-	UK	BA	-	1	0	99
73.03	314.19	A	N	-	314.55	A	N	-	UK	BA	DD	0	0	99
73.04	314.55	A	N	-	314.88	A	N	-	UK	BA	BD	1	0	99
73.05	314.88	A	N	-	315.16	A	N	-	UK	BA	DD	0	0	99
73.06	315.16	A	N	-	315.78	A	N	-	UK	BA	DD	1	0	99
73.07	315.78	A	N	-	316.59	A	N	-	MG	UK	DD	0	0	99
73.08	316.59	A	N	80	323.69	A	N	-	MF	UK	DD	2	1	99
75.01	323.69	A	N	-	325.22	A	N	-	MF	UK	DD	3	1	99
75.02	325.22	A	N	-	325.60	A	N	-	DY	UK	BD	1	0	99
75.03	325.60	A	N	-	326.98	A	N	-	DY	BA	DD	1	0	99
76.01	326.98	A	N	-	328.15	A	N	-	DY	BA	DD	7	1	99
76.02	328.15	A	N	-	328.53	A	N	-	UK	BA	DD	5	1	99
76.03	328.53	A	N	-	330.75	A	N	-	UK	BA	DD	4	1	99
76.04	330.75	A	N	-	331.18	A	N	-	UK	BA	DD	0	0	99
77.01	331.18	A	N	-	331.90	T	N	87	UK	BA	DD	2	0	99
77.02	331.90	I	N	-	332.98	A	N	-	DY	BA	DD	2	0	99
77.03	332.98	A	N	-	333.40	A	N	-	UK	BA	DD	2	0	99
77.04	333.40	A	N	-	338.95	A	N	-	DY	BA	DD	5	1	99
78.01	338.95	A	N	-	341.45	A	N	-	UK	BA	DD	4	1	99
79.01	341.45	I	N	70	341.68	A	N	-	DY	BA	DD	3	0	99
79.02	341.68	A	N	-	342.69	A	N	-	UK	BA	DD	2	1	99
79.03	342.69	A	N	-	342.89	A	N	-	BR	BA	DD	0	0	99
79.04	342.89	A	N	-	350.85	I	A	-	DY	BA	DD	4	1	99
81.01	350.85	T	N	-	352.55	T	N	-	UK	BA	DG	1	4	99
81.02	352.55	I	N	-	352.93	A	N	-	DY	BA	DD	1	0	99
81.03	352.93	T	N	-	355.12	F	N	-	UK	BA	DD	1	0	99
82.01	355.12	F	N	-	360.88	T	N	-	UK	BA	DD	2	1	99
83.01	360.88	I	A	-	361.48	T	N	-	DY	BA	GD	2	1	99
83.02	361.48	I	A	50	361.61	I	A	65	DY	BA	DD	4	1	99
83.03	361.61	T	N	65	372.30	I	A	70	DY	BA	DD	2	1	95
85.01	372.30	T	N	-	374.12	A	N	-	UK	BA	DD	1	1	99
86.01	374.12	A	N	-	375.20	A	N	-	UK	BA	GD	1	1	99
86.02	375.20	A	N	-	376.03	I	N	-	DY	BA	DD	1	1	99
86.03	376.03	T	N	-	380.80	A	N	-	UK	BA	GD	3	1	99
87.01	380.80	A	N	-	381.16	A	N	-	UK	BA	BD	1	1	99
87.02	381.16	A	N	-	383.30	A	N	-	UK	BA	DD	2	1	99
88.01	383.30	A	N	-	393.07	A	N	-	MF	BA	DD	5	0	99
90.01	393.07	A	N	-	393.16	A	N	-	MF	DI	DD	0	0	99
90.02	393.16	A	N	-	395.33	A	N	-	DY	BA	GD	3	0	99
91.01	395.33	A	N	-	401.10	T	N	-	MF	BA	DD	4	0	99
92.01	401.10	I	N	-	401.75	A	N	-	DY	BA	DD	2	0	99
92.02	401.75	A	N	-	403.80	I	A	45	DY	BA	DD	3	0	99
92.03	403.80	T	N	-	405.58	T	N	-	UK	BA	GD	1	1	99
93.01	405.58	I	N	85	405.69	I	N	85	DY	BA	GG	0	0	99

CY-2a	Upper Contact				Lower Contact				Lithology			Vesicles	Veins	Gma
Unit	Depth(m)	Nat	G	Dip(°)	Depth(m)	Nat	G	Dip(°)	Ut	Rt	Cl	(%)	(%)	(%)
93.02	405.69	T	N	85	406.53	D	N	15	UK	BA	GD	3	0	99
93.03	406.53	D	N	15	407.31	D	N	-	PI	BA	GD	10	0	99
93.04	407.31	D	N	25	407.95	D	A	15	PI	BA	GD	3	0	99
93.05	407.95	D	A	-	408.52	A	N	-	PI	BA	GD	2	0	99
93.06	408.52	A	N	-	409.00	A	N	-	PI	BA	DG	2	0	99
93.07	409.00	A	N	-	410.22	A	N	-	PI	BA	GD	12	1	99
93.08	410.22	A	A	-	410.40	A	N	-	UK	UK	GD	4	0	99
94.01	410.40	A	N	-	411.04	A	N	-	UK	BA	GD	1	1	99
94.02	411.04	A	N	-	411.90	F	N	-	UK	BA	GD	2	1	99
94.03	411.90	F	N	-	413.23	T	N	-	MF	BA	GD	2	0	99
94.04	413.23	A	N	-	424.65	A	N	-	DY	BA	GD	3	1	99
97.01	424.65	A	N	-	426.13	I	N	-	DY	BA	GD	2	0	99
97.02	426.13	T	N	70	426.29	T	N	25	UK	BA	GD	10	1	99
97.03	426.29	I	N	25	426.79	I	N	55	DY	BA	GD	2	1	90
97.04	426.79	T	N	55	427.12	D	N	50	UK	BA	GD	7	0	95
97.05	427.12	D	A	55	427.74	D	A	25	PI	BA	GD	1	0	99
97.06	427.74	A	N	25	427.98	A	N	-	PI	BA	GD	8	1	95
97.07	427.98	A	N	-	428.10	D	N	65	PI	BA	GD	8	1	90
97.08	428.10	D	N	65	428.56	D	N	10	PI	BA	GD	8	1	90
97.09	428.56	D	A	10	428.80	D	A	40	PI	BA	GD	11	1	95
97.10	428.80	D	A	40	429.35	D	A	25	PI	BA	GD	12	0	95
97.11	429.35	D	A	25	430.66	D	A	30	PI	BA	GD	12	0	95
98.01	430.66	D	N	30	431.85	A	N	-	PI	BA	GD	8	0	99
98.02	431.85	D	A	-	432.85	D	N	-	PI	BA	GD	10	1	99
98.03	432.85	D	A	-	433.90	D	A	-	PI	BA	GD	3	5	99
98.04	433.90	D	A	-	436.59	D	A	-	PI	BA	GD	4	1	99
99.01	436.59	D	A	-	437.39	A	N	-	PI	BA	GD	6	0	99
99.02	437.39	A	N	-	438.75	D	A	-	PI	BA	DD	12	0	95
99.03	438.75	D	A	-	439.24	A	N	-	PI	BA	DD	4	1	99
99.04	439.24	A	N	-	439.70	A	A	-	PI	BA	GD	2	0	99
99.05	439.70	A	N	-	441.41	A	A	-	PI	BA	DG	5	1	99
100.01	441.41	D	A	-	441.91	D	A	-	PI	BA	GD	8	1	99
100.02	441.91	D	A	-	442.32	D	A	-	PI	BA	GD	8	1	99
100.03	442.32	D	A	-	442.83	D	A	5	PI	BA	GD	10	1	99
100.04	442.83	D	A	5	443.34	D	A	-	PI	BA	GD	7	1	99
100.05	443.34	D	A	-	449.35	D	A	-	MF	BA	DD	3	1	99
101.01	449.35	D	A	-	452.78	D	A	-	MF	BA	GD	5	0	99
102.01	452.78	D	A	-	454.24	D	A	15	MF	BA	GD	10	1	99
102.02	454.24	D	A	15	454.86	D	A	10	PI	BA	GD	2	1	99
102.03	454.86	D	A	10	455.29	A	A	-	PI	BA	GD	3	1	99
102.04	455.29	A	A	-	456.38	A	A	-	PI	BA	DG	4	0	99
102.05	456.38	A	A	-	457.10	D	A	10	PI	BA	GD	4	1	99
102.06	457.10	D	A	10	457.35	D	A	50	PI	BA	GD	5	0	99
103.01	457.35	A	A	-	458.10	D	A	-	PI	BA	GD	9	0	99
103.02	458.10	D	A	-	458.50	D	A	-	PB	BA	GD	2	1	99
103.03	458.50	D	A	-	459.50	D	A	-	PI	BA	GD	2	2	99
103.04	459.50	D	A	-	459.90	D	A	-	PI	BA	DG	2	1	99
103.05	459.90	D	A	-	460.22	D	A	-	PI	BA	DD	10	1	99
103.06	460.22	D	A	-	460.46	D	A	-	PB	BA	GG	0	0	99
103.07	460.46	D	A	-	461.15	D	A	-	PI	BA	DG	10	1	99
103.08	461.15	D	A	-	462.20	D	A	-	PB	BA	DG	4	2	99
103.09	462.20	D	A	-	462.59	D	A	25	PI	BA	GD	2	0	96
104.01	462.59	D	A	60	463.05	D	N	-	PI	BA	GD	7	1	99
104.02	463.05	D	A	-	463.54	D	A	-	PB	BA	DG	3	0	99

CY-2a Unit	Upper Contact Depth(m)	Nat	G	Dip(°)	Lower Contact Depth(m)	Nat	G	Dip(°)	Lithology Ut	Rt	Cl	Vesicles (%)	Veins (%)	Gma (%)
104.03	463.54	D	A	-	463.94	D	A	-	PI	BA	DG	8	0	99
104.04	463.94	D	A	-	464.83	D	A	-	PB	BA	DG	2	4	99
104.05	464.83	D	A	-	465.30	D	A	-	PI	BA	GD	3	1	99
104.06	465.30	D	A	-	466.00	D	A	-	PI	BA	DG	10	2	99
104.07	466.00	D	A	-	476.78	I	N	40	DY	BA	DG	1	2	99
106.01	476.78	A	N	-	477.78	A	N	-	PB	BA	DG	3	1	99
106.02	477.78	A	N	-	478.41	D	A	70	PI	BA	GD	3	1	99
106.03	478.41	D	A	70	480.65	A	A	-	PI	BA	GD	1	1	99
107.01	480.65	A	A	-	481.50	F	N	-	UK	BA	GD	1	0	99
107.02	481.50	F	N	-	482.09	A	A	-	MF	BA	GD	2	1	99
107.03	482.09	A	A	-	483.61	D	N	-	UK	BA	GD	7	1	80
107.04	483.61	D	N	-	483.95	D	A	65	PB	BA	GD	1	4	80
107.05	483.95	D	A	65	484.58	D	A	-	PI	BA	DG	4	1	99
108.01	484.58	A	A	-	485.24	D	N	-	PI	BA	DG	3	1	99
108.02	485.24	D	A	-	485.68	A	N	-	PB	BA	DG	0	1	99
108.03	485.68	A	N	-	488.30	D	A	50	MF	BA	GD	5	1	99
108.04	488.30	D	A	50	489.69	D	A	10	PI	BA	GD	4	1	99
108.05	489.69	D	A	5	490.90	D	A	70	PI	BA	DG	4	1	99
109.01	490.90	D	A	80	493.26	D	A	-	MF	BA	GD	4	1	99
109.02	493.26	D	N	-	496.85	T	N	-	MF	BA	GD	3	2	99
110.01	496.85	A	N	60	499.99	I	N	45	DY	BA	GD	1	3	99
110.02	499.99	T	N	45	503.66	T	N	25	UK	BA	GD	8	2	99
111.01	503.66	I	N	20	505.76	I	N	5	DY	BA	GD	1	1	99
111.02	505.76	T	N	-	507.18	D	A	-	MF	BA	GD	2	1	99
112.01	507.18	D	N	-	508.50	D	N	-	PI	BA	GD	2	1	99
112.02	508.50	D	N	60	510.50	D	N	-	PB	BA	GD	2	1	99
112.03	510.50	D	N	-	512.19	D	N	-	MF	BA	GD	14	1	99
112.04	512.19	D	N	-	513.88	A	N	70	MF	BA	GD	2	2	99
113.01	513.88	A	N	70	514.08	A	N	70	UK	UK	WW	0	0	99
113.02	514.08	A	N	70	515.68	D	A	-	MF	BA	GD	1	1	99
113.03	515.68	D	A	-	517.70	D	N	12	MF	BA	DG	1	1	99
113.04	517.70	D	N	-	524.59	D	N	-	MF	BA	DD	15	1	99
115.01	524.59	A	N	-	526.43	A	N	-	MF	BA	DG	5	0	99
115.02	526.43	A	N	-	527.26	A	N	-	MF	BA	DG	2	1	99
115.03	527.26	A	N	-	528.50	A	A	-	MF	BA	DG	1	1	99
115.04	528.50	A	N	-	528.90	T	N	-	MF	BA	DG	1	1	99
115.05	528.90	I	N	85	529.25	I	N	45	DY	BA	GD	1	1	99
116.01	529.25	T	N	45	529.36	T	N	50	UK	BA	DG	15	0	99
116.02	529.36	I	N	45	532.46	I	N	50	DY	BA	GD	5	1	99
116.03	532.46	T	N	50	532.83	T	N	50	MF	BA	DG	10	0	99
116.04	532.83	I	N	50	534.20	I	N	68	DY	BA	DG	4	1	99
116.05	534.20	T	N	68	534.31	T	N	65	UK	BA	GD	4	0	99
116.06	534.31	I	N	65	535.35	I	N	65	DY	BA	GD	12	1	99
117.01	535.35	T	N	65	538.98	I	N	55	DY	BA	GF	10	1	99
117.02	538.98	T	N	55	539.32	T	N	80	UK	BA	DG	1	0	99
117.03	539.32	I	N	80	539.55	I	N	70	DY	BA	GD	2	1	99
117.04	539.55	T	N	70	540.75	I	N	15	DY	BA	DG	2	1	99
118.01	540.75	T	N	15	545.64	I	A	75	DY	BA	GD	1	1	99
118.02	545.64	A	N	-	545.94	A	N	-	VB	BA	GG	0	0	99
118.03	545.94	A	N	80	547.42	I	N	60	DY	-	GD	2	2	99
119.01	547.42	T	N	-	547.53	T	N	10	VB	BA	GD	2	0	99
119.02	547.53	I	N	10	547.78	I	N	-	DY	BA	DD	7	1	99
119.03	547.78	T	N	-	549.70	T	N	-	VB	BA	GD	5	0	99
119.04	549.70	I	N	40	553.20	I	N	60	DY	BA	GD	3	1	99

CY-2a Unit	Upper Contact Depth(m)	Nat	G	Dip(°)	Lower Contact Depth(m)	Nat	G	Dip(°)	Lithology Ut	Rt	Cl	Vesicles (%)	Veins (%)	Gma (%)
120.01	553.20	T	N	65	553.55	T	N	45	VB	BA	GD	3	0	99
120.02	553.55	I	A	60	555.30	A	N	-	DY	BA	GD	2	1	99
120.03	555.30	A	N	-	557.66	I	A	70	DY	BA	GD	1	1	80
121.01	557.66	A	N	60	560.53	I	N	45	DY	BA	GD	2	1	99
121.02	560.53	T	N	45	556.93	I	A	0	DY	BA	GD	1	2	99
122.01	556.93	T	N	5	576.36	I	N	70	DY	BA	GD	1	1	80
124.01	576.36	T	N	70	577.17	I	N	70	DY	BA	DD	4	5	99
124.02	577.17	T	N	70	581.30	I	N	-	DY	BA	DD	0	10	99
125.01	581.30	A	N	-	582.00	I	N	15	DY	BA	DD	1	1	99
125.02	582.00	T	N	45	582.12	T	N	60	UK	BA	DD	0	0	99
125.03	582.12	I	N	-	583.60	I	N	-	DY	BA	GD	5	1	99
125.04	583.60	T	N	70	587.02	A	N	-	UK	BA	DD	1	1	99
					Core Lost 587.02 - 587.35 m									
126.01	587.35	A	N	-	589.72	T	N	70	UK	BA	GD	4	2	99
126.02	589.72	I	N	70	589.88	T	N	30	DY	BA	GG	0	60	99
126.03	589.88	I	N	30	590.49	I	A	65	DY	BA	GD	1	1	99
127.01	590.49	T	N	75	591.80	T	N	85	UK	BA	GD	3	1	99
127.02	591.80	I	N	85	593.10	I	N	68	DY	BA	GD	1	1	99
127.03	593.10	T	N	68	595.39	A	N	0	DY	BA	GD	5	1	99
127.04	595.39	A	N	0	605.50	A	N	60	DY	BA	GD	5	1	99
129.01	605.50	A	N	-	607.77	T	N	-	UK	BA	GD	5	1	99
130.01	607.77	I	A	80	631.53	I	N	85	DY	BA	DD	4	1	99
134.01	631.53	T	N	85	634.43	I	N	10	DY	BA	GD	2	3	99
135.01	634.43	T	N	10	642.70	I	N	80	DY	BA	DD	3	1	99
136.01	641.70	T	N	80	645.53	I	N	80	DY	BA	GD	1	1	99
137.01	645.53	T	N	80	646.32	I	A	20	DY	BA	DD	0	1	99
137.02	646.32	T	N	20	646.99	T	N	55	UK	BA	GD	2	0	99
137.03	646.99	T	N	-	647.72	A	N	55	UK	BA	GD	5	0	99
137.04	647.72	A	N	68	650.48	I	N	80	DY	BA	GD	2	1	99
138.01	650.48	T	N	80	650.83	I	N	40	DY	BA	GD	15	1	99
138.02	650.83	I	N	60	651.30	T	N	70	DY	BA	GD	1	1	99
138.03	651.30	I	N	70	651.67	I	A	35	DY	BA	DD	2	0	99
138.04	651.67	T	N	30	653.23	I	A	15	DY	BA	GD	1	1	99
138.05	653.23	T	N	15	653.90	T	N	50	UK	BA	GD	10	2	99
138.06	653.90	I	N	70	659.92	I	N	60	DY	BA	GD	2	1	99
139.01	659.92	T	N	60	660.01	T	N	70	UK	BA	GD	1	0	99
139.02	660.01	I	N	70	661.11	I	N	80	DY	BA	GD	10	1	99
140.01	661.11	T	N	80	661.42	T	N	75	UK	BA	DG	2	3	99
140.02	661.42	I	N	75	662.03	I	N	75	DY	BA	DG	1	1	99
140.03	662.03	T	N	75	662.50	I	N	68	DY	BA	GD	1	1	99
140.04	662.50	T	N	68	663.05	T	N	60	UK	BA	GD	1	1	99
140.05	663.05	I	N	60	668.12	T	N	40	DY	BA	DG	3	5	99
141.01	668.12	I	A	40	668.73	I	N	40	DY	BA	GD	1	1	99
141.02	668.73	T	N	40	669.93	A	N	-	UK	BA	GD	0	1	99
141.03	669.93	A	N	50	671.80	A	N	-	VB	BA	GD	0	1	99
142.01	671.80	A	N	-	676.93	I	N	60	DY	BA	DD	1	1	99
142.02	676.93	T	N	60	677.83	A	N	60	BR	BA	DG	2	0	99
143.01	677.83	A	N	60	678.35	I	N	80	DY	BA	GD	4	0	99
143.02	678.35	T	N	80	680.62	T	N	50	VB	BA	DG	1	1	99
143.03	680.62	I	N	50	685.70	I	N	70	DY	BA	DG	1	0	99
144.01	685.70	T	N	70	687.85	A	N	-	VB	BA	DG	1	1	99
144.02	687.85	A	A	-	688.81	T	N	75	UK	BA	DG	1	1	99
145.01	688.81	I	N	80	689.15	A	N	-	UK	BA	DG	2	1	99

REFERENCES

Constantinou, G.
1980: Metallogenesis associated with the Troodos ophiolite; *in* Ophiolites: Proceedings of the International Ophiolite Symposium, Cyprus, 1979, ed. A. Panayiotou; Cyprus Geological Survey Department, Ministry of Agriculture and Natural Resources, p. 663-674.

Gass, I.G. and Smewing, J.D.
1973: Intrusion, extrusion and metamorphism at constructive margins: evidence from the Troodos massif, Cyprus; Nature, v. 242, p. 26-29.

Hynes, A.
1975: Comment on "The Troodos ophiolitic complex was probably formed in an island arc", by A. Miyashiro; Earth and Planetary Science Letters, v. 25, no. 2, p. 213-216.

Johnson, H.P., Karsten, J.L., Vine, F.J., Smith, G.C. and Schoenharting, G.
1982: A low level magnetic survey over a massive sulphide orebody in the Troodos ophiolite complex, Cyprus; Marine Technology Society Journal, v. 16, no. 3, p. 76-80.

Miyashiro, A.
1973: The Troodos ophiolitic complex was probably formed in an island arc; Earth and Planetary Science Letters, v. 19, no. 2, p. 218-224.

Moores, E.M.
1975: Discussion of "Origin of Troodos and other ophiolites: a reply to Hynes", by Akiho Miyashiro; Earth and Planetary Science Letters, v. 25, no. 2, p. 223-226.

Oudin, E. and Constantinou, G.
1984: Black smoker chimney fragments in Cyprus sulphide deposits; Nature, v. 308, p. 349-353.

Smewing, J.D., Simonian, K.O. and Gass, I.G.
1975: Metabasalts from the Troodos Massif, Cyprus: genetic implications deduced from petrography and trace element geochemistry; Contributions to Mineralogy and Petrology, v. 51, p.49-64.

Spooner, E.T.C.
1977: Hydrodynamic model for the origin of the ophiolitic cupriferous pyrite ore deposits of Cyprus; *in* Volcanic Processes in Ore Genesis; Geological Society of London, Special Publication, no. 7, p. 58-71.

Spooner, E.T.C. and Bray, C.J.
1977: Hydrothermal fluids of seawater salinity in ophiolitic sulphide ore deposits in Cyprus; Nature, v. 266, no. 5605, p. 808-812.

Spooner, E.T.C., Chapman, H.J. and Smewing, J.D.
1977: Strontium isotopic contamination and oxidation during ocean floor hydrothermal metamorphism of the ophiolitic rocks of the Troodos Massif, Cyprus; Geochimica et Cosmochimica Acta, v. 41, no. 7, p. 873-890.

The Geology and Geophysics of the Area surrounding the CY-2 and CY-2a Drill Holes of the Cyprus Crustal Study Project

JOHN MALPAS

Department of Earth Sciences, Memorial University, Newfoundland, A1B 3X5

Malpas, J., The geology and geophysics of the area surrounding the CY-2 and CY-2a Drill Holes of the Cyprus Crustal Study Project; in *Cyprus Crustal Study Project: Initial Report, Holes CY-2 and 2a, ed. P.T. Robinson, I.L. Gibson and A. Panayiotou; Geological Survey of Canada, Paper 85-29, p. 19-28, 1987.*

Abstract

Drill holes CY-2 and CY-2a of the Cyprus Crustal Study Project are situated in an area underlain by rocks representing the highest, extrusive parts of the Troodos ophiolite and their sedimentary cover. The basement rocks consist of a series of pillow lavas and thin flows, hyaloclastites, and an underlying sequence of diabase dykes with lava screens. Overlying sedimentary rocks are dominated by marls and chalks with minor cherts and, immediately overlying the igneous rocks, intermittent occurrences of ferromanganiferous shales and umbers. Sulphide mineralization in the form of Cyprus-type ore bodies (70,000-5,000,000 tonnes) is restricted to the pillow lavas and has been mined both by open-pit and underground methods. The present distribution of the ore is structurally controlled and is delineated by low seismic velocity bodies surrounded by high seismic velocity zones paralleling the alteration halos of highly silicified rocks.

Résumé

Les forages CY-2 et CY-2a du Projet d'Etude de la Croûte Cyprus sont situés dans la région dont les roches sous-jacentes représentent les plus hautes des parties extrusives de l'ophiolite de Troodos et leur couvert sédimentaire. Les roches du socle consistent en une série de coulées de laves en coussins et de coulées liquides, d'hyaloclastites et d'une séquence sous-jacente de dykes de diabase avec écrans de lave. Les roches sédimentaires trouvées au-dessus sont principalement des marles et craies avec du chert en quantité mineure et immédiatement par-dessus des roches ignées se trouvent de façon intermittente des shales ferromanganifères et des terres. La minéralisation en sulfures sous la forme de minerai de type Cyprus (70.000-5.000.000 tonnes) est limitée aux coulées de laves en coussins et a été exploitée à la surface et sous terre. La présente distribution du minerai est controllée par la structure et est délimitée par des roches à faible vitesse séismique entourées par des zones à haute vitesse séismique parallèles aux halos d'altération des roches hautement silicifiées.

INTRODUCTION

Drill holes CY-2 and CY-2a were designed to penetrate rocks affected by the hydrothermal systems that gave rise to the Agrokipia ore bodies. These ore bodies, together with a number of associated occurrences at Kambia, Mitsero (Kokkinopezoula) and Kapedhes may all be found in the Akaki-Lythrodondha map area of Bear (1960) and Figure 1.

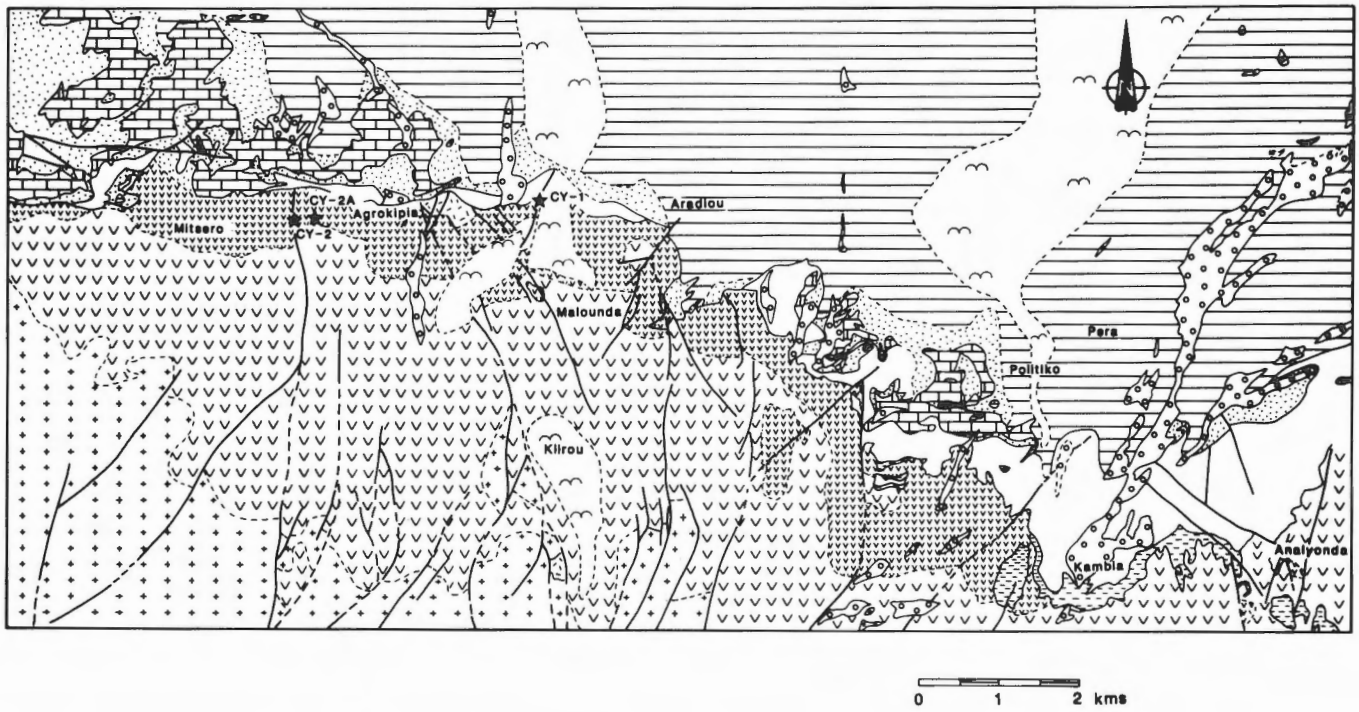

LEGEND

SEDIMENTARY ROCKS

RECENT			Alluvium
PLEISTOCENE		Fanglomerate Series	Boulder beds & secondary limestone
PLIOCENE	Mesaoria Group		Buff & grey marl, sands & calcareous siltstones
MIOCENE	Dhali Group	Koronia Limestone	Reef limestone
		Pakhna Formation	Chalks, marls & limestones
MIOCENE TO UPPER CRETACEOUS	Lapithos Group		White flaggy & cleaved chalk. Chalk with chert bands & pink marls
JURRASIC?	Troya Group	Perapedhi Formation	Umberous shales, radiolarian shales & radiolarites

VOLCANIC ROCKS

Upper Pillow Lavas	Pillow lavas. Olivine-basalt, picrite-basalt, glassy basalt, mugearites & limburgites
Lower Pillow Lavas	Pillow lavas & contemporaneous intrusives. Andesites, dacites & keratophyres
Basal Group	Diabase intrusives with screens of pillow lava

INTRUSIVES

High level intrusives

Figure 1: Regional geology in the vicinity of the CY-2 and CY-2a drill holes. Modified after Bear (1960).

This area consists of roughly equal proportions of sediments and underlying igneous rocks, with the boundary marked by numerous small inliers and outliers along a line from Mitsero to Analyonda. The basement rocks of the area consist of the Upper and Lower Pillow Lava suites and the underlying Basal Group of Bear (1960). The Basal Group differs from the underlying Sheeted Diabase only in that narrow pillow lava screens are recognizable between diabasic material. In places the screens are essentially absent and multiple intrusives dominate the succession. Periods of volcanic quiescence are marked by restricted sedimentation between successive lava flows and there appears to have been considerable relief on the pillow lava surface prior to the deposition of the major sedimentary succession. The Perapedhi Formation consists of sediments that fill in the hollows on this irregular surface and comprises manganiferous shales and radiolarites with limited ongoing volcanicity evidenced by the presence of bentonites. Although there is no discernible unconformity, there is a marked difference between the Perapedhi Formation and the overlying Lapithos Group. Marked differences in thickness of the sedimentary pile occur in closely adjacent areas (Figure 2) but sedimentation appears to have been fairly continuous during Upper Cretaceous through to Lower Miocene times and is dominated by marls and chalks with minor chert horizons.

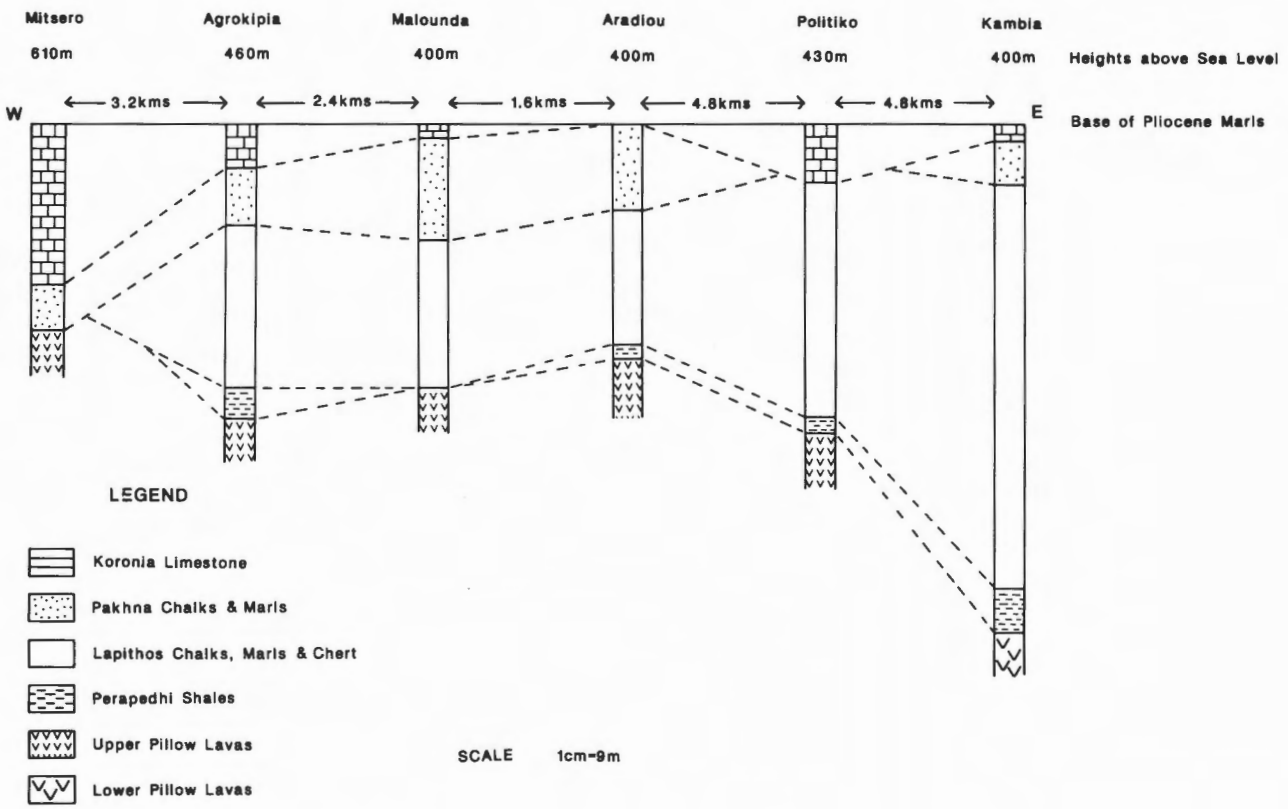

Figure 2: Variations in thickness of the Supra-ophiolite sedimentary succession on the north flank of the Troodos Complex. After Bear (1960).

THE SEDIMENTARY COVER SUCCESSION

a) The Perapedhi Formation

Radiolaria (*Meyenella meyeni*) indicate a Jurassic age for this Formation, and suggest a correlation with the Mamonia Formation (Trypa Group) to the south which contains a similar lithology and fauna. The thickness of the Formation rarely exceeds 40-50 feet and its disposition in depressions on the irregular pillow lava surface means that occurrences are intermittent and somewhat dispersed, but generally lie along the main igneous-sedimentary map boundary.

The lavas underlying these sediments typically are highly decomposed and iron-stained and in some areas are completely altered to a soft yellow clay. The full sedimentary sequence of the Formation as revealed in the Kambia area is as follows from top to bottom:

Marl with chert intercalations
Bentonite
Radiolarian shales
Manganiferous shales and umber

However, in most localities in the Agrokipia area all but the manganiferous and radiolarian shales are absent. The manganiferous shales are widespread and may locally grade into true umbers or black laminated clays with pyrolusite and psilomelane concretions. The shales are intercalated with, and gradually merge up section into radiolarian shales, distinguished by their salmon-pink colour. This results essentially from a decrease in the amounts of manganese and argillaceous material and an increase in radiolarian and silty material.

At Agrokipia, the Perapedhi Formation is in faulted contact with the Upper Pillow Lavas. In the inclined shaft of the underground workings the Formation is represented by 3 metres of brown shales with some subordinate clays of bentonitic affinity. Sediments of similar lithology to those of the Perapedhi Formation occur as thin intercalations within the Pillow Lava Series. North of Mitsero the following succession was recorded by Bear (1960) within the pillow lavas from top to bottom:

8cm	Sheared brown serpentine
8cm	Pink radiolarian shales
10cm	White papery shales
5cm	Pink papery shales
20cm	Black manganiferous shales

The manganiferous sediments were formed by precipitation from hydrothermal waters venting onto the ocean floor. The erratic distribution of these sediments in the Akaki-Lythrodondha area results from ponding in basins and troughs on the irregular pillow lava surface. There is an almost total absence of detrital and calcareous material at this stage of geological evolution.

b) The Lapithos Group

Lapithos sediments are exposed in a discontinuous belt running east-west immediately north of the igneous rocks. The succession thins considerably from east to west and around Agrokipia small patches of Lapithos sediments occur as faulted inliers within both the Koronia limestone and Pakhna chalks of the overlying Dhali Group. Outliers of Lapithos rocks are also associated with the Perapedhi sediments west of Kambia. The Lapithos sediments either overlie the Perapedhi sediments or, more commonly where the latter are absent, rest directly on the Upper Pillow Lavas.

The Lapithos Group in general has an age range from Upper Cretaceous to Lower Miocene but in the immediate area of the drill holes only the middle and upper units of the Group are exposed. These range from Palaeocene to Eocene and Oligocene to Lower Miocene in age, respectively.

The Middle Lapithos consists at its base of pink, chert-bearing marls which grade upward into chalks with a more compact texture. The proportion of chert increases upwards in the succession and it is not unusual for the contact between the Middle and Upper Lapithos sediments to be marked by jasper veins. At one exposure near Agrokipia, Lower and Middle Eocene chalks rest directly on the Upper Pillow Lavas, and contain the faunal assemblage: *Robulus, Cibicides pseudoungerianus, Eponides umbonatus* var. *stellatus* and *Truncorotalia aragonensis* (Bear, 1960).

Whereas the Middle Lapithos has an extremely patchy distribution, the Upper Lapithos is more continuous. In places it transgresses onto pillow lavas to the total exclusion of the Middle Lapithos, but the succession again thins drastically to the west. The assemblage consists almost entirely of foraminiferal chalks with numerous intercalations of fissile black shale near the top which is also characterized by large numbers of limonite nodules. Abundantly fossiliferous, the chalks contain a large number of benthonic genera as well as *Globigerina, Globigerinoides, Globorotalia* and *Orbulina* (Bear, 1960).

c) The Dhali Group

The Dahli Group consists of the Pakhna Formation and the Koronia limestone. The Pakhna Formation forms the base of the Group and is best developed just north of Mitsero where a unique evaporite facies of some 150 metres thickness is present including some large gypsum lenses. In

general, however, the Pakhna Formation is a succession of marls and chalks with only subordinate gypsum. The general dip of the beds is moderate and to the north but where large amounts of evaporite are present remobilization of the salts has produced modified dips, in some cases steep and to the south. Drilling in the Mitsero area has revealed three horizons of gypsum of various sizes and shapes, one immediately below the overlying reefoidal Koronia Limestone and another, as a result of faulting, in contact with the Lapithos.

Northeast of Agrokipia, the Pakhna Formation is less than 15 metres thick and consists predominantly of grey and fawn coloured marls. In the inclined shaft of the underground working, en echelon faulting reveals a 7 metre thick zone of carbonaceous shales which is closely associated with small pockets of disseminated sulphide and strontianite (Bear, 1960). An intraformational conglomerate appears immediately above the shale horizon and consists of fragments of marlstone, black shale and comminuted fossils including fossil fish which date the assemblage as Lower Helvetian (Henson et al., 1949).

The Koronia Limestone forms the upper portion of the Dhali Group and occurs as a series of outcrops which transgressively overlie the Perapedhi and Lapithos sediments between Mitsero and Agrokipia, and in some places lie directly on the Upper Pillow Lavas. It is easily recognized as the sedimentary element that forms the scarps on the hills immediately surrounding Agrokipia, but decreases rapidly in occurrence and thickness from this point eastwards. In the Mitsero area, thicknesses of 150 metres are recorded in bore holes. The Koronia Limestone is a hard, semi-crystalline rock composed of masses of broken shells and casts of small gastropods. Breccias are not uncommon and large scale recrystallization, extensive dolomitization and zones of local silicification are found everywhere. Lateral to the reef core a softer sandy limestone is developed. This facies is oolitic, devoid of stratification and contains but little arenaceous matter in the form of quartz, feldspar, epidote, diopside and iron oxide grains. East of Agrokipia the base of the massive reef limestone is separated from the Pakhna chalks by coralline limestones up to 1 metre thick.

d) The Mesaoria Group

The only sediments of the Mesaoria Group represented in the immediate area of the drill holes are the Myrtou Marls and sandy and shelly limestones of the Nicosia Formation. The marls were the first deep water deposits of the Lower Pliocene and are intercalated at their base with more sandy arenaceous sediments. They appear to have been derived from the underlying Lapithos and Dhali sediments and reach a total thickness of some 700 metres. The sandy and shelly limestones of the Nicosia Formation overlie the marls but rarely reach thicknesses in excess of 50 metres in the area under consideration. The limestones are medium grained rocks with a speckled appearance due to the large number of iron-stained shell fragments. Heavy mineral analyses reported in Bear (1960) indicate that the source of these sediments was to the north and probably related to that which supplied detritus to the Kythrea flysch.

THE VOLCANIC BASEMENT SUCCESSION

a) The Pillow Lava Sequence

The extrusive sequence of the Troodos Ophiolite in the Agrokipia area, as exposed for example along the Akaki River canyon, is from 1,100 to 1,500 metres thick and consists of pillow or sheet flow lavas and associated breccias. Intrusive rocks are represented by thin dykes and sills and some larger stocks and there are thin interflow layers of hyaloclastic tuffs. The lower 300-500 metres of the extrusive sequence consist of aphyric or poorly phyric andesites and dacites with rare microphenocrysts of plagioclase, clinopyroxene and iron oxides. These are referred to as the Lower Zone Lavas by Robinson et al. (1983) and Schmincke et al. (1983). The remainder of the sequence consists of basalts and basaltic andesites which are sparsely porphyritic towards their base but become highly phyric higher in the section. Olivine phenocrysts are usually accompanied by chromite, clinopyroxene and rare orthopyroxene, making picritic rocks a fairly common occurrence particularly at the bases and centres of pillow tubes and some sheet flows. On the basis of phenocryst content, the same authors have referred these rocks to the Middle and Upper Zone Lavas, respectively. Whereas the boundary between the Middle and Upper Zones is essentially gradational, that between the Middle and Lower Zone varies from being relatively sharp, for example in the Akaki Canyon to being transitional as a result of interdigitation of lava types, for example in the Pedeios Canyon. Earlier workers (Bear, 1960; Gass, 1960; Gass and Smewing, 1973) used similar mineralogical features and a perceived metamorphic break to divide the lava pile into the Upper Pillow Lavas and the Lower Pillow Lavas. Their line of division essentially coincides with the Upper/Middle Zone boundaries described by Robinson et al. (1983) and Schmincke et al. (1983). It is now clear that the more fundamental break occurs at the Lower/Middle Zone boundary since the Lower Zone rocks resemble island arc tholeiites geochemically whilst the Middle and Upper Zone lavas are a series of depleted tholeiites with relatively high SiO_2 at high MgO/FeO ratios, low Ti, Zr, Y, Nb, Ni etc. (Figure 3). The

latter rocks have boninitic affinity but rocks resembling true boninites are found only on the southern side of the Troodos Massif in the Arakapas Fault valley.

Pillow lavas form most of the extrusive sequence and occur in units that may exceed 100 metres in thickness. Individual pillows generally have a diameter of 0.5 metres but are very often tube-like. Vesicular pillows are common and suggest a magma relatively rich in volatiles as is also suggested by low totals of glass analyses (Robinson et al., 1983) and the occurrence in places of quench amphiboles. Feeders to overlying pillow lavas have been recorded by Schmincke et al. (1983) as large, irregular lava bodies up to 6 metres in width and 4 metres in height. They often have lobate lateral margins which interdigitate with each other or with piles of the smaller, normal pillows. Pillows with smaller than average dimensions preferentially occur towards the top of each of the pillowed units together with lapilli-tuffs, lava stringers and hyaloclastites.

Massive lava flows are common in the sequence, especially in the lower parts. Individual flows are quite variable in thickness but can generally be traced for distances of several hundred metres. The distribution and type of vesicles in these flows permits their distinction from sheet-like intrusions, small pipe vesicles and vesicle sheets appearing in defined basal colonnades and large, flow-deformed vesicles in the top parts of the flows. The tops of many flows are marked by brecciated, glassy cooling surfaces.

Extrusive breccias are common in the lower parts of the sequence, occurring near the tops of pillow lava units, interbedded with sheet flows and apparently filling fissures. Thin hyaloclastic lapilli tuffs consisting of black volcanic glass are sparsely distributed throughout the pillowed sequence.

Intrusions in the form of both sills and dykes are found throughout the sequence although sills are more common in the upper parts. Most dykes are aphyric but there are olivine-phyric varieties associated with late intrusions. The dykes are generally of the order of 0.5 metres wide although there are massive diabases up to several tens of metres wide which have an apparent layered aspect throughout the pillow lava pile. Dykes increase downward into the Basal Group with, in places, a relatively abrupt transition at the base of the section.

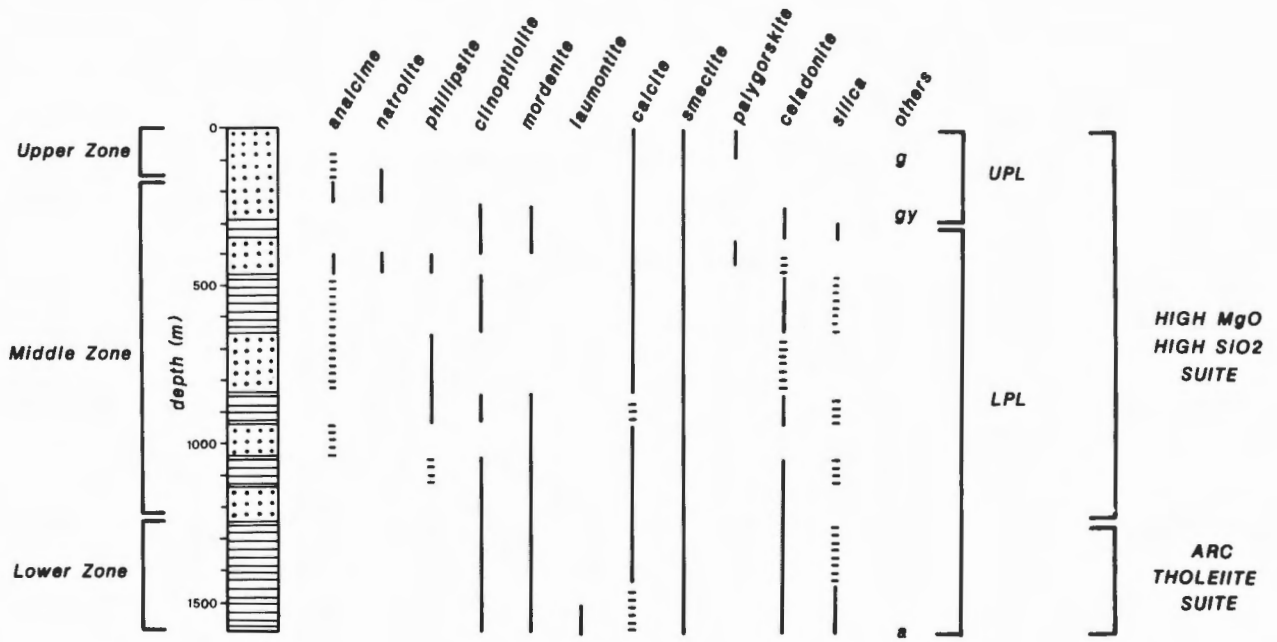

Figure 3: Distribution of secondary minerals in the lava succession of the Troodos ophiolite in the vicinity of the CY-2 and CY-2a drill holes. The distribution of dominantly pillow flows and dominantly sheet flows are shown by dots and horizontal lines respectively. The subdivision of the lava stratigraphy into lithological zones and geochemical units is also shown. See text for detail. UPL and LPL are upper pillow lavas and lower pillow lavas of Gass (1960), g = gmelinite, gy = gypsum, a = aragonite. After Gillis and Robinson (1985).

Swarms of small faults spaced at distances of a few tens of metres occur throughout the section and appear in many cases to be growth faults which operated penecontemporaneously with volcanic activity. They often appear to have controlled the production of open fissures that were subsequently filled with hyaloclastites. Most of the observed faults do not cut the overlying sediments, and where they do, it is probably a result of reactivation.

The pillow lava sequence has been altered primarily by low-temperature interaction with sea water and locally by active hydrothermal upwellings. Below the sea-floor weathered surface containing abundant calcite and smectite, the pillow lavas are characterized by assemblages of analcime, natrolite, phillipsite, chabazite and gmelinite whilst the sheet flows have assemblages of clinoptilolite, mordenite and celadonite (Figure 3). The basal andesites and dacites have abundant secondary silica. There is no good correlation of alteration with depth and the variations are perhaps best explained by local variations in permeability, rate of cooling, water/rock ratio and possibly initial lava composition (Gillis and Robinson, 1985).

b) The Basal Group and Sheeted Dyke Section

The Basal Group forms a considerable portion of the foothills of the Troodos Range in the southern portion of the study area. Bear (1960) also mapped a small fault-bounded inlier within the pillow lavas immediately west of Klirou. Besides diabase dykes which form the bulk of the intrusive material, pillow lavas are intruded by and form blocks within gabbroic, microgabbroic and plagiogranitic rocks. Within the screens, pillow breccias are common and glassy selvages are often preserved. The widths and number of pillow screens vary considerably from one area to another. They often appear as small lenticular relics without lateral continuity. Other screens may be up to 20 metres wide and much more continuous. The density of pillow screens, as would be expected, increases upward in the succession towards the transition to the Lower Pillow Lavas.

The bulk of the pillow lavas in the Basal Group appear to have been considerably altered, in some places by autometasomatism, but in others by alteration associated with upwelling hydrothermal circulation. Both the primary and secondary mineralogy suggest that the composition of the original flows varied from andesite to dacite. They therefore appear to fall into the category of Lower Zone lavas as described above. The assemblage actinolite - epidote - albite - chlorite is most common in the Basal Group lavas and most original rock textures have been replaced by a granoblastic mosaic.

The intrusives within the Basal Group are merely the vertical extension of the diabase dykes of the Sheeted Complex below. There is no difference structurally, petrologically or genetically between the two except that the Basal Group dykes appear on average more vesicular. The Sheeted Complex consists of a series of multiple dyke swarms with individual dykes varying in width from 0.5 metres to 3 metres, the sheeted aspect being enhanced by major joint surfaces parallel to the dyke strike. Chill margins are often preserved but only rarely as glass. Measurements of chilling statistics undertaken during this project do not confirm the preferential chilling model of Kidd and Cann (1974) and, with the available data, there is no clear relationship between the time of intrusion of the dyke and its chemistry, although the mineralogy and chemistry of the dykes cover the range exhibited by the pillow lavas. Dykes with Upper/Middle Zone Lava chemistry do, however, cluster as swarms, which may be fault controlled during intrusion.

MASSIVE SULPHIDE MINERALIZATION

a) General Considerations

The massive sulphide ore bodies of the Troodos ophiolite which are the original examples of Cyprus-type occurrences, are restricted to the pillow lavas where they occur in clusters of four or more bodies which define five mining districts. They range in size from about 50,000 tonnes to over 20,000,000 tonnes and have an average copper content that varies from 0.5% to 4.5% (Constantinou, 1980). In addition to these massive sulphide occurrences, many small gossans and zones of hydrothermal alteration occur throughout the extrusive sequence and some minor mineralization occurs in the upper parts of the Basal Group.

Constantinou (1980) notes that the massive ores typically have a conglomeratic structure consisting of variously shaped blocks of colloform sulphide material in a matrix of sandy sulphide. The principal ore minerals are pyrite, chalcopyrite, marcasite and sphalerite and gossan zones are characterized by limonite, haematite, jarosite, native sulphur, gypsum and silica. Directly overlying some of the ore bodies is a thin layer of ochre, a manganese-poor, iron-rich sediment containing abundant sulphide material and derived by leaching of the massive sulphide. Beneath each massive orebody lies a stockwork zone consisting of mineralized and hydrothermally altered breccias and pillow lavas. The sulphide in these zones is associated with quartz in veins and the sulphur content ranges from as much as 30% close to the orebody to 10% in the deeper parts.

It is now generally considered that the orebodies formed as exhalative deposits on the seafloor. Spooner (1977) suggested a model involving the

circulation of sea water hydrothermal cells at and below an active spreading centre with the recharge zones penetrating as deep as the gabbros and plagiogranites of the plutonic ophiolite stratigraphy. At these depths the water reached temperatures in excess of 300°C. The hot fluids then returned to the surface, in many cases being directed along narrow planes of weakness, causing massive alteration in the stockwork zones and the precipitation of massive sulphide ores on the seafloor. Based on the spacing of the orebodies, Spooner (1977) postulated that they formed from a series of axially symmetrical convection cells from 3 to 5 km deep and with half widths approximately equal to this thickness of the permeable layer.

b) The Agrokipia Orebodies

The Agrokipia orebodies form part of the Tamasos Mining District in which four major groups of deposits and a large number of prospects and gossans occur. The principal structure in the area is the Agrokipia Fault which strikes at N30°W through the Agrokipia 'B' workings and offsets the orebody. Three ore bodies were originally discovered in the Agrokipia area. Two were shallow lensoid structures that were exploited by open-cast methods and form the Agrokipia 'A' mine. Their upper levels were well marked by gossan and reserves were estimated at the time of discovery at about 700,000 tonnes. The third ore body, Agrokipia 'B', is centred about 300 metres east of Agrokipia 'A' and is located about 150 metres deeper in the section in the aphyric Lower Zone Lavas. No indication of Agrokipia 'B' was seen at the surface - discovery was made by Hellenic Mining Company through percussion drilling on a gravity anomaly. The main body is pyramidal in form extending downwards from a depth 170 metres below the surface for another 160 metres. Other smaller associated ore bodies occur and are interpreted as downthrown segments to the north of the Agrokipia Fault. Ore reserves were estimated at 5,000,000 tonnes of which about 500,000 tonnes are high grade Cu-Zn ore. A small amount of this was removed by underground mining some 25 years ago (Figure 4).

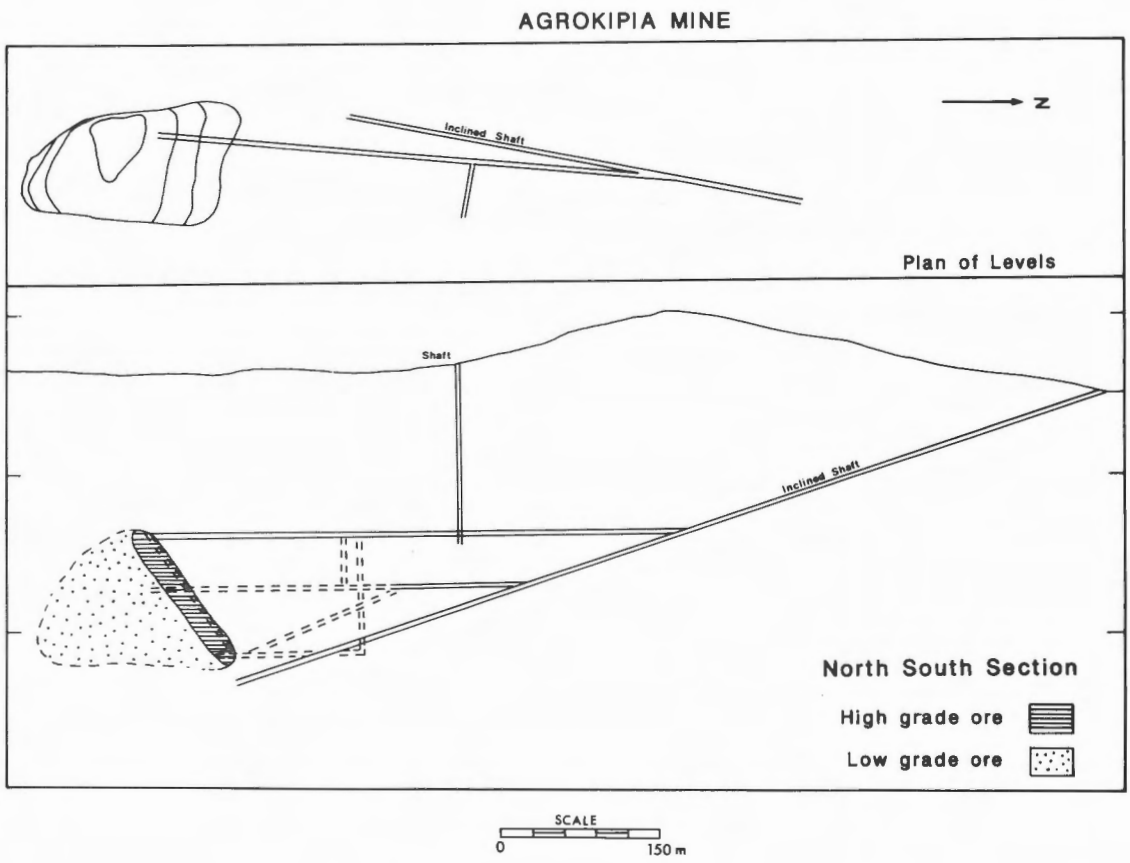

Figure 4: The Agrokipia B mine plan. After Bear (1960).

Specific site selection for the CY-2 and CY-2a bore holes was based upon geological mapping and interpretation of drilling logs from the Hellenic Mining Company. Detailed geophysical surveying was carried out immediately prior to site selection (Johnson et al., 1982).

GEOPHYSICAL SURVEYS

Magnetic, gravity and seismic surveys have been carried out over the area surrounding the Agrokipia ore bodies. A pronounced magnetic low is observed over the Agrokipia 'A' body and a weaker, broader low over the deeper Agrokipia 'B' body. To the west of the open pit a major N-S fault is delineated by a ridge of magnetic high, and the Agrokipia Fault is recorded as a trough of magnetic low with an adjacent high running NW-SE through Agrokipia 'B'. Simple modelling shows this later signature to be due to uplift of mineralized rocks on the SW side of the fault as interpreted from field mapping.

The gravity survey of the area was completed before mining took place by the Hellenic Mining Company. Gravity highs, once thought to be due to the presence of denser mineralized material now appear to be caused by intrusions into the pillow lava section close to the surface. These have been intersected by drilling in a number of exploratory holes. A small local positive anomaly is seen offset east of Agrokipia 'A' and there is a second smaller positive anomaly associated with Agrokipia 'B'. The structures defined in the field and recognized as magnetic anomalies also appear as steep gravity gradients (Smith and Vine, 1987).

Seismic velocities recorded in the area are variable. The average gradient for the upper 800 metres of the extrusive section appears rather high when compared to sections of the oceanic crust (e.g. White, 1984). This essentially results because of especially low velocities in the upper 300 metres which result from high porosity, open fractures and low lithostatic pressure within the extrusives. The velocities recorded in rocks between 3,000 and 800 metres in depth are, however, much closer to oceanic layer 2 values at about 2 km/sec. The local velocity structure over the ore bodies departs significantly from the structure of unmineralized lavas. The ore deposit is characterized by a low velocity body surrounded by a high velocity zone that parallels the alteration zone of highly silicic rocks. A similar velocity discontinuity approximately marked by the 4 km/sec velocity contour (Eleftheriou and Schoenharting, 1987) and at a depth of 550 to 650 metres might correlate with the pillow lava/Basal Group boundary below which dykes essentially dominate the lithology.

ACKNOWLEDGEMENTS

Thanks are due to Mr. T. Brace for the drafting of the diagrams. This work was supported in part by an operating grant from NSERC, Canada.

REFERENCES

Bear, L.M.
1960: The geology and mineral resources of the Akaki-Lythrodondha Area; Cyprus Geological Survey Department, Ministry of Agriculture and Natural Resources, Memoir, no. 3, p. 1-122.

Constantinou, G.
1980: Metallogenesis associated with the Troodos Ophiolite; *in* Ophiolites: Proceedings of the International Ophiolite Symposium, Cyprus, 1979, ed. A. Panayiotou, Cyprus Geological Survey Department, Ministry of Agriculture and Natural Resources, p. 663-674.

Eleftheriou, S. and Schoenharting, G.
1987: A seismic survey at the Agrokipia mine, Cyprus: the velocity structure of a hydrothermally altered extrusive section of the Troodos ophiolite; *in* Cyprus Crustal Study Project Initial Report Hole CY2-2a, ed. P.T. Robinson, I.L. Gibson and A. Panayiotou; Geological Survey of Canada, Paper 85-29.

Gass, I.G.
1960: The geology and mineral resources of the Dhali area; Cyprus Geological Survey Department, Ministry of Agriculture and Natural Resources, Memoir, no. 4, p. 1-116.

Gass, I.G. and Smewing, J.D.
1973: Intrusion, extrusion and metamorphism at constructive margins: evidence from the Troodos Massif, Cyprus; Nature, v. 242, p. 26-29.

Gillis, K.M. and Robinson, P.T.
1985: Low-temperature alteration of the extrusive sequence, Troodos ophiolite, Cyprus; Canadian Mineralogist, v. 23, p. 431-441.

Henson, F.R.S., Browne, R.V. and McGinty, J.
1949: A synopsis of the stratigraphy and geological history of Cyprus; Geological Society of London, Quarterly Journal, v. 105, p. 1-41.

Johnson, H.P., Karsten, J.L., Vine, F.J., Smith, G.C. and Schoenharting, G.
1982: A low level magnetic survey over a massive sulphide orebody in the Troodos ophiolite complex, Cyprus; Marine

Technology Society Journal, v. 16, no. 3, p. 76-80.

Kidd, R.G.W. and Cann, J.R.
1974: Chilling statistics indicate an ocean-floor spreading origin for the Troodos complex, Cyprus; Earth and Planetary Science Letters, v. 24, no. 1, p. 151-155.

Robinson, P.T., Melson, W.G., O'Hearn, T. and Schmincke, H.-U.
1983: Volcanic glass compositions of the Troodos ophiolite, Cyprus; Geology, v. 11, no. 7, p. 400-404.

Schmincke, H.-U., Rautenschlein, M., Robinson, P.T. and Mehegan, J.M.
1983: Troodos extrusive series of Cyprus: a comparison with oceanic crust; Geology, v. 11, no. 7, p. 405-409.

Smith, G.C. and Vine F.J.
1987: Gravity and magnetic studies of the Agrokipia sulphide ore bodies, Cyprus; *in* Cyprus Crustal Study Project Initial Report Hole CY2-2a, ed. P.T. Robinson, I.L. Gibson and A. Panayiotou; Geological Survey of Canada, Paper 85-29.

Spooner, E.T.C.
1977: Hydrodynamic model for the origin of the ophiolitic cupriferous pyrite ore deposits of Cyprus; *in* Volcanic Processes in Ore Genesis; Geological Society of London, Special Publication, no. 7, p. 58-71.

White, R.S.
1984: Atlantic oceanic crust: seismic structure of a slow spreading ridge; *in* Ophiolites and Oceanic Lithosphere, ed. I.G. Gass, S.J. Lippard and A.W. Shelton; Geological Society of London, Special Publication, no. 13, p. 101-112.

Evidence Relevant to the Hydrothermal Discharge Pattern during Formation of the Agrokipia 'B' Ore Deposit, Cyprus

JAMES M. HALL[1] AND MONA BOTROS[2]

[1]Centre for Marine Geology, Dalhousie University, Halifax, Nova Scotia, Canada, B3H 3J5
[2]Department of Oceanography, University of Washington, Seattle, Washington, U.S.A., 98195

Hall, J.M. and Botros, M., Evidence relevant to the hydrothermal discharge pattern during formation of the Agrokipia 'B' Ore Deposit, Cyprus; in *Cyprus Crustal Study Project: Initial Report, Holes CY-2 and 2a, ed. P.T. Robinson, I.L. Gibson and A. Panayiotou; Geological Survey of Canada, Paper 85-29, p. 29-38, 1987.*

Abstract

Where drill hole CY-2a samples the unexposed Agrokipia 'B' deposit, Cyprus, clear evidence is found for locally arrested upwelling of hydrothermal fluid in a zone of alternating massive flows and massive glass. In order to provide additional evidence for models for the origin of the deposit as a whole, a detailed survey has been made of a well exposed gossan of similar cross sectional area to the Agrokipia 'B' deposit. The survey revealed several zones of locally arrested upwelling at the margins of the gossan. Some of these zones occur only a few tens of metres laterally from well defined channels in the gossan that appear to have been principal conduits for the rising hydrothermal fluids. The gossan observations allow the possibility that the Agrokipia 'B' ore body represents part of a hydrothermal upwelling system that vented onto the sea floor, with drill hole CY-2a sampling a peripheral area of locally arrested upwelling.

Résumé

Les échantillons du trou de forage CY-2a prélevés dans le gîte 'B' d'Agrokipia de subsurface montrent nettement qu'il y a eu localement arrêt du fluide hydrothermal ascendant dans une zone où alternent les coulées de lave massive et de verre massif. Une étude détaillée d'un chapeau ferrugineux bien exposé, lequel présente une coupe tranversale similaire au gîte 'B' d'Agrokipia, a été réalisée dans le but d'apporter des preuves additionnelles appuyant les modèles qui cherchent à expliquer la formation du gisement entier. L'étude a révélé qu'il existait dans les marges du chapeau ferrugineux plusieurs zones où plafonnait localement l'ascension des fluides. Certaines de ces zones apparaissent à seulement quelques dizaines de mètres latéralement à des chenaux bien définis au sein du chapeau ferrugineux, lesquels semblent avoir servi de conduits principaux à la montée des fluides hydrothermaux. Les observations sur le chapeau ferrugineux suggèrent que le gîte 'B' d'Agrokipia représente une portion du système hydrothermal ascendant dont les fluides s'échappaient par des évents sur le plancher océanique, et que le forage CY-2a a permis d'échantillonner une région périphérique où se produisit localement un arrêt des fluides ascendants.

INTRODUCTION

One of the objectives of the Cyprus Crustal Study Project (CCSP) is to investigate the hydrothermal upwelling systems that gave rise to the Fe-Cu-Zn bearing massive sulfide ore bodies located at various levels within the Extrusive Sequence of the Troodos ophiolite. Such an objective is timely in view of the strong current interest in the setting of the high temperature vents that occur at intervals along the spreading ridges of the Pacific Ocean and elsewhere. These geothermal vents have become rather well known from extensive submersible and deep-tow camera observations, and from analyses of the discharged fluids and the sulfide and other minerals formed at the vent sites as hydrothermal fluids mix with cold sea water. The existence of vents that discharge acidic fluids at up to 350-400°C at rates of up to several metres per second (Macdonald et al., 1980; Goldie and Bottrill, 1981) prompts interest in the location and geometry of the flow channels beneath the vents, and the interactions between the fluids and the rocks with which they come into contact. Such flow channels are little known from the present ocean floors. Sections of rock altered by high temperature fluids are rare in DSDP ocean basement drill holes, the 18 m stockwork-like mineralized interval in the 1075.5 m basement section at DSDP Hole 504B being the best example (Honnorez et al., 1985). This suggests that fluid flow conduits are of relatively limited cross section, as was postulated by Spooner (1977) and others. Examination of the sulfide ore bodies of the Troodos, ophiolite, and their underlying stockwork zones, provides an alternative means of examining these flow channels. Evidence such as the occurrence of probable vent fragments and traces of fauna similar to those found in new present-day vents (Oudin and Constantinou, 1984), as well as the physical conditions prevailing during the sea floor construction of the Troodos ophiolite (ICRDG, 1984), suggests that the ore bodies are analogous to those occurring presently on spreading centres. For these reasons, study of Troodos massive sulfide ore bodies and stockworks is likely to provide insights into the conditions beneath the vents of in-situ oceanic crustal spreading centres.

The intention of this report is to describe, using outcrop examples, possible settings for the continuous but areally very limited section through one such ore body recovered from CCSP drill hole CY-2a. This is achieved by examining evidence for the distribution of former high temperature mineralizing fluid flow in a number of gossans, particularly that near the village of Klirou.

TROODOS MASSIVE SULFIDE OREBODIES AND STOCKWORKS

The sulfide deposits of the Troodos ophiolite are located at various levels within the Extrusive Sequence, with different bodies located at the contact of the Lower Pillow Lavas with the Basal Group, i.e. directly above epidote-bearing rocks, within the Lower Pillow Lavas, between the Lower and Upper Pillow Lavas, or at the extrusive-sediment interface (Constantinou, 1980). There is evidence that many of the deposits were formed in fault controlled basins, with the ore material accumulating on the coeval sea floor (Constantinou, 1980; Adamides, 1980). The underlying stockworks are zones of disseminated mineralization and extensive alteration of the country rock. The stockwork extent is unknown, but at Skouriotissa the zone is more than 700 m in vertical extent.

THE AGROKIPIA OREBODIES AND STOCKWORKS

Three ore bodies occur within a 500 m by 150 m area directly to the west of Agrokipia village (Bear, 1960: p. 97-99). The two more westerly Agrokipia 'A' deposits are in close proximity to each other and were worked by opencast methods in the 1950's. The Agrokipia 'B' deposit, investigated by CCSP drill hole CY-2a, is located within the Lower Pillow Lavas 400 m to the east and 150 m lower stratigraphically than the Agrokipia 'A' deposits. The description of the B body by Bear (1960) emphasizes features of economic interest, such as shape, size, structural setting, and ore grade. The body was mined by underground methods during the 1960's but is no longer accessible. The asymmetrical, 150 m high and 150 m wide, pyramidal shape of the body and its geological setting within the Lower Pillow Lavas is well documented by extensive percussion drilling by the Hellenic Mining Company (N.G. Adamides, pers. comm.). However, no information relevant to the process of formation of the body at or below the sea floor was previously available. Almost complete core recovery in drill hole CY-2a (Figure 1) has resulted in unequivocal evidence for the process of formation of the part of the ore body at this location. In particular, a transition in the type of alteration style in an alternating massive lava and massive glass sequence occurs within the 149 to 154 m depth interval. Above this interval, alteration of both lava and glass is of the smectite-carbonate type which is familiar from many of the extrusive sections in oceanic crust recovered during the Deep Sea Drilling Project. Honnorez (1981) reviews evidence for the physical and chemical conditions required to produce this style of alteration and concludes that contact with sea water at less than

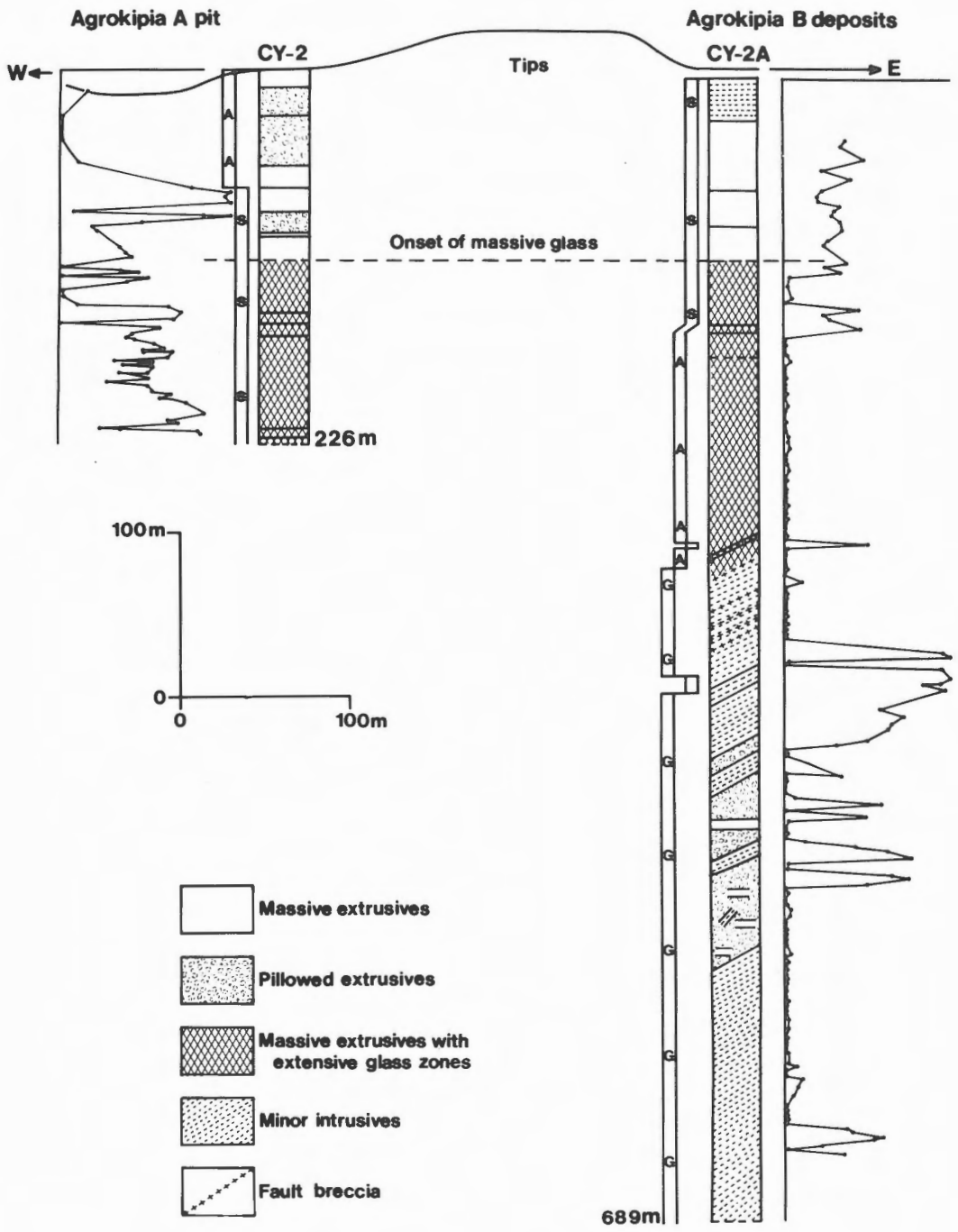

Figure 1: The two broad columns show primary lithologies identified by drill holes into stockwork zones beneath the massive sulfide ore deposits at Agrokipia, Cyprus. Narrow columns represent in simplified form the present state of alteration or metamorphism of the rocks: S - smectite style (green and brown smectites, celadonite, carbonate, zeolites). A - argillic style (complete replacement of primary phases by quartz, illite, chlorite, pyrite, sphene and sphalerite). G - greenschist style (complete replacement of primary phases by chlorite, epidote, quartz, albite and minor pyrite). Graphs running along the columns show the initial magnetic susceptibility in arbitrary units. From ICRDG, 1984.

10°C is the mechanism involved. Below 154 m both lava and glass are intensely or entirely argillized, as is indicated by the presence of quartz, illite and chlorite; pyrite, sphene and sphalerite are also present. Massive pyrite ore only occurs as occasional bands, typically about 10 cm in thickness. Alteration of this type requires temperatures of 200°C or higher (Spooner and Bray, 1977).

Several lines of evidence point clearly to a replacement origin for the Agrokipia 'B' deposit throughout most of the mineralized 154 m to 297 m section penetrated by drill hole CY-2a. The presence of an unusual pairing of massive lava and massive glass primary lithologies in both smectite and argillite alteration zones, rather than a sharp change of primary lithology with the onset of mineralization points to a replacement origin for the argillized and mineralized zone. This interpretation is confirmed by features of the transition zone. For example, between 153.00 and 153.20 m a transition in primary lithology from dark grey-green massive lava (above) to blue-black massive glass (below) occurs, within which is seen the first indication of argillic alteration. This is in the form of a number of veins in the massive basalt, which is in the smectite-carbonate facies of bulk alteration. The most prominent, subvertical vein has a 0.5 mm infilling containing sulfides and is bordered by 2 mm wide zones of pale grey argillic alteration of the massive lava. This vein appears to be rooted in a brecciated, permeable zone in the uppermost part of the underlying massive glass unit. Very pale-grey to off-white mineralized argillic material fills most of the spaces between the fragmented primary material, which also appears to have undergone local argillic alteration. A 4 cm by 1 cm open cavity at 153.10 m is lined by botryoidal surfaces of secondary phases and represents the remainder of a larger cavity, now partly infilled by off-white secondary phases, pyrite, and orange-brown sphalerite.

Below 297 m, a sequence of dikes with occasional screens of pillowed or massive lava is in a greenschist state of alteration, characterized by the complete replacement of primary phases of chlorite, epidote, quartz, albite and minor pyrite.

In light of this clear evidence for replacement and infilling, the question arises as to whether the Agrokipia 'B' ore body was formed entirely or only in part, by these mechanisms. One possibility is that the replacement/infilling zone formed laterally adjacent to a channelway which carried the ore forming fluid to vents at the sea floor. Since it is presently impossible to examine other parts of the Agrokipia 'B' body, the relative feasibility of different models for the formation of the ore body may be assessed by studying exposed areas of mineralized ground. Since previous literature descriptions of such areas have been intended to provide information for economic assessment, we have undertaken a detailed study of a mineralized area from a fluid flow viewpoint. This type of study is readily carried out as both the primary and secondary colouration of areas of rocks that have been altered by contact with high temperature mineralizing fluids are very distinctive, and field observation is sufficient to distinguish them from less altered zones.

THE KLIROU GOSSAN

(a) General Features

The mineralized area selected for study was one of the many gossans that occur in the Extrusives and Basal Group within the Akaki-Lythrodondha map area. The gossan was formed by oxidation of sulfide minerals due to subaerial exposure. The fact that it occurs within the Troodos ophiolite, a well documented fragment of oceanic crust containing numerous orebodies formed by hydrothermal convection, suggests that this and other gossans mark the site of a former upwelling zone. The gossan selected for study has an almost completely exposed cross section in the banks of a branch stream of the Akaki-Maroulena river system near the villages of Klirou and Kalokhario. The gossan is located at 35°00″36′N, 33°08″30′E, approximately 4 km south-southeast of, and one kilometer stratigraphically below, the Agrokipia ore bodies (Figure 2). Where presently exposed, this zone of upwelling is located close to the base of the Lower Pillow Lavas. The gossan extends over the whole 40 m of vertical exposure. The approximately 7,000 m^2 (120 m by 60 m) cross sectional area of the gossan is similar to the average cross sectional area of the Agrokipia 'B' deposit, which has basal dimensions of 150 m by 100 m (Bear, 1960, Figure 14). The gossan was examined in early 1983 by J.M. Hall for evidence of the pattern of fluid flow and a detailed topographic and geological survey was carried out by M. Botros during the summer of 1983. Mapping and photography were used to construct a three-dimensional model of the gossan area on a horizontal scale of 1:200 and a vertical scale of 1:315. Figures 3 and 4 show general views of the gossan and the model, respectively. The medium grey coloured surface areas in both plates are light tan coloured in the field. These represent the oxidized surfaces of very distinctive light grey, pervasively altered and mineralized volcanics with the dominant mineralization being pyrite. Oxidation of the pyrite as a result of subaerial weathering processes gives rise to the tan coloured surface coating of iron oxy-hydroxides. The unweathered, very distinctive mineralized light grey material closely resembles in both colour and softness the pervasively argillized and mineralized extrusives occurring between 154 m and

297 m depth in drill hole CY-2a. In the model, the darker coloured, surrounding volcanics are dark grey brown in the field and appear to have undergone only low temperature clay-carbonate or mild zeolite facies hydrothermal alteration. The colour contrast between argillized and less altered rocks is very marked and, in conjunction with the typical narrow transitions between the two types of alteration, allows the highly altered material to be mapped with confidence using only macroscopic examination in the field. The strike of the long axis of the gossan is E-W, in contrast with the average N-S strike of the dikes in the vicinity and the 220/70°NW orientation of the major fault cutting the gossan. The geologic history of the gossan area began with submarine basic volcanism, perhaps originating from a small vent now marked by a plug-like intrusive body directly to the southwest of the main area of the gossan. The hydrothermal upwelling event then followed. Some of the dikes present in the area of the gossan are also in an argillic state of alteration. Both earlier intrusion or intrusion during the hydrothermal event would be consistent with this observation. Diking also took place after the termination of the event as indicated by the presence of the relatively unaltered basic dike (no. 5 in Figure 4) crosscutting the gossan. Fault activity occurred in the area both before and during the hydrothermal event.

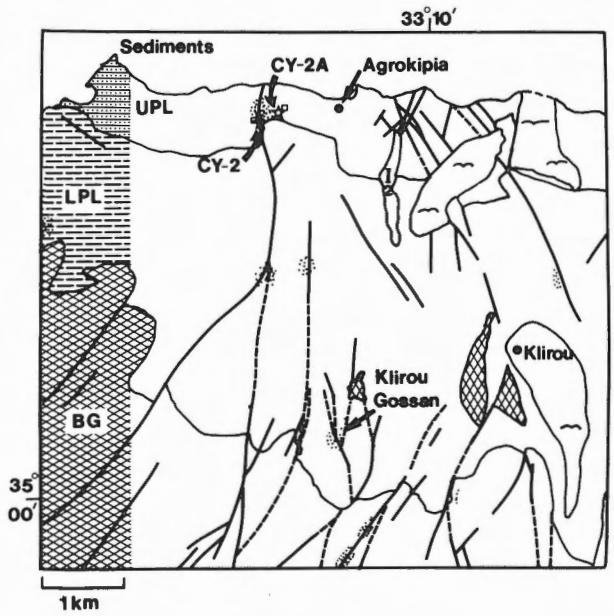

Figure 2: Location of the Klirou gossan in relationship to CCSP drill hole CY-2a. UPL: Upper Pillow Lavas; LPL: Lower Pillow Lavas; B.G.: Basal Group. Faults are indicated by heavy continuous or broken lines and gossans by dotted pattern.

(b) Fluid-Flow Related Features

A number of features of the Klirou gossan can be interpreted in terms of fluid penetration and flow through the section, some of which in turn bear on the interpretation of the CY-2a section. Alteration-based evidence for fluid penetration or flow occurs on a wide variety of scales, ranging from mm-scale around fractures and joints in massive and pillowed flows, to the apparent pervasive penetration of the whole body of pre-existing volcanics.

Several different relationships between areas with and without argillic alteration occur near the boundaries of the gossan. A number of pillowed flows, of which no. 3 in Figure 4 is an example, occur about 10 m from the southern margin of the gossan, and again in the stream banks close to the lowest exposures of the gossan. These show intense high-temperature alteration of pillow margins and inter-pillow material grading to distinctly less altered pillow cores. In the pillow cores, alteration is limited to zones immediately adjacent to fractures (Figure 5). A similar example of incomplete high temperature alteration is seen in a massive flow located within 1-2 metres of the southern edge of the gossan between the post-mineralization dike and the stream. In this case, intense alteration is restricted to within a few centimeters of the subvertical joints defining the columnar structure part of the flow (Figure 6).

Other examples of locally restricted high-temperature (>200°C) alteration on a larger scale are seen where volcanics which are partly or largely pervasively altered are overlain by little-altered material. Two clear examples of this situation are at locations 2.1 and 2.2 in Figure 4. At location 2.1, a 5 m extension of high temperature alteration southwards of the gossan terminates upwards in a massive flow. This situation is comparable with the upwards termination of argillic alteration in drill hole CY-2a. While gossan-type alteration at location 2.1 appears on the outcrop as a branch from the main area of alteration, if it were continuous downwards, it would resemble the situation in drill hole CY-2a. A second example of upwards termination of gossan-type alteration is seen at location 2.2 of Figure 4. A plug-like body of massive basalt, 15 m by 10 m in cross section and at least 10 m in vertical extent, occurs at this location. The bulk of this massive material shows only smectite-carbonate alteration, but the lowermost metre or so of the two faces of the body exposed in the stream bank has experienced high temperature alteration (Figure 7). This situation again resembles that in drill hole CY-2a, and, as at location 2.1, also occurs at or near the periphery of the main gossan area.

Figure 3: General view of Klirou gossan, facing north from the southern end of the gossan.

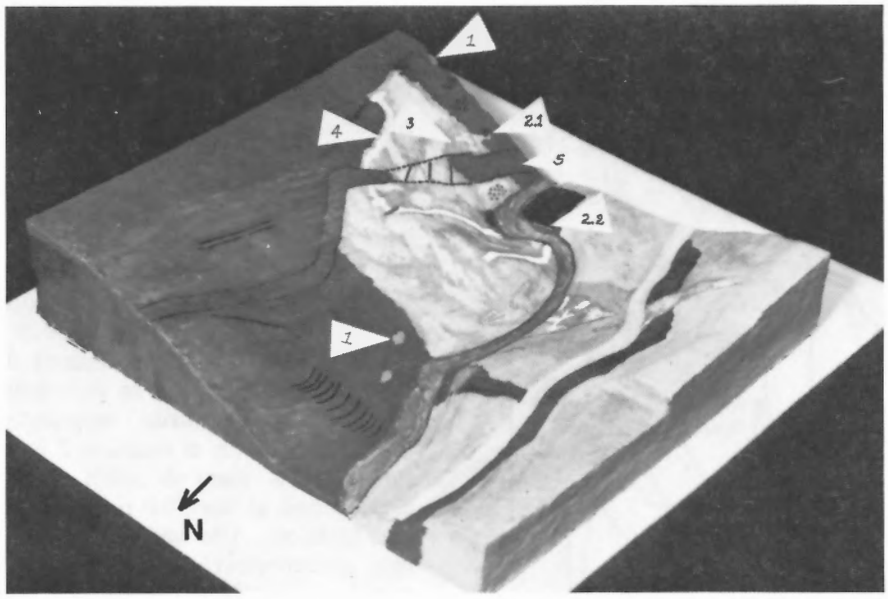

Figure 4: Model of Klirou gossan. The numbered arrows refer to examples of the following features: (1) Small satellite upwelling zones separated from the main gossan area by little-altered rocks. (2.1) Gossan area that terminates upwards in massive flows. (2.2) Gossan area that terminates upwards within a small plug-like mass. (3) Pillowed flows in which pillow peripheries are intensely altered and pillow cores much less so. (4) Narrow sinuous zone of most intense alteration. (5) Post-mineralization dike. Note: the different general colouration of the opposite stream banks represents rock exposure on the NE (darker) bank and soil and vegetation on the SW (lighter) bank. The intermediate grey represents weathered gossan material.

Figure 5: Peripheral high temperature alteration of pillows, Klirou gossan.

Figure 6: Massive flow in the vicinity of location 2.1 in Figure 4 showing high temperature hydrothermal alteration limited to material adjacent to jointing: Klirou gossan.

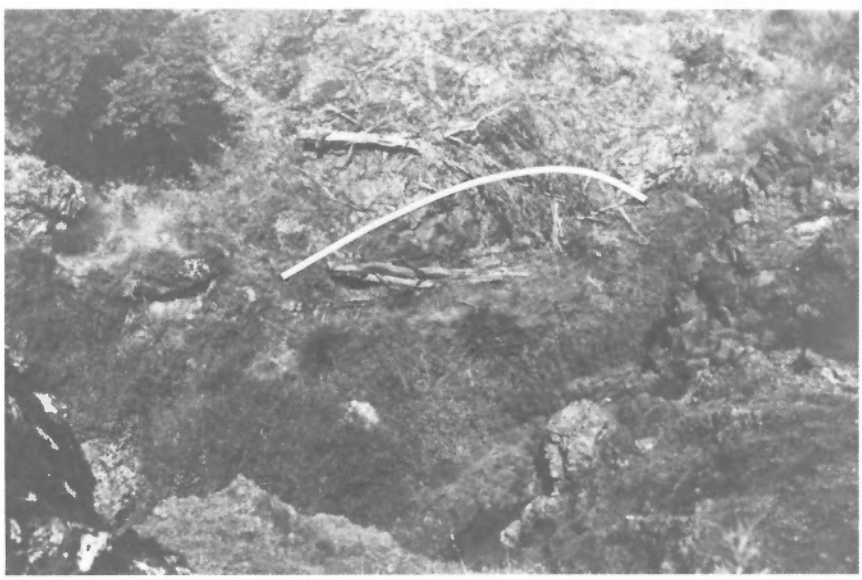

Figure 7: High temperature hydrothermal alteration at the base of a plug-like mass (Location 2.2 in Figure 4): Klirou gossan. View is from 2.1 looking towards 2.2. Argillic alteration occurs in the area below the white line near the base of exposure.

Further evidence of the irregularity in the lateral limits of upwelling is provided by four small gossan areas separated from the main area, at least at the present erosional level, by volcanics showing only low temperature alteration. Three of these occurrences, with an average area of 6 m^2, are in lavas, while the fourth is a 5 m by 8 m dike segment. These isolated areas are all within 20 m of the boundaries of the main gossan body.

Within the main body of the gossan, high temperature alteration is largely pervasive with both disseminated, and poorly defined vein-like, sulfide occurrences. Although primary structures are often sufficiently well retained for the original lithology to be readily recognizable within most of the area of pervasive alteration, there are a number of regions where alteration has been so intense that the primary lithology is now indeterminate (locations such as no. 4 in Figure 4). The most prominent of these regions are a series of irregular but continuous zones that wander sinuously (Figure 8) through the pervasively altered material. Within these typically 1-2 m wide zones, the gossan material is relatively structureless, very light in colour, and has a soft, clay-like consistency leading to its relatively rapid erosion. These zones are not obviously restricted to a particular lithology or structural feature. The principal structureless zone extends in an overall upwards direction throughout the 40 m of vertical exposure, except where it is cut by the post-mineralization dike. Two possible origins can be suggested for these features. Firstly, since they tend to be located centrally within the gossan and show no recognizable primary structures, they may represent the principal pathways for fluid flow. Secondly, their texture resembles that of the most intensely argillized massive glass zones in drill hole CY-2a, and thus their highly altered nature may reflect an origin as primary glass.

THE KAMBIA AREA

During a survey of the volcanics and their immediate sediment cover in the area directly to the east of Kambia village (Yang et al., 1984), examination was made of a series of gossans located along the north-northeast trending fault that passes through the Kambia Mine (Bear, 1960: p. 91-94), and is observed to continue in the volcanics to the edge of the sediment cover. At a location close to 35°00′N, 33°16′E a small domelike, upwards-terminating occurrence of orange-weathering, gossan material in sheet flows was noted (Figure 9). The general alteration of the sheet flows in the vicinity appears to be of a low temperature type. However, it is notable that just above the zone of gossan type, celadonitic clays are locally very common, giving the basalts a green-blue hue. This upwards termination of argillic alteration in sheet flows also resembles the upwards termination of alteration in the glassy massive basalts of drill hole CY-2a, as does the occurrence of celadonitic clays a short distance above the zone of argillic alteration.

Figure 8: The base of the southernmost sinuous zone of structureless, pale coloured clay-like material: Klirou gossan.

DISCUSSION

The relative spatial location of the various features observed in the Klirou gossan extend the possible interpretations for the original setting of the Agrokipia 'B' ore body. With the evidence of the ore body shape provided by mining and percussion drilling as well as the single vertical profile from the CY-2a drill hole, there is no compelling reason to suggest other than a replacement origin for the body. The model for the formation of the ore deposit would involve upwelling of a hot fluid that was prevented from reaching the sea floor by an impermeable layer.

The contribution from the study of the Klirou and other gossans is to show that locally arrested upwelling can occur only a few tens of metres from what may be a principal upward fluid flow pathway. It is then possible to suggest that a comparable situation occurs within the Agrokipia 'B' ore body. In such a model, major upwelling, possibly venting on the sea floor would have followed a generally vertical zone perhaps only a few tens of metres from the drill hole. Drill hole CY-2a would then have penetrated an area of locally arrested peripheral upwelling on the lower flank of the general area of upwelling.

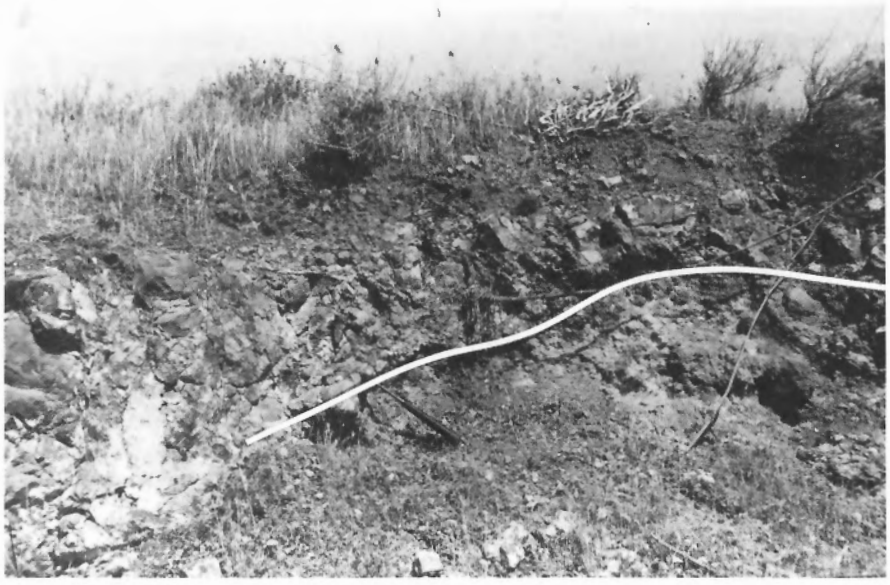

Figure 9: The upwards termination of high temperature gossan-type alteration in celadonite-bearing massive basalts in the Kambia area. Argillic alteration occurs below the white line and extends to the bottom of the exposure.

ACKNOWLEDGEMENTS

We should like to acknowledge the assistance of the Geological Survey Department of Cyprus, and in particular Mr. Costas Stavrides, Mr. Dimitris, and Dr. Costas Xenophontos for advice, equipment and help in mapping the Klirou gossan. An earlier photographic reconnaissance of considerable value was made by Mr. Charles Walls. Comments from John Delaney were greatly appreciated. Support from the Natural Sciences and Engineering Research Council (Canada) is gratefully acknowledged for a summer studentship for M. Botros, for support of the drilling operations at Agrokipia, and for subsequent field and laboratory investigations through Strategic/Oceans Grant no. G0741 and Operating Grant no. A7812 to J.M. Hall.

REFERENCES

Adamides, N.G.
1980: The form and environment of formation of the Kalavasos ore deposits, Cyprus; *in* Ophiolites: Proceedings of the International Ophiolite Symposium, Cyprus, 1979, ed. A. Panayiotou; Cyprus Geological Survey Department, Ministry of Agriculture and Natural Resources, p. 117-127.

Bear, L.M.
1960: The geology and mineral resources of the Akaki-Lythrodondha area; Cyprus Geological Survey Department, Ministry of Agriculture and Natural Resources, Memoir, no. 3, p. 1-122.

Constantinou, G.
1980: Metallogenesis associated with the Troodos ophiolite; *in* Ophiolites: Proceedings of the International Ophiolite Symposium, Cyprus, 1979, ed. A. Panayiotou, Cyprus Geological Survey Department, Ministry of Agriculture and Natural Resources, p. 663-674.

Goldie, R. and Bottrill, T.J.
1981: Seminar on sea-floor hydrothermal systems; Geoscience Canada, v. 8, no. 3,

p. 93-104.

Honnorez, J.
1981: The aging of oceanic crust at low temperature; *in* The Sea; Ideas and Observations on Progress in the Study of the Seas, Volume 7, The Oceanic Lithosphere, ed. C. Emiliani; John Wiley and Sons, New York, p. 525-587.

Honnorez, J., Alt, J.C., Honnorez-Guerstein, B.-M., Laverne, C., Muehlenbachs, K., Ruiz, J. and Saltzman, E.
1985: Stockwork-like sulfide mineralization in young oceanic crust: Deep Sea Drilling Project Hole 504B; *in* Initial Reports of the Deep Sea Drilling Project, Volume 83, ed. R.N. Anderson, J. Honnorez, K. Becker, et al.; U.S. Government Printing Office, Washington, D.C., v. 83, p. 263-282.

ICRDG
1984: Are Troodos deposits an East Pacific analog?; Geotimes, v. 29, no. 5, p. 12-14.

Macdonald, K.C., Becher, K., Spiess, F.N. and Ballard, R.D.
1980: Hydrothermal heat flux at the 'black smoker' vents on the East Pacific Rise; Earth and Planetary Science Letters, v. 48, p. 1-7.

Oudin, E. and Constantinou, G.
1984: Black smoker chimney fragments in Cyprus sulphide deposits; Nature v. 308, p. 349-353.

Spooner, E.T.C.
1977: Hydrodynamic model for the origin of the ophiolitic cupriferous pyrite ore deposits of Cyprus; *in* Volcanic Processes in Ore Genesis; Geological Society of London, Special Publication, no. 7, p. 58-71.

Spooner, E.T.C. and Bray, C.J.
1977: Hydrothermal fluids of seawater salinity in ophiolitic sulfide ore deposits in Cyprus; Nature, v. 266, no. 5605, p. 808-812.

Yang, J., Tesfazghi, G.-E. and Venkataramana, P.
1984: Report on the geology of the area east of Kambia, Nicosia district, Cyprus; *in* Report to IDRC on the Second Training Program in Marine Geology; Centre for Marine Geology, Dalhousie University, Halifax, Nova Scotia.

Cyprus Crustal Study Project.
Hole CY-2 Lithologic Unit Summaries

PAUL T. ROBINSON[1] AND IAN L. GIBSON[2]

[1]Department of Geology, Dalhousie University,
Halifax, Nova Scotia, Canada, B3H 3J5
[2]Department of Earth Sciences, University of Waterloo,
Waterloo, Ontario, Canada, N2L 3G1

Robinson, P.T. and Gibson, I.L., Cyprus Crustal Study Project. Hole CY-2 lithologic unit summaries; in *Cyprus Crustal Study Project: Initial Report, Holes CY-2 and 2a, ed. P.T. Robinson, I.L. Gibson and A. Panayiotou; Geological Survey of Canada, Paper 85-29, p. 39-44, 1987.*

Abstract

Hole CY-2 is located at Lat. 35°02′43″N, Long. 33°08′48″E near the Agrokipia Ore body on the North side of the Troodos Ophiolite, Cyprus. The hole was drilled to a depth of 222.16 m. Core recovery was 91.8%. More than one hundred cooling units were identified in the field and these have been grouped into fourteen major lithologic units, varying in thickness from 2.85 m (Unit VII) to 56.90 m (Unit XII). For each of these major units, the following information is given: the position and nature of the upper and lower contact, the unit thickness, the dominant lithology, and the identification numbers of the cooling units grouped within the major lithologic unit. For each major lithologic unit, this heading is followed by a description detailing the lithology, texture, alteration mineralogy and major megascopic features.

Résumé

Le forage CY-2 est situé à Lat. 35°02′43″N, Long. 33°08′48″E près du dépôt de minerai d'Agrokipia sur le côté nord de l'Ophiolite de Troodos, Cyprus. Le forage a atteint une profondeur de 222,16 m. La récupération fut de 91,8%. Plus de cent unités de refroidissement furent identifiées sur le terrain et celles-ci ont été groupées en quatorze unités lithologiques majeures, variant en épaisseur de 2,85 m (Unité VII) à 56,90 m (Unité XII). Pour chacune de ces unités majeures, l'information suivante est donnée: la position et nature du contact supérieur et inférieur, l'épaisseur de l'unité, la lithologie dominante et les numéros d'identification des unités de refroidissement groupées à l'intérieur des unités lithologiques majeures. Pour chaque unité lithologique majeure, cette entête est suivie par une description détaillée de la lithologie, texture, minéralogie d'altération et charactéristiques mégascopiques majeures.

UNIT I

Upper contact:	4.40 m, ambiguous
Lower contact:	9.70 m, ambiguous
Thickness:	5.30 m
Lithology:	Highly altered lava
Cooling units:	1.01 to 1.02

Unit I is a sequence of light grey, highly altered lava. The upper contact is the top of the core and the lower contact is drawn at a gap in the core across which the color and degree of alteration change markedly. The rock is fine grained without any evidence of the former texture or mineralogy. No vesicles are apparent but it is not clear whether they were absent in the original rock or whether they were obliterated by alteration. Brown limonite staining occurs along abundant fractures but there are no well developed veins. The groundmass is completely altered to light gray clay minerals and is impregnated with minor disseminated pyrite. The rock is slightly less altered and darker gray in the basal 50 cm than in the upper part of the unit.

UNIT II

Upper contact:	9.70 m, ambiguous
Lower contact:	27.70 m, ambiguous
Thickness:	18.00 m
Lithology:	Altered pillowed(?) lavas
Cooling units:	1.03 to 3.06

The upper contact is drawn at a 2.30-m-wide gap in the core across which the color and degree of alteration change markedly. The lower contact is drawn at the top of a much more highly altered and pyritized sequence than that comprising Unit II. Overall, the rocks are light gray to medium gray in color but brown limonite staining is common in the upper 30 cm. Most specimens are aphanitic to very fine grained with a devitrified glassy texture, and contain minute laths of plagioclase. A few narrow, curved zones of hydrated and altered glass now composed of bluish-gray clay minerals are believed to represent pillow rinds. Most of the rocks in this unit are aphyric but cooling unit 3.05 has 1 to 2% of small olivine(?) phenocrysts completely replaced by clay minerals and iron oxides. Vesicles make up less than 1% of the rock and are up to 1 mm across. About one-half of them are open and the remainder are filled with dark clay minerals locally accompanied with small red crystals of an unknown mineral. Sparse veins are hairline fractures lined or filled with gypsum(?) and a lavender-colored unknown mineral. Groundmass alteration with clay minerals and minor disseminated pyrite is moderate and the original texture is usually well preserved. The lower 2 m of rock are lighter gray and more altered than the remainder of the unit, but the original pillow structure is still recognizable.

UNIT III

Upper contact:	27.70 m, ambiguous
Lower contact:	57.50 m, ambiguous
Thickness:	29.80 m
Lithology:	Highly altered pillowed(?) lava
Cooling units:	4.01 to 6.04

A 29.60-m-thick sequence of light gray, highly altered and pyritized, pillowed(?) lavas comprise Unit III. The upper contact is drawn at a sharp increase in the intensity of alteration, and the lower contact at a change from pillowed to massive flow. In most parts of the unit the original texture has been destroyed but in a few relatively fresh areas the rock appears to be very fine grained and aphyric with a devitrified, originally glassy texture, suggestive of pillows. A few zones (e.g., 37.20-37.90 m) consist of altered, brecciated material, possibly hyaloclastite or fine-grained pillow breccia. Vesicles comprise about 1% of the unit and average about 1 mm in diameter. Most are filled with quartz and/or clay minerals usually associated with small quantities of pyrite. Veins are sparse (less than 1% of the unit) but some may have been destroyed due to brecciation during drilling. Small, irregular veins are filled with pyrite, silica, and clay minerals whereas larger veins, up to 1 cm across, are typically filled with gypsum or jasper. These minerals appear to represent a later, separate veining episode. The groundmass is highly altered throughout, consisting largely of light gray clay minerals with 1 to 2% of disseminated pyrite. Between 48.60 and 48.74 m there is a zone of hard, red jasper with a rather open porous texture.

UNIT IV

Upper contact:	57.50 m, ambiguous
Lower contact:	70.50 m, ambiguous
Thickness:	13.00 m
Lithology:	Altered massive flows
Cooling units:	7.01 to 8.04

Unit IV consists of 13.00 m of moderately to highly altered massive lava flows. A change to pillowed lavas marks the upper contact and a sharp decrease in the intensity of alteration marks the lower boundary. The rock is light gray, often highly vesicular, fine grained, and aphyric. Vesicles range up to 15 percent in the upper parts of individual flows but are sparse to absent elsewhere. They range from 1 to 12 mm and average about 8 mm across. Most of them are open,

the remainder contain a few% of clay minerals, pyrite, quartz, and gypsum. Veins are sparse (about 1% of the unit) and range from 1 to 10 mm wide. They are filled with about equal amounts of clay minerals and gypsum, and only rarely contain pyrite or hematite. Alteration of the groundmass is high, with 50 to 70% of the rock replaced with clay minerals, silica, sparse hematite, and minor disseminated pyrite. The latter is usually found in small, irregular, vuggy cavities.

UNIT V

Upper contact:	70.50 m, ambiguous
Lower contact:	85.80 m, depositional
Thickness:	15.30 m
Lithology:	Massive(?) flow
Cooling units:	8.05

Unit V is a single cooling unit of fine-grained, aphyric, relatively fresh, massive basalt. The upper contact is marked by a sharp decrease in alteration from the overlying unit and the lower contact is marked by a decrease in grain size toward a small breccia zone. Grain size variations within the unit suggest the presence of additional boundaries but none are clearly preserved in the core. Vesicles average less than 1% and never exceed 5% of the rock. They range up to 1 cm across but average about 2 to 3 mm; many are flattened and elongate. Most are filled with calcite but some are open or have minor clay minerals or pyrite. Veins are sparse except in the lower 1 to 5 m where they make up about 20% of the rock. They range from hairline fractures lined with clay minerals to veins up to 3 mm across filled with carbonate and pyrite with minor clay minerals and hematite. The groundmass is relatively fresh, showing minor iron oxide staining along some fractures and minor replacement by clay minerals.

UNIT VI

Upper contact:	85.80 m, depositional
Lower contact:	97.45 m, ambiguous
Thickness:	11.65 m
Lithology:	Pillowed lavas and a massive flow
Cooling units:	11.01 to 14.01

Unit VI consists of a massive lava flow overlain by a series of pillowed lavas, both composed of fine-grained, aphyric, relatively fresh basalt. The upper contact is taken as the bottom of the thick massive flow of cooling unit 8.05. The base of the unit is drawn at the top of a dark gray, clinopyroxene-rich lava flow. A 100-cm-thick layer of highly altered basalt between 96.45 and 97.45 m is included as the base of the massive flow of Unit VI. The pillowed lavas, which extend from 85.80 to 93.30 m in the core, are recognized by their very fine-grained texture and by the presence of numerous steeply dipping and curved chilled margins, which are often associated with small patches of breccia. Six cooling units are recognized in this sequence indicating an average vertical thickness of about 1.25 m. Some pillow margins may have been destroyed by drilling and thus the average thickness may be less. The pillowed lavas are medium-gray, very fine-grained, aphyric basalts. Vesicles average 1 to 2% of these rocks but may comprise 10 to 15% in the upper parts of some pillows. They average about 2 mm across but range up to 15 mm in the zones of highest abundance. About half of the vesicles are filled with zeolite and minor clay minerals. Veins make up about 1% of the pillows and range from 1 to 3 mm in width. They are filled with quartz, hematite, and minor clay minerals. Groundmass alteration is highly variable, ranging from 10% or less in pillow interiors up to 100% in glassy and brecciated pillow rinds. In the altered rinds the glass is replaced predominately by green clay minerals, accompanied by minor quartz and hematite. The massive flow is about 4.15 m thick and consists of medium-gray, fine-grained, relatively fresh, aphyric basalt. The highly altered material at the base (cooling unit 14.01) consists of light gray, fairly porous, partly brecciated basalt. Vesicles average about 2% of the flow and range up to 15 mm across. They are largest and most abundant in the upper 1.5 m of the flow. Most vesicles are empty but others contain small amounts of zeolite, pyrite, quartz, and calcite. Between 95.20 and 95.70 m there are numerous large elongate vugs up to 4 cm wide and 7 cm long. They are flattened in a plane inclined about 50 degrees to the core axis. Most are lined with minor calcite, sometimes accompanied by pyrite. Veins average about 1% of the flow, range from 1 to 3 mm wide, and are filled mostly with calcite accompanied by minor clay minerals and pyrite. The groundmass is medium to light gray with some alteration to clay minerals. In the lower 100 cm the rock is completely altered to clay, silica(?), and minor disseminated pyrite.

UNIT VII

Upper contact:	97.45 m, ambiguous
Lower contact:	100.30 m, ambiguous
Thickness:	2.85 m
Lithology:	Massive(?) flow
Cooling units:	14.02

A 2.85-m-thick sequence of dark brownish-gray, clinopyroxene-phyric basalt comprises Unit VII. A marked difference in mineralogy and intensity of

alteration distinguishes this unit from the overlying massive flow. The lower contact is drawn at a sharp change to gray, aphyric lava. Clinopyroxene phenocrysts make up 2 to 3% of the rock and form fresh, glassy, green, anhedral crystals, 1 to 2 mm across. They are set in a very fine-grained, almost glassy, groundmass. Vesicles comprise about 3% of the unit, and range from 0.5 to 2 mm across. Most are filled with white calcite. Veins are very rare and consist of hairline fractures filled with calcite. The groundmass is fresh except in the lower 50 cm where several pieces of highly pyritized and altered rock are present. These appear to consist of pyrite, silica, and hematite, and are so altered that no trace of their original texture or mineralogy remains. They may have fallen into the hole from a higher level, or they may represent a narrow altered zone within Unit VII.

UNIT VIII

Upper contact:	100.30 m, ambiguous
Lower contact:	114.55 m, depositional
Thickness:	14.25 m
Lithology:	Massive flows
Cooling units:	14.03 to 17.02

Unit VIII is a sequence of aphyric, massive lava flows with numerous zones and layers of red jasper. The upper contact is drawn at the base of the clinopyroxene-phyric flow of cooling unit 14.02. The lower contact is at the top of a thick glassy, lava flow. The rocks are light gray to greenish-gray, moderately to highly vesicular, and moderately altered. Vesicles range up to 20% of the rock but average about 3 to 4%. The are concentrated in definite layers , generally in the upper and lower parts of individual flows. They vary from 1 to 25 mm and average about 3 mm across. Most vesicles are open but some are lined or filled with celadonite, zeolite, or minor pyrite. Veins make up less than 1% of the unit and range up to 3 mm wide. They are filled with celadonite and hematite, sometimes accompanied by minor zeolite. The groundmass is fine- to medium-grained with a glassy chilled margin preserved at 106.00 m. Alteration in the groundmass is moderate, largely involving replacement by clay minerals, including some celadonite. Several zones of brick red jasper are present (101.80 - 101.90 m, 103.60 - 103.70 m, 107.35 - 107.45 m, 109.75 - 110.35 m, 111.30 m, 112.20 - 112.25 m, 112.45 - 112.50 m, and 112.60 - 112.70 m), and these probably represent parts of the core that have been completely silicified. The jasper is associated with green clay minerals (celadonite?) in what may have originally been glassy zones. In a few locations the jasper fills veins up to 1 cm wide but generally it appears to have formed by replacement. A few vug-like cavities in the jasper are lined with clear quartz crystals.

UNIT IX

Upper contact:	114.55 m, depositional
Lower contact:	146.45 m, depositional
Thickness:	31.90 m
Lithology:	Glassy massive flows
Cooling units:	18.01 to 25.01

Unit IX is a thick sequence of massive, sometimes glassy, flows which contain abundant green celadonite and red jasper. These basalts are fresher than those of Unit VIII and commonly have thick glassy zones in the upper and lower parts of individual flows. The upper contact is drawn at the first occurrence of such a glassy zone. The rocks become fresher with depth, and the lower contact is arbitrarily placed at the base of cooling unit 25.01, the last one in which abundant jasper and silica occur. There is no significant change in rock type or cooling unit type between Units IX and X and the distinction is based on the degree of alteration and secondary mineralization. A typical section from top to bottom of a single flow in Unit IX includes an upper zone, a few centimeters to several meters thick, of dark gray, glassy lava that breaks into thin pieces along fractures perpendicular to the core axis. This material passes downward, usually with a sharp contact, into greenish-gray, often highly vesicular and somewhat rubbly basalt up to several meters thick, which in turn is underlain by another glassy zone. Fifteen cooling units have been logged in Unit IX for an average vertical thickness of just over 2 m. However, the actual number of cooling units is probably somewhat less because many glassy zones were logged as separate units when they could not be definitely related to a given flow. All of the basalts in Unit IX are fine grained and aphyric. Vesicles are abundant in the crystallized flow interiors, often comprising up to 15% of these zones and ranging up to 1 cm across. Most are open but some are lined or filled with variable mixtures of celadonite, zeolite, minor pyrite, and minor silica. Clearly defined veins are rare, generally comprising less than 1% of any given flow. They range from 1 mm to 1 cm wide, and are filled largely with celadonite and minor zeolite. Some jasper occurs in poorly defined veins but it more commonly replaces large patches in the groundmass. Groundmass alteration in the glassy zones is very high, with 80 to 90% of the rock being replaced by brownish- to dark greenish-gray clay minerals. Extensive alteration to celadonite is most pronounced in the vesicular crystalline zones but it also occurs sporadically in the glassy lavas. Red or yellowish-brown jasper is widely distributed in Unit IX although it usually occurs in smaller and more irregular zones than in Unit VIII. It is invariably

associated with green celadonite in broad, diffuse, vein-like masses or in irregular patches replacing the groundmass. Like the celadonite, the jasper is most abundant in the crystalline interiors of individual flows.

UNIT X

Upper contact:	146.45 m, depositional
Lower contact:	152.65 m, depositional
Thickness:	6.20 m
Lithology:	Massive flow
Cooling units:	26.01

A single massive lava flow comprises Unit X. It is distinguished from the overlying and underlying units by being generally non-glassy. The upper contact is marked by a 3-cm-thick glassy chilled zone and the lower contact by about 15 cm of broken glassy material. Otherwise, the flow is holocrystalline and relatively fresh. Thin breccia zones occur at both the upper and lower contacts. The unit consists of light gray, fine-grained, aphyric basalt. Vesicles are generally small and sparse, averaging about 1 mm across and about 1% of the unit. A few irregular cavities up to 1 cm across are scattered through the rock. An abundance of minute vesicles in the central part of the flow gives the rock a porous appearance. About one-third of the vesicles are filled with clay minerals and minor amounts of calcite and zeolite. Veins comprise about 1% of the unit and range from 1 to 15 mm wide. They are filled with clay minerals and minor silica. Groundmass alteration is weak, being concentrated in the glassy and brecciated zones. Here, about one-half of the rock is replaced by celadonite. Elsewhere, the rock shows little megascopic alteration.

UNIT XI

Upper contact:	152.65 m, depositional
Lower contact:	159.60 m, depositional
Thickness:	6.95 m
Lithology:	Glassy massive flows
Cooling units:	28.01 to 29.04

Unit X is a relatively thin sequence of glassy, massive lava flows. It differs from the overlying and underlying units in being glass-rich and somewhat more altered. The upper contact is drawn at the top of cooling unit 28.01, a glass-rich flow, and the lower unit is drawn arbitrarily at the base of cooling unit 29.04, at the top of a thick sequence of non-glassy flows. Individual flows are varied but most appear to have upper and lower glassy zones and crystalline interiors. The glass is dark greenish-gray, non-vesicular material, now largely altered to clay minerals. It has a pronounced planar jointing roughly perpendicular to the core axis. The crystalline flow interiors consist of light gray, fine-grained, aphyric, moderately to highly vesicular basalt. In these zones vesicles range from 2 to 15% of the rock and are up to 1 cm across. A few are lined with clay minerals and partly filled with zeolites. Veins make up less than 1% of the unit and are mostly in the crystalline zones. They range from about 1 to 8 mm wide, and are filled with green clay minerals and minor zeolite. Groundmass alteration of the glassy material is high (80-90%) and involves replacement by clay minerals. The crystalline rocks are relatively fresh except in some highly vesicular zones where the groundmass is partly replaced by clay minerals.

UNIT XII

Upper contact:	159.60 m, depositional
Lower contact:	216.50 m, depositional
Thickness:	56.90 m
Lithology:	Massive flows
Cooling units:	29.05 to 43.03

Unit XII is a thick sequence of massive lava flows containing only small amounts of glass along the cooling unit contacts. The upper contact is taken as the base of the glassy lava flow of cooling unit 29.04 and the lower contact is drawn at the top of another glassy flow (cooling unit 44.01). The rocks are medium gray to greenish-gray, aphyric basalts without any apparent changes in lithology with depth. Twenty nine cooling units are recognized in Unit XII suggesting an average thickness of just under 2 m. However, several flows have thicknesses in excess of 5 m. Individual cooling units typically have chilled margins, often with thin glassy layers. These pass into central zones of fine- to medium-grained, crystalline basalt, most of which is quite fresh. Vesicles average 2 to 3% of the unit but show a highly irregular distribution within individual flows. The largest and most abundant vesicles occur in the upper one-third of individual flows whereas the smallest and fewest are in the chilled margins. Vesicles are between 1 and 5 mm across but in a few flows (e.g. cooling unit 34.02) large vesicles up to 2 cm across are common. In most of Unit XII vesicles and larger cavities are open, often being lined with clay minerals and minor zeolites, particularly heulandite and mordenite(?). In a few flows, however, abundant white silica completely fills some vesicles (e.g. cooling unit 34.02). In these rocks completely filled vesicles commonly exist side by side with open ones. Veins are sparse in the massive flows, comprising less than 1% of the unit. They are randomly distributed and generally less than 2 mm wide. They are filled with about equal amounts of

clay minerals and zeolites, and rarely by silica. Groundmass alteration is weak to moderate and is highest in the glassy margins where the glass is 80 to 90% replaced by clay minerals. In the crystalline flow interiors only minor bleaching and alteration to clay minerals has occurred.

UNIT XIII

Upper contact:	216.50 m, depositional
Lower contact:	221.95 m, depositional
Thickness:	5.45 m
Lithology:	Glassy massive flow
Cooling units:	44.01

A single massive lava flow with a thick glassy zone at the top comprises Unit XIII. A sharp chilled margin at the base of the overlying unit marks the top of the flow. Below this is about 1.7 m of somewhat brecciated, vesicular, and altered glass. The glass is dark gray where fresh but very light gray to tan where bleached and altered. Unlike many other flows in Hole CY-2 the glassy material in cooling unit 44.01 does not display a horizontal parting. The lower 3.77 m of the unit consist of medium gray to greenish-gray, fine-grained, aphyric, crystalline basalt. A thin glassy zone, 5 to 10 cm thick, marks the base of the flow. Vesicles comprise about 2% of the unit as a whole but are concentrated in the upper 2 m and in the basal 30 cm. Vesicles in the upper glassy zone are mostly filled with silica and minor zeolite whereas those in the lower 30 cm are filled with dark green clay minerals, accompanied by rare zeolites. Veins make up 1 to 2% of the unit, and are typically less than 5 mm wide. They are filled chiefly with clay minerals and/or zeolites. Groundmass alteration is high in the upper glassy zone where about 90% of the rock is replaced by clay minerals, silica, and minor zeolite. The silica and zeolite occur in irregular patches, perhaps filling spaces between small breccia fragments. The crystalline parts of the flow are relatively fresh except in a 1.2-m-thick zone between 218.40 and 219.60 m. Here, the rock is bleached and extensively replaced by silica, celadonite, and minor zeolite. Porous, vuggy areas are filled with celadonite and heulandite accompanied by minor mordenite.

UNIT XIV

Upper contact:	221.95 m, depositional
Lower contact:	226.16 m, base of core
Thickness:	4.21 m
Lithology:	Massive flows
Cooling units:	45.01 to 46.02

Unit XIV consists of 3 massive flows of light gray to greenish-gray, fine-grained, aphyric basalt. The upper contact is drawn at the base of the glass-rich flow of cooling unit 44.01, and the lower contact is the bottom of the hole at 226.16 m. Most of the flows have thick glassy zones but cooling unit 45.01 is characterized by numerous irregular glassy patches separated by crystalline zones. In most cases, these glassy patches do not extend through the core and hence are not logged as flow margins. They appear to be flow lobes or irregular masses in which local chilling has occurred. Vesicles are generally sparse, averaging about 1% of the unit and never exceeding 5% of the rock. Several small vesicle zones occur in the interval between 225.00 and 225.10 m. The vesicles average about 1 mm and range up to 15 mm across. Most are empty or lined with minor clay minerals and/or zeolites. A few large silica-filled vesicles occur between 224.45 and 224.60 m. Groundmass alteration is moderate to high, especially in the most glassy cooling unit (45.01). Here, the glass is 70 to 80% replaced by dark green clay minerals and some celadonite. In the crystalline zones 30 to 40% of the rock is altered to clay minerals, particularly celadonite.

ACKNOWLEDGEMENTS

This summary was produced from the detailed core descriptions prepared in Cyprus during the Spring and Summer of 1982 by the Cyprus Crustal Study Project laboratory staff. The assistance of the many individual scientists in the preparation of these detailed descriptions is gratefully acknowledged.

Cyprus Crustal Study Project.
Hole CY-2a Lithologic Unit Summaries

PAUL T. ROBINSON[1] AND IAN L. GIBSON[2]

[1]Department of Geology, Dalhousie University,
Halifax, Nova Scotia, Canada, B3H 3J5
[2]Department of Earth Sciences, University of Waterloo,
Waterloo, Ontario, Canada, N2L 3G1

Robinson, P.T. and Gibson, I.L., Cyprus Crustal Study Project. Hole CY-2a lithologic unit summaries; in *Cyprus Crustal Study Project: Initial Report, Holes CY-2 and 2a, ed. P.T. Robinson, I.L. Gibson and A. Panayiotou; Geological Survey of Canada, Paper 85-29, p. 45-55, 1987.*

Abstract

Hole CY-2a is located at Lat. 35°02′40″N, Long. 33°08′55″E near the Agrokipia Ore body on the North side of the Troodos Ophiolite, Cyprus. The hole was drilled to a depth of 689.15 m. Core recovery was 93.4%. More than three hundred and fifty cooling units were identified in the field and these have been grouped into twenty-two major lithologic units, varying in thickness from 0.43 m, a thin sedimentary layer, (Unit II) to 160.25 m, a section of altered basaltic dykes at the base of the hole (Unit XII). For each of these major units, the following information is given: the position and nature of the upper and lower contact, the unit thickness, the dominant lithology, and the identification numbers of the cooling units grouped within the major lithologic unit. For each major lithologic unit, this heading is followed by a description detailing the lithology, texture, alteration mineralogy and major megascopic features.

Résumé

Le forage CY-2a est situé à Lat. 35°02′40″N, Long. 33°08′55″E près du dépôt de minerai d'Agrokipia sur le côté nord de l'Ophiolite de Troodos, Cyprus. Le forage a atteint une profondeur de 689,15 m. La récupération fut de 93,4%. Plus de trois cent cinquante unités de refroidissement furent identifiées sur le terrain et celles-ci ont été groupées en vingt-deux unités lithologiques majeures, variant en épaisseur de 0,43 m, une mince couche sédimentaire (Unité II), à 160,25 m, une section de dykes basaltiques altérés à la base du forage (Unité XII). Pour chacune de ces unités majeures, l'information suivante est donnée: la position et nature du contact supérieur et inférieur, l'épaisseur de l'unité, la lithologie dominante et les numéros d'identification des unités de refroidissement groupées à l'intérieur des unités lithologiques majeures. Pour chaque unité lithologique majeure, cette entête est suivie par une description détaillée de la lithologie, texture, minéralogie d'altération et charactéristiques mégascopiques majeures.

UNIT I

Upper contact:	3.35 m, ambiguous
Lower contact:	30.72 m, intrusive(?)
Thickness:	27.37 m
Lithology:	Basalt sill(?)
Cooling units:	1.01

Unit I is a 26.37-m-thick sequence of gray to greenish-gray, medium- to coarse-grained, massive basalt tentatively interpreted as a sill. The upper contact is the top of the core and the lower contact is drawn at the top of a thin layer of greenish-gray, bedded sediments. The base of the unit is marked by a subhorizontal chill zone with 1 to 2 mm of altered glass(?), but this contact is not clearly intrusive. The upper 23.80 m of the unit are aphyric whereas the lower 2.5 m are sparsely to highly olivine-phyric, suggesting olivine accumulation at the base. Olivine phenocrysts are 10 to 25% of the rock between 27.15 and 30.00 m, decreasing to 1% at the base of the unit. The olivine is euhedral to subhedral, up to 5 mm across, and completely replaced by brown to light gray clay minerals and by minor carbonate in the lower meter of the unit. The groundmass increases from medium grained in the upper several meters to coarse grained in the central part of the unit and then decreases quickly to fine grained in the basal 50 cm. It consists of subhedral plagioclase laths and anhedral clinopyroxene up to 2 mm across in the coarsest parts of the unit. Vesicles average about 1% of the unit but are concentrated in zones a few tens of centimeters thick where they comprise 5-15% of the rock. Most vesicles are 1 to 2 mm across, irregular in shape, and open. A few are lined or filled with dark green clay minerals and rarely by calcite. The calcite-filled vesicles occur only in the lower meter of the unit. Veins make up $<$ 1% of the rock, are generally 1 mm wide, and are filled with clay minerals and minor calcite. A few thick veins, up to 1 cm wide, are filled with light gray, greasy appearing, often slickensided, clay minerals. The groundmass is generally fresh with 5% or less of interstitial clay minerals. In a few zones groundmass alteration is 10 to 15% or even up to 25% of the rock. In these zones dark green clay minerals form small irregular spots in the groundmass and completely fill the vesicles.

UNIT II

Upper contact:	30.72 m, truncated(?)
Lower contact:	31.15 m, ambiguous
Thickness:	0.43 m
Lithology:	Sediment
Cooling units:	7.01

Unit II consists of about 0.5 m of light green to chocolate brown, fine- to coarse-grained sediment. The basal 25 cm consist of poorly bedded, grayish-green, medium- to coarse-grained hyaloclastite composed largely of sand-size platy fragments of altered glass. This sequence is overlain gradationally by fine-grained, well bedded, light green to brown hyaloclastite composed of silt-size and smaller pieces of altered glass. The unit appears to be truncated by the massive basalt of cooling unit 1.01, but the upper contact could be depositional. The lower contact is placed arbitrarily at the lowest occurrence of sediment in a zone of drilling rubble.

UNIT III

Upper contact:	31.15 m, ambiguous
Lower contact:	67.50 m, ambiguous
Thickness:	36.35 m
Lithology:	Massive basalt flows
Cooling units:	7.02 to 10.01

A 36.35-m-thick sequence of predominately dark gray, massive, basalt flows makes up Unit III. Cooling unit 8.01 consists of fragments of green, coarse-grained hyaloclastite which are interpreted as having slumped into the hole from Unit II. The upper contact is drawn in a zone of drilling rubble below the lowest occurrence of hyaloclastite of Unit II. The lower contact is arbitrarily placed in a breccia zone at the top of a thick, coarse-grained, non-vesicular, massive basalt. Cooling units 8.02, 9.01, 9.02, and 10.01 are separated by thin zones of altered glass indicating definite cooling breaks between flows. The basalts are fine-grained, aphyric, and highly vesicular suggesting a series of massive flows. Vesicles make up about 2 to 3% overall but are concentrated in zones where they comprise up to 10% of the rock. The vesicles range from 1 to 15 mm across and average about 3 mm. Most are subspherical and are partly to completely filled with white calcite (90%) and colorless zeolite (10%). The largest and most abundant vesicles are concentrated in the middle and upper parts of individual flows. Veins make up $<$ 1% of the unit but comprise up to 10% of a few intervals. They range from about 1 to 10 mm wide and are filled entirely with white calcite. A few veins have vuggy cavities lined with euhedral calcite crystals. The groundmass is dark gray and generally fresh, but in a few zones it is partly replaced by clay and celadonite. A few zones have 5 to 10% carbonate in the groundmass replacing interstitial material or filling minute vesicles. The glassy chilled margins of the flows are replaced by green smectite.

UNIT IV

Upper contact:	67.50 m, ambiguous
Lower contact:	89.90 m, ambiguous
Thickness:	22.40 m
Lithology:	Massive basalt, probably intrusive
Cooling units:	15.01

Unit IV is a single cooling unit, 22.40 m thick, of greenish- to brownish-gray, medium-grained, aphyric basalt. The upper contact is drawn arbitrarily in a breccia zone between the fine-grained, dark gray, vesicular basalt of Unit III and the coarser-grained, greenish-gray basalt of Unit IV. The lower contact is drawn at a transition to another fine-grained basalt with abundant large vesicles. The basalt of Unit IV is very uniform in character but the grain size decreases somewhat in the lower 15 cm. There are no chilled or glassy margins preserved but the core is highly broken and these may have been lost. The massive basalt of this unit lacks the large and abundant vesicles which are characteristic of the overlying and underlying units. Instead, the rocks have many small irregular pits or cavities giving the rock a highly porous appearance. These small vesicles range from about 5 to 10% of the rock and are filled with dark green clay minerals and minor white calcite. A few larger vesicles, up to 4 mm across, are also present and these are completely filled with calcite. Veins comprise < 1% of the unit and consist of clay-lined fractures, often with well developed slickensides. Several thick veins, up to 1 cm wide, occur between 87.30 and 87.60 m. The groundmass is soft, highly altered (50-60%), and contains abundant dark green clay minerals and minor calcite. Although the contacts are not preserved the relatively coarse-grained nature of the unit, its lack of large vesicles, and its very uniform character suggest an intrusive origin.

UNIT V

Upper contact:	89.90 m, ambiguous
Lower contact:	109.00 m, ambiguous
Thickness:	19.10 m
Lithology:	Massive basalt flows
Cooling units:	21.01 to 24.01

A series of light gray, fine-grained, aphyric, massive basalt flows comprises Unit V. The upper contact is placed at the base of the massive, generally non-vesicular basalt of cooling unit 15.01 and the lower contact is drawn at the top of a sequence of massive basaltic glass. Seven cooling units are recognized in this 19.10-m-thick sequence indicating an average vertical thickness of about 2.7 m. Individual flows generally have thin glassy selvedges and are sometimes separated by a few centimeters of altered glassy breccia (e.g. cooling unit 21.03). A particularly well developed chilled margin is preserved at 98.10 m. Much of the core has been fractured and broken during drilling so that some contacts may be missing. Vesicles average 3-4 percent of the rock but exhibit systematic variations in abundance. The largest and most abundant vesicles typically occur in the middle and upper parts of individual flows and some accumulations of small vesicles occur close to the lower contacts. Most vesicles are 2-3 mm across but some range up to 10 mm. Rare vug-like cavities up to 3 cm across are also present locally. About half of the vesicles are open; the remainder are filled with approximately equal proportions of calcite and zeolite (analcime?). Veins are sparse (< 1% of the unit) and consist chiefly of discontinuous, hairline stringers of calcite. Groundmass alteration in the flows is variable, probably in the range of 20 to 100 percent. All of the glassy rinds and the brecciated material between flows is altered to green smectite with minor calcite and zeolite(?). The gray, massive flow interiors are much fresher but even here the rocks are soft, suggesting alteration of interstitial material to smectite. In a few locations (e.g., 97.80-97.85 m) the breccia matrix is replaced by calcite and zeolite (analcime?). Because of their relatively thick and massive character and their abundance of vesicles the rocks of Unit V are interpreted as massive, crystalline lava flows.

UNIT VI

Upper contact:	109.00 m, ambiguous
Lower contact:	149.22 m, ambiguous
Thickness:	40.22 m
Lithology:	Alternating layers of massive glass and massive crystalline basalt
Cooling units:	25.01 to 33.01

Unit VI is a 40.22-m-thick sequence of alternating layers of massive, partly altered, basaltic glass and massive, crystalline basalt. The first glassy layer is taken as the top of the unit and the lower contact is drawn at the top of a massive basalt containing veins of hydrothermal minerals. The base of the unit also marks the lowest occurrence of fresh glass in the core. Thirteen separate layers of glass are recognized (cooling units 25.01, 25.03, 26.02, 26.04, 27.01, 27.03, 27.05, 28.02, 29.02, 30.02, 32.01, 32.03, 33.01) and these comprise about 35% of the total thickness. Individual layers range from 0.12 to 5.07 m and average about 1.3 m in vertical thickness. The glassy layers are composed of black to brownish-gray, aphyric, highly altered glass with prominent horizontal fractures. Highly variable alteration of the glass has

produced a brecciated appearance with irregular patches of generally fresh material being surrounded by black or greenish-gray smectite. Overall about 80% of the glass is altered but locally the alteration ranges from about 60 to 100%. Although smectite is the most common alteration product, celadonite is locally abundant, particularly in cooling unit 33.01. Where fresh, the glass is black and vitreous and has a well developed perlitic texture. It appears to be massive with no primary brecciation or fragmentation. Small (<1 mm) vesicles filled with calcite, zeolite, and minor pyrite comprise about 1% of these rocks. Hairline fractures filled with zeolite are locally present but extremely rare. Twelve layers of massive crystalline basalt are present in Unit VI, comprising about 65% of the total (cooling units 25.02, 26.01, 26.03, 26.05, 27.02, 27.04, 28.01, 29.01, 30.01, 31.01, 32.02, 32.04, 33.02). These range from 0.10 to 6.32 m and average about 2.3 m in vertical thickness. The crystalline basalts are greenish- to brownish-gray, very fine-grained, and often highly vesicular. The brownish-gray layers are aphanitic, non vesicular, and often have waxy surfaces. The greenish-gray zones are slightly coarser-grained and typically contain 10-15% of large vesicles. Most of the vesicles (70-80%) are open; others are partly to completely filled with zeolites, green smectite, and traces of quartz. Veins are almost completely absent and consist of hairline fractures filled with zeolites. Most of the crystalline basalts have a dull, highly altered appearance suggesting significant replacement of interstitial groundmass material by smectite and locally by celadonite. The origin of these crystalline and glassy lavas is not clear. There is no evidence of pillow structures and the crystalline zones are similar to massive lava flows observed in outcrop. The boundaries between the crystalline and glassy zones are transitional but occur over just a few centimetres. These boundaries may be flat or dip up to about 60 degrees. Very thin glassy layers may simply be chilled margins of massive flows but the thicker glassy layers are difficult to explain in this way. Alternatively, the sequence may have formed by ponding of lavas on the sea floor with periodic chilling due to episodic eruption or by frequent incursions of water into the ponded lava.

UNIT VII

Upper contact:	149.22 m, ambiguous
Lower contact:	154.24 m, ambiguous
Thickness:	5.02 m
Lithology:	Massive lavas with hydrothermal veins
Cooling units:	33.02

Unit VII is a single cooling unit of massive basalt which differs from the overlying units only in the presence of veins of argillic and zeolitic material representing the first evidence of hydrothermal alteration in Hole CY-2a. The unit is underlain by weakly altered and mineralized lavas which grade downward into intensely altered lavas. The rocks of Unit VII are medium-gray, fine-grained, aphyric, and moderately vesicular. Vesicles comprise only about 1% of the entire unit but are concentrated in layers or zones where they range up to 10% of the rock. The maximum vesicule diameter is about 8 mm and the average about 3 mm. About 10% of the vesicles are lined with smectite or celadonite and partly filled with zeolite. Veins also occur in distinct zones where they make up as much as a third of the rock but they comprise less than 1% of the unit as a whole. Individual veins range from hairline stringers up to several millimeters wide and they typically form an anastomosing pattern that gives the rock a brecciated appearance. The veins are filled largely with white argillic material accompanied by minor quartz, pyrite, and sphalerite. Groundmass alteration is moderate outside the zones of net veining and involves replacement of interstitial material by smectite and celadonite. Unit VII is lithologically similar to the overlying massive lava flows but is distinguished by its hydrothermal veining and alteration.

UNIT VIII

Upper contact:	154.24 m, ambiguous
Lower contact:	281.05 m, ambiguous
Thickness:	126.81 m
Lithology:	Highly altered and argillized massive lava flows and massive glass(?)
Cooling units:	35.01 to 60.02 (61.01 to 66.02) The units in parentheses represent a duplicate section drilled from 258.20 to 282.85 m when the hole was wedged past an obstruction.

Unit VIII consists of a sequence of highly altered and mineralized, non-pillowed, lava flows about 126.81 m thick. The upper contact is drawn at the first occurrence of significant hydrothermal alteration in the core and the lower contact is marked by the top of a dark gray relatively fresh basalt dike that was intruded after the major stage of hydrothermal activity. Two subunits are recognized on the basis of differing degrees of alteration and bleaching. Subunit VIIIa (cooling units 35.01 to 38.01; 154.24 to 167.74 m) consists of light brown to grayish-brown, hydrothermally altered lavas in which some of the original texture of the rock is preserved. Subunit VIIIb (cooling units 38.02 to 60.02; 167.74 to 281.05

m) consists of highly bleached and altered lavas in which the original character has been largely destroyed. Two principal lithologic types are recognized in both units. The first is a series of light gray, generally vesicular, completely altered but weakly mineralized massive lavas. Generally, these rocks have 1-2%, and rarely up to 7%, vesicles which average 4 to 5 mm across. A few larger vesicles, up to 1-2 cm across, are probably solution cavities enlarged by hydrothermal activity. About half of the vesicles are filled, predominantly with quartz, pyrite, and minor sphalerite. Veins usually comprise less than 1% of these rocks and range up to about 3 mm across. They are filled with approximately equal amounts of quartz and pyrite, occasionally accompanied by sphalerite. Thirty three such layers are recognized in Unit VIII constituting about 40 percent of the total (cooling units 35.01, 35.02, 36.02, 37.01, 38.01, 38.03, 39.01, 40.02, 42.01, 42.04, 42.06, 43.03, 44.01, 46.01, 47.01, 48.02, 50.01, 50.04, 51.01,51.04, 52.01, 52.03, 53.02, 53.04, 53.06, 54.03, 55.02, 56.02, 56.04, 57.01, 57.03, 59.02, 59.04). They have an average vertical thickness in the core of about 1.5 m. Alternating regularly with these massive lavas are cream colored to very light gray, extremely leached and altered, typically brecciated, highly mineralized lavas. These rocks contain few or no vesicles but a few have rough, bumpy surfaces due to the presence of numerous small, quartz-filled cavities. These lavas make up about 50 percent of the unit and occur in 33 distinct layers (36.01, 36.03, 38.02, 38.04, 40.01, 41.01, 42.03, 42.05, 43.01, 43.05, 44.02, 46.03, 48.01, 48.03, 49.02, 50.02, 50.05, 51.02, 51.05, 52.02, 53.01, 53.03, 53.05, 54.01, 54.04, 55.01, 56.01, 56.03, 57.02, 57.04, 59.01, 60.01). Groundmass alteration in both the massive and brecciated zones is similar and involves complete replacement by cream-colored argillic material, quartz, pyrite, and minor sphalerite. The massive lavas are less bleached and generally have no more than 1-2% of disseminated pyrite. The brecciated and bleached lavas typically have up to 10% of pyrite and in a few cases grade into massive pyrite ore. Eleven such intervals of massive, silicified ore occur in this sequence (cooling units 42.02, 43.02, 43.04, 46.02, 49.01, 50.03, 54.02, 54.06, 58.01, 59.03, 60.02) and they range from 0.17 to 3.56 m in thickness. These highly mineralized zones consist of gray, porous masses of pyrite, often with significant amounts of silica. In some cases the silica occurs as red jasper, in others as gray, aphanitic material. A few highly silicified zones occur without significant mineralization (e.g., cooling unit 51.03). Overall, the silicified and highly mineralized zones comprise about 10 % of the unit. The alternating sequence of massive and brecciated altered lavas described above is interpreted as the altered and mineralized equivalent of Unit VI which consists of alternating layers of crystalline basalt and massive glass. The coherent, vesicular zones in Unit VIII are believed to be altered massive lava flows whereas the highly bleached, brecciated, and mineralized zones are thought to represent zones of altered massive glass. Presumably the glass is more bleached and mineralized than the crystalline flows because it reacted more extensively with the hydrothermal fluids. The brecciated nature of the altered glassy zones is thought to reflect alteration patterns in the original glass rather than fragmentation during formation or during hydrothermal alteration. As described for unit VI, the glass develops an apparent brecciation by partial alteration to smectite. This texture is apparently preserved and enhanced by the later hydrothermal alteration.

UNIT IX

Upper contact:	281.05 (280.86) m, ambiguous
Lower contact:	282.85 (282.56) m, ambiguous
Thickness:	1.80 m (1.70 m)
Lithology:	Massive basalt dike(?)
Cooling units:	60.03 (66.02). The units in parentheses represent a duplicate section drilled from 258.20 to 282.85 m when the hole was wedged past an obstruction.

Unit IX is a single cooling unit of gray to brownish-gray, non-vesicular, massive basalt. The upper contact is marked by a sharp color change and a decrease in the degree of alteration. The base is drawn at a change to cream-colored, highly brecciated, highly altered lava. Unit IX was penetrated twice because of the duplicate section drilled between 258.20 m and 282.85 m in Hole CY-2a. The depths and thickness given in parentheses above are from the second section. The basalt of Unit IX is fine- to medium-grained, massive, and sparsely porphyritic. Olivine phenocrysts, up to 2 mm across, are scattered throughout the rock. These are euhedral crystals completely replaced by carbonate and chlorite. The groundmass is medium grained throughout except in the lower 50 centimeters of the unit where it fines toward the lower contact. Rare veins of calcite and gypsum are present but they make up much less than 1% of the unit. Alteration of the groundmass is much less than in the overlying and underlying units and consists largely of replacement by smectite and minor carbonate. Pyrite is conspicuously absent although a few grains occur in the upper 10 cm of the unit. Because of the weakly altered and non-mineralized nature of this unit it is interpreted as a dike intruded into the sequence after the major phase of hydrothermal alteration had ceased. The presence of sparse olivine phenocrysts suggests that this dike was a feeder for the uppermost olivine-phyric lavas

exposed in the area of the borehole.

UNIT X

Upper contact:	282.56 m, ambiguous
Lower contact:	297.14 m, ambiguous
Thickness:	14.58 m
Lithology:	Highly altered and bleached lavas
Cooling units:	66.03 - 68.03

A 14.58-m-thick sequence of intensely altered and bleached lavas similar to those of Unit VIII comprises Unit X. The upper contact is drawn at the base of the dark gray, relatively fresh basalt of cooling unit 66.02 and the base is marked by a 0.35-m-thick interval of fault breccia separating this unit from a series of altered, mineralized dikes. The bulk of Unit X consists of very highly brecciated, altered, and bleached lava with many zones of red jasper. Only cooling units 67.04 and 68.02 are massive and coherent. Cooling unit 67.04 is believed to be a massive flow whereas 68.02 is probably a small dike intruded before or during the major phase of hydrothermal activity. Vesicles are sparse in Unit X and are present only in the massive, coherent intervals. They range up to 10 mm across and are about one-half filled with quartz and pyrite in approximately equal proportions. Veins are sparse and consist of masses of pyrite and quartz which grade into groundmass material. The rocks are pervasively bleached and altered and are replaced by variable mixtures of argillic material, gray silica, jasper, and pyrite. Pyrite mineralization averages 5-10% for the entire unit but is unevenly distributed. The two massive zones are the least obviously altered and mineralized but both contain pyrite veins and disseminated pyrite in the groundmass. Unit X is lithologically similar to Unit VIII and the two are separated only by the post-mineralization dike of Unit IX. Hence, Units VIII and XI are considered to be part of the same sequence. Judging from the extensive brecciation and the intensive alteration, most of Unit X was probably originally glassy material.

UNIT XI

Upper contact:	297.14 m, ambiguous
Lower contact:	297.49 m, ambiguous
Thickness:	0.35 m
Lithology:	Fault breccia
Cooling units:	69.01

Unit XI consists of 0.35 m of light gray to brownish-gray fault breccia and gouge with well developed slickensides. The breccia consists of angular fragments of altered lava up to 1 cm across in a comminuted matrix of the same material. Along the most strongly slickensided zones there are several millimeters of brownish-gray, very fine-grained gouge. Veins and vesicles are absent, but the rock is intensely altered and weakly mineralized. Both the clasts and the matrix are replaced by argillic material and quartz, accompanied by 3-5% of disseminated pyrite.

UNIT XII

Upper contact:	297.49 m, ambiguous
Lower contact:	361.61 m, intrusive
Thickness:	64.12 m
Lithology:	Altered dikes
Cooling units:	69.02 - 83.02

Unit XII is a sequence of gray to brownish-gray, altered massive basalts interpreted as dikes. The upper contact is drawn at the base of a small fault breccia that separates highly bleached and altered lavas from the gray massive lavas of Unit X. The lower contact is placed at the top of a thick dike of dark gray, relatively fresh basalt (cooling unit 83.03). Forty five cooling units are recognized in Unit XII and most of these are separated by chilled but ambiguous contacts. Where contacts are well preserved (cooling units 71.02, 77.02, 79.04, 81.02, 83.01, 83.02) they are intrusive. However, even where the contacts between cooling units are ambiguous, small pieces of fine-grained to aphanitic material are present suggesting a chilled margin. The rocks of Unit XII are very uniform in color, texture, and degree of alteration. Most are medium-grained, massive lavas with intergranular to subophitic textures but many become finer grained toward their margins. Most cooling units are aphyric but a few (e.g., 76.01, 76.03, 77.04, 78.01) have 1-2% of small patches of chlorite up to 2 mm across, some of which may be altered crystals of clinopyroxene and/or olivine. A few thin cooling units (69.05, 69.07, 72.01, 73.05, 75.02, 77.02, 77.04, 79.01, 81.02) consist of light brown, aphanitic, aphyric lava, lithologically similar to the chilled margins of the thicker units. A few highly brecciated intervals (cooling units 73.02, 73.07, 76.04, 79.03), consist of gray, angular basalt fragments up to 4 cm across set in a comminuted matrix of the same material. Some of the fragments are aphanitic but there is no good evidence of chilling in these rocks. They are often in sharp contact with more massive basalt and are interpreted as fault breccias, although most do not have slickensides. All of the rocks of Unit XII are sparsely vesicular. Where present the vesicles are usually relatively large (up to 1 cm) but widely spaced. Only a few cooling units have small, closely spaced vesicles. These small vesicles are usually filled with chlorite whereas the larger ones are

often rimmed with chlorite and only partly filled with quartz and pyrite. Veins are also very rare but fracture surfaces are commonly coated with chlorite and pyrite. The groundmass is pervasively altered to mixtures of chlorite (possibly with some epidote), quartz, albite, and minor disseminated pyrite. Although these rocks are completely altered, their style of alteration and their secondary mineral assemblages are completely different from those of Unit X. The secondary mineralogy of the aphanitic cooling units is not known but is probably dominated by clay minerals. Of the 45 cooling units recognized in this sequence only 6 have unambiguous contacts. These preserved contacts are intrusive or faulted. However, even in the absence of clear-cut intrusive relationships, the massive, relatively coarse-grained, non-vesicular nature of these rocks strongly suggests that they are a series of hydrothermally altered dikes underlying the argillized lavas of Unit X. The two units appear to be separated by a small fault but the differences in alteration style are believed to be due to differences in the original textures and permeabilities of the rocks rather than to formation in different hydrothermal systems.

UNIT XIII

Upper contact:	361.61 m, truncated
Lower contact:	372.30 m, intrusive
Thickness:	10.69 m
Lithology:	Basalt dike
Cooling units:	83.03

A single 10.69-m-thick cooling unit of light to dark gray, aphyric, massive basalt comprises Unit XIII. It is interpreted as a dike based on a lower intrusive contact. Both contacts are recognized by abrupt changes in the degree and type of alteration. The color varies from light gray in the upper and lower parts of the unit to dark gray in the central portions. The rock is fine-grained in the upper 3 m, but grades downward into a medium grained interior at about 364.20 where the color changes from light to dark gray. At the base the grain size decreases abruptly at about 370.53 m and then decreases gradually to the chilled margin at 372.30 m. Vesicles comprise about 1-2% of the unit but they are irregularly distributed and most occur in a zones 1 to 2 cm thick. The largest vesicles, up to 6 mm across, occur in the central portions whereas those near the base of the unit are about 1 mm across. All of the vesicles are filled with calcite and traces of pyrite. In the central part of the unit there are up to 20% of large, vesicle-like features filled with slightly coarser-grained groundmass material which are interpreted as varioles. Veins are very rare and consist of hairline cracks filled with calcite, minor pyrite, and traces of quartz. A few of the pyrite-filled veins have narrow bleached halos up to 2 mm wide. The degree of groundmass alteration is difficult to determine but the primary mafic minerals appear to be largely replaced by chlorite and minor carbonate. The absence of pyrite and the different style and intensity of alteration suggest that this is a post-mineralization dike.

UNIT XIV

Upper contact:	372.30 m, truncated
Lower contact:	403.80 m, intrusive
Thickness:	31.50 m
Lithology:	Massive basalts, probably dikes
Cooling units:	85.01 - 92.02

Unit XIV consists of 12 cooling units of light gray, to greenish-gray, massive, aphyric basalt, interpreted as dikes. The upper contact is drawn at the base of the dark gray, post-mineralization dike of cooling unit 83.03 and the base is taken at the top of a sequence of altered glassy material. Individual cooling units have an average vertical thickness of 2.6 m and range from 0.36 to 9.77 m. Cooling unit 90.01 is a thin zone of coarse-grained diorite with amphibole crystals which grades abruptly into the diabase above and below. It is thought to be a coarse-grained segregation in the center of a thick dike (cooling units 88.01 and 90.02) but it could possibly be an inclusion. The basalts of Unit XIV are very uniform with fine- to medium-grained textures grading into chilled zones at several margins. The chilled zones are light green and aphanitic but do not appear to have been glassy. Definitely intrusive margins are rare (cooling units 86.02, 92.01, and 92.02) but the uniform nature of the basalts and the general lack of vesicles are more suggestive of dikes than massive flows. Thin breccia zones occur in the intervals 376.05 - 376.15 m and 381.15 - 381.25 m. These consist of angular fragments of basalt in a comminuted matrix of the same composition. Because of their location in the core and the absence of slickensides these zones are interpreted as brecciated dike margins. At 376.10 m a chilled margin is in contact with the breccia. Vesicles comprise 1% or less of the entire sequence and occur in small clusters near the centers of individual cooling units. A few vesicles are up to 1 cm across but most are less than 3 mm. The smaller vesicles are generally filled with calcite and pyrite, sometimes accompanied by lesser amounts of chlorite and quartz. The larger vesicles are open or are lined with small quartz crystals. In the interval 393.40 - 393.50 m there are numerous large solution cavities up to 3 cm across, lined and partly filled with calcite. Veins comprise much less than 1% of the unit and consist of hairline stringers of calcite and pyrite. Groundmass alteration is apparently pervasive

although the rocks are still generally gray in color. Primary minerals are replaced by various mixtures of chlorite, albite, and quartz with 1-2% of disseminated pyrite.

UNIT XV

Upper contact:	403.80 m, truncated(?)
Lower contact:	413.23 m, truncated(?)
Thickness:	9.43 m
Lithology:	Altered pillowed lava
Cooling units:	92.03 to 94.03

Unit XV is a 9.43-m-thick sequence of greenish-gray, often vesicular, highly altered, pillowed lava. The upper contact is drawn at the top of a dark gray, altered glassy layer and the lower contact at the intrusive margin of cooling unit 94.04. The uppermost cooling unit is ambiguous, appearing to have a relict perlitic texture at the top and a brecciated character near the base. This cooling unit could be a glassy pillow or a zone of altered massive glass similar to those in Unit VI. A small dike (cooling unit 93.01) is present between 405.58 and 405.69 m, but it does not cut completely across the core. Cooling unit 94.03 has a narrow, nearly vertical, breccia zone running through it which is interpreted as a small fault. Ten cooling units (excluding 93.01) are recognized in this sequence indicating an average vertical pillow thickness of about 1 m. All of the lavas are fine grained and aphyric with variable vesicle contents. Overall, vesicles average 1-2% of the rock but range up to 20% in some pillow interiors. In these highly vesicular zones individual vesicles range up to 1 cm or more across. Many of the large cavities are irregular and appear to have been enlarged by solution. Most of the small vesicles are completely filled with quartz; the larger ones are open or lined with quartz, pyrite, and epidote. Discontinuous hairline stringers of chlorite are present locally but comprise $<<$ 1% of the unit. Fracture surfaces are commonly coated with quartz and pyrite. The generally green color of the rocks indicates that groundmass alteration is high, with the primary minerals having been completely replaced by mixtures of chlorite, epidote, quartz, and albite. Most rocks also contain 1-2% of disseminated pyrite.

UNIT XVI

Upper contact:	413.23 m, intrusive(?)
Lower contact:	426.13 m, intrusive
Thickness:	12.90 m
Lithology:	Basalt dikes
Cooling units:	94.04 - 97.01

Two cooling units of light greenish-gray, medium-grained, aphyric basalt interpreted as dikes make up Unit XVI. The upper contact is drawn at an intrusive contact marking the top of a uniform massive basalt and the lower contact is placed at the top of a brecciated sequence. The upper and lower contacts are not very clear but are probably intrusive. The thicknesses and massive character of these cooling units indicate that they are not pillows and their sparsely vesicular nature suggests that they are dikes rather than flows. On average vesicles comprise $<1\%$ of the unit and never exceed 2% of the rock. Most vesicles are about 2 mm across, and they are filled with quartz and minor pyrite. Between 417.80 and 418.40 m vesicles range up to 2.5 cm across and are largely open or lined with quartz. A few are completely filled with gypsum. Narrow veins of quartz and pyrite are present but make up much less than 1% of the unit. A few of these veins have bleached zones up to 1 cm wide on either side. Fracture surfaces are often coated with quartz, pyrite, and sphalerite(?). The rocks are pervasively altered to chlorite, epidote, albite, and quartz, and they usually contain 1-2% of disseminated pyrite. In a few zones (e.g. 421.90 - 422.40 m) steeply dipping white streaks of quartz(?) are present.

UNIT XVII

Upper contact:	426.13 m, truncated(?)
Lower contact:	443.34 m, depositional(?)
Thickness:	17.21 m
Lithology:	Altered pillowed lava
Cooling units:	97.02 - 100.04

Unit XVII is a sequence of light greenish-gray, fine-grained, aphyric, altered pillows. The upper contact is drawn at the base of the massive dike of cooling unit 97.01 and the lower contact is placed at the top of a thick massive unit interpreted as a lava flow (cooling unit 100.05). Twenty three cooling units are recognized in this 17.21-m-thick sequence indicating an average vertical pillow thickness of 0.75 m. Cooling unit 97.03 is somewhat more massive and less vesicular than the overlying and underlying units, and it may possibly be a small dike or flow. All of the other units are interpreted as definite pillows based on their thickness, vesicle distribution, and contact relationships. Most units have sharp chilled margins about 1 cm thick with little or no intervening breccia. Where present, breccias consist of masses of altered glassy material up to 10 cm thick. Vesicles range from about 2 to 10% and average about 7-8% of the rock. Most vesicles are 2-3 mm across but some large vesicles are up to 2 cm in diameter. Some of the large vesicles are irregular in shape and they may have been enlarged by solution. On average, the

vesicles are about one-half filled with quartz and calcite. Small quantities of pyrite are usually present and a few vesicles contain minor zeolite and/or gypsum. Veins are small and sparse, averaging much less than 1% of the rock and rarely exceeding 1 mm in width. They are filled largely with chlorite, quartz, pyrite, and rare sphalerite, sometimes followed by calcite and gypsum. Groundmass alteration is pervasive and chiefly involves replacement of primary minerals by mixtures of chlorite, epidote, albite, and quartz. In the breccia zones the glassy fragments are completely replaced by chlorite accompanied by minor quartz and pyrite. A few small, irregular patches of gypsum and calcite occur in the groundmass, particularly in breccia zones. Disseminated pyrite is sparse and rarely exceeds 1% of the rock.

UNIT XVIII

Upper contact:	443.34 m, depositional(?)
Lower contact:	452.78 m, depositional
Thickness:	9.44 m
Lithology:	Altered massive lava flows
Cooling units:	100.05 - 101.01

Two massive lava flows with a combined thickness of 9.44 m comprise Unit XVIII. The upper contact is placed at the base of the lowest pillow in Unit XVI (cooling unit 100.04) and the lower contact at the bottom of cooling unit 101.01, a thick, massive flow. The underlying cooling unit (102.01) is 1.46 m thick and could be another massive flow, however, it has altered glassy material at the top and bottom and is interpreted here as a pillow. The massive lavas of Unit XVIII are interpreted as flows rather than dikes because they appear to have depositional contacts and are locally highly vesicular. A possible cooling break between 444.80 and 445.00 m is suggested by grain size variations and by the distribution of vesicles. However, this is a zone of drilling rubble and such a contact, if present, is not preserved. The flows consist of light greenish-gray, fine-grained, aphyric, altered lava, probably originally basalt. The grain size is quite uniform but appears to coarsen slightly in the center of the thickest cooling unit (100.05). Vesicles average about 3% of the entire sequence but range up to 20% in some intervals. Most vesicles are oval in cross-section and vary from 1 mm to 3 cm across. The smallest vesicles are completely filled with chlorite, quartz, or gypsum whereas the larger ones are open or lined with thin coatings of chlorite, quartz, and rarely calcite. A few large irregular cavities (e.g. 445.50 m) contain abundant epidote and quartz, followed by gypsum. Pyrite is locally intergrown with the quartz. Veins are very rare and consist of discontinuous, irregular streaks of quartz or gypsum. A few subparallel streaks of white quartz(?) occur in the central portion of cooling unit 101.01, but these are not true veins. The groundmass is pervasively altered to a mixture of chlorite, epidote, albite, and quartz with 1% or less of disseminated pyrite. Small, irregular patches of gypsum are also locally present.

UNIT XIX

Upper contact:	452.78 m, depositional
Lower contact:	466.00 m, truncated(?)
Thickness:	13.22 m
Lithology:	Altered pillowed lava
Cooling units:	102.01 - 104.06

A 13.22-m-thick sequence of pillowed lava comprises Unit XIX. The upper contact is drawn at the base of a thick massive flow (cooling unit 101.01) and the lower contact is drawn at the top of another thick massive cooling unit (104.07) interpreted as a dike. Twenty one cooling units are recognized in this sequence indicating an average vertical pillow thickness of 0.63 m. Fourteen of these units are clearly individual pillows, 6 are thin breccia sequences and 1 (102.01) is probably a pillow but it is thicker and more massive in character than the other pillows and could be a thin flow or a dike. The pillows consist of light greenish-gray, fine-grained, aphyric, altered lava that was probably originally basalt. Generally, the altered glass rinds are 2-3 cm thick and not highly brecciated. In a few cases, however, breccia zones between pillows are more than a meter thick. These breccias consist of fragments of altered crystalline and glassy basalt in a finer-grained matrix of similar material. Vesicles average 2-3% of the overall unit but range from $<1\%$ to 15 or 20% in thin zones. In most pillows the vesicles are concentrated near the upper and lower margins. The maximum vesicle diameter is about 1.5 cm but these large cavities are irregular in shape and may have been enlarged by solution. Most vesicles are between 1 and 5 mm in diameter and average about 2 mm. The smaller vesicles are typically filled with chlorite or quartz whereas the larger ones are completely open or lined with quartz, minor chlorite, and minor pyrite. A few larger vesicles are filled with gypsum. Veins always comprise much less than 1% of the rock and consist of narrow, discontinuous streaks of quartz, chlorite, and minor pyrite, sometimes followed by gypsum or calcite. Groundmass alteration to chlorite, epidote, quartz and albite is pervasive. Disseminated pyrite comprises $<1\%$ of the rocks but is locally more abundant in some breccias. Late calcite and gypsum also occur in small, irregular patches in the groundmass.

UNIT XX

Upper contact:	466.00 m, intrusive(?)
Lower contact:	476.78 m, intrusive(?)
Thickness:	10.78 m
Lithology:	Massive basalt dike
Cooling units:	104.07

A single cooling unit of massive, altered basalt interpreted as a dike comprises Unit XX. The upper and lower contacts are somewhat ambiguous but appear to be intrusive. The upper contact is marked by a sharp change in color and grain size and is characterized by a series of steeply dipping white streaks similar to those seen along other intrusive contacts. The lower margin has a distinct chill zone, 2-3 mm wide, and is characterized by a number of small vesicles in the overlying 15 cm. The lavas are gray to faintly greenish-gray, fine- to medium-grained, and aphyric. The unit is fine- to very fine-grained near the top and bottom but becomes medium-grained within a half a meter of the contacts. A relict intergranular to subophitic texture is clearly visible in the medium-grained zone. In the lower 15 cm of the unit vesicles make up 7-8% of the rock but they are nearly absent elsewhere. The maximum vesicle diameter is about 3 mm and most are <1 mm across. The smallest vesicles are filled with chlorite whereas the larger ones are lined and rarely filled with pyrite and minor quartz. Veins are conspicuously absent but a few hairline fractures are coated with chlorite and pyrite. The groundmass appears to be pervasively altered to chlorite, epidote, quartz, and albite although in the central part of the unit the rock is grayer and fresher appearing than the pillow lavas above and below. Traces of pyrite are also disseminated in the groundmass.

UNIT XXI

Upper contact:	476.78 m, truncated(?)
Lower contact:	528.90 m, truncated
Thickness:	52.12 m
Lithology:	Pillowed(?) lavas and massive flows cut by several dikes
Cooling units:	106.01 - 115.04

Unit XXI is a thick sequence of altered lavas in which 31 cooling units of varied character are recognized. Two of these (110.01 and 111.01) are identified as dikes based on their massive, generally non-vesicular, character and the presence of clearly identifiable intrusive contacts. Two other cooling units (107.05 and 109.01) are tentatively identified as dikes on the basis of lithology but the contact relationships are ambiguous. Unit 113.01 is a 0.20 m thick quartz/gypsum/pyrite vein. The remaining 26 cooling units are tentatively interpreted as massive lava flows and pillows on the basis of their lithology. They range from 6.89 to 0.34 m and average 1.65 m in vertical thickness. The thickest units (1.5 m or more) are tentatively identified as massive flows and the thinner units as pillows or pillow breccias. In unequivocally pillowed sequences such as Units XV, XVII, and XIX the average vertical pillow thickness is between 0.5 and 1.0 m and only three exceed 1.5 m in thickness. Thus, cooling units thicker than 1.5 m are likely to be massive flows. However, both thick pillows and thin massive flows occur in some exposed sequences on Troodos so thickness alone is not a reliable indicator of cooling unit character. Lithologic features commonly used to distinguish pillows from flows (vesicle size and abundance, presence of interunit breccia, etc.) are variable in Unit XXI and their occurrence does not correlate closely with cooling unit thickness. Using all of the available criteria 14 cooling units are tentatively identified as massive flows (106.03, 108.03, 109.02, 110.02, 111.02, 112.01, 112.02, 112.04, 113.02, 113.03, 113.04, 115.01, 115.02, 115.04) and 12 as probable pillows (106.01, 106.02, 107.01, 107.02, 107.03, 107.04, 108.01, 108.02, 108.04, 108.05, 112.03, 115.03). The pillows and massive flows are lithologically similar and consist of gray to grayish-green, uniformly fine-grained, aphyric lava. The flows are massive with little or no brecciation. Pillows on the other hand show considerable internal brecciation and are typically separated by zones of altered hyaloclastite. Cooling unit 107.03 is an unusual sequence of thin pillows or pillow lobes, each about 10 cm thick. Cooling units interpreted as pillows have clusters of small (1-2 mm) vesicles near their upper and lower contacts and are nearly vesicle-free in their central parts. The thicker cooling units interpreted as flows have larger (up to 10 mm) and more abundant vesicles which are distributed more or less uniformly through the rock. About one-half of the vesicles are filled, chiefly with chlorite, quartz, pyrite, and gypsum. Veins are common in the pillows and flows, averaging about 1% of the rock and ranging up to 1 cm wide. They are filled largely with pyrite and quartz and some have small patches of late gypsum. The dikes are light gray to greenish-gray, fine- to medium-grained, aphyric basalts with sparse vesicles. Their contacts are sharp and chilled and the rocks often have streaks and vesicle trains parallel to the contacts. The rocks grade from aphanitic at the chilled margins through fine-grained zones, 10-15 cm thick, into medium-grained interiors. Vesicles make up <1% of these rocks and have a maximum diameter of about 2 mm. About half are filled with quartz, pyrite, and chlorite in the proportions 2:2:1. Pyrite-quartz veins are unusually abundant in the dikes, commonly making up 2-3% of the rock and ranging up to 1 cm in width. Groundmass alteration

in dikes, pillows, and lava flows is pervasive, producing a generally greenish tint to the rocks. Primary minerals are replaced by mixtures of chlorite, epidote, quartz, and albite. Disseminated pyrite is always present but never exceeds 1% of the rock. The small pillows or pillow lobes of cooling unit 107.03 are darker gray in color than the other units and may be somewhat less altered. On the other hand, the hyaloclastites and breccias are typically green in color and are completely replaced by chlorite. Both quartz and late gypsum locally replace the breccia matrix. Overall, Unit XXI is a complex sequence of largely extrusive material cut by a few dikes. There is no particular pattern to the occurrence of pillows and massive flows but identification of individual units is difficult.

UNIT XXII

Upper contact:	528.90 m, intrusive
Lower contact:	689.15 m, bottom of the hole
Thickness:	160.25 m
Lithology:	Altered basalt dikes
Cooling units:	115.05 - 145.01

Unit XXII consists of a thick sequence composed chiefly of altered dikes which presumably were originally basaltic in composition. In the upper 10 m there are a few thin screens of altered lava between the dikes but in the remainder of the unit dikes appear to intrude dikes. The upper contact is placed at the point where dikes constitute over 90% of the sequence and the unit extends to the base of the hole. Sixty nine cooling units are recognized in this 160.23-m-thick sequence and most of these have distinct boundaries. Forty five cooling units have at least one definitely intrusive contact indicating that they are dikes. Seventeen of these are complete dikes with intrusive contacts on the top and bottom. Of the 28 dikes with a single chill zone 22 (78%) have the lower contact preserved and 6 (22%) have the upper contact preserved. Most of the remaining cooling units are lithologically similar to the dikes and these are also interpreted as intrusions. A few thin units truncated on both sides (116.01, 116.03, 116.05, 117.02, 119.01, 119.03, 120.01, 141.03) are brecciated and often rather vesicular suggesting that they are screens of lava flows or pillows. The 61 cooling units interpreted as dikes range from 0.15 to 23.76 m in vertical thickness and average 2.54 m. The dike swarm has an average dip in the core of 65 degrees indicating true thicknesses between 0.09 m and 13.63 m with an average of 1.46 m. The dikes are light greenish-gray, fine- to medium-grained, aphyric, altered rocks which probably were basalts originally. Vesicles average about 1% of the rocks and are scattered more or less uniformly through the unit. Most are 1-3 mm across but a few larger solution cavities are also present. The smallest vesicles are typically filled with chlorite whereas the larger ones are lined with chlorite and partly to completely filled with quartz, epidote, and pyrite. In most cooling units veins are small and sparse but locally pyrite-quartz veins comprise up to 5 % of the rock. Primary minerals in the groundmass are completely replaced by chlorite, epidote, quartz, and albite, and most rocks also contain 1-2 % of disseminated pyrite. The sparse lava screens are light grayish-green, fine-grained, aphyric rocks that contain abundant vesicles. Vesicles make up 10-15% of most of these units and range up to 1.5 cm across. They are about two-thirds filled with epidote, quartz, chlorite, and pyrite. Veins are generally absent but a few units have streaks of quartz or chlorite. The groundmass is completely altered to quartz, epidote, chlorite, albite, and minor pyrite.

ACKNOWLEDGEMENTS

This summary was produced from detailed core descriptions prepared in Cyprus during the Summer of 1982 by the Cyprus Crustal Study Project laboratory staff. The assistance of the many individual scientists in the preparation of these detailed descriptions is gratefully acknowledged.

Alteration Mineralogy of a Fossil Ore-Solution Aquifer: Petrography and Mineral Chemistry from the Lower Portion of Research Drill Hole CY-2a, Agrokipia, Cyprus

HEATHER E. JAMIESON[1], J.W. LYDON[2] AND G.M. LECHEMINANT[2]

[1]Department of Geological Sciences, Queen's University, Kingston, Ontario, Canada, K7L 3N6
[2]Geological Survey of Canada, 601 Booth Street, Ottawa, Ontario, Canada, K1A 0E8

Jamieson, H.E., Lydon, J.W. and LeCheminant, G.M., Alteration mineralogy of a fossil ore-solution reservoir: petrography and mineral chemistry from the lower portion of research drill hole CY-2a, Agrokipia, Cyprus; in *Cyprus Crustal Study Project: Initial Report, Holes CY-2 and 2a, ed. P.T. Robinson, I.L. Gibson and A. Panayiotou; Geological Survey of Canada, Paper 85-29, p. 57-68, 1987.*

Abstract

The secondary minerals present in the lower 300 m of core from the Cyprus Crustal Study Project drill hole CY-2a have been studied by petrographic examination and electron microprobe analysis. These dykes and lavas underlie the Agrokipia 'A' orebody, and may have been hydrothermally altered by the same fluids that deposited the copper-zinc sulphide ore. From a depth of 400 to 650 m, all rocks consist of the assemblage chlorite-albite-quartz-sphene-pyrite, with minor epidote, calcite, and anhydrite, and several zones of trace chalcopyrite, galena and sphalerite. From 650 m to the base of the drillhole at 680 m, all fragmental rocks, such as pillow breccias, contain patches of monomineralic epidote within chloritized basalt, while massive lavas and dykes consist of the greenschist assemblage described above. Plagioclase composition was found to be consistently albitic throughout the core interval. The relative abundance and degree of crystallinity of epidote increases with depth but the composition varies little. Chlorite in veins and vesicles is compositionally indistinguishable from chlorite in the groundmass (average Fe/(Fe+Mg) = 0.44). Within the lower zone of patchy alteration, chlorite composition, like that of epidote, exhibits a wider range of composition within a single thin section than it does in other samples. In general, fragmental rocks contain chlorite with lower Fe/(Fe+Mg) than do massive rocks.

Résumé

Une étude au microscope pétrographique et une analyse à la microsonde a porté sur les minéraux secondaires inclus dans les carottes des derniers 300 m du fond du trou de forage CY-2a du Cyprus Crustal Study Project. Ces dykes et laves sont sous-jacents au gîte Agrokipia 'A', et il semble que leur altération hydrothermale résulte de l'action des mêmes fluides qui formèrent le dépôt de minerai de sulfures de cuivre et zinc. Dans l'intervalle de 400 à 650 m, toutes les roches sont composées de l'assemblage chlorite-albite-quartz-sphène-pyrite, avec en quantité subordonnée de l'épidote, de la calcite, et de l'anhydrite, et des zones de traces de chalcopyrite, galène et sphalérite. De 650 m jusqu'au fond du trou, à 680 m, toutes les roches fragmentées, telles les coussins bréchifiés, contiennent des plages d'épidote monominéralique dans le basalte chloritisé, tandis que les laves massives et les dykes sont formés de l'assemblage de schistes verts décrit ci-dessus. La composition albitique du plagioclase est constante au travers la section représentée par les carottes. L'abondance relative et le degré de cristallinité de l'épidote augmentent avec la profondeur, mais la composition demeure stable. Les compositions de la chlorite dans les veines et vacuoles et de la chlorite dans la matrice sont indistinctes (moyenne Fe/(Fe+Mg) 0,44). Dans la zone inférieure caractérisée par les plages d'altération, la composition de la chlorite et de l'épidote exhibe dans une lame mince particulière plus variable que celle observée dans les autres échantillons. En général, les roches fragmentées renferment de la chlorite avec un rapport Fe/(Fe+Mg) plus faible que pour les roches massives.

INTRODUCTION

Research hole CY-2a of the Cyprus Crustal Study Project is located above the Agrokipia 'A' massive sulphide orebody. As illustrated in Figure 1, the drill hole intersects 150 m of relatively unaltered massive flows and dikes, followed by another 150 m of brecciated mineralized lavas rich in pyrite, chlorite and muscovite, followed in turn by 400 m of altered dykes, with screens of fragmented flows and pillows, extending to the base of the hole. This lower core interval of altered rocks is the subject of the research reported in this paper and in the companion paper in this volume (Jamieson and Lydon, 1987).

From a depth of 400 to 650 m, all the rocks, including massive flows, dikes and breccias, are completely altered to the assemblage chlorite - albite - quartz - sphene that is a typical 'greenschist' assemblage of metabasalts. Pyrite is present in veins, vesicles and the groundmass throughout the interval and constitutes as much as ten percent of the rock. In several zones within this core interval, chalcopyrite, sphalerite and galena accompany pyrite in trace amounts. Below 650 m, sections of fragmental rocks record the effect of a fluid-rock interaction that caused the replacement of chloritized basalt with patches of coarse epidote. The massive dikes and lavas, however, retain the greenschist alteration assemblage.

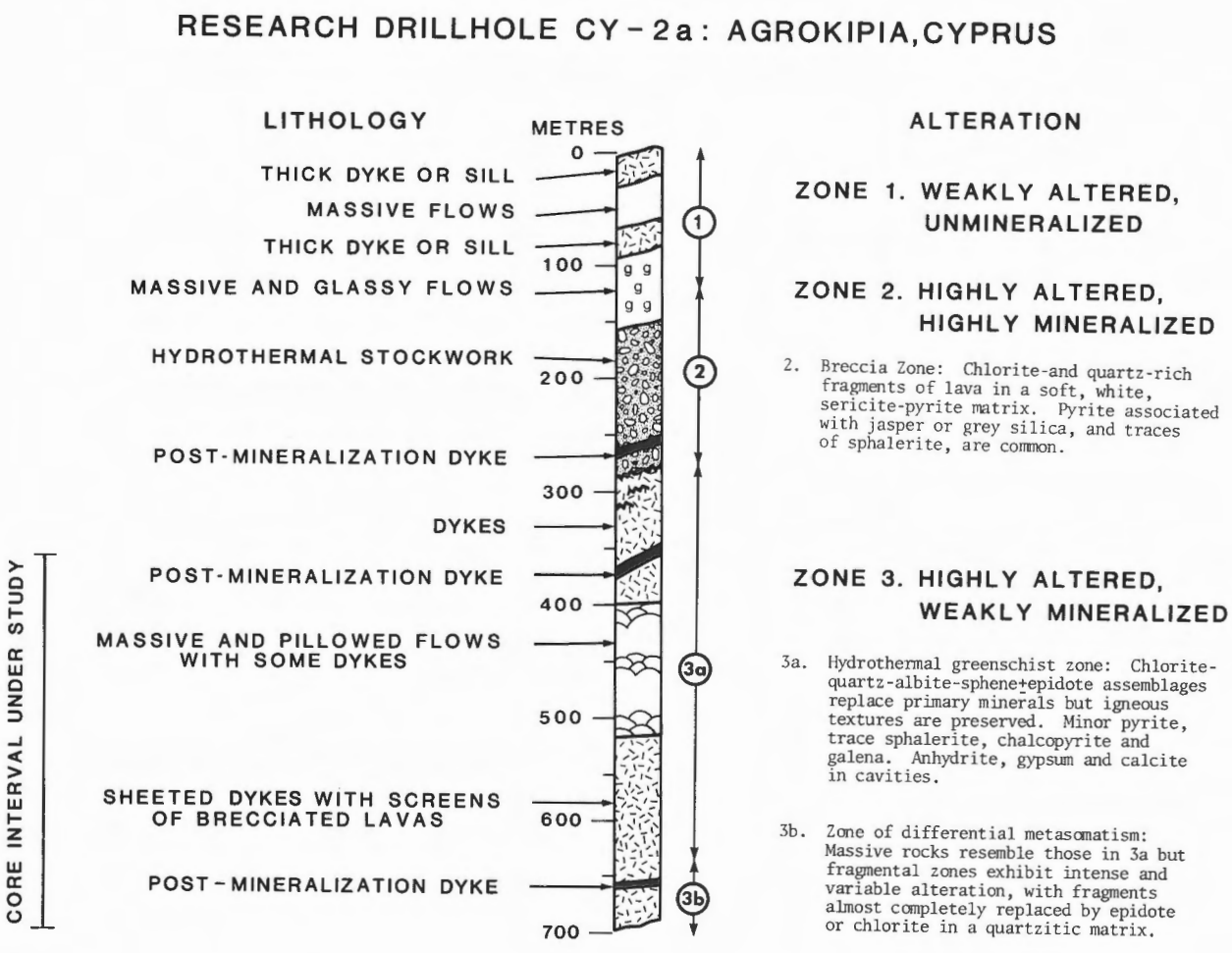

Figure 1: Generalized log of the CY-2a drill hole.

The position of these intensely altered fragmental zones more or less vertically below the stockwork of the Agrokipia deposits suggests that these rocks represent a fossil aquifer system that acted as either a reservoir within which ore-forming fluids were generated, or a conduit through which the fluids passed. If so, then these samples provide the opportunity for research on the origin of ore-forming hydrothermal solutions which has not been possible by studying either, (a) modern hydrothermal systems, which are either not metalliferous (e.g. most modern hydrothermal systems), or else the reservoir zones are inaccessible (e.g. sulfide-precipitating hot springs at submarine ridges), or, (b) ancient ore deposits, in which neither the fossil aquifer zones nor the fluid compositions have been positively identified. In particular, the CY-2a core samples of hydrothermally altered rocks have not been affected by subsequent regional metamorphism and deformation, as is the case of most ancient deposits such as those in the Canadian Precambrian, nor by the supergene alteration observed in many surface samples from Cyprus (Lydon, 1984).

In order to assess the possibility that the 650-690 m core interval represents a fossil hydrothermal system that interacted with the ore-forming fluids, the mineralogy and chemistry of approximately forty samples were examined in detail. This paper reports the mineralogy, textures and mineral chemistry determined from petrographic examination, X-ray diffraction and electron microprobe analysis. The major and trace element geochemistry of the same samples and the sulphur isotope compositions of the pyrite and sulphate are reported in the companion paper (Jamieson and Lydon, 1987).

GENERAL OBSERVATIONS

The alteration state of the basalts underlying the Agrokipia sulfide mineralization can be summarized by the following four observations.

1) Mineralogical Zones

The core interval examined is readily divisible into two alteration zones. The upper section, from a depth of 370 to 650 m, is identified as the hydrothermal greenschist zone. In this interval, massive flows, fragmental rocks, and dikes all consist of the assemblage albite - chlorite - quartz - pyrite - sphene. Minor amounts of epidote, calcite, and anhydrite (partially hydrated to gypsum) are also present in some samples, as shown in the mineral distribution table in Figure 2. Igneous textures are well-preserved. As described in the companion paper (Jamieson and Lydon, 1987), igneous compositions, in terms of major element proportions, are also generally preserved except for calcium depletion and iron sulphide addition. In contrast, the lower section, from 650 to 690 m, is described as the zone of differential metasomatism. Here, local migration of most major elements has produced patches of extremely epidote-rich rocks in fragmental horizons. These epidote-rich fragmental sections are several centimetres to several metres in length, and are separated by sections of massive rocks that retain the same greenschist assemblage that dominates the upper zone.

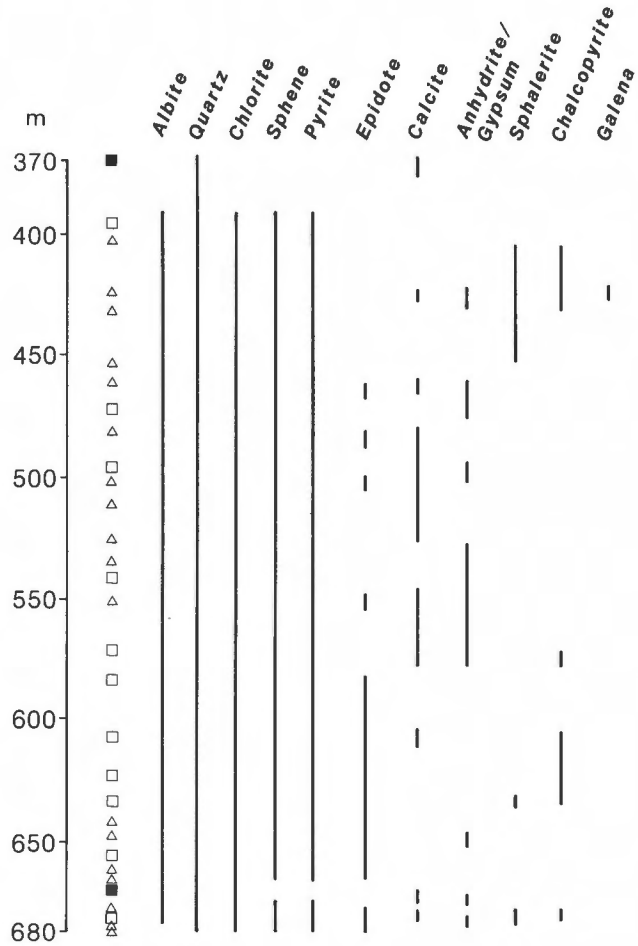

Figure 2: Distribution of minerals within core interval under study. Symbols mark sample locations: triangles refer to fragmental rocks, mainly pillow breccias, open squares refer to dikes and massive flows, and solid squares refer to relatively unaltered, post-mineralization dikes.

2) Degree of Alteration

Throughout the core interval under study, the samples examined were found to consist entirely of secondary minerals. Even where delicate volcanic features such as chilled margins, tiny felted microlites and perlitic fractures are preserved, the primary mineralogy is completely replaced except for the occasional area of partially devitrified glass. The general alteration pattern consists of albitization of plagioclase phenocrysts and microlites, pseudomorphic replacement of ferromagnesian phenocrysts by chlorite, and alteration of microcrystalline interstitial material to a mixture of chlorite, quartz and sphene. The only samples preserving some primary igneous mineralogy are the two post-mineralization dikes indicated in Figure 1.

3) Mineral Paragenesis

Within the hydrothermal greenschist zone, secondary minerals appear to have formed directly from the primary igneous assemblage. No remnants of pre-existing, lower-temperature alteration phases, characteristic of the extrusive volcanic sequence elsewhere in the Troodos complex, have been observed. In samples such as those taken at depths of 426.0 m and 455.9 m, chlorite appears have formed directly from glass, rather than from an alteration product of glass, such as smectite. In addition, vein-vesicle fillings do not appear to replace other open-space deposits such as zeolites or clays which are found in the extrusive sequence at other locations (Gillis, 1983; Botros, 1983). Furthermore, the identity and relative proportions of minerals found as vein and vesicle fillings vary so much on the scale of a few millimeters that a generalization as to the patterns of mineral paragenesis is not possible. The only evidence of replacement reactions observed in this suite is, (a) the replacement of both chlorite-albite fragments and calcium sulfate veins by epidote within the zone of differential metasomatism, and, (b) the hydration of anhydrite to gypsum.

4) Mineral Distribution Patterns

The distribution and relative proportions of the major alteration minerals (chlorite, albite, quartz and pyrite) are generally uniform, and appears to be unrelated to either stratigraphy or precursor porosity.

Epidote, however, shows two patterns of distribution. As a minor phase in the greenschist assemblage, epidote increases both in abundance and in degree of crystallinity with depth, indicating, from comparison with active geothermal systems, a modest thermal gradient over the 400 m examined. Figure 2 suggests that, with increasing depth, epidote takes the place of calcite and anhydrite as the calcium-bearing minor phase, although there is no textural evidence of simple replacement. The onset of extreme epidote replacement in the lowest 20 m may have been stimulated by a number of mechanisms, as discussed in a later section.

The distribution of chalcopyrite and sphalerite is related to neither depth nor porosity but rather concentrated in three horizons at approximately 420-460 m, 570-640 m and near 685 m depth. The chlorite in these base metal-rich horizons is enriched in manganese.

HYDROTHERMAL GREENSCHIST ZONE

Massive Crystalline Rocks

Macroscopically, massive crystalline rocks of the hydrothermal greenschist zone are fine-grained, grey-green samples with uniform textures. They are distinctly paler than the two examples of post-mineralization dikes described below. In thin section, holocrystalline rocks such as dikes and massive flows display a uniform texture of randomly-oriented or, less commonly, pilotaxitic feldspar laths in a groundmass of chlorite, quartz, sphene, pyrite. Except for the uppermost samples, minor epidote is also present. In contrast to dikes away from the vicinity of ore deposits, (W.R.A. Baragar, pers. comm., 1984) actinolite is not present. The feldspar occurs as subhedral blades with ragged terminations that range in size from microlites to rare phenocrysts. Albite twinning is present but extinction is obscured by alteration. In some samples feldspar is replaced by epidote or a mixture of chlorite and quartz but most commonly the feldspar is albitized. In a few dikes near the 600 m depth, potassium-rich feldspar is found as rims on albite, probably indicating a late, low-temperature enrichment of potassium. This is manifested as local K_2O-enrichment in the corresponding chemical analyses (Jamieson and Lydon, 1987). Chlorite forms pale green, weakly pleochroic, massive or acicular aggregations interstitial to feldspar, and is usually associated with quartz. Chlorite also pseudomorphically replaces pyroxene or olivine phenocrysts. Quartz is usually subequant, subhedral and frequently includes apatite laths. Sphene forms tiny saccharoidal grains dispersed in the groundmass.

Although on the scale of a thin section the texture of these crystalline rocks is uniform, the distribution of pyrite is inhomogeneous even at the scale of a hand specimen because of its common occurrence in centimetre-wide veins. However, the amount of pyrite in the groundmass, where it forms subhedral to euhedral equant grains, is consistently about five per cent by volume. Chalcopyrite and sphalerite occur as trace amounts, spatially associated

with pyrite, in veins or as disseminations in wall rocks adjacent to veins. Most of the sulfides are found as veins and vesicle fillings. Highly corroded grains of remnant aluminum-rich spinel are found in the groundmass of a few samples.

Glassy Rocks

Cryptocrystalline to glassy fragmental samples from the hydrothermal greenschist zone represent brecciated pillow margins, flow tops, or dike margins. In some cases brownish-yellow glass is either well preserved or is partially devitrified to chlorite and sphene. In other cases, the fragments consist of an extremely fine-grained version of the texture and secondary assemblages typical of the massive rocks found in this zone. The presence of remanent chill margins and perlitic cracks at fragment boundaries suggest that the fragmentation is primary, even though the matrix assemblage of chlorite - quartz - pyrite appears to be entirely of a secondary, hydrothermal origin. A frequent and spectacular texture seen in these rock types consists of concentrically-zoned ellipsoidal structures made up of chlorite and sphene, as shown in Figure 3. These are thought to be the result of cooling and alteration of glass. The curved fractures defining the ellipsoid boundaries are interpreted as perlitic fractures and the concentric banding is probably the result of diffusion-controlled alteration. Cores of ellipsoids consist of coarser grains of quartz, pyrite or, rarely, analcime.

Vesicles and Veins

Both flows and dikes contain vesicles and veins. Vesicles are usually round, up to 4 mm in diameter and constitute as much as 8% of a thin section. The abundance, texture, and contained phases of vesicles appear independent of host lithology. Vesicles are usually completely filled, most commonly with massive or fibrous chlorite, anhedral or drusy quartz, and euhedral pyrite. Fine-grained calcite and sheafs of coarse epidote may also occur in minor amounts. Sphalerite and chalcopyrite are concentrated within broad sections (400-465 m and 570-640 m), and in a single sample near the base (684.8 m). Both are always in close association with pyrite, whether in veins or in the groundmass, and are usually in contact with each other. Mutual equilibrium textures, such as chalcopyrite rimming sphalerite, or included as tiny blebs in sphalerite are common. Rare grains of galena were observed in hand specimen in vesicles containing sphalerite and quartz. Digenite was observed in a single specimen.

Mineral proportions and habit vary from vesicle to vesicle in the same thin section, and do not exhibit a simple or consistent paragenesis. Thus, the vesicles appear to record very localized conditions of hydrothermal precipitation.

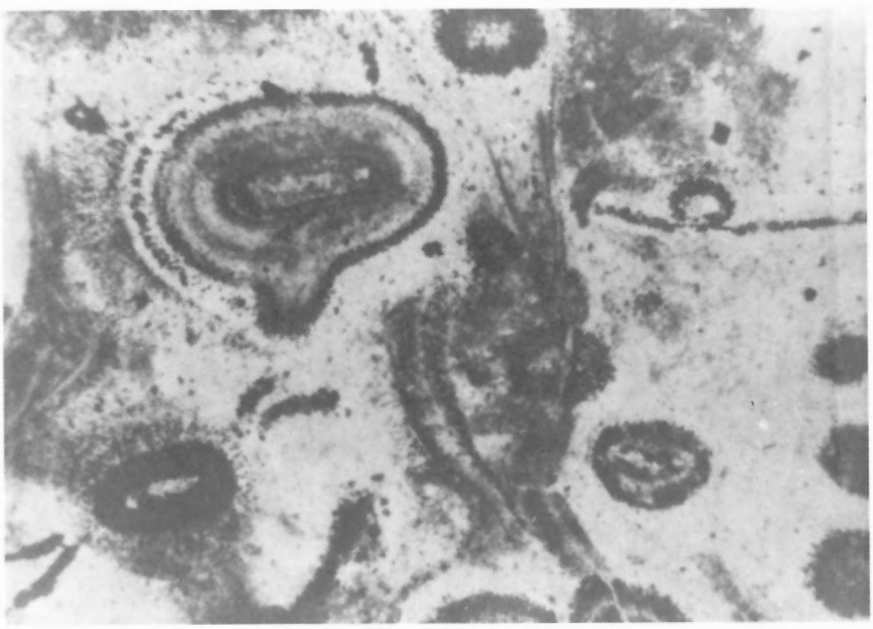

Figure 3: Sample from a depth of 553.5 m. Texture interpreted to be a result of devitrification and alteration of glass. The width of the photograph represents approximately 0.6 mm.

Larger, irregular cavities interpreted as solution-enlarged vesicles are found between approximately 400 and 470 m depth. This interval corresponds to the upper mineralized zone, in which cavity fillings contain sphalerite, chalcopyrite and/or galena. Rarely, large cavities in this region are filled with fibrous gypsum with relicts of the precursor anhydrite.

Veins are most commonly infilled by subhedral to euhedral pyrite grains with interstitial anhydrite, or anhydrite partially replaced by gypsum. Tiny grains of anhydrite are completely enclosed by pyrite. Although gypsum is the most abundant form of calcium sulfate seen, the following textural observations confirm that anhydrite is the primary mineral: (a) optically aligned 'islands' of anhydrite occur within sheets of fibrous gypsum (Figure 4), (b) the sulfate enclosed within pyrite is, without exception, anhydrite, and (c) 'explosion' textures, in which cleavage fragments of anhydrite appear to have been bent and broken in order to accommodate the volume expansion of hydration, are common. Sulfate is clearly not the product of pyrite oxidation, as the pyrite is fresh and unaltered and there are no iron oxides present. Where epidote is closely associated with calcium sulfate (e.g. Figure 4), the consistent alignment of gypsum fibres in apparently unconnected interstices between the epidote grains suggests that the epidote replaced the gypsum, but the relative age of these two minerals is not certain and does not affect the general interpretation of the aquifer history (Jamieson and Lydon, 1987).

Other vein minerals are quartz, chlorite, calcite and epidote. Dolomite was identified by microprobe in one sample. All veins appear to be of the same age. All minerals that occur in veins also occur in vesicles.

ZONE OF DIFFERENTIAL METASOMATISM

Below 650 m, fragmental rocks record the effect of a water-rock reaction that produced only epidote or epidote with minor quartz. Textural evidence demonstrates that this near-monomineralic precipitate replaced chloritized fragments. The replacement appears to have been selective, as shown by the co-existence of epidotized patches, recognizable as fragments by their shape and size, and chlorite-rich fragments which show only incipient epidotization. Coarse epidote also appears to replace veins of anhydrite, which are partially hydrated (Figure 4).

The general texture of the fragmental horizons affected by epidote-producing metasomatism indicates that they were glassy or cryptocrystalline pillow breccias, as seen higher in the core interval. This is demonstrated by comparing Figure 5, which shows a chloritic fragmental pillow rim from the hydrothermal greenschist zone, with Figure 6, which shows a fragmental from the zone of differential metasomatism in which most of the fragments have been replaced by epidote. The matrix of breccias in the zone of differential metasomatism consists mainly of quartz and pyrite. In some samples, the fragmental character has been obscured by extreme epidotization.

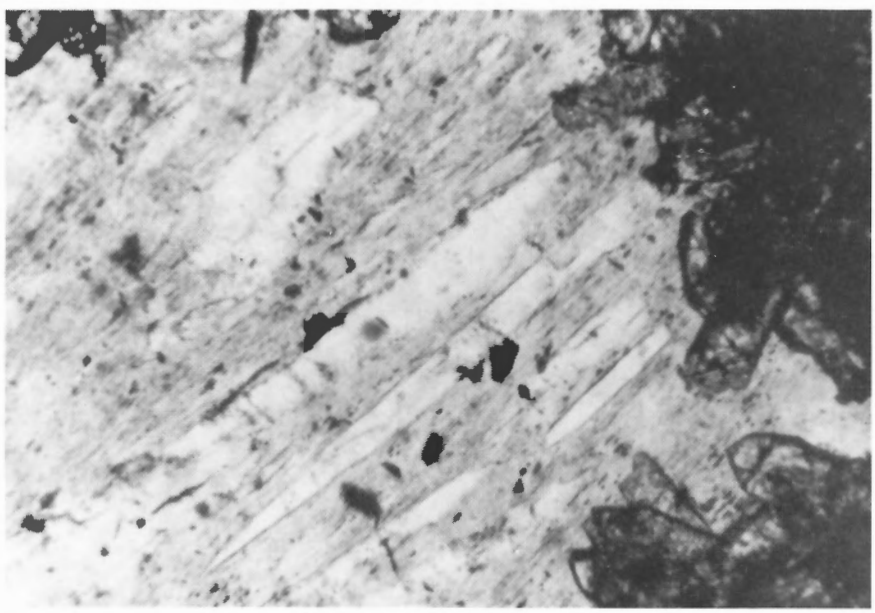

Figure 4: Sample from a depth of 686.6 m. Islands of optically-aligned, remnant anhydrite in fibrous gypsum. Coarse epidote at left. The width of the photograph represents approximately 0.6 mm.

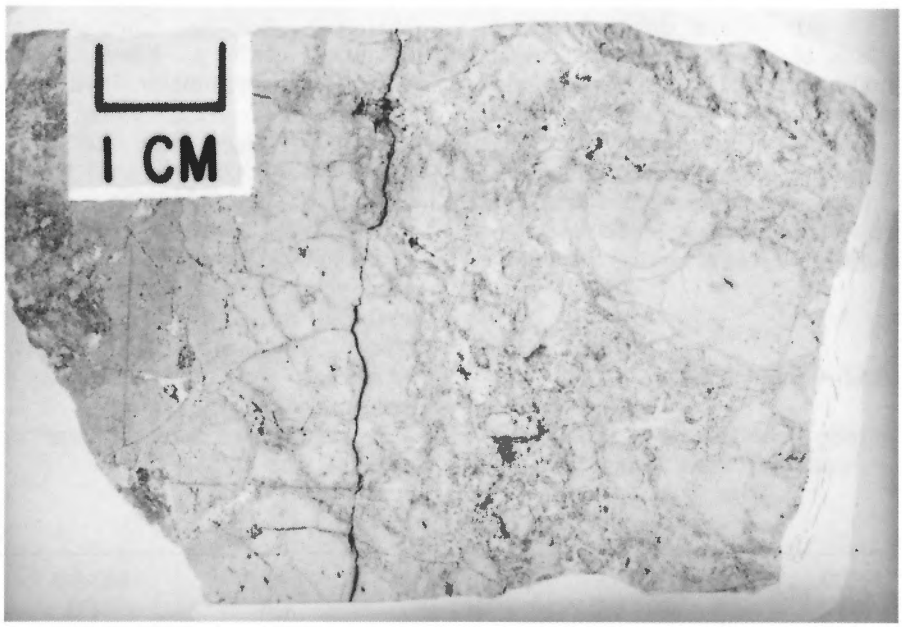

Figure 5: Sample from a depth of 434.5 m. Typical fragmental pillow rim from the Hydrothermal Greenschist Zone. The fragments consist of glass and chlorite-rich assemblages in a matrix of quartz and pyrite.

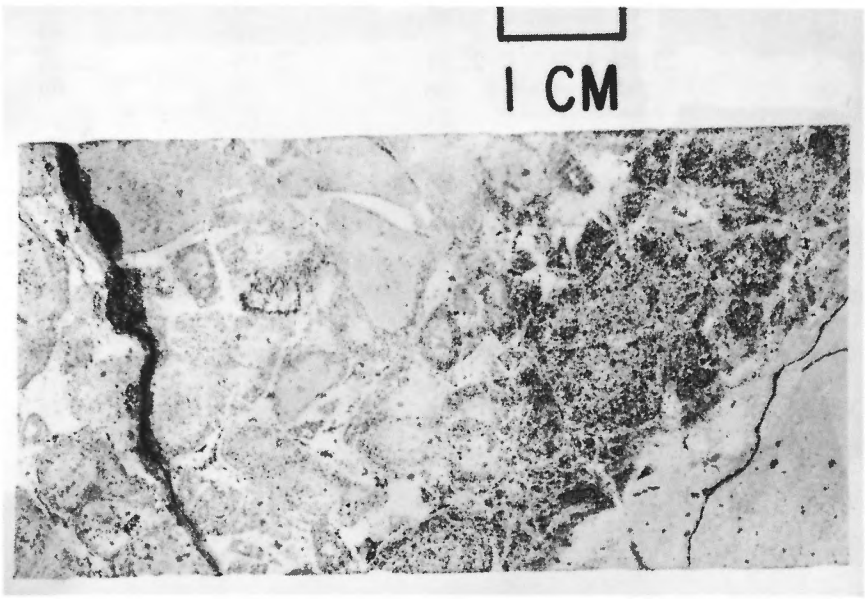

Figure 6: Sample from a depth of 670.0 m. Typical fragmental rock from the Zone of Differential Metasomatism. Fragments are dominated pale epidote, in some cases rimmed by chlorite, in a quartz-rich matrix. Dark band near base of fragmental zone is chlorite-rich.

POST-MINERALIZATION DIKES

There are two noticeably less altered dikes, one at the top of the sample interval (370.5 m), and one near the bottom (673.0 m). These differ from all other rocks by their lack of pyrite, other than trace amounts in the groundmass, and by their relatively dark colour in hand specimen. The sample from 370.5 m contains fresh plagioclase (An 63), clinopyroxene and spinel in a groundmass of smectite. The sample from 673.0 m possesses feldspars that are only partially albitized, retains primary spinel but also contains abundant secondary chlorite and groundmass carbonate.

MINERAL CHEMISTRY

Electron microprobe analysis was used to establish the range in composition of major phases. Several grains from each thin section were analyzed in order to test both grain-to-grain homogeneity and analytical reproducibility.

The mineral analyses were obtained using a Materials Analysis Company electron microprobe equipped with a Kevex Model 5000A energy dispersive spectrometer, and automated to produce simultaneous multi-element analysis and data reduction (Plant and Lachance, 1973), through program SICOM on a Hewlett Packard 1000 computer. Operating conditions are 20kV accelerating voltage, specimen current of 10 nanoamperes measured on a standard kaersutite, and a counting time of 100 seconds. The chlorites were analyzed for 10 elements using kaersutite (Na, Ca), biotite (Mg, Si, Ti, Mn, Fe), labradorite (Al), orthoclase (K), and chromite (Cr) as standards. Analyses have an accuracy of 1-2% of the amount present for major elements, and up to 10% for minor elements.

TABLE 1. Epidote Analyses

Depth No. of grains	462.0 (6)	544.0 (3)	670.0B (3)	673.0 (3)	685.8B (7)	687.6 (6)
wt.%						
SiO_2	38.11	37.99	38.07	39.19	38.84	38.97
TiO_2	.04	.15	.14	.10	.19	.03
Al_2O_3	23.08	23.72	25.58	23.97	24.53	24.43
Cr_2O_3	.08	.16	.05	.11	.08	.06
FeO	13.27	12.85	10.33	11.26	12.37	12.36
MnO	.21	.48	.51	.24	.53	.20
MgO	.46	.64	.39	.52	.53	.62
CaO	23.16	22.00	22.91	21.99	23.09	23.19
Na_2O	.01	.00	.06	.49	.00	.05
K_2O	.06	.02	.07	.06	.07	.09
TOTAL	98.48	98.01	98.11	97.94	100.23	100.00
IONS for 25 0						
Si	6.19	6.17	6.10	6.30	6.15	6.18
Ti	.01	.02	.02	.01	.02	.00
Al	4.42	4.54	4.83	4.54	4.58	4.56
Cr	.01	.02	.01	.01	.01	.01
Fe	1.80	1.75	1.38	1.51	1.64	1.64
Mn	.03	.07	.07	.03	.07	.03
Mg	.11	.16	.09	.13	.13	.15
Ca	4.02	3.83	3.94	3.79	3.92	3.94
Na	.00	.00	.02	.15	.00	.00
K	.01	.00	.01	.01	.01	.02
ION RATIO						
Fe/(Fe+Al)	.29	.28	.22	.25	.26	.26
Range	.26-.31	.27-.28	.22-.22	.22-.28	.24-.28	.22-.30

Tables 1, 2 and 3 list mineral analyses for epidote, feldspar and chlorite respectively. Epidote from six samples was analyzed; the Fe/(Fe+Al) molar ratio varies from 0.19 to 0.31. The range of composition is highest in the monomineralic epidote patches, where distinct zoning can be observed optically. Plagioclase from ten altered samples was analyzed, and found to be consistently albitic, with the mole proportion of Ab ranging from 89 to 99 per cent. Based on this preliminary work, variation in feldspar composition appears to be as great within a sample as between samples. The post-mineralization dike at 370.5 m retains its primary plagioclase composition of 63 mole per cent plagioclase. Carbonates from several samples were found to be pure calcite, except for rare dolomite, coexisting with calcite, in a vein at 462.0 m. Sphalerite could not be successfully analyzed because of the many tiny inclusions of chalcopyrite.

Compositional variation in chlorite has been explored more throughly than for any other mineral because chlorite is ubiquitous, and appears to be particularly sensitive to changes in alteration conditions. Figure 7 shows the average composition, in terms of the atomic ratio Fe/(Fe+Mg), of several chlorite grains from each of fourteen samples. These selected samples represent a wide range of rock Fe/(Fe+Mg) and lithology. In most cases, the Fe/(Fe+Mg) ratio of chlorite is remarkably consistent (Table 3) within a thin section despite the analytical challenge presented by the fine grain size. This permits the recognition of systematic minor changes. Furthermore, within the hydrothermal greenschist zone, the composition of chlorites in veins and vesicles is indistinguishable from that of groundmass chlorites in the same thin section (see Figure 7). This is strong evidence that both groundmass and vein-vesicle minerals were in equilibrium with the same fluid, and thus the mineralogy of the entire thin section can be considered in the assessment of fluid composition. However, within the zone of differential metasomatism, chlorite compositions are variable which suggests variability in fluid composition and disequilibrium between grains.

TABLE 2. Feldspar Analyses

Depth	370.5	398.5	434.5	462.0	497.4	544.0	624.6	624.0*	670.08	673.0	685.8B
No. of grains	(7)	(2)	(7)	(2)	(4)	(4)	(5)	(3)	(5)	(3)	(4)
wt.%											
SiO_2	52.40	66.23	68.59	65.50	67.57	68.31	65.99	65.11	68.56	66.09	67.76
Al_2O_3	29.39	20.03	20.43	19.12	20.82	20.58	21.17	19.26	19.63	20.86	19.48
FeO	.94	.64	.14	.32	.67	.70	.45	.35	.16	.32	.66
CaO	12.85	.97	.68	.49	1.00	.69	1.94	.62	.25	1.77	.15
Na_2O	4.02	10.49	10.96	10.78	10.62	11.18	9.99	2.52	11.18	10.25	11.20
K_2O	.09	.13	.13	.08	.56	.13	.22	12.73	.09	.11	.06
TOTAL	99.70	98.49	100.94	96.28	101.24	101.60	99.7	100.59	99.86	99.41	99.30
IONS for 32 0											
Si	9.61	11.83	11.88	11.92	11.77	11.84	11.65	11.87	11.99	11.69	11.98
Al	6.35	4.22	4.18	4.10	4.28	4.20	4.04	4.14	4.05	4.35	4.06
Ca	2.53	.19	.13	.10	.64	.13	.37	.12	.05	.34	.03
Na	1.43	3.68	3.80	3.80	3.59	3.76	3.42	.89	3.79	3.52	3.84
K	.02	.03	.03	.02	.13	.03	.05	2.96	.02	.02	.01
MOLE PROPORTIONS											
An	63.5	4.8	3.3	2.4	4.8	3.3	9.5	3.1	1.2	8.7	.7
Ab	35.9	94.4	96.0	97.1	91.9	96.0	89.2	22.4	98.3	90.7	98.9
Or	.5	.8	.7	.4	3.2	.7	1.3	74.5	.5	.6	.3
Range of Ab	30-44	93-96	91-98	97-98	86-95	93-98					

*Potassic rims on albite grains

TABLE 3. Chlorite Analyses

Depth	398.5	434.5	462.0	497.4	503.4	544.0	624.0	647.6A*	647.6A+	670.0B	673.0	680.0	680.1B	687.6
No. of grains	(4)	(4)	(3)	(5)	(5)	(4)	(5)	(8)	(4)	(10)	(5)	(11)	(5)	(3)
wt.%														
SiO_2	27.51	26.60	28.26	26.70	27.21	28.10	27.68	27.34	27.83	27.75	27.55	27.19	28.44	26.98
TiO_2	.11	.10	.11	.12	.10	.10	.08	.12	.09	.09	.09	.09	.10	.12
Al_2O_3	17.54	17.16	19.03	20.00	19.32	18.17	18.53	19.58	18.13	18.74	18.35	18.83	18.95	18.44
Cr_2O_3	.08	.04	.10	.06	.05	.04	.04	.04	.06	.04	.04	.07	.09	.07
FeO	27.92	20.78	23.23	24.87	24.61	23.94	27.39	22.82	23.28	23.28	27.07	23.61	19.41	23.24
MnO	.97	1.60	.59	.69	.62	.63	.94	.75	.74	.65	.74	.71	.57	.67
MgO	13.93	14.74	17.44	15.26	16.26	18.56	15.11	18.51	18.50	17.51	15.55	17.78	20.94	16.56
CaO	.09	.14	.10	.16	.12	.02	.04	.04	.03	.09	.08	.03	.07	.08
Na_2O	0.00	.37	0.00	0.00	.03	.00	.00	.00	.00	.00	.00	.00	.00	.00
K_2O	.03	.10	.04	.01	.06	.02	.01	.02	.01	.02	.02	.02	.04	.04
TOTAL	88.19	81.63	88.89	87.87	88.49	89.54	89.82	89.22	88.67	88.18	89.47	88.33	88.59	89.20
IONS for 28 0														
Si	5.86	5.96	5.80	5.61	5.67	5.76	5.76	5.59	5.75	5.75	5.74	5.65	5.74	5.77
Ti	.02	.01	.02	.02	.02	.01	.01	.02	.01	.01	.01	.01	.01	.02
Al	4.41	4.52	4.60	4.95	4.74	4.39	4.54	4.72	4.41	4.58	4.51	4.61	4.51	4.60
Cr	.01	.01	.02	.01	.01	.01	.01	.01	.01	.01	.01	.01	.01	.01
Fe	4.98	3.90	3.98	4.37	4.28	4.10	4.77	3.90	4.02	4.04	4.72	4.10	3.28	4.12
Mn	.18	.31	.10	.12	.11	.11	.17	.13	.13	.11	.13	.12	.10	.12
Mg	4.43	4.93	5.33	4.78	5.08	5.66	4.69	5.64	5.69	5.41	4.83	5.50	6.30	5.23
Ca	.02	.03	.02	.04	.03	.00	.01	.01	.01	.02	.02	.01	.01	.02
Na	.00	.16	0.00	0.00	.01	.00	.00	.00	.00	.00	.00	.00	.00	.00
K	.01	.03	.01	.00	.02	.01	.00	.01	.00	.01	.00	.00	.01	.01
ION RATIO														
Fe/ (Fe+Mg)	.53	.43	.42	.48	.46	.42	.50	.40	.41	.42	.49	.42	.34	.44
Range	.50-.54	.42-.43	.42-.43	.46-.50	.44-.46	.40-.42	.49-.50	.40-.44	.40-.41	.39-.46	.45-.51	.34-.48	.33-.38	.42-.46

*Chlorite in devitrified glass, +Chlorite in holocrystalline groundmass

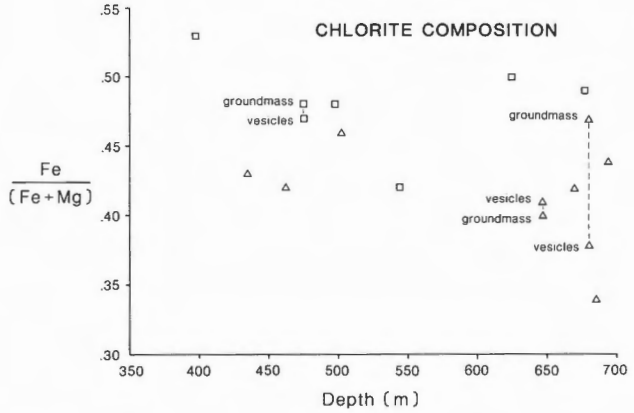

Figure 7: Chlorite composition in relation to depth and lithology. Triangles refer to chlorite from fragmental rocks, and squares to chlorite from massive dikes.

Figure 7 demonstrates that chlorite composition does not vary with depth, but does vary with lithology. In general, fragmental rocks contain chlorite with lower Fe/(Fe+Mg) than do massive rocks. However, there is no corresponding pattern of relatively lower Fe/(Fe+Mg) in the whole-rock analyses of the fragmental samples, and, given that chlorite is the dominant Mg-Fe mineral present, this suggests that either, (a) rock geochemistry is not sufficiently sensitive to small compositional variations recorded by chlorite, or, (b) the Fe not present in the chlorite of the fragmental samples is taken up in epidote, or, in the case of samples from the hydrothermal greenschist zone, in alteration solutions which precipitate epidote lower in the section.

It was also observed that chlorites in samples where chalcopyrite and sphalerite occur contain approximately 0.5 to 1.0 weight percent more MnO than chlorites from other samples. This confirms the positive correlation of MnO with Zn and Cu indicated by the whole-rock analyses (Jamieson and Lydon, 1987).

CONCLUSIONS

The following conclusions on hydrothermal alteration can be drawn from petrographic evidence.

Alteration of these lavas and dikes is pervasive, in terms of complete mineralogical change from primary igneous assemblages, but not progressive in the sense that secondary minerals do not replace other secondary minerals formed under lower-grade conditions. Evidence of, and exceptions to, this general pattern are given in point (3) of the general observations listed above. This pattern indicates that the hydrothermal alteration system was superimposed on lavas and dikes that were relatively unaltered, and that all the rocks, with the exception of the post-mineralization dykes, predated the establishment of the hydrothermal system. Moreover, the presence of anhydrite, which exhibits retrograde solubility under hydrothermal conditions, suggests that the hydrothermal system was terminated by sudden death, rather than slow decay with progressively cooling waters.

Within the core interval under study, there is no systematic mineralogical variation with depth. Mineralogical variation with lithology appears to be confined to magnesium-enrichment of chlorite in fragmental rocks relative to that in massive rocks, and the epidotization of fragmental zones below a depth of 650 metres. Rock textures, the monomineralic or near-monomineralic product assemblage, the variability of composition of both chlorite and the zonation of epidote all indicate that the metasomatism was a multi-stage or disequilibrium process. The impression is that the epidote was 'dumped' in response to some triggering mechanism specific to those locations. Arnórsson et al. (1983) have shown that geothermal fluids from Iceland are supersaturated with respect to epidote. A high nucleation energy for epidote has also been suggested by reluctant nucleation in experiments modelling greenschist metamorphism (Moody et al., 1983; Liou, 1973). Since epidotization involves considerable addition of calcium, the observation that epidote appears to replace calcium sulfate suggests that the presence of anhydrite or gypsum may well have caused a local enrichment in calcium activity in the pore fluid during hydrothermal alteration, which triggered the rapid nucleation and dumping of epidote within the fragmental sections of the lower part of CY-2a.

ACKNOWLEDGEMENTS

This research was accomplished while the senior author held a Natural Sciences and Engineering Research Council Visiting Fellowship at the Geological Survey of Canada. H.E.J. is particularly grateful to Dr. W.R.A. Baragar of the Geological Survey of Canada, who facilitated her involvement with the ICRDG, and who provided useful comments on earlier versions of both this and the companion paper. Valuable suggestions were also contributed by Dr. E. Froese and Dr. F. Chandler of the Geological Survey of Canada, K. Gillis of Dalhousie University and Dr. J.A. Hanes of Queen's University.

REFERENCES

Arnórsson, S., Gunnlaugsson, E. and Svavarsson, H.
1983: The chemistry of geothermal waters in Iceland. II. Mineral equilibria and independent variables controlling water compositions; Geochimica et Cosmochimica Acta v. 47, no. 3, p. 547-566.

Botros, M.
1983: A petrographic study of the hydrothermal alteration and ore mineral deposition in drill core samples from Agrokipia, Cyprus; unpublished B.Sc. thesis, Dalhousie University, Halifax, Canada.

Gillis, K.M.
1983: Low temperature alteration of the extrusive sequence, Troodos ophiolite, Cyprus; Geological Association of Canada - Mineralogical Association of Canada, Annual Meeting, Victoria, Canada, 1983, Program with Abstracts, v. 8, p. A27.

Jamieson, H.E. and Lydon, J.W.
1987: Geochemistry of a fossil ore-solution aquifer: chemical exchange between rock and hydrothermal fluid recorded in the lower portion of research drill hole CY-2a, Agrokipia, Cyprus; *in* Cyprus Crustal Study Project Initial Report Hole CY2-2a, ed. P.T. Robinson, I.L. Gibson and A. Panayiotou; Geological Survey of Canada, Paper 85-29.

Liou, J.G.
1973: Synthesis and stability relations of epidote, $Ca_2Al_2FeSi_3O_{12}(OH)$; Journal of Petrology v. 14, p. 381-413.

Lydon, J.W.
1984: Some observations on the mineralogical and chemical zonation patterns of volcanogenic sulphide deposits of Cyprus; *in* Current Research, Part A, Geological Survey of Canada, Paper 84-1A, p. 611-616.

Moody, J.B., Meyer, D. and Jenkins, J.E.
1983: Experimental characterization of the greenschist/amphibolite boundary in mafic systems; American Journal of Science, v. 283, no. 1, p. 48-92.

Plant, A.G. and Lachance, G.R.
1973: Quantitative electron microprobe analysis using an energy dispersive spectrometer; Proceedings of the Eighth National Conference on Electron Probe Analysis, New Orleans, Paper 13.

Secondary Minerals in the CCSP Drill Holes CY-2 and CY-2a, Agrokipia, Cyprus

VICTOR B. KURNOSOV[1], PAUL T. ROBINSON[2], OLEG V. CHUDAEV[1],

IGOR V. KHOLODKEVICH[1] AND EUGENE D. PETRACHENKO[1]

[1]The Far East Geological Institute of the Far East Science Centre,
of the Academy of Sciences of the USSR, Vladivostok, 690022, USSR
[2]Centre For Marine Geology, Dalhousie University, Halifax,
Nova Scotia, Canada, B3H 3J5

Kurnosov, V.B., Robinson, P.T., Chudaev, O.V., Kholodkevich, I.V. and Petrachenko, E.D., Secondary minerals in the CCSP Drill Holes CY-2 and CY-2a, Agrokipia, Cyprus; in *Cyprus Crustal Study Project: Initial Report, Holes CY-2 and 2a, ed. P.T. Robinson, I.L. Gibson and A. Panayiotou; Geological Survey of Canada, Paper 85-29, p. 69-78, 1987.*

Abstract

Two types of alteration have been recognized in the extrusive part of the Troodos ophiolite, sampled in holes CY-2 and CY-2a: background alteration and high-temperature hydrothermal alteration. Replacement of the glassy mesostasis in the lavas by trioctahedral smectite under 'non-oxidizing' conditions is typical of background alteration. However, in highly permeable intervals, the mesostasis is replaced by celadonite, formed under oxidizing conditions. Smectite, hydromica, sepiolite, palygorskite, calcite, cristobalite, quartz, heulandite and barite were also depositied in veins and vesicles during this stage of alteration. Hydrothermal assemblages are characterized by chlorite and quartz, with variable sulphide mineralization. In veins and vesicles of this zone, chlorite, hydromica, gypsum, anhydrite, calcite, quartz, albite, epidote, zoisite, pyrite, chalcopyrite, and sphalerite were recognized. A low grade greenschist facies assemblage of chlorite, epidote, albite occurs in the lower part of hole CY-2a. The upper part of hole CY-2 penetrated an oxidized ore zone about 20 m thick with the following secondary minerals: smectite, gypsum, delafossite, cuprite, native copper, and parabutlerite.

Résumé

Deux types d'altération ont été reconnues dans la partie extrusive de l'ophiolite de Troodos échantillonnée par les forages CY-2 et CY-2a: une altération d'arrière-plan et une altération hydrothermale de haute température. Le remplacement de la mésostasis vitreuse de la lave par de la smectite trioctahédrale dans des conditions non-oxidantes est typique de l'altération d'arrière-plan. Cependant, dans les intervalles hautement perméable, le mésostasis est remplacée par de la céladonite formée dans des conditions oxidantes. Les minéraux smectite, hydromica, sépiolite, palygorskite, calcite, cristobalite, quartz, heulandite et barite ont aussi été déposés dans des veines et vésicules pendant cette étape de l'altération. Les assemblages hydrothermaux sont charactérisés par de la chlorite et du quartz, avec une minéralisation en sulfures variable. Dans les veines et vésicules de cette zone, les minéraux suivants ont été reconnus: chlorite, hydromica, gypse, anhydrite, calcite, quartz, albite, épidote, zoisite, pyrite, chalcopyrite et sphalérite. Un assemblage de chlorite, épidote et albite du faciès schiste vert de faible intensité est présent dans la partie inférieure du forage CY-2a. La partie peu profonde du forage CY-2 a pénétré une zone de minerai oxidé d'environ 20 m d'épaisseur contenant les minéraux secondaires suivants: smectite, gypse, delafossite, cuprite, cuivre natif, et parabutlérite.

INTRODUCTION

Holes CY-2 and CY-2a were drilled into and beneath the Agrokipia ore bodies of Cyprus in order to investigate the hydrothermal processes leading to formation of sulphide ore bodies in oceanic crust. The Agrokipia ore deposits lie about 1 km west of Agrokipia village on the northern flank of the Troodos ophiolite. Details of the geologic setting are given in Malpas (1987).

The Agrokipia 'A' deposit was a massive sulphide body which has been removed by open cast techniques. The Agrokipia 'B' deposit lies about 300 m east of Agrokipia 'A' and about 150 m deeper in the section. It has been partly mined by underground techniques.

Holes CY-2 and CY-2a were intended to sample the hydrothermal conduit or stockwork zone beneath the ore bodies. Hole CY-2 was spudded in the pit from which the Agrokipia 'A' deposit had been removed. It penetrated an upper zone of alteration and mineralization about 100 m thick. Below this level alteration decreases rapidly until fresh volcanic glass appears at 105 m. The hole was terminated voluntarily at 226 m when it became apparent that it had passed from the stockwork zone. Hole CY-2a was spudded 280 m east of CY-2, directly above the Agrokipia 'B' deposit. Relatively fresh lavas were penetrated to a depth of 154 m. Between 154 and 297 m a sequence of highly altered and mineralized massive lavas was encountered. Below this level is a section of altered lavas and dykes with sulphide-filled veins and vesicles.

We studied the secondary minerals in the altered lavas in order to determine the paleotemperatures, oxygen fugacities and mineral paragenesis in the ascending limb of a hydrothermal system. Active hydrothermal systems have yet to be studied in this fashion because they have not been sampled by drilling.

METHODS OF INVESTIGATION

In holes CY-2 and CY-2a secondary minerals replace the groundmass of altered rocks and fill veins and vesicles. Mineral identification was by petrographic and X-ray diffraction analysis. An electron microscope was used to classify clay minerals as dioctahedral or trioctahedral. X-ray diffraction patterns were obtained from oriented smear slides using a DRON-2 and DRON-3 X-ray diffractometer with CuKα and FeKα radiation. Clay minerals were air dried, treated with ethylene-glycol or glycerol, and heated at 550°C for 1 to 2 hours. An X-ray photometer with FeKα radiation was used to identify certain sulphide grains. Electron diffraction patterns were obtained with an EG-100M electron microscope using an accelerating voltage of about 100 kv. Minerals in veins and vesicles and secondary minerals replacing olivine phenocrysts were hand picked under a binocular microscope. Groundmass minerals were separated from powdered samples.

GROUNDMASS ALTERATION OF VOLCANIC ROCKS

Groundmass alteration of volcanic rocks largely involves replacement of the glassy mesotasis by clay minerals, particularly smectite, hydromica, and chlorite. These are locally accompanied by cristobalite, opal C-T, and quartz. Smectites are mainly uniform, trioctahedral varieties of the saponite group. The *b* cell parameter ranges from 9.19 to 9.20 Å (Table 1). X-ray diffraction patterns of specimens treated with ethylene glycol show a narrow and strong symmetric (001) reflection at 16.8 to 17 Å. After heating the (001) reflection shifts to 9.5-9.9 Å. The only exceptions are smectites from the uppermost part of hole CY-2 (4.40 to 10.40 m) whose X-ray diffraction patterns show extremely wide and weak reflections. We have previously obtained similar diffraction patterns for smectites from weathered basalts from tropical Pacific islands. Fe-smectite with a *b* cell parameter of 9.06 Å was also identified in hole CY-2 at 11 m (Table 1). Hydromica from the groundmass of altered lavas has clearly defined reflections which are integrals of the reflection at 10 Å. The (060) reflections suggest that the hydromica from holes CY-2 and CY-2a is generally a dioctahedral variety of the 1M polytype (Table 1). It belongs to the glauconite-celadonite group. Hydromica of the $2M_1$ type occurs in the lowermost part of hole CY-2a. Members of the chlorite family, such as chlorite, chlorite with a hydrated brucitic layer, swelling chlorite and a mixed-layer variety (chlorite-swelling chlorite) were also recognized. The ratio of the first four chlorite basal reflections and a *b* cell parameter ranging from 9.23 to 9.25 Å (Table 1) suggest a trioctahedral Fe-Mg variety. The X-ray diffraction pattern of the chlorite with a hydrated brucite layer shows a (001) reflection of 13.5 Å when heated to 550°C. The basal reflection (001) of swelling chlorite saturated with ethylene glycol shifts to about 17 Å. After heating it returns to 13.8 Å, as in common chlorite. The chlorite-swelling chlorite mixed-layer variety is characterized by the following reflections obtained from air-dried specimens; 29.2 Å (001); 14.4 Å (002); 96 Å (003); 7.1 Å (004); 4.75 Å (006); 3.56 Å (008). After saturation with glycerol it swells, thus increasing the *c* cell parameter. This is indicated by the shift of the (001) reflection to 31.7 Å and the (002) reflection to 15.4 Å. The (002) reflection of heated specimens is 13.8 Å, suggesting that the swelling phase is chlorite. The chlorite-

swelling chlorite is not a strictly ordered mixed-layer mineral because it has no integral succession of basal reflections which are multiples of 31-32 Å.

Several varieties of silica were identified. Cristobalite was recognized from reflections at 4.04 to 4.08 Å. Opal C-T shows split reflections with peaks at 4.08 and 4.30 Å. Quartz was identified by two reflections at 3.34 and 4.25 Å.

DISTRIBUTION OF SECONDARY GROUNDMASS MINERALS

Hole CY-2

Smectite occurs as a groundmass mineral throughout most of the profile. It is either the principal or sole secondary mineral in most samples. However, between 27.70 and 97.45 m (Units III-VI) chlorite and quartz are the dominant secondary minerals. This zone is also one of extensive enrichment in pyrite. Within this interval there are systematic variations in the chlorite phases. In the lowermost parts of Unit VI a mixed layer chlorite-swelling chlorite prevails. In the central parts of each unit chlorite is the most abundant mineral whereas in the marginal parts chlorite with a hydrated brucite layer (Unit IV, 57.85 m), or swelling chlorite with smectite (Unit V, 80.20 m) predominate. Chlorite prevails or becomes the only secondary clay mineral in the centers of the units. The appearance of quartz in the chlorite-rich zone is most obvious in Unit III, which contains a layer of pink-red jasper composed of quartz with fine pyritic impregnations at 48.65 m. Epidote and albite were also identified petrographically in Units III and IV.

Thus, in hole CY-2, chloritization, albitization and silicification are confined to the main stockwork zone through which hydrothermal ore solutions passed, as indicated by the widespread disseminated pyrite. In the lower half of hole CY-2, beginning at 112.25 m, directly beneath the chlorite-quartz-pyrite zone, green or dark green celadonite is common. The celadonite occurs in the marginal parts of Units VIII, XII and XIV, and at the very top (161.70 m) and base of Unit XII (213.64 m)(Table 2). It also occurs near the base of Units VIII and XIV (112.25 m and 225.50 m, respectively). In most samples the celadonite is accompanied by silica in the form of cristobalite or rare opal C-T and quartz (Table 2). Between the celadonite-rich zones the rocks are completely or largely replaced by brown smectite. In some samples, for example at 161.70 m, dioctahedral celadonite co-exists with trioctahedral smectite. The close association of celadonite which reflects oxidizing conditions and smectite, which probably formed under 'non-oxidizing' conditions coupled with the presence of celadonite in the lower parts of several units indicates that the celadonite did not form by halmyrolysis after the lavas were erupted onto the sea floor. Rather we suspect that the distribution of celadonite reflects penetration of sea water into the extrusive complex along permeable zones. This would explain the occurrence of celadonite at the margins of flows, which are zones of relatively high porosity and permeability. In some zones, the green celadonite-rich rocks are closely associated with red-brown, hematite-rich layers (e.g. 112.25 m), confirming that the celadonite-bearing rocks formed under oxidizing conditions. Thus, our observations are consistent with those of Gillis and Robinson (1985), suggesting that smectite is the most common low-temperature secondary mineral in the Troodos lavas and that celadonite formed in zones of high permeability. Zones of higher temperature alteration are locally superimposed on the lavas where ore-bearing solutions passed through the stockwork zones beneath the pyrite ore bodies. Smectite is typically absent from these zones indicating that alteration occurred under significantly different conditions that those that prevailed in the lava pile as a whole.

Hole CY-2a

In hole CY-2a three distinct alteration zones are recognized. An upper zone (0-154 m) contains a low temperature secondary mineral assemblage composed chiefly of smectite, locally replaced by celadonite in permeable zones (Table 3). From about 154 to 297 m, the rocks are highly bleached and altered. Most specimens are white to light grey, poorly consolidated, and composed largely of chlorite and quartz with variable sulphide mineralization, largely in the form of pyrite and sphalerite. In some samples swelling chlorite and mixed-layer chlorite-swelling chlorite were identified (Table 3). Smectite occurs locally as an impurity or as a subordinate mineral. Hydromica was identified in the upper part of Unit III. This hydromica differs from the celadonite produced by low temperature background alteration of rocks. It is a $2M_1$ polytype of the muscovite group with a *b* cell parameter of 8.97 Å (Table 1). In this zone it is consistently associated with chlorite, quartz and various sulphide minerals. Also in this zone, epidote appears as a minor constituent beginning at about 200 m and increasing in abundance toward the base of the hole. It is locally accompanied by zoisite in the lowest parts. Secondary albite occurs in the interval from 346.9 to 650.6 m.

TABLE 1. The *b* Cell Parameter of Clay Minerals from the Groundmass of Rocks in Extrusive Series, Holes CY-2 and CY-2a

Depth (m)	Unit Number	*b* cell (Å)	Polytype	Minerals
Hole CY-2				
11.00	II	9.06; 9.20		smectite
35.70	III	9.22		chlorite
80.20	IV	9.22; 8.98		smectite and swelling chlorite
95.78	VI	9.25		chlorite and mixed-layer chlorite-swelling chlorite
112.25	VIII	9.03		smectite and hydromica
118.95	IX	9.19		smectite
138.75	IX	9.01; 9.19		smectite
143.63	IX	9.19		smectite
145.80	IX	9.20		smectite
161.70	XII	9.05	1M	hydromica
161.70	XII	9.01; 9.19		smectite, hydromica
Hole CY-2a				
30.18	I	9.22		smectite from olivine
43.75	III	9.18		smectite
46.30	III	9.03; 9.26		smectite, hydromica
118.75	VI	9.05; 9.20	1M	hydromica and smectite
204.60	VIII	9.25; 8.97	2M	chlorite and hydromica
216.60	VIII	9.02; 9.20		chlorite and hydromica
265.00	VIII	9.27; 9.22	1M+2M	chlorite and hydromica
375.14	XIV	9.23; 9.01		chlorite and mixed-layer chlorite-swelling chlorite
382.44	XIV	9.29		mixed-layer chlorite-swelling chlorite
446.25	XVIII	9.30		chlorite
617.13	XXII	9.34; 9.21		chlorite
650.60	XXII	9.22		chlorite

TABLE 2. Secondary Minerals from the Groundmass of Rocks in Extrusive Series, Hole CY-2

Unit Number (interval in m)	Depth (m)	Sm	Hm	Chl	Qtz	Other Minerals
I(4.40-9.70)	4.40	X				
II(9.70-27.70)	10.40	X				
	11.00	X				
III(27.70-57.30)	35.70			X	0	trace epidote
	48.65	X				
IV(57.30-70.50)	57.85			X	0	
	59.50			X	0	
V(70.50-85.80)	80.20	+				abundant swelling chlorite
VI(85.20-97.45)	91.00	0		X	0	trace mixed layer chlorite-swelling chlorite
	95.78			+	+	abundant mixed layer chlorite-swelling chlorite, trace albite
VII(97.45-100.30)	98.60	X		0		
VIII(100.30-114.50)	112.25	X	0			trace cristobalite
IX(114.50-146.45)	118.95	X				
	123.20	X				trace cristobalite
	138.75	X				
	143.63	X		0		
	145.80	X	0			trace Opal C-T
XII(159.60-216.50)	161.70	X				
	161.70		X			
	161.70		X			trace cristobalite ?
	162.60	X				
	163.00		X			
	172.35	X		0		
	198.60	X				
	213.64		X			
	214.10	X				
XIV(221.95-226.16)	225.50	X	0			
	225.50	+	X			

Sm: smectite, Hm: hydromica, Chl: chlorite, Qtz: quartz, X: abundant, +: moderate, 0: trace

NOTE: Units I, II and III are from the oxidizing zone. Units IV, V and VI are from the ore zone. The remainder of the units are from the unmineralized, country rock zone.

TABLE 3. Secondary Minerals from the Groundmass of Rocks in Extrusive Series, Hole CY-2a

Unit Number (interval in m)	Depth (m)	Sm	Hm	Chl	SwChl	MixChl	Qtz	Ep	Ab
I(3.35-30.72)	6.85	X		0	0			0	
	30.18	X							
III(31.15-67.50)	43.75	X							
	46.30	X	+						
	46.30	X							
IV(67.50-89.95)	75.40	X							
	88.85	X							
VI(109.00-149.22)	118.75	X							
	118.75	+	X						
	131.20	X							
	147.50	X							
VIII(154.23-280.63)	157.90	+			+		0		
	160.20	+			+	X			
	204.60		+	X			0	0	
	216.60		+	X			+	0	
	248.70						X		
	265.00		+	+			0		
	272.10						X		
XII(297.49-361.61)	301.24	0		X			+	0	
	346.95	0		X			0		0
	352.10			X					
XIII(361.61-372.30)	364.59	+		0	+		0	0	0
XIV(372.30-403.80)	375.14			X		+	0	0	0
	382.44			0		X			
	382.44			X			0	0	0
XVII(426.13-443.34)	428.70			X			0	0	0
XVIII(443.34-452.78)	446.25			X			0		
	446.25			X				0	0
	452.90	0?		X			0	0	0
XIX(452.78-466.00)	458.65			X			+		
XXI(476.78-528.92)	484.95			X			0	0	0
	512.80			X			+		
XXII(528.92-689.15)	543.80			X			+	0	0
	576.78			X			+	0	0
	613.55			X			+		
	617.13			X			+	0	0
	650.60			X				0	0
	680.60						X	+	
	680.60						+	X	
	689.10			X					
	689.10						X	+	

Sm: smectite, Hm: hydromica, Chl: chlorite, Sw Chl: swelling chlorite, Mix Chl: mixed layer chlorite-swelling chlorite, Qtz: quartz, Ep: epidote, Ab: albite, X: abundant, +: moderate, 0: trace

NOTE: Units I, III, IV and VI are from the unmineralized, country rock zone. The remainder of the units are from the ore zone.

SECONDARY MINERALS IN VEINS AND VESICLES

Identification of Minerals in Veins and Vesicles

The following minerals fill veins and vesicles in the core recovered from holes CY-2 and CY-2a: smectite, hydromica, chlorite, gypsum, anhydrite, sepiolite, palygorskite, cristobalite, quartz, heulandite, barite, pyrite, chalcopyrite, sphalerite, delafossite, cuprite, native copper, and parabutlerite. The clay minerals filling veins and vesicles have X-ray characteristics similar to those replacing groundmass material. Both trioctahedral saponites (b = 9.23 Å) and dioctahedral nontronites (b = 9.01 Å) are present. Likewise two types of hydromica were identified; celadonite (b = 9.92-9.06 Å; 1M polytype) and muscovite (b = 8.98 Å; $2M_1$ polytype). In addition, small amounts of trioctahedral hydromica (b = 9.21-9.23 Å) are present in veins and vesicles, accompanied by trioctahedral chlorite (Table 4). Gypsum and anhydrite were identified in X-ray patterns from strong reflections at 7.6 Å (for gypsum) and 3.5 Å (for anhydrite). Sepiolite was identified by a strong reflection between 11.8 and 12.3 Å, that is unchanged after saturation with ethylene-glycol. Upon heating to 350°C, this peak shifts to about 10 Å and its intensity decreases. Palygorskite has a strong reflection at 10.5 Å which shifts to 10 Å upon glycolation. After heating, the peak shifts to approximately 9.5 Å and its intensity sharply decreases. The strongest reflection for heulandite is at 8.9 Å. Barite was identified by a series of strong reflections at 3.90; 3.44; 3.32; 3.10; 2.83; 2.73; 2.12 and 2.10 Å. Pyrite and sphalerite were identified by X-ray reflections at 1.63; 2.71; 2.42 Å (pyrite) and at 3.12; 1.90 and 1.63 Å (sphalerite). One sulphide grain was extracted from vesicles of each of two samples (hole CY-2). Reflections obtained by the Debay's X-ray method (most strong at 3.03; 1.85; 1.59 Å) suggest chalcopyrite. Several oxides were also identified in the mineralized zone of hole CY-2: delafossite (2.51; 2.23; 2.86 Å), cuprite (2.46; 2.13 Å), native copper (2.087; 1.80; 1.28 Å), and parabutlerite (5.89; 5.04; 3.09; 3.06 Å).

Distribution Of Secondary Minerals In Veins and Vesicles

Hole CY-2

Smectite and celadonite fill veins and vesicles in the zone of low temperature alteration below 100 m. These minerals are accompanied by lesser amounts of sepiolite, calcite, cristobalite, quartz, and heulandite (Table 5). The mineralized zone from 0-100 m is characterized by abundant quartz, chlorite, gypsum, pyrite, chalcopyrite, and sphalerite. An upper oxidized zone (0-20 m) also contains gypsum, delafossite, cuprite, native copper, and parabutlerite (Table 5).

TABLE 4. The b Cell Parameter of Clay Minerals from Veins and Vesicles of Extrusive Rocks, Holes CY-2 and CY-2a

Depth (m)	Unit Number	b cell (Å)	Polytype	Minerals
Hole CY-2				
57.85	IV	9.27		chlorite from vesicles
123.20	IX	9.20; 9.06		hydromica from vesicles
143.63	IX	9.07; 9.22		hydromica and smectite from vesicles
162.60	XII	9.21; 9.01		hydromica and smectite from vesicles
172.35	XII	9.23		smectite from vesicles
188.40	XII	9.23		hydromica from vein
188.40	XII	9.21		hydromica from vesicles
Hole CY-2a				
6.85	I	8.99; 9.25		smectite from vesicle
17.20	I	9.06; 9.21	1M	smectite and hydromica from vein
43.75	III	9.28; 8.98	1M+2M	smectite and trace from vesicles, hydromica
131.20	VI	9.25; 9.08		smectite from vesicles
275.30	VII	9.02		hydromica from white matter
301.24	XII	9.30; 9.00		chlorite from vesicles
452.90	XVIII	9.30		chlorite from vein

TABLE 5. The Minerals from Veins and Vesicles of Rocks in Extrusive Series, Hole CY-2

Unit Number (interval in m)	Depth (m)	Sm	Hm	Crist	Qtz	Other Minerals	Sample Type
I(4.40-9.70)	4.40					parabutlerite	crust
II(9.70-27.70)	11.00					gypsum	vein
	11.00					delafossite, cuprite, parabutlerite	vein
	11.00					cuprite, native copper	red crystals
III(27.70-57.30)	35.70					pyrite	sulphide in vesicle
IV(57.30-70.50)	57.85				+	chlorite	vesicle
	57.85					gypsum	sulphide in vesicle
	57.85					pyrite	sulphide in vesicle
	57.85					chalcopyrite	sulphide in vesicle
	57.85					chalcopyrite	sulphide in vesicle
	57.85					pyrite	sulphide in vesicle
	57.85				+	chlorite, chalcopyrite?	vesicle
	59.50					gypsum	vein
VI(85.20-97.45)	91.00				+		vein fragment
	91.99				+		vein fragment
	91.00					sphalerite	vein fragment
	91.00				+	chlorite, pyrite?, sphalerite	whole vein
IX(114.50-146.45)	123.20		+	+			crust
	123.20		+	+			vesicle
	143.63	+	+			sepiolite?	green vein
	143.63					heulandite	vein
	145.80					sepiolite	vein
	145.80	+	+			heulandite?	green vein
XII(159.60-216.50)	162.60	+	+				vesicle
	163.00			+	+		vein
	172.35	+				calcite	vesicle
	188.40		+	+		calcite	green vein
	188.40		+	+			vesicle
	213.64			+	+		vein
	213.64					heulandite	vein
	213.64	+	+	+?			green vein
	214.10	+	+				vesicle
XIV(221.95-226.16)	225.50					heulandite	crystals

Sm: smectite, Hm: hydromica, Crist: cristobalite, Qtz: quartz

Hole CY-2a

In hole CY-2a the upper parts of the core (0-154 m) contain an assemblage of low temperature vein minerals similar to that found in the lower part of hole CY-2 (Table 6). Smectite, celadonite, sepiolite, calcite, quartz, and heulandite are the most abundant and are locally accompanied by smaller amounts of palygorskite and barite. The mineralized zone of hole CY-2a (154-297 m) contains abundant chlorite, gypsum, quartz, pyrite and sphalerite. In addition, muscovite, calcite, and anhydrite are present locally. Quartz is consistently more abundant and widespread in the mineralized zone than in the overlying zone of low temperature alteration. Sphalerite is more common in hole CY-2a than in CY-2 where only one sample at a depth of 91 m was found with sphalerite (Table 5).

TABLE 6. The Minerals from Veins and Vesicles of Rocks in Extrusive Series, Hole CY-2a

Unit Number (interval in m)	Depth (m)	Sm	Qtz	Pyr	Sph	Other Minerals	Sample Type
I(3.35-30.72)	6.85	+				swelling chlorite	vesicle
	17.20	+				hydromica	green vein
	17.20	+				palygorskite	yellow vein
	17.20	+				sepiolite	grey vein
	17.20	+				sepiolite	brown crust
III(31.15-67.50)	43.75	+				hydromica	vesicle
	43.74					calcite	vesicle
	46.30					calcite, heulandite	vesicle
IV(67.50-89.95)	75.40	+				sepiolite	vein
VI(109.00-149.22)	118.75					barite	crystals
	131.20	+					vesicle
	147.50	+	+			calcite	vesicle
	147.50					calcite	white matter with sulphide
VIII(154.23-280.63)	157.90		+			swelling chlorite	vesicle
	160.20			+	+		sulphide in vesicles
	193.10						sulphide in vesicles
	193.10			+		gypsum	crystals
	193.10		+	+		hydromica	white matter with sulphide
	248.70		+	+			sulphide from vein
	255.10		+	+			sulphide from vein
	255.10		+	+	+		white matter with sulphide
	272.10		+				sulphide from vein
	272.10		+	+	+	calcite	sulphide from vein
	272.10		+	+	+		white matter with sulphide
	275.30		+	+	+		quartz with sulphide
	275.30		+		+	hydromica	white matter with sulphide
XII(297.49-361.61)	301.24		+	+		chlorite, calcite	vesicle
	346.95		+			chlorite, calcite	vein
XVII(426.13-443.34)	428.70		+	+			vesicle
	428.70		+	+		chlorite	vein with sulphide
XVIII(443.34-452.78)	446.25		+		+?		vesicle
	446.25		+			chlorite	vesicle
	452.90			+	+	chlorite	vein with sulphide
XIX(452.78-466.00)	458.65			+	+		vein with sulphide
XXI(476.78-528.92)	512.80			+			vein with sulphide
XXII(528.92-689.15)	576.78			+	+		vein with sulphide
	680.60						vein

Sm: smectite, Qtz: quartz, Pyr: pyrite, Sph: sphalerite

SUMMARY

We distinguish two basic types of alteration in holes CY-2 and CY-2a; low temperature sea water-rock interaction and higher temperature hydrothermal alteration. The low temperature, background alteration is found in lower parts of hole CY-2 and the upper parts of CY-2a. It is non-pervasive with fresh volcanic glass preserved locally. Permeability appears to be the most important factor in controlling the distribution of this type of alteration. The secondary mineral assemblages are dominated by smectite in zones of low permeability and by celadonite in zones of higher permeability. These clay minerals are accompanied by varying proportions of calcite, cristobalite, quartz, heulandite, barite, sepiolite, and palygorskite deposited in veins or vesicles.

Based on comparisons with low temperature zeolite facies assemblages from Iceland (Kristmannsdottir and Tomasson, 1978) and the Del Puerto Ophiolite (Evarts and Schiffmann, 1983), we estimate temperatures of formation to have been between about 50 and 100°C. On the one hand, zeolites such as phillipsite are absent, suggesting temperatures in excess of 25°C. On the other, higher temperature zeolites, such as laumontite, are found only in veins at the transition to higher temperature hydrothermal zones. The presence of celadonite in these rocks suggests locally oxidizing conditions, probably reflecting penetration of seawater into the lava pile. Secondary mineral assemblages dominated by smectite probably formed under less oxidizing conditions.

Two zones of higher temperature, pervasive hydrothermal alteration are recognized. In the upper parts of hole CY-2 and the middle parts of CY-2a (154-297 m) the rocks are highly bleached and mineralized. Secondary minerals in these zones are chiefly chlorite, muscovite, quartz, and pyrite. Traces of epidote occur in the lower part of this zone in hole CY-2a. In the lower parts of hole CY-2a (below 297 m) higher temperature hydrothermal alteration has produced low grade greenschist facies assemblages composed chiefly of epidote, chlorite, albite and quartz. Sulphide minerals are commonly present in veins. Temperatures of this subgreenschist facies probably ranged between about 250 and 300°C (cf. Anderson et al., 1982; Evarts and Schiffmann, 1983). In active hydrothermal systems, epidote forms at temperatures as low as 230°C but does not become abundant below about 260°C. The absence of actinolite suggests that temperatures did not exceed 300°C (Ellis, 1979). The abundance of sulphide minerals indicates generally reducing conditions.

A zone of later oxidation is superimposed on the altered and mineralized rocks in the upper part of hole CY-2. This is recorded in minerals such as cuprite, delafossite, and parabutlerite, which presumably formed after exposure of the Agrokipia 'A' ore body at the surface.

REFERENCES

Anderson, R.N., Honnorez, J., Becker, K., Adamson, A.C., Alt, J.C., Emmermann, R., Kempton, P.D., Kinoshita, H., Laverne, C., Mottl, M.J. and Newmark, R.L.
1982: DSDP hole 504B, the first reference section over 1 km through Layer 2 of the oceanic crust; Nature, v. 300, p. 589-594.

Ellis, A.J.
1979: Explored geothermal systems; *in* Geochemistry of Hydrothermal Ore Deposits, 2nd Edition, ed. H.L. Barnes; John Wiley and Sons, New York, p. 632-683.

Evarts, R.C. and Schiffmann, P.
1983: Submarine hydrothermal metamorphism on the Del Puerto ophiolite, California; American Journal of Science, v. 283, p. 289-340.

Gillis, K.M. and Robinson, P.T.
1985: Low-temperature alteration of the extrusive sequence, Troodos ophiolite, Cyprus; Canadian Mineralogist, v. 23, p. 431-441.

Kristmannsdottir, H. and Tomasson, J.
1978: Zeolite zones in geothermal areas in Iceland; *in* Natural Zeolites: Occurrence, Properties, Use; ed. L.B. Sand and F.A. Mumpton, Pergamon Press, Oxford, p. 277-284.

Malpas, J.
1987: The geology and geophysics of the area surrounding the CY-2 and CY-2a drill holes of the Cyprus Crustal Study Project; *in* Cyprus Crustal Study Project Initial Report Hole CY2-2a, ed. P.T. Robinson, I.L. Gibson and A. Panayiotou; Geological Survey of Canada, Paper 85-29.

The Geochemistry and Nature of Unusual Glassy Lavas from CCSP Holes CY-2 and CY-2a, Troodos Ophiolite, Cyprus

IAN L. GIBSON[1], GLEN C. MCGILL[1] AND PAUL T. ROBINSON[2]

[1]Department of Earth Sciences, University of Waterloo,
Waterloo, Ontario, Canada, N2L 3G1
[2]Centre for Marine Geology, Dalhousie University,
Halifax, Nova Scotia, Canada, B3H 3J5

Gibson, I.L., McGill, G.C. and Robinson, P.T., The geochemistry and nature of unusual glassy lavas from CCSP Holes CY-2 and CY-2a, Troodos Ophiolite, Cyprus; in *Cyprus Crustal Study Project: Initial Report, Holes CY-2 and 2a, ed. P.T. Robinson, I.L. Gibson and A. Panayiotou; Geological Survey of Canada, Paper 85-29, p. 79-85, 1987.*

Abstract

Unusually thick and abundant layers of volcanic glass were penetrated in holes CY-2 and CY-2a, drilled in the vicinity of the Agrokipia ore deposits. Petrographic examination revealed that these are massive, flow banded rocks, presumably formed by quenching of fluid lavas. What appears in hand specimen to be a fragmental texture, is the result of perlitic cracks and differential alteration. Fresh glasses are andesitic in composition, ranging from about 57 to 61 wt.% SiO_2. Petrographically and geochemically, they belong to the andesite-dacite-rhyodacite assemblage that makes up the lower part of the extrusive sequence. With increasing hydration and alteration the glasses exhibit losses of CaO, Al_2O_3 and FeO, and gains in K_2O. Incompatible trace elements were relatively immobile during the low temperature alteration that affected these rocks. Stratigraphic relations suggest that the Agrokipia ore deposits are associated with a local volcanic centre that may have localized the hydrothermal alteration.

Résumé

Des couches inhabituellement épaisses et abondantes de verre volcanique ont été pénétrées par les forages CY-2 et CY-2a, forés dans les environs des dépôts de minerai d'Agrokipia. L'examination pétrographique a revélé que celles-ci sont de massives roches à rubannement d'écoulement, présumément formées par le refroidissement de laves fluides. Ce qui apparaît dans l'échantillon macroscopique être une texture fragmentaire est le résultat de fentes perlitiques et d'altération différentielle. Les verres frais sont de composition andésitique, avec SiO_2 formant de 57 à 61% du poids. D'après leur pétrographie et géochimie, ils appartiennent à l'assemblage andésite-dacite-rhyodacite qui compose la partie inférieure de la séquence extrusive. Avec une augmentation de l'hydratation et de l'altération, les verres montrent des pertes en CaO, Al_2O_3 et FeO, et des gains en K_2O. Des éléments trace incompatibles étaient relativement immobiles pendant l'altération de basse température qui a affecté ces roches. Les relations stratigraphiques suggèrent que les dépôts de minerai d'Agrokipia sont associés à un centre volcanique local qui peut avoir localisé l'altération hydrothermale.

INTRODUCTION

As part of the Cyprus Crustal Study Project, two holes were drilled into and beneath the Agrokipia ore bodies of the Troodos ophiolite. These ore bodies are located in the extrusive sequence on the north flank of Troodos about 1 km northwest of the village of Agrokipia. The geologic setting of the Agrokipia deposits is described in Malpas (1987).

Hole CY-2 penetrated 226 m of lavas on the eastern margin of the Agrokipia 'A' orebody. Hole CY-2a was spudded in about 280 m east of CY-2, directly above the Agrokipia 'B' deposit. It penetrated 689 m of lavas and dykes, including a highly altered and mineralized zone between 154 and 297 m.

One of the striking features of the lavas penetrated by these two holes is the abundance of thick, massive layers of volcanic glass. Glassy pillow lavas are well known in the Troodos ophiolite (Adamides, 1980; Robinson et al., 1983; Bailey, 1984; Thy et al., 1985), although they have commonly been misidentified as limburgites. However, massive layers of glass have not been previously reported. Because the glassy lavas are highly altered, the routine analyses carried out on CY-2 and CY-2a drillcore failed to provide accurate geochemical data. Therefore, a detailed study of these lavas was undertaken in order to determine their primary textures and compositions, and to shed more light on their mode of formation.

CORE DESCRIPTION AND PETROGRAPHY

In hole CY-2 the massive glassy lavas occur throughout the lower 116 m of the drilled section (Robinson and Gibson, 1983). Forty-seven glassy layers were recovered from this interval, ranging from a few centimetres to over 3 metres in thickness. In hole CY-2a, massive glassy lavas first appear at 109 m, at almost the same stratigraphic level as in hole CY-2. Fourteen glassy layers, ranging from 12 cm to over 5 m thick, were recovered between 109 and 149 m, the lowest level in hole CY-2a at which fresh glass occurs. From 154 to 297 m, the rocks are highly altered and mineralized and the original lithology has been largely destroyed. However, the rocks are interpreted as a series of alternating massive crystalline and originally glassy flows. Below 297 m the drilled sequence consists chiefly of dykes with some screens of pillow lavas.

The thinnest glassy layers appear to represent chilled tops and bottoms of massive lava flows. They grade into crystalline flow interiors over distances of 1-2 cm, and in some cases exhibit sharp breaks between glassy layers. The thicker layers are more difficult to interpret. Like the thin layers, they lie between massive, crystalline zones and grade into them. However, there are typically no sharp cooling breaks either within the glassy layers or at their contacts with the crystalline material.

The glassy material is extensively altered to clay minerals along closely spaced fractures, causing the core to split into disk-shaped pieces. The fractures follow a primary flow fabric in the rock which is parallel to the upper and lower flow surfaces. When immersed in water the altered glass swells and disintegrates rapidly.

Because the alteration is irregular and patchy, many of the glassy rocks have a fragmental appearance which is enhanced by the development of perlitic textures. However, petrographic examination indicates that none of the glasses are hyaloclastites. Some glasses show minor brecciation along flow margins but in most cases the fragmental appearance in hand specimen is due to differential alteration resulting in patches of fresh glass surrounded by clay minerals. Flow banding within the glass is continuous between the fresh glassy zones indicating little or no rotation of individual patches.

Fresh samples consist of light brown, isotropic glass, with or without microlites. Where present, the microlites consist chiefly of plagioclase with minor pyroxene. They typically define a crude flow banding. Approximately half of the samples examined also have microphenocrysts of plagioclase, clinopyroxene, and orthopyroxene, although these never exceed 1% of the rock. Plagioclase is the most abundant and occurs as euhedral laths or prisms up to 1 mm long. Clinopyroxene forms small granules or laths, generally less than 0.25 mm across. Orthopyroxene occurs as rare subhedral crystals about 0.15 mm across.

Vesicles comprise 5-15% of most specimens and range from 0.2 to 1 mm in diameter. They are spherical to ovoid in shape and are randomly distributed. Most are partly or completely filled with yellowish-brown clay minerals.

The isotropic glass grades into crystalline material through a partially devitrified zone. Small, irregular patches of devitrification in the glass become larger and coalesce toward the crystalline zones to form dark, opaque masses. Alteration to clay minerals and iron oxides is rare in the devitrified zones but common elsewhere.

ANALYTICAL METHODS AND RESULTS

Bulk rock samples were analyzed for major elements by X-Ray Assay Laboratories of Toronto. The values for ferric iron are total iron expressed as Fe_2O_3. Microprobe analyses of the glass were carried out at Dalhousie University and in this case total iron is expressed as FeO. Instrumental neutron activation procedures were used for the determination of Hf, Th,

Ta and the rare earth elements at the University of Waterloo, following the methods of Gordon et al. (1968), Hertogen and Gijbels (1971) and Gibson and Jagam (1980). Major and trace element results for 14 whole rock samples are presented in Table 1. Table 2 contains 19 microprobe analyses of 5 fresh and altered glass samples.

DISCUSSION

Initial Lava Compositions

Microprobe analyses of the petrographically freshest glasses (Analyses 1, 2, 3, 10, 11, 12, and 15 of Table 2) indicate that these are andesites which range from about 57 to 61 wt.% SiO_2. Petrographically and geochemically, the analyzed glasses belong to the andesite-dacite-rhyodacite assemblage defined by Robinson et al. (1983). This assemblage forms the lower part of the Troodos extrusive sequence and appears to represent the evolved portion of an arc tholeiite suite.

Element Mobility During Alteration

All of the analyzed specimens are from the zone of low-temperature alteration, outside the hydrothermal conduits associated with the Agrokipia ore deposits. The glasses have undergone varying degrees of hydration and alteration, allowing us to assess the major and trace element mobility under these conditions.

Hydration of the glass is manifested petrographically, largely in colour changes. Fresh glass is light brown, whereas incipiently altered material is bleached to very pale brown or yellowish brown. Yellowish-brown varieties are commonly slightly birefringent, indicating incipient crystallization. The final stage is complete replacement by dark yellowish-brown, crystalline clay minerals.

TABLE 1. Whole-Rock Chemical Analyses of Glassy Units from Hole CY-2

Unit	17.02	17.02	18.01	19.02	19.05	20.01	21.02	23.01	23.03	23.05	24.01	27.01	28.03	29.01
Depth(m)	112.6	112.8	115.2	119.2	121.0	123.4	126.2	133.5	134.7	136.4	138.2	152.6	153.7	157.5
Major Elements														
SiO_2	64.7	52.5	51.7	70.5	51.4	52.5	53.1	54.0	51.8	53.4	53.3	51.1	51.0	53.3
Al_2O_3	9.19	11.6	12.2	7.00	12.1	12.4	12.3	12.9	12.2	13.0	13.1	11.8	12.0	12.4
Fe_2O_3	10.9	14.4	11.5	10.2	11.4	11.3	10.3	10.3	10.6	10.1	10.8	12.6	11.4	11.7
MgO	2.17	3.78	4.19	2.00	4.67	3.99	3.71	3.28	4.22	4.01	3.90	4.33	4.44	3.63
CaO	3.16	4.53	1.98	2.28	2.45	3.30	2.73	3.83	2.74	3.43	4.46	2.30	2.44	3.84
Na_2O	1.70	2.04	2.09	1.50	1.96	2.12	2.25	2.44	2.09	2.26	2.37	1.89	1.90	2.37
K_2O	0.91	1.02	1.06	2.00	0.95	0.89	0.73	0.52	0.60	0.50	0.49	0.96	1.01	0.67
TiO_2	0.67	0.85	0.98	0.53	0.88	0.96	0.94	1.09	1.03	1.04	1.01	1.01	1.01	1.05
P_2O_5	0.08	0.06	0.06	0.07	0.05	0.07	0.08	0.08	0.06	0.07	0.08	0.05	0.05	0.08
MnO	0.09	0.17	0.16	0.08	0.18	0.17	0.19	0.18	0.20	0.20	0.20	0.19	0.19	0.20
LOI	5.77	8.47	14.8	4.08	13.8	12.2	13.3	11.7	14.2	11.8	9.93	14.2	14.2	10.7
Trace Elements														
Ce	6.09	4.08	5.86	5.26	4.16	5.26	6.74	6.10	4.48	5.18	6.31	2.99	3.71	4.91
Nd	6.51	4.34	5.88	5.33	4.13	5.01	6.28	6.06	4.20	5.03	6.11	3.10	3.30	4.66
Sm	2.05	1.51	1.89	1.96	1.60	1.80	–	2.26	–	1.81	–	–	–	–
Eu	0.88	0.67	0.77	0.72	0.58	0.73	0.86	0.85	0.59	0.70	0.85	0.42	0.51	0.68
Gd	–	2.51	–	3.04	2.04	–	–	–	2.55	–	–	1.84	–	2.95
Tb	0.70	0.54	0.65	0.60	0.50	0.60	0.68	0.66	0.48	0.52	0.65	0.36	0.41	0.53
Tm	0.47	0.44	–	0.64	0.49	–	–	–	–	–	–	–	–	–
Yb	2.74	2.75	2.91	3.99	2.90	2.86	2.90	2.75	2.20	2.33	2.76	1.96	1.71	2.47
Th	0.24	0.26	0.35	0.23	0.32	0.36	0.41	0.38	0.32	0.34	0.36	0.26	0.24	0.30
Ta	0.06	0.06	0.08	–	0.03	0.10	0.08	0.09	0.06	0.06	0.08	0.06	0.04	0.07
Hf	1.13	1.49	1.95	1.16	1.75	1.90	1.99	1.77	1.68	1.67	1.64	1.19	1.19	1.54

TABLE 2. Microprobe Analyses of Volcanic Glasses From Holes CY-2 and CY-2a

Analysis No.	1	2	3	4	5	6	7	8	9	10
Hole	CY-2	CY-2	CY-2	CY-2a	CY-2a	CY-2a	CY-2a	CY-2a	CY-2a	CY-2a
Unit	43.03	43.03	43.03	27.01	27.01	27.01	27.03	27.03	27.03	27.05
Depth(m)	216.43	216.43	216.43	118.75	118.75	118.75	119.80	119.80	119.80	123.10
SiO_2	57.04	57.08	56.71	59.05	59.31	58.78	56.94	56.64	53.59	61.64
TiO_2	1.25	1.28	1.09	0.94	0.55	0.90	0.90	0.95	0.87	1.07
Al_2O_3	15.17	14.86	15.19	16.42	16.47	15.91	13.54	13.12	12.82	14.48
FeO	11.29	11.12	10.99	9.13	8.54	9.33	7.46	7.80	6.22	9.10
MnO	0.06	0.00	0.08	0.19	0.10	0.14	0.07	0.00	0.11	0.00
MgO	2.98	2.87	2.89	4.77	4.63	4.39	1.81	1.68	1.74	1.87
CaO	7.68	7.34	7.53	2.10	1.94	1.94	5.45	5.25	4.76	6.25
Na_2O	3.84	3.92	3.66	1.63	1.43	1.31	3.71	3.20	3.54	4.01
K_2O	0.16	0.08	0.15	0.25	0.29	0.14	0.33	0.21	0.30	0.19
P_2O_5	0.00	0.00	0.00	0.00	0.00	0.00	0.11	0.00	0.13	0.00
TOTAL	99.47	98.54	93.30	94.48	93.25	92.83	90.33	88.84	84.08	98.63
LOI	.53	1.45	1.71	5.52	6.74	7.16	9.68	11.15	15.92	1.39

Analysis No.	11	12	13	14	15	16	17	18	19
Hole	CY-2a	CY-2a	CY-2a	CY-2a	CY-2a	CY-2a	CY-2a	CY-2a	CY-2a
Unit	27.05	27.05	27.05	27.05	30.02	30.02	30.02	30.02	30.02
Depth(m)	123.10	123.10	123.10	123.10	136.70	136.70	136.70	136.70	136.70
SiO_2	61.50	61.39	60.92	60.04	59.30	57.97	58.48	57.23	57.08
TiO_2	0.96	0.89	0.92	1.01	1.09	1.06	0.94	1.02	0.96
Al_2O_3	14.51	14.33	14.19	14.14	14.61	14.42	14.35	14.35	14.18
FeO	8.97	9.07	8.97	8.82	9.02	8.68	8.76	8.77	8.26
MnO	0.06	0.00	0.00	0.08	0.11	0.11	0.00	0.00	0.04
MgO	1.71	1.60	1.65	1.72	2.36	2.28	2.11	2.25	2.16
CaO	6.34	6.15	6.12	6.09	6.57	6.50	6.38	6.35	6.16
Na_2O	3.95	3.80	3.89	3.68	4.24	4.23	3.90	3.60	3.91
K_2O	0.27	0.18	0.18	0.28	0.26	0.24	0.16	0.24	0.15
P_2O_5	0.00	0.00	0.00	0.00	0.09	0.13	0.00	0.00	0.00
TOTAL	98.28	97.42	96.82	95.90	97.67	95.64	95.09	93.81	92.90
LOI	1.73	2.59	3.16	4.14	2.35	4.38	4.92	6.19	7.1

Table 2 presents major oxide data on fresh and altered material from the same samples so that direct comparisons are possible. The variable totals of the microprobe analyses are believed to reflect variable degrees of secondary hydration. Thus, the differences between these totals and 100 percent are assumed to represent loss on ignition (LOI). These values are taken as a crude measure of secondary hydration and alteration, keeping in mind that fresh glasses have 1-4% of volatiles. (Robinson et al., 1983; Rautenschlein et al., 1985). In Figure 1, oxide values have been plotted against the calculated LOI to show trends with increasing hydration. Each set of points represents multiple microprobe analyses from variably altered parts of the same sample.

With increasing hydration most samples show losses of SiO_2, CaO, Al_2O_3 and FeO, and increases in K_2O. No significant gains or losses are observed in MgO and Na_2O, whereas TiO_2 shows different trends for different samples.

Because the trace elements were determined only for bulk rock samples, direct comparisons of fresh and altered samples are not possible. However, when the values reported here are compared with those determined for fresh andesitic glasses by Rautenschlein et al. (1985), there appears to have been little trace element mobility during alteration. Chondrite normalized abundances of K, P, Ti, and the analyzed trace elements, are shown in Figure 2, along with the abundances in the fresh andesite glasses reported by Rautenschlein et al. (1985). The fresh andesites have incompatible element abundances within the range of the analyzed samples, confirming that with the exception of K, these elements are

relatively immobile during low temperature alteration and hydration (cf. Pearce, 1975; Bednarz et al., 1987; Sunkel et al., 1987). It should be noted that the more mobile incompatible elements, such as Rb, Ba and Sr were not analyzed in this investigation.

Stratigraphic Position of the Glassy Lavas

On the northern flank of Troodos there are two lithostratigraphic sequences (Mehegan, 1987) corresponding to the geochemical division recognized by Robinson et al. (1983). The lower unit (unit I) is a sequence of pillows, massive lavas, and hyaloclastites ranging in composition from andesite to rhyodacite. Some basaltic members of this series have been recognized in the Basal Group as pillow screens between dykes. An overlying sequence of relatively depleted basaltic andesites, basalts and picrites comprises unit II. Holes CY-2 and CY-2a were spudded in close to the contact between these two units. The lithostratigraphic units vary greatly in thickness along strike. In the Agrokipia area, the lavas of unit II are about 150 m thick, whereas in the Akaki Canyon, located about 3 km to the east, they are nearly 1200 m thick. Thus, the Agrokipia ore deposits overly a thick accumulation of differentiated lavas (unit I), perhaps marking a local volcanic centre. This interpretation is strengthened by the occurrence of a dyke swarm at relatively shallow levels beneath the Agrokipia 'B' ore deposit. This swarm was penetrated at about 300 m in hole CY-2a at a depth of less than 500 m below the top of the lava pile. In the nearby Akaki Canyon, exposed dyke swarms of this type are found only at much lower levels.

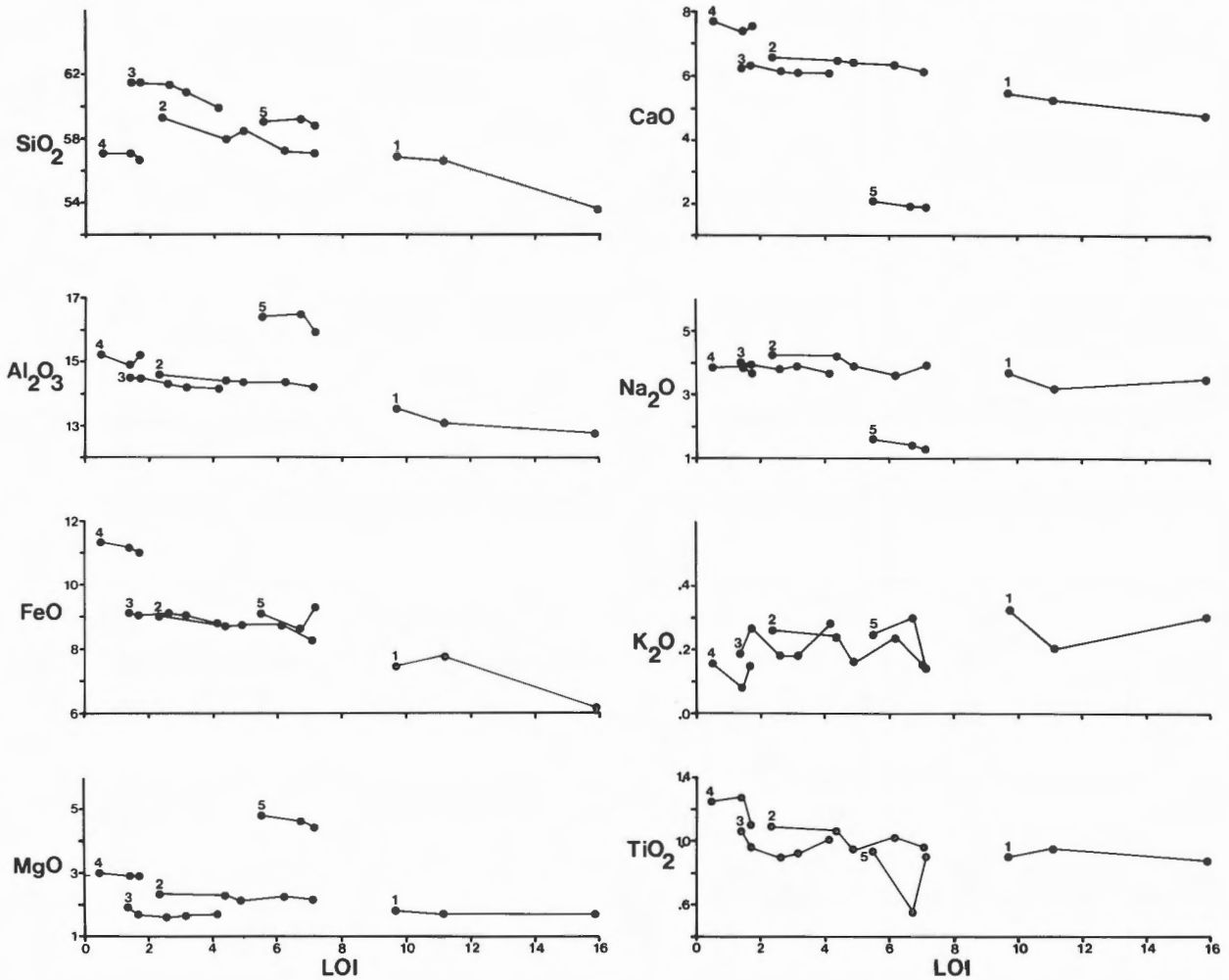

Figure 1: Plots of oxide values versus loss on ignition showing chemical variation with increasing hydration and alteration (all values in weight percent). Points connected by lines represent multiple microprobe analyses from a single sample. (1) Hole CY-2a, depth 119.80 m; (2) Hole CY-2, depth 136.70 m; (3) Hole CY-2a, depth 123.10 m; (4) Hole CY-2, depth 216.43 m; (5) Hole CY-2a, depth 118.75 m.

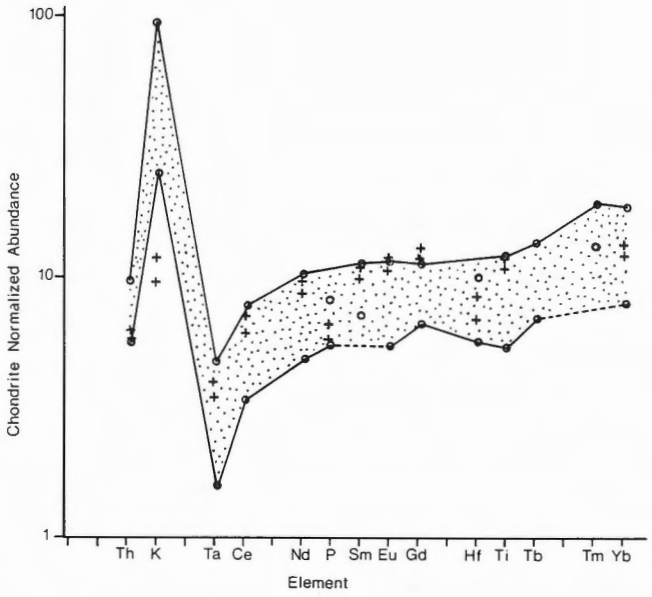

Figure 2: Chondrite normalized incompatible element plot showing the range of compositions for the analyzed hydrated glasses. Superimposed on this range are data for two fresh andesite glasses from Rautenschlein et al. (1985).

A considerable thickness of massive lavas was penetrated in both holes CY-2 and CY-2a, and the abundance of these massive units suggests possible ponding of the lavas in a topographic depression. Such depressions have been reported in the axial zone of modern spreading ridges, such as the East Pacific Rise, and on small seamounts associated with the ridges. The glassy layers may represent chilled margins of the ponded flows.

The other alternative is that sea water somehow penetrated at many different levels into a pond of molten lava, perhaps during partial draining of such a pond. Such drained ponds have been reported from the East Pacific Rise but there is no evidence in the Troodos core material to indicate that such a process occurred in the lavas of Agrokipia.

Whatever process was involved, it is clear that unusually thick masses of lava were rapidly quenched to form the glasses. Such quenching may have been aided by the high volatile contents of the lavas.

It is interesting to speculate on the relationship of copper sulphide mineralization to the volcanic processes suggested here. If the unusual thickness of differentiated lavas marks the position of a volcanic centre there may have been a relatively shallow magma chamber beneath the Agrokipia area. Lavas, fed by the dyke swarm, penetrated in hole CY-2a, would have preferentially erupted near such a centre, leading to the development of a volcanic edifice. The local thermal anomaly associated with such a volcanic centre may have driven a hydrothermal convection system leading to copper sulphide mineralization. The Agrokipia 'A' deposit is an exhalative deposit formed when hot fluids reached the seafloor, whereas the Agrokipia 'B' deposit appears to have formed by replacement of pre-existing lavas. The thick section of massive lavas overlying the Agrokipia 'B' deposits may have inhibited upward flow of the mineralizing fluids causing alteration and mineralization within the lava pile.

The stratigraphic relationships indicate that after hydrothermal circulation and ore deposition ceased, the dormant volcanic centre was 'drowned' by eruption of the basaltic lavas of lithostratigraphic unit II.

SUMMARY

The glassy lavas penetrated in holes CY-2 and CY-2a appear to be massive flows formed by ponding of fluid lavas in a topographic depression. Their fragmental appearance in hand specimen is due to development of perlitic textures and differential alteration. All analyzed specimens are evolved andesites belonging to the lower arc tholeiite suite recognized by Robinson et al. (1983). The lava stratigraphy along the northern flank of Troodos supports a model involving development of a local volcanic centre, with an associated dyke swarm, that served to localize hydrothermal alteration and ore formation. Very comparable associations have been reported from many massive sulphide bodies in Archean greenstone terrains (e.g. Goodwin, 1982).

ACKNOWLEDGEMENTS

Drilling investigations of the Troodos ophiolite were supported by the Natural Sciences and Engineering Research Council of Canada (NSERC) as well as by funding agencies in Cyprus, Denmark, West Germany, Great Britain and the United States. The authors particularly thank the many members of the Cyprus Geological Survey, particularly G. Constantinou, A. Panayiotou and C. Xenophontos for their generous assistance. Ongoing investigations by ILG on volcanism in extensional environments and by PTR on the oceanic lithosphere are supported by NSERC operating grants.

REFERENCES

Adamides, N.G.
1980: The form and environment of formation of the Kalavasos ore deposits, Cyprus; *in* Ophiolites: Proceedings of the International Ophiolite Symposium, Cyprus, 1979, ed. A. Panayiotou; Cyprus Geological Survey Department, Ministry of Agriculture and Natural Resources, p. 117-128.

Bailey, D.G.
1984: Stratigraphy and geochemistry of the Troodos ophiolite extrusive sequence in the Mangi area, Cyprus; unpublished M.Sc. thesis, Dalhousie University, Halifax, Nova Scotia, Canada, p. 1-215.

Bednarz, U., Sunkel, G. and Schmincke, H.-U.
1987: The basaltic andesite-andesite and the andesite-dacite series from ICRDG drill holes CY-2 and CY-2a. I. Lithology, petrology, and geochemistry; *in* Cyprus Crustal Study Project Initial Report Hole CY2-2a, ed. P.T. Robinson, I.L. Gibson and A. Panayiotou; Geological Survey of Canada, Paper 85-29.

Gibson, I.L. and Jagam, P.
1980: Instrumental neutron activation analysis of rocks and minerals; *in* Short Course in Neutron Activation Analysis in the Geosciences, Halifax, May 1980, ed. G.K. Muecke; Mineralogical Association of Canada, Short Course Handbook, v. 5.

Goodwin, A.M.
1982: Archean volcanoes in southwestern Abitibi Belt, Ontario and Quebec: form, composition, and development; Canadian Journal of Earth Sciences, v. 19, no. 6, 1140-1155.

Gordon, G.E., Randle, K., Goles, G.G., Corliss, J.B., Beeson, M.H. and Oxley, S.S.
1968: Instrumental activation analysis of standard rocks with high-resolution gamma-ray detectors; Geochimica et Cosmochimica Acta, v. 32, no. 4, p. 369-396.

Hertogen, J. and Gijbels, R.
1971: Instrumental neutron activation analysis of rocks with a low-energy photon detector; Analytica Chimica Acta, v. 56, p. 61-82.

Malpas, J.
1987: The geology and geophysics of the area surrounding the CY-2 and CY-2a drill holes of the Cyprus Crustal Study Project; *in* Cyprus Crustal Study Project Initial Report Hole CY2-2a, ed. P.T. Robinson, I.L. Gibson and A. Panayiotou; Geological Survey of Canada, Paper 85-29.

Mehegan, J.M.
1987: Temporal, spatial and chemical evolution of the Troodos Ophiolite lavas, Cyprus: supra-subduction zone volcanism in the Tethys Sea; unpublished Ph.D. thesis, Dalhousie University, Halifax, Nova Scotia, Canada, p. 1-300.

Pearce, J.A.
1975: Basalt geochemistry used to investigate past tectonic environments on Cyprus; Tectonophysics, v. 25, no. 1-2, p. 41-67.

Rautenschlein, M., Jenner, G.A., Hertogen, J., Hofmann, A.W., Kerrich, R., Schmincke, H.-U. and White, W.M.
1985: Isotopic and trace element composition of volcanic glasses from the Akaki Canyon, Cyprus: implications for the origin of the Troodos ophiolite; Earth and Planetary Science Letters, v. 75, no. 4, p. 369-383.

Robinson, P.T. and Gibson, I.L.
1983: Cyprus Crustal Study Project. Hole CY-2a Lithologic Unit Summaries.

Robinson, P.T., Melson, W.G., O'Hearn, T. and Schmincke, H.-U.
1983: Volcanic glass compositions of the Troodos ophiolite, Cyprus; Geology, v. 11, no. 7, p. 400-404.

Sunkel, G., Bednarz, U. and Schmincke, H.-U.
1987: The basaltic andesite-andesite and the andesite-dacite series from ICRDG drill holes CY-2 and CY-2a. II. Alteration; *in* Cyprus Crustal Study Project Initial Report Hole CY2-2a, ed. P.T. Robinson, I.L. Gibson and A. Panayiotou; Geological Survey of Canada, Paper 85-29.

Thy, P., Brooks, C.K. and Walsh, J.N.
1985: Tectonic and petrogenetic implications of major and rare earth element chemistry of Troodos glasses, Cyprus; Lithos, v. 18, no. 3, p. 165- 178.

Geochemistry of Hydrothermally Altered Rocks from Cyprus Drill Holes CY-2 and CY-2a compared with other Cyprus Stockworks

J.R. CANN, P.J. OAKLEY, H.G. RICHARDS AND C.J. RICHARDSON

Department of Geology, The University of Newcastle upon Tyne, England, NE1 7RU

Cann, J.R., Oakley, P.J., Richards, H.G. and Richardson, C.J., Geochemistry of hydrothermally altered rocks from Cyprus Drill Holes CY-2 and CY-2a compared with other Cyprus Stockworks; in *Cyprus Crustal Study Project: Initial Report, Holes CY-2 and 2a, ed. P.T. Robinson, I.L. Gibson and A. Panayiotou; Geological Survey of Canada, Paper 85-29, p. 87-102, 1987.*

Abstract

Eighty-four samples selected from the core of Holes CY-2 and CY-2a, drilled as part of the Cyprus drilling project, were analyzed for major and some trace elements. The holes were drilled to intersect stockwork zones underlying Cyprus-type sulphide deposits, and penetrated three different alteration facies: (l) background zeolite facies, (2) a white-rock facies with the assemblage quartz-pale chlorite-pyrite-illite-anatase which formed the core of the stockworks, and (3) a propylitic facies with the assemblage albite-green chlorite-quartz-sphene-epidote-carbonate, which appears to have formed an envelope around the core zone. These facies are imposed on different volcanic protoliths, in particular a unit of interbedded hyaloclastite and lava flows, and a pillowed unit. The latter is only recognizable by the pieces of jasper, now largely replaced by pyrite-quartz, which were originally interpillow sediments. Comparison with compositions of fresh glasses shows that the white-rock and propylitic alteration processes involved large scale element transport, in particular addition of Mg, Fe, S, K, Si, Cu and Zn to the rock, and overall removal of Ca. During white-rock alteration Ca and Na are almost completely removed and in this facies variable addition of Fe and S to produce pyrite is accompanied by progressive replacement of chlorite by illite.

Résumé

Une groupe sélectionné de 84 échantillons de carottes des trous de forages CY-2 et CY-2a faisant partie du projet de forages de Chypre fut analysé pour les éléments majeurs et en trace. L'orientation des trous de forages recoupait les zones du stockwerk sous-jacentes aux gîtes de sulfures du type Chypre, et trois faciès d'altération différents furent rencontrés: (1) un faciès à zéolites d'arrière-plan, (2) un faciès blanc formé d'un assemblage de quartz-chlorite pâle-pyrite-illite-anatase composant les carottes des stockwerks, et (3) un faciès propylitique avec un assemblage albite-chlorite verte-quartz-sphène-épidote-carbonate, qui semble avoir enrobé la zone forée. Ces faciès sont superposés à différents protolites de volcanites, particulièrement à une unité formée d'hyaloclastites et de coulées de laves intercalées, et à une unité de laves en coussinets. Cette dernière est reconnue grâce à des fragments de jaspe, qui sont actuellement remplacés en majeure partie par pyrite-quartz, et qui constituaient initialement des sédiments intercalés entre les coussinets. Une comparaison avec les compositions de verres inaltérés révèlent que les processus responsables du développement des faciès blanc et propylitique ont impliqué une migration des éléments à grande échelle, particulièrement pour les ajouts à la roche de Mg, Fe, S, K, Si, Cu, et Zn, et pour le lessivage du Ca dans l'ensemble. Le Ca et Na furent lessivés quasi totalement durant l'épisode d'altération du faciès blanc et simultanément des ajouts variables de Fe et de S ont produit la pyrite accompagnée du remplacement progressif de la chlorite par l'illite.

INTRODUCTION

Holes CY-2 and CY-2a were drilled during the summer of 1982 in the course of the International Cyprus Research Drilling Project. The holes were drilled to give a fully cored record of stockworks beneath two neighbouring Cyprus sulphide ore deposits for comparison with surface observations and previously drilled uncored holes. The results may be compared with observations of currently-active hydrothermal springs on the crest of the East Pacific Rise (Ballard et al., 1981; Converse et al., 1984; Edmond et al., 1982; Haymon and Kastner, 1981; Michard et al., 1984; Mottl, 1983).

The ideal Cyprus cupriferous sulphide deposit is composed of a lens of massive pyritic sulphide, underlain by a stockwork of sulphide veins developed in altered basalt, and overlain in turn by limonitic sediments (ochres) and unaltered, lava flows. This structure, first fully described in Cyprus by Constantinou and Govett (1972, 1973), was interpreted by them as evidence that the ores had formed by exhalation at the ocean floor, of hydrothermal solutions rising from depth through the stockwork zone. This model is widely accepted for Cyprus sulphide ores and other volcanogenic massive sulphide deposits.

Constantinou (1972) was the first to conduct a detailed study of Cyprus stockworks, and this was summarized and extended later (Constantinou, 1977, 1980). He showed that the characteristic alteration assemblage in the Cyprus stockworks is quartz (chalcedony) - chlorite - pyrite - illite - leucoxene, and demonstrated that the chemical changes in rock composition accompanying formation of the stockwork involved a systematic increase in Fe, S, and sometimes Si, and decrease in Ca and Na.

Hole CY-2 was sited within the pit left after the extraction of the Agrokipia 'A' ore body, located at UTM grid reference WD 133781, about 1 km west of Agrokipia village. The ore body was a concordant lens of massive pyrite, yielding about 700,000 tons of ore with low, non-economic values of Cu (Bear, 1960). The tapering edge of the ore body still remains in the north-west part of the pit, where it is overlain by unmineralized lavas. The floor of the pit is made up of highly altered pillow flows and pillow breccias (perhaps once a talus pile), and the hole was sited in what appears to be the centre of the alteration pipe. Altered lavas were drilled in the upper 50 m, but below the lavas are progressively less altered. The hole was terminated at a depth of 226 m in unmineralized lavas that had only been affected by low grade zeolite facies alteration. Clearly the hole failed to remain within the alteration pipe. The geometry of the pipe remains unclear, though uncored drill holes of the Hellenic Mining Company indicate that a pipe is present, perhaps inclined to the south (Adamides, 1984).

Hole CY-2a was spudded above the nearby concealed Agrokipia 'B' ore deposit, sited on the basis of records of uncored holes drilled during exploration of the deposit. The Agrokipia 'B' deposit has no surface indication and was discovered by drilling on a gravity anomaly observed during survey around Agrokipia 'A'. The deposit was small by Cyprus standards, though it did contain significant levels of Zn and some Cu (Bear, 1960). Adamides (1984) points out that the Hellenic Mining Company's drilling records show the deposit to be overlain by a unit of glassy lavas about 30 m thick, the lower part of which shows progressively increasing alteration with depth. He records a gradual increase in sulphide grade with depth, and considers that the Agrokipia 'B' deposit was formed below the sea floor, and not at the sea floor itself, as is the case with Agrokipia 'A'. A modern analogue of the 'A' deposit would be the exhalative black smoker springs of 21°N on the East Pacific Rise, and for the 'B' deposit the warm springs emerging at the axis of the Galapagos Rift (Corliss et al., 1979). The waters of the latter, at present at 2-15°C, have been shown to have evolved by sub-surface mixing of cold sea water with 300°C hydrothermal waters (Edmond et al., 1979). Any sulphides present in the hot solutions would have been precipitated at depth within the lavas. None are forming at the sea floor now.

Hole CY-2a confirmed and extended the record of the original uncored holes. The upper 109 m is made up of unmineralized lavas of uniform aphyric nature. Between 109 and 154 m is a unit of unmineralized glassy lavas, with a transitional base 1-2 m thick. Below this transition zone, between 154 and 297 m, is a zone of intensely altered pale lavas, where hard silicified lavas alternate with soft clay-rich rocks. Sulphide-rich zones occur within this unit, often associated with red jasper. The lower part of the hole, between 297 and 689 m, is made up of less intensely altered rocks, of dark grey to greenish lavas intruded by dykes. This unit contains sulphide veins throughout. The transition at 297 m between the intensely altered lavas and the lower unit is apparently sharp.

Rocks similar to those drilled in CY-2a are present beneath several other ore deposits in Cyprus, and as root zones of ore deposits that have been removed by erosion. The type of alteration found at Agrokipia is close to one end member of a wide spectrum of alteration types. At one extreme are the highly silicified stockworks, such as that of the Mathiati deposit, and at the other the poorly silicified stockworks of Pitharokhoma and Sha. The Agrokipia stockworks are similar to the poorly silicified types.

PETROGRAPHY AND MINERALOGY

The altered basalts of Holes CY-2 and CY-2a fall essentially into three alteration facies:

1. Low grade zeolite facies assemblages, dominated by smectites, with some zeolites, characteristic of the lower part of the CY-2 section and the upper 154 metres of CY-2a.
2. Highly altered white rock facies assemblages, dominated by pale chlorite, illite, pyrite and quartz, characteristic of the upper part of CY-2 and the section of CY-2a, between 154 m and 297 m.
3. Propylitic assemblages, with green chlorite, albite, carbonate and other minerals stable under greenschist facies conditions, found between 297 m and the base of Hole CY-2a.

Though the surrounding unmineralized rocks are now altered into zeolite facies assemblages, it is unlikely that they were altered to this degree when the white rock and propylitic alteration took place. Results of drilling very young ocean crust (Pritchard et al., 1978; Humphris et al., 1980) suggest that, unless thick sediments are present, basalt within a few kilometres of a spreading centre shows very little alteration at all.

Zeolite Facies Alteration

Rocks of this facies are dull brown in hand specimen. In thin section the dominant mineral is smectite, which replaces olivine, fills vesicles and replaces both glass and ferromagnesian minerals in the groundmass of these usually fine-grained rocks. The smectite ranges from dark brown to pale brown. It is frequently accompanied by bluish green celadonite which gives a characteristic 10 Angström units line in X-ray diffraction patterns of the clay concentrate. Phenocrysts of plagioclase and augite are less affected by alteration than the groundmass. Glassy units, perhaps hyaloclastites, below 100 m depth in CY-2a, show partial replacement of massive glass by yellow smectite and phillipsite, which also fill the vesicles in the glass. Calcite occurs sporadically through the rocks as veins or partial fillings of vesicles.

Interstitial grains of quartz are scattered through the groundmass of the crystalline lavas, and there is some controversy as to whether the quartz is primary or not. Gass et al. (1975) argued that most if not all of the quartz is secondary and introduced during alteration. However, recent analyses from Troodos (Robinson et al., 1983) have shown high Si levels to be characteristic of many fresh glasses and thus presumably of the fresh crystalline basalts. It seems unlikely, however, that the excess silica originally crystallized in these fine grained basalts in the form of such coarse-grained areas, and some redistribution of silica within the rock must have occurred during the alteration to give the quartz its present form.

White Rock Facies Alteration

The white rock facies is so termed because freshly-exposed surfaces are very pale grey to white. The facies is characterized by the assemblage pale chlorite-quartz-pyrite-illite. The interval between 154 m and 297 m in Hole CY-2a over which this alteration type was encountered contains three different groups of lithologies distinguishable in hand specimen. One is a tough brittle altered basalt, containing a high proportion of quartz. This is marked by the occurrence of large empty vesicles lined with euhedral quartz and pyrite. The vesicles are up to several centimetres across, much larger than is typical in the zeolite facies basalts, and have probably been enlarged by bulk solution of the rock during alteration. The second lithological group is also made up of altered basalt, but is much softer and contains a smaller proportion of quartz. Enlarged vesicles are absent. The third group of lithologies is not basaltic in origin. It is made up of red haematitic jaspers grading into pyrite-quartz mineralization. It can be shown that jaspers in other Cyprus stockwork zones represent altered interstitial ferruginous metalliferous sediments, and that the gradation from jasper to pyrite-quartz mineralization is the result of recrystallization and pyritization of jasper (Richards and Boyle, 1985). In particular, zones of pyrite-quartz mineralization that occur within intensely mineralized basalts in the Pitharokhoma stockwork can be clearly identified from their shape as replacements of pockets of inter-pillow sediment (H.G. Richards et al., submitted for publication). The pyrite-quartz mineralization in CY-2a, of similar texture and associated with jasper and recrystallized jasper, probably formed in the same way.

We thus interpret the white rock section in Hole CY-2a to be two units, an upper unit in which the alternations of soft and hard altered basalt may represent the altered equivalent of the alternations of glassy and crystalline basalts in the zeolite facies unit above the altered zone, and a lower unit of altered pillow lava.

In thin section, the altered basalts are all texturally similar. The igneous texture is well preserved, mainly as a felted network of plagioclase laths now pseudomorphed by illite and polycrystalline quartz. These are set in a matrix of pale chlorite studded with variable amounts of flakes of sericite. Pyrite occurs as disseminations throughout the rock and as thin veins and vesicle fillings. Clusters of minute highly birefringent grains are scattered through the groundmass. Most are of sphene, but others are composed of small square plates. Optical

properties microprobe analyses and X-ray diffraction identify this as anatase.

Electron microprobe analyses of the chlorite show it to be a ripidolite (Hey, 1954) of very constant composition throughout the section, approximately $[Mg_{5.5}Fe_{3.5}Al_{3.0}]_{12.0}[Al_{2.4}Si_{5.7}]_{8.1}O_{20}(OH)_{16}$.
The sericite is also constant in composition, close to $K_{1.5}Al_{4.0}[Si_{6.6}Al_{1.3}]_{7.9}O_{20}(OH)_4$.

Overall the white rock section is composed of a very simple mineral assemblage consisting of only four major phases, each of these with a very restricted composition range, though different samples contain these phases in very different proportions.

The upper contact of the white rock is gradational, with veins of this type of alteration cutting the overlying zeolite facies unit, demonstrating that the white rock alteration developed after that unit had been erupted.

Propylitic Alteration

Below 300 m in Hole CY-2a, the alteration style is propylitic. The rocks show very well-preserved igneous textures. Plagioclase laths are usually entirely replaced by albite, though rims of original sodic plagioclase are in places retained. Ferromagnesian minerals are entirely replaced by green chlorite, which also replaces glass and other interstitial material. Originally more glassy rocks show extensive development of chlorite and only vestigial albite laths. Sphene is scattered as minutely granular aggregates throughout the groundmass, apparently replacing titanomagnetite. Pyrite cubes are disseminated through the rocks, though in some samples the pyrite pseudomorphs iron oxides, and in others occurs as a spongy interstitial material. The habit of quartz is rather like that in the zeolite facies: it occurs as coarse anhedral grains in the groundmass, and also as fillings of vesicles and veins. Epidote is almost completely absent in the upper hundred metres of propylitic alteration, but it appears more regularly at greater depth, normally as small granular crystals in the groundmass. Near the bottom of the hole epidote is more abundant. Carbonate in the form of calcite is developed sporadically in the section, usually as large poikiloblastic plates preferentially replacing chlorite and enclosing albite laths. The rocks for analysis were chosen to avoid specimens containing carbonate.

GEOCHEMICAL ANALYSIS

The 24 samples selected for analysis from Hole CY-2 were those designated for geochemical analysis by UK laboratories, as were the upper 25 samples of Hole CY-2a (those taken from above 275 m). The samples from the section of Hole CY-2a below 275 m had not been specifically designated as national responsibilities, so 35 samples were selected on the basis of thin section observations to represent the different petrographic types observed, and to give a uniform spacing through the section.

All 84 samples were analyzed for major elements (Si, Al, Fe, Mg, Ca, Na, K, Ti, Mn) and for selected trace elements (Cr, Ag, Li, Ni, Co, Zr, Cu, V, Pb) by atomic absorption methods. P was determined by colorimetry, and total sulphur by iodometric titration of SO_2 following combustion. The methods used were those current in our analytical laboratory at Newcastle, and full details may be obtained from P.J. Oakley on request. The presence of pyrite in the rocks interfered with the determination of ferrous iron, and our determinations in rocks with more than about 1% of pyrite were not satisfactory, since a small, but unpredictable, fraction of the pyrite dissolves during analysis for ferrous iron. For this reason, values for ferrous iron have only been quoted for rocks of zeolite facies. The quality of the chemical analyses can be assessed by the comparative analyses of international standard rocks given in Table 1. The results from the analyses are given in full in the data tables in this volume. Representative analyses from each alteration facies are given in Tables 2, 3 and 4. In Hole CY-2, the upper part, down to 67 m, is in white-rock facies and the rest in zeolite facies. In Hole CY-2a, the section above 157 m is in zeolite facies, that between 154 and 297 m in white rock facies and the bottom of the hole in propylitic facies.

CHEMICAL CHARACTERISTICS OF ALTERATION FACIES

The lavas of the Troodos complex show a range of composition, from lavas with a generally boninitic chemistry to others with trace element characteristics close to MORB, but with a more evolved major element composition (Miyashiro, 1973; Pearce, 1975, 1980; Robinson et al., 1983). From the patterns of less mobile elements it is apparent that the majority of the rocks drilled in Holes CY-2 and CY-2a belong to a single, rather restricted group of composition. This is best seen from the abundances of Ti and Cr. Below about 50 m depth in the Hole CY-2 and below about 90 m depth in Hole CY-2a, almost all of the analyses (excepting for two short sections of Hole CY-2) show a consistent pattern of moderate to high TiO_2 (1.0-1.6%) and very low values of Cr (4-30 ppm). Also characteristic is the very low level of Ni (<l-20 ppm). The contrasting group of analyses, from the upper parts of the holes, contain TiO_2 at about 0.5-0.7%, Cr at 80-300 ppm and Ni at 40-150 ppm. Because the great majority of the altered basalts came so clearly from one protolith, chemical comparisons will be normally made on that basis. Table 5 gives

means of the high-Ti rocks of each alteration facies, so that comparisons can be made between rocks of generally similar original compositions. Standard deviations are not given, because of the grossly non-normal distribution of some of the elements. The means should be used only as an indication of the bulk composition of each facies group, and not as an estimate of a typical analysis from each group.

Zeolite Facies

Representative analysis from this facies are given in Table 2. Some of the characteristics of the high-Ti protolith can be deduced from the analyses of Troodos glass reported by Robinson et al. (1983). A group of those analyses come very close in their content of immobile elements to the zeolite facies rocks reported here (see the mean in Table 5). Extrapolating the graphs of Robinson et al. (1983) to appropriate compositions suggests that the main changes during zeolite facies alteration were to the relative abundances of Ca, Na and K, with depletion in CaO from an initial level of about 8.5% to 5.8% and enrichment in Na_2O from 2.7 to 3.1 and of K_2O from 0.2 to 0.6. The contents of the other major elements have probably been altered very little. Of the trace elements, the levels of V, Cr and probably Ni seem to remain relatively unaffected by even rather severe alteration in other basalts. Though Co and, particularly, Cu, Zn and Pb are mobile during intense alteration, their levels here seem entirely appropriate for basalts of this composition. Li is highly mobile under most kinds of alteration. Though the values here are consistent (range 7-13 ppm), they probably do not represent an original value.

On the Ca-Mg-Na diagram (Figure 1), the points corresponding to zeolite facies basalts fall in a field between the protolith composition and the Na-Mg edge of the triangle, showing depletion in Ca and some enrichment in Na.

TABLE 1. Partial Analyses of some International Standard Rocks

	TB	(shale)	BM	(basalt)	BOB1	(basalt)	MRG1	(gabbro)
SiO_2	60.00	(60.24)	Std	(49.51)	50.30	(50.10)	38.80	(39.32)
Al_2O_3	Std	(20.60)	Std	(16.23)	16.80	(16.50)	8.80	(8.50)
FeO*	6.22	(6.22)	8.63	(8.71)	Std	(7.58)	Std	(16.03)
MnO	0.05	(0.05)	0.14	(0.15)	0.14	(0.14)	Std	(0.17)
MgO	1.94	(1.94)	Std	(7.46)	7.44	(7.48)	Std	(13.49)
CaO			Std	(6.44)	11.20	(11.3)	Std	(14.77)
Na_2O	1.34	(1.31)			3.16	(3.14)	0.72	(0.71)
K_2O			0.18	(0.20)	0.34	(0.36)	0.16	(0.18)
TiO_2			Std	(1.14)	1.26	(1.27)		
P_2O_5					0.16	(0.16)	0.07	(0.06)
Li			73	(70)	7		4	(4)
V			200	(180)				
Cr			129	(121)	288	(280)		
Co			40	(34)	54	(55)	86	(86)
Ni			63	(56)	98	(105)	180	(195)
Cu			40	(45)	59	(62)	133	(135)
Zn			120	(113)	60	(65)	199	(190)
Ag								
Pb			7	(11)	<4	(4)		

*Total iron as FeO, Std: value used as standard in analysis, bracketed numbers are standard values, those for TB, BM and MRG1 are 1984 values from the Geostandards Newsletter, Special Issue, July 1984, those for BOB1 are 1978 standard values, analyses performed by P.J. Oakley at Newcastle at the same time as the unknowns from Holes CY-2 and CY-2a.

TABLE 2. Representative Analyses of Zeolite Facies Basalts

Hole CY-2 Depth (m)	110.75	130.90	150.35	169.45	189.40	214.10
SiO_2	56.6	54.6	57.8	56.7	56.4	63.1
Al_2O_3	16.4	15.5	15.3	15.8	16.8	14.1
Fe_2O_3	7.7	8.8	5.5	6.9	7.62	4.80
FeO	2.59	3.06	4.80	3.60	1.97	3.33
MnO	0.22	0.17	0.26	0.25	0.17	0.22
MgO	3.49	4.63	4.16	4.16	3.41	2.48
CaO	6.02	5.30	6.64	6.56	5.00	5.75
Na_2O	3.35	2.97	2.96	3.26	3.94	2.97
K_2O	0.38	0.44	0.18	0.18	0.28	0.62
TiO_2	1.22	1.25	1.27	1.36	1.33	1.28
P_2O_5	0.13	0.10	0.10	0.10	0.20	0.12
S	0.02	0.02	0.08	0.07	0.03	0.03
H_2O+	2.40	3.30	1.40	1.84	3.90	1.35
	100.52	100.14	100.45	100.78	101.05	100.15
Less O for S	0.01	0.01	0.02	0.02	0.01	0.01
Total	100.51	100.13	100.43	100.76	101.04	100.14
ppm						
Li	10	11	9	9	10	8
V	210	340	370	310	70	270
Cr	14	9	9	7	4	11
Co	23	27	31	29	14	19
Ni	5	10	16	11	10	7
Cu	36	78	111	62	36	34
Zn	125	106	106	106	114	100
Ag	<1	<1	<1	<1	<1	<1
Pb	7	3	3	3	3	<3

All samples are from Hole CY-2, and are selected to have similar TiO_2, Cr and Ni, and hence presumably similar protolith composition.

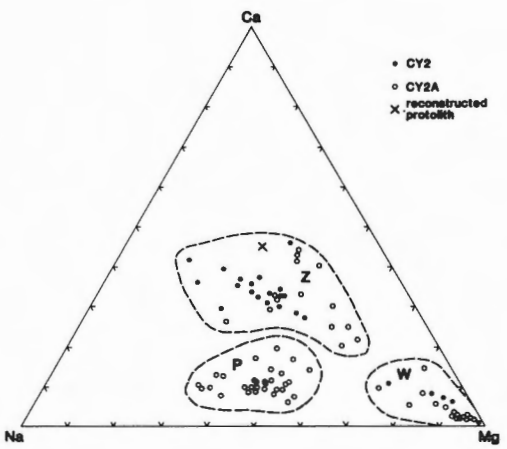

Figure 1: Ca-Na-Mg (atomic) proportions in zeolite facies basalts (Z), white-rock facies basalts (W) and propylitic facies basalts (P) from Holes CY-2 and CY-2a. X marks the position of the reconstructed protolith for the majority of the samples (see text).

White-Rock Facies

Table 3 gives representative analyses from this facies, and shows that the white-rock facies lavas have undergone much more severe alteration. The mean shows severe depletion in both CaO and Na_2O, essentially to trace levels, enrichment in both FeO* and S, consistent with pyrite precipitation, and moderate enrichment in MgO. Among the trace elements, Cu and Zn are strongly enriched, while Ag appears above detection limit and Pb is in places over 10 ppm. On Figure 1, the white rocks lie very near the Mg corner, because of their strong depletion in Ca and Na, coupled with some enrichment in Mg.

The group of analyses also shows pronounced internal variation in composition. The most variable trace elements are Cu, Zn and Pb, which show ranges of 11-1390 ppm, 83-2360 ppm and <3-100 ppm respectively. This variation, though, is very specific. High values in one element are not correlated with either high or low values of the others. High values probably correspond to small pockets of specific mineralization. Some of the samples most enriched in pyrite show lowest values of Cu, Zn and Pb (see 189.85).

TABLE 3. Representative Analyses of White-Rock Facies Basalts

Hole CY-2a Depth (m)	174.20	199.20	219.40	245.80	252.90	285.30
SiO_2	59.0	56.3	43.9	33.7	57.3	59.5
Al_2O_3	13.7	12.5	10.9	18.8	12.1	12.9
FeO*	10.5	14.9	23.8	21.3	14.0	10.60
MnO	0.42	0.10	0.05	0.14	0.20	0.19
MgO	7.32	4.21	1.75	7.19	3.90	4.97
CaO	0.26	0.18	0.16	0.22	0.20	1.30
Na_2O	0.12	0.21	0.24	0.28	0.16	0.28
K_2O	1.12	1.65	1.97	2.40	1.71	0.86
TiO_2	1.38	1.24	1.11	1.55	1.23	1.02
P_2O_5	0.10	0.09	0.04	0.11	0.11	0.11
S	1.20	8.67	18.9	13.0	8.34	4.11
H_2O+	6.09	4.35	2.83	6.62	4.44	4.94
	101.21	104.40	105.65	105.31	103.69	100.78
Less O for S	0.30	2.16	4.72	3.24	2.08	1.03
Total	100.91	102.24	100.93	102.07	101.61	99.75
ppm						
Li	7	5	3	6	4	2
V	140	290	240	300	190	166
Cr	14	12	8	4	6	4
Co	20	26	38	27	20	22
Ni	<1	7	2	<1	7	4
Cu	900	58	46	43	38	51
Zn	610	260	490	460	1730	1730
Ag	<1	1	1	<1	<1	<1
Pb	<3	<3	<3	<3	<3	<3

All samples are from Hole CY-2a, and are selected to have similar TiO_2, Cr and Ni, and hence presumably similar protolith composition.

The major elements, on the other hand, show very regular correlations with one another. Since these correlations are partly the result of the rather restricted mineralogy of the white rocks, it is convenient to recalculate the analyses into white-rock norms, in which pyrite is calculated stoichiometrically from S, chlorite from MgO (using the electron probe composition), illite from K_2O similarly, TiO_2 is taken to be present as a separate phase, and quartz is calculated by difference. The other elements are assumed to substitute into chlorite and illite. The result of this calculation (Table 6) shows that a considerable variation exists. This is displayed graphically in Figure 2, where normative chlorite and illite are plotted against normative pyrite. The graphs show a broad trend with increasing normative pyrite from rocks containing about 5% pyrite, 40% chlorite, 15% illite and 40% quartz, to rocks with 35% pyrite, 10% of chlorite, 25% of illite and 30% of quartz. This trend may have been caused by subsequent transformation of some initial form of white rock to a later one.

Propylitic Facies

Table 4 gives representative analyses from this facies. Table 5 shows that the mean composition of the propylites is enriched in MgO and especially in Na_2O, and depleted in CaO relative to the protolith. Fe and S are both enriched as are the trace elements Cu, Zn and Pb. Table 3 (CY-2a, 297-689 m) shows that enrichment in Cu is again sporadic, but enrichment in Zn and Pb is more uniform throughout the propylitic section. Ag is consistently below detection limit. On Figure 1, the propylitic samples fall towards the Mg-Na side of the triangle, as would be expected from the major element changes.

TABLE 4. Representative Analyses of Propylitic Facies Basalts

Hole CY-2a Depth (m)	346.50	434.78	445.70	495.20	583.20	641.60
SiO_2	49.4	58.7	59.8	46.6	49.9	54.6
Al_2O_3	14.9	14.3	15.0	12.6	15.0	13.9
FeO*	11.1	8.97	9.09	19.6	16.9	14.0
MnO	0.28	0.56	0.34	0.2	0.36	0.36
MgO	5.52	5.43	4.37	5.48	5.23	4.40
CaO	5.88	1.96	1.63	2.02	1.24	1.61
Na_2O	2.23	4.10	5.17	2.36	3.33	3.21
K_2O	1.27	0.10	0.10	0.26	0.14	0.67
TiO_2	1.31	1.22	1.34	1.01	1.11	1.14
P_2O_5	0.09	0.14	0.13	0.10	0.10	0.12
S	0.05	1.15	0.02	9.65	2.71	1.44
H_2O+	6.09	4.35	3.47	4.82	5.79	4.17
	98.12	100.98	100.46	104.74	101.81	99.62
Less O for S	0.01	0.29	0.01	2.41	0.68	0.36
Total	98.11	100.69	100.45	102.33	101.13	99.26
ppm						
Li	8	5	3	4	3	2
V	520	194	149	330	375	393
Cr	14	2	4	5	9	11
Co	37	22	19	61	26	27
Ni	15	4	4	10	15	11
Cu	57	54	48	13	867	209
Zn	149	730	500	170	142	160
Ag	<1	<1	<1	<1	<1	<1
Pb	7	130	15	9	7	22

All samples are from Hole CY-2a, and are selected to have similar TiO_2, Cr and Ni, and hence presumably similar protolith composition.

TABLE 5. Means of Rock Groups Altered in Different Facies

	(a) 18 zeolite facies basalts from Hole CY-2	(b) 15 white rock basalts from Hole CY-2a	(c) 24 propylitic basalts from Hole CY-2a	(d) Estimated protolith
SiO_2	56.3	52.1	55.5	55.4
Al_2O_3	15.7	13.9	14.3	16.2
FeO*	9.9	14.4	12.3	10.0
MnO	0.28	0.20	0.32	–
MgO	4.15	6.35	5.13	4.2
CaO	5.80	0.36	1.86	8.5
Na_2O	3.08	0.23	3.83	2.7
K_2O	0.56	1.52	0.16	0.2
TiO_2	1.30	1.24	1.18	1.3
P_2O_5	0.13	0.10	0.13	
S	0.04	7.04	1.83	
H_2O+	2.69	5.55	4.41	
Li	9	6	3	
V	270	240	280	
Cr	10	10	6	
Co	26	26	29	
Ni	11	4	7	
Cu	57	186	143	
Zn	118	705	248	
Ag	<1	1	<1	
Pb	4	6	15	

*Total Fe calculated as FeO, (a) CY-2 76.45-223.80 inclusive except for 96.75 and 135.15, (b) CY-2a 160.45-291.20 inclusive, (c) CY-2a 414.00-687.85 inclusive. All of these rocks have been selected to have similar contents of TiO_2, Cr and Ni, which are normally nearly immobile elements. The original magmatic compositions were thus probably broadly similar between the groups.

Again, the major elements show some consistency. When the chemical analyses are recalculated in terms of normative minerals, using a more iron-rich chlorite than for the white-rocks, the samples range in general from rocks with about 40% of chlorite, 25% of albite and 25% of quartz, to rocks with a higher albite content calculating to about 30% of chlorite, 40% of albite and 25% of quartz. Pyrite is normally low in these rocks, and enrichment in pyrite does not seem to be related to any other variation. Quartz is highly variable in amount. Calcite is present in a few samples.

This broad trend is seen in Figure 3, and probably related to varying mineralogy of the protolith. As was indicated in the section on petrography, propylitic alteration shows a strong effect of congruence, the specific relation of one secondary phase to one or more primary phases (Cann, 1969, 1979). Here, albite is clearly restricted to replacing original plagioclase crystals, whereas chlorite can replace both original ferromagnesian minerals and original glass or interstitial matrix. The result is that rocks originally more rich in glass or interstitial groundmass, such as pillow or dyke margins, eventually contain a much higher proportion of chlorite than rocks that were originally holocrystalline. The chemical variation seen here would thus reflect such an original variation in primary mineral composition.

CHEMICAL CHANGES ACCOMPANYING ALTERATION

Though gross chemical changes during alteration can be estimated from Figure 1 and Table 5, a knowledge simply of initial composition and final composition is not enough to define chemical changes unambiguously. We assume in addition that one element has remained immobile during alteration,

TABLE 6. Alteration Norms of White Rock Samples from CY-2a

Sample	pyrite	chlorite	illite	TiO_2	quartz
160.45	1.6	44.5	36.8	1.1	16.1
165.40	12.1	74.5	9.2	1.4	14.9
174.20	2.3	41.6	14.5	1.4	40.1
181.15	4.9	35.6	17.4	1.1	41.0
189.85	32.0	16.0	24.9	1.1	25.9
199.20	16.2	23.9	21.4	1.2	37.2
219.40	35.4	10.0	25.6	1.1	28.0
228.70	7.5	51.9	15.1	1.5	24.1
238.26	8.7	49.2	17.9	1.5	22.7
245.80	24.3	40.9	31.2	1.6	2.0
252.90	15.6	22.2	22.2	1.2	38.8
262.40	12.4	22.0	23.0	1.1	41.6
273.65	6.6	36.1	14.3	1.2	41.9
285.30	7.7	28.3	11.2	1.0	51.8
291.20	10.4	44.9	11.9	1.2	31.6
mean	13.2	36.1	19.8	1.3	30.5

Norms calculated using electron probe analyses of illite and chlorite and stoichiometric pyrite, quartz and TiO_2, Pyrite = S x 1.871, chlorite = MgO x 5.688, sericite = K_2O x 12.99, TiO_2 = TiO_2, quartz by difference.

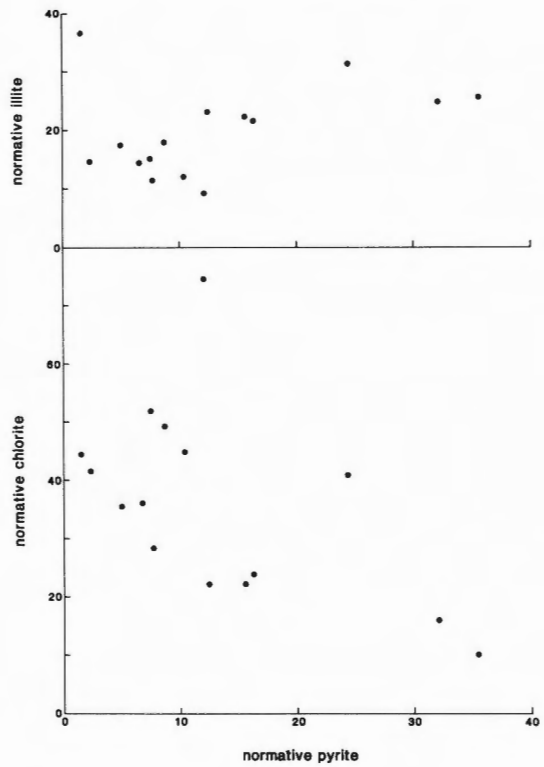

Figure 2: Hole CY-2a white-rock facies alteration. Plots of white-rock facies normative minerals (see text), illite against pyrite and chlorite against pyrite to show correlations.

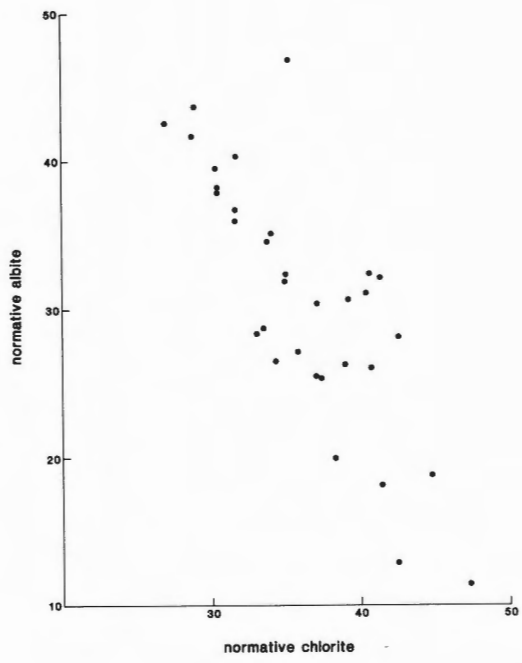

Figure 3: Hole CY-2a propylitic facies alteration. Plot of propylitic facies normative albite versus normative chlorite (see text for explanation of calculation).

since a number of studies that have indicated only slight mobility of some components during similar alteration (Cann, 1970; Humphris and Thompson, 1978; Smith and Smith, 1976). Within the group of elements analyzed here, Al_2O_3 is the component that appears to have shown least original magmatic variation while at the same time being likely to have remained relatively immobile.

Composition of the protolith was primarily calculated using the less-altered zeolitic facies basalts of Table 2, supplemented for Ca, Na, Mg and K by the results of Robinson et al. (1983). This estimated composition is given in Table 5. Because it is based on rather indirect evidence, this composition cannot be considered very precise, and there would, in any case, have been some original magmatic variation. Details of chemical changes may thus not be well constrained, but the general picture should be accurate.

Chemical fluxes were calculated by normalizing each altered rock to an Al_2O_3 content of 16.2 and then subtracting from the result the precursor composition given above. This gives the total change in moving from protolith to altered rock. The calculation yields very small changes for TiO_2, which is probably also immobile, thus justifying the particular protolith composition chosen.

Table 7 gives the results of calculations of chemical changes for the white rocks of Hole CY-2a. As would be expected from the original analyses, the chemical changes vary from rock to rock, as is shown in Figure 4. Here the relationships between the differences for K_2O, MgO, FeO and S are seen. The difference in FeO shows a strong positive correlation with that in S. At one end of the line are white rocks to which little Fe or S has been added, and at the other are rocks to which 55% of pyrite has been added. In parallel with this difference in pyrite addition, the change in MgO is about +5g/100g of parent rock in rocks to which little pyrite has been added and -2g/100g, corresponding to a net removal of MgO from the rock, in rocks to which much pyrite has been added. K_2O shows the opposite trend, ranging from an addition of 1g/100g at low S levels to an addition of 3g/100g at high S levels (though one or two samples do not follow the trend). SiO_2 shows a mean influx of 6.9g/100g, varying between a net addition of 21.3g/100g and a net subtraction of 26.4g/100g, but this variation is not correlated with the variation in pyrite addition. Presumably the range in SiO_2 reflects local differences in temperature and flow rate in the upflow zone, since the precipitation of SiO_2, though slow, is essentially temperature controlled.

TABLE 7. Chemical Changes during Alteration of Protolith Basalt to White Rock (CY-2a)

Sample	ΔSiO_2	ΔMgO	ΔK_2O	ΔFeO^*	ΔS	ΔCaO	ΔNa_2O
160.45	+9.6	+4.9	+3.1	+1.6	+1.0	-7.7	-2.1
165.40	-11.7	+9.7	+0.6	+6.5	+6.8	-8.1	-2.5
174.20	+14.4	+4.5	+1.1	+2.6	+1.4	-8.2	-2.6
181.15	+19.2	+3.4	+1.4	+1.6	+1.3	-8.2	-2.4
189.85	+5.0	-0.3	+2.4	+20.2	+23.3	-8.0	-2.4
199.20	+17.6	+1.3	+1.9	+9.4	+11.2	-8.3	-2.4
219.40	+9.9	-1.6	+2.7	+25.6	+28.1	-8.3	-2.3
228.70	-2.6	+5.3	+1.0	+2.4	+4.1	-8.2	-2.5
238.26	-12.8	+3.8	+1.1	+3.1	+4.3	-8.3	-2.4
245.80	-26.4	+2.1	+1.9	+8.6	+11.2	-8.3	-2.5
252.90	+21.3	+1.1	+2.1	+8.9	+11.2	-8.2	-2.5
262.40	+19.7	+0.8	+2.1	+6.9	+8.4	-8.1	-2.4
273.65	+12.1	+3.2	+1.1	+4.1	+4.1	-8.2	-2.6
285.30	+19.3	+2.1	+0.9	+3.5	+5.1	-6.9	-2.3
291.20	+9.2	+5.4	+0.9	+6.5	+6.7	-8.2	-2.5
mean g/100g	+6.9	+3.1	+1.6	+7.4	+8.6	-8.1	-2.4
mg ats/100g	+115	+77	+34	+103	+269	-144	-77

*Total change of iron calculated as FeO, data indicates g/100 g of original rock, + is addition to rock, - is removal from rock

The chemical fluxes calculated for alteration of protolith basalt to propylite do not show the same systematic relations on those for the white rocks. Overall, in g/100g, SiO_2 shows an addition of 9.0, FeO of 4.2, MgO of 1.7, Na_2O of 1.5, K_2O of 0.1 and S of 2, while CaO shows a removal of 6.3. Influx of Na_2O is variable, depending on whether the rock is chlorite-rich or albite-rich (and thus probably on its original mineralogy, as discussed above). The relationship between influx of Fe and S is different from the case of the white rocks. There (Figure 4) the ratio of addition of S to that of Fe was greater than the ratio in FeS_2. Here (Figure 5) the relationship is less well defined, but the ratio of addition of S to that of Fe lies generally between 1 and 2.

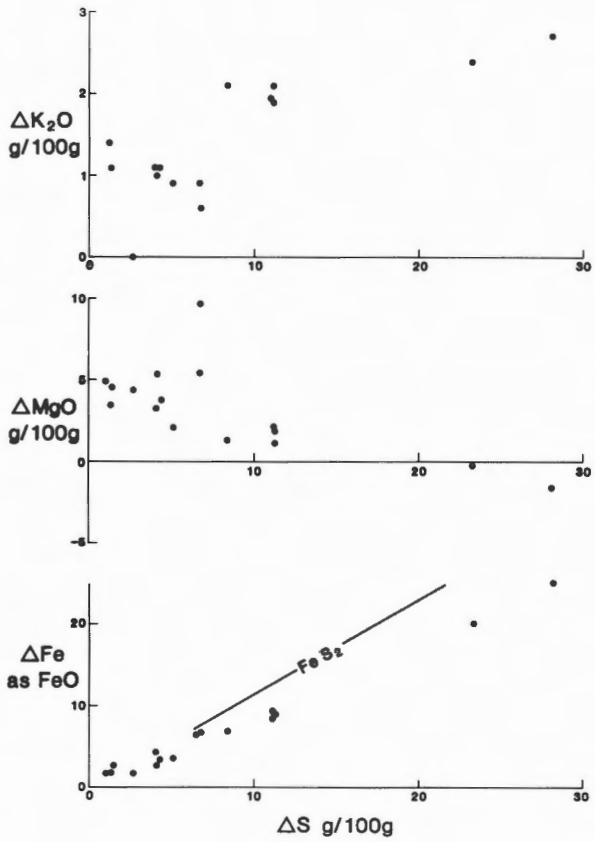

Figure 4: Chemical fluxes during white-rock alteration, Hole CY-2a. Values are of grams of component added per 100 grams of original rock, assuming immobile Al and TiO_2 and the protolith composition quoted in the text. The line marked FeS_2 is the line for stoichiometric addition of pyrite.

COMPARISON WITH OTHER STOCKWORKS

This work on Hole CY-2a is only part of a wider investigation of Cyprus stockworks. This investigation has shown that stockworks show a considerable range in their petrology and geochemistry (H.G. Richards et al., submitted for publication). Three distinct types of stockwork were identified. One type is similar to that drilled by Hole CY-2a, with the development of white-rock facies alteration with the assemblage chlorite + illite + quartz + pyrite and enrichment of Mg and K in the altered rock. The second type is exemplified by the Kokkinopezoula stockwork, in which instead of illite is developed a Ca, Na-bearing illite-smectite mixed layer, containing little K. The altered rock is still very pale and shows Mg enrichment, but little increase in K. The third type is represented by the Mathiati stockwork (Lydon and Galley, 1986). Here the climax of alteration is represented by the assemblage Fe-chlorite + quartz + pyrite. The altered rocks show strong silicification but no addition of Mg or K.

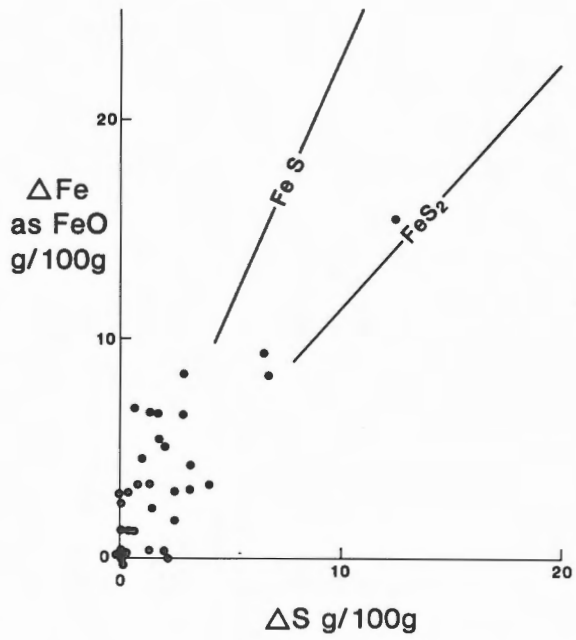

Figure 5: Chemical fluxes during propylitic alteration, Hole CY-2a. Values are of grams of component added per 100 grams of original rock, assuming immobile Al and TiO_2 and the protolith composition quoted in the text. The lines marked FeS and FeS_2 are those that would be followed by stoichiometric addition of these components.

The type of stockwork corresponding to that described here from Hole CY-2a is best exemplified by the partly-mined stockwork at Pitharokhoma near the village of Kambia. This stockwork is described in detail by H.G. Richards et al. (submitted for publication). It shows a clear concentric arrangement of alteration zones. The stockwork is 200 x 100 m in plan at outcrop, and the outer zone of the alteration (about 50 m wide) is made up of grey-green rock with the assemblage albite + chlorite-smectite mixed layer minerals + quartz + sphene. Within this zone are two areas of more intense alteration, 30-80 m across. These highly altered zones are composed of the white-rock facies assemblage chlorite + illite + quartz + pyrite. At the centre of the larger of these zones are two small areas of yet more intense alteration about 20 m across, in which the assemblage is illite + quartz + pyrite, where chlorite is absent, Mg is consequently depleted and K strongly enriched. Al has been mobile at these intense degrees of alteration, and is markedly depleted relative to still-immobile elements such as Ti and Zr, but in the less intensely altered rocks Al has behaved apparently as an immobile element.

Through this sequence of alteration types the inter-pillow hydrothermal sediments can be distinguished by their characteristic cuspate morphology. Beyond the influence of the stockwork they are composed of brown iron-manganese oxides. Within the chlorite-smectite zone these have been transformed to bright red jasper, sometimes with sparse disseminated pyrite. Within the zones of more intense alteration the amount of disseminated pyrite increases and clear crystalline quartz replaces the cryptocrystalline silica, giving eventually a pyrite-quartz assemblage still morphologically recognizable as originally inter-pillow sediment.

The bodies of massive sulphide in this type of deposit are enclosed within the highly-altered zones and have clearly not been formed by exhalation at the sea floor but by precipitation below the sea floor in voids or as a replacement product. Faults cut through the stockwork and bring different alteration facies abruptly into contact. Dykes cut the stockwork, some of them clearly post-dating the alteration, but many apparently either intruded before the alteration occurred, or during the alteration phase.

Hole CY-2a is interpreted as having penetrated such a stockwork. The white-rock section of the hole between 154 and 297 m corresponds to the core zone of highly altered basalt, with the jasper and pyrite-quartz assemblages representing original inter-pillow hydrothermal sediment. The abrupt transition at 297 m to propylitic alteration probably corresponds to penetration through a fault separating the inner from the outer zone of alteration, since in the absence of a fault the transition is gradual, through intermediate mineral assemblages. The mineralogy of the propylitic lower section of the hole does not correspond precisely to that of the outer zone at Pitharokhoma, since it contains chlorite and epidote, rather than chlorite-smectite mixed layers. However, the assemblages in Hole CY-2a can be paralleled closely by those in a similarly zoned stockwork near Kalokhorion south of Kambia, which is at a deeper structural level in the ophiolite than the Pitharokhoma stockwork.

CONCLUSIONS

The mineralized stockwork drilled below the Agrokipia 'A' and 'B' ore deposits in Holes CY-2 and CY-2a can be divided into three alteration facies, a background low-grade zeolite facies, an intensely altered white-rock facies (with the metabasaltic assemblage quartz + chlorite + illite + pyrite) and a propylitic facies (albite + chlorite + quartz + epidote). The chemical alteration pattern is different for each facies. Relative to a reconstructed protolith composition, the zeolite facies alteration has resulted in removal of Ca and addition of Na and K to the rock, but in little other change. The white-rock facies samples show a strong depletion in Ca and Na, and enrichment in K, Mg, Fe and S, as well as in the trace elements Cu, Zn, Pb and Ag. These samples form a spectrum from rocks poor in pyrite and rich in chlorite to rocks containing over 30% of pyrite, and almost entirely chlorite-free. The propylites show strong Ca depletion, together with enrichment in Mg, Na, Cu, Zn and Pb.

Similar stockworks can be seen at different structural levels in other parts of Cyprus. They show a clear concentric pattern of alteration facies (Constantinou, 1972, 1977, 1980; Lydon and Galley, 1986), as is seen in stockworks below volcanogenic massive sulphides in many parts of the world (Franklin et al., 1981; Shirozu, 1978; Larson, 1984). The zeolite facies is developed as a background, probably later, alteration outside the zone of influence of the hydrothermal fluid rising through the stockwork. The propylitic facies of Hole CY-2a finds parallels in the outer zones of many stockworks, which are characterized by the presence of albite replacing plagioclase, though the layer silicates present vary from smectite through mixed layers to chlorite, apparently depending on structural level. White-rock facies assemblages are found in the core zones of one of the three major types of stockwork, as exemplified by that at Pitharokhoma, where the most intense alteration is represented by the illite-rich, chlorite-poor assemblages that form one end of the spectrum of white-rock compositions in Hole CY-2a.

In Hole CY-2a, the upper part of the section, altered to zeolite facies, may, at least in part, represent post-mineralization volcanism. However, the

lower part of this unit, at about 154 m into the hole, shows a rapid transition to the underlying white-rock facies, over 1-2 m of vertical section, so that part at least of the zeolite facies section must predate the hydrothermal episode. No propylitic zone intervenes between the zeolite and white rock zones here, suggesting an unusually sudden decrease in the intensity of hydrothermal alteration with height in the hole. A similar boundary, with the opposite sense, occurs in Hole CY-2, where the white-rock facies alteration seen in the top of the section rapidly gives way to zeolite facies alteration with depth. At 297 m into Hole CY-2a, the abrupt transition from white rock to propylitic facies suggests that the hole has passed suddenly from the core of a stockwork into the outer zone, probably by crossing a fault, similar to those seen to cut the stockwork at Pitharokhoma.

Most of the sulphide-rich portions of the core from Hole CY-2a are associated with diffuse areas of jasper, and can be seen to have formed by replacement of jasper, itself formed from hydrothermal sediment occurring interstitially to pillows, as can be demonstrated at Pitharokhoma (H.G. Richards et al., submitted for publication). Larger zones of massive sulphide occur enclosed within the intensely altered white-rock facies material in the Agrokipia 'B' deposit penetrated by Hole CY-2a, as shown by the records of the Hellenic Mining Company (Adamides, 1984), and similar enclosed bodies of massive sulphide exist at Pitharokhoma (H.G. Richards et al., submitted for publication). Such bodies cannot have formed by exhalation at the sea floor but must have been precipitated either as void filling or replacement, within the upwelling zone itself.

Sub-sea-floor precipitation of sulphide, when taken together with the transitional nature of the upper boundary of the white rock zone, suggests that in the Agrokipia 'B' deposit, and at Pitharokhoma, the hot fluids did not vent directly onto the sea floor, but were mixed beneath the sea floor with entrained cold sea water. Such mixing would cool and dilute the hydrothermal waters and induce precipitation of sulphides primarily by changing pH. Sub-sea-floor mixing can be demonstrated at the axis of the Galapagos Spreading Centre, where warm solutions emerging at the sea floor can be shown geochemically to have originated by mixing of 300°C hydrothermal solutions with cold sea water (Corliss et al., 1979; Edmond et al., 1979). A model of this kind for Agrokipia 'B' was proposed by Adamides (1984), and has been elaborated with additional evidence by H.G. Richards et al. (submitted for publication).

ACKNOWLEDGEMENTS

This study would not have been possible without the help of members of the Cyprus Geological Survey, especially Dr. G. Constantinou, A. Panayiotou and Dr. C. Xenophontos. Their practical assistance, advice, experience of the terrain, leadership in the field, and past researches have all been invaluable. We are very grateful for much advice and helpful discussion with Dr. N. Adamides. Pam Foster typed the manuscript and Christine Jeans drew the diagrams.

REFERENCES

Adamides, N.G.
1984: Cyprus volcanogenic sulphide deposits in relation to their environment of formation; unpublished Ph.D. thesis, University of Leicester, England, p. 1-383.

Ballard, R.D., Francheteau, J., Juteau, T., Rangan, C. and Normark, W.
1981: East Pacific Rise at 21°N: the volcanic, tectonic and hydrothermal processes of the central axis; Earth and Planetary Science Letters, v. 55, p. 1-10.

Bear, L.M.
1960: The geology and mineral resources of the Akaki-Lythrodondha area; Cyprus Geological Survey Department, Ministry of Agriculture and Natural Resources, Memoir, no. 3, p. 1-122.

Cann, J.R.
1969: Spilites from the Carlsberg Ridge, Indian Ocean; Journal of Petrology, v. 10, pt. 1, p. 1-19.
1970: Rb, Sr, Y, Zr and Nb in some ocean floor basaltic rocks; Earth and Planetary Science Letters, v. 10, no. 1, p. 7-11.
1979: Metamorphism in the ocean crust; *in* Deep Drilling Results in the Atlantic Ocean: Ocean Crust, ed. M. Talwani, C.G. Harrison, and D.E. Hayes; Maurice Ewing Series 2, American Geophysical Union, Washington, D.C.

Constantinou, G.
1972: The geology and genesis of the sulphide ores of Cyprus; unpublished Ph.D. thesis, University of London, England.
1977: Hydrothermal alteration of basaltic lavas of the Troodos ophiolite complex associated with the formation of the massive sulphide deposits; *in* Volcanic Processes in Ore Genesis; Geological Society of London, Special Publication, no. 7.
1980: Metallogenesis associated with the

Troodos ophiolite; *in* Ophiolites, Proceedings of the International Ophiolite Symposium, Cyprus, 1979, ed. A. Panayiotou; Cyprus Geological Survey Department, Ministry of Agriculture and Natural Resources, p. 663-674.

Constantinou, G. and Govett, G.J.S.
1972: Genesis of sulphide deposits, ochre and umber of Cyprus; Institution of Mining and Metallurgy, London, Transactions and Bulletin, Section B; Applied Earth Sciences, v. 81, Bulletin no. 783, p. B34-B46.
1973: Geology, geochemistry, and genesis of Cyprus sulfide deposits; Economic Geology, v. 68, no. 6, p. 843-858.

Converse, D.R., Holland, H.D. and Edmond, J.M.
1984: Flow rates in the axial hot springs of the East Pacific Rise (21°N): implications for the heat budget and the formation of massive sulfide deposits; Earth and Planetary Science Letters, v. 69, no. 1, p. 159-175.

Corliss, J.B., Dymond, J., Gordon, L.I., Edmond, J.M., Von Herzen, R.P., Ballard, R.D., Green, K., Williams, D., Bainbridge, A., Crane, K. and Van Andel, T.H.
1979: Submarine thermal springs on the Galapagos Rift; Science, v. 203, no. 4385, p. 1073-1083.

Edmond, J.M., Measures, C., McDuff, R.E., Chan, L.H., Collier, R., Grant, B., Gordon, L.I. and Corliss, J.B.
1979: Ridge crest hydrothermal activity and the balances of the major and minor elements in the ocean: the Galapagos data; Earth and Planetary Science Letters, v. 46, p. 1-18.

Edmond, J.M., Von Damm, K.L., McDuff, R.E. and Measures, C.I.
1982: Chemistry of hot springs on the East Pacific Rise and their effluent dispersal; Nature, v. 297, p. 187-191.

Franklin, J.M., Lydon, J.W. and Sangster, D.F.
1981: Volcanic-associated massive sulphide deposits; Economic Geology, 75th Anniversary Volume, p. 485-627.

Gass, I.G., Neary, C.R., Plant, J., Robertson, A.H.F., Simonian, K.O., Smewing, J.D., Spooner, E.T.C. and Wilson, R.A.M.
1975: Comments on 'The Troodos Ophiolitic Complex was probably Formed in an Island Arc', by A. Miyashiro and subsequent correspondence by A. Hynes and A. Miyashiro; Earth and Planetary Science Letters, v. 25, no. 2, p. 236-238.

Haymon, R.M. and Kastner, M.
1981: Hot spring deposits on the East Pacific Rise at 21°N: preliminary description of mineralogy and genesis; Earth and Planetary Science Letters, v. 53, no. 3, p. 363-381.

Hey, M.H.
1954: A new review of the chlorites; Mineralogical Magazine and Journal of the Mineralogical Society, v. 30, p. 277.

Humphris, S.E., Melson, W.G. and Thompson, R.N.
1980: Basalt weathering on the East Pacific Rise and the Galapagos Spreading Center, Deep Sea Drilling Project, Leg 54; *in* Initial Reports of the Deep Sea Drilling Project, Volume 54, ed. B.R. Rosendahl, R. Hekinian, et al.; U.S. Government Printing Office, Washington, D.C., v. 54, p. 773-787.

Humphris, S.E. and Thompson, G.
1978: Trace element mobility during hydrothermal alteration of oceanic basalts; Geochimica et Cosmochimica Acta, v. 42, no. 1, p. 127-136.

Larson, P.B.
1984: Geochemistry of the alteration pipe at the Bruce Cu-Zn volcanogenic massive sulfide deposit, Arizona; Economic Geology, v. 79, no. 8, p. 1880-1896.

Lydon, J.W. and Galley, A.
1986: The chemical and mineralogical zoning of the Mathiati alteration pipe, Cyprus, and its genetic significance; *in* Metallogeny of Basic and Ultrabasic Rocks; Institution of Mining and Metallurgy, London (in press).

Michard, G., Albarède, F., Michard, A., Minster, J.-F., Charlou, J.-L. and Tan, N.
1984: Chemistry of solutions from the 13°N East Pacific Rise hydrothermal site; Earth and Planetary Science Letters, v. 69, no. 3, p. 297-307.

Miyashiro, A.
1973: The Troodos ophiolite complex was probably formed in an island arc; Earth and Planetary Science Letters, v. 19, no. 2, p. 218-224.

Mottl, M.J.
1983: Metabasalts, axial hot springs and the structure of hydrothermal systems at mid-ocean ridges; Geological Society of America, Bulletin, v. 94, no. 2, p. 161-180.

Pearce, J.A.
1975: Basalt geochemistry used to investigate past tectonic environments on Cyprus; Tectonophysics, v. 25, no. 1-2, p. 41-67.
1980: Geochemical evidence for the genesis and eruptive setting of lavas from Tethyan ophiolite; *in* Ophiolites,

Proceedings of the International Ophiolite Symposium, Cyprus, 1979, ed. A. Panayiotou; Cyprus Geological Survey Department, Ministry of Agriculture and Natural Resources, p. 261-272.

Pritchard, R.G., Cann, J.R. and Wood, D.A.
1978: Low-temperature alteration of oceanic basalts, DSDP Leg 49; *in* Initial Reports of the Deep Sea Drilling Project, Volume 49, ed. B.P. Luyendyk, J.R. Cann, et al.; U.S. Government Printing Office, Washington, D.C., v. 49, p. 709-714.

Richards, H.G. and Boyle, J.F.
1985: Origin, alteration and mineralization of inter-lava metalliferous sediments of the Troodos ophiolite, Cyprus; *in* Metallogeny of Basic and Ultrabasic Rocks, Proceedings, Edinburgh, 1985; Institution of Mining and Metallurgy, London.

Robinson, P.T., Melson, W.G., O'Hearn, T. and Schmincke, H.-U.
1983: Volcanic glass compositions of the Troodos ophiolite, Cyprus; Geology v. 11, no. 7, p. 400-404.

Shirozu, H.
1978: Wall-rock alteration of Kuroko deposits; *in* Clays and Clay Minerals of Japan: Developments in Sedimentology, Volume 26, ed. T. Sudo and S. Shimoda; Kodansha-Elsevier, Tokyo, v. 26, p. 127-145.

Smith, R.E. and Smith, S.E.
1976: Comments on the use of Ti, Zr, Y, Sr, K, P and Nb in classification of basaltic magmas; Earth and Planetary Science Letters, v. 32, no. 2, p. 114-120.

Sulphide Mineralization, Hydrothermal Alteration and Chemistry in the Drill Hole CY-2a, Agrokipia, Cyprus

PETER M. HERZIG AND GUNTHER H. FRIEDRICH

Institut für Mineralogie und Lagerstättenlehre
Rheinisch-Westfälische Technische Hochschule Aachen
D-5100 Aachen, Federal Republic of Germany

Herzig, P.M. and Friedrich, G.H., Sulphide mineralization, hydrothermal alteration and chemistry in the drill hole CY-2a, Agrokipia, Cyprus; in *Cyprus Crustal Study Project: Initial Report, Holes CY-2 and 2a, ed. P.T. Robinson, I.L. Gibson and A. Panayiotou; Geological Survey of Canada, Paper 85-29, p. 103-138, 1987.*

Abstract

The Agrokipia sulphide deposit, a fossil sub-seafloor hydrothermal system, is located in pillow lavas of the Troodos ophiolite. Hole CY-2a intersected uppermost lavas, stockwork sulphides, and underlying altered rocks to a depth of 689 m. Based on the alteration mineral distribution, four major alteration zones were distinguished. The absence of actinolite from the assemblage epidote + chlorite + albite + sphene + calcite indicates a paleotemperature of about 300°C at the base of the hole. The ore mineral paragenesis predominantly consists of pyrite, intergrown with sphalerite, less chalcopyrite and minor, but widespread, pyrrhotite. Pyrite shows As concentrations up to 1.87 wt.% and Co/Ni ratios between 2.0 and 8.0. Sphalerite is Fe-rich, showing an average of 9.7 mol % FeS above and 19.7 mol % FeS below 270 m depth. Greenschist facies and propylitic altered rocks are K and Ca depleted and Na enriched, relative to fresh lava composition. The ore zone is enriched in Fe, Zn, Cu, As, Si and K, the latter incorporated into sericite/illite, whereas Ca, Na and Sr are considerably leached. A significant Ba anomaly is associated with the sulphide zone, caused by leaching of Ba from plagioclase and redeposition mainly within sericite/illite.

Résumé

Le gîte de sulfures d'Agrokipia, un système hydrothermal fossile de sous-plancher océanique, est localisé dans les laves en coussinets de l'ophiolite de Troodos. Le trou de forage CY-2a recoupait les laves sommitales, le stockwerk de sulfures, et les roches altérées sous-jacentes jusqu'à la profondeur de 689 m. La distribution des minéraux d'altération permet de distinguer quatre zones majeures d'altération. L'absence d'actinolite dans l'assemblage épidote + chlorite + albite + sphène + calcite indique une paléotempérature d'environ 300°C au fond du trou de forage. La paragenèse des minéraux opaques est dominée par la pyrite, des intercroissances avec la sphalérite, de la chalcopyrite subordonnée et de la pyrrhotite accessoire mais répandue. La pyrite est caractérisée par des teneurs en As jusqu'à 1,87% et des rapports Co/Ni entre 2,0 et 8,0. La sphalérite est riche en Fe, la moyenne étant de 9,7 mole % FeS au-dessus et 19,7 mole % au-dessous de 270 m. Les faciès des schistes verts et les roches propylitiques altérées sont appauvries en K et Ca et enrichies en Na, relativement à la composition des laves inaltérées. La zone minéralisée est enrichie en Fe, Zn, Cu, As, Si et K, ce dernier élément est incorporé dans la séricite/illite, tandis que Ca, Na et Sr ont été considérablement lessivés. Une anomalie significative de Ba est associée à la zone de sulfures, due au lessivage du Ba du plagioclase et refixé principalement dans la séricite/illite.

INTRODUCTION

The Agrokipia 'B' Fe-Zn-Cu sulphide deposit, located in the northern extrusive belt of the Troodos ophiolite complex, Cyprus (Figure 1), was selected by the International Crustal Research Drilling Group (ICRDG) as the drillsite for Hole CY-2a of the Cyprus Crustal Study Project (Robinson et al., 1984). The continuously cored 689 m borehole intersected unaltered lavas, the stockwork mineralization of Agrokipia 'B' and then penetrated about 400 m into the extensive alteration pipe beneath the deposit (Figure 2). The drilled section allowed investigation of the secondary mineral distribution, the ore mineralogy and the chemical characteristics of a fossil sulphide deposit, formed by sub-seafloor hydrothermal activity.

Fluid inclusion and stable isotope studies indicate that the Cyprus volcanogenic sulphide deposits were formed by seawater convection cells, probably driven by high level magma chambers (Spooner and Fyfe, 1973; Spooner et al., 1974; Heaton and Sheppard, 1977; Spooner, 1977; Spooner and Bray, 1977). It is supposed that these hydrothermal systems operated during spreading above a subduction zone, probably in an early stage of island arc development (Robinson et al., 1983; Schmincke et al., 1983; Rautenschlein et al., 1985; Bednarz et al., 1987) in late Cretaceous ocean crust (Robertson and Woodcock, 1980). The Agrokipia system can be compared to recent and subrecent hydrothermal systems, discovered at diverging oceanic plate boundaries (Francheteau et al., 1979; Hekinian et al., 1980; Lonsdale et al., 1980; Anderson et al., 1982; Bischoff et al., 1983; Normark et al., 1983; Koski et al., 1984; Rona, 1984). Also, some metamorphosed massive sulphide ore bodies in the Canadian Shield are similar to recent hydrothermal deposits and are interpreted as ancient Cyprus-type mineralization (Duke and Hutchinson, 1974; Large, 1977; Beaty and Taylor, 1982; Hall, 1982; Lydon, 1983; Franklin, 1984).

This paper describes the results of bulk rock major and trace element geochemistry, X-ray analyses of alteration minerals and microscopical examination of sulphide and silicate phases of CY-2a samples. Systematic studies were carried out on pyrite, chalcopyrite and sphalerite to determine variations in the trace element spectrum of sulphides with depth. Epidote was analyzed from the lower section of the core, and electron microprobe data for chlorite were obtained between 161 and 671 m.

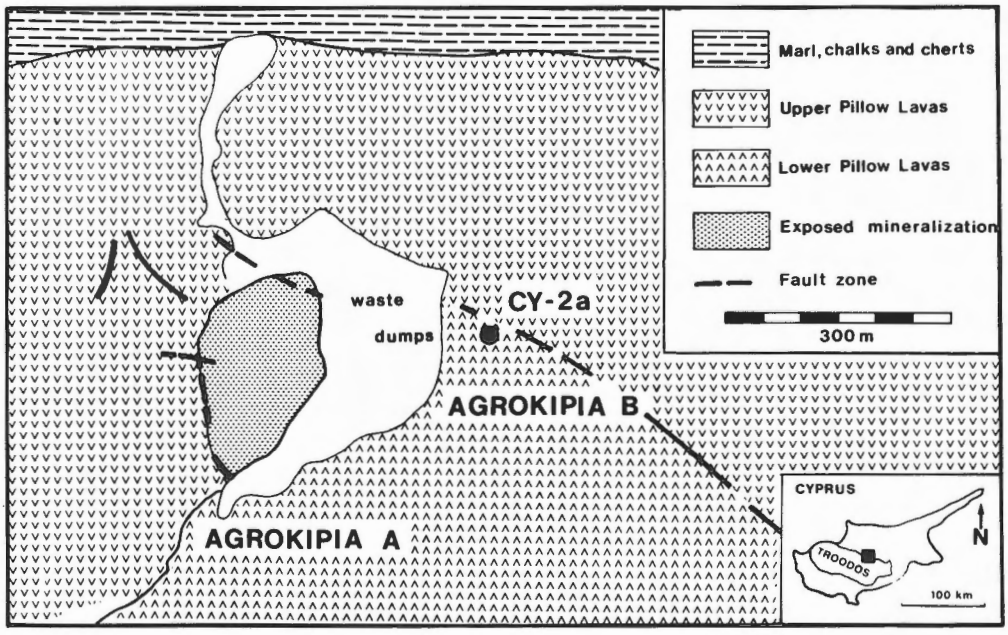

Figure 1: Geological map of the Agrokipia mining area. Drillsite CY-2a is located east of the Agrokipia 'A' open pit, directly above the buried Agrokipia 'B' ore body (modified after N.G. Adamides, unpub. rep., 1983).

GEOLOGICAL SETTING

The Agrokipia deposit, near the village of Agrokipia, Cyprus consists of the 'A' and 'B' ore bodies (Figure 1), which represent massive and stockwork-type mineralization, respectively (Herzig, 1982). The nearly mined-out massive ore of Agrokipia 'A' was located at the boundary between the conventionally called (Bear, 1963; Gass, 1960) Upper and Lower Pillow Lavas (Adamides, 1984). The stockwork mineralization of Agrokipia 'B' (avg. 20% S; 3% Zn+Cu) occurs at a depth of 154 m below surface at a lower stratigraphic level and is described as having been formed within the Lower Pillow Lavas (Adamides, 1984) or below this unit (D.L. Searle and G. Constantinou, unpub. rep., 1968). Adamides (1984) considered the Agrokipia 'A' deposit as a typical example of an exhalative massive ore body, in contrast to Agrokipia 'B', which represents a replacement deposit, entirely enclosed in the lava pile. Neither deposit shows evidence of major structural control, as is typical for most of the Cyprus deposits, but they may be linked by a fracture zone and therefore generated by the same hydrothermal fluid.

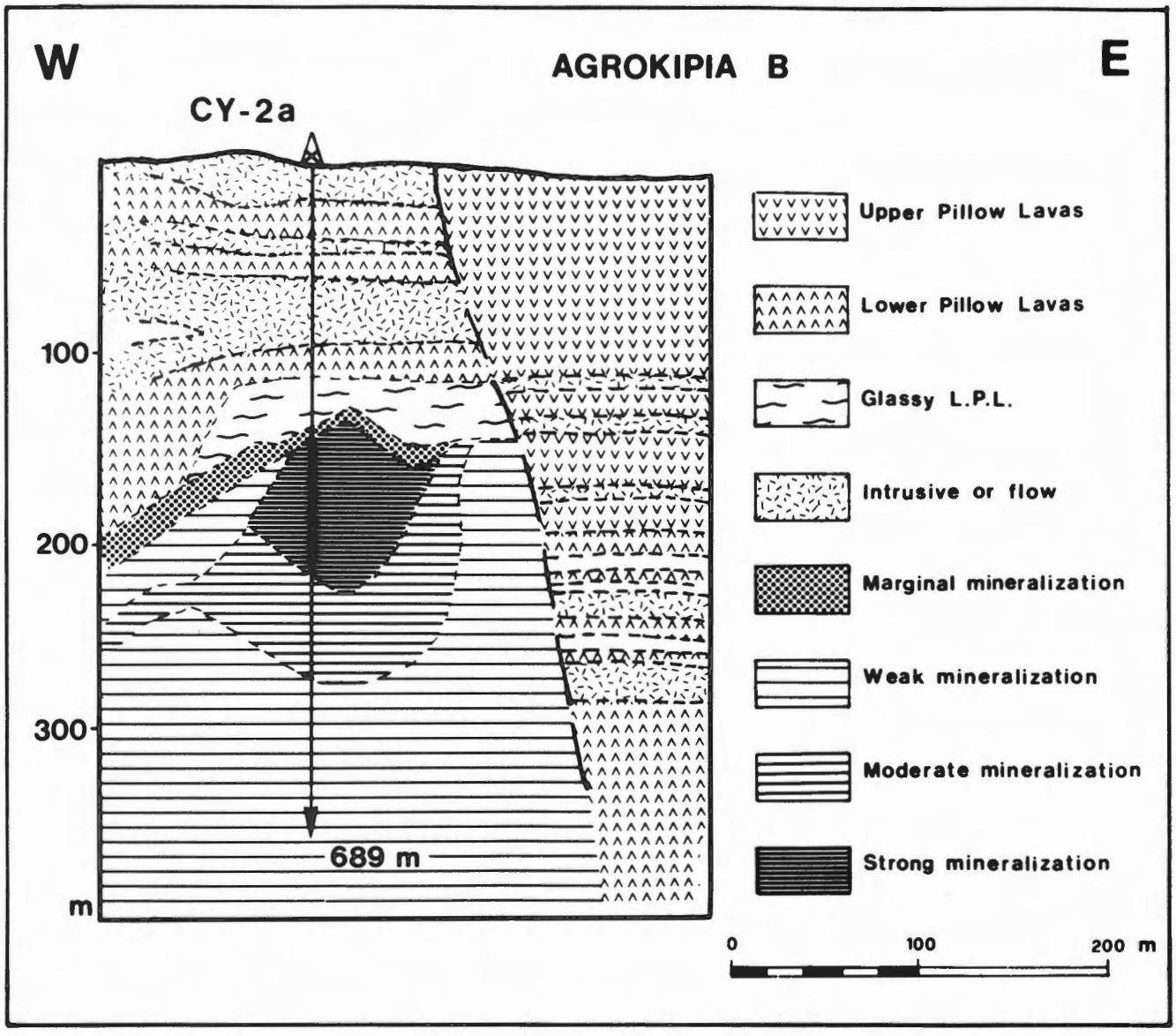

Figure 2: Geological cross section of the Agrokipia 'B' deposit, showing the position of Hole CY-2a. All data based on percussion exploration borehole information (modified after N.G. Adamides, unpub. rep., 1983).

DRILLSITE AND LITHOLOGY

The CY-2a drillsite is located at 35°02′40″N, 33°08′55″E in Lower Pillow Lavas east of the Agrokipia 'A' pit, south of a NW-SE tending fault zone (Figure 1). As shown in Figure 3, CY-2a penetrated six major lithological intervals (Robinson and Gibson, 1983; Robinson and Hall, 1983):

0-109 m:	concordant sills, flows and massive basalts
110-154 m:	alternating glassy and crystalline basalts
155-299 m:	highly altered sequences of massive flows and hyaloclastites
300-406 m:	altered dykes underlain by massive basalt
407-531 m:	pillowed and massive flows cut by dykes
532-689 m:	steeply inclined dykes

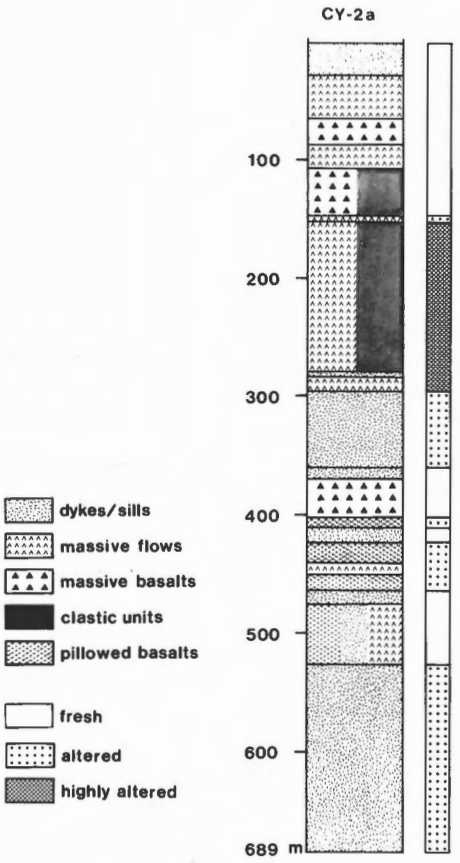

Figure 3: Lithological units and alteration zones of Hole CY-2a.

Low to medium grade stockwork-type mineralization with abundant fracture, cavity and groundmass sulphides is concentrated in the highly altered zone between 154 and 300 m and strongly decreases towards the base of the hole. Based on type and intensity of alteration, two basalt dykes cored at 281 m and 362 m, are interpreted as post-mineralization feeders for the uppermost lavas. According to Bednarz et al. (1987) the drilled sequence can be divided into an uppermost basaltic-andesitic (0-90 m) and a lower andesitic-dacitic series (90-689 m).

METHODS

Results described in this paper are based on the study of 330 minicores (2.5 cm in diameter), obtained by drilling perpendicular to the main core. From these minicores 38 thin sections and 45 polished sections were examined and described.

Further identification of secondary minerals was done on about 100 powdered bulk samples by X-ray diffraction using a Siemens D 500 unit with Cu Kα radiation. Selected samples were glycolated and heated for clay mineral determination.

About 70 silicate and 550 sulphide analyses were carried out on polished thin sections and polished sections using an ARL-SEMQ electron microprobe. Routine operating conditions were 15 or 20 kV initiation energy, 10 nA sample current, 10-20 sec. counting time, and a focused beam. The analyses were corrected using the modified program MAGIC IV (Colby, 1968). The reproducibility of the results is better than ±2%.

Bulk rock chemical analyses were carried out using a Philips PW 1400 X-ray fluorescence spectrometer with an on-line Philips PM 851 computer. For major element determination, samples were ignited at 1000°C for two hours to oxidize sulphide sulfur and the loss on ignition was determined. From the ignited samples, glass disks incorporating lithium tetra- and metaborate (rock to flux ratio 1:10) were made. The major element analyses have been recalculated using the LOI values. Trace element determinations were done on pressed powder pellets of the original samples. The analytical programs for major and trace element analyses are calibrated against a series of 20 international standard rock samples. For analytical quality control the internal ICRDG standards TRS 1-7 were analyzed.

Evaluation of microprobe and XRF data was done using the computer program MAX (Kottrup and Rehder, 1983) of the Federal Institute of Geosciences and Natural Resources (BGR), Hannover, FRG.

SECONDARY MINERAL DISTRIBUTION

To study the type and intensity of hydrothermal alteration and to estimate the paleotemperature gradient of the Agrokipia hydrothermal system, the distribution of secondary minerals in CY-2a has been determined (Figure 4). Four major alteration zones were established:

1. A low temperature alteration interval from 0-154 m ('uppermost lavas').
2. A mineralized, silicified and strongly argillized zone between 154-300 m ('mineralization').
3. A transition zone of propylitic alteration between 300-400 m ('propylitic zone').
4. A zone of lower greenschist facies alteration between 400-689 m ('greenschist facies zone').

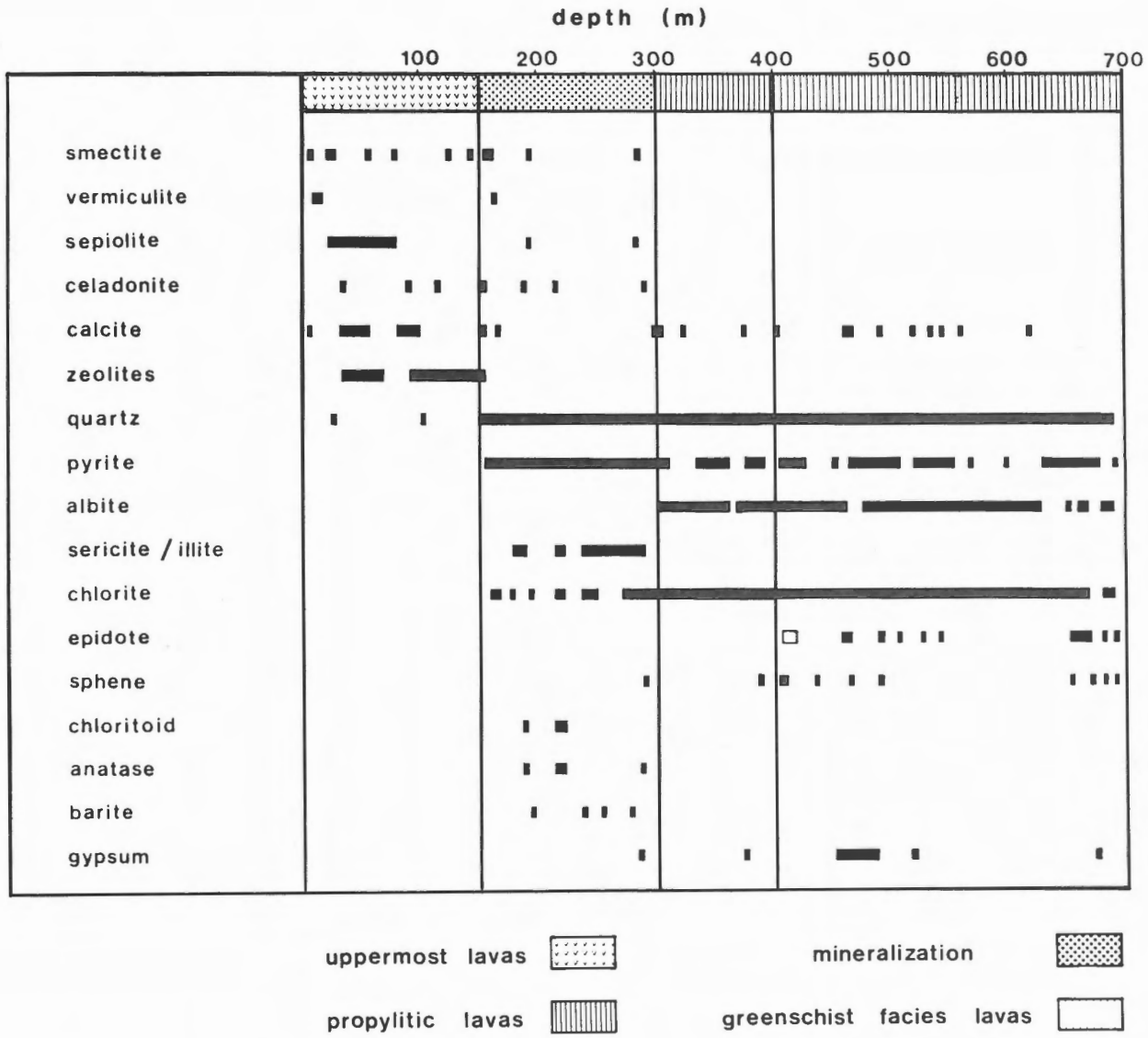

Figure 4: Downhole mineral distribution in Hole CY-2a. Alteration zones correspond to different mineral assemblages occurring with depth. The boundary between the propylitic and greenschist facies was drawn using the first occurrence of epidote at about 400 m.

Zone 1

Alteration in zone 1 is restricted to the formation of smectite-vermiculite, sepiolite, celadonite, zeolites and calcite occurring in veins and void spaces and replacing the groundmass. Smectite and celadonite replace most glassy and chilled margins, but fresh glass is preserved in places. Primary phases such as Ca-plagioclase, magnetite and rare pyroxene still occur. The distribution of zeolites is from Robinson and Gibson (1983), as zeolites were not identified in the study reported in this paper. Robinson et al. (1984) described laumontite from the transition between zones 1 and 2. Sodium and Ca-Na-K zeolites including analcime, natrolite, phillipsite and gmelinite were described by Gillis and Robinson (1985) from a stratigraphic level in the extrusive sequence SE of Agrokipia, equivalent to zone 1 of CY-2a. Sunkel et al. (1987) report heulandite and laumontite from the upper 154 m in CY-2a. The observed secondary minerals are typical of seawater-basalt interaction under relatively low temperature and oxidic to suboxidic conditions. Cann (1981) considered the development of celadonite as characteristic for sub-seafloor weathering of basalts. This type of basalt alteration is commonly described from shallow DSDP basement holes (Honnorez, 1981) and also from the upper zone of the DSDP hole 504B (Anderson et al., 1982).

Zone 2

Zone 2 represents an intensively altered and silicified horizon with abundant sulphide mineralization and almost complete destruction of the primary host rock minerals. Pyrite-quartz veins, locally associated with sphalerite, minor chalcopyrite and red jasper predominate in the extensively bleached and argillized lavas. Massive pyrite ore is restricted to highly leached and brecciated zones of altered glass. In less altered, originally massive lavas, both disseminated pyrite and pyrite in vesicles are common. Locally, the ore is pervasively silicified, but concentrations of quartz also occur with minor mineralization. Red jasper and hematite-bearing quartz replace sulphides between 165-186 m, 234-272 m and 283-297 m in the core (cf. Figure 10), but disseminated pyrite in red jasper also occurs. Throughout zone 2, the sulphide-quartz assemblage is commonly accompanied by sericite/illite and abundant chlorite. The secondary mineral assemblage and the almost complete destruction of primary phases indicate alteration under elevated temperatures and high water/rock ratios. This coincides with Sr-isotope data of Rommel and Friedrichsen (1987) who calculated water/rock ratios of 2.8 ± 1.7 above and 12.1 ± 3.0 below 154 m. In addition, chloritoid (186-223 m), barite (192-275 m), gypsum (282 and 286 m), and prehnite (186 m) were identified. Anatase and/or rutile replace titanomagnetite. Native sulfur was detected by XRD at 235 m depth in highly altered host rock, on both sides of a 5 mm thick pyrite vein.

Low temperature minerals like smectite-vermiculite, sepiolite, celadonite, zeolites, calcite and mixed layers are also found in the high temperature alteration environment of zone 2. These secondary minerals are considered as late stage, low temperature products, which are superimposed on the previously formed high temperature mineral suite, probably during the waning stage of hydrothermal activity.

Zone 3

A propylitic style of alteration predominates in zone 3, superimposed on a dyke sequence between 300-400 m. The main alteration products are chlorite and quartz, accompanied by albite and low grade disseminated pyrite. Albite replacing Ca-plagioclase was first observed at 300 m. Various mixtures of this alteration assemblage replace the primary minerals. Vesicles are lined or partly to completely filled with chlorite. Also quartz, pyrite, minor calcite and gypsum occur in void spaces. The groundmass is uniformly altered to chlorite, quartz, albite and disseminated pyrite.

Zone 4

In zone 4, from about 400 m to the base of the hole at 689 m, the mineral assemblage epidote + chlorite + albite + sphene + calcite is developed, associated with fracture-filling quartz and minor sulphides. In thin sections and X-ray diffraction diagrams epidote was first positively identified at 462 m. Robinson and Gibson (1983) indicated that epidote was first observed in the core at about 400 m. Thus, it can be assumed that epidote first appears somewhere in the interval between 400-462 m. Veins in deeper levels of this alteration zone are filled with chlorite, epidote, quartz and pyrite, followed by calcite and gypsum. Vesicle fillings commonly consist of early chlorite, lining or partly filling the vesicles and later epidote, overgrowing the chlorite. Some vesicles almost completely filled with chlorite and minor epidote or quartz + chlorite + epidote are present. Epidote and sphene, as well as chlorite, albite and quartz, replace the groundmass. Gypsum is concentrated between 450-516 m, and is associated with anhydrite between 452-458 m. The assemblage of secondary minerals found in zone 4 indicates lower greenschist facies conditions (Elthon, 1981). This alteration grade starts about 100 m above the extrusive/intrusive boundary at about 530 m.

ALTERATION TEMPERATURES

Based on magnetic properties, Hall et al. (1987) divided the uppermost 154 m of the core into two alteration zones, assuming cold (about 10°C) seawater alteration for the interval between 0-149 m and alteration temperatures of about 200°C for the transition zone (149-154 m).

The occurrence of laumontite (Robinson et al., 1984) in this transition zone also points to elevated alteration temperatures. Palmason et al. (1979) assigned a stability range of 100-200°C for laumontite found in geothermal areas of Iceland. Henley and Ellis (1983) observed laumontite to be stable between about 140-230°C in active geothermal systems, whereas experimental data of Liou (1971) indicate a stability range of 150-300°C.

Oxygen and hydrogen isotope ratios of whole rock and mineral separates (smectite, chlorite/illite, quartz) have revealed alteration temperatures between 60-150°C for the upper 154 m of the hole (Rommel and Friedrichsen, 1987). The absence of very low temperature zeolites in the uppermost zone (Sunkel et al., 1987) also indicates a minimum temperature of 50°C (Evarts and Schiffmann, 1983). These findings, to some extent, support the temperature estimates of Hall et al. (1987) for the transition zone, but suggest much higher temperatures than they assumed for the upper 149 m. Heulandite reported from 126 m by Hall et al. (1987) indicates alteration temperatures of 100-115°C (Henley and Ellis, 1983) at this depth, which agrees with the isotope data reported by Rommel and Friedrichsen (1987). Nevertheless a rise in alteration temperature from about 125°C to approximately 150°C can be estimated for the interval between 149 and 154 m (Figure 5).

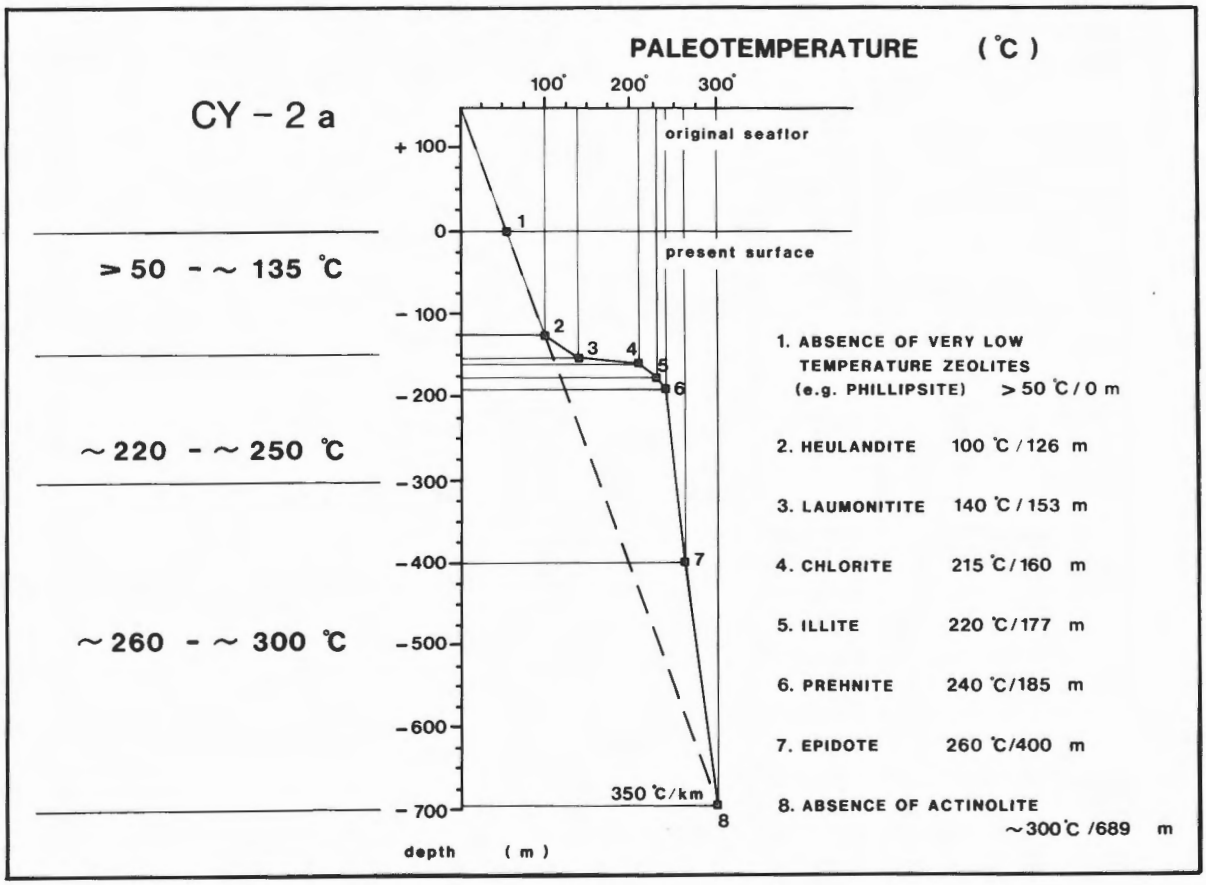

Figure 5: Paleotemperature curve based on the occurrence of various secondary minerals in Hole CY-2a. A fossil geothermal gradient of 350°C/km was calculated assuming that the top of the hole was about 150 m below the original seafloor.

The first appearance of chlorite at 160 m points to a minimum alteration temperature of 200-230°C (Tomasson and Kristmannsdottir, 1972; Steiner, 1968; Kristmannsdottir, 1976). In natural geothermal systems, illite first becomes stable at about 210-230°C (Henley and Ellis, 1983; Ellis, 1979). The first occurrence of illite at 177 m and prehnite at 185 m with formation temperatures about 240°C (Exley, 1982) supports the temperature estimation of about 225°C for the upper level (160-190 m) of the mineralized zone. Anatase, first observed at 186 m in CY-2a, coincides with an alteration temperature of probably more than 250°C, estimated by Hall (1985) for Fe-Ti oxide alteration in Iceland.

Epidote first occurs between 400 and 465 m depth, indicating paleotemperatures of at least 260°C (Browne and Ellis, 1970; Liou, 1973; Palmason et al., 1979), whereas oxygen and hydrogen isotope data indicate alteration at 310-430°C for the zone below 154 m (Rommel and Friedrichsen, 1987). Due to the absence of actinolite, which was identified neither in thin sections nor in XRD analyses, alteration temperatures at the base of CY-2a should not have exceeded 300-320°C (Ellis, 1979; Elthon, 1981). Anderson et al. (1982) estimated an alteration temperature of at least 230°C for the paragenesis chlorite + sphene + albite + epidote + quartz, and >280°C where actinolite is present. According to the average isotope data of Rommel and Friedrichsen (1987), the ascending hydrothermal fluids had initial temperatures of about 390°C.

Based on the above calculations using the first occurrence of various temperature sensitive secondary minerals, a paleothermal gradient of 350°C/km can be assumed for the hydrothermal system of Agrokipia 'B' (Figure 5). The alteration mineral stability temperatures used in this calculation are from experimental equilibrium reactions (e.g. Liou, 1971; 1973), and measured temperatures in geothermal bore holes (e.g. Palmason et al., 1979). A linear extrapolation of the temperature gradient would imply a maximum depth of the magma chamber at about 3.5 km, but most likely the magma occurred at a much shallower level. Reid et al. (1977) and Lewis and Garmany (1982), show that segments of the East Pacific Rise are underlain by a magma chamber at a depth of about 1.5 km.

COMPOSITIONS OF CHLORITE AND EPIDOTE

Chlorite and epidote compositions were studied by electron microprobe analyses. About 70 measurements on epidote between 488 and 681 m were carried out. Forty-one chlorites from six samples between 161-671 m were analyzed to obtain variations in chlorite composition with depth.

Chlorite

Chlorites predominantly occur as groundmass replacements and vesicle linings or fillings. Optically, they are light green and show brownish to bluish interference colour.

Selected analyses of representative chlorite are presented in Table 1, and Table 2 shows data on mean, maximum and minimum values. In Figure 6 the variability in the average Mg/(Mg+Fe) ratios of the analyzed chlorites is shown. No compositional variation with depth was found. Following the classification given by Riverin (1977) and Exley (1982), all chlorites can be classified as Mg-rich (Figure 6). In Figure 7, which shows Si atoms per formula unit against $Fe^{2+}/(Mg+Fe^{2+})$ per formula unit, the chlorites plot in the compositional fields of pycnochlorites and subordinate brunsvigites (Hey, 1954), showing $Fe^{2+}/(Mg+Fe^{2+})$ ratios of 0.37-0.58.

The average CaO content of the chlorites ranges from 0.05-0.26 wt.%. As already pointed out by Exley (1982), chlorite is the most important depositional site for Mn amongst the hydrothermal alteration minerals. Compared to chlorites from the Reydarfjordur drillcore, Iceland, with a mean of 0.47 wt.% MnO (Exley, 1982), the chlorites from CY-2a are considerably enriched in MnO with a mean of 0.75 wt.% and a maximum of 1.10 wt.%.

In the Al_2O_3-FeO_t-MgO ternary plot, the chlorites from CY-2a show a relatively close grouping (Figure 8) with FeO_t of 20.60-28.63 wt.%, MgO ranging from 10.65-20.67 wt.% and Al_2O_3 between 17.19-21.36 wt.%. Compared to chlorites from hydrothermal quartz- and sulphide-bearing greenstones from the Mid Atlantic Ridge (Delaney et al., 1980) and chlorites from DSDP metabasalts (Pritchard, 1979), the chlorites analyzed from CY-2a are characterized by intermediate FeO_t and similar MgO values. Chlorites from experimental seawater/basalt reactions in a water dominated system with water/rock ratios between 50-125 (Seyfried and Mottl, 1982) and from oceanic metabasalts (Pritchard, 1979) differ from those analyzed from CY-2a by their higher MgO contents (Figure 8). This suggests that the Mg/Fe ratio of chlorites is related to the seawater/fluid ratio; Mg-rich chlorites form under conditions where large amounts of seawater are heated up during wall rock reaction with hot, ore-forming fluids, or simply by the high geothermal gradient, whereas Mg-poor chlorites form by ascending, pure hydrothermal fluids, which carry dissolved Fe but almost no Mg (Edmond et al., 1982; Michard et al., 1984).

TABLE 1. Representative Microprobe Data of Chlorite from Drillcore CY-2a.

	1	2	3	4	5	6	7	8	9
				Analyses as Oxides, wt.%					
SiO_2	27.26	27.48	27.42	27.39	27.86	27.29	27.92	28.73	27.96
Al_2O_3	19.31	19.51	19.27	20.40	18.60	19.90	18.48	17.55	17.90
FeO	28.17	27.75	28.63	21.98	22.24	22.41	27.09	25.94	26.35
MnO	0.82	0.80	0.76	0.67	0.73	0.59	1.10	0.88	0.94
MgO	11.81	11.42	10.73	17.59	18.34	17.46	15.20	16.43	16.02
CaO	0.28	0.20	0.20	0.08	0.04	0.09	0.08	0.09	0.08
Total	87.65	87.16	87.00	88.12	87.81	87.73	89.87	89.62	89.25
				Structural Formula Based on 28 Oxygens					
Si	5.835	5.893	5.919	5.634	5.770	5.655	5.797	5.936	5.826
Al(IV)	2.165	2.107	2.081	2.366	2.230	2.345	2.203	2.064	2.174
Al(VI)	2.707	2.824	2.822	2.537	2.310	2.515	2.320	2.210	2.223
Fe^{2+}	5.043	4.977	5.169	3.872	3.851	3.884	4.704	4.482	4.592
Mn	0.149	0.145	0.139	0.117	0.128	0.104	0.193	0.154	0.166
Mg	3.768	3.650	3.453	5.394	5.661	5.393	4.705	5.060	4.976
Ca	0.064	0.046	0.046	0.018	0.008	0.020	0.018	0.020	0.018
Total	19.729	19.641	19.629	19.891	19.959	19.915	19.940	19.926	19.975

	10	11	12	13	14	15	16	17	18
				Analyses as Oxides, wt.%					
SiO_2	27.26	27.52	27.51	28.49	27.96	27.28	27.94	27.66	26.72
Al_2O_3	19.12	19.11	18.60	21.24	20.52	20.84	19.90	18.81	19.77
FeO	21.30	21.02	21.02	25.04	24.35	24.48	24.94	24.14	23.81
MnO	0.73	0.70	0.73	0.67	0.68	0.65	0.79	0.65	0.75
MgO	20.67	20.34	20.08	16.70	17.10	16.97	15.98	17.18	16.13
CaO	0.06	0.05	0.05	0.06	0.04	0.04	0.06	0.03	0.08
Total	89.13	88.75	87.99	92.21	90.64	90.25	89.62	88.46	87.26
				Structural Formula Based on 28 Oxygens					
Si	5.546	5.609	5.660	5.658	5.645	5.544	5.732	5.739	5.622
Al(IV)	2.454	2.391	2.340	2.342	2.355	2.456	2.268	2.261	2.378
Al(VI)	2.131	2.200	2.171	2.630	2.529	2.536	2.544	2.199	2.525
Fe^{2+}	3.624	3.583	3.617	4.159	4.112	4.161	4.279	4.189	4.190
Mn	0.126	0.121	0.127	0.113	0.116	0.112	0.137	0.114	0.134
Mg	6.268	6.180	6.159	4.944	5.147	5.141	4.887	5.313	5.059
Ca	0.013	0.011	0.011	0.013	0.008	0.008	0.013	0.006	0.018
Total	20.161	20.095	20.084	19.856	19.912	19.958	19.861	19.960	19.926

Total Fe expressed as FeO, Samples 1-3: 161.00 m depth, samples 4-6: 297.90 m depth, samples 7-9: 386.45 m depth, samples 10-12: 487.88 m depth, samples 13-15: 541.15 m depth, samples 16-18: 670.99 m depth.

TABLE 2. Average and Range of Composition of Chlorite from Drillcore CY-2a.

Depth (m)	n	SiO_2 mean	min max	Al_2O_3 mean	min max	FeO mean	min max	MnO mean	min max	MgO mean	min max	CaO mean	min max
			25.97		18.89		25.94		0.72		10.65		0.20
161.00	7	27.59	30.10	19.21	19.51	27.35	28.63	0.77	0.82	11.12	11.81	0.26	0.31
			26.81		18.60		20.64		0.59		17.46		0.04
297.90	6	27.38	27.86	19.78	20.40	21.67	22.41	0.67	0.73	18.12	18.88	0.08	0.10
			26.66		17.19		25.71		0.85		15.20		0.08
386.45	6	27.83	28.73	17.92	18.48	26.42	27.18	0.97	1.10	15.89	16.43	0.13	0.32
			26.87		17.79		20.60		0.69		19.23		0.01
487.88	6	27.36	27.82	18.51	19.12	20.90	21.30	0.72	0.74	20.09	20.67	0.07	0.22
			26.69		20.09		23.98		0.65		15.89		0.04
541.15	7	27.52	28.49	20.93	21.36	24.45	25.04	0.66	0.69	16.60	17.10	0.05	0.07
			24.98		18.54		22.15		0.65		15.18		0.03
670.99	9	26.83	27.94	19.02	19.90	23.22	24.94	0.70	0.79	16.68	17.21	0.07	0.10

Total Fe expressed as FeO, n: number of analyses

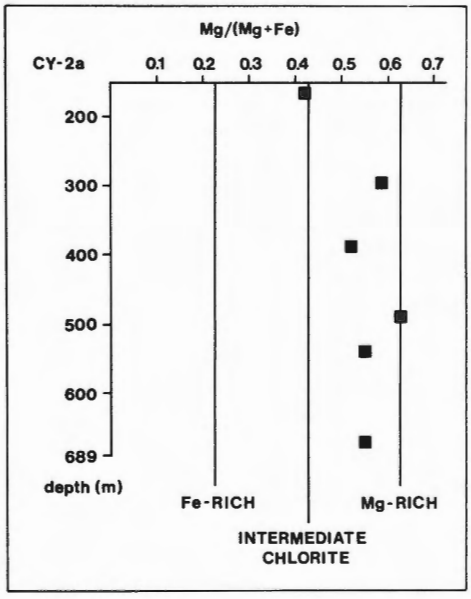

Figure 6: Variation in the Mg/(Mg+Fe) ratio of chlorites from Hole CY-2a. Chlorite classification according to Riverin (1977).

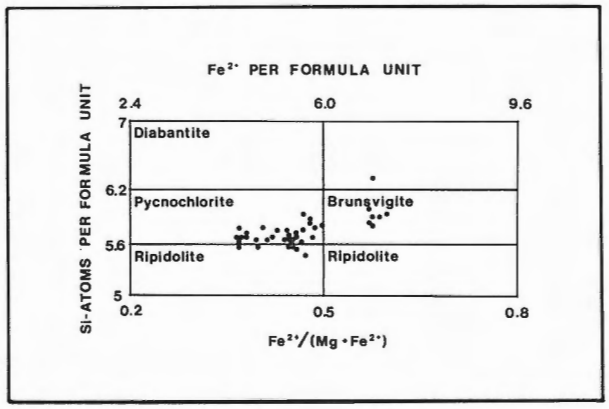

Figure 7: Compositional variation of chlorites from Hole CY-2a. Classification after Hey (1954).

Epidote

Epidotes occur mainly as fan-shaped and six-sided, prismatic crystals up to 100 μm across in vesicles where they are often associated with chlorite. Granular aggregates are less common. Greenish-yellow to bluish-pink interference colours are characteristic.

Representative analyses are listed in Table 3, and mean, maximum and minimum values in Table 4. The epidotes vary in Fe_2O_3 and Al_2O_3 contents between 12.04-19.14 wt.% (mean 15.19 wt.%) and 19.25-26.44 wt.% (mean 22.82 wt.%), respectively. MnO has a maximum of 0.77 wt.% with an average of 0.36 wt.%. Mg-rich epidote, with up to 1.0 wt.% MgO, occurs at 488 m depth, but the mean value is 0.16 wt.%. Like chlorite, epidote is an important carrier of Mn. However, the amount of MnO incorporated in chlorite (mean 0.75 wt.%) is about twice the average content of epidote (0.36 wt.%).

The data on epidote chemistry suggest a decrease of the Fe/Al ratio with depth. However, some of this variation may be due to zonation within individual crystals, as described by Viereck et al. (1982). In many cases, the variation in the Fe/Al ratio in individual epidote crystals is larger than the variation between averaged ratios from different epidote samples (Exley, 1982).

Holdaway (1972) used the P_s value, calculated from the cation ratio $(Fe^{3+}/(Fe^{3+}+Al))*100$, to describe epidote composition, and demonstrated that it largely varies as a function of oxygen fugacity (Keith et al., 1968). This is supported by Liou (1973) who showed that epidote is most Fe-rich (P_s 33 ± 2) at high fO_2, and becomes progressively more aluminous (P_s 25 ± 3) in a reducing environment. Liou (1973) also pointed out that increasing fO_2 causes an enlargement of the epidote stability field and a considerable decrease in the minimum formation temperature. Epidote zonation or Fe-depleted rims as observed by Exley (1982) and Viereck et al. (1982) may therefore be due to variation in the oxygen fugacity of the altering solutions with time.

The data obtained from the epidotes of CY-2a coincide with the conclusions drawn by Liou (1973). The P_s value within the Sheeted Dyke Complex (i.e. below 530 m) decreases from P_s 36 at 555 m to P_s 23 at 681 m (Figure 9), which is consistent with lower oxygen fugacity assumed for deeper levels of the hydrothermal system. However, data between 488-516 m indicate an inconsistent variation in the Fe/Al ratio, which may be attributed to the change in lithology from a well permeable sequence of pillows, flows and dykes to a pure dyke series.

Oxygen fugacity, temperature and fluid composition all control the stability and composition of epidote, but wall rock composition, reactivity and permeability are additional important factors for the introduction of elements into secondary minerals like epidote. High pressure is not required for the formation of epidote in hydrothermal environments. As shown in active geothermal areas, epidote occurs at pressures of less than 500 bars (Keith et al., 1968).

ORE MINERAL PARAGENESIS

In order to obtain data on the ore mineral paragenesis occurring in CY-2a samples, 45 selected polished sections from 31-669 m were examined. The distribution of different ore minerals and red jasper in relation to depth and alteration zones of CY-2a is shown in Figure 10.

The ore mineral assemblage of the stockwork zone consists predominantly of pyrite, accompanied by varying amounts of sphalerite, less chalcopyrite and minor but widespread pyrrhotite. No abrupt changes in the ore mineral assemblage with depth were observed. Pyrite occurs continuously below 154 m, either in veins and vesicles or disseminated in the groundmass. Chalcopyrite and sphalerite are mainly restricted to the highly mineralized zone between 154-300 m, but in the greenschist facies zone they occur chiefly as minute inclusions in pyrite. Pyrrhotite was found exclusively as inclusions in pyrite, particularly from 198-334 m and below 550 m. Marcasite and galena are accessory minerals. Sulphide veins associated with red jasper or hematite-bearing quartz are common between 165-297 m. Generally, the intensity of mineralization decreases with depth, though pyrite with minor inclusions of chalcopyrite, sphalerite or pyrrhotite is present down to the bottom of CY-2a.

Pyrite

Pyrite occurs as early euhedral and late anhedral grains up to 500 μm in diameter. The grains are massive or highly porous and locally brecciated, but with only minor displacement of the fragments. Also, distinctly zoned crystals of alternating massive and porous pyrite were observed. Melnikovite pyrite occurs in large grains of massive pyrite (Figure 11a) and concentric shrinkage cracks of colloform pyrites are commonly filled with sphalerite and silicate minerals. Early pyrite is often replaced by quartz and red jasper, whereas late pyrite contains euhedral quartz crystals and is disseminated in red jasper. Both chalcopyrite (Figure 11b) and sphalerite (Figure 11c) marginally replace pyrite in several cases. Inclusions of chalcopyrite, sphalerite and silicate minerals are generally common and pyrite also carries minor inclusions of pyrrhotite (< 30 μm). Silicate mineral inclusions are often concentrated in the cores of pyrite crystals. Marcasite may occur as anhedral masses intergrown with pyrite or as individual grains. Optically, the majority of the pyrite grains show unusual anisotropy.

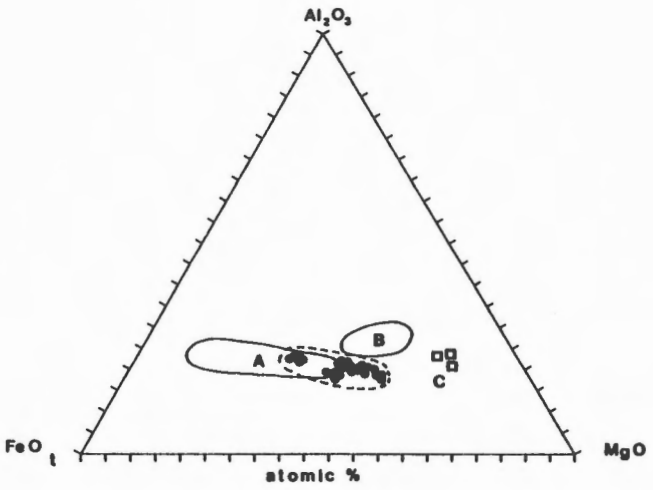

Figure 8: Al_2O_3-FeO_t-MgO ternary diagram of chlorites from Hole CY-2a (black dots). For comparison, sulphide-bearing greenstones (A) (Delaney et al., 1980), chlorites from DSDP-metabasalts (B) (Pritchard, 1979) and chlorites from experimental seawater/basalt reactions (C) (Seyfried and Mottl, 1982) are plotted. Total Fe expressed as FeO.

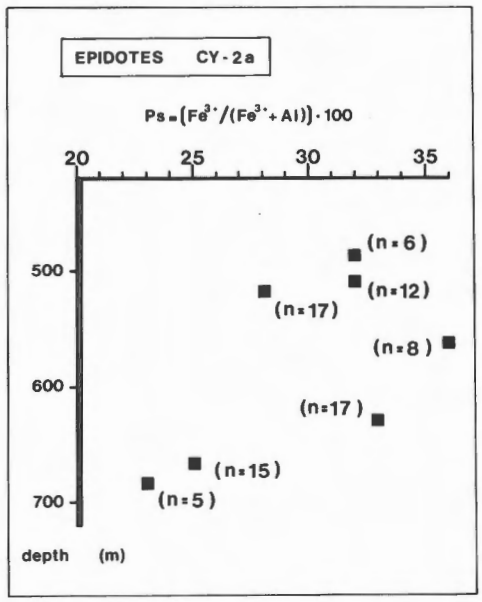

Figure 9: Variation in the P_s value (P_s = $(Fe^{3+}/(Fe^{3+}+Al))*100$; Holdaway, 1972) of epidotes between 488 m and 681 m in Hole CY-2a.

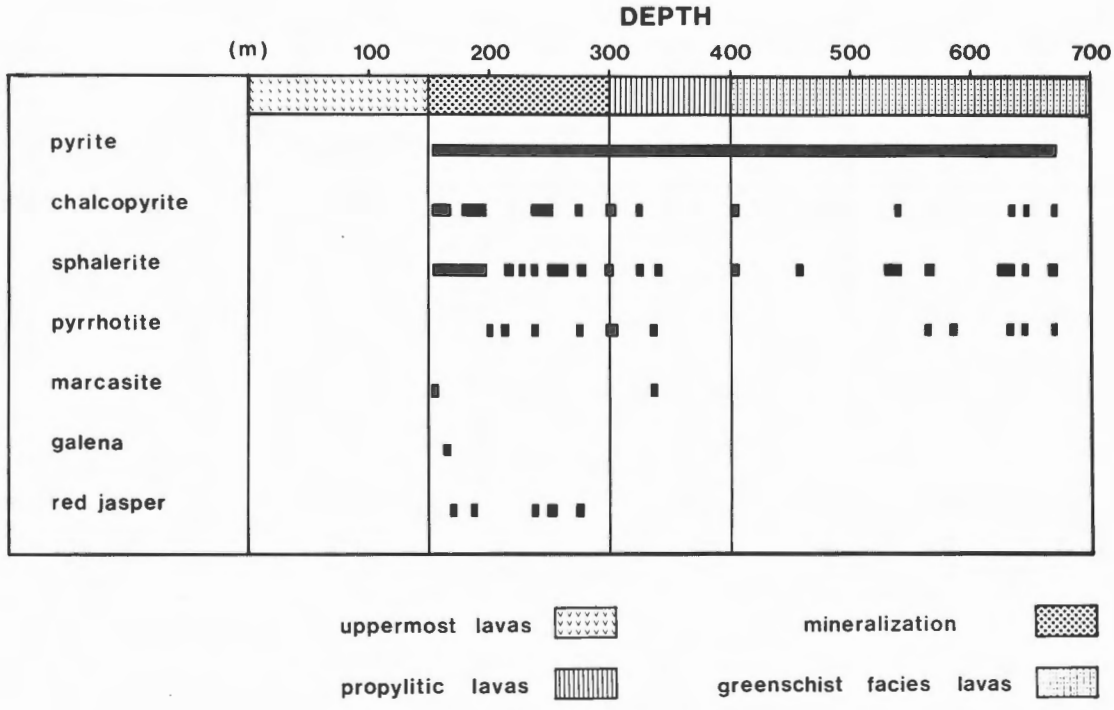

Figure 10: Ore mineral paragenesis and occurrence of red jasper in Hole CY-2a.

TABLE 3. Representative Microprobe Data of Epidote from Drillcore CY-2a.

	1	2	3	4	5	6	7	8	9
				Analyses as Oxides, wt.%					
SiO_2	38.77	38.39	37.68	37.00	36.76	38.39	38.16	37.31	38.61
Al_2O_3	22.55	22.24	21.62	22.40	21.28	21.52	22.34	22.81	24.14
Fe_2O_3	15.76	15.94	17.03	15.74	17.41	17.04	16.10	15.58	13.82
MnO	0.34	0.35	0.24	0.40	0.18	0.43	0.72	0.33	0.31
MgO	1.00	0.41	0.21	0.32	0.25	0.05	0.11	0.06	0.09
CaO	21.39	21.89	22.55	22.33	22.46	22.46	22.09	22.71	22.90
Total	99.81	99.23	99.32	98.20	98.33	99.89	99.52	98.80	99.87
				Structural Formula Based on 25 Oxygens					
Si	6.062	6.057	5.981	5.925	5.914	6.053	6.040	5.932	6.033
Al	4.156	4.136	4.045	4.228	4.035	3.999	4.143	4.274	4.445
Fe^{3+}	1.854	1.893	2.035	1.897	2.108	2.022	1.906	1.864	1.625
Mn	0.045	0.047	0.032	0.054	0.025	0.057	0.096	0.044	0.041
Mg	0.233	0.096	0.050	0.076	0.060	0.012	0.026	0.014	0.021
Ca	3.583	3.701	3.836	3.832	3.872	3.794	3.724	3.869	3.767
Total	15.933	15.928	15.978	16.012	16.013	15.937	15.935	15.998	15.932

	10	11	12	13	14	15	16	17	18
				Analyses as Oxides, wt.%					
SiO_2	37.96	37.28	38.07	36.92	36.09	38.15	37.45	36.68	39.06
Al_2O_3	23.72	23.79	20.38	20.55	19.26	22.22	19.86	21.70	25.60
Fe_2O_3	14.50	15.14	17.47	16.87	18.55	15.20	17.58	15.59	13.19
MnO	0.40	0.16	0.33	0.28	0.14	0.34	0.26	0.36	0.37
MgO	0.10	0.08	0.19	0.22	0.14	0.10	0.11	0.14	0.09
CaO	22.67	23.11	22.71	22.81	22.98	22.32	22.16	22.09	22.62
Total	99.35	99.56	97.40	95.97	95.31	98.33	97.42	96.56	100.94
				Structural Formula Based on 25 Oxygens					
Si	5.968	5.872	6.070	5.985	5.934	6.071	6.080	5.974	5.992
Al	4.396	4.416	3.830	3.926	3.732	4.168	3.800	4.165	4.629
Fe^{3+}	1.716	1.794	2.096	2.058	2.295	1.820	2.148	1.911	1.523
Mn	0.053	0.021	0.045	0.038	0.020	0.046	0.036	0.050	0.048
Mg	0.023	0.019	0.045	0.054	0.025	0.024	0.027	0.034	0.021
Ca	3.819	3.900	3.880	3.961	4.048	3.806	3.855	3.855	3.718
Total	15.975	16.022	15.967	16.022	16.053	15.935	15.946	15.989	15.931

	19	20	21	22	23	24	25	26	27
					Analyses as Oxides, wt.%				
SiO_2	38.16	38.59	38.88	38.81	38.96	38.55	38.28	38.26	36.94
Al_2O_3	25.32	25.71	25.72	23.81	27.03	25.76	26.64	25.30	24.83
Fe_2O_3	13.38	12.34	13.12	14.32	10.08	12.27	11.27	12.69	13.54
MnO	0.77	0.46	0.51	0.54	0.49	0.61	0.63	0.49	0.11
MgO	0.10	0.14	0.13	0.14	0.02	0.22	0.02	0.14	0.02
CaO	23.17	23.34	22.86	22.92	22.61	22.23	22.26	22.18	22.79
Total	100.90	100.59	101.22	100.53	99.19	99.64	99.10	99.05	98.22
					Structural Formula Based on 25 Oxygens				
Si	5.895	5.949	5.957	6.022	6.021	5.980	5.952	5.979	5.859
Al	4.611	4.672	4.645	4.355	4.924	4.710	4.882	4.661	4.642
Fe^{3+}	1.556	1.432	1.513	1.672	1.172	1.432	1.319	1.493	1.616
Mn	0.101	0.060	0.066	0.071	0.064	0.080	0.083	0.065	0.015
Mg	0.023	0.032	0.030	0.032	0.004	0.051	0.004	0.033	0.004
Ca	3.836	3.855	3.753	3.811	3.744	3.695	3.708	3.714	3.873
Total	16.020	15.999	15.963	15.963	15.929	15.948	15.947	15.943	16.010

Total Fe expressed as Fe_2O_3 (recalculated from FeO), samples 1-5: 487.88 m depth, samples 6-8: 508.09 m depth, samples 9-11: 516.09 m depth, samples 12-14: 554.54 m depth, samples 15-17: 631.20 m depth, samples 18-22: 666.49 m depth, samples 23-27: 680.60 m depth.

TABLE 4. Average and Range of Composition of Epidote from Drillcore CY-2a.

Depth (m)	n	SiO_2 mean	min max	Al_2O_3 mean	min max	Fe_2O_3 mean	min max	MnO mean	min max	MgO mean	min max	CaO mean	min max
			36.57		21.28		15.74		0.18		0.19		21.39
487.88	6	37.53	38.77	21.93	22.55	16.43	17.41	0.28	0.40	0.40	1.00	22.21	22.64
			37.31		21.52		15.42		0.33		0.02		22.09
508.09	12	37.99	38.40	22.39	22.97	16.09	17.04	0.43	0.72	0.06	0.11	22.50	22.71
			37.28		23.31		13.61		0.14		0.07		22.47
516.09	17	37.95	38.61	23.77	24.21	14.42	15.14	0.31	0.47	0.10	0.14	22.80	23.22
			36.09		19.25		16.08		0.14		0.13		21.81
554.54	8	37.03	38.07	19.86	20.55	17.75	19.14	0.20	0.33	0.23	0.72	22.70	23.07
			36.68		19.86		13.64		0.26		0.05		21.69
631.20	17	37.43	38.15	21.66	22.87	15.41	17.82	0.35	0.48	0.12	0.16	22.10	22.57
			37.69		22.55		12.34		0.17		0.09		22.05
666.49	15	38.70	39.67	24.46	25.72	13.72	15.74	0.45	0.77	0.13	0.18	22.89	23.46
			36.36		24.83		12.04		0.11		0.02		21.87
680.60	5	37.40	38.55	25.70	26.44	12.53	13.54	0.47	0.69	0.10	0.22	22.25	22.79

Total Fe expressed as Fe_2O_3, n: number of analyses

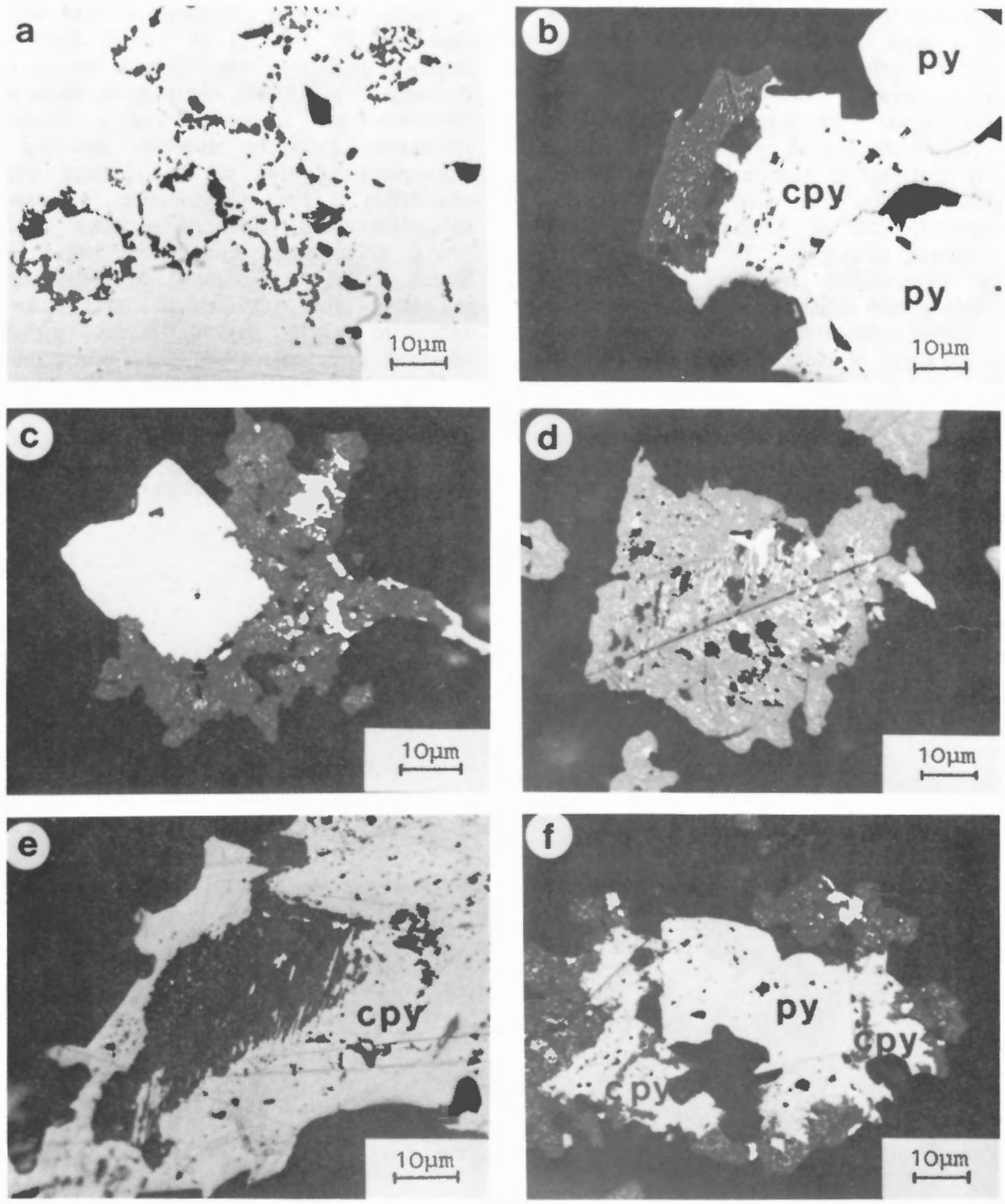

Figure 11: Photomicrographs (PPL, oil immersion) of sulphides from Hole CY-2a. a) 192.95 m: Early melnikovite pyrite surrounded by shrinkage cracks and embedded in later massive pyrite. b) 166.42 m: Subhedral pyrite (py) partly replaced by chalcopyrite (cpy) which is intergrown with sphalerite (dark grey) within quartz gangue. The sphalerite has abundant orientated blebs and spindles of chalcopyrite. c) 166.42 m: Sphalerite (dark grey) replacing euhedral pyrite. Sphalerite is associated with chalcopyrite and carries abundant chalcopyrite inclusions. d) 166.42 m: Sphalerite twin showing a herring-bone texture of chalcopyrite laths and blebs. e) 166.42 m: Comb-like intergrown texture of anhedral sphalerite (dark-grey) and chalcopyrite (cpy). Sphalerite carries orientated chalcopyrite blebs and laths. f) 166.42 m: Anhedral pyrite (py), partly replaced by chalcopyrite (cpy) and sphalerite (dark-grey). Chalcopyrite in turn is replaced by sphalerite, carrying blebs of chalcopyrite.

Chalcopyrite

Chalcopyrite is the only Cu-sulphide observed in the core. It is most abundant between 155-323 m, where it may form anhedral grains up to 200 μm in diameter in a quartz matrix. It also occurs interstitially to pyrite and sphalerite, enclosed in sphalerite, or filling cavities in pyrite. Below 530 m chalcopyrite is restricted to minute blebs (< 20 μm) in pyrite. Chalcopyrite often corrodes and replaces pyrite between 150-200 m (Figure 11b) and is replaced by quartz throughout the whole zone, as indicated by quartz-filled fractures or marginal corrosion. Chalcopyrite lamellae (< 10 μm) occur in sphalerite in three orientations. Also chalcopyrite inclusions in the form of blebs or fine dust (<< 1 μm) are common between 161-198 m. A twinned crystal of sphalerite displays a herring-bone texture of chalcopyrite laths and blebs which are orientated at 120 degrees and bisected by the trace of the twin plane (Figure 11d). Commonly, the chalcopyrite laths or spindles are concentrated in the central parts of sphalerite grains, whereas the margins are almost free of them. Almost identical features were recently described by Ixer et al. (1984) from the Oman sulphide deposits. According to Barton (1978) and Eldridge et al. (1983), chalcopyrite blebs and rods in sphalerite are interpreted as a replacement of sphalerite, probably due to leaching and the subsequent addition of Cu reacting with FeS in sphalerite. For chalcopyrite to exsolve from sphalerite, fluid temperatures must have been > 650°C (Hutchinson and Scott, 1981; Kojima and Sugaki, 1985). Complex comb-like intergrowths, indicating the replacement of chalcopyrite by sphalerite along crystallographic directions, are observed in several cases (Figures 12a and 12b), as well as chalcopyrite replacement by sphalerite along fractures and grain margins. In a few cases sphalerite appears to have been replaced by chalcopyrite. Sphalerite stars (< 1 μm) are found, within chalcopyrite, between 298-300 m.

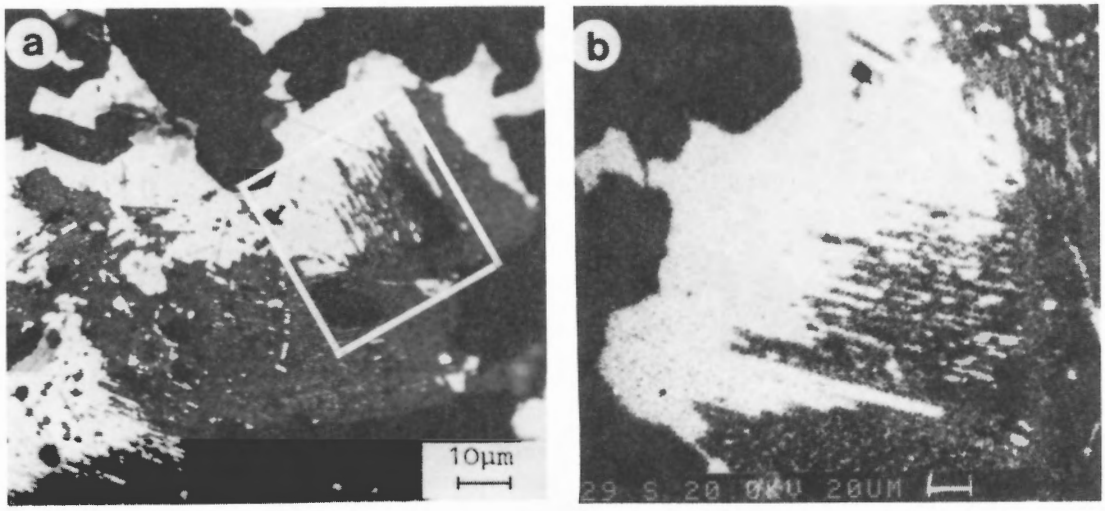

Figure 12: Photomicrograph (PPL, oil immersion) of sulphides from Hole CY-2a. a) 166.42 m: Complex intergrowths of sphalerite and chalcopyrite (white), interpreted as replacement of chalcopyrite by sphalerite along crystallographic directions. Sphalerite carries laths and blebs of chalcopyrite. b) 166.42 m: Microprobe scan showing the Cu distribution (white) of the area indicated by a square in Figure 12a.

Sphalerite

Sphalerite is abundant between 154-334 m and occurs interstitially to pyrite and chalcopyrite or as individual anhedral masses up to 200 μm in diameter. Twinned or euhedral sphalerite crystals were seldom observed. From 400-689 m, sphalerite fills cavities in pyrite. Pyrite and chalcopyrite are both corroded and replaced by sphalerite (Figures 11c and 12a). Between 161-198 m extensive replacement of chalcopyrite by sphalerite took place along crystallographic planes. Sphalerite apparently also replaces chalcopyrite (Figure 11e), as indicated by relics of resorbed chalcopyrite entirely enclosed in sphalerite. Cavities in chalcopyrite are sometimes filled with sphalerite. Shrinkage cracks of former colloform pyrite are impregnated with later sphalerite. Sphalerite, between 161-198 m, carries abundant orientated chalcopyrite blebs (Figures 11b and 12a) and lamellae. Pure sphalerite grains are also found. Minute sphalerite stars within chalcopyrite were observed between 298-300 m, and these probably reflect exsolution or simultaneous crystallization (Ramdohr, 1975; Wiggins and Craig, 1980). Oudin (1983) states that sphalerite exsolution lamellae in chalcopyrite are absent in samples from the East Pacific Rise 21°N, but present in equivalent Cyprus samples, probably due to late unmixing of a Cu-Fe-Zn-S phase. According to Soen and Pauly (1967) temperatures of about 500°C are necessary for Zn to be soluble in sufficient amounts in chalcopyrite.

Pyrrhotite, Marcasite, Galena

Discrete minute inclusions (< 30 μm) of pyrrhotite exclusively occur within pyrite, particularly in the interval between 198-334 m and below 550 m. Pyrite also contains small pyrrhotite-chalcopyrite inclusions below 580 m. In two cases (154 and 334 m) marcasite was detected as anhedral masses associated with pyrite. Traces of galena occur in only two polished sections (161 and 166 m), where it replaces pyrite and is replaced by sphalerite. Sphalerite with chalcopyrite blebs and laths is found within galena. One discrete, almost submicroscopic grain of native gold was found enclosed in pyrite in a sample from 166 m. Primary Fe-Ti oxides generally have been leached and replaced by sulphides. They are characterized by a grid pattern of rutile needles, associated with hematite, sphene, anatase, leucoxene clouds and sometimes pyrite blebs. The secondary origin of the rutile is indicated by the absence of twin lamellae. At about 386 m, magnetite grains up to 30 μm in diameter were found, which are considered by Hall et al. (1987) to be of secondary origin.

Textural relations of ore and gangue minerals suggest that pyrite was the first sulphide precipitated, followed by chalcopyrite and sphalerite (Figure 11f). Quartz was deposited during the waning stages of hydrothermal activity.

The small chalcopyrite-pyrrhotite inclusions in pyrite below 580 m can be used as a 'fixed-point' geothermometer and suggest a formation temperature less than 334 ± 17°C (Ixer et al., 1984). According to Yund and Kullerud (1966), Barton and Skinner (1979) and Sugaki et al. (1975), at this temperature the tie line of pyrite + intermediate solid solutions (iss) in the Cu-Fe-S system switches to chalcopyrite + pyrrhotite. Formation temperatures of about 300°C are consistent with isotope studies by Heaton and Sheppard (1977), but contrast with Large's (1977) estimation of < 275°C for the formation of the Agrokipia 'B' ore.

SULPHIDE CHEMISTRY

In order to establish variations in the stoichiometry of the different sulphides in relation to depth, systematic quantitative microprobe analyses were carried out on pyrite (255), chalcopyrite (72), sphalerite (180) and pyrrhotite (34) between 154-666 m.

Pyrite

Pyrite was analyzed for Fe, S, As, Co, Ni, Au and Se in seventeen polished sections from 154-666 m. Nine to 32 grains were measured in each sample (Table 5).

Pyrites from CY-2a show a variation of 32.1-37.3 atomic% Fe (mean 33.9%, std. dev. 0.87) and are thus slightly Fe enriched compared to the theoretical value of 33.3 atomic% Fe for a standard pyrite and 33.4 atomic% Fe determined on average for 119 pyrites from the East Pacific Rise 21°N (Lafitte and Maury, 1983). They correspond to the average formula $Fe_{1.03}S_2$. Similar Fe-enriched pyrites (mean 33.8 atomic% Fe) were recently described by Hekinian and Fouquet (1985) from an off-axis seamount southeast of the East Pacific Rise at 12°50'N. According to Gordon-Smith (1942), an excess in the Fe content of pyrite can imply the transformation of the normal cubic lattice to a ditrigonal structure, due to the presence of Fe atoms in S positions. Similar moderate to distinctly anisotropic pyrites were observed in sulphides from the East Pacific Rise at 21°N (Oudin, 1983).

Cobalt concentrations range up to 0.30 wt.%, whereas Ni is generally around the detection limit of 100 ppm. Cobalt and Ni usually substitute for Fe in the pyrite structure. The Co/Ni ratio varies between 2.0 and 8.0 (avg. 0.05 wt.% Co, 0.01 wt.% Ni) which is typical of pyrite formed under volcanogenic conditions (Bralia et al., 1979). Significant concentrations of As up to 1.87 wt.% are characteristic for the pyrites of CY-2a, in contrast to the lack of As in samples from the East Pacific Rise

21°N (Oudin, 1983). The As content therefore is not responsible for the observed anisotropy. Arsenic generally substitutes for S in the pyrite lattice. Gold values of 0.12-0.33 wt.% were detected in individual pyrites from 198-279 m and at 457 m depth. As only traces of Au have been found in chalcopyrite (see below), pyrite must be the main Au carrying sulphide phase. Selenium does not reach concentrations above the detection limit of 400 ppm.

No variation in the composition of different pyrite types (e.g. porous, dense, colloform) or of vein, vesicle and disseminated pyrite was observed. Thus, it is not possible to distinguish pyrite generations using Co, Ni or As.

Figure 13 shows average concentrations of Ni, Co and As in pyrite with depth in CY-2a (Table 5). Arsenic varies over a narrow range of 0.64 to 1.20 wt.%, with a mean of 0.87 wt.% (std. dev. 0.20). The Co content of pyrite increases slightly with depth, as already noted from various Cyprus ore bodies by Johnson (1972), who suggested that cobalt-rich pyrites may be generated under elevated temperatures (Loftus-Hill and Solomon, 1967). Nickel averages 100 ppm below 300 m, but shows erratically higher values (up to 700 ppm) in the most intensively mineralized interval between 150-300 m.

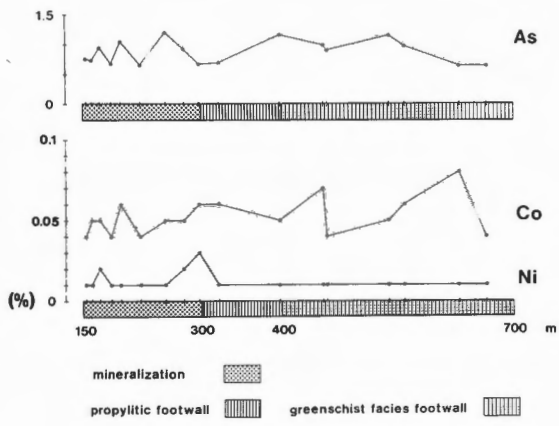

Figure 13: Downhole variation in As, Co and Ni content of pyrites in Hole CY-2a. Each point represents an average of 9-32 individual analyses (cf. Table 5).

TABLE 5. Average Microprobe Analyses of Pyrite from Drillcore CY-2a.

Depth (m)	n	Fe	S	As	Co	Ni	Total	Fe	S	As	Co	Ni
		Analyses, wt.%						atomic %				
153.60	25	47.82	50.84	0.76	0.04	0.01	99.47	34.91	64.65	0.41	0.03	0.01
161.00	11	47.62	50.98	0.74	0.05	0.01	99.40	34.75	64.81	0.40	0.03	0.01
171.05	10	46.37	53.22	0.95	0.05	0.02	100.61	33.16	66.29	0.51	0.03	0.01
185.70	32	46.63	52.89	0.68	0.04	0.01	100.35	33.47	66.13	0.36	0.03	0.01
197.75	17	47.60	50.50	1.05	0.06	0.01	99.22	34.89	64.48	0.57	0.04	0.01
223.10	12	46.75	53.16	0.66	0.04	0.01	100.62	33.42	66.20	0.35	0.03	0.01
255.10	10	47.52	51.08	1.20	0.05	0.01	99.86	34.57	64.74	0.65	0.03	0.01
278.50	13	45.04	53.48	0.92	0.05	0.02	99.51	32.41	67.04	0.49	0.03	0.01
297.90	13	46.69	52.80	0.67	0.06	0.03	100.25	33.53	66.05	0.36	0.04	0.02
323.20	17	46.88	53.89	0.69	0.06	0.01	101.53	33.17	66.42	0.36	0.04	0.01
401.40	9	47.52	49.62	1.16	0.05	0.01	98.36	35.23	64.08	0.64	0.04	0.01
456.95	18	47.28	52.33	0.99	0.07	0.01	100.68	33.95	65.46	0.53	0.05	0.01
462.05	10	46.75	53.30	0.90	0.04	0.01	101.00	33.32	66.17	0.48	0.03	0.01
541.15	12	47.33	51.27	1.15	0.05	0.01	99.81	34.41	64.93	0.62	0.03	0.01
561.03	18	46.83	53.47	0.97	0.06	0.01	101.34	33.27	66.17	0.51	0.04	0.01
631.20	16	47.26	51.70	0.64	0.08	0.01	99.69	34.28	65.32	0.35	0.05	0.01
666.49	12	46.39	52.95	0.64	0.04	0.01	100.03	33.34	66.29	0.34	0.03	0.01
min		44.23	48.20	0.56	0.02	0.00		32.14	62.27	0.30	0.01	0.00
max	255	50.22	54.55	1.87	0.30	0.07		37.25	67.31	1.02	0.20	0.05
mean		46.96	52.22	0.84	0.05	0.01		33.89	65.61	0.45	0.04	0.01

n: number of analyses

Chalcopyrite

Chalcopyrite, coexisting with pyrite and sphalerite, was analyzed from depths between 154-666 m for Cu, Fe, S, As, Co, Ni and Au (Table 6). Selected samples were also analyzed for Ag, Se, Mn and As, but with the exception of Se (up to 0.60 wt.%), only traces of these elements were detected.

Most of the chalcopyrites are very homogeneous in composition (Figure 14), and reveal a stoichiometry almost the same as examples from modern oceanic crust (Lafitte and Maury, 1983). Chalcopyrites from 197.75 m are characterized by a lower average Cu value of 17.95 atomic% (25.38 wt.%) and are slightly enriched in Fe and S relative to the other samples (Figure 14). These phases may represent iss-related exsolution products. A maximum substitution of Cu by Fe of about 2.5% was found. Copper substitution by Fe in the range of about 2-3% was also noted by Oudin (1983) from chalcopyrites associated with chalcopyrrhotites of the East Pacific Rise at 21°N. Lafitte et al. (1985) mentioned Fe-enriched chalcopyrites from the same site. Sugaki et al. (1975) proved by experimental work in the system Cu-Fe-S, that Fe-enriched chalcopyrites form under hydrothermal conditions between 350 and 300°C.

The average formula calculated for all analyzed chalcopyrites except those from 197.75 m is $Cu_{0.96}Fe_{1.01}S_2$. Considering that 'high temperature chalcopyrites' range from $Cu_{1.25}/Fe_{1.00}$ to $Cu_{1.00}/Fe_{1.25}$ (Ramdohr, 1975), the chalcopyrites analyzed here show a metal depletion and may be classified as 'low temperature chalcopyrites'.

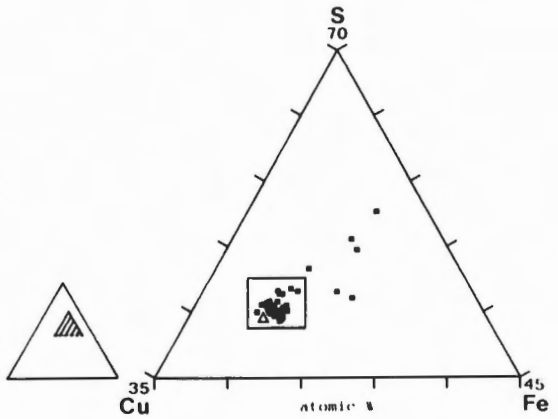

Figure 14: Cu-Fe-S ternary diagram of chalcopyrites from Hole CY-2a. For comparison the compositional field of chalcopyrite from the East Pacific Rise at 21°N (square) (Lafitte and Maury, 1983) and the position of theoretical chalcopyrite (open triangle) are shown. Units are 5 atomic % each.

Cobalt and Ni concentrations are generally low (both averaging 0.02 wt.%) and vary only slightly with depth (Figure 15). In contrast to the slightly increasing Co contents of pyrite at depth, the Co contents of chalcopyrite shows almost no variation below 300 m. Average As values reach 0.21 wt.% and elevated As concentrations are restricted to the uppermost zone of the highly mineralized stockwork. Below 300 m the As values are extremely low. Gold was not detected in concentrations above 0.10 wt.%.

Sphalerite

Some 180 sphalerite grains from 17 samples between 154-666 m depth were analyzed for Zn, S, Fe, Cu, Cd, Mn and Au (Table 7).

Copper was found in several sphalerites in significant concentrations up to 7.2 atomic% (9.5 wt.%) (Figure 16), whereas others carry only minor Cu or are completely free of Cu. Copper and Fe in these cupriferous sphalerites are generally positively correlated, indicating that elevated Cu concentrations in sphalerite result from minute chalcopyrite inclusions. Wiggins and Craig (1980) have shown that most natural sphalerites contain less than 0.5 wt.% Cu in solid solution and that higher Cu-concentrations result from chalcopyrite inclusions in sphalerite. Copper zonation in a euhedral sphalerite grain is shown in Figure 17 in the form of a microprobe element scan. As evident from this traverse (A-B), there is also a significant positive correlation between Cu and Fe, due to the occurrence of disseminated chalcopyrite ('chalcopyrite disease') in sphalerite. In this example, chalcopyrite is concentrated in the centre of the sphalerite.

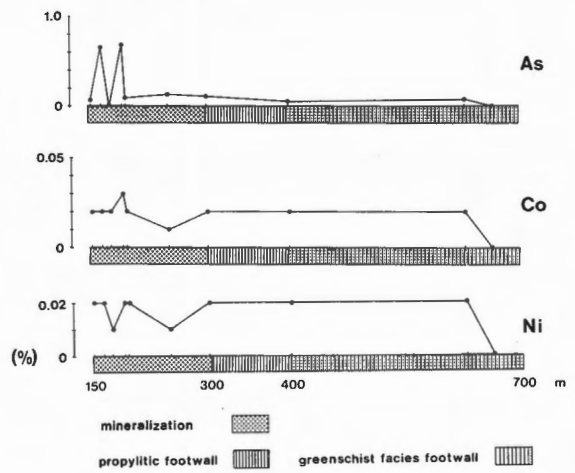

Figure 15: Downhole variation of As, Co and Ni content of chalcopyrites from Hole CY-2a. Each point represents an average of 3-12 individual analyses (cf. Table 6).

TABLE 6. Average Microprobe Data of Chalcopyrite from Drillcore CY-2a.

Depth (m)	n	Fe	Cu	S	Co	Ni	As	Total	Fe	Cu	S	Co	Ni	As
		Analyses, wt.%							atomic %					
153.60	12	30.46	33.46	34.63	0.02	0.02	0.07	98.66	25.32	24.45	50.15	0.02	0.02	0.04
166.42	13	30.22	33.40	34.47	0.02	0.02	0.66	98.83	25.15	24.43	49.98	0.02	0.02	0.41
177.30	3	30.67	32.53	35.53	0.02	0.01	0.00	98.75	25.31	23.59	51.07	0.02	0.01	0.00
192.95	3	31.38	31.76	34.12	0.03	0.02	0.69	98.00	26.31	23.40	49.82	0.02	0.02	0.43
197.75	7	35.19	25.38	38.28	0.02	0.02	0.09	98.98	28.31	17.95	53.65	0.02	0.02	0.05
251.60	6	30.72	33.95	35.31	0.01	0.01	0.13	100.11	25.14	24.42	50.34	0.01	0.01	0.08
301.18	10	31.29	33.05	34.81	0.02	0.02	0.11	99.31	25.84	23.99	50.07	0.02	0.02	0.07
405.66	6	31.65	33.71	35.18	0.02	0.02	0.05	100.61	25.81	24.16	49.97	0.02	0.02	0.03
631.20	9	30.59	33.71	35.02	0.02	0.02	0.08	99.44	25.23	24.42	50.28	0.02	0.02	0.05
666.49	3	30.88	32.13	36.00	0.00	0.00	0.00	99.27	25.35	23.18	51.47	0.00	0.00	0.00
min		29.22	19.65	33.63	0.00	0.00	0.00		24.48	13.47	49.34	0.00	0.00	0.00
max	72	37.28	34.57	42.42	0.05	0.06	0.76		30.37	25.47	57.64	0.04	0.05	0.48
mean		31.19	32.53	35.21	0.02	0.02	0.21		25.71	23.59	50.54	0.01	0.01	0.13

n: number of analyses

TABLE 7. Average Microprobe Data of Sphalerite from Drillcore CY-2a.

Depth (m)	n	Zn	Fe	S	Cd	Mn	Cu	Total	FeS mole %	Zn	Fe	S	Cd	Mn	Cu
		Analyses, wt.%								atomic %					
153.60	13	61.98	4.36	33.93	0.11	0.08	0.01	100.47	7.60	45.43	3.74	50.71	0.05	0.07	0.01
161.00	33	57.15	6.49	33.44	0.08	0.09	2.79	100.05	11.72	42.04	5.59	50.15	0.03	0.08	2.11
166.42	13	58.32	4.30	33.25	0.13	0.04	3.55	99.60	7.94	43.22	3.73	50.25	0.06	0.04	2.71
177.30	12	58.02	6.22	34.91	0.11	0.09	0.31	99.65	11.14	42.36	5.32	51.97	0.05	0.08	0.23
192.95	12	61.51	4.13	32.62	0.17	0.00	0.17	98.60	7.28	46.20	3.63	49.96	0.07	0.00	0.13
197.75	9	58.15	5.72	33.67	0.08	0.11	0.99	98.71	10.32	43.17	4.97	50.97	0.03	0.10	0.76
249.88	13	57.25	8.75	34.04	0.10	0.08	0.02	100.24	15.16	41.77	7.47	50.64	0.04	0.07	0.02
251.60	10	62.12	3.31	34.20	0.10	0.15	0.28	100.18	5.87	45.59	2.84	51.18	0.04	0.13	0.21
272.30	10	54.19	11.96	33.65	0.07	0.55	0.02	100.43	20.52	39.41	10.18	49.89	0.03	0.48	0.01
323.20	10	52.77	12.42	32.86	0.06	0.98	0.01	99.11	21.59	38.94	10.73	49.44	0.03	0.86	0.01
405.66	6	53.33	12.61	32.32	0.08	0.36	0.00	98.70	21.66	39.66	10.98	49.01	0.03	0.32	0.00
526.45	7	53.65	11.87	32.86	0.11	0.26	0.05	98.81	20.56	39.75	10.29	49.64	0.05	0.23	0.04
530.93	4	54.31	10.63	35.65	0.05	0.10	0.02	100.75	18.63	38.90	8.91	52.07	0.02	0.09	0.01
561.03	9	59.57	6.23	33.44	0.17	0.12	0.02	99.55	10.90	44.03	5.39	50.39	0.07	0.11	0.02
631.20	6	49.15	13.69	34.47	0.11	0.46	2.22	100.12	24.57	35.52	11.58	50.80	0.05	0.40	1.65
643.89	6	51.34	13.66	34.69	0.18	0.04	0.02	99.93	23.73	37.14	11.57	51.17	0.08	0.03	0.01
666.49	7	55.69	6.21	34.24	0.50	0.05	3.59	100.27	11.54	40.70	5.31	51.03	0.21	0.04	2.70
min		46.20	2.25	31.51	0.00	0.00	0.00		4.04	33.44	1.96	48.52	0.00	0.00	0.00
max	180	63.19	15.95	36.06	0.59	2.97	9.54		28.87	47.19	13.51	52.41	0.25	2.61	7.17
mean		57.12	7.55	33.68	0.12	0.19	1.09		14.02	42.01	6.48	50.47	0.05	0.16	0.83

n: number of analyses

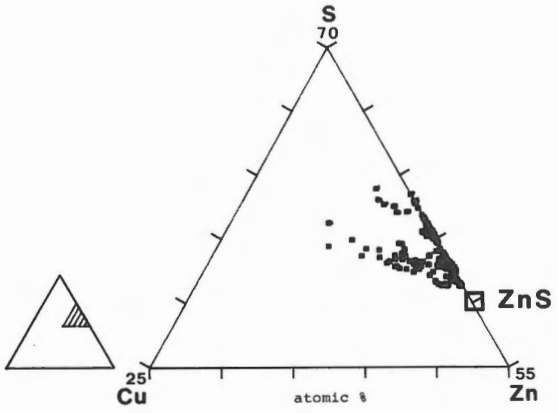

Figure 16: Cu-Zn-S ternary diagram of sphalerite from Hole CY-2a. For comparison the position of theoretical sphalerite is plotted. Units are 5 atomic % each.

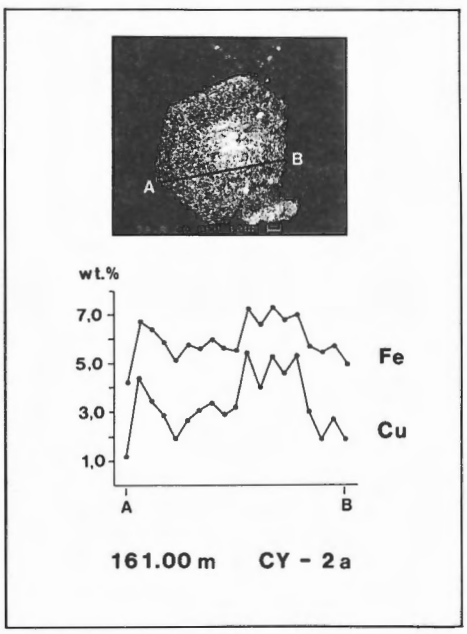

Figure 17: Electron microprobe scan, showing the zonal distribution of Cu (white) in an euhedral sphalerite grain from 161 m in Hole CY-2a. A and B indicate a microprobe traverse. Note the positive correlation between Cu and Fe.

A general feature of all sphalerites from CY-2a is a high Fe content, varying between 2.3-16.0 wt.% (avg. 7.6 wt.%) or 4.0-28.9 mol % FeS (avg. 14.0 mol %), respectively. High Fe content in sphalerite is generally not associated with high Cu concentrations. Very Fe-rich sphalerites (> 10.0 wt.% Fe) typically show extremely low Cu contents of about 0.02 wt.% on average. In some cases, elevated S values probably point to submicroscopic pyrite inclusions, but the majority of sphalerites reveal normal S, low to zero Cu and significantly elevated Fe. The average formula corresponds to $Zn_{0.85}Fe_{0.13}S_1$. Samples with inclusions of chalcopyrite (positive Cu-Fe correlation) also show a negative correlation of Zn and Fe, which suggests that Fe also substitutes for Zn in sphalerite. Compared to theoretical sphalerite and sphalerite from the East Pacific Rise at 21°N (Lafitte and Maury, 1983), the CY-2a sphalerites show slightly elevated S values, but the variation in the Fe content is similar to the East Pacific Rise sphalerites (Figure 18). A large variation in the Fe content of the sphalerites resembles that in samples analyzed from the Juan de Fuca Ridge (Koski et al., 1984) and the East Pacific Rise at 13°N (Hekinian and Fouquet, 1985) and appears to be a typical feature of oceanic sphalerites.

The distribution of average Fe, Cd, Mn and Cu concentrations in sphalerite with depth in CY-2a is shown in Figure 19. Significant amounts of Cu occur in sphalerite only in the uppermost and lowest levels in the core. The Mn concentrations in sphalerite from below 250 m are generally higher than in those from 154-250 m. Up to 3.0 wt.% Mn was found in sphalerite at 323 m. According to Stoiber (1940), the substitution of Mn for Zn in the sphalerite lattice, takes place at elevated temperatures. The average contents of Cd in sphalerite increase with depth, reaching a maximum of 0.50 wt.% at 666 m. Mookherjee (1962) demonstrated that the incorporation of Cd in the sphalerite structure is buffered by the concentration of chloride in solution. At low formation temperatures, increasing Cd contents in sphalerite can be explained by a decrease of chloride concentration in the hydrothermal fluid. Probably Cd is preferentially incorporated in sphalerite at higher temperatures, but this is a controversial subject in the literature (Stoiber, 1940; Fleischer, 1955; Mookherjee, 1962). Sphalerites from CY-2a show a positive correlation between Mn and Fe (Stoiber, 1940; Fleischer, 1955; Skinner, 1958; Krause, 1961; Sims and Barton, 1961; Craig et al., 1984), whereas the Cd content shows no relation to Fe. High average Fe concentrations (avg. 19.7 mol % FeS) in sphalerite are restricted to depths below 270 m. Sphalerites containing lower Fe values (avg. 9.7 mol % FeS) are found in the upper zone of mineralization.

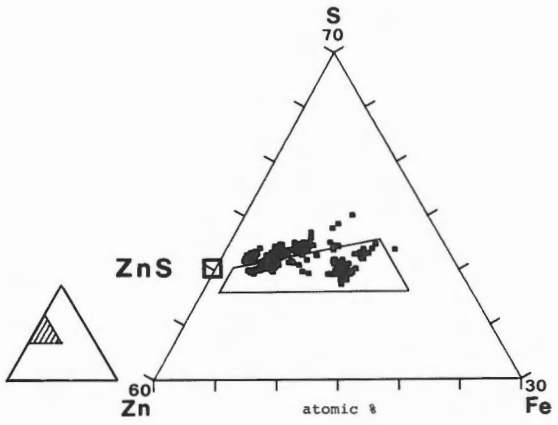

Figure 18: Zn-Fe-S ternary diagram for sphalerites from Hole CY-2a. For comparison the compositional field of sphalerite from the East Pacific Rise at 21°N (Lafitte and Maury, 1983) and the position of theoretical sphalerite are shown.

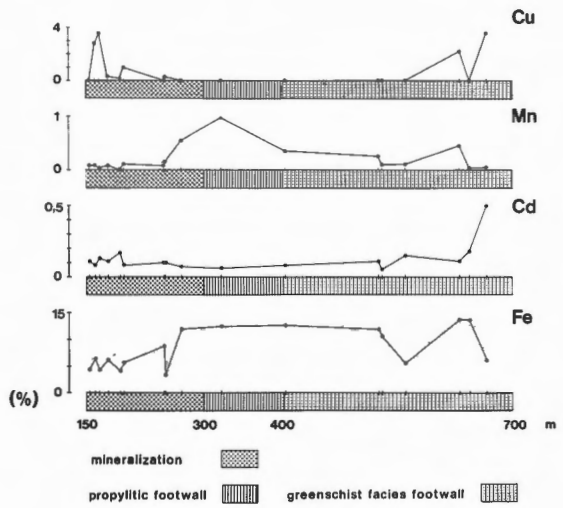

Figure 19: Downhole variation in Cu, Mn, Cd and Fe content of sphalerites from Hole CY-2a. Each point represents an average of 4-33 individual analyses (cf. Table 7).

The amount of Fe in the sphalerite structure is a function of the temperature of formation and the fugacity of S (Scott and Barnes, 1971; Scott, 1973; Hutchinson and Scott, 1981) and thus related to the coexisting Fe-sulphides which serve to buffer the a_S and hence the a_{FeS} in sphalerite (Barton and Toulmin, 1966; Craig et al., 1984). High S concentrations and a constant Fe supply result in the formation of pyrite (Sims and Barton, 1961). Therefore, sphalerite in equilibrium with pyrite is mostly characterized by relatively low Fe concentrations. In contrast, sphalerite coexisting with pyrite + (hexagonal) pyrrhotite has a higher Fe content because pyrrhotite and pyrite effectively buffer the S fugacity in the system and force the incorporation of FeS into the sphalerite lattice (Barton and Toulmin, 1966; Skinner et al., 1967; Scott and Kissin, 1973). Assuming that sphalerite in CY-2a is in true equilibrium with the coexisting Fe-sulphides, the relatively high average FeS concentration of 19.7 mol % in sphalerite associated with pyrite + (hexagonal) pyrrhotite below 270 m depth may indicate formation temperatures above 250°C. Sphalerites from the interval 154-252 m, coexisting with pyrite (154-177 m) or pyrite + (monoclinic) pyrrhotite (193-252 m) is characterized by an average value of 9.7 mol % FeS, which points to formation temperatures below 250°C (Browne and Lovering, 1973; Scott and Kissin, 1973; Willan and Hall, 1980).

Pyrrhotite

Thirty-four analyses were obtained from pyrrhotite inclusions in pyrite at 234 m, 272 m, 584 m, 631 m and 644 m. The gap between 271 and 584 m is due to an absence of pyrrhotite, or to a grain size below that necessary for microprobe analyses.

Copper concentrations reach up to 1.5 wt.%, probably due to close association with chalcopyrite. In addition, Co up to 0.07 wt.%, Ni up to 0.04 wt.% and maximum As concentrations of 0.31 wt.% were detected. The Fe content of pyrrhotite at 234 and 272 m averages 46.95 and 46.34 atomic%, respectively, whereas the pyrrhotites from 584 m, 631 m and 644 m show average Fe concentrations of 47.27, 47.12 and 47.16 atomic%. According to Kissin and Scott (1982), hexagonal and monoclinic pyrrhotites can be distinguished by the Fe-content of $>$ 47.0 atomic% (hexagonal) and 46.4-47.0 atomic% (monoclinic). Therefore, pyrrhotites above 272 m are considered to show a monoclinic and below 584 m a hexagonal symmetry. Due to the general small size of the pyrrhotite grains, it was not possible to determine the symmetry by means of diffractometry. Kissin and Scott (1982) reported that hexagonal pyrrhotite becomes stable above 254°C, whereas the monoclinic phase exists below this temperature. Hexagonal pyrrhotite is also the dominant Fe-monosulphide phase

found in high temperature sulphide deposits on the East Pacific Rise (Haymon, 1983; Oudin, 1983; Hekinian and Fouquet, 1985; Lafitte et al., 1985).

WHOLE ROCK GEOCHEMISTRY

Major oxides and trace elements have been determined for 330 samples between 3.60 and 688.88 m (Table 8), using X-ray fluorescence techniques. Each analysis listed in the table corresponds to 5-16 samples, analyzed per 20 m unit.

Major Elements

In Table 9 the concentrations of selected major oxides are summarized for the alteration zones, as defined by the secondary mineral distribution.

Assuming that Al is relatively immobile during hydrothermal alteration (Humphris and Thompson, 1978; Honnorez, 1981; Lydon, 1983), the major elements have been normalized with respect to Al according to the method described by Krauskopf (1979). The average of 32 analyses of 'Lower Pillow Lavas', unaffected by hydrothermal alteration, have been taken from Desmet et al. (1980) and used for data normalization. The downhole variation of the normalized elements is shown in Figure 20 as gains and losses compared to the 'standard'. Each of the 35 values plotted in this figure represents the average of a 20 m interval.

TABLE 8. Major and Trace Element Content of Drillcore CY-2a in Form of 20 m Interval Averages.

Sample	Depth	SiO_2	TiO_2	Al_2O_3	Fe_2O_3	MnO	MgO	CaO	Na_2O	K_2O	P_2O_5	Cr_2O_3	V_2O_5	LOI	Total
1	10.00	52.53	0.55	15.54	9.21	0.11	7.86	7.56	1.94	1.25	0.05	0.02	0.04	2.85	99.52
2	30.00	50.25	0.69	13.79	9.73	0.15	8.61	8.63	1.98	1.35	0.06	0.04	0.04	4.41	99.73
3	50.00	50.48	1.06	15.96	11.03	0.12	6.59	5.49	2.37	1.92	0.10	0.01	0.06	4.77	99.95
4	70.00	47.43	0.59	14.32	8.01	0.12	7.02	10.92	2.01	1.14	0.06	0.03	0.04	5.42	97.08
5	90.00	50.52	0.74	15.28	8.82	0.13	7.05	8.74	1.93	1.40	0.06	0.02	0.04	3.87	98.61
6	110.00	50.84	1.18	16.32	10.66	0.19	6.02	4.98	2.62	1.70	0.13	0.01	0.05	3.27	97.97
7	130.00	55.16	1.20	14.84	10.78	0.27	4.33	4.65	2.68	0.75	0.08	0.01	0.03	4.25	99.04
8	150.00	58.06	0.99	11.73	10.77	0.17	4.29	4.42	2.43	0.95	0.07	0.03	0.05	3.52	97.49
9	170.00	53.22	1.10	12.53	15.47	0.23	6.29	0.56	0.80	1.22	0.10	0.04	0.03	7.62	99.20
10	190.00	33.29	0.76	8.65	35.17	0.09	2.89	0.60	0.39	1.25	0.07	0.02	0.03	18.19	101.38
11	210.00	49.12	0.89	9.45	24.38	0.07	2.96	0.16	0.44	1.38	0.06	0.01	0.04	12.51	101.47
12	230.00	38.77	0.75	7.98	32.70	0.10	3.26	0.15	0.46	0.97	0.06	0.01	0.03	16.49	101.73
13	250.00	48.03	0.68	7.84	26.13	0.12	3.28	0.19	0.48	0.89	0.07	0.03	0.03	13.41	101.17
14	270.00	49.78	0.65	7.49	25.45	0.11	2.96	0.20	0.44	0.91	0.07	0.01	0.03	13.21	101.32
15	290.00	62.89	0.74	10.73	12.00	0.30	4.97	1.86	0.79	0.71	0.07	0.01	0.03	6.28	101.38
16	310.00	58.44	0.94	13.72	13.05	0.48	5.07	1.65	1.62	0.87	0.09	0.01	0.04	5.14	101.10
17	330.00	57.24	1.10	14.68	10.25	0.28	5.25	2.27	2.55	0.73	0.08	0.01	0.05	5.02	99.51
18	350.00	55.79	1.20	14.58	12.30	0.30	5.35	1.88	3.46	0.56	0.09	0.01	0.05	5.10	100.66
19	370.00	52.34	1.21	15.14	12.43	0.22	6.50	3.83	3.29	0.33	0.07	0.01	0.07	5.22	100.67
20	390.00	58.24	1.03	14.59	11.20	0.36	5.05	1.64	4.48	0.35	0.09	0.01	0.03	3.87	100.94
21	410.00	56.31	1.22	14.53	12.74	0.54	5.82	1.16	3.65	0.22	0.10	0.01	0.05	4.77	101.10
22	430.00	54.99	1.16	13.52	12.14	0.67	5.61	2.01	3.44	0.11	0.09	0.01	0.05	4.76	98.53
23	450.00	60.32	1.15	13.00	11.13	0.25	4.02	1.91	4.61	0.10	0.10	0.01	0.03	4.43	101.05
24	470.00	53.45	1.03	12.87	14.42	0.28	4.55	3.11	3.86	0.13	0.08	0.01	0.05	5.77	99.62
25	490.00	48.81	1.10	12.81	17.66	0.28	5.56	3.24	3.23	0.12	0.08	0.01	0.05	6.95	99.89
26	510.00	58.51	1.10	12.53	13.26	0.25	4.35	2.29	3.48	0.17	0.08	0.01	0.04	4.83	100.91
27	530.00	49.00	1.15	13.13	20.26	0.26	4.84	1.58	3.06	0.16	0.08	0.01	0.04	7.88	101.43
28	550.00	49.17	1.00	12.47	19.13	0.22	4.37	2.52	2.88	0.26	0.07	0.01	0.04	8.49	100.61
29	570.00	42.69	1.03	12.59	24.14	0.35	4.49	2.14	2.57	0.21	0.07	0.01	0.05	9.88	100.20
30	590.00	42.56	1.07	11.98	25.77	0.34	4.81	1.57	2.34	0.10	0.07	0.01	0.05	10.01	100.70
31	610.00	49.29	1.14	15.37	17.53	0.50	5.88	1.40	3.37	0.10	0.07	0.01	0.07	4.78	99.52
32	630.00	52.42	1.04	13.47	16.19	0.41	5.29	1.67	2.68	0.29	0.07	0.01	0.07	5.22	98.84
33	650.00	46.50	1.15	12.42	19.48	0.30	5.60	2.55	3.04	0.09	0.07	0.01	0.08	7.97	99.27
34	670.00	45.24	1.13	12.16	20.26	0.31	5.71	2.39	2.84	0.17	0.09	0.01	0.07	8.56	98.94
35	690.00	52.74	1.24	13.21	14.93	0.32	5.82	4.30	2.83	0.14	0.11	0.01	0.08	5.70	101.44

TABLE 8 (cont.)

Sample	Depth	Pb	Ba	Sb	As	Ga	Zn	Cu	Ni	Co	Zr	Y	Sr	Rb
1	10.00	10	31	20	10	15	143	280	39	39	40	13	84	13
2	30.00	10	30	20	10	14	98	47	101	38	48	18	82	20
3	50.00	10	36	20	10	18	96	58	31	36	69	28	90	17
4	70.00	10	32	20	10	15	64	64	52	31	45	18	87	17
5	90.00	10	39	20	10	16	69	32	49	33	52	21	85	17
6	110.00	10	53	20	10	20	111	35	20	31	79	34	87	19
7	130.00	10	185	20	10	18	129	40	20	26	81	30	90	15
8	150.00	62	143	24	29	17	10987	304	57	29	57	29	79	32
9	170.00	32	138	21	47	20	2960	1383	20	24	72	31	23	13
10	190.00	34	480	24	214	18	942	77	24	35	61	26	12	18
11	210.00	25	634	20	184	16	795	145	20	29	52	22	12	16
12	230.00	14	673	21	105	17	865	97	23	41	51	20	12	13
13	250.00	12	302	20	26	15	283	41	22	31	54	23	11	12
14	270.00	11	426	21	78	14	1644	77	22	36	56	24	14	12
15	290.00	10	160	20	35	14	284	90	25	24	55	22	30	10
16	310.00	10	60	20	10	17	220	235	20	21	74	31	33	10
17	330.00	10	30	20	12	17	228	38	20	27	75	33	55	10
18	350.00	12	34	20	10	18	378	218	20	27	77	34	60	10
19	370.00	10	30	20	10	18	219	64	20	37	67	29	73	10
20	390.00	11	30	20	10	18	602	230	20	24	77	34	73	10
21	410.00	12	32	20	11	19	834	219	20	25	85	35	57	10
22	430.00	339	30	20	36	15	2626	132	20	27	82	34	73	10
23	450.00	63	30	21	162	15	331	46	20	25	84	32	67	10
24	470.00	24	30	25	111	17	296	49	20	31	70	30	72	10
25	490.00	10	30	20	13	17	218	27	20	35	70	29	66	10
26	510.00	10	34	20	15	16	161	68	20	27	70	28	70	10
27	530.00	10	30	20	17	19	174	21	20	38	75	30	57	10
28	550.00	10	30	20	13	17	126	26	20	57	68	27	54	10
29	570.00	10	35	20	10	18	158	173	20	57	65	25	41	10
30	590.00	10	30	20	11	19	173	747	21	66	73	23	41	10
31	610.00	10	30	20	10	19	309	297	20	26	69	27	60	10
32	630.00	10	30	20	10	17	224	193	20	25	65	26	64	10
33	650.00	10	30	20	11	19	192	79	20	34	70	27	60	10
34	670.00	10	30	20	13	19	183	45	20	47	74	29	52	10
35	690.00	10	30	20	10	18	132	124	20	29	82	32	83	10

Total Fe expressed as Fe_2O_3, oxides in wt.%, traces in ppm, lower detection limits for P_2O_5 = 0.05%, Cr_2O_3 = 0.01%, Pb, As, and Rb = 10 ppm, Sb and Ni = 20 ppm, Ba = 30 ppm. For element concentrations below the lower detection limit, the value of the lower detection limit is listed.

Data normalization using Ti as the stable element (Pearce and Cann, 1973; Floyd and Winchester, 1978; Finlow-Bates and Stumpfl, 1981) reveals a similar distribution curve to that obtained using Al (Figure 20), but individual values are generally slightly lower. Normalization based on Ti from glass analyses of the horizon 113.20-141.60 m in CY-2a (Bednarz et al., 1987), instead of the Ti-value from average LPL analyses of Desmet et al. (1980), gave a downhole element distribution, which, except for the uppermost 90 m, is almost identical to that shown in Figure 20. The values above 90 m are generally higher than those in Figure 20, because the 'glass standard' only reflects the primary composition of rocks below 90 m depth (cf. Bednarz et al., 1987).

TABLE 9. Average Content of Fe_2O_3, CaO, K_2O, SiO_2, MgO and Na_2O (wt.%) in 330 Rock Samples from Uppermost Lavas (0-150 m), Mineralization (150-300 m), Propylitic Lavas (300-400 m) and Greenschist Facies Lavas (400-689 m) in the Drillcore CY-2a.

		Fe_2O_3	CaO	K_2O	SiO_2	Al_2O_3	MgO	Na_2O
Uppermost Lavas	mean	9.64	7.35	1.41	51.53	14.91	6.75	2.17
(0-150 m)	min	3.46	0.49	0.14	19.33	3.05	1.66	0.48
n = 68	max	16.52	24.23	4.71	81.61	17.44	15.50	4.32
	s.d.	1.88	3.58	1.14	6.23	2.38	2.37	0.86
Mineralization	mean	21.79	0.82	1.00	49.61	9.65	4.10	0.70
(150-300 m)	min	8.27	0.01	0.06	1.13	0.12	0.09	0.05
n = 87	max	61.33	7.01	2.73	88.41	16.59	10.22	2.98
	s.d.	14.63	1.54	0.72	18.17	5.82	3.07	0.65
Propylitic Lavas	mean	11.86	2.25	0.56	56.42	14.54	5.44	3.10
(300-400 m)	min	5.58	0.46	0.09	43.39	12.08	1.16	0.53
n = 49	max	18.54	6.50	1.55	66.31	19.14	10.24	6.17
	s.d.	2.20	1.51	0.33	4.98	1.41	1.79	1.37
Greenschist Facies	mean	16.99	2.20	0.16	51.03	13.12	5.13	3.22
Lavas (400-689 m)	min	8.48	0.41	0.08	19.60	1.61	1.47	0.47
n = 126	max	43.74	11.76	0.93	70.67	18.35	9.40	6.10
	s.d.	6.92	1.57	0.14	8.88	2.66	1.46	1.11

s.d.: standard deviation

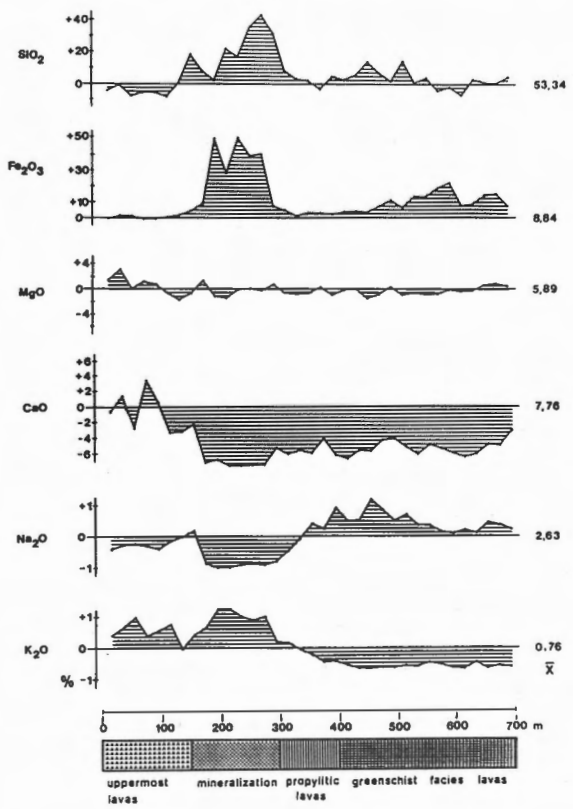

Figure 20: Aluminum normalized element gains and losses in Hole CY-2a in relation to the average values (indicated at the right) of hydrothermally almost unaffected 'Lower Pillow Lavas' (Desmet et al., 1980). Individual points represent the average of 20 m intervals, corresponding to a total of 330 analyses.

Potassium

Potassium shows a significant increase upward in CY-2a from the depleted greenschist facies rocks at base (avg. 0.16% K_2O; Table 9) through the propylitic rocks (avg. 0.56%) to the upper lavas (avg. 1.41%). The mineralized zone is distinctly enriched in K_2O (Figure 20) with a maximum content of 2.73%. The apparent relatively low average value of 1.00% K_2O (Table 9) for this interval is due to the masking effect of large increases of SiO_2 and Fe_2O_3. Feldspar alteration in deeper levels, coupled with mobilization and introduction of K into the highly altered zone is considered to be the principal process of K_2O enrichment. Mineralogically, the high K values of the mineralized zone (150-300 m) are reflected in an abundance of sericite/illite (Figure 4). In the uppermost lavas, K is fixed mainly in zeolites, celadonite and primary plagioclase.

Sodium, Calcium

The propylitic and greenschist facies altered rocks in CY-2a are distinctly depleted in Ca (avg. 2.25% and 2.20% CaO, respectively) and enriched in Na (avg. 3.10% and 3.22% Na_2O, respectively; Figure 20; Table 9). The reverse distribution of Ca and Na is explained by the transformation of primary Ca-plagioclase to oligoclase-albite. Sodium for this process is probably obtained from seawater with some from chloritization of volcanic glass. In addition to albitization, glass and pyroxene alteration liberates Ca. This results in a high Ca concentration of the hydrothermal fluids and a Ca depletion in the leached rocks as demonstrated in the lower section of CY-2a. In addition, leaching of Ca from basalt balances the precipitation of Mg from seawater and is therefore also related to this process (Mottl, 1983). Due to the almost complete breakdown of the primary minerals by alteration, the mineralized zone between 150-300 m is strongly depleted in Ca and Na, as demonstrated by the average values of 0.82% CaO and 0.70% Na_2O (Table 9). Some samples are almost completely free of Na and Ca, with only 0.05% Na_2O and 0.01% CaO, respectively, which indicates alteration under high water/rock ratios (cf. Rommel and Friedrichsen, 1987). The higher values of CaO between 0-100 m is reflected in the occurrence of zeolites, calcite and primary bytownite-labradorite.

Magnesium

The MgO concentrations show relatively constant average values of 5.13% in the greenschist facies, 5.44% in the propylitic zone, and 4.10% in the mineralized zone (Figure 20; Table 9). A slightly higher average of 6.75% MgO was determined for the lavas above 154 m. No distinct gains or losses of Mg relative to the 'standard' were observed in the alteration pipe (Figure 20). As indicated by experimental work (Seyfried and Mottl, 1982) and the discharge of Mg-free solutions at the East Pacific Rise (Edmond et al., 1982; Michard et al., 1984), the Mg concentration within hydrothermal systems at higher temperatures is largely controlled by the uptake by basalt of $Mg(OH)_2$ from downwelling seawater and incorporation of MgO into chlorite and smectite. Microprobe studies have shown that Fe-rich chlorite is the dominant species in CY-2a. This contrasts the low Mg concentration of the lower alteration zone. Magnesium is probably higher at deeper levels in the Sheeted Complex below the base of Hole CY-2a, where strong heating of downward percolating seawater took place. Elevated MgO values in the upper 100 m of the core are due to the occurrence of olivine-bearing basaltic-andesitic lavas (Bednarz et al., 1987).

The generally low Mg concentration observed in CY-2a contrasts with Mg-rich chloritic cores reported from alteration pipes of several Canadian deposits (Sangster, 1972; Franklin et al., 1981).

Iron

High Fe concentrations with an average content of 21.79% and a maximum of 61.33% Fe_2O_3 within the mineralized zone (Table 9) are closely related to the extensive sulphide mineralization between 150-300 m (Figure 20). Iron is also enriched in deeper levels of the alteration zone due to the existence of disseminated and vein pyrite.

Silica

Silica is enriched in the feeder channel and the pervasively mineralized zone (Figure 20), as indicated by quartz-sulphide-jasper assemblages. A maximum SiO_2 value of 88.41% was determined in one such zone. The average values of 51.53% (0-154 m), 49.61% (154-300 m), 56.42% (300-400 m) and 51.03% SiO_2 (400-689 m) listed in Table 9, only reveal relative SiO_2 concentrations resulting from normalizing the analyses to 100%. The true SiO_2 enrichment factors are evident from Figure 20. The highest SiO_2 values occur just below and at the top of the main ore zone (Figure 20). The latter may be explained by the strong temperature contrast which prevailed at this level, whereas the strong silicification associated with the lower level of the sulphide zone is most likely due to the precipitation of late stage quartz. The formation of this late stage quartz took place during cooling of the hydrothermal system below the critical temperature of quartz solubility. Silicification of the feeder zone during the waning stage of hydrothermal activity was also suggested by Bowers et al. (1985), who compared the chemical composition of fluids and chimneys at the East Pacific Rise 21°N with Cyprus ore deposits.

The element combination Ca-Na-K was found to be discriminative for different degrees of hydrothermal alteration in CY-2a (Figure 21).

Samples of the greenschist facies and propylitic altered zone group at the Na_2O apex, whereas the uppermost lavas, relatively unaffected by alteration, tend towards elevated CaO values. Samples from the mineralized and highly altered zone form an individual group with low CaO and Na_2O, but high K_2O content.

Trace Elements

The trace element distribution of CY-2a samples is given, in the form of averages for 20 m intervals, in Table 8 and shown graphically in Figure 22. The averages, ranges and standard deviations for each element with respect to the different alteration zones are given in Table 10.

In addition to the trace elements presented here, Pb, Bi, Sb, Mo, Ga, Nb, Zr and Y have been analyzed. Generally, the concentrations detected for Bi, Sb and Mo were found to be below the detection limit of 20 ppm for Bi and Sb, and 10 ppm for Mo. Elevated concentrations of Bi (up to 24 ppm), Sb (up to 62 ppm) and Mo (up to 42 ppm) were found only in the top zone of mineralization between 154 and 200 m. Elevated Pb values occur between 155 and 235 m (maximum 270 ppm) and between 416-462 m, where up to 1200 ppm Pb was detected. Gallium has relatively uniform values, varying between 10-30 ppm. Yttrium and Zr concentrations vary between 10-50 ppm and 20-115 ppm, respectively.

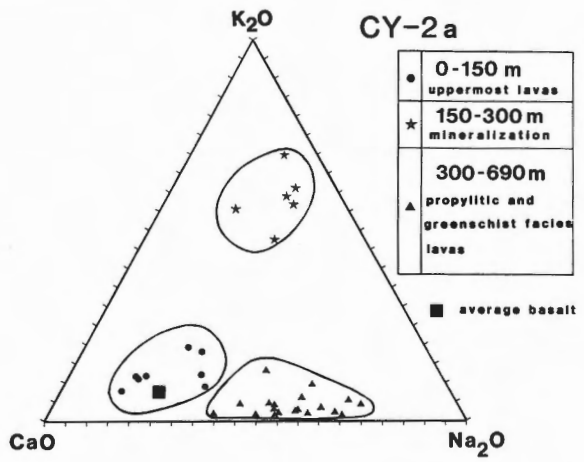

Figure 21: Ternary CaO-NaO-K_2O diagram showing 20 m interval averages of unaltered, mineralized and propylitic-greenschist facies samples from Hole CY-2a, corresponding to a total of 330 analyses. Average basalt according to Desmet et al. (1980).

Thallium was analyzed in 21 samples by AAS, following the method described by Ikramuddin (1983). Concentrations up to 2.19 ppm were found between 186-208 m depth in contrast to an average of 0.17 ppm for the upper 170 m. Between 260-420 m extremely low values (avg. 0.09 ppm) occur, whereas an average of 0.80 ppm was detected for samples below 450 m.

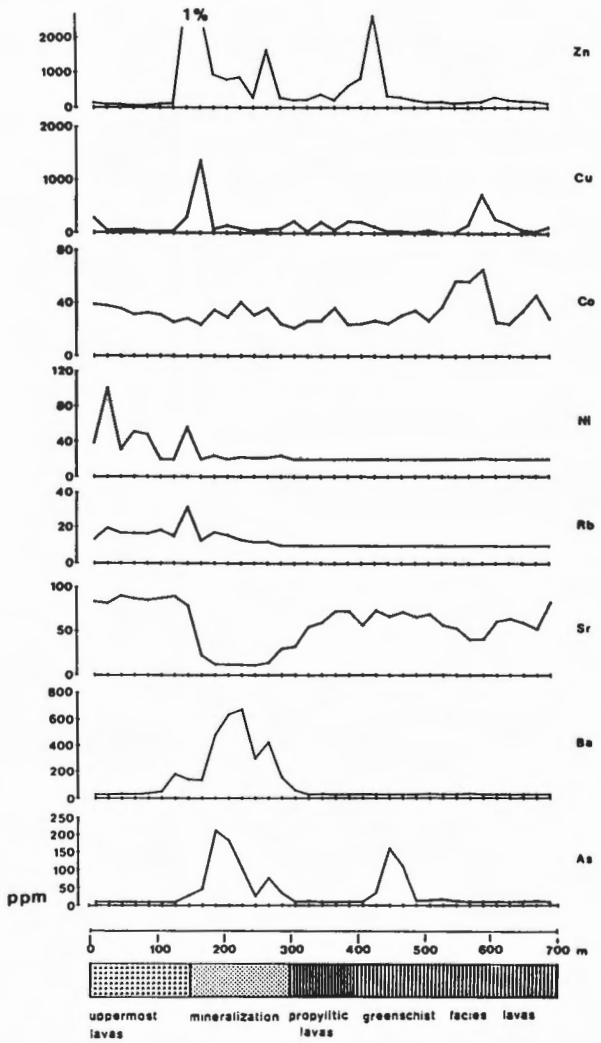

Figure 22: Distribution of selected trace elements in Hole CY-2a. Individual points represent the averages of 20 m intervals corresponding to a total of 330 analyses (cf. Table 10).

TABLE 10. Average Content of Ba, As, Zn, Cu, Ni, Co, Sr and Rb (ppm) in 330 Rock Samples from Uppermost Lavas (0-150 m), Mineralization (150-300 m), Propylitic Lavas (300-400 m) and Greenschist Facies Lavas (400-689 m) in the Drillcore CY-2a.

		Ba	As	Zn	Cu	Ni	Co	Sr	Rb
Uppermost Lavas	mean	46.43	10.20	111.71	77.23	46.29	33.14	85.12	19.88
(0-150 m)	min	30	10	46	20	20	20	16	10
n = 68	max	803	24	438	1522	325	55	106	187
	s.d.	93.64	1.69	74.84	189.92	51.45	7.19	14.38	22.81
Mineralization	mean	367.21	89.40	2561.10	326.50	26.94	31.67	20.14	13.18
(150-300 m)	min	30	10	21	20	20	20	10	10
n = 87	max	2130	807	110428	15220	412	114	130	33
	s.d.	366.58	170.47	12235.00	1664.90	42.63	16.77	22.17	5.54
Propylitic Lavas	mean	36.54	10.40	348.88	181.59	20.00	26.77	58.92	10.04
(300-400 m)	min	30	10	23	20	20	20	10	10
n = 49	max	303	30	2525	1140	20	44	97	11
	s.d.	37.92	2.77	379.58	275.42	0.00	7.72	20.88	0.19
Greenschist Facies	mean	30.81	29.40	426.35	144.47	20.08	36.56	60.51	10.00
Lavas (400-689 m)	min	24	10	52	20	20	20	16	10
n = 126	max	68	863	17508	2603	26	196	168	10
	s.d.	4.73	98.85	1572.00	342.13	0.61	30.45	20.50	0.00

s.d.: standard deviation

The mineralized zone is characterized by higher Zn (avg. 2561 ppm, max. 11%) than Cu (avg. 327 ppm, max. 1.5%) values (Figure 22; Table 10). The Cu/Zn average ratio decreases from 0.43 between 300-689 m to 0.13 between 154-300 m, indicating a decreasing temperature gradient (Franklin et al., 1981). However, no distinct zoning from a Cu-rich base to a Zn-rich top, typical of other volcanogenic sulphide deposits (Franklin et al., 1981) was observed.

Below 154 m Ni shows low average concentrations between 27 ppm (154-300 m) and less than 20 ppm (detection limit) between 300-689 m (Table 10). Elevated Ni concentrations up to 325 ppm occur in the uppermost, olivine-phyric lavas (Bednarz et al., 1987).

Cobalt displays the opposite behavior, showing a slight increase in concentration below 500 m, where a maximum of 196 ppm Co was detected. This reflects the higher Co content of pyrite in the lower part of the section.

In the greenschist facies and propylitized zones Sr is slightly depleted (avg. 61 and 59 ppm, respectively), mainly due to release of Sr during albitization. Strontium is strongly leached from the ore zone (avg. 20 ppm), which coincides with the complete decomposition of primary Ca minerals. Strontium-depleted rocks typically indicate proximity to hydrothermal activity (Govett, 1983).

The Rb values in the propylitic and greenschist facies zones were found to be generally below the detection limit of 10 ppm, but a slight increase in Rb can be observed in the mineralized zone (avg. 13 ppm) and the uppermost lavas (avg. 20 ppm). The positive correlation of Rb and K in the mineralized zone indicates, that Rb is bound to sericite and illite. The zone of mineralization is distinctly outlined by high Rb/Sr ratios.

The ore zone is clearly defined by the distribution of As, which shows an average value of 89 ppm, and a maximum value of 807 ppm between 154-300 m. High As concentrations up to 863 ppm were also found between 410-490 m.

A strong positive correlation is shown between sulphide mineralization and the distribution of Ba (Figure 22). Maximum values of more than 2000 ppm (Table 10) were found in the mineralized interval, which is characterized by a distinct Ba anomaly. Leaching of Ba from plagioclase, and to a lesser degree from pyroxene, by hydrothermal alteration, may be the principal process of Ba mobilization. The leached Ba was transported in upwelling hydrothermal fluids and redeposited during sulphide precipitation at higher levels. Barium depletion in the source rock is demonstrated in Figure

23, where the Ba values from 530-689 m are plotted against Zr. The stippled area in this figure was defined by Adamides (1984) and represents Ba-Zr values of hydrothermally unaffected gabbros and Lower Pillow Lavas from the Troodos ophiolite, which reveal a typical fractionation pattern with late stage incorporation of Ba in alkali plagioclase. Obviously, the Sheeted Complex samples from CY-2a (530-689 m) do not reflect this fractionation and show a distinct depletion in Ba due to later hydrothermal leaching.

A statistically significant positive correlation of r=0.7 (n=87) between K_2O and Ba occurs in the zone of mineralization indicating that Ba is bound to K-bearing minerals. Sericite/illite and celadonite are the only K silicates occurring in this interval. It can be concluded, that during sulphide precipitation, hydrothermally transported Ba was redeposited in the sericite/illite structure, where it substituted for K, and not in celadonite, which is of post-mineralization age. The occurrence of barite, identified by XRD in trace amounts in the sulphide zone, may be explained by the temporary dominance of sulfate-rich seawater in the horizon of sulphide precipitation, as suggested for the formation of hematite-bearing quartz and red jasper.

The association of Ba and sulphide mineralization has been further proven by the investigation of exploration boreholes from various mining areas in Cyprus (Herzig, 1986). Analyses of soil and surface rock samples have shown that Ba should be considered as a proximity indicator for exploration of Cyprus-type deposits (Friedrich et al., 1984; Herzig, 1986).

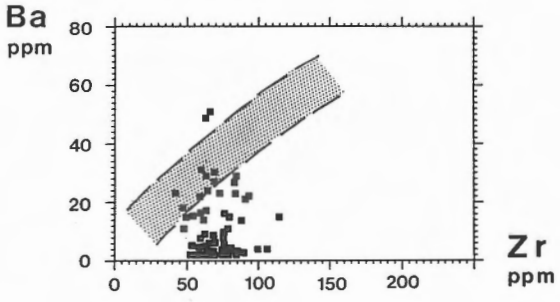

Figure 23: Ba-Zr diagram showing Ba depletion of rock samples between 530-689 m ('Sheeted Complex') in Hole CY-2a (squares) in relation to the Ba distribution pattern of equivalent rocks, unaffected by hydrothermal alteration (stippled area; after N.G. Adamides, unpub. rep., 1983).

SUMMARY AND CONCLUSIONS

Mineralogical and geochemical studies of core from the 689-m-deep Hole CY-2a within the Agrokipia hydrothermal sulphide deposit have led to a subdivision of the basaltic-andesitic-dacitic sequence into four major alteration zones.

Smectite-vermiculite, sepiolite, celadonite and zeolites are the principal secondary minerals occurring in the uppermost lavas of zone 1 between 0-154 m. This mineral assemblage is typical for alteration by seawater-basalt interaction within the zeolite facies. Temperatures between 50 and 135°C are estimated.

Zone 2 between 154-300 m, is characterized by sulphide-quartz-jasper mineralization associated with chlorite and sericite/illite. Alteration took place at maximum temperatures of about 250°C under high water/rock ratios. Iron, Si, K, Ba, As, Cu and Zn are considerably enriched in this zone, whereas Ca, Na and Sr are drastically depleted due to almost complete destruction of the primary minerals. The intensive alteration and abundant mineralization of zone 2 can be explained by the lithological characteristics of this interval. Hyaloclastites intercalated with massive lava flows and capped by a thick massive flow, permitted high water/rock ratios and thus were most favourable for sub-seafloor mixing of ascending hydrothermal fluids with downward penetrating seawater, causing pervasive replacement of glass and flows during intensive fluid/rock interaction, and precipitation of sulphides. Low temperature minerals found in the high temperature environment of zone 2 are considered to be late stage products, superimposed on the previously formed high temperature assemblage during the waning stages of hydrothermal activity.

Zone 3 between 300-400 m, represents a transition zone of propylitic alteration and is characterized by the first occurrence of albite at 300 m. In zone 4, from 400 to 689 m, the mineral assemblage epidote + chlorite + albite + sphene + calcite indicates lower greenschist facies conditions. Due to the absence of actinolite, alteration temperatures at the base of the hole did not markedly exceed 300°C. The propylitic and greenschist facies rocks of zones 3 and 4 are distinctly depleted in K and Ca and enriched in Na largely due to albitization processes.

Temperature estimates based on the distribution of secondary silicate minerals are supported by studies of chalcopyrite-pyrrhotite inclusions in pyrite, which indicate formation temperatures of $< 334 \pm 17$°C (Sugaki et al., 1975) below 580 m depth. The Fe-content of sphalerite points to formation temperatures < 250°C above and > 250°C below 270 m depth (Browne and Lovering, 1973; Scott and Kissin, 1973).

The chemical composition of silicate minerals (chlorite and epidote) and sulphides (pyrite,

chalcopyrite and sphalerite) shows no significant vertical variation within the alteration pipe of Agrokipia 'B'. Chlorites are Mg-rich (pycnochlorite) and are interpreted as having been formed in an environment of high seawater/fluid ratios, largely during reactions of wall rock with progressively heated downward percolating seawater. Iron-rich epidote occurring at high levels and more aluminous epidote at lower levels of the greenschist facies point to a decrease in fO_2 towards deeper zones of the hydrothermal system (cf. Liou, 1973). Pyrite, chalcopyrite and sphalerite throughout show a stoichiometry which is very similar to sulphides from the modern oceanic crust. The homogeneous stoichiometry of silicates and sulphides within CY-2a suggests a relatively uniform composition of the hydrothermal solutions with depth and time.

However, the presence of jasper, hematite-bearing quartz, barite and native sulfur in zone 2 indicates a temporary dominance of 'fresh' seawater in the zone of ore formation. Sudden mixing of large amounts of oxygen-rich seawater with hydrothermal fluids resulted in a temporary rise in fO_2 and pH, and caused the formation of oxidative minerals. Textural relations suggest that jasper and hematite-bearing quartz were formed relatively late, after the main period of sulphide deposition, probably during the waning stage of hydrothermal activity. Repeated fracturing of the oceanic crust during spreading would explain the sudden introduction of such large amounts of oxygenating seawater in the regime of sulphide formation. The resulting physico-chemical conditions persisted until the fractures were sealed by alteration minerals, or the passage ways were closed by further faulting. Pyrite, occurring disseminated in red jasper, was probably precipitated when anoxic conditions were re-established.

The mode of alteration and the secondary mineral paragenesis observed in CY-2a indicate at least two stages of hydrothermal activity:

1. An early stage of high temperature activity below 154 m with initial fluid temperatures of about 300°C.
2. A late stage of low temperature ($<$ 100°C) activity within the whole sequence during the waning stage of hydrothermal circulation.

The uppermost lavas were altered by seawater-basalt interaction and possibly by ascending hydrothermal fluids, previously cooled by sub-surface mixing.

The sulphide mineralization observed in the fossil hydrothermal system penetrated by Hole CY-2a is believed to be similar to sulphide formation in the modern oceanic crust. Agrokipia 'B' does not represent an exhalative deposit, where hydrothermal fluids discharged onto the seafloor, but is considered to be a typical example of a sulphide deposit, formed by sub-seafloor mixing of hot fluids with cold seawater. Present day analogues of those types of deposits may occur below hydrothermal mound areas, i.e. sites of emanation of low temperature fluids which previously cooled during sub-surface contact with seawater, as discovered at the East Pacific Rise at 21°N (Spiess et al., 1980) and recently during cruise SO-39 of RV SONNE at the Galapagos Spreading Center (H. Bäcker et al., in prep.). This suggests that economic sulphide deposits like Agrokipia 'B' may exist below the seafloor in areas of recent low temperature hydrothermal activity.

ACKNOWLEDGEMENTS

This study is part of a Ph.D. thesis in preparation by P.M.H. and was funded by a grant of the European Community Research & Development Program 'Raw Materials' given to G.H.F. The authors wish to thank the International Crustal Research Drilling Group for the opportunity to participate in the Cyprus Crustal Study Project. We thank K. Becker and D. Schöps for assistance with XRF analyses and data management, S. Keyssner and A. Germann for help during sampling in Cyprus, and H. Aghazadeh and A. O'Kelly for drawing the diagrams. We are grateful to P.T. Robinson, U. Bednarz and two anonymous referees for their constructive criticism on the manuscript.

REFERENCES

Adamides, N.G.
1984: Cyprus volcanogenic sulfide deposits in relation to their environment of formation; unpublished Ph.D. thesis, University of Leicester, p. 1-383.

Anderson, R.N., Honnorez, J., Becker, K., Adamson, A.C., Alt, J.C., Emmermann, R., Kempton , P.D., Kinoshita, H., Laverne, C., Mottl, M.J. and Newmark, R.L.
1982: DSDP hole 504 B, the first reference section over 1 km through Layer 2 of the oceanic crust; Nature, v. 300, p. 589-594.

Barton, P.B., Jr.
1978: Some ore textures involving sphalerite from the Furutobe mine, Akita Prefecture, Japan; Mining Geology, v. 28, p. 293-300.

Barton, P.B., Jr. and Skinner, B.J.
1979: Sulfide mineral stabilities; *in* Geochemistry of Hydrothermal Ore Deposits, 2nd Edition, ed. H.L. Barnes; John Wiley and Sons, New York, p.

278-403.

Barton, P.B., Jr. and Toulmin, P., III.
1966: Phase relations involving sphalerite in the Fe-Zn-S system; Economic Geology, v. 61, p. 815-849.

Bear, L.M.
1963: The mineral resources and mining industry of Cyprus; Cyprus Geological Survey Department, Ministry of Agriculture and Natural Resources, Bulletin, no. 1, p. 1-208.

Beaty, D.W. and Taylor, H.P., Jr.
1982: Some petrologic and oxygen isotopic relationships in the Amulet Mine, Noranda, Quebec, and their bearing on the origin of Archean massive sulfide deposits; Economic Geology, v. 77, p. 95-108.

Bednarz, U., Sunkel, G. and Schmincke, H.-U.
1987: The basaltic andesite-andesite and the andesite-dacite series from ICRDG drill-holes CY-2 and CY-2a. I. Lithology, petrology, and geochemistry; *in* Cyprus Crustal Study Project Initial Report Hole CY2-2a, ed. P.T. Robinson, I.L. Gibson and A. Panayiotou; Geological Survey of Canada, Paper 85-29.

Bischoff, J.L., Rosenbauer, R.J., Aruscavage, P.J., Baedecker, P.A. and Crock, J.G.
1983: Seafloor massive sulfide deposits from 21°N, East Pacific Rise, Juan de Fuca Ridge, and Galapagos Rift: bulk chemical composition and economic implications; Economic Geology, v. 78, p. 1711-1720.

Bowers, T.S., Von Damm, K.L. and Edmond, J.M.
1985: Chemical evolution of mid-ocean ridge hot springs; Geochimica et Cosmochimica Acta, v. 49, p. 2239-2252.

Bralia, A., Sabatini, G. and Troja, F.
1979: A revaluation of the Co/Ni ratio in pyrite as a geochemical tool in ore genesis problems; Mineralium Deposita, v. 14, p. 353-374.

Browne, P.R.L. and Ellis, A.J.
1970: The Ohaki-Broadlands hydrothermal area, New Zealand: mineralogy and related geochemistry; American Journal of Science, v. 269, p. 97-131.

Browne, P.R.L. and Lovering, J.F.
1973: Composition of sphalerites from the Broadland geothermal field and their significance to sphalerite geothermometry and geobarometry; Economic Geology, v. 68, p. 381-387.

Cann, J.R.
1981: Basalts from the ocean floor; *in* The Sea; Ideas and Observations on Progress in the Study of the Seas, Volume 7, The Oceanic Lithosphere, ed. C. Emiliani; John Wiley and Sons, New York, p. 363-390.

Colby, J.W.
1968: Quantitative microprobe analyses of thin insulating films; Advances in X-ray Analysis, v. 11, p. 287-305.

Craig, J.R., Ljøkjell, P. and Vokes, F.M.
1984: Sphalerite compositional variations in sulfide ores of the Norwegian Caledonides; Economic Geology, v. 79, p. 1727-1735.

Delaney, J.R., Mogk, D.W. and Mottl, M.J.
1980: High-temperature, sulfide-bearing hydrothermal system on the Mid-Atlantic Ridge at 23.6°North; Geological Society of America, Abstracts, v. 12, p. 411.

Desmet, A., Gagny, C., Lapierre, H. and Rocci, G.
1980: Organisation spatio-temporelle du complexe filonien du Troodos: son enracinement dans la chambre magmatique; *in* Ophiolites, Proceedings of the International Ophiolite Symposium, Cyprus, 1979, ed. A. Panayiotou; Cyprus Geological Survey Department, Ministry of Agriculture and Natural Resources, p. 66-72.

Duke, N.A. and Hutchinson, R.W.
1974: Geological relationships between massive sulfide bodies and ophiolitic volcanic rocks near York Harbour, Newfoundland; Canadian Journal of Earth Sciences, v. 11, p. 53-64.

Edmond, J.M., Von Damm, K.L., McDuff, R.E. and Measures, C.I.
1982: Chemistry of hot springs on the East Pacific Rise and their effluent dispersal; Nature, v. 297, p. 187-191.

Eldridge, C.S., Barton, P.B., Jr. and Ohomoto, H.
1983: Mineral textures and their bearing on formation of the Kuroko orebodies; Economic Geology, Monographs, v. 5, p.241-281.

Ellis, A.J.
1979: Explored geothermal systems; *in* Geochemistry of Hydrothermal Ore Deposits, 2nd Edition, ed. H.L. Barnes; John Wiley and Sons, New York, p. 632-683.

Elthon, D.
1981: Metamorphism in oceanic spreading centers; *in* The Sea; Ideas and Observations on Progress in the Study of the Seas, Volume 7, The Oceanic Lithosphere, ed. C. Emiliani; John Wiley and Sons, New York, p. 285-303.

Evarts, R.C. and Schiffmann, P.

1983: Submarine hydrothermal metamorphism on the Del Puerto ophiolite, California; American Journal of Science, v. 283, p. 289-340.

Exley, R.A.
1982: Electron microprobe studies of the Island Research Drilling Project high-temperature hydrothermal mineral geochemistry; Journal of Geophysical Research, v. 87, no. B8, p. 6547-6557.

Finlow-Bates, T. and Stumpfl, E.F.
1981: The behaviour of so called immobile elements in hydrothermally altered rocks associated with volcanogenic submarine-exhalative ore deposits; Mineralium Deposita, v. 16, p. 319-328.

Fleischer, M.
1955: Minor elements in some sulfide minerals; Economic Geology, 50th Anniversary Volume, p. 970-1024.

Floyd, P.A. and Winchester, J.A.
1978: Identification and discrimination of altered and metamorphosed volcanic rocks using immobile elements; Chemical Geology, v. 21, p. 291-306.

Francheteau, J., Needham, H.D., Choukroune, P., Juteau, T., Séguret, M., Ballard, R.D., Fox, P.J., Normark, W., Carranza, A., Cordoba, D., Guerrero, J., Rangin, C., Bougault, H., Cambon, P. and Hekinian, R.
1979: Massive deep-sea sulfide ore deposits discovered on the East Pacific Rise; Nature, v. 277, no. 5697, p. 523-528.

Franklin, J.M.
1984: Volcanic-associated massive sulfide deposits recent to Precambrian; Irish Association for Economic Geology, Abstracts.

Franklin, J.M., Lydon, J.W. and Sangster, D.F.
1981: Volcanic-associated massive sulfide deposits; Economic Geology, 75th Anniversary Volume, p. 485-627.

Friedrich, G., Herzig, P., Keyssner, S. and Maliotis, G.
1984: The distribution of Hg, Ba, Cu and Zn in the vicinity of cupriferous sulfide deposits, Troodos Complex, Cyprus; Journal of Geochemical Exploration, v. 21, p. 167-174.

Gass, I.G.
1960: The geology and mineral resources of the Dhali area; Cyprus Geological Survey Department, Ministry of Agriculture and Natural Resources, Memoir, no. 4, p. 1-116.

Gillis, K.M. and Robinson, P.T.
1985: Low-temperature alteration of the extrusive sequence, Troodos ophiolite, Cyprus; Canadian Mineralogist, v. 23, p. 431-441.

Gordon-Smith, F.
1942: Variation in the properties of pyrite; American Mineralogist, v. 27, p. 1-19.

Govett, G.J.S.,
1983: Rock geochemistry in mineral exploration; *in* Handbook of Exploration Geochemistry, Volume 3; Elsevier, p. 1-396.

Hall, B.V.
1982: Geochemistry of the alteration pipe at the Amulet upper A deposit, Noranda, Quebec; Canadian Journal of Earth Sciences, v. 19, p. 2060-2084.

Hall, J.M.
1985: The Iceland Research Drilling Project crustal section: variation of magnetic properties with depth in Icelandic-type oceanic crust; Canadian Journal of Earth Sciences, v. 22, no. 1, p. 85-101.

Hall, J.M., Ward, T. and Fisher, B.E.
1987: Rock magnetism, oxide petrography and alteration state in Samples from CCSP Hole CY-2a through the Agrokipia B ore body and stockwork, Cyprus; *in* Cyprus Crustal Study Project Initial Report Hole CY2-2a, ed. P.T. Robinson, I.L. Gibson and A. Panayiotou; Geological Survey of Canada, Paper 85-29.

Haymon, R.M.
1983: Growth history of hydrothermal black smoker chimneys; Nature, v. 301, p. 695-698.

Heaton, T.H.E. and Sheppard, S.M.F.
1977: Hydrogen and oxygen isotope evidence for sea-water hydrothermal alteration and ore deposition, Troodos complex, Cyprus; *in* Volcanic Processes in Ore Genesis; Geological Society of London, Special Publication, no. 7, p. 42-57.

Hekinian, R., Fevrier, M., Bischoff, J.L., Picot, P. and Shanks, W.C.
1980: Sulfide deposits from the East Pacific Rise near 21°N; Science, v. 207, p. 1433-1444.

Hekinian, R. and Fouquet, Y.
1985: Volcanism and metallogenesis of axial and off-axial structures on the East Pacific Rise near 13°N; Economic Geology, v. 80, p. 221-249.

Henley, R.W. and Ellis, A.J.
1983: Geothermal systems ancient and modern: a geochemical review; Earth Science Reviews, v. 19, p. 1-50.

Herzig, P.M.
1982: Geochemical investigation of cupriferous pyrite deposits in the Troodos ophiolite

complex, Cyprus; unpublished Dipl. thesis, Aachen Technical University, p. 1-231.

1986: Barium in seafloor hydrothermal processes and its significance for exploration of Cyprus sulfide deposits; *in* Metallogeny of Basic and Ultrabasic Rocks, Proceedings; Institution of Mining and Metallurgy, London.

Hey, M.H.

1954: A new review of the chlorites; Mineralogical Magazine, v. 30, p. 277.

Holdaway, M.J.

1972: Thermal stability of Al-Fe-epidote as a function of fO_2 and Fe content; Contributions to Mineralogy and Petrology, v. 37, p. 307-340.

Honnorez, J.

1981: The aging of the oceanic crust at low temperature; *in* The Sea; Ideas and Observations on Progress in the Study of the Seas, Volume 7, The Oceanic Lithosphere, ed. C. Emiliani; John Wiley and Sons, New York, p. 525-587.

Humphris, S.E. and Thompson, G.

1978: Hydrothermal alteration of oceanic basalts by seawater; Geochimica et Cosmochimica Acta, v. 42, no. 2, p. 107-125.

Hutchinson, M.N. and Scott, S.D.

1981: Sphalerite geobarometry in the Cu-Fe-Zn-S system; Economic Geology, v. 76, p. 143-153.

Ikramuddin, M.

1983: A rapid and precise method for the determination of thallium in geological materials at the one nanogram per gram level; Atomic Spectroscopy, v. 4, p. 101-102.

Ixer, R.A., Alabaster, T. and Pearce, J.A.

1984: Ore petrography and geochemistry of massive sulfide deposits within the Semail ophiolite, Oman; Institution of Mining and Metallurgy, London, Transactions and Bulletin, Section B; Applied Earth Sciences, v. 93, p. 114-124.

Johnson, A.E.

1972: Origin of the Cyprus pyrite deposits; International Geological Congress, Report, 24th Session, Section 4, Montreal, p. 291-298.

Keith, T.E.C., Muffler, L.J.P. and Cremer, M.

1968: Hydrothermal epidote formed in the Salton Sea geothermal system, California; American Mineralogist, v. 53, p. 1635-1644.

Kissin, S.A. and Scott, S.D.

1982: Phase relations involving pyrrhotite below 350°C; Economic Geology, v. 77, p. 1739-1754.

Kojima, S. and Sugaki, A.

1985: Phase relations in the Cu-Fe-Zn-S system between 500°C and 300°C under hydrothermal conditions; Economic Geology, v. 80, p. 158-171.

Koski, R.A., Clague, D.A. and Oudin, E.

1984: Mineralogy and chemistry of massive sulfide deposits from the Juan de Fuca Ridge; Geological Society of America, Bulletin, no. 95, p. 930-945.

Kottrup, G. and Rehder, S.

1983: MAX Program Description; Bundesanstalt für Geowissenschaften und Rohstoffe, Hannover, p. 1-109.

Krause, H.

1961: Analytische und röntgenographische Untersuchungen natürlicher Zinkblenden; Neues Jahrbuch für Mineralogie, Abhandlungen, v. 97, p. 143-164.

Krauskopf, K.B.

1979: Introduction to Geochemistry; McGraw-Hill, Tokyo, p. 1-617.

Kristmannsdottir, H.

1976: Types of clay minerals in hydrothermally altered basaltic rocks; Reykjanes, Iceland, Jökull, v. 26, p. 30-39.

Lafitte, M. and Maury, R.

1983: The stoichiometry of sulfides and its evolution: a chemical study of pyrites, chalcopyrites and sphalerites from terrestrial and oceanic environments; Earth and Planetary Science Letters, v. 64, p. 145-152.

Lafitte, M., Maury, R., Perseil, E.A. and Boulegue, J.

1985: Morphological and analytical study of hydrothermal sulfides from 21°North East Pacific Rise; Earth and Planetary Science Letters, v. 73, p. 53-64.

Large, R.R.

1977: Chemical evolution and zonation of massive sulfide deposits in volcanic terrains; Economic Geology, v. 72, p. 549-572.

Lewis, B.T.R. and Garmany, J.D.

1982: Constraints on the structure of the East Pacific Rise from seismic refraction data; Journal of Geophysical Research, v. 87, no. B10, p. 8417-8425.

Liou, J.G.

1971: Synthesis and stability relations of prehnite, $Ca_2Al_2Si_3O_{10}(OH)_2$; American Mineralogist, v. 56, p. 507-531.

1973: Synthesis and stability relations of epidote, $Ca_2Al_2FeSi_3O_{12}(OH)$; Journal

of Petrology, v. 14, p. 381-413.

Loftus-Hills, G. and Solomon, M.
1967: Cobalt, nickel and selenium in sulphides as indicators of ore genesis; Mineralium Deposita, v. 2, p. 228-242.

Lonsdale, P.F., Bischoff, J.L., Burns, V.M., Kastner, M. and Sweeney, R.E.
1980: A high-temperature hydrothermal deposit on the seabed at a Gulf of California spreading center; Earth and Planetary Science Letters, v. 49, no. 1, p. 8-20.

Lydon, J.W.
1984: Some observations on the mineralogical and chemical zonation patterns of volcanogenic sulphide deposits of Cyprus; *in* Current Research, Part A, Geological Survey of Canada, Paper 84-1A, p. 611-616.

Michard, G., Albarede, F., Michard, A., Minster, J.-F., Charlou, J.-L. and Tan, N.
1984: Chemistry of solutions from 13°N East Pacific Rise hydrothermal site; Earth and Planetary Science Letters, v. 67, p. 297-307.

Mookherjee, A.
1962: Certain aspects of the geochemistry of cadmium; Geochimica et Cosmochimica Acta, v. 26, p. 351-360.

Mottl, M.J.
1983: Metabasalts, axial hot springs, and the structure of hydrothermal systems at mid-ocean ridges; Geological Society of America, Bulletin, no. 94, p. 161-180.

Mottl, M.J. and Holland, H.D.
1978: Chemical exchange during hydrothermal alteration of basalt by seawater. I. Experimental results for major and minor components of seawater; Geochimica et Cosmochimica Acta, v. 42, no. 8, p. 1103-1115.

Normark, W.R., Morton, J.L., Koski, R.A., Clague, D.R. and Delaney, J.R.
1983: Active hydrothermal vents and sulfide deposits on the southern Juan de Fuca Ridge; Geology, v. 11, p. 158-163.

Oudin, E.
1983: Hydrothermal sulfide deposits of the East Pacific Rise (21°N). Part I: Descriptive mineralogy; Marine Mining, v. 4, p. 39-72.

Palmason, G.S., Arnorsson, I.B., Fridleifsson, H., Kristmannsdottir, K., Saemundsson, V., Stefansson, B., Steingrimsson, J., Tomasson, J. and Kristjansson, L.
1979: The Iceland crust: evidence from drill hole data on structure and processes; *in* Deep Drilling Results in the Atlantic Ocean: Ocean Crust, Maurice Ewing Series, Volume 2, ed. M. Talwani, C.G. Harrison and D.E. Hayes; American Geophysical Union, Transactions, v. 2, p. 43-65.

Pearce, J.A. and Cann, J.R.
1973: Tectonic setting of basic volcanic rocks determined using trace element analyses; Earth and Planetary Science Letters, v. 19, no. 1, p. 290-300.

Pritchard, R.G.
1979: Alteration of basalts from DSDP legs 51, 52, and 53, holes 417 A and 418 A; *in* Initial Reports of the Deep Sea Drilling Project, Volumes 51-53, Part 2, U.S. Government Printing Office, Washington, D.C., v. 51-53, pt. 2, p. 1185-1200.

Ramdohr, P.
1975: Die Erzminerale und ihre Verwachsungen; Akademie-Verlag, Berlin, p. 1-1277.

Rautenschlein, M., Jenner, G.A., Hertogen, J., Hofmann, A.W., Kerrich, R., Schmincke, H.-U. and White, W.M.
1985: Isotopic and trace element composition of volcanic glasses from the Akaki Canyon, Cyprus: implications for the origin of the Troodos ophiolite; Earth and Planetary Science Letters, v. 75, no. 4, p. 369-383.

Reid, I., Orcutt, J.A. and Prothero, W.L.
1977: Seismic evidence for a narrow zone of partial melting underlying the East Pacific Rise at 21°N; Geological Society of America, Bulletin, no. 88, p. 678-682.

Riverin, G.
1977: Wall-rock alteration at the Millenbach mine, Noranda area, Quebec; unpublished Ph.D. thesis, Queen's University, Kingston, p. 1-255.

Robertson, A.H.F. and Woodcock, N.H.
1980: Tectonic setting of the Troodos massif in the east Mediterranean; *in* Ophiolites, Proceedings of the International Ophiolite Symposium, Cyprus, 1979, ed. A. Panayiotou; Cyprus Geological Survey Department, Ministry of Agriculture and Natural Resources, p. 36-49.

Robinson, P.T. and Gibson, I.L.
1983: Cyprus Crustal Study Project. Hole CY-2a lithologic unit summaries.

Robinson, P.T. and Hall, J.M.
1983: Hydrothermal circulation and base metal sulfide deposition in oceanic crust: results of research drilling in the Agrokipia ore deposits, Cyprus; Geological Association of Canada, Program with Abstracts, v. 9, p. 58.

Robinson, P.T., Hall, J.M. and Malpas, J.
1984: The principle results of the Cyprus Crustal Study Project to May 1984; Geological Association of Canada, Program with Abstracts, v. 9, p. 100.
Robinson, P.T., Melson, W.G., O'Hearn, T. and Schmincke, H.-U.
1983: Volcanic glass compositions of the Troodos ophiolite, Cyprus; Geology, v. 11, no. 7, p. 400-404.
Rommel, U. and Friedrichsen, H.
1987: The alteration chemistry of CY-2a: a stable and radiogenic isotope study; *in* Cyprus Crustal Study Project Initial Report Hole CY2-2a, ed. P.T. Robinson, I.L. Gibson and A. Panayiotou; Geological Survey of Canada, Paper 85-29.
Rona, P.A.
1984: Hydrothermal mineralization at seafloor spreading centers; Earth-Science Reviews, v. 20, p. 1-104.
Sangster, D.F.
1972: Precambrian volcanogenic massive sulphide deposits in Canada: a review; Geological Survey of Canada, Paper 72-22, p. 1-44.
Schmincke, H.-U., Rautenschlein, M., Robinson, P.T. and Mehegan, J.M.
1983: Troodos extrusive series of Cyprus: a comparison with oceanic crust; Geology, v. 11, no. 7, p. 405-409.
Scott, S.D.
1973: Experimental calibration of the sphalerite geobarometer; Economic Geology, v. 68, p. 466-474.
Scott, S.D. and Barnes, H.L.
1971: Sphalerite geothermometry and geobarometry; Economic Geology, v. 66, p. 653-669.
Scott, S.D. and Kissin, S.A.
1973: Sphalerite composition in the Zn-Fe-S system below 300°C; Economic Geology, v. 68, p. 475-479.
Seyfried, W.E., Jr. and Bischoff, J.L.
1979: Low temperature basalt alteration by seawater: an experimental study at 70°C and 150°C; Geochimica et Cosmochimica Acta, v. 43, p. 1937-1947.
Seyfried, W.E., Jr. and Mottl, M.J.
1982: Hydrothermal alteration of basalt by seawater under seawater-dominated conditions; Geochimica et Cosmochimica Acta, v. 46, p. 985-1002.
Sims, P.K. and Barton, P.B., Jr.
1961: Some aspects of the geochemistry of sphalerite, Central City district, Colorado; Economic Geology, v. 56, p. 1211-1237.
Skinner, B.J.
1958: The geology and metamorphism of the Nairne pyritic formation, a sedimentary sulfide deposit in south Australia; Economic Geology, v. 53, p. 546-563.
Skinner, B.J., White, D.E., Rose, H.J. and Mays, R.E.
1967: Sulfides associated with the Salton Sea geothermal brine; Economic Geology, v. 62, p. 316-330.
Soen, O.I. and Pauly, H.
1967: A sulphide paragenesis with pyrrhotite and marcasite in the siderite-cryolite ore of Ivigtut, South Greenland; Meddelelser om Gronland, v. 175, p. 1-55.
Spiess, F.N., Macdonald, K.C., Atwater, T., Ballard, R., Carranza, A., Cordoba, D., Cox, C., Diaz Garcia, V.M., Francheteau, J., Guerrero, J., Hawkins, J., Haymon, R., Hessler, R., Juteau, T., Kastner, M., Larson, R., Luyendyk, B., MacDougall, J.D., Miller, S., Normark, W., Orcutt, J. and Rangin, C.
1980: East Pacific Rise: hot springs and geophysical experiments; Science, v. 207, no. 4438, p. 1421-1433.
Spooner, E.T.C.
1977: Hydrodynamic model for the origin of the ophiolitic cupriferous pyrite ore deposits of Cyprus; *in* Volcanic Processes in Ore Genesis; Geological Society of London, Special Publication, no. 7, p. 58-71.
Spooner, E.T.C., Beckinsale, R.D., Fyfe, W.S. and Smewing, J.D.
1974: O^{18} enriched ophiolitic metabasic rocks from E. Liguria (Italy), Pindos (Greece), and Troodos (Cyprus); Contributions to Mineralogy and Petrology, v. 47, p. 41-62.
Spooner, E.T.C. and Bray, C.J.
1977: Hydrothermal fluids of seawater salinity in ophiolitic sulfide ore deposits in Cyprus; Nature, v. 266, no. 5605, p. 808-812.
Spooner, E.T.C. and Fyfe, W.S.
1973: Sub-sea-floor metamorphism, heat and mass transfer; Contributions to Mineralogy and Petrology, v. 42, p. 287-304.
Steiner, A.
1968: Clay minerals in hydrothermally altered rock at Wairakei, New Zealand; Clays and Clay Minerals, v. 16, p. 193-213.
Stoiber, R.E.
1940: Minor elements in sphalerite; Economic Geology, v. 35, p. 501-519.
Sugaki, A., Shima, H., Kitakaze, A. and Harada, H.
1975: Isothermal phase relations in the system Cu-Fe-S under hydrothermal conditions

at 350°C and 300°C; Economic Geology, v. 70, p. 806-823.

Sunkel, G., Bednarz, U. and Schmincke, H.-U.
1987: The basaltic andesite-andesite and the andesite-dacite series from the ICRDG drill holes CY-2 and CY-2a. II. Alteration; *in* Cyprus Crustal Study Project Initial Report Hole CY2-2a, ed. P.T. Robinson, I.L. Gibson and A. Panayiotou; Geological Survey of Canada, Paper 85-29.

Tomasson, J. and Kristmannsdottir, H.
1972: High temperature alteration minerals and thermal brines, Reykjanes, Iceland; Contributions to Mineralogy and Petrology, v. 36, p. 123-134.

Viereck, L.G., Griffin, B.J., Schmincke, H.-U. and Pritchard, R.G.
1982: Volcaniclastic rocks of the Reydarfjordur drill hole, Eastern Iceland. 2. Alteration Journal of Geophysical Research, v. 87, no. B8, p. 6459-6476.

Wiggins, L.B. and Craig, J.R.
1980: Reconnaissance of the Cu-Fe-Zn-S system: sphalerite phase relationships; Economic Geology, v. 75, p. 742-751.

Willan, R.C.R. and Hall, A.J.
1980: Sphalerite geobarometry and trace-element studies on stratiform sulphide from McPhun's Cairn, Loch Fyne, Argyll, Scotland; Institution of Mining and Metallurgy, London, Transactions and Bulletin, Section B; Applied Earth Sciences, v. 89, p. B31-B40.

Yund, R.A. and Kullerud, G.
1966: Thermal stability of assemblages in the Cu-Fe-S system; Journal of Petrology, v. 7, p. 454-488.

Geochemistry of a Fossil Ore-Solution Aquifer: Chemical Exchange Between Rock and Hydrothermal Fluid Recorded in the Lower Portion of Research Drill Hole CY-2a, Agrokipia, Cyprus

HEATHER E. JAMIESON[1] AND J.W. LYDON[2]

[1]Department of Geological Sciences, Queen's University, Kingston, Ontario, Canada, K7L 3N6
[2]Geological Survey of Canada, 601 Booth Street, Ottawa, Canada, K1A 0E8

Jamieson, H.E. and Lydon, J.W., Geochemistry of a fossil ore-solution aquifer: chemical exchange between rock and hydrothermal fluid recorded in the lower portion of research drill hole CY-2a, Agrokipia, Cyprus; in *Cyprus Crustal Study Project: Initial Report, Holes CY-2 and 2a, ed. P.T. Robinson, I.L. Gibson and A. Panayiotou; Geological Survey of Canada, Paper 85-29, p. 139-152, 1987.*

Abstract

Thirty-six samples of hydrothermally altered rock from the lower portion of the Cyprus Crustal Study Project drill hole CY-2a have been analyzed for major, minor and selected trace elements. Because these pervasively altered dykes and lavas underlie the Agrokipia 'A' orebody, and contain minor sulphide mineralization, they may represent a fossil aquifer in which the ore-forming hydrothermal solutions once resided. The geochemical results indicate that both the iron and the sulphur contained in pyrite were added to the rocks. Calcium has been depleted from most of the samples, but locally enriched in epidote-rich patches. Trace amounts of copper, zinc, lead and manganese are concentrated together in sulphides and Mn-rich chlorites. These patterns suggest that the lower portion of CY-2a interacted with either several hydrothermal fluids, or with a single fluid that underwent several changes in its chemical behaviour. Sulphur isotope values from anhydrite and gypsum, which coexist with pyrite in veins, indicate that sulfate was precipitated from seawater of the same age as the host lavas.

Résumé

Une analyse d'éléments majeurs, mineurs, et de certains éléments traces a porté sur 36 échantillons de roches altérées par des solutions hydrothermales provenant de la partie inférieure du trou de forage CY-2a du Cyprus Crustal Study Project. Ces dykes et ces laves profondément altérés et sous-jacents au gîte Agrokipia 'A', lesquels contiennent de faibles quantités de sulfures, représentent possiblement un aquifère fossile dans lequel résidaient les solutions hydrothermales qui formèrent le gîte. Les données géochimiques révèlent que le fer et le soufre contenus dans la pyrite furent ajoutés à la roche. Dans la majorité des échantillons on note un appauvrissement du calcium, mais il y a localement un enrichissement dans les plages fortement épidotisées. Le cuivre, le zinc, le plomb et le manganèse à l'état de trace sont concentrés et groupés dans les sulfures et les chlorites enrichies en manganèse. Ces modes de distribution suggèrent une interaction de la partie inférieure du trou de forage CY-2a avec les fluides hydrothermaux, ou avec un liquide unique dont le comportement chimique aurait été modifié à plusieurs reprises. Les analyses des isotopes du soufre dans l'anhydrite et le gypse, lesquels minéraux accompagnent la pyrite dans les veines, indiquent une précipitation du sulfate à partir d'une eau de mer de même âge que les laves qui portent la minéralisation.

INTRODUCTION

Hydrothermally altered rock present in the lower 300 metres of the 700 m deep research drill hole CY-2a has been tentatively identified as a fossil aquifer in which the fluids responsible for depositing the overlying Agrokipia sulfide orebodies once resided. To test this hypothesis, the mineralogy and geochemistry of this core interval has been examined in detail. The mineralogy is discussed in the companion paper to this one, published elsewhere in this volume (Jamieson et al., 1987). The dykes and interstitial lavas are divided into two alteration zones: the hydrothermal greenschist zone, where the mineral assemblage is consistently dominated by albite - chlorite - quartz - sphene, and the zone of differential metasomatism, where fragmental rocks have been replaced by monomineralic patches of epidote. In this paper, the results of chemical analysis of whole rock samples is discussed in the context of chemical exchange between reservoir rock and hydrothermal fluid.

METHODS

Table 1 lists the results of chemical analysis of thirty-six rock samples from the CY-2a core. The major elements and zirconium were determined by X-ray fluorescence, volatiles by chemical methods, and the trace elements by atomic absorption. Sulphur is assumed to exist as a sulphide in all cases, so that the amount of oxygen-equivalent sulphur anions has been subtracted from the total. This is not completely valid for those samples that contain significant calcium sulphate, and, in those cases, this method of calculation produces artificially low totals.

The number of significant figures shown for each element is an indication of the reproducibility for that element as determined in routine laboratory analysis. Samples 474.9 and 475.0 are duplicates of a macroscopically homogeneous dyke that were submitted in order to test reproducibility, which appears to be satisfactory. The only element for which the results are less reproducible than expected is sulphur, which is the result of the inhomogeneous distribution of pyrite, rather than analytical problems.

Samples selected for analysis include pillow breccias, massive flows and dykes. No attempt was made to avoid pyrite veins, so that the mobilization of other elements along with pyrite could be determined. This led to the problem of irregularly-distributed pyrite obscuring other chemical variations as discussed below. For sites within the zone of differential metasomatism, pairs of adjacent samples (at depths of 667.0 m, 670.0 m, and 680.0 m) were chosen so that one was rich in epidote and the other poor, providing the opportunity to test the mobility of all elements involved in producing the epidote patches.

GENERAL OBSERVATIONS

The following general insights into the nature of alteration processes in the rocks underlying the Agrokipia orebody are provided by the geochemical data in Table 1, and supported by the petrographic observations reported in the companion paper (Jamieson et al., 1987). The differences in chemical composition between variably altered samples is discussed in relative terms. In the absence of density measurements, or firm identification of immobile components, absolute gains and losses are uncertain.

1. Both the iron and the sulphur in pyrite were introduced from elsewhere.
2. All the rocks with greenschist-type assemblages have been depleted in calcium to about the same degree.
3. Local patches of epidote-rich rock are enriched in calcium, and depleted in magnesium, sodium and titanium.
4. Copper, zinc, lead and manganese have been locally concentrated together in sulfides and Mn-enriched chlorites.
5. Apart from the four processes described above, there has apparently been little element migration. Notably, magnesium contents appear to be little changed from the primary igneous values.

THE PYRITE PROBLEM

Before the whole-rock analyses can be interpreted in a useful manner, the problem of the irregular distribution of pyrite veins must be resolved. Macroscopic examination of the core reveals that pyrite is distributed in a highly inhomogeneous manner on the scale of a hand specimen or a sample used for chemical analysis. Analyzed sulphur values range from negligible to 18 weight percent. This obscures systematic variations in other elements that are contained in phases distributed in a more homogeneous manner. (Epidote is also distributed in irregular patches within the zone of differential metasomatism, but in order to identify other elements segregated by epidotization, epidote-rich samples and adjacent epidote-poor samples were segregated, as described above.) Because virtually all sulphur is contained in pyrite, the analyses can be corrected by subtracting the sulphur together with an appropriate amount of iron, and renormalizing the remaining elements (Table 2). This correction increases the similarity of FeO values for the duplicate analyses (474.9 and 475.0). Chalcopyrite and sphalerite are

TABLE 1. Chemical Analyses of Rock Samples from the Lower Portion of CY-2a Drill Hole

Depth	370.5	398.5	406.3	426.0	434.5-1	434.5-2	455.9	462.0	474.9*
SiO_2 (wt.%)	53.2	63.1	53.6	49.0	46.5	57.0	48.6	48.6	56.1
TiO_2	1.30	1.02	1.18	1.11	1.16	1.29	1.45	1.00	1.01
Al_2O_3	14.7	13.9	13.2	12.8	13.6	15.2	15.3	10.6	12.5
FeO	10.7	8.1	11.8	13.0	10.9	9.2	13.2	14.3	10.3
MnO	0.37	0.38	0.39	0.55	1.02	0.79	0.76	0.19	0.29
MgO	5.29	4.39	6.77	5.52	6.52	5.61	8.24	3.84	3.77
CaO	6.54	1.38	0.38	1.49	1.50	1.88	1.63	2.23	2.24
Na_2O	2.0	4.1	1.7	2.7	2.2	3.4	2.3	2.7	2.6
K_2O	0.06	0.19	0.26	0.09	0.07	0.13	0.02	0.06	0.14
H_2O	4.5	3.6	7.1	7.1	6.9	5.0	7.0	7.8	5.5
CO_2	0.8	0.0	0.2	0.3	0.2	0.2	0.5	0.9	0.1
P_2O_5	0.07	0.12	0.09	0.07	0.10	0.13	0.07	0.09	0.12
S	0.05	0.09	2.44	4.74	1.55	0.91	0.72	8.88	3.79
O equiv.	0.0	0.0	0.95	1.77	0.58	0.34	0.27	3.32	1.42
TOTAL	99.7	100.4	98.3	96.7	95.5	100.5	99.6	97.9	97.1
Cu (ppm)	48	11	52	94	129	38	45	35	8
Pb	7	3	5	73	6570	338	13	58	9
Zn	106	552	480	558	1760	610	620	236	217
Cr	4	4	4	4	8	7	6	8	4
Mn	3100	2900	3200	4000	9500	7200	7000	1400	2200
Ba	65	30	40	30	35	20	35	45	35
Sr	88	74	34	42	66	76	46	48	56
Zr	60	80	60	60	80	80	70	40	70

Depth	475.0*	483.8	497.4	503.4	515.7	528.3	539.4	544.0	553.5
SiO_2 (wt.%)	55.8	52.8	41.2	49.6	55.4	50.4	43.5	51.8	54.8
TiO_2	0.97	1.31	0.90	1.40	1.18	1.11	1.19	1.12	1.13
Al_2O_3	12.7	15.6	8.9	14.1	13.7	11.7	13.7	13.1	13.1
FeO	11.4	11.0	22.5	12.9	11.2	15.3	16.1	13.6	11.7
MnO	0.27	0.31	0.17	0.34	0.28	0.22	0.25	0.25	0.21
MgO	3.63	6.13	2.63	6.84	4.83	3.99	4.56	5.15	4.96
CaO	2.34	1.39	2.16	1.91	1.63	1.62	1.55	1.49	1.51
Na_2O	2.7	4.1	1.6	2.5	2.8	2.2	3.0	2.5	2.7
K_2O	0.16	0.03	0.16	0.10	0.10	0.10	0.34	0.26	0.23
H_2O	6.0	5.0	2.4	7.4	5.4	8.3	8.6	7.5	6.2
CO_2	0.1	0.1	0.0	0.2	0.2	0.2	0.1	0.0	0.3
P_2O_5	0.11	0.12	0.07	0.10	0.10	0.10	0.12	0.12	0.08
S	5.06	0.72	17.80	3.22	1.95	7.47	8.38	5.28	3.34
O equiv.	1.89	0.27	6.66	1.20	0.73	2.80	3.14	1.98	1.25
TOTAL	99.4	98.3	93.8	99.5	98.2	100.0	98.3	100.2	99.1
Cu (ppm)	7	4	8	6	5	5	8	4	7
Pb	8	7	8	4	5	4	10	6	6
Zn	206	210	128	208	146	127	145	130	105
Cr	4	4	6	6	4	4	5	4	4
Mn	2150	2400	1180	2600	2200	1520	1650	1850	1700
Ba	30	30	25	20	25	25	35	25	25
Sr	56	42	42	56	48	32	40	40	42
Zr	50	80	30	70	70	50	40	50	70

Depth	576.5	587.6	610.7	624.0	635.1	647.6	650.1	658.1	667.0-1
SiO_2 (wt.%)	50.9	55.2	51.6	53.9	54.4	46.1	47.9	54.5	50.1
TiO_2	0.86	1.26	1.14	1.18	1.06	1.33	1.15	1.12	1.01
Al_2O_3	8.5	13.3	15.3	15.6	13.4	13.5	10.9	12.4	12.5
FeO	17.9	11.5	13.8	11.0	13.1	14.8	16.3	10.4	13.2
MnO	0.22	0.34	0.52	0.44	0.40	0.39	0.23	0.28	0.26
MgO	3.51	4.14	5.60	6.92	4.22	7.26	3.84	4.26	5.09
CaO	1.55	1.54	1.55	1.90	2.12	1.59	2.17	2.16	3.17
Na_2O	1.3	3.1	2.8	2.0	2.0	2.6	2.7	3.0	2.5
K_2O	0.07	0.13	0.07	0.85	0.91	0.03	0.03	0.15	0.02
H_2O	3.5	5.9	6.0	5.1	5.0	8.7	3.2	5.7	7.4
CO_2	0.0	0.1	0.1	0.0	0.1	0.1	0.0	0.1	0.2
P_2O_5	0.06	0.09	0.09	0.08	0.06	0.08	0.11	0.08	0.09
S	11.60	2.93	0.93	0.13	1.48	5.34	10.10	3.13	6.17
O equiv.	4.34	1.10	0.35	0.00	0.55	2.00	3.78	1.17	2.31
TOTAL	95.7	98.52	99.2	99.2	98.0	99.8	94.9	97.5	99.5
Cu (ppm)	243	82	285	100	179	9	9	6	16
Pb	7	6	5	5	7	15	4	5	9
Zn	128	142	251	382	158	206	113	150	118
Cr	4	4	8	7	6	8	4	4	12
Mn	1650	2400	4100	3800	3400	2800	1550	2080	1860
Ba	20	30	15	20	25	55	30	30	20
Sr	30	48	48	64	46	20	30	56	38
Zr	40	60	30	70	40	50	60	50	40

Depth	667.0-2	670.0-1	670.0-2	673.0	680.1-1	680.1-2	684.8	685.8	687 6
SiO_2 (wt.%)	52.0	53.4	61.3	51.3	55.8	63.6	56.1	52.4	41.3
TiO_2	1.24	0.85	1.14	1.32	0.74	0.88	1.26	1.24	1.03
Al_2O_3	13.1	14.4	14.6	15.4	13.3	12.3	12.5	13.6	14.8
FeO	11.9	9.0	7.4	11.0	8.4	6.6	11.5	12.2	10.5
MnO	0.27	0.26	0.24	0.36	0.24	0.20	0.30	0.37	0.34
MgO	5.57	1.82	3.62	5.22	1.80	2.79	4.89	6.63	3.77
CaO	1.43	10.3	1.59	5.73	10.5	3.18	1.87	2.81	14.3
Na_2O	3.3	1.0	4.5	2.2	0.9	3.5	2.4	2.1	0.0
K_2O	0.02	0.02	0.04	0.82	0.04	0.03	0.02	0.05	0.05
H_2O	6.5	3.6	3.6	4.2	4.7	3.7	5.6	4.2	7.2
CO_2	0.1	0.1	0.1	7.1	0.1	0.1	0.1	0.2	1.4
P_2O_5	0.06	0.14	0.20	0.11	0.19	0.19	0.09	0.07	0.07
S	4.70	2.08	0.92	0.21	3.02	1.71	2.53	2.05	2.55
O equiv.	1.76	0.78	0.34	0.0	1.13	0.64	0.95	0.77	0.95
TOTAL	98.5	96.3	98.9	99.9	98.6	98.3	98.4	97.1	96.5
Cu (ppm)	11	5	159	19	30	13	33	37	25
Pb	8	11	8	4	9	8	9	7	12
Zn	138	56	95	131	41	56	112	122	87
Cr	10	7	9	9	6	8	8	8	8
Mn	1800	2130	2070	3100	2000	1370	2100	2130	2800
Ba	25	45	20	55	65	30	20	20	50
Sr	10	244	22	76	258	56	22	34	300
Zr	50xx	80	110	60	90	130	60	50	60

*Duplicate Samples

TABLE 2. Pyrite-Free Rock Geochemistry*

Depth	370.50	398.50	406.30	426.00	434.5-1	434.5-2	455.90	462.00	474.90
wt.%									
SiO_2	53.94	63.04	56.93	53.39	52.24	57.75	49.64	58.14	61.51
TiO_2	1.31	1.01	1.25	1.20	1.30	1.30	1.48	1.19	1.10
Al_2O_3	14.90	13.88	14.02	13.94	15.27	15.40	15.62	12.68	13.70
Fe_2O_3	0.00	0.00	0.00	0.00	0.00	0.00	0.00	0.00	0.00
FeO	10.80	8.01	10.15	12.43	10.71	8.49	12.87	7.84	7.72
MnO	0.37	0.37	0.41	0.59	1.41	0.80	0.77	0.22	0.31
MgO	5.36	4.38	7.19	6.01	7.32	5.68	8.41	4.59	4.13
CaO	6.63	1.37	0.04	1.62	1.68	1.90	1.66	2.66	2.45
Na_2O	2.02	4.09	1.90	2.94	2.47	3.44	2.34	3.23	2.85
K_2O	0.06	0.18	0.27	0.09	0.07	0.13	0.02	0.07	0.15
H_2O	4.56	3.59	7.54	7.73	7.75	5.06	7.15	9.33	6.03
S	0.00	0.00	0.00	0.00	0.00	0.00	0.00	0.00	0.00
SUM	100.00	100.00	100.00	100.00	100.00	100.00	100.00	100.00	100.00

Depth	475.00	483.80	497.40	503.40	515.70	528.30	539.40	544.00	553.50
wt.%									
SiO_2	60.92	54.42	61.42	52.63	58.39	57.00	50.88	56.21	58.53
TiO_2	1.05	1.35	1.34	1.48	1.24	1.25	1.39	1.21	1.20
Al_2O_3	13.86	16.07	13.26	14.96	14.44	13.23	16.02	14.21	13.99
Fe_2O_3	0.00	0.00	0.00	0.00	0.00	0.00	0.00	0.00	0.00
FeO	7.65	10.66	10.36	10.66	10.06	9.92	10.28	9.74	9.38
MnO	0.29	0.31	0.25	0.36	0.29	0.24	0.29	0.27	0.22
MgO	3.96	6.31	3.92	7.25	5.09	4.51	5.33	5.58	5.29
CaO	2.55	1.43	3.22	2.02	1.71	1.83	1.81	1.61	1.61
Na_2O	2.94	4.22	2.38	2.65	2.95	2.48	3.50	2.71	2.88
K_2O	0.17	0.03	0.23	0.10	0.10	0.11	0.39	0.28	0.24
H_2O	6.55	5.15	3.57	7.85	5.69	9.38	10.06	8.13	6.62
S	0.00	0.00	0.00	0.00	0.00	0.00	0.00	0.00	0.00
SUM	100.00	100.00	100.00	100.00	100.00	100.00	100.00	100.00	100.00

Depth	576.50	587.60	610.70	624.00	635.10	647.60	650.10	658.10	667.0-1
wt.%									
SiO_2	65.09	58.80	52.90	54.57	57.04	50.32	60.18	59.70	55.73
TiO_2	1.09	1.34	1.16	1.19	1.11	1.45	1.44	1.22	1.12
Al_2O_3	10.87	14.16	15.68	15.79	14.05	14.73	13.69	13.58	13.90
Fe_2O_3	0.00	0.00	0.00	0.00	0.00	0.00	0.00	0.00	0.00
FeO	9.95	9.54	13.28	11.00	12.42	11.02	9.38	8.44	8.72
MnO	0.28	0.36	0.53	0.44	0.41	0.42	0.28	0.30	0.28
MgO	4.48	4.41	5.74	7.00	4.42	7.92	4.82	4.66	5.66
CaO	1.98	1.64	1.58	1.92	2.22	1.73	2.72	2.36	3.52
Na_2O	1.66	3.30	2.87	2.02	2.09	2.83	3.39	3.28	2.78
K_2O	0.08	0.13	0.07	0.86	0.95	0.03	0.03	0.16	0.02
H_2O	4.47	6.28	6.15	5.16	5.24	9.49	4.02	6.24	8.23
S	0.00	0.00	0.00	0.00	0.00	0.00	0.00	0.00	0.00
SUM	100.00	100.00	100.00	100.00	100.00	100.00	100.00	100.00	100.00

Depth	667.0-2	670.0-1	670.0-2	673.00	680.1-1	680.1-2	684.80	685.80	687.60
wt.%									
SiO_2	57.01	57.52	63.06	52.69	59.51	66.76	59.52	55.88	45.38
TiO_2	1.35	0.91	1.17	1.35	0.78	0.92	1.33	1.32	1.13
Al_2O_3	14.96	15.51	15.01	15.81	14.18	12.91	13.26	14.50	16.26
Fe_2O_3	0.00	0.00	0.00	0.00	0.00	0.00	0.00	0.00	0.00
FeO	8.52	7.72	6.76	11.09	6.11	5.32	9.87	11.04	9.02
MnO	0.29	0.28	0.24	0.36	0.25	0.20	0.31	0.39	0.37
MgO	6.10	1.96	3.72	5.36	1.91	2.92	5.18	7.07	4.14
CaO	1.56	11.09	1.63	5.88	11.19	3.33	1.98	2.99	15.71
Na_2O	3.61	1.07	4.62	2.25	0.95	3.67	2.54	2.23	0.00
K_2O	0.02	0.02	0.04	0.84	0.04	0.03	0.02	0.05	0.05
H_2O	7.12	3.87	3.70	4.31	5.01	3.88	5.94	4.47	7.91
S	0.00	0.00	0.00	0.00	0.00	0.00	0.00	0.00	0.00
SUM	100.00	100.00	100.00	100.00	100.00	100.00	100.00	100.00	100.00

*'Pyrite-free' rock compositions calculated by subtracting all the sulphur and an appropriate amount of iron from the data in Table 1

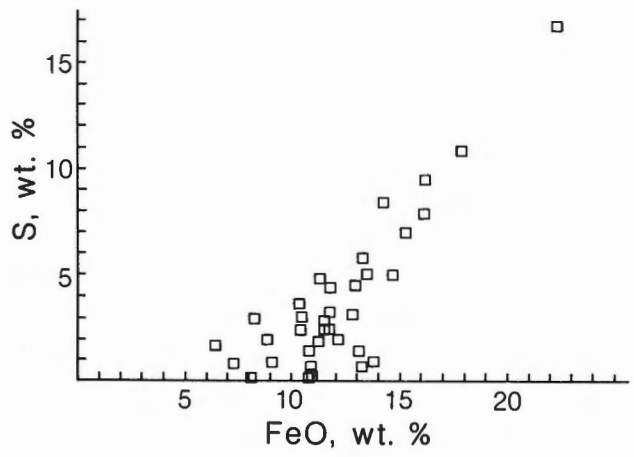

Figure 1: The variation of S with FeO for all samples.

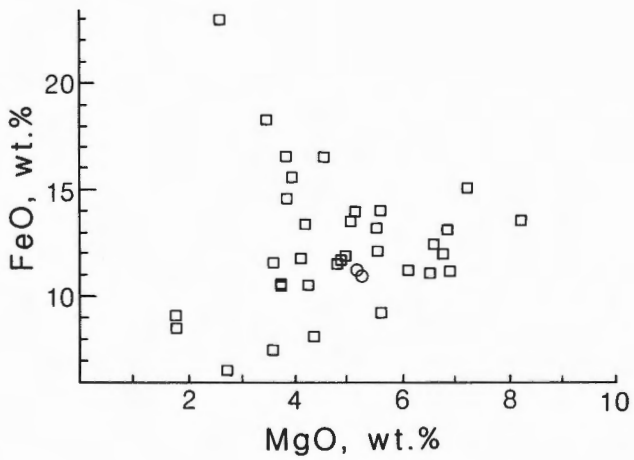

Figure 2: The variation of FeO with MgO for all samples. The two post-mineralization dykes are identified by open circles.

present in only trace amounts and, although calcium sulphate is locally present in minor amounts, removal of the sulphate-bearing samples from the data set does not change the following observations.

Figure 1 demonstrates the high correlation between iron and sulphur in the uncorrected data. This distribution could be produced by starting with a rock of approximately 8 per cent FeO and adding various amounts of both iron and sulphur in proportions appropriate for the stoichiometry of pyrite. Comparison of element ratios from the uncorrected data with those from the 'pyrite-free' calculated compositions reveal that this is probably exactly what happened.

There is no significant correlation of FeO and MgO indicated by the uncorrected, or pyrite-bearing data set (Figure 2). However, Figure 3 shows that there is a positive correlation of the same elements for the pyrite-free calculated compositions. This suggests that both the sulphur and the iron (in pyrite) were added together, and the irregular distribution of the pyrite has masked the pre-existing FeO-MgO correlation. This differs from the conclusion of Mottl (1983), who suggested that most of the iron required for sulphide precipitation in altered basalts recovered from the seafloor was produced by very local remobilization and not introduced with the sulphur-bearing fluid. All chemical compositions discussed and and illustrated in the remainder of the paper are the pyrite-free calculated rock compositions.

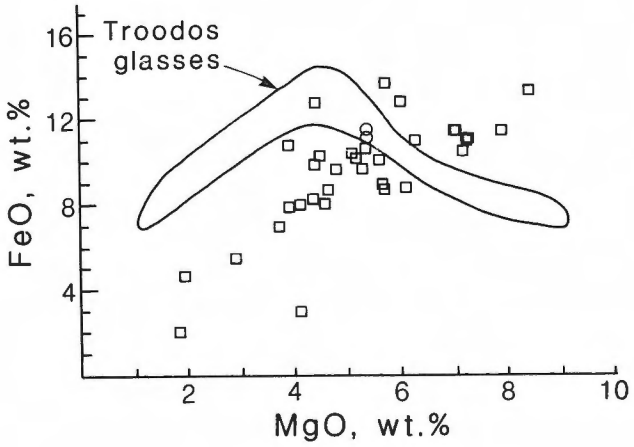

Figure 3: The variation of FeO with MgO for 'pyrite-free' calculated compositions. The post-mineralization dykes are identified by open circles. The loci of Troodos glass compositions reported by Robinson et al. (1983) are also shown.

CHANGES IN CHEMISTRY WITH DEPTH

Rather than the systematic variations of chemical composition with depth that might result from a constant geothermal gradient, the CY-2a interval under study records (a) abrupt changes corresponding to epidotization, and, (b) several horizons where metal and other minor elements are enriched.

In the former case, the paired samples, in which one represents an epidote-rich portion and the other an adjacent epidote-poor portion, are particularly useful in determining which elements are mobilized during this type of metasomatism. Figures 4, 5, 6 and 7 show the variation of calcium, magnesium, sodium and titanium with depth for the lowest 10 samples of the core interval, that is, the zone of differential metasomatism. There is significantly more variation of these elements within this zone than within the hydrothermal greenschist zone. The epidotizing process appears to enrich the rocks in calcium, and deplete them in magnesium, sodium and titanium. Total iron is lower in these ten samples than in samples from the hydrothermal greenschist zone, but appears to be relatively enriched in the epidote-rich member of the paired samples. Silicon and aluminum vary little throughout the entire core interval under study.

Figures 8, 9 and 10 indicate the horizons where copper, zinc and manganese are all enriched. The dotted lines bracketing the two major zones are based on the distribution pattern of copper. These intervals correspond directly with the samples exhibiting trace amounts of chalcopyrite and sphalerite, and increased manganese content in chlorite (Jamieson et al., 1987). A single elevated lead value matches the sample containing a few grains of galena. The correlation between zinc and manganese is particularly strong, as shown in Figure 11, suggesting that the rocks interacted with a highly evolved solution that had already leached significant Mn and Zn from the basalt. It should be noted that there is no correlation between sulphur and copper, or sulphur and zinc contents. That is, pyrite-rich samples are not necessarily rich in other sulphides, indicating that the copper and zinc were deposited independently from the constituents of the pyrite. Potassium is enriched sporadically in the same general interval as is copper and, to a lesser extent, zinc, as shown in Figure 12. However, the samples that contain potassium-rich feldspar contain no visible chalcopyrite, and close examination of the chemical data confirms the lack of good correlation between K_2O and base metals. Thus whatever process precipitated potassium locally may have been unrelated to that which precipitated copper.

Calcium and strontium vary sympathetically and thus the latter is strongly enriched during epidotization.

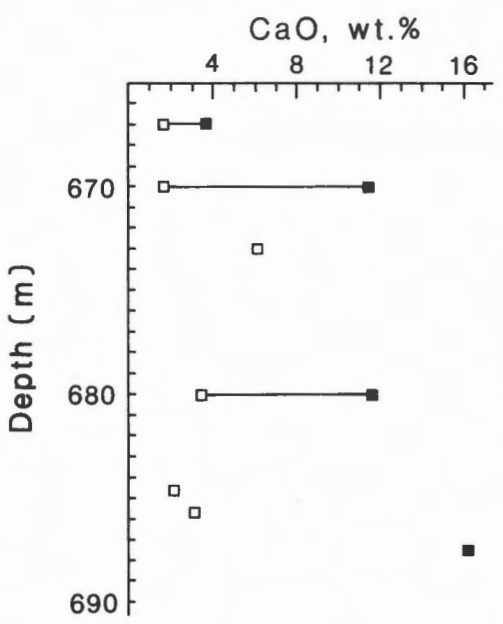

Figure 4: CaO content of samples within the zone of differential metasomatism. In this, and the following three diagrams, solid squares represent epidote-rich samples and vertical lines join pairs of samples from the same depth.

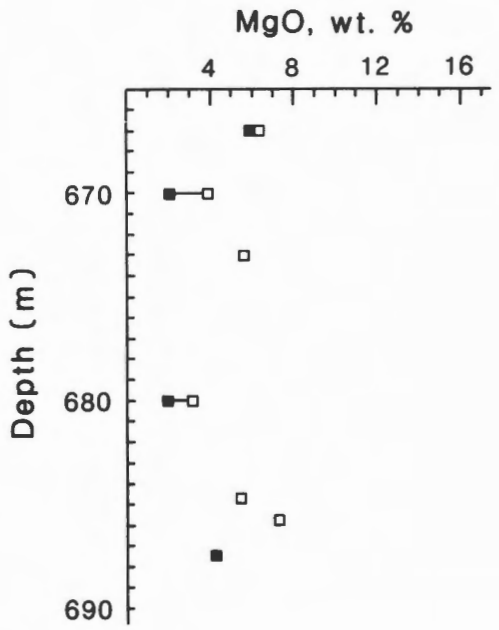

Figure 5: MgO content of samples within the zone of differential metasomatism.

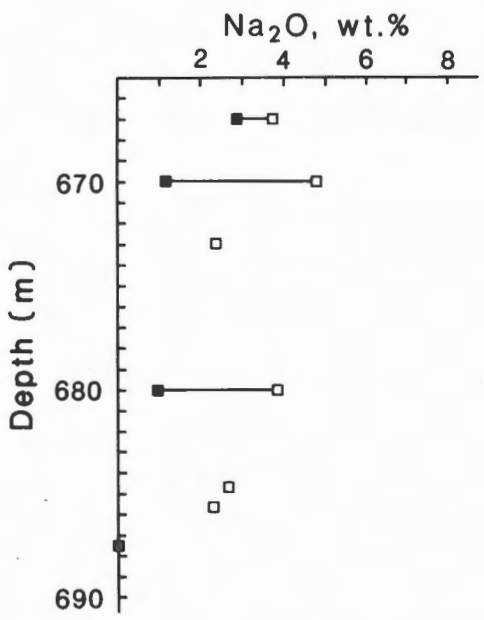

Figure 6: Na_2O content of samples within the zone of differential metasomatism.

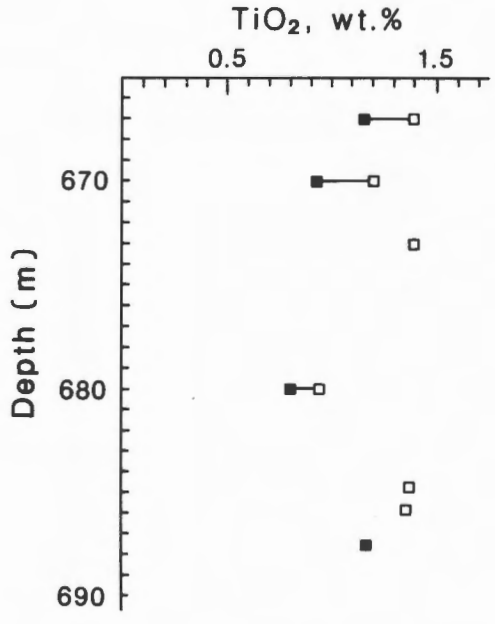

Figure 7: TiO_2 content of samples within the zone of differential metasomatism.

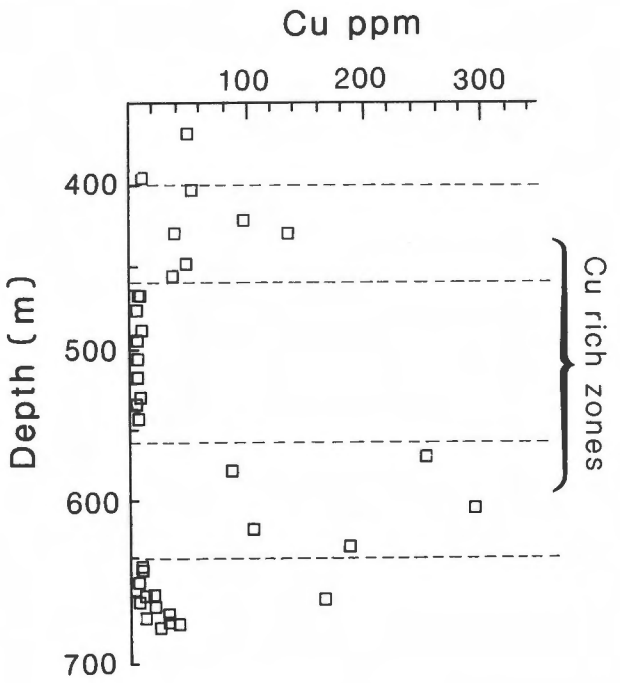

Figure 8: Cu content of all samples.

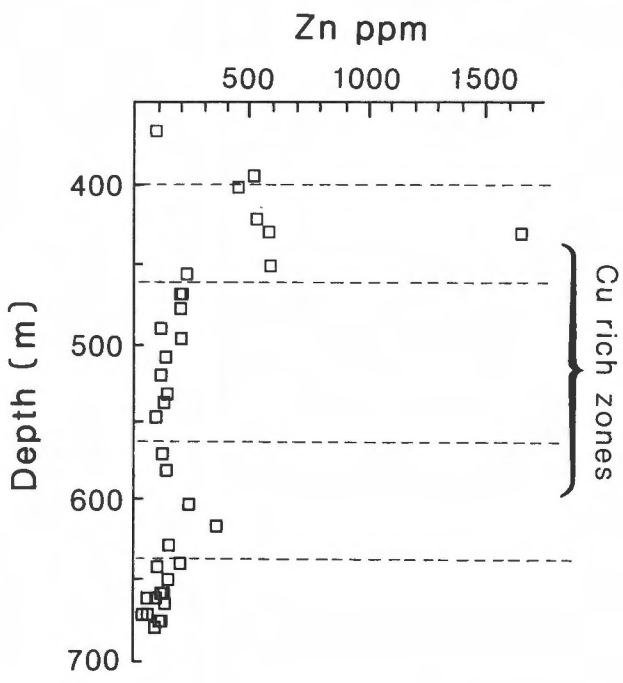

Figure 9: Zn content of all samples.

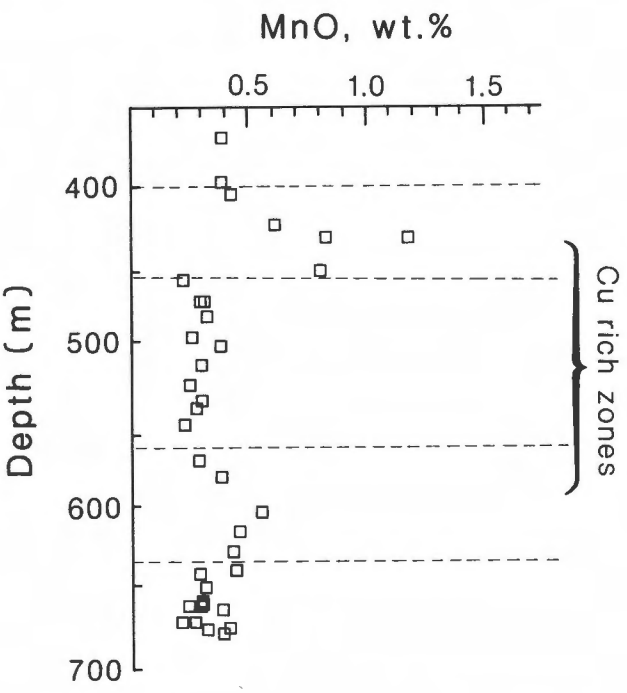

Figure 10: MnO content of all samples.

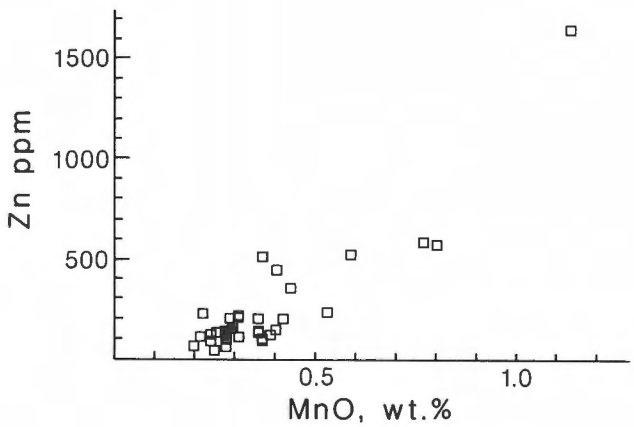

Figure 11: The variation of Zn with MnO for all samples.

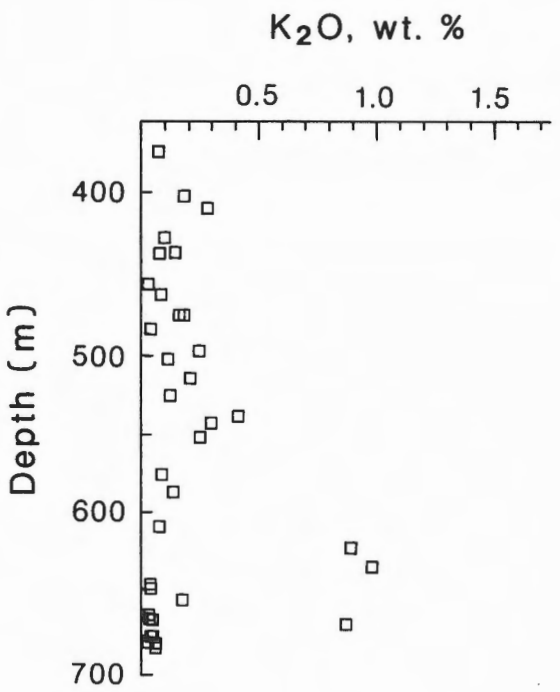

Figure 12: K_2O content of all samples.

IGNEOUS VERSUS METAMORPHIC CHEMICAL VARIATIONS

That the deposition of pyrite is superimposed on, and possibly postdates, the sympathetic MgO-FeO pattern shown in Figure 3, does not confirm that this latter relationship is a result of primary igneous processes. In fact, the distinction between igneous and metamorphic chemical variation patterns can only be made by, (a) comparing the compositions of a suite of altered rocks with unaltered rocks that can be confidently considered as precursors, and, (b) relating chemical changes to observed mineralogical changes. For this study, the best available data that can be used to represent unaltered rocks are the 59 glass compositions of Robinson et al. (1983). Baragar et al. (1984) report that several hundred analyses of comprehensively sampled sheeted dykes from Troodos closely resemble the glass compositions, although there is more scatter, and less distinctive breaks in composition between the magma types recognized by Robinson et al. (1983). These dykes, which are not in the vicinity of sulphide mineralization, consist of plagioclase - actinolite - chlorite - magnetite - quartz - clinopyroxene, assemblages with only trace epidote (W.R.A. Baragar, pers. comm., 1984).

Figure 13 shows the variation of CaO with MgO in the CY-2a samples. Also shown are the fields corresponding to Troodos glasses, and to altered seafloor basalts. The unaltered lavas show a positive correlation, probably due to the fractionation of clinopyroxene (Robinson et al., 1983). In comparison, the samples from this study appear considerably depleted in CaO, except for the epidotized samples, which are, of course, considerably enriched in CaO. The low CaO content of the majority of the dykes and lavas is manifested mineralogically by the lack of actinolite in the greenschist assemblage. The two post-mineralization dykes are more CaO-rich than the main group of samples, and are probably undepleted or partly so. Since one of the principal characteristics of these two dykes is the lack of pyrite, it can be concluded that pyrite addition and calcium depletion both predated the emplacement of these dikes, and may be part of a single process. Figure 13 also shows the MgO-CaO distribution of fresh and altered basalts from mid-ocean ridges compiled by Mottl (1983). These altered oceanic basalts have been depleted in calcium during alteration, but they have been systematically enriched in magnesium at the same time. Mottl explains how both the laboratory experiments on basalt-seawater interaction and the chemistry of the seafloor basalts demonstrate that the major chemical exchange is seawater Mg for basalt Ca, on a nearly mole for mole basis, producing the negative correlation seen as the wide band in Figure 13. However, the CY-2a samples do not follow this simple pattern. Calcium depletion is unrelated to magnesium content, suggesting that the range in MgO values may be primary.

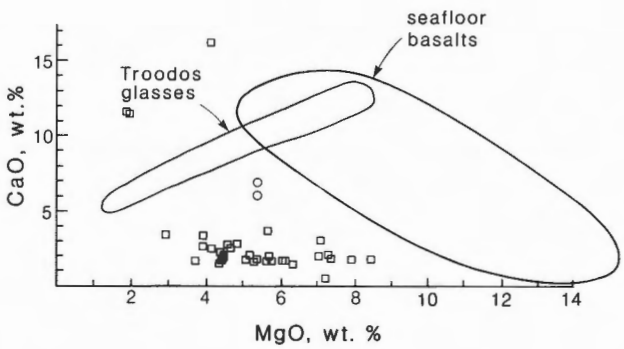

Figure 13: The variation of CaO with MgO for all samples. The post-mineralization dykes are indicated by open circles. The compositional fields for Troodos glasses analyzed by Robinson et al. (1983) and seafloor basalts compiled by Mottl (1983) are also shown.

As seen in Figure 14, SiO_2 and MgO constants of the altered rocks exhibit a negative correlation, which resembles that of the glass compositions in a general way. The low magnesium content of the epidotized samples displaces them from the general distribution.

In Figure 3, the field of glass compositions is superimposed on the FeO-MgO distribution of pyrite-free CY-2a samples. The positive correlation of the CY-2a samples resembles the low-Mg portion of the complicated glass distribution, but extends to higher Mg values.

The distribution of other major elements with respect to magnesium is similar to patterns displayed by the glasses but more scattered. Although the CY-2a samples exhibit a range in Mg values that extend from the andesites to the basalts of the glass suites of Robinson et al. (1983), the titanium content is consistently higher than 0.85 percent, a value which is considered as a discriminant between the low-Mg, high-Ti andesite-dacites and the relatively high-Mg, low-Ti basalts and basaltic andesites (Baragar et al., 1984).

The compatibility between the chemical analyses and the observed mineralogy can be illustrated by using an ACF diagram. Since:

$$A = Al_2O_3 + Fe_2O_3 - Na_2O - K_2O,$$
$$F = MgO + FeO + MnO, \text{ and}$$
$$C = CaO,$$

the alumina content has been corrected for the presence of alkali feldspar. No correction has been made for CaO in sphene, calcite or gypsum. In order to plot the rock compositions, the Fe_2O_3 content must also be known. This could not be determined by chemical analysis because of the presence of pyrite, but a crude estimation has been made by considering all iron in the greenschist samples to be ferrous, and using the CaO content and epidote composition to calculate Fe_2O_3 for the epidotized samples. Figure 15 shows that all the rock compositions lie very near the chlorite-epidote join. Any excess CaO beyond that in epidote is contained in carbonate, sulfate, sphene or the plagioclase component of feldspar, rather than in actinolite. Baragar (pers. comm., 1984) reports that the dikes he and co-workers have studied (Baragar et al., 1984) are somewhat depleted in calcium relative to the glass compositions of Robinson et al. (1983), but the mineral assemblage includes actinolite and only trace epidote. Figure 15 indicates that, in the case of the Agrokipia rocks, actinolite is precluded by lack of calcium.

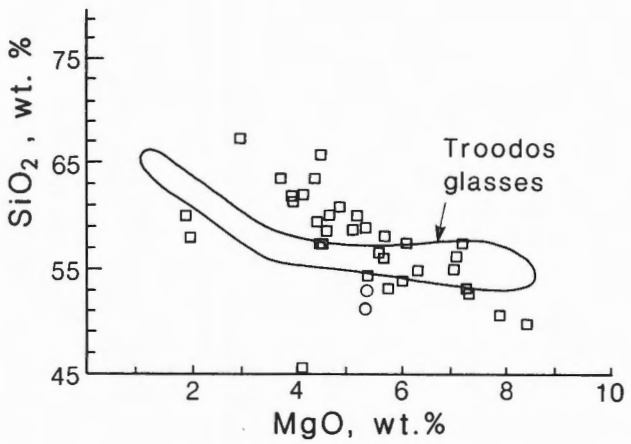

Figure 14: The variation of SiO_2 with MgO for all samples. The post-mineralization dykes are indicated by open circles. The Troodos glasses analyzed by Robinson et al. (1983) are also shown.

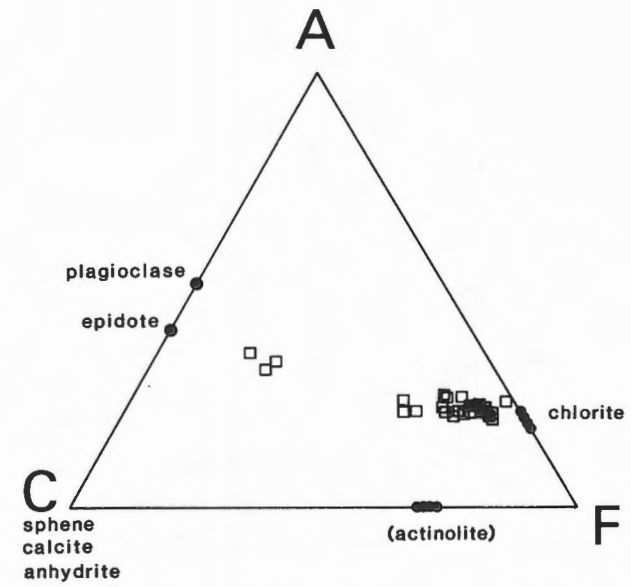

Figure 15: An ACF diagram showing all samples plotted by the method described in the text.

SULPHATE-SULPHIDE RELATIONS

Anhydrite, a mineral rare in ancient massive sulfide deposits (Franklin et al., 1981), but common in modern ocean-floor sulphide deposits (e.g. Oudin, 1979) and in active geothermal systems (e.g. Tómasson and Kristmannsdottir, 1972), occurs frequently in the pyrite veins throughout the core interval and less commonly in the vesicles near the top of the interval. Most of the sulphate now present is gypsum, but textural evidence confirms that anhydrite was the primary phase, and that the anhydrite was in equilibrium with pyrite in the same veins (Jamieson et al., 1987). Thus, the anhydrite appears to have been precipitated from the same hydrothermal solution as was the pyrite.

The average δS value determined from twenty samples of pyrite selected from various depths throughout the core interval under study is 4.2‰, with a range of -1.1 to 6.1‰. Duplicate samples indicate high reproducibility with values of 2.8 and 2.9‰. There is no systematic variation with depth, host-rock lithology or host-rock alteration. Seven samples of calcium sulphate were also analyzed isotopically, and produced an average δS value of 21.8‰ and a range of 20.9 to 22.7‰. Duplicate samples have values of 21.8 and 22.3‰. There was insufficient material to analyze anhydrite alone, but samples known to contain both anhydrite and gypsum did not differ from those which contained only gypsum, suggesting that hydration did not alter isotopic ratios. As in the case of the pyrite, there was no variation with depth or type of rock hosting the vein or vesicle.

Gypsum is present elsewhere in the Troodos lavas, and both sulphur and strontium isotopic evidence from other studies suggest that, in some cases, this sulphate is later than other secondary minerals and may be precipitated at low temperatures (Lydon, 1984; Staudigel et al., 1984). Gypsum from the ochre and stockwork zone of the Mathiati ore deposit, which is considered by Lydon (1984) to have formed from oxidation of sulfides, has δS values of approximately 5 to 8‰, just slightly heavier than the pyrite in the ore. However, the calcium sulphate from the lower portion of CY-2a is clearly of a different origin. The sulphur isotopic composition of the sulphates sampled in this study (21.8‰) are closer to that predicted by Lydon and Jamieson (1984) for gypsum precipitated from seawater of the same age as the host lavas (17‰) than it is to the Mathiati gypsum.

CONCLUSIONS

The altered rocks of the lower portion of CY-2a appear to have interacted with at least three fluids. Alternatively, these rocks interacted with a single fluid, and that fluid evolved over time or in space in such a way that it acquired three different geochemical characters.

Fluid I attended the development of the greenschist assemblage of chlorite - albite - quartz - sphene. All rocks were depleted in calcium. If the MgO-SiO_2 and MgO-FeO variations have been correctly identified as the products of magmatic processes, then there were no other chemical changes involved in the greenschist alteration itself. This alteration postdates all igneous events except the intrusion of the two 'post-mineralization' dikes.

Pyrite was precipitated in all rocks affected by Fluid I, and may have been precipitated by Fluid I. However, both the iron and the sulphur were supplied from external sources. Quartz, chlorite, calcite, epidote and anhydrite all coexist with pyrite in veins and vesicles. The textural relations show no evidence of one mineral replacing another. The simplest explanation is that they were deposited from the same fluid, and the fact that vein chlorite is identical to groundmass chlorite in the same thin section suggests that this fluid was Fluid I. The relative proportion of pyrite present is highly inhomogeneous on the scale of a hand sample.

Fluid II 'dumped' epidote in fragmental horizons in the lower 20 m of the core interval in areas that may have been localized by the presence of calcium sulfate. The solid product of this stage of alteration was essentially monomineralic epidote, and thus the precursor rocks were leached of magnesium, sodium, and titanium but generally unchanged in silicon and aluminum. This reaction clearly postdates that which involved Fluid II, as epidote replaces chloritized basalt.

Fluid III produced the zones enriched in chalcopyrite, sphalerite and manganese-enriched chlorite. These rocks contain the same minerals as the greenschist assemblages, except for the minor amounts of additional sulfides. Therefore, it is probable that this alteration was later than that produced by Fluid I, and that manganese was added to pre-existing chlorite. Chalcopyrite, sphalerite and pyrite appear to all be in textural equilibrium, and Fluid III may have deposited pyrite as well.

Yet another fluid may have been responsible for the local enrichment of potassium in the lower dikes. No other element is clearly correlated with this development of potassium feldspar.

Both Fluids II and III may have been derived from Fluid I by reaction with basalt. According to Mottl (1983), progressive basalt-seawater interaction produces solutions enriched in calcium, manganese,

copper, and zinc, amongst other elements. In this case, the elements appear to be segregated further. The products of Fluid III suggest a highly evolved solution except that there is no enrichment of calcium at all, whereas Fluid II must have been rich in calcium but did not precipitate any other elements in significant amounts. The localization of epidote precipitation, producing monomineralic patches rather than even disseminations, may have been due to the high nucleation energy of that mineral (Jamieson et al., 1987) Epidote-rich rocks have been implicated in the formation of massive sulfide deposits as marking fluid channelways (MacGeehan, 1978), or as a source of constituents found in proximate alteration pipes and sulfide deposits (Gibson et al., 1983; Stephens, 1980). In the case of the Agrokipia orebody, the relation between epidote precipitation and the generation of ore-bearing solutions remains unresolved.

ACKNOWLEDGEMENTS

Most of this research was completed while the senior author held a Natural Sciences and Engineering Research Council Visiting Fellowship at the Geological Survey of Canada. All analytical data were provided by the Geological Survey of Canada laboratories, except for sulphur isotope data, which were determined at McMaster University. H.E.J. is indebted to Dr. W.R.A. Baragar of the Geological Survey of Canada for valuable discussion and to an anonymous reviewer for useful comments.

REFERENCES

Baragar, W.R.A., Lambert, M.B., Baglow, N. and Gibson, I.L.
1984: Sheeted dike complex, Troodos ophiolite; Geological Association of Canada - Mineralogical Association of Canada, Annual Meeting, London, Ontario, Canada, 1984, Program with Abstracts, v. 9, p. 44.

Franklin, J.M., Lydon, J.W. and Sangster, D.F.
1981: Volcanic-associated massive sulfide deposits; Economic Geology, 75th Anniversary Volume, p. 485-627.

Gibson, H.L., Watkinson, D.H. and Comba, C.D.A.
1983: Silicification: hydrothermal alteration in an Archean geothermal system within the Amulet Rhyolite formation, Noranda, Quebec; Economic Geology, v. 78, no. 5, p. 954-971.

Jamieson, H.E., Lydon, J.W. and LeCheminant, G.M.
1987: Alteration mineralogy of a fossil ore-solution aquifer: petrography and mineral chemistry from the lower portion of research drill hole CY-2a, Agrokipia, Cyprus; *in* Cyprus Crustal Study Project Initial Report Hole CY2-2a, ed. P.T. Robinson, I.L. Gibson and A. Panayiotou; Geological Survey of Canada, Paper 85-29.

Lydon, J.W.
1984: Some observations on the mineralogical and chemical zonation patterns of volcanogenic sulphide deposits of Cyprus; *in* Current Research, Part A, Geological Survey of Canada, Paper 84-1A, p. 611-616.

Lydon, J.W. and Jamieson, H.E.
1984: The generation of ore-forming hydrothermal solutions in the Troodos ophiolite complex: some hydrodynamic and mineralogical considerations; *in* Current Research, Part A, Geological Survey of Canada, Paper 84-1A, p. 617-625.

MacGeehan, P.J.
1978: The geochemistry of altered volcanic rocks at Matagami, Quebec: a geothermal model for massive sulphide genesis; Canadian Journal of Earth Sciences, v. 15, no. 4, p. 551-570.

Mottl, M.J.
1983: Metabasalts, axial hot springs and the structure of hydrothermal systems at mid-ocean ridges; Geological Society of America, Bulletin, v. 94, no. 2, p. 161-180.

Oudin, E.
1979: Etude mineralogiques et géochimiques des dépots sulfures sous-marins actuels de la ride est-pacifique (21°N) 'Campagne Rise'; Bureau de Recherches Géologiques et Minières, Mémoires, no. 25, p. 1-241.

Robinson, P.T., Melson, W.G., O'Hearn, T. and Schmincke, H.-U.
1983: Volcanic glass compositions of the Troodos ophiolite, Cyprus; Geology, v. 11, no. 7, p. 400-404.

Staudigel, H., Gillis, K. and Robinson, P.T.
1984: Isotopic composition of some secondary phases in the Troodos ophiolite; Geological Association of Canada - Mineralogical Association of Canada, Annual Meeting, London, Ontario, Canada, 1984, Program with Abstracts, v. 9, p. 108.

Stephens, M.B.
1980: Spilitization, element release and the formation of massive sulphides in the Stekenjokk volcanites, Central Swedish Caledonides; Norges Geologiske

Undersoekelse, no. 360, p. 159-163.
Tómasson, J. and Kristmannsdottir, H.
1972: High temperature alteration minerals and thermal brines, Reykjanes, Iceland; Contributions to Mineralogy and Petrology, v. 36, p. 123-134.

Diverse Modes of Occurrence of Cyprus Sulphide Deposits and Comparison with Recent Analogues

N.G. ADAMIDES

Astromerites Village, Nicosia, Cyprus

Adamides, N.G., Diverse modes of occurrence of Cyprus sulphide deposits and comparison with recent analogues; in *Cyprus Crustal Study Project: Initial Report, Holes CY-2 and 2a, ed. P.T. Robinson, I.L. Gibson and A. Panayiotou; Geological Survey of Canada, Paper 85-29, p. 153-168, 1987.*

Abstract

Extensive studies of Cyprus sulphide deposits suggest that their size and nature, i.e. exhalative vs. replacement, are related to the regional structure of the area at the time of their formation. Deposits located close to transform faults such as those of Kalavasos, are small and exhalative in nature as a result of the abundance of structures through which ore fluids could reach the sea floor. These are closely comparable to the deposits of the East Pacific Rise. Larger deposits and a wider spacing between mineralized zones are found in areas of less intense tectonism and, where favourable structures exist, as in the Limni mining district, such deposits may also form on the sea floor. In the absence of such structures, ore deposition may take place completely within the lavas. The Agrokipia 'A' and 'B' deposits are used as examples and it is concluded that they are genetically related in the sense that 'A' has formed on the sea floor by percolation of ore fluids to higher levels along a fracture and 'B' by veining and replacement of favourable horizons within the lavas. The Skouriotissa orebody is very similar to black smoke deposits presently forming along spreading ridges, in its very limited alteration pipe and extensive pyritic lens, but the size of the deposit is greater than known sea floor occurrences. Comparison with recent examples and the observed relationships between ores and associated lavas and sediments on Cyprus suggest that all the volcanic rocks formed in a spreading environment and that the sulphide deposits and the umberous sediments are genetically related.

Résumé

Les études approfondies des gîtes de sulfures de Chypre révèlent que leur dimension et leur nature, i.e. exhalation vs. remplacement, dépendent de la structure régionale de l'aire au moment de leur formation. Les gîtes localisés près des failles transformantes comme ceux de Kalavasos, sont petits et produits par exhalation, ils doivent leur origine à de nombreuses structures qui devaient autoriser la migration des fluides minéralisants vers le plancher océanique. Ces gîtes présentent beaucoup de traits communs avec ceux de la dorsale sous-marine du Pacifique Est. Les gîtes de plus grande dimension et dont les zones minéralisées sont séparées par des espaces plus larges sont localisés dans des régions d'activité tectonique moins intense et, où les structures favorables existent, par exemple dans le district minier de Limni, il est probable que les gîtes se soient également formés sur le plancher océanique. En absence de telles structures, le minérai aurait pu se former complètement dans les laves. Les gîtes d'Agrokipia 'A' et 'B' servent d'exemples et nous en déduisons qu'ils sont génétiquement reliés dans le sens que 'A' s'est formé sur le plancher océanique par une percolation ascendante des fluides minéralisants le long d'une fracture et que 'B' est dû à la formation de filons et au remplacement des horizons favorables dans les laves. Le gîte de Skouriotissa ressemble de très près aux dépôts de fumeurs noirs qui se forment actuellement le long des crêtes d'expansion océanique, par le fait que l'altération est très serrée sur la cheminée et par la présence de lentilles étendues de pyrite, cependant le gîte est de plus grande dimension que ceux connus de plancher océanique. Une comparaison avec des exemples récents et les relations observées entre minerais, laves et sédiments associés sur Chypre suggèrent que toutes les roches volcaniques formées dans une zone d'expansion océanique et les gîtes de sulfures et sédiments noirâtres sont génétiquement reliés.

INTRODUCTION

The Troodos ophiolite, Cyprus, (Figure 1) is now almost universally regarded as a fragment of oceanic crust created in a spreading environment (Gass, 1968; Moores and Vine, 1971). This inference is strongly supported by its stratigraphy (Figure 2), and, in particular, by the evidence of major crustal extension provided by the sheeted dyke complex (Pearce, 1975). Numerous studies of the ophiolite have resulted in a model in which the harzburgite, flooring the cumulate sequence, represents a refractory residue produced by partial melting of a plagioclase lherzolite mantle (Allen, 1975), the cumulate sequence represents the product of solidification of that melt in a sub-axial chamber (Greenbaum, 1972) or chambers (Moores and Vine, 1971; Allen, 1975; Gass, 1980; Malpas and Langdon, 1984), and the sheeted complex and pillow lavas are the intrusive-extrusive products of volcanic processes at the spreading axis or axes (Gass and Smewing, 1973).

Based on their structural and mineralogical characteristics the volcanogenic sulphide deposits, primarily associated with the pillow lavas and the higher parts of the sheeted complex, have been interpreted as the result of hydrothermal processes at a spreading axis, (Adamides, 1975; 1980; Oudin et al., 1981). The discovery that similar sulphide deposits are presently forming along active spreading axes, such as the East Pacific Rise (Spiess et al., 1980; Hekinian et al., 1980; Haymon and Kastner, 1981) and the Juan de Fuca Ridge (Koski et al., 1982), reinforced this conclusion (Malahoff, 1982; Malahoff and Embley, 1983; Oudin et al., 1981).

The purpose of this paper is to provide detailed information on the structural controls and rock associations of several Cyprus deposits and to examine to what extent the analogies to modern examples apply.

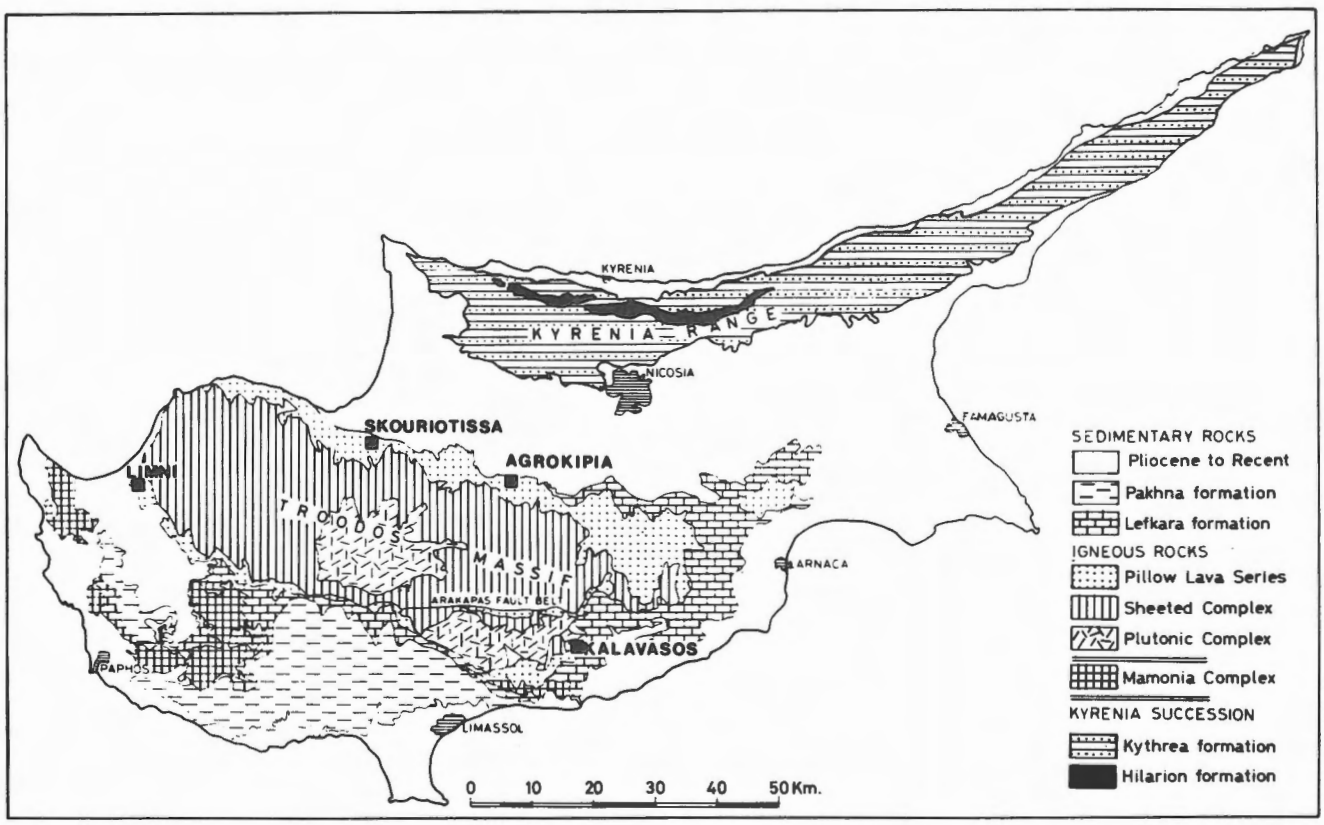

Figure 1: Generalized geological map of Cyprus showing location of areas described in text.

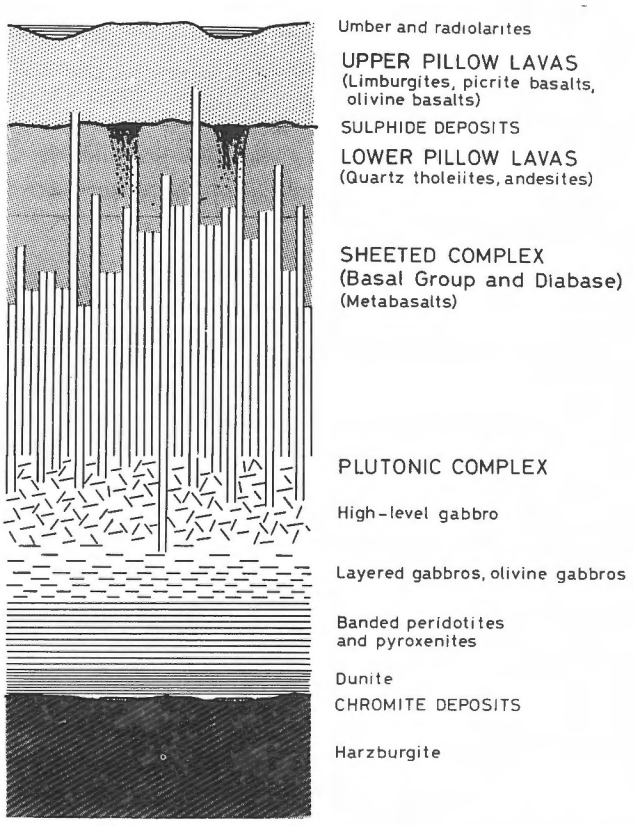

Figure 2: The stratigraphic sequence of the Troodos ophiolite (mainly after Allen, 1975).

BRIEF REVIEW OF CYPRUS SULPHIDE DEPOSITS

A Cyprus sulphide deposit ideally consists of a lens-like upper zone of massive sulphide, which grades downward through a zone composed essentially of quartz and pyrite into a stockwork in which sulphides fill fractures and cavities in pervasively altered country rock (Figure 3). In still deeper levels the mineralization is primarily represented by veinlets and disseminations of sulphide, mainly pyrite, in altered and commonly strongly epidotized volcanic rocks. Such mineralization is typically associated with the Basal Group, a transitional sequence between the sheeted complex and the pillow lavas.

A thin zone of laminated iron hydroxides and intercalated clastic pyritic bands, termed ochre overlies the massive sulphide zone in some deposits. Constantinou (1972) suggested that the ochre formed by submarine weathering of the massive sulphides prior to their burial by lavas, whereas Hutchinson and Searle (1971) favour an interpretation involving oscillation between oxidizing and reducing conditions at the final stages of ore deposition.

The massive sulphide zone typically comprises pure sulphide with a conglomeratic structure in which the ore consists of blocks of solid sulphide enclosed in friable, dark, sandy-textured pyrite. Colloform textures, delicate banding and high porosity are also characteristic of the upper parts of the massive ore zone. At deeper levels, the sulphides become coarser grained and commonly contain cavities lined by well crystallized pyrite.

Intense brecciation is characteristic. The upper parts of the underlying stockwork zones are intensely brecciated with angular fragments cemented by sulphide and silica. In the marginal parts of ore zones, brecciation decreases and relic structures of the lavas, such as pillow outlines, are commonly observed. In these marginal parts glassy pillow margins are completely replaced by sulphide and sulphide veinlets cut pillows and dykes. The host rocks are typically completely replaced by an assemblage of quartz and chlorite.

Pyrite is the most abundant sulphide in all deposits. Chalcopyrite is second in abundance and textural relationships suggest that it is paragenetically later than pyrite. It typically occurs as pools between pyrite grains, as interstitial material between collomorphic bands of pyrite, and as inclusions in pyrite, normally along growth zones (Constantinou and Govett, 1973). In the zone of supergene enrichment the chalcopyrite is commonly altered peripherally to bornite and chalcocite (Bear, 1963). Intergrowths of valleriite are in rare cases contained in the chalcopyrite (Hutchinson, 1965). Sphalerite is present in most orebodies but rarely reaches significant amounts.

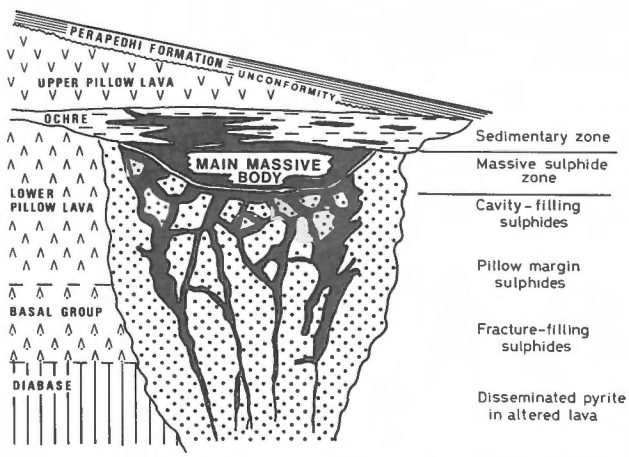

Figure 3: Diagrammatic illustration of the form of a typical Cyprus massive sulphide orebody (after Hutchinson and Searle, 1971).

Cyprus sulphide deposits vary in size from large ore bodies measuring a few million tons to sliver-like concentrations measured in thousands of tons (Table 1).

TABLE 1. The Size and Grade of some Economic Orebodies in the Troodos Ophiolite

Orebody	Tonnage	S (%)	Cu (%)	Zn (%)
Mavrovouni	15,000,000	47	4.0	0.5
Skouriotissa	6,000,000	48	2.2	–
Limni	16,000,000	14	1.0	X
Apliki	1,650,000	36	1.8	–
North Mathiatis	2,800,000	33	0.2	–
Kinousa Underground	300,000	44	2.4	3.4
Kinousa Opencast	220,000	47	2.2	–
Memi	1,500,000	26	–	–
Sha	350,000	25	1.0	–
Ambelikou	16,000	45	1.0	–
Klirou East	420,000	23	1.1	1.4
Klirou West	77,000	21	0.5	0.5
Phoenix	15,000,000	3	0.5	–

X: trace amounts

GEOLOGICAL ASPECTS OF REPRESENTATIVE DEPOSITS

A) The Limni Mining District

The Limni district, situated in western Cyprus (Figure 1), is located in the pillow lavas close to the boundary with the Sheeted Complex.

The region is dominated by two major northwesterly faults which are aligned parallel to the dykes of the Sheeted Complex (Adamides, 1975). These have been termed the Limni and Kinousa faults and have acted as the main controls in the localization of mineralization in the area. Other directions of faulting trend north-south, northeast and west-northwest.

Limni and Evloimeni Deposits

The Limni orebody, amounting to 16 million tons of cupriferous stockwork mineralization, was localized by the Limni fault (Figures 4 and 5) and truncated in its southeasterly continuations by a transcurrent north-south structure, the Eastern Boundary fault.

Extensive hydrothermal alteration, concomitant with the introduction of sulphides, has converted the wall rocks in an area measuring 700 by 200 metres into a predominantly quartz-chlorite assemblage. The lavas close to the Limni fault are thoroughly brecciated but pillow outlines may still be discerned in outlying areas.

The orebody is located within the Lower Pillow Lavas and passes laterally from thoroughly mineralized ground into unmineralized lavas. It was covered by unmineralized olivine-rich basalts which attain great thicknesses in the region surrounding the mine.

A second orebody, Evloimeni, is located along the continuation of the Limni fault. In contrast to Limni, this deposit is characterized by low copper values and predominantly pyritic mineralization (Figure 6). Its structural position suggests that this, also, was controlled by the Limni fault. Mineralization is similarly within the Lower Pillow Lavas and gradations into the unmineralized representatives of these lavas are common.

The only other noteworthy mineralization along the Limni fault is the Ayii Saranta prospect located 1 km southeast of Evloimeni. Several small gossans within the Lower Pillow Lavas, suggests the presence of limited mineralization. Lead values have been reported in the past from this occurrence (Bear, 1963) and drilling indicated the presence of minor disseminated copper and zinc mineralization.

Kinousa and Uncle Charles

These orebodies are located in the hanging wall of the Kinousa fault and are linked by a zone of stockwork mineralization (Figure 7). Kinousa underground was covered by 100 metres of clayey sediments of the Kannaviou and Perapedhi formations, whereas Uncle Charles (Kinousa opencast), was located beneath a small thickness of scree.

Both orebodies exhibit the typical pattern of Cyprus deposits with an upper zone of massive pyrite, underlain by a stockwork zone of cavity fillings and disseminations. The ore zone is offset by a fault sub-parallel to the Kinousa fault in such a way that most of the stockwork zone of Uncle Charles was removed.

Kinousa underground shows high copper and zinc values, reflected in abundant chalcopyrite and sphalerite. The deposit averaged 3.5% Zn and 3.5% Cu and differed greatly from Uncle Charles which was predominantly copper-rich. Fractionation of these elements is suggested by regular variation of the Cu/Cu + Zn ratio within the orebody and testifies to the influence of physicochemical parameters on the final mineralogical composition of the deposits.

B) The Kalavasos Mining District

Great tectonic complexity characterizes this region, which is situated in the southern parts of the island. This complexity is in most part due to the proximity of a major synvolcanic fracture zone, the Arakapas Fault Belt (Figure 1), considered to be a fossil transform structure (Moores and Vine, 1971). The influence of this structure on the geology of the

area is reflected in the presence of thick intervolcanic sediments, particularly developed at the contact between the basal facies of the Upper Pillow Lavas and the olivine basalts which form the upper parts of the Upper Pillow Lavas. These sediments attain a great thickness in the valley of the Arakapas Fault Belt but thin gradually to the south, being totally absent in the region south of Kalavasos.

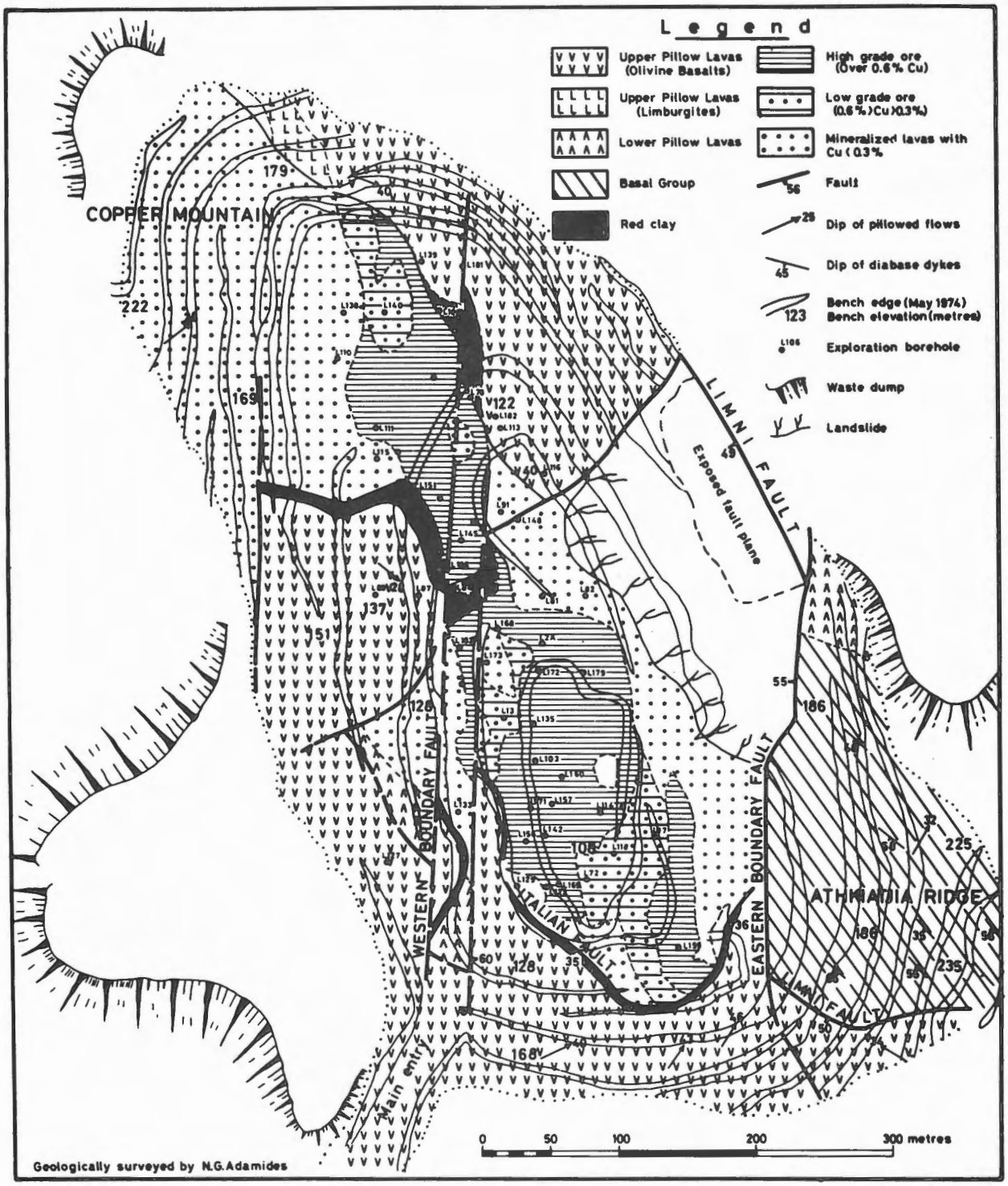

Figure 4: Geological map of the Limni opencast mine.

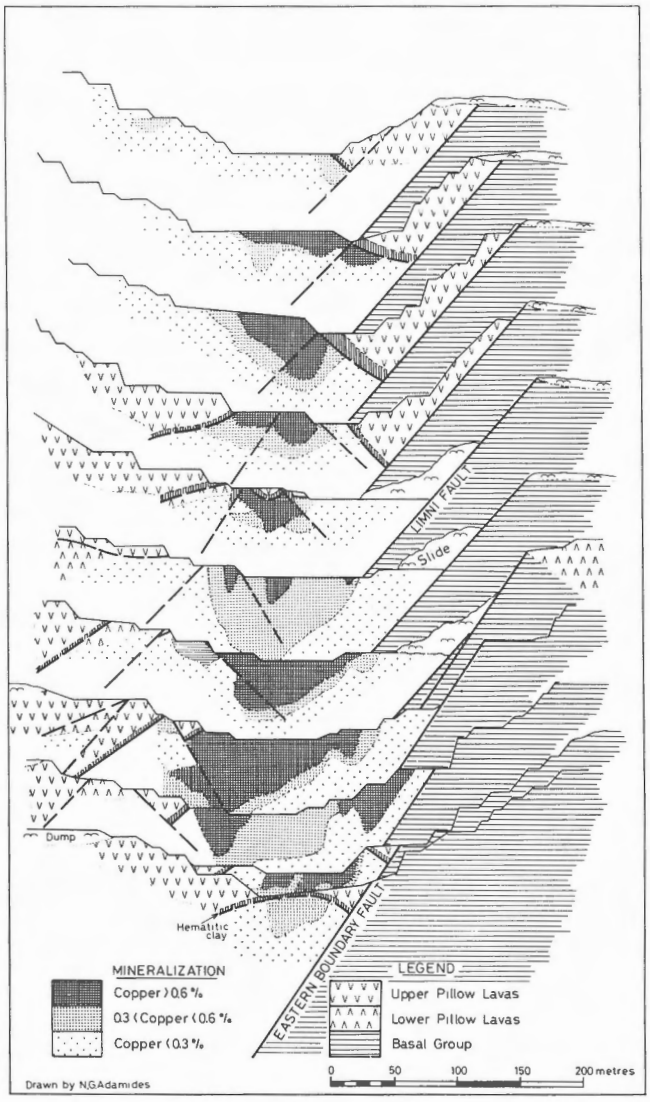

Figure 5: Series of geological sections through the Limni orebody (looking north), illustrating rock relationships and distribution of copper.

Figure 6: Geological section through Evloimeni mine.

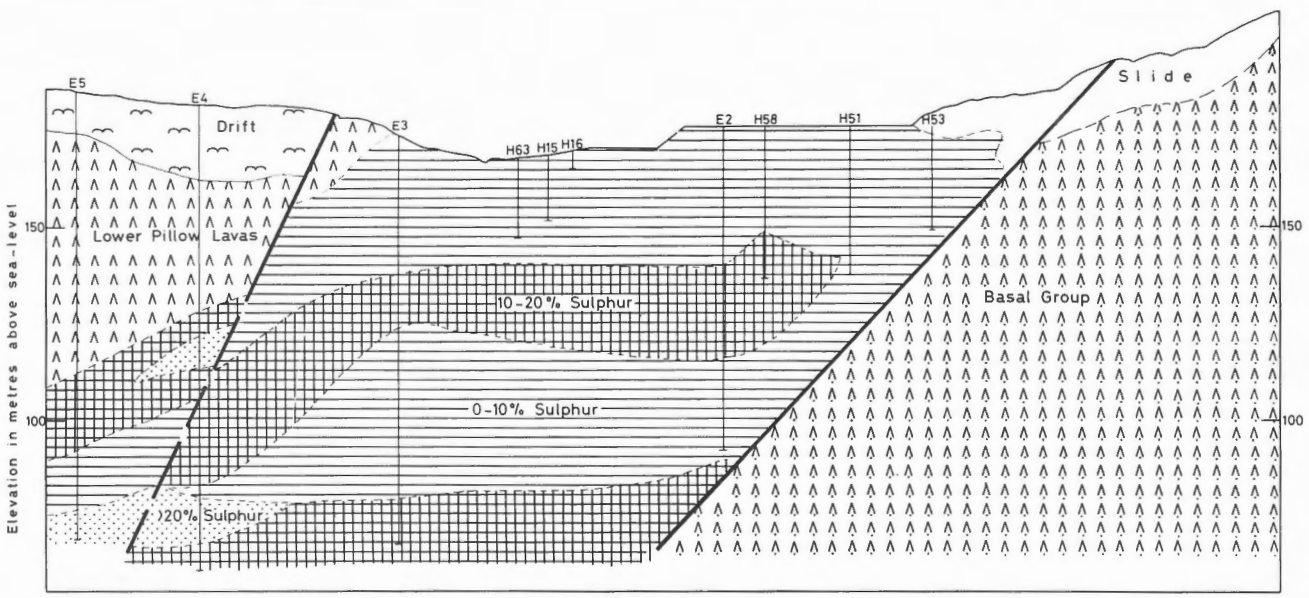

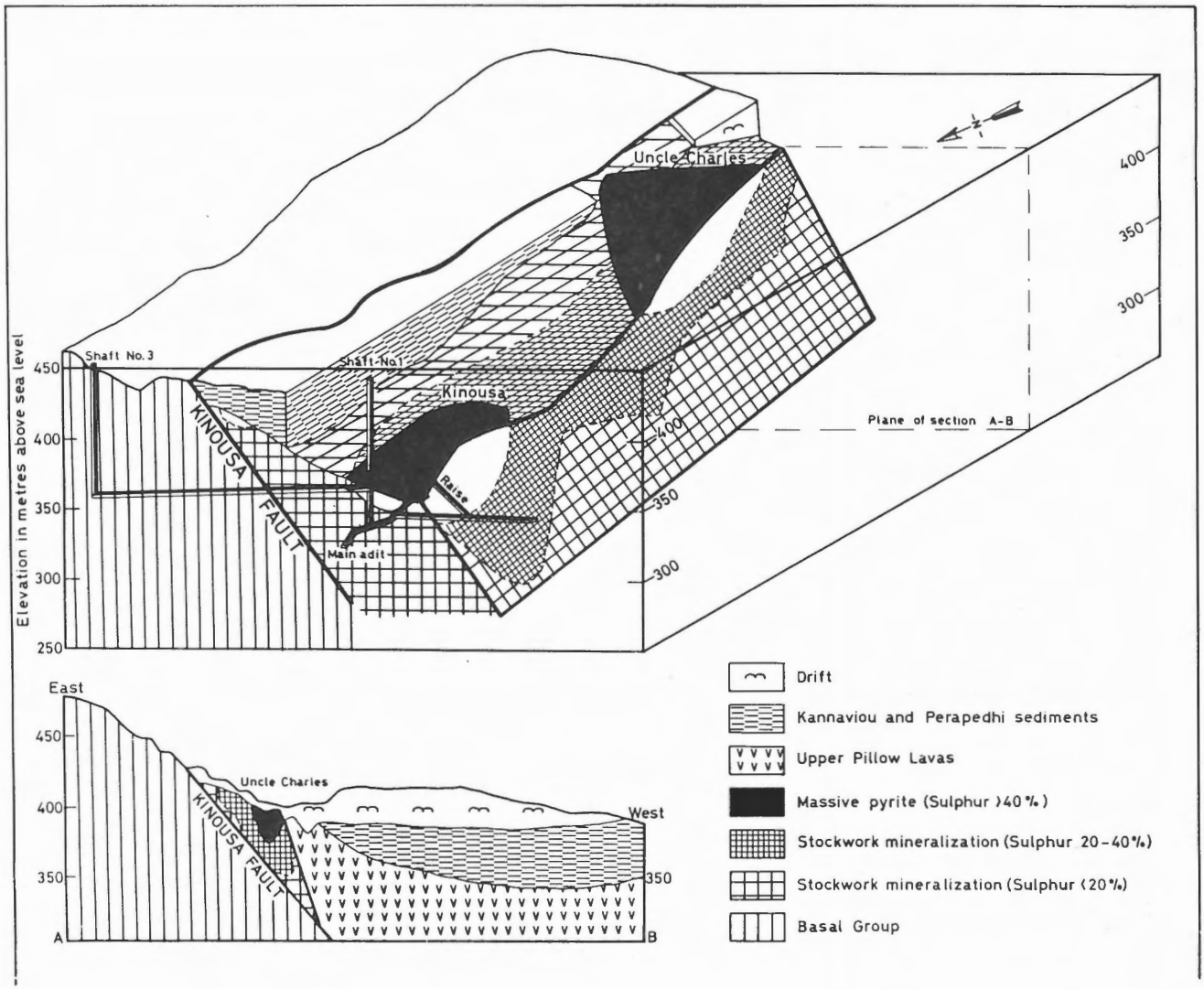

Figure 7: Isometric projection of the Kinousa deposits.

A result, probably, of the situation of the area close to the transform structure is the tilting of the volcanic formations in the area to near vertical attitudes and their disruption by a series of late, low-angle gravity faults which dislocate the formations and enclosed sulphide deposits (Figure 8).

The ore bodies are localized along northeasterly faults, parallel to the predominant dyke direction in the Sheeted Complex (Adamides, 1980). Four such fault zones have been recognized, each containing one or more deposits (Figure 9).

A major east-trending fault, the Mavridia fault, considered a subsidiary of the Arakapas Fault, apparently played a role in the channeling of ore fluids, as indicated by hydrothermal alteration along the fault plane. However, the northeast-trending faults are considered to have been the primary control of the mineralization. This is inferred from the concentration of massive mineralization in the downthrow sides of these structures, the absence of hydrothermal alteration in their footwall sides, and the concentration of higher copper values along the faults. These are relatively minor structures that appear to have acted as passive recipients of the ore fluids, which were rising from depth.

Stratigraphically, the mineralization appears to be confined to the Lower Pillow Lavas, the olivine basalts of the Upper Pillow Lavas being devoid of any hydrothermal alteration.

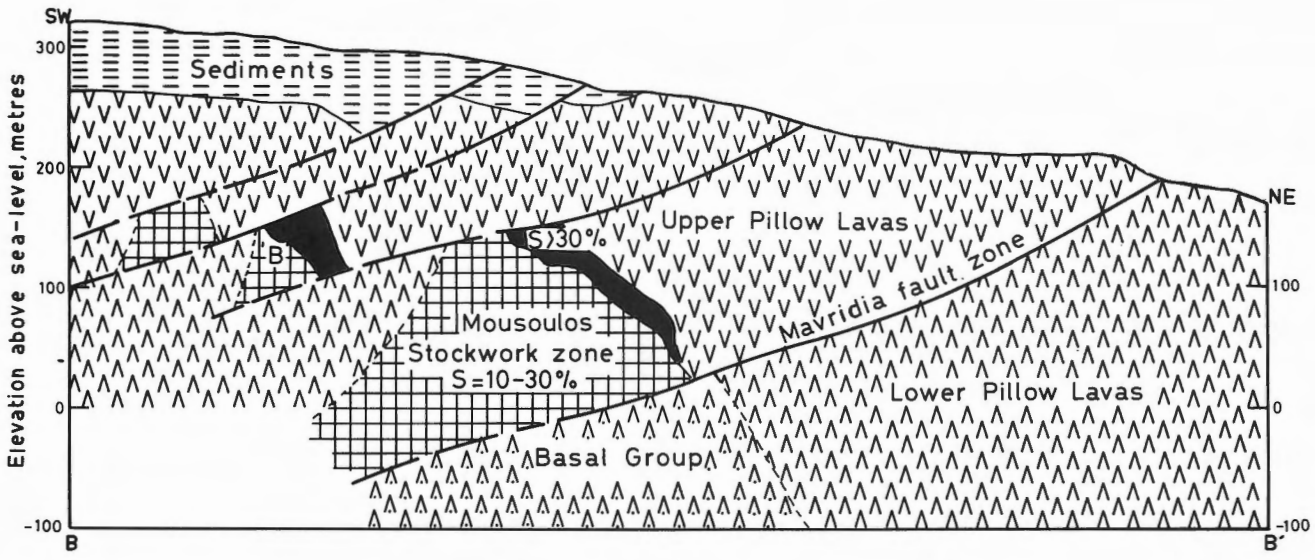

Figure 8: Geological section through Mousoulos and 'B' orebodies, illustrating the function of low angle faults in the final localization of the deposits.

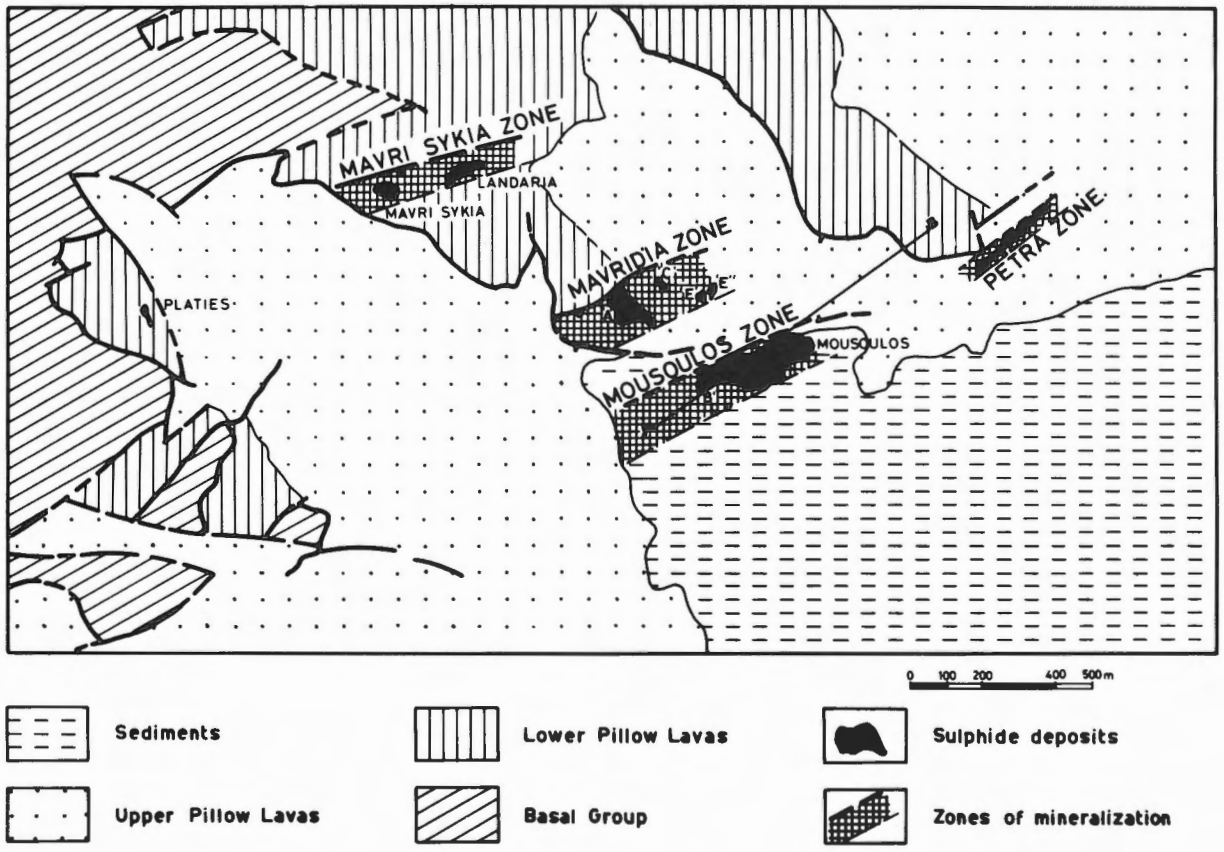

Figure 9: Generalized geological map of the Kalavasos mining district showing the relationship of sulphide deposits to northeasterly-trending faults.

C) Skouriotissa and Phoenix

The Skouriotissa orebody (Figure 1), one of the largest deposits on the island, is located in pillow lava terrain at the intersection of north-trending structures, parallel to the structural grain of the Sheeted Complex and a major east-trending structure which is reflected on the surface by a ridge of hydrothermally altered lavas.

The deposit is characterized by a central pipe of stockwork mineralization and an extensive flat lens of massive pyrite, directly located above the pipe and thinning laterally away. The alteration pipe grades laterally into unmineralized Lower Pillow Lavas (Figure 10) and is limited in extent compared to the overlying massive pyritic lens so that the latter is resting on completely unmineralized lavas in its lateral extensions.

The massive pyrite was locally covered by a layer of ochre or umber, with no intervening pillow lavas. Laterally away from the deposit the same continuous bed of umber rests on unmineralized olivine basalts.

The Phoenix occurrence located west of the Skouriotissa orebody is a mass of stockwork mineralization (Figure 10). This is separated from Skouriotissa by a considerable tract of ground comprising unmineralized Lower Pillow Lavas.

The two occurrences are considered as distinct concentrations of ore, although partly localized by similar structures. Borehole evidence indicates that the alteration pipe underlying the massive Skouriotissa deposit extends to considerable depth and no structure may be invoked to transport the massive pyrite from an original situation above the Phoenix orebody as previous workers suggested (Constantinou, 1972; 1980).

The Phoenix orebody has all the characteristics of a vein-type deposit and most probably never had an associated massive pyritic zone. Intense chloritic alteration of the host rocks is characteristic but sulphide veining is weak and the deposit has a high chalcopyrite/pyrite ratio. The orebody is envisaged as a broad linear zone of sulphide veining and propylitization with ore deposition taking place within the lava pile. Relationships in the opencast pit suggest that propylitized but otherwise unmineralized lavas in the upper parts of the ore zone pass gradually at deeper levels into sulphide-impregnated ground.

The development of thick Upper Pillow Lavas in the area laterally away from the massive pyrite and the cover by a common blanket of umber testifies to penecontemporaneous volcanism and ore deposition, followed by a prolonged period of umber sedimentation probably related to the same cycle of hydrothermal activity which deposited the sulphides. This inference accords with earlier views (Hutchinson, 1965; Clark, 1971; Hutchinson and Searle, 1971) which envisage genetic relationships between the umbers and the sulphide deposits.

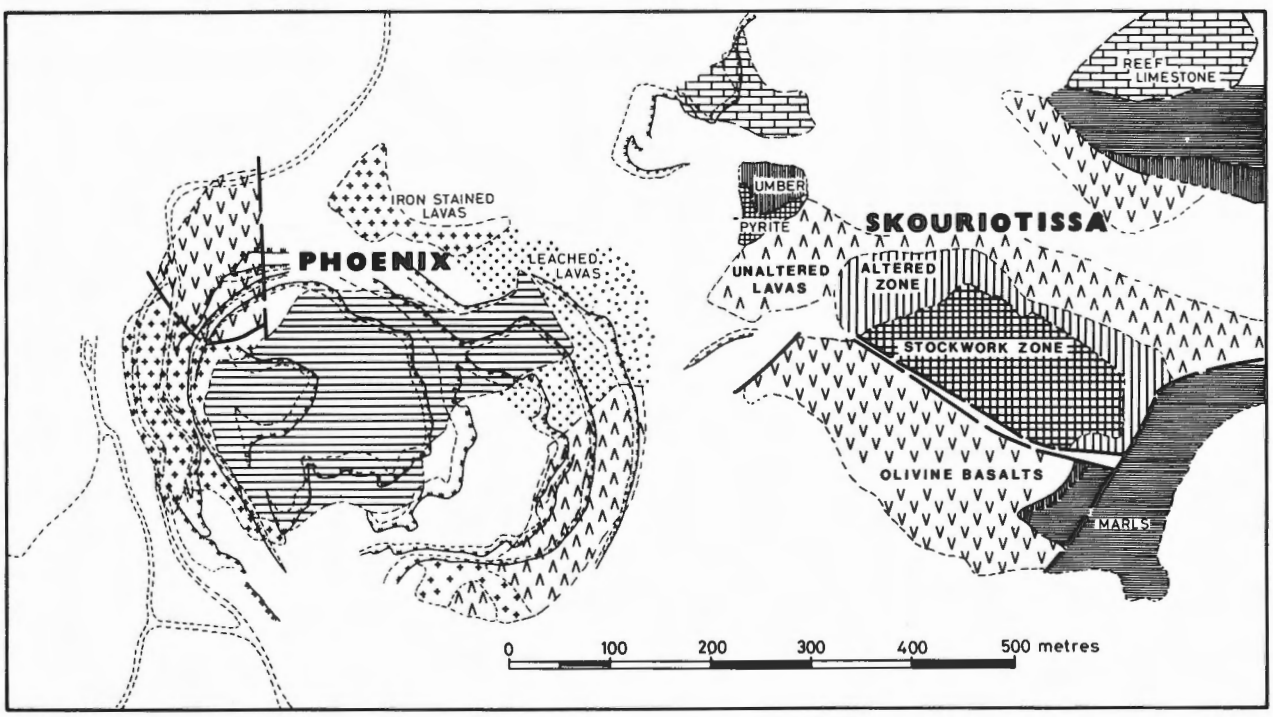

Figure 10: Geological map of Skouriotissa and Phoenix mineralized occurrences.

D) The Agrokipia Deposits - Tamasos Area

Geological investigations in the area of Agrokipia deposits (Figure 1) indicate no obvious structural control for ore deposition but rather a predominance of concordant sills and flows which may have dammed the ore fluids and led to precipitation of sulphides within the lavas.

The Agrokipia 'B' orebody (Figure 11), for example, is completely enclosed within the Lower Pillow Lavas at a considerable depth below the top of the lava pile. The passage from unmineralized to mineralized lavas is effected gradually through a zone of sulphide veining in otherwise very little altered lavas. A large thickness of glassy lavas is present directly above the mineralized zone.

The adjacent Agrokipia 'A' orebody is an exhalative deposit localized at the contact between Lower and Upper Pillow Lavas. The stockwork zone of Agrokipia 'A', however, is diffuse and shows frequent gradations into weakly altered and little mineralized lavas. This probably reflects the absence of structures along which the ore fluids could be focused.

South of the Agrokipia deposits weak iron staining and oxidation mark the site of the Mathiatis (Mitsero) occurrence. Drilling in the area disclosed that unmineralized Lower Pillow Lavas at the surface grade downward into pervasively chloritized rocks. The mineralization is weak and pyritic, but with locally high zinc contents. In many cases Zn exceeds 1% and in exceptional situations ranges up to 15%. Contacts with the surrounding lavas are gradational and the ore fluids probably never reached the sea floor.

This type of mineralization may be widespread in Cyprus and similar ore-host rock relationships are envisaged for the recently discovered mineralization at Klirou (Christoforou, pers. comm., 1981) and Sha (Maliotis, pers. comm., 1982).

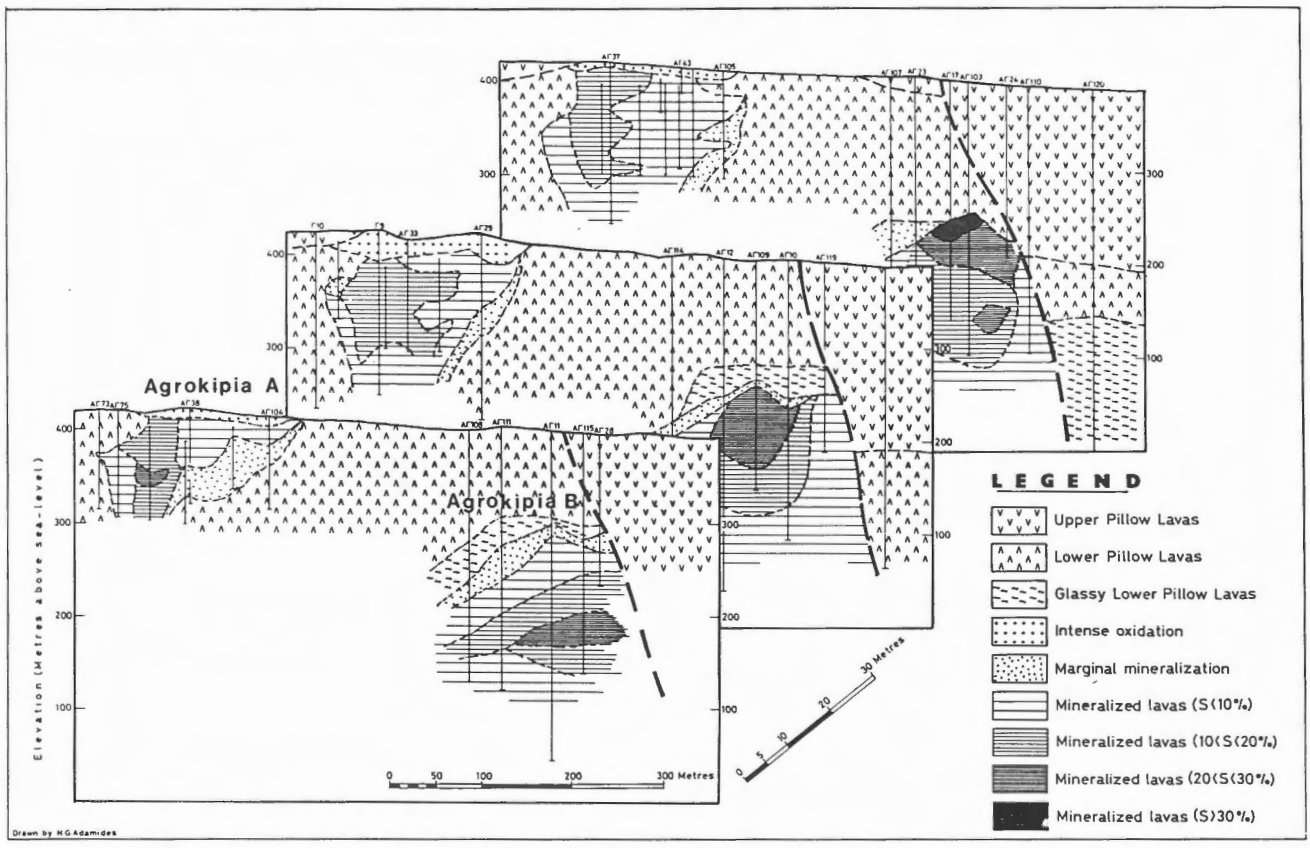

Figure 11: Isometric projection of the Agrokipia deposits (viewed from the southeast).

SOME FEATURES OF MODERN SPREADING CENTRES

The structural pattern of modern oceanic spreading centres is broadly similar irrespective of spreading rate. At the Mid-Atlantic Ridge, e.g., normal faults trend parallel to the axis (Aumento, 1972; Ballard and Van Andel, 1977) and their throws increase from simple fractures at the central depression to faults with downthrows of 100 metres or more at the flanks. The same pattern characterizes the fast spreading East Pacific Rise, where a central extrusion zone is flanked by zones 0.5 to 1.5 km wide characterized by numerous fissures and faults and a horst and graben topography (Crane and Normark, 1977). All tectonic features are oriented parallel to the spreading axis.

In contrast to the tectonic pattern, mineralization associated with modern oceanic ridges is diverse. The Mid-Atlantic Ridge is characterized by limited formation of manganese crusts (Rona, 1980), sulphide mineralization generally being confined to sparse sulphide veining in partly altered basalts (Bonatti et al., 1976). However, recent discoveries of layered sulphides and sulphide chimneys suggest hydrothermal vents on the sea floor. Active 'Black-smoker' vents were observed recently in the Mid-Atlantic Ridge rift valley just south of the Kane Fracture Zone (Detrick et al., in press). Intense sulphide mineralization, on the other hand, characterizes the East Pacific Rise (Spiess et al., 1980; Hekinian et al., 1980; Haymon and Kastner, 1981), with numerous chimneys and mounds of sulphides built on the bare oceanic crust. These chimneys are narrow, with orifice diameters generally less than 1 metre (Cann and Strens, 1982), and are mineralogically zoned, with chalcopyrite-rich centres and zinc-rich rims (Haymon, 1982). Identical sulphide mounds have also been described from the Galapagos spreading centre (Malahoff, 1982) and the Juan de Fuca Ridge (Koski et al., 1982; Normark et al., 1982).

The vent waters giving rise to the black smoker deposits are significantly enriched in manganese but no manganese compounds are precipitated with the sulphides due to sluggishness of oxidation of Mn^{2+} to Mn^{4+} (Haymon and Kastner, 1981).

A special form of hydrothermal activity, observed at the Galapagos spreading centre, relates to the emergence of warm fluids enriched in calcium, barium, silica and potassium and strongly depleted in magnesium. Regular variations with temperature are interpreted as indicative of sulphide precipitation at depth (Corliss et al., 1979; Edmond et al., 1979).

COMPARISON OF TROODOS SULPHIDE DEPOSITS AND MODERN ANALOGUES STRUCTURAL PARALLELS

Direct structural analogies may be recognized in the control of ore deposition at Troodos and modern spreading centres. The localization of Cyprus deposits by faults which were predominantly parallel to the structural grain of the Sheeted Complex may be directly correlated with similar control exercised by axial faults along modern spreading axes. However, in contrast to modern environments where mineralization appears to be linked primarily to such axial faults, some Cyprus deposits (e.g. Agrokipia and Mathiatis Mitsero) apparently formed in unfaulted areas. In the Kalavasos region numerous small, narrowly localized deposits occur at high levels, although, at deeper levels, the ore zones coalesce, suggesting a single causative factor for the uprise of ore fluids.

It is inferred from the above observations that faults were not the major determining factor in ore deposition in Cyprus. Faults are believed to act as passive recipients of hydrothermal fluids whose circulation is triggered by deeper seated heat sources. Where faulting is active the ore fluids reach the ocean floor and exhalative deposits form. Where faulting is negligible ore deposition may take place within the lavas.

The above conclusions are in direct contrast with the mode of formation of black smoker deposits, where penetration of axial faults into the sub-axial magma chamber is considered instrumental in ore deposition (Cann and Strens, 1982), an inference supported by the strict control imposed on the mineralization by such faults and the lateral persistence of hydrothermal activity (Koski et al., 1982).

A major difference between Cyprus deposits and black smoker accumulations relates to the scale of processes involved. The Limni orebody alone testifies to hydrothermal activity over an area of 140,000 m^2 the rocks within that zone being thoroughly altered almost uniformly to a quartz-chlorite assemblage impregnated and veined by sulphides. The pipe-like orifice which vented the fluids for the formation of the Skouriotissa massive orebody is 250 metres in maximum diameter (Figure 11) and is represented by intensely silicified, chloritized and sulphide impregnated lavas. In the stockwork zones of all deposits intense brecciation is observed which may have formed by a process similar to that elaborated by Phillips (1972) whereby widening of faults by hydraulic fracturing results from accumulation of hydrothermal fluid at pressures exceeding pore water pressures.

It is concluded from the above that some significant differences exist in the mode of formation of black smoker deposits and the Cyprus ore bodies.

Major deposits may form at spreading axes in exceptional situations by mound coalescence (Malahoff and Embley, 1983) but such deposits will be characterized by their narrow localization along the controlling structures and the lack of the regional pervasive alteration observed in Cyprus.

STRATIGRAPHIC IMPLICATIONS

The Sheeted Complex (Basal Group and Diabase) and the lower part of the Lower Pillow Lavas exhibit affinities to island arc andesites and dacites (Robinson et al., 1983) and have generally been associated with axial volcanism (Gass and Smewing, 1973), a conclusion in most part supported by the evidence of crustal extension provided by the Sheeted Complex (Pearce, 1975). By contrast, the primitive extrusives representing the Upper Pillow Lavas have been associated with off-axis volcanism (Gass and Smewing, 1973) at the flanks of a spreading axis. The origin of these high magnesium, low-Ti lavas has been linked to extreme partial melting of a depleted source above a subduction zone (Sun and Nesbitt, 1978), with introduction of water facilitating formation of such melts by lowering the solidus (Crawford et al., 1981).

Chemical studies carried out by the author (Adamides, 1984) on the sulphide deposits of Limni and Kalavasos, suggest that in these areas the period of sulphide mineralization coincided with the onset of primitive volcanism. Such volcanism is represented by lavas which, although, on the basis of field characteristics and alteration, are mapped as Lower Pillow Lavas, are chemically identical to the typical members of the Upper Pillow Lavas. Similar data suggest that the parental magma for all members of the ophiolite was the same, chemical differences being explained as the result of fractional crystallization taking place at the spreading axis and the diapiric uprise of unfractionated magma at a slightly off-axis regime. However, Mehegan and Robinson (1985) suggest the presence of three principal lava suites, each represented by a different parental magma.

The association of sulphide deposits with the initial stages of primitive volcanism suggests that the orebodies are contained within the Lower Pillow Lavas but they are most common in the upper parts of the lava pile. They related to the emplacement of the low-Ti lavas. Although some propose slow spreading rate for the Troodos ophiolite (Nisbet and Pearce, 1973) and the extent of fractional crystallization of the Lower Pillow Lavas suggest an environment in which hydrothermal activity was limited, the association of the Troodos orebodies with the upper primitive volcanic rocks suggests that both may reflect slightly off axis processes.

Formation of the umbers has been linked to the same processes which formed the sulphide deposits (Spooner and Fyfe, 1973; Robertson and Fleet, 1977). At modern spreading centres these precipitates form in close proximity to, but not directly in, the sulphide deposits. The hydrothermal fluids are enriched in manganese but direct precipitation with the sulphides is prevented by the sluggish oxidation of manganese compounds (Haymon and Kastner, 1981). In Cyprus, these umberous precipitates are best developed above the Upper Pillow Lavas, and are commonly separated from the sulphide orebodies by a considerable thickness of unmineralized lavas. Incipient formation of umbers however, has been observed between the Upper and Lower Pillow Lavas in the Kalavasos region and Margi areas (Adamides, 1980; Bailey, 1984) and between lava flows within the Upper Pillow Lavas in Tamasos. Umber formation, therefore, was not a process which simply followed Upper Pillow Lava volcanism but was directly linked with the history of the ophiolite.

The occurrence of umber directly overlying massive pyrite at Skouriotissa, and the fact that the same bed of umber rests laterally on Upper Pillow Lavas, coupled with the evidence from modern spreading centres on the rapid removal of sulphides by submarine oxidation, suggest that the interval between sulphide precipitation and umber deposition was very brief. This implies that formation of sulphide deposits was followed by very rapid extrusion of Upper Pillow Lavas, development of thick umbers taking place after the cessation of igneous activity. The spatial separation, therefore, between sulphides and umbers testifies to the rapidity of volcanic processes and not the presence of a significant time gap.

PROPOSED MODEL

A model which adequately explains the observed petrological and field aspects of the Troodos sulphide deposits is illustrated diagrammatically in Figure 12. Formation of the Sheeted Complex and the tholeiitic member of the Lower Pillow Lavas is envisaged to take place at a spreading axis located above a subduction zone (Malpas and Robinson, 1983; Adamides, 1984; Moores et al., 1984). Open system fractionation and replenishment characterizes formation of the Sheeted Complex, as opposed to closed system fractionation characterizing the more evolved Lower Pillow Lavas, in sub-axial chambers arranged around the main axis. This model has been proposed for the formation of some Chilean ophiolites (Stern and de Wit, 1980).

Diapiric uprise of unfractionated melt in the flanks of the spreading axis promotes intense hydrothermal circulation contemporaneous with the initial stages of primitive volcanism. Such circulation is responsible for the metamorphism of the ophiolite

and the formation of hydrothermal fluid enriched in ore metals, in accord with the seawater circulation hypothesis (Elder, 1965; Spooner and Fyfe, 1973).

The observed clustering of orebodies into mining districts is fully in accord with development of secondary cells at the higher levels of the Sheeted Complex (Solomon, 1976). Varga and Moores (1985) suggest that the ore bodies are located along graben structures reflecting old spreading centres. Channeling of ore fluids is effected mostly by structures inherited from the tensional environment of the spreading axis, whereas, in the absence of severe tectonism, sulphide precipitation may take place within the lava pile. Mixing of hydrothermal fluid with ambient seawater played a significant role in ore deposition, and formation of deposits such as Agrokipia 'B', Mathiatis (Mitsero) and Phoenix. Such deposits may have been originally expressed on the surface by the emergence of warm, calcium-enriched, magnesium-depleted fluids in a situation comparable to that described at the Galapagos spreading centre (Corliss et al., 1979; Edmond et al., 1979; Edmond, 1982).

Formation of the sulphide deposits, localized within the early products of primitive volcanism, was followed by extrusion of the olivine basalts and picrites, representing products of continuing evolution within the magma chambers. These lavas rapidly covered the deposits and preserved them from destruction. Prolonged umber deposition from late stage exhalations persisted after volcanic activity ceased.

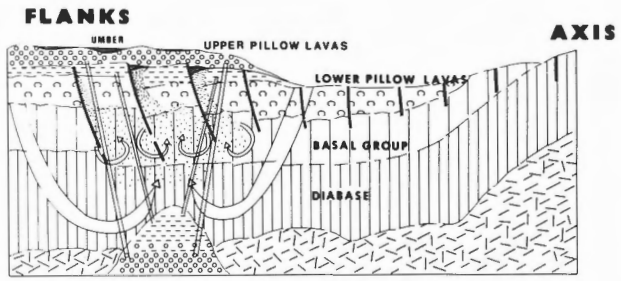

Figure 12: Diagrammatic illustration of the environment of formation of Cyprus sulphide deposits. Formation of the Sheeted Complex and Lower Pillow Lavas in an axial regime is envisaged, and of the Upper Pillow Lavas and sulphide deposits at the flanks of the spreading axis by intrusion of primitive magma to high levels and resultant hydrothermal circulation. Localization of the deposits takes place primarily in structures inherited from the tensional axial environment. The model incorporates ideas of Spooner and Fyfe (1973) and Solomon (1976).

ACKNOWLEDGEMENTS

Much of the data presented above form part of a Ph.D. thesis submitted to the University of Leicester. The help received in this respect from the staff of the above institution and, in particular, from Dr M.J. Le Bas, is gratefully acknowledged. Thanks are also extended to the managements of Limni Mines and Hellenic Mining Company for permission to make free use of data collected during employment, and to Prof. P.T. Robinson who made publication of this work possible.

REFERENCES

Adamides, N.G.
1975: Geological history of the Limni concession, Cyprus, in the light of the plate tectonics hypothesis; Institution of Mining and Metallurgy, London, Transactions and Bulletin, Section B; Applied Earth Sciences, v. 84, p. B17-B23.
1980: The form and environment of formation of the Kalavasos ore deposits, Cyprus; *in* Ophiolites: Proceedings of the International Ophiolite Symposium, Cyprus, 1979, ed. A. Panayiotou; Cyprus Geological Survey Department, Ministry of Agriculture and Natural Resources, p. 117-127.
1984: Cyprus volcanogenic sulfide deposits in relation to their environment of formation; unpublished Ph.D. thesis, University of Leicester, p. 1-383.

Allen, C.R.
1975: The petrology of a portion of the Troodos plutonic complex, Cyprus; unpublished Ph.D. thesis, University of Cambridge, p. 1-161.

Aumento, F.
1972: The oceanic crust of the mid-Atlantic Ridge at 45°N; *in* The Ancient Oceanic Lithosphere, Canadian Contributions Nos. 1-11 to the Geodynamics Project, Papers presented at a Short Symposium held at Carleton University, Ottawa, October, 1970; Department of Energy, Mines and Resources, Publications of the Earth Physics Branch, Ottawa, v. 42, no. 3, p. 49-52.

Bailey, D.G.
1984: Stratigraphy and geochemistry of the Troodos ophiolite extrusive sequence in the Margi area, Cyprus; unpublished M.Sc. thesis, Dalhousie University, Halifax, Nova Scotia, Canada.

Ballard, R.D. and Van Andel, T.H.
1977: Morphology and tectonics of the inner rift valley at lat 36°50'N on the Mid-Atlantic Ridge; Geological Society of America, Bulletin, v. 88, p. 507-530.

Bear, L.M.
1963: The mineral resources and mining industry of Cyprus; Cyprus Geological Survey Department, Ministry of Agriculture and Natural Resources, Bulletin, no. 1, p. 1-208.

Bonatti, E., Honnorez-Guerstein, M.B., Honnorez, J. and Stern, C.
1976: Hydrothermal pyrite concretions from the Romanche trench (equatorial Atlantic): metallogenesis in oceanic fracture zones; Earth and Planetary Science Letters, v. 32, no. 1, p. 1-10.

Cann, J.R. and Strens, M.R.
1982: Black smokers fuelled by freezing magma; Nature, v. 298, no. 5870, p. 147-149.

Clark, L.A.
1971: Volcanogenic ores; comparison of cupriferous pyrite deposits of Cyprus and Japanese Kuroko deposits; *in* International Association of the Genesis of Ore Deposits, Tokyo-Kyoto Meetings, Papers and Proceedings; Mining Geology (Society of Mining Geologists of Japan), Special Issue (Tokyo), no. 3, p. 206-215.

Constantinou, G.
1972: The geology and genesis of the sulphide ores of Cyprus; unpublished Ph.D. thesis, University of London, p. 1-275.
1980: Metallogenesis associated with the Troodos ophiolite; *in* Ophiolites: Proceedings of the International Ophiolite Symposium, Cyprus, 1979, ed. A. Panayiotou, Cyprus Geological Survey Department, Ministry of Agriculture and Natural Resources, p. 663-674.

Constantinou, G. and Govett, G.J.S.
1973: Geology, geochemistry, and genesis of Cyprus sulfide deposits; Economic Geology, v. 68, no. 6, p. 843-858.

Corliss, J.B., Dymond, J., Gordon, L.I., Edmond, J.M., Von Herzen, R.P., Ballard, R.D., Green, K., Williams, D., Bainbridge, A., Crane, K. and Van Andel, T.H.
1979: Submarine thermal springs on the Galapagos Rift; Science, v. 203, no. 4385, p. 1073-1083.

Crane, K. and Normark, W.R.
1977: Hydrothermal activity and crestal structure of the East Pacific Rise at 21°N; Journal of Geophysical Research, v. 82, no. 33, p. 5336-5348.

Crawford, A.J., Beccaluva, L. and Serri, G.
1981: Tectono-magmatic evolution of the West Philippine-Mariana region and the origin of boninites; Earth and Planetary Science Letters, v. 54, no. 2, p. 346-356.

Detrick, R.S., Honnorez, J., Adamason, A.C., Brass, G., Gillis, K., Humphris, S.E., Mevel, C., Meyer, P., Petersen, N., Rautenschlein, M., Shibata, T., Staudigel, H., Yamamoto, K. and Wooldridge, A.L.
–: Drilling the Snake Pit hydrothermal sulfide deposit on the Mid-Atlantic Ridge; Geology (in press).

Edmond, J.M.
1982: The chemistry of ridge crest hot springs; Marine Technology Society, Journal, v. 16, no. 3, p. 23-25.

Edmond, J.M., Measures, C., McDuff, R.E., Chan, L.H., Collier, R., Grant, B, Gordon, L.I. and Corliss, J.B.
1979: Ridge crest hydrothermal activity and the balances of the major and minor elements in the ocean: the Galapagos data; Earth and Planetary Science Letters, v. 46, p. 1-18.

Elder, J.W.
1965: Physical processes in geothermal areas; *in* Terrestrial Heat Flow; American Geophysical Union, Monographs, no. 8, p. 211-239.

Gass, I.G.
1968: Is the Troodos Massif of Cyprus a fragment of Mesozoic ocean floor?; Nature, v. 220, no. 5162, p. 39-42.
1980: The Troodos Massif: its role in the unravelling of the ophiolite problem and its significance in the understanding of constructive margin processes; *in* Ophiolites: Proceedings of the International Ophiolite Symposium, Cyprus, 1979, ed. A. Panayiotou, Cyprus Geological Survey Department, Ministry of Agriculture and Natural Resources, p. 23-35.

Gass, I.G. and Smewing, J.D.
1973: Intrusion, extrusion and metamorphism at constructive margins: evidence from the Troodos Massif, Cyprus; Nature, v. 242, p. 26-29.

Greenbaum, D.
1972: Magmatic processes at ocean ridges: evidence from the Troodos Massif, Cyprus; Nature, Physical Science, v. 238, no. 80, p. 18-21.

Haymon, R.M.
1982: Hydrothermal deposition on the East Pacific Rise at 21°N; unpublished Ph.D. thesis, University of California, San Diego, California, U.S.A.

Haymon, R.M. and Kastner, M.
1981: Hot spring deposits on the East Pacific Rise at 21°N: preliminary description of mineralogy and genesis; Earth and Planetary Science Letters, v. 53, no. 3, p. 363-381.
Hekinian, R., Fevrier, M., Bischoff, J.L., Picot, P. and Shanks, W.C.
1980: Sulfide deposits from the East Pacific Rise near 21°N; Science, v. 207, p. 1433-1444.
Hutchinson, R.W.
1965: Genesis of Canadian massive sulphides reconsidered by comparison to Cyprus deposits; Canadian Institute of Mining and Metallurgy, Transactions, v. 68, p. 286-300.
Hutchinson, R.W. and Searle, D.L.
1971: Stratabound pyrite deposits in Cyprus and relations to other sulphide ores; *in* International Association of the Genesis of Ore Deposits, Tokyo-Kyoto Meetings, Papers and Proceedings; Mining Geology (Society of Mining Geologists of Japan), Special Issue (Tokyo), no. 3, p. 198-205.
Koski, R.A., Normark, W.R., Morton, J.L. and Delaney, J.R.
1982: Metal sulfide deposits on the Juan de Fuca ridge; Oceanus, v. 25, no. 3, p. 42-48.
Malahoff, A.
1982: A comparison of the massive submarine poly-metallic sulphides of the Galapagos rift with some continental deposits; Marine Technology Society, Journal, v. 16, no. 3, p. 39-45.
Malahoff, A. and Embley, R.W.
1983: The Galapagos rift polymetallic sulfide deposit; a possible marine structural analogue to the Cyprus ore bodies; *in* Geological Association of Canada; Mineralogical Association of Canada; Canadian Geophysical Union, Joint Annual Meeting, Program with Abstracts - Geological Association of Canada, v. 8, p. A44.
Malpas, J. and Langdon, G.
1984: Petrology of the upper pillow lava suite, Troodos ophiolite, Cyprus; *in* Ophiolites and Oceanic Lithosphere, ed. I.G. Gass, S.J. Lippard and A.W. Shelton; Geological Society of London, Special Publication, no. 13, Blackwell Scientific Publications, Oxford, p. 155-167.
Malpas, J. and Robinson, P.T.
1983: Geology of the Troodos ophiolite, Cyprus; *in* Geological Association of Canada; Mineralogical Association of Canada; Canadian Geophysical Union, Joint Annual Meeting, Program with Abstracts - Geological Association of Canada, v. 8, p. A44.
Mehegan, J.M. and Robinson, P.T.
1985: Lava compositions of the Troodos ophiolite, Cyprus; EOS, American Geophysical Union, v. 66, no. 46, p. 1123.
Moores, E.M., Robinson, P.T., Malpas, J. and Xenophontos, C.
1984: Model for the origin of the Troodos Massif, Cyprus, and other mideast ophiolites; Geology, v. 12, p. 500-503.
Moores, E.M. and Vine, F.J.
1971: The Troodos Massif, Cyprus, and other ophiolites as oceanic crust: evaluation and implications; *in* A Discussion on the Petrology of Igneous and Metamorphic Rocks from the Ocean Floor; Philosophical Transactions of the Royal Society of London, Series A, v. 268, p. 443-466.
Nisbet, E. and Pearce, J.A.
1973: TiO_2 and a possible guide to past oceanic spreading rates; Nature, v. 246, no. 5434/5, p. 468-469.
Normark, W.R., Lupton, J.E., Murray, J.W., Delaney, J.R., Johnson, H.P., Koski, R.A., Clague, D.A. and Morton, J.L.
1982: Polymetallic sulfide deposits and water-column of active hydrothermal vents on the southern Juan de Fuca Ridge; Marine Technology Society, Journal, v. 16, no. 3, p. 46-53.
Oudin, E., Picot, P. and Pouit, G.
1981: Comparison of sulphide deposits from the East Pacific Rise and Cyprus; Nature, v. 291, no. 5814, p. 404-407.
Pearce, J.A.
1975: Basalt geochemistry used to investigate past tectonic environments on Cyprus; Tectonophysics, v. 25, no. 1-2, p. 41-67.
Phillips, W.J.
1972: Hydraulic fracturing and mineralization; Geological Society of London, Quarterly Journal, v. 128, p. 337-359.
Robertson, A.H.F. and Fleet, A.J.
1977: Rare-earth element evidence for the genesis of the metalliferous sediments of Troodos, Cyprus; *in* Volcanic Processes in Ore Genesis, Geological Society of London, Special Publication, no. 7, p. 78-79.
Robinson, P.T., Melson, W.G., O'Hearn, T. and Schmincke, H.-U.
1983: Volcanic glass compositions of the Troodos ophiolite, Cyprus; Geology, v.

11, no. 7, p. 400-404.

Rona, P.
1980: TAG hydrothermal field: Mid-Atlantic Ridge crest at latitude 26°N; Geological Society of London, Journal, v. 137, pt. 4, p. 385-402.

Solomon, M.
1976: 'Volcanic' massive sulphide deposits and their host rocks - a review and an explanation, *in* Handbook of Strata-Bound and Stratiform Ore Deposits. II. Regional Studies and Specific Deposits, Volume 6. Cu, Zn, Pb, and Ag Deposits, ed. K.H. Wolf; Elsevier, Amsterdam, pt. 2, v. 6, p. 21-50.

Spiess, F.N., Macdonald, K.C., Atwater, T., Ballard, R., Carranza, A., Cordoba, D., Corx, C., Diaz Garcia, V.M., Francheteau, J., Guerrero, J., Hawkins, J., Haymon, R., Hessler, R., Juteau, T., Kastner, M., Larson, R., Luyendyk, B., MacDougall, J.D., Miller, S., Normark, W., Orcutt, J. and Rangin, C.
1980: East Pacific Rise: hot springs and geophysical experiments; Science, v. 207, p. 1421-1433.

Spooner, E.T.C. and Fyfe, W.S.
1973: Sub-sea-floor metamorphism, heat and mass transfer; Contributions to Mineralogy and Petrology, v. 42, p. 287-304.

Stern, C. and de Wit, M.J.
1980: The role of spreading centre magma chambers in the formation of phanerozoic oceanic crust: evidence from Chilean ophiolites; *in* Ophiolites: Proceedings of the International Ophiolite Symposium, Cyprus, 1979, ed. A. Panayiotou, Cyprus Geological Survey Department, Ministry of Agriculture and Natural Resources, p. 497-506.

Sun, S.-S. and Nesbitt, R.W.
1978: Geochemical regularities and genetic significance of ophiolitic basalts; Geology, v. 6, no. 11, p. 689-693.

Varga, R.J. and Moores, E.M.
1985: New field mapping results, Troodos sheeted complex, Cyprus; EOS, American Geophysical Union, v. 66, no. 46, p. 1123.

The Alteration Chemistry of CCSP Hole CY-2a: A Stable and Radiogenic Isotope Study

U. ROMMEL AND H. FRIEDRICHSEN

Mineralog.-Petrograph. Inst. der Universität Tübingen, Abteilung Geochemie, D-7400 Tübingen, FRG

Rommel, U. and Friedrichsen, H., The alteration chemistry of CCSP Hole CY-2a: a stable and radiogenic isotope study; in *Cyprus Crustal Study Project: Initial Report, Holes CY-2 and 2a, ed. P.T. Robinson, I.L. Gibson and A. Panayiotou; Geol. Survey of Canada, Paper 85-29, p. 169-181, 1987.*

Abstract

This study investigates the temperatures and extent of seawater-rock interaction during the hydrothermal alteration and mineralization of the rocks from drill hole CY-2a. δD values of whole rock samples range from -35 to -102 and at 154 m, the upper boundary of mineralization, they increase from -89 ± 8 to -44 ± 8. Two post-mineralization dykes which cross-cut the mineralized part of CY-2a have δD values of -95 and -82. Conversely the $\delta^{18}O$ of phyllosilicate separates decreases across this contact. Above 154 m and in the post-mineralization dykes $\delta^{18}O$ values for smectite range from 9.2 to 18.2; below 154 m chlorite/illite values range from -0.3 to 7.2. Quartz separates from the mineralized units yielded $\delta^{18}O$ values between 3.6 and 8.7. The isotope data suggest alteration temperatures of 60 to 150°C for the unmineralized parts of CY-2a, and temperatures of 280 to 485°C for the mineralized zones. The Sr isotope ratios show an increase from 0.7043 ± 0.0003 to 0.7058 ± 0.0003 at a depth of 154 m. Compared to initial Sr isotope ratios of 0.7035 for fresh Troodos basalts and of 0.7076 for Upper Cretaceous seawater, these data show that mineralization took place under high water/rock ratios. Both Sr and O isotope data change gradually across the mineralized-unmineralized boundary at 154 m, suggesting that Agrokipia 'B' is a replacement deposit. The hydrogen isotope data, however, suggest a sharp change in temperature across the boundary and are compatible with formation of the body at a former seawater-ocean floor interface.

Résumé

L'objectif de la présente étude était d'estimer les températures et l'importance de l'interaction eau de mer-roche durant les épisodes d'altération hydrothermale et de minéralisation des roches récupérées dans le trou de forage CY-2a. Les valeurs de δD des échantillons de roches totales varient de -35 à -102 et à 154 m, la limite supérieure de la minéralisation, elles accroissent de -89 ± 8 à -44 ± 8. Deux dykes postérieurs à la minéralisation qui recoupent la section minéralisée du forage CY-2a possèdent des valeurs δD de -95 et -82. Au contraire, les valeurs de $\delta^{18}O$ des concentrés de phyllosilicates décroissent au travers ce contact. Au-dessus de 154 m et dans les dykes postérieurs à la minéralisation, les valeurs de $\delta^{18}O$ pour la smectite varient de 9,2 à 18,2; sous les 154 m les valeurs pour chlorite/illite oscillent de -0,3 à 7,2. Les concentrés de quartz extraits des unités minéralisés fournissent des valeurs de $\delta^{18}O$ comprises entre 3,6 et 8,7. Les données sur les isotopes révèlent des températures d'altération de 60 à 150°C pour les parties nonminéralisées du CY-2a, et des températures de 280 à 485°C pour les zones minéralisées. Les rapports des isotopes du Sr montrent un accroissement de 0,7043 ± 0,0003 à 0,7058 ± 0,0003 à la profondeur de 154 m. Une comparaison avec les rapports initiaux des isotopes du Sr de 0,7043 pour les basaltes sains de Troodos et de 0,7076 pour l'eau de mer du Crétacé supérieur, indiquent que la minéralisation s'est développée dans des conditions de rapports eau/roche élevés. Les données sur les isotopes du Sr et également de l'oxygène varient graduellement au travers la limite qui sépare les zones minéralisée et nonminéralisée à 154 m, ce qui suggère que le gîte 'B' d'Agrokipia est un dépôt de substitution. Les données sur les isotopes de l'hydrogène, cependant, indiquent un changement brusque des températures en traversant la limite et elles s'accordent avec l'hypothèse de formation du corps minéralisé sur une ancienne interface eau de mer-plancher océanique.

INTRODUCTION

Hydrothermal convection of seawater at spreading centres has been postulated for many years, based on theoretical considerations (Elder, 1965; Lister, 1972; Williams et al., 1974) and geochemical studies of basalts from the oceanic crust and ophiolites (Corliss, 1971; Spooner and Fyfe, 1973). The discovery of hydrothermal vent fields at the Galapagos Spreading Centre (Corliss et al., 1979) and of the black smokers at the East Pacific Rise at 21°N (Spiess et al., 1980) was a spectacular confirmation of those theories. Sulphide ore deposits are one of the most important products of the hydrothermal convection of seawater, formed when the hot solutions were cooled by seawater. The Cyprus-type sulphide ore deposits, which occur in the volcanic section of many ophiolites, are regarded as fossil examples of this kind of ore-forming processes (Oudin and Constantinou, 1984).

In order to study these sulphide deposits in more detail, the Agrokipia 'B' ore body was selected as one drill site (CY-2a) as part of a research drilling project in Cyprus by the International Crustal Research Drilling Group. The complete section through Agrokipia 'B' offered the opportunity to study a continuous suite of rocks, not affected by weathering, which has been partly recrystallized during post-magmatic large-scale water-rock interaction.

It was the purpose of this study to investigate the thermal history of these hydrothermal processes and to obtain more detailed information about the temperatures and water/rock ratios. Experimental work on the interaction of basalt with seawater indicates that the water/rock ratio is one of the most important factors controlling the chemistry of hydrothermal solutions (Seyfried et al., 1978; Mottl and Seyfried, 1980). Therefore, knowledge of the water/rock ratios involved in the alteration of the basalts of CY-2a should shed light on the conditions which lead to the formation of Cyprus-type ore deposits.

For this purpose $^{87}Sr/^{86}Sr$ and stable isotope investigations were carried out on whole rock samples as well as mineral separates. Hydrogen and oxygen isotope ratios of secondary minerals, formed during the ore-forming processes, can be used to estimate the temperatures during sulphide deposition assuming simultaneous deposition of secondary silicates. Estimates for effective water/rock ratios during hydrothermal alteration can be derived from Sr isotope compositions of whole rock samples.

Furthermore, we wanted to study the chemical alteration of major and trace elements and balance the transport of ore-forming elements during the different stages of hydrothermal seawater-rock interaction.

For many years, the Troodos ophiolite complex was regarded as typical ancient oceanic lithosphere which was generated at an oceanic ridge (Gass, 1968; Moores and Vine, 1971). Although Miyashiro (1973) pointed out geochemical similarities with an island arc, based mainly on geochemical data, other workers have suggested a back-arc environment (Pearce, 1975; Smewing et al., 1975), or a fore-arc environment for the formation of Troodos (Cameron et al., 1980; Leitch, 1984). Now there seems to be evidence that the Troodos ophiolite formed in an embryonic island-arc (Robinson et al., 1983; Schmincke et al., 1983; Moores et al., 1984).

In any case, a magma chamber below a zone of tension in oceanic crust will cause a temperature anomaly, which in turn will initiate hydrothermal convection cells of seawater. The chemical changes during the hydrothermal activity of seawater completely obliterate primary magmatic compositions in rocks like those recovered by CY-2a, except for a few relatively immobile elements like Ti, Y or Zr.

EXPERIMENTAL PROCEDURES

Mineral separation was done by standard heavy liquid and magnetic techniques, and purity was checked by X-ray diffraction. For whole-rock samples we tried to select splits which were free of veins and large vesicles.

For the O isotopic analyses samples were treated with ClF_3 at 550 to 650°C for 12 hours in nickel bombs. The oxygen released was converted to CO_2. The $^{18}O/^{16}O$ ratio was measured with a McKinney-type mass spectrometer.

Hydrogen was extracted at about 1,000°C, as a mixture of H_2 and H_2O. The water was reduced with uranium at 750°C, and hydrogen was sampled on activated charcoal at -180°C. Prior to hydrogen extraction, samples were treated at 150°C for 12 hours in vacuum to remove adsorbed and interlayer water.

Water from fluid inclusions in quartz and pyrite was extracted by crushing in evacuated stainless steel tubes. The water released was converted to hydrogen. Thermal decrepitation of quartz at about 1,000°C yielded concordant results.

Isotope analyses on replicates, in general, yielded an analytical uncertainty of less than ± 0.2 for $\delta^{18}O$ values and ± 2.5 for δD values. The isotope data are reported relative to SMOW (Standard Mean Ocean Water).

For Sr isotope studies, 100-500 mg of the sample were decomposed with HF and HNO_3 in a closed system vented by N_2 from liquid nitrogen. Strontium was extracted by standard ion exchange methods and measured on a MAT 261 solid source mass spectrometer. Typical errors are less than 0.0001.

Chemical analyses of whole rock samples were

performed by X-ray fluorescence (Siemens SRS 300).

RESULTS

Lithology and Chemistry

Based on the style of alteration, the rocks of CY-2a can roughly be divided into 3 groups.

The upper 154 m (Units I to VII, according to the Hole CY-2a Lithologic Unit Summaries by Robinson and Gibson, 1983), mainly consist of massive lava flows and glass intervals capped by a thick sill. They have been subjected to clay-type, low-grade alteration (ICRDG, 1984).

Below 154 m, the sequence of alternating glass and flows continues, but in this section the rocks are highly altered and mineralized. The groundmass is completely replaced by chlorite, illite, quartz, sphene, pyrite, and minor sphalerite. There are some layers which only consist of massive pyrite and red jasper or grey silica. This style of intensive alteration continues down to 297 m, except for one post-mineralization dyke which cross-cuts this sequence.

Below 297 m, the rocks are altered to low grade greenschist mineralogy with chlorite, quartz, albite, and epidote. The rocks are less mineralized, and mineralization is restricted to veins, fractures and cavity fillings, with minor disseminated pyrite. In this part of CY-2a the lithologic units are mainly dykes with minor pillow lavas and a few intercalated flows. From 362 to 372 m, another post-mineralization dyke cross-cuts this sequence.

In Figure 1, CaO, Na_2O, and K_2O contents of 27 whole rock samples are plotted. These are the major elements which show the most systematic variation with depth. From the variation of these elements, we define three characteristic styles of alteration. In the upper part we notice a rather variable chemical composition, which is due to the low grade of alteration, and may well reflect primary differences in composition. At 154 m, there is a remarkable decrease of CaO and Na_2O, and an increase in K_2O. This reflects the breakdown of plagioclase and the occurrence of varying amounts of illite in this highly altered zone. Below 300 m, the CaO content increases rather uniformly. Na_2O strongly increases due to varying contents of albite, and K_2O decreases again to values around 0.5%.

The transition zone from 138 to 154 m in which the first hydrothermal veins occur does not show significant changes in chemical composition.

The two post-mineralization dykes have CaO, Na_2O, and K_2O contents similar to those of the rocks from the upper part of the hole.

The rocks above 154 m and the two post-mineralization dykes can be further distinguished by comparing their TiO_2, Y, and Zr contents. Samples from Units I and IV have an average TiO_2 content of $0.56 \pm 0.14\%$, compared to a mean TiO_2 of $1.27 \pm 0.16\%$ for the samples from all other units, except for the two later dykes. The low-Ti samples are also low in Y (14 ± 4 ppm) and Zr (36 ± 10 ppm), whereas the high-Ti samples are high in Y (27 ± 5 ppm) and Zr (65 ± 10 ppm) as well. These mean values correspond very well to the data given by Smewing et al. (1975) for rocks from the Upper Pillow Lavas with low Ti, Y, and Zr (the Upper pillow Lavas are more or less equivalent to the depleted tholeiite suite defined by Robinson et al., 1983 and Schmincke et al., 1983), and for rocks from the underlying Axis Sequence with high Ti, Y, and Zr (corresponding to the andesite - dacite - rhyodacite suite defined by Robinson et al., 1983, and Schmincke et al., 1983). So the upper post-mineralization dyke with TiO_2 = 0.56%, Y = 9 ppm, and Zr = 34 ppm clearly belongs to the depleted lavas, and the lower one with TiO_2 = 1.35%, Y = 22 ppm, and Zr = 56 ppm is a late dyke belonging to the andesite - dacite - rhyodacite suite. This is not meant as a strict classification. It just shows that the upper post-mineralization dyke intruded later than the lower one, and the fact that the lower one is not mineralized suggests that mineralization ceased before the production of andesite - dacite - rhyodacite rocks had stopped.

Sr Isotopes

Fresh rocks derived from the same magmatic source have a very uniform Sr isotope composition. As has been shown in previous studies on recent and fossil hydrothermal convection cells, an isotope exchange of basalt-Sr and seawater-Sr takes place during the hydrothermal circulation of seawater through oceanic crust (Dasch et al., 1973; Spooner et al., 1977; Barrett and Friedrichsen, 1982; Albarède et al., 1981; Michard et al., 1984). This isotope exchange is independent of alteration temperatures and yields mixed values of basalt and seawater $^{87}Sr/^{86}Sr$ ratios, which depend on the effective water/rock ratio during the hydrothermal event.

As seawater is enriched in ^{87}Sr compared to fresh basalts, the basalts become enriched in ^{87}Sr during hydrothermal alteration. The co-existing water, on the other hand, will be depleted in ^{87}Sr. It is possible to estimate the water/rock ratios of hydrothermal events by simple balance calculations, if the Sr isotope compositions of fresh and altered basalt and of seawater are known.

Fresh basalts and gabbros from the Troodos ophiolite have $^{87}Sr/^{86}Sr$ ratios of 0.7033 to 0.7037 (Spooner et al., 1977). This is somewhat higher than the initial magmatic value of 0.70265 reported for fresh MORB (Hart, 1976) and indicates some addition of ^{87}Sr-enriched material, probably by

previously altered subducted oceanic crust to the magma source of the Troodos rocks. According to Peterman et al. (1970), the Sr isotope composition of seawater was 0.7076 ± 0.0003 during the Upper Cretaceous.

One requirement for estimating water/rock ratios is that the Sr content of basalt and seawater remain constant during hydrothermal alteration. Chemical analyses of the vent waters from the Galapagos Spreading Centre and from the East Pacific Rise at 21°N showed that the Sr content of the vent waters was indistinguishable from that of fresh seawater, indicating that no loss or addition of Sr occurred during the circulation of hot seawater through oceanic crust.

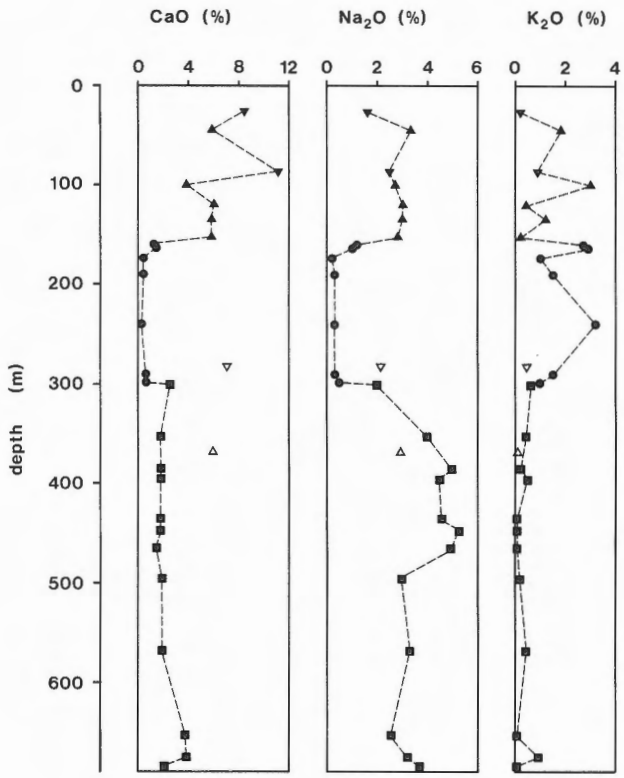

Figure 1: CaO, Na_2O, and K_2O contents of whole rock samples from Hole CY-2a versus depth. Symbols: black triangles = unmineralized samples from the upper part of CY-2a above a depth of 154 m, open triangles: post-mineralization dykes (angle down: Upper Pillow Lavas, angle up: Lower Pillow Lavas); black dots = samples from the strongly altered and mineralized zone from 154 to 300 m; black squares = samples from the greenschist zone below 300 m.

However, this was not the case during the alteration of the rocks of CY-2a. Figure 2 shows the Sr contents of the analyzed samples versus depth of drill hole, and it is obvious that the rocks of the highly altered and mineralized zone have strongly been depleted in Sr, down to contents below the limit of detection (11 ppm). The loss of Sr is a consequence of the breakdown of plagioclase and of the even more effective leaching of the former glass layers.

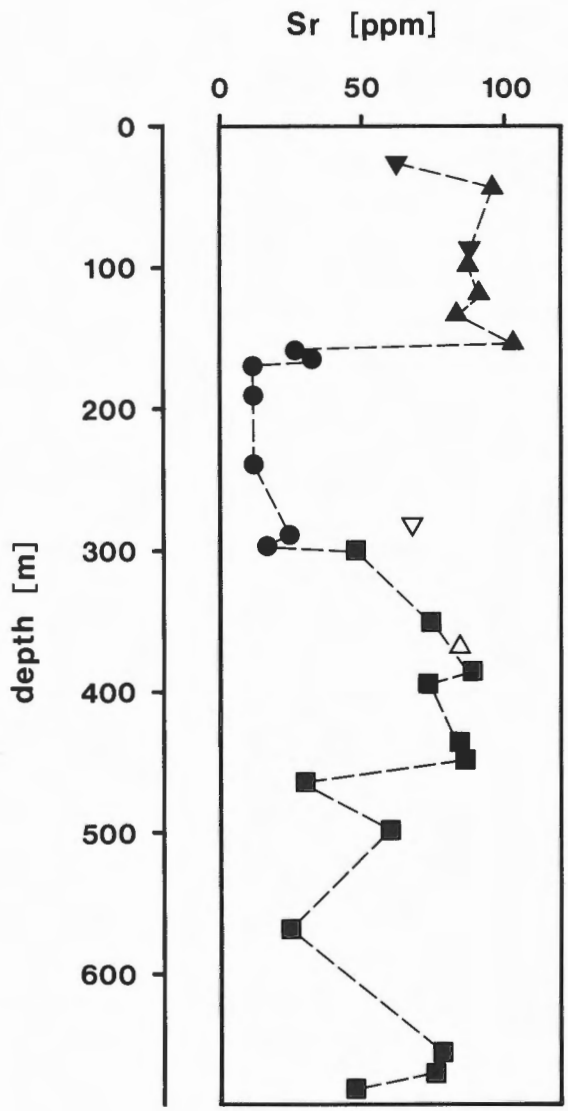

Figure 2: Sr contents of whole rock samples versus drilled depth (symbols as in Figure 1).

The $^{87}Sr/^{86}Sr$ ratios of CY-2a show a very consistent picture (Figure 3) and do not correlate with the variable Sr contents. The Sr isotope composition of the samples from the low-grade altered upper part of CY-2a, and from the two post-mineralization dykes, is 0.7044 ± 0.0003, whereas the samples from the highly mineralized zone and the greenschist zone have rather uniform $^{87}Sr/^{86}Sr$ ratios of 0.7058 ± 0.0003. The sample from the transition zone at 138 to 154 m has an intermediate Sr isotope ratio of 0.7048.

Because of the loss of Sr, it is impossible to calculate water/rock ratios for the highly mineralized samples, but the high Sr isotope ratios indicate that water/rock ratios were much higher during the event which caused mineralization and greenschist alteration than during the low-grade alteration of the upper part of CY-2a and the later dykes.

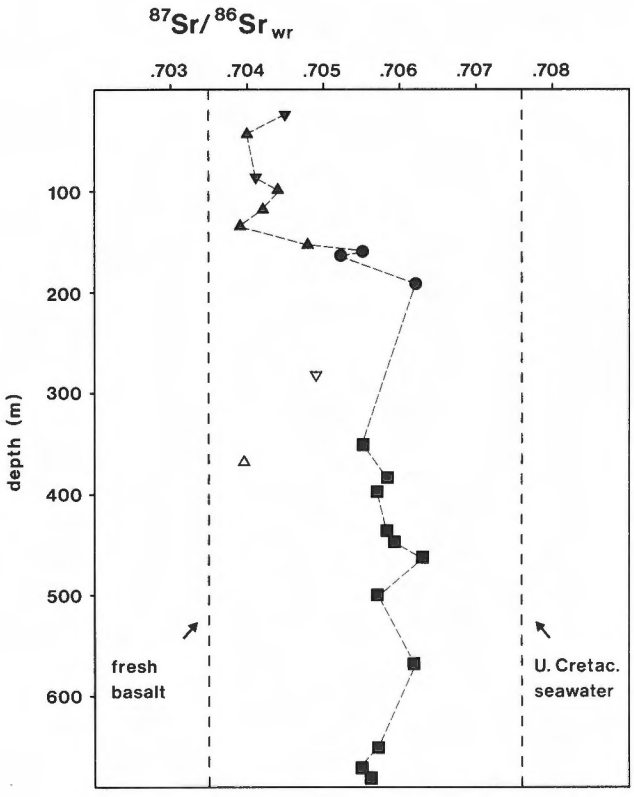

Figure 3: $^{87}Sr/^{86}Sr$ ratios of whole rock samples versus depth (symbols as in Figure 1). The dashed lines represent the Sr isotope composition of fresh basalts from Troodos (Spooner et al., 1977) and of Upper Cretaceous seawater (Peterman et al., 1970).

We calculated water/rock ratios only for those samples with a Sr content >70 ppm. For the unmineralized rocks we found ratios of 2.1 ± 0.9, in the greenschist zone the ratios lie around 12.1 ± 3. The calculated water/rock ratio for the alteration of the upper post-mineralization dyke is 4.3, for the lower one it is 2.6. The sample from the transition zone yielded a water/rock ratio of 5.9.

However, one should keep in mind that the calculated water/rock ratios are only minimum values for the water/rock ratios which prevailed during the hydrothermal processes. As McCulloch et al. (1981) point out, an appreciable amount of water may move through fractures in the rock during hydrothermal circulation without exchanging isotopes with the host rock. So the actual water/rock ratios probably were much higher than the calculated values.

Stable Isotopes

In Figure 4 the hydrogen isotope composition of whole rock samples and the oxygen isotope composition of smectite, chlorite, and mixtures of chlorite and illite are plotted versus depth in the drill hole. Since smectites are the main H-bearing minerals in the units above 154 m and the two later dykes, and chlorites in the units below 154 m, the hydrogen isotopic composition of whole rock samples corresponds with the isotopic composition of these phases.

Both the δD and $\delta^{18}O$ values vary with the occurrence of highly altered and mineralized lavas. The δD values rise abruptly from -89 ± 9 to -44 ± 8. The $\delta^{18}O$ values show a more continuous decrease from 12.0 to 18.2 down to 2.6 ± 2.1. The isotopic composition of the samples does not reflect the chemical difference between the highly mineralized zone and the greenschist zone.

The oxygen and hydrogen isotope composition of the post-mineralization dykes is similar to that of the unmineralized upper part of CY-2a.

The hydrogen and oxygen isotope composition of a mineral depends on the isotopic composition of the fluid phase with which the mineral equilibrated, and on the temperature of equilibration. In general, high-temperature reactions yield small isotope fractionations between minerals and water, and vice versa. This temperature dependence has been calculated or experimentally determined for many mineral-water systems (Friedman and O'Neil, 1977). It is possible to calculate formation or equilibration temperatures of minerals by determining their isotopic composition, if the isotopic composition of the reacting fluid phase is known.

The fluid phase, which caused the alteration of the Troodos ophiolite, was Upper Cretaceous seawater. This was shown by fluid inclusion studies, as well as Sr and stable isotope investigations (Heaton and

Sheppard, 1977; Spooner and Bray, 1977; Spooner et al., 1977). Present-day ocean water, by definition, has a δD and $\delta^{18}O$ of 0. Shackleton and Kennett (1975) have estimated that, prior to the formation of the currently existing ice sheets in the Miocene, the oxygen isotope composition of seawater was about -1. For the same reason Heaton and Sheppard (1977) assumed that Cretaceous seawater had a δD value of -7.

The samples from the unmineralized units with a mean δD of -89 show a larger fractionation relative to the co-existing seawater than the samples from the mineralized units with an average δD of -44, indicating that the alteration, which affected the upper part of CY-2a and the two later dykes, took place at much lower temperatures.

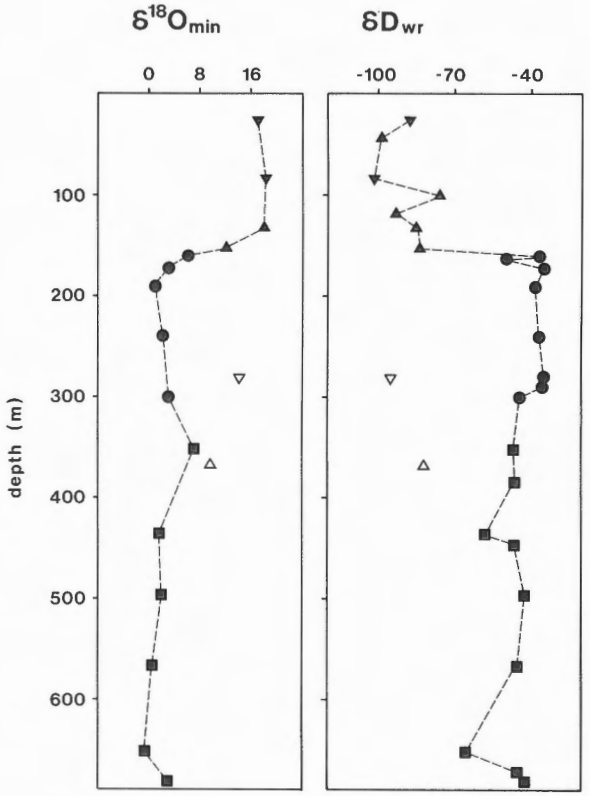

Figure 4: δD values of whole rock samples (symbols as in Figure 1) and $\delta^{18}O$ values of smectite (triangles) and chlorite (dots and squares) versus drilled depth.

One problem is whether or not the isotopic composition of the fluid phase remains constant during the hydrothermal processes. This is more likely to be correct for the hydrogen isotope composition of the fluid phase, for even highly altered basalts contain only a small amount of hydrogen compared to water. So the hydrogen isotope composition of the fluid phase will hardly be affected by water-rock interaction even at small water/rock ratios.

However, basalt-seawater reactions at high temperatures will tend to enrich the fluid phase in ^{18}O, whereas low temperature reactions will lower the $\delta^{18}O$-value of the fluid phase. Apart from temperature, the magnitude of this isotope shift largely depends on the effective water/rock-ratios. Craig et al. (1980) have investigated the oxygen isotope composition of the black smoker fluids from the East Pacific Rise and found that the hot end member of the solutions is enriched by 1.6 in ^{18}O compared to ambient seawater. However, Sr isotope investigations by Albarède et al. (1981) and Michard et al. (1984) indicate rather low water/rock ratios of 1 to 5 for the East Pacific Rise hydrothermal systems. As shown above, one has to assume higher water/rock ratios for the alteration of the mineralized rocks from CY-2a. So the oxygen isotope composition of the hydrothermal fluids was probably close to the initial seawater value of -1.

One way to calculate the temperatures of alteration and mineralization is to determine the oxygen isotope composition of quartz which formed during those processes. We analyzed 13 quartz separates, 4 from the highly mineralized and argillized zone, 8 from the greenschist zone, and 1 from the lower (earlier) post-mineralization dyke. The $\delta^{18}O$ values range from 3.6 to 8.7, without any systematic variation with depth. Quartz from the post-mineralization dyke yielded a $\delta^{18}O$ value of 10.7.

Assuming an oxygen isotope composition of -1 for the hydrothermal fluids and using the equation given by Bottinga and Javoy (1973), quartz formation temperatures ranging from 280 to 430°C were calculated (Figure 5). This is in good agreement with data of Spooner and Bray (1977), who measured homogenization temperatures up to 350°C for fluid inclusions in quartz intergrown with stockwork sulphides, and with unpublished data of Poty (cf. Heaton and Sheppard, 1977), who found fluid inclusion homogenization temperatures up to 400°C in stockwork quartz. Homogenization temperatures are always minimum temperatures for the formation of fluid inclusions, and the formation temperature of the host mineral can be higher.

The D values of the chloritized rocks can also be used to calculate the actual temperatures by using the equation for hydrogen isotope fractionation between OH-bearing minerals and water given by Suzuoki and

Epstein (1976). The fractionation factor of OH-bearing minerals is influenced by their content of Fe, Mg, and Al in the octahedral sites. Taking an average chlorite composition of $Mg_{5.06}Fe_{4.25}Mn_{0.13}Ca_{0.02}Al_{2.44}(Si_{5.72}Al_{2.78})O_{20}(OH)_{16}$ (mean of 18 analyzes of 6 chlorites from CY-2a, Herzig and Friedrich, 1987), we calculated chlorite formation temperatures from 320 to 485°C for the samples from the greenschist zone (Figure 5). The small enrichment in D of the strongly mineralized and argillized zone of CY-2a (mean δD: -39 ± 5) relative to the samples from the greenschist zone (mean δD: -49 ± 8) probably does not reflect a difference in alteration temperatures. More likely, it is due to the presence of illite, which, like muscovite (Suzuoki and Epstein, 1976), incorporates more D than chlorite does at the same temperature.

The various temperature intervals for chlorite and quartz formation indicate that the formation of chlorite took place at an earlier, hotter stage of the hydrothermal processes, while the formation of quartz went on during the cooling of the convection cell. This is supported by a formation temperature of 243°C for quartz from the post-mineralization dyke at 368 m. This dyke probably was affected by the waning stages of the high-temperature event.

To calculate the alteration temperatures of the unmineralized rocks (above 154 m and the two post-mineralization dykes), we used the oxygen isotope fractionation of smectite and water given by Yeh and Savin (1977). For a $\delta^{18}O$ value of -1 for seawater, the oxygen isotope ratios of 3 smectite separates from Unit I, IV, and VI yield alteration temperatures of 62 to 66°C (Figure 5). Smectite from Unit VII, the unit with the first occurrence of hydrothermal veins in only slightly altered rocks, yields an alteration temperature of 115°C.

Smectite from the upper post-mineralization dyke formed at 95°C; smectite from the lower one at 148°C. These low temperatures are maximum temperatures, for they were determined assuming a $\delta^{18}O$ of seawater of -1. Basalt-seawater reactions at low temperatures tend to decrease the $\delta^{18}O$ of seawater (Lawrence et al., 1975), and assuming lower $\delta^{18}O$ values than -1 would lead to even lower temperatures than those calculated above.

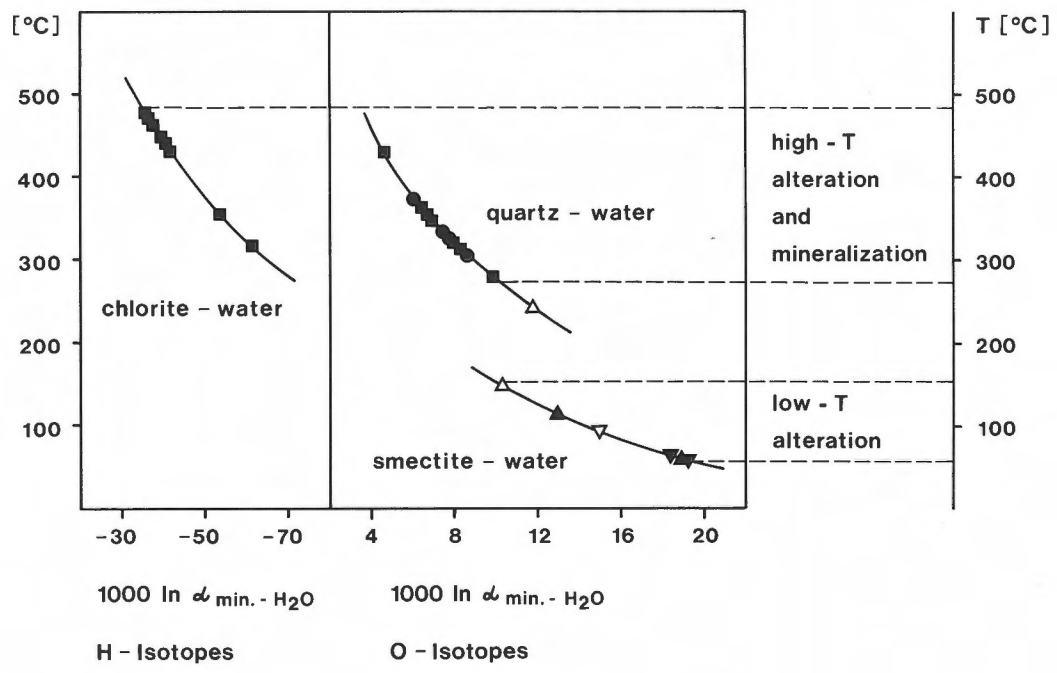

Figure 5: Hydrogen isotope fractionation between chlorite and water (Suzuoki and Epstein, 1976) and oxygen isotope fractionation between quartz and water (Bottinga and Javoy, 1973) and between smectite and water (Yeh and Savin, 1977) as a function of temperature. Data points plotted on the fractionation curves represent the isotope fractionation between chlorite, quartz or smectite analyzed in this study and seawater, assuming a δD value of -7 and a $\delta^{18}O$ value of -1 for the reacting seawater. Symbols as in Figure 1; see text for discussion.

Fluid inclusions in quartz from the silicified pyritic zones yielded δD values of -30 using different techniques. Fluid inclusions in pyrite from the same sample had a hydrogen isotope composition of -50. These data cannot represent the original composition of the ore-forming fluid, because there should be no difference between the fluid composition of quartz and pyrite which formed at about the same time. If there had been any change in the hydrogen isotope composition of the reacting seawater during the high-temperature hydrothermal processes, only a shift to more positive values should be expected, because reactions forming OH-bearing minerals can only lead to an enrichment of the fluid phase in D (Suzuoki and Epstein, 1976).

It is evident that either an isotope fractionation occurred during trapping, or that the fluid inclusions have leaked. The former assumption seems to be more likely, for leaking should preferably deplete the trapped fluid in H, and not, as observed, in D.

DISCUSSION

Stable isotope ratios and Sr data of the samples from CY-2a show a prominent change at 154 m depth with the onset of mineralized rocks. Above 154 m, there is evidence for low-temperature alteration at low water/rock ratios; below 154 m, stable isotopes suggest that alteration and mineralization took place at temperatures between 280 and 485°C, and Sr isotope data indicate higher water/rock ratios.

This is shown very clearly by Figure 6, where samples from CY-2a can be divided into two distinct groups by their hydrogen isotope composition and their Sr isotope ratios. The samples from the two later dykes belong to the low temperature, low water/rock ratio group.

According to Adamides (1984), the Agrokipia 'B' deposit is not a typical exhalative Cyprus-type sulphide deposit, but should be regarded as a kind of replacement deposit in proximity to a truly exhalative deposit. This is evidenced by the absence of a well-defined massive pyrite zone and a regular decrease of grade with depth.

One of the strongest arguments in favour of this view is that, so far, all the contacts between the mineralized and unmineralized lavas found at Agrokipia 'B' are gradational ones, with sulphide veins in otherwise slightly altered lavas. Adamides (1984) further states that the Agrokipia 'A' deposit, which lies about 300 m to the west of Agrokipia 'B', is a truly exhalative ore deposit, for here mineralization is concentrated at the boundary between Upper and Lower Pillow Lavas (Constantinou and Govett, 1973). He concludes that the ore fluids, which formed the Agrokipia 'B' deposit, followed a fracture zone to higher levels in the sequence and deposited Agrokipia 'A' at a former seafloor-ocean interface. So Agrokipia 'B' perhaps represents a replacement deposit which, however, formed about 100 to 200 m below the former seafloor.

Stable isotope and Sr isotope data indicate that the rocks of Hole CY-2a underwent at least two different stages of alteration. Hot ascending hydrothermal solutions caused mineralization and high-grade alteration. The gradual increase of whole rock $^{87}Sr/^{86}Sr$ ratios and the gradual decrease of $\delta^{18}O$-values of smectite at the boundary between unmineralized and mineralized lavas support Adamides' view that Agrokipia 'B' represents a replacement deposit. The whole rock hydrogen isotope data, however, reflect a very sudden increase in temperature at 154 m and not a gradual transition to higher temperatures. So the hydrogen data suggest that Agrokipia 'B' was deposited from hot ascending solutions at a former seawater-basalt interface, which soon was covered by additional extrusive and intrusive sequences.

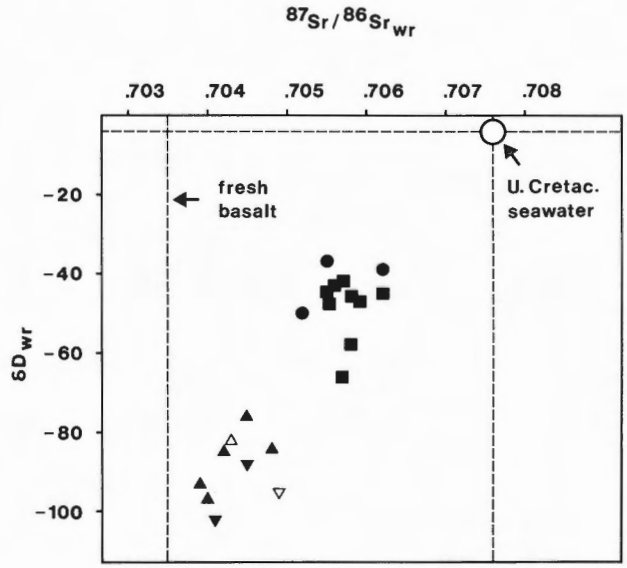

Figure 6: $^{87}Sr/^{86}Sr$ ratios of whole rock samples versus their hydrogen isotope composition. The dashed vertical lines represent the Sr isotope composition of fresh basalts from Troodos and of Upper Cretaceous seawater. The dashed horizontal line represents the hydrogen isotope composition of Upper Cretaceous seawater (symbols as in Figure 1).

TABLE 1. Sample Description and Strontium, Hydrogen and Oxygen Isotope Analyses of Minerals and Whole Rocks

No.	Depth/Units	Lithology	$^{87}Sr/^{86}Sr$	δD	$\delta^{18}O$
1	28.35-40 I 1.01	dark greenish-grey, medium-grained, phyric, massive basalt	0.70450	-88	17 .5 sm 3 .0 ma 5 .4 di 5.3 pl
3	41.85-90 III 9.02	dark grey, fine-grained, aphyric basalt	0.70396	-97	
9	85.55-60 IV 15.01	greenish-grey, medium-grained aphyric, massive basalt	0.70411	-102	9 .5 wr 18 .2 sm
11	97.40-45 V 22.01	medium grey, fine-grained, aphyric basalt	0.70449	-76	
16	118.10-15 VI 26.05	brownish-grey, very fine-grained, sparsely phyric, massive basalt	0.70421	-85	
20	131.44-51 VI 29.01	highly broken and fractured, brownish- to greenish-grey, fine-grained, aphyric basalt	0.70388	-93	9 .1 wr 18 .0 sm 2 .3 ma
26	153.80-85 VII 33.02	grey- to brownish-grey, fine-grained to aphanitic, aphyric basalt	0.70483	-84	9 .7 wr 12 .0 sm 2 .6 ma
27	159.58-68 VIII 36.02	light grey, aphyric, intensely altered lava cut by zones of intense dissolution and mineralization	0.70549	-37	8 .5 wr 5 .9 ch 6 .4 qu
29	161.53-58 VIII 36.03	light grey, fine-grained, highly altered, aphyric lava cut by veins of irregular masses of quartz and sulphide	0.70522	-50	
32	169.85-90 VIII 38.04	light grey, highly altered, aphyric lava; probably originally massive glass		-35	2 .9 ch 5 .0 qu
39	189.25-30 VIII 42.06	light grey, fine-grained, altered massive lava	0.70619	-39	1 .4 il 0 .8 ch
52	240.40-45 VIII 51.05	very light grey, highly argillized lava; probably altered massive glass		-37 -36 il -40 cl	3.5 il 1.9 ch
63	275.30-35 VIII 59.03	grey, intensly altered and silicified volcanic, strongly mineralized	f.i. qu: f.i. py:	-34 -51	7 .5 qu

No.	Depth/Units	Lithology	$^{87}Sr/^{86}Sr$	δD	$\delta^{18}O$
65	279.70-75 VIII 60.01	light grey, highly altered lava, probably altered massive glass		-35	
67	282.00-05 IX 60.03	brownish-grey, medium-grained, aphyric, relatively fresh basalt	0.70488	-95	9 .5 wr 14 .0 sm
73	289.45-50 X 68.01	light grey, fine-grained, aphyric lava with pyrite and gypsum vein		-36	4 .7 wr
74	297.25-30 XI 69.01	fault breccia; brownish-grey volcanic breccia with slickensides		-44	8 .7 wr 3 .1 ch 6 .7 qu
85	351.69-82 XII 81.02	Massive, grey-green, fine-grained, aphyric, pervasively altered basalt	0.70547	-47	8 .3 wr 7 .2 ch 5 .8 qu
88	368.06-21 XIII 83.03	dark grey, medium-grained, aphyric, unmineralized, massive basalt	0.70430	-82	8 .4 wr 9 .2 sm 10 .7 qu 1.6 ma
91	384.35-50 XIV 88.01	light grey, fine-grained, sparsely phyric, altered, massive basalt	0.70583	-46	7 .2 wr 6 .9 qu 0 .9 ma
93	393.10-15 XIV 90.01	coarse-grained, aphyric microdiorite	0.70569		5 .4 qu
102	434.78-92 XVII 98.04	light greenish-grey, fine-grained, aphyric basalt	0.70576	-58	6 .1 wr 1 .5 ch 8 .7 qu
104	445.82-94 XVIII 100.05	light grey, fine-grained, aphyric, massive basalt	0.70589	-47	6 .2 wr -1.3 ma
106	464.86-92 XIX 104.05	faintly mineralized, pervasively altered pillow breccia	0.70628		
114	494.83-97 XXI 109.02	greenish-grey, fine-grained, aphyric, altered basalt	0.70571	-42	4 .0 wr 2 .0 ch 5 .7 qu
130	568.30-40 XXII 121.01	greenish-grey, medium-grained, sparsely vesicular dyke	0.70617	-45	4 .0 wr 0 .5 ch 3 .6 qu

No.	Depth/Units	Lithology	$^{87}Sr/^{86}Sr$	δD		$\delta^{18}O$
141	653.41-54 XXII 138.06	greyish-green, fine- to medium-grained, altered and mineralized, aphyric basalt	0.70568	-66		3 .3 wr -0.3 ch 7 .2 qu 0 .4 ep
143	672.15-27 XXII 142.01	dark grey, fine- to medium-grained, massive, altered dyke	0.70547	-45		
146	688.55-70 XXII 144.02	altered, mineralized, medium-grained basalt, probably pillow	0.70557	-43 -49 -8	 ch ep	7 .2 wr 2.8 ch 7.0 qu 1.3 ma

ch: chlorite, di: diopside, ep: epidote, f.i. qu: fluid inclusions in quartz, f.i. py: fluid inclusions in pyrite, il: illite, ma: magnetite, pl: plagioclase, qu: quartz, sm: smectite, wr: whole rock, $^{87}Sr/^{86}Sr$ ratios and δD values refer to whole rock analyses, except where specified.

The high-temperature activity of the convection cell, which caused the formation of the Agrokipia 'B' orebody, slowed down before the production of rocks from the andesite - dacite - rhyodacite suite had ceased. The whole sequence of Hole CY-2a was affected by at least one low-temperature event, which involved smaller effective water/rock ratios than the high-temperature event. This is suggested by the Sr isotope ratios of the unmineralized rocks and the post-mineralization dykes. The secondary minerals which were formed at high temperatures, however, have completely retained their high-temperature isotope composition, even though they must have been affected by the low-temperature event.

ACKNOWLEDGMENTS

The authors would like to thank the International Crustal Research Drilling Project for the opportunity to participate in the Cyprus Crustal Study Project. We are also indebted to G. Bartholomae, M. Feth, M. Schumann, and J. Zimmermann for analytical assistance. This study was funded by a grant from the European Community Research & Development Program Raw Materials and by the German Science Foundation.

REFERENCES

Adamides, N.
1984: Cyprus volcanogenic sulfide deposits in relation to their environment of formation; unpublished Ph.D. thesis, University of Leicester, p. 1-383.

Albarède, F., Michard, A., Minster, J.-F. and Michard, G.
1981: $^{87}Sr/^{86}Sr$ ratios in hydrothermal waters and deposits from the East Pacific Rise at 21°N; Earth and Planetary Science Letters, v. 55, no. 2, p. 229-236.

Barrett, T.J. and Friedrichsen, H.
1982: Strontium and oxygen isotopic composition of some basalts from Hole 504 B, Costa Rica Rift, DSDP Legs 69 and 70; Earth and Planetary Science Letters, v. 60, no. 1, p. 27-38.

Bottinga, Y. and Javoy, M.
1973: Comments on oxygen isotope geothermometry; Earth and Planetary Science Letters, v. 20, no. 2, p. 250-265.

Cameron, W.E., Nisbet, E.G. and Dietrich, V.J.
1980: Petrographic dissimilarities between ophiolitic and ocean-floor basalts; *in* Ophiolites, Proceedings of the International Ophiolite Symposium, Cyprus, 1979, ed. A. Panayiotou; Cyprus Geological Survey Department, Ministry of Agriculture and Natural Resources, p. 182-192.

Constantinou, G. and Govett, G.J.S.

1973: Geology, geochemistry, and genesis of Cyprus sulfide deposits; Economic Geology, v. 68, no. 6, p. 843-858.

Corliss, J.B.
1971: The origin of metal-bearing submarine hydrothermal solutions; Journal of Geophysical Research, v. 76, no. 33, p. 8128-8138.

Corliss, J.B., Dymond, J., Gordon, L.I., Edmond, J.M., Von Herzen, R.P., Ballard, R.D., Green, K., Williams, D., Bainbridge, A., Crane, K. and Van Andel, T.H.
1979: Submarine thermal springs on the Galápagos Rift; Science, v. 203, no. 4385, p. 1073-1083.

Craig, H., Welhan, J.A., Kim, K., Poreda, R. and Lupton, J.E.
1980: Geochemical studies of the 21°N EPR hydrothermal fluids; EOS, v. 61, no. 46, p. 992.

Dasch, E.J., Hedge, C.E. and Dymond, J.
1973: Effect of sea water interaction on strontium isotope composition of deep-sea basalts; Earth and Planetary Science Letters, v. 19, no. 2, p. 177-183.

Elder, J.W.
1965: Physical processes in geothermal areas; American Geophysical Union, Monographs, no. 8, p. 211-239.

Friedman, I. and O'Neil, J.R.
1977: Compilation of stable isotope fractionation factors of geochemical interest; United States Geological Survey, Professional Paper, p. 1-440.

Gass, I.G.
1968: Is the Troodos Massif of Cyprus a fragment of Mesozoic ocean floor?; Nature, v. 220, no. 5162, p. 39-42.

Hart, S.R.
1976: LIL-element geochemistry, Leg 34 basalts; *in* Initial Reports of the Deep Sea Drilling Project, Volume 34, ed. R.S. Yeats, S.R. Hart, et al.; U.S. Government Printing Office, Washington D.C., v. 34, p. 283-288.

Heaton, T.H.E. and Sheppard, S.M.F.
1977: Hydrogen and oxygen isotope evidence for sea-water hydrothermal alteration and ore deposition, Troodos Complex, Cyprus; *in* Volcanic Processes in Ore Genesis, Geological Society of London, Special Publication, no. 7, p. 42-57.

Herzig, P.M. and Friedrich, G.H.
1987: Sulphide mineralization, hydrothermal alteration and chemistry in the drill hole CY-2a, Agrokipia, Cyprus; *in* Cyprus Crustal Study Project Initial Report Hole CY2-2a, ed. P.T. Robinson, I.L. Gibson and A. Panayiotou; Geological Survey of Canada, Paper 85-29.

ICRDG
1984: Are Troodos deposits an East Pacific analog? Geotimes, v. 29, no. 5, p. 12-14.

Lawrence, J.R., Gieskes, J.M., Broecker, W.S.
1975: Oxygen isotope and cation composition of DSDP pore waters and the alteration of Layer II basalts; Earth and Planetary Science Letters, v. 27, no. 1, p. 1-10.

Leitch, E.C.
1984: Island arc elements and arc-related ophiolites; Tectonophysics, v. 106, no. 3/4, p. 177-203.

Lister, C.R.B.
1972: On the thermal balance of a mid-ocean ridge; Geophysical Journal of the Royal Astronomical Society, v. 26, p. 515-535.

McCulloch, M.T., Gregory, R.T., Wasserburg, G.J. and Taylor, Jr., H.P.
1981: Sm-Nd, Rb-Sr, and $^{18}O/^{16}O$ isotopic systematics in an oceanic crustal section: evidence from the Samail ophiolite; Journal of Geophysical Research, v. 86, no. B4, p. 2721-2735.

Michard, G., Albarède, F., Michard, A., Minster, J.-F., Charlou, J.-L., Tan, N.
1984: Chemistry of solutions from the 13°N East Pacific Rise hydrothermal site; Earth and Planetary Science Letters, v. 67, no. 3, p. 297-307.

Miyashiro, A.
1973: The Troodos ophiolitic complex was probably formed in an island arc; Earth and Planetary Science Letters, v. 19, no. 2, p. 218-224.

Moores, E.M., Robinson, P.T., Malpas, J. and Xenophontos, C.
1984: Model for the origin of the Troodos Massif, Cyprus, and other mideast ophiolites. Geology, v. 12, p. 500-503.

Moores, E.M. and Vine, F.J.
1971: The Troodos Massif, Cyprus, and other ophiolites as oceanic crust: evaluation and implications; *in* A Discussion on the Petrology of Igneous and Metamorphic Rocks from the Ocean Floor; Philosophical Transactions of the Royal Society of London, Series A, v. 268, p. 443-466.

Mottl, M.J. and Seyfried, W.E.
1980: Sub-seafloor hydrothermal systems rock-vs. seawater-dominated; *in* Seafloor Spreading Centres. Hydrothermal systems, ed. P.A. Rona, R.P. Lowell; Benchmarc Papers in Geology, Dowden, Hutchinson and Ross, Stroudsburg, Pa., p. 66-82.

Oudin, E. and Constantinou, G.
1984: Black smoker chimney fragments in Cyprus sulphide deposits; Nature, v. 308, p. 349-353.
Pearce, J.A.
1975: Basalt geochemistry used to investigate past tectonic environments on Cyprus; Tectonophysics, v. 25, no. 1-2, p. 41-67.
Peterman, Z.E., Hedge, C.E. and Tourtelot, H.A.
1970: Isotopic composition of strontium in sea water throughout Phanerozoic time; Geochimica et Cosmochimica Acta, v. 34, no. 1, p. 105-120.
Robinson, P.T. and Gibson, I.L.
1983: Cyprus Crustal Study Project. Hole CY-2a Lithologic Unit Summaries.
Robinson, P.T., Melson, W.G., O'Hearn, T. and Schmincke, H.-U.
1983: Volcanic glass compositions of the Troodos ophiolite, Cyprus; Geology, v. 11, no. 7, p. 400-404.
Schmincke, H.-U., Rautenschlein, M., Robinson, P.T. and Mehegan, J.M.
1983: Troodos extrusive series of Cyprus: a comparison with oceanic crust; Geology, v. 11, no. 7, p. 405-409.
Seyfried, Jr., W.E., Mottl, M.J. and Bischoff, J.L.
1978: Seawater/basalt ratio effects on the chemistry and mineralogy of spilites from the ocean floor; Nature, v. 275, no. 5676, p. 211-213.
Shackleton, N.J. and Kennett, J.P.
1975: Paleotemperature history of the Cenozoic and the initiation of Antarctic glaciation: oxygen and carbon isotope analyses in DSDP sites 277, 279 and 281; *in* Initial Reports of the Deep Sea Drilling Project, Volume 29, ed. J.P. Kennett, R.E. Houtz, et al.; U.S. Government Printing Office, Washington D.C., v. 29, p. 743-755.
Smewing, J.D., Simonian, K.O. and Gass, I.G.
1975: Metabasalts from the Troodos Massif, Cyprus: genetic implications deduced from petrography and trace element geochemistry; Contributions to Mineralogy and Petrology, v. 51, p. 49-64.
Spiess, F.N., Macdonald, K.C., Atwater, T., Ballard, R., Carranza, A., Cordoba, D., Corx, C., Diaz Garcia, V.M., Francheteau, J., Guerrero, J., Hawkins, J., Haymon, R., Hessler, R., Juteau, T., Kastner, M., Larson, R., Luyendyk, B., MacDougall, J.D., Miller, S., Normark, W., Orcutt, J. and Rangin, C.
1980: East Pacific Rise: hot springs and geophysical experiments; Science, v. 207, p. 1421-1433.
Spooner, E.T.C. and Bray, C.J.
1977: Hydrothermal fluids of seawater salinity in ophiolitic sulphide ore deposits in Cyprus; Nature, v. 266, no. 5605, p. 808-812.
Spooner, E.T.C., Chapman, H.J. and Smewing, J.D.
1977: Strontium isotopic contamination and oxidation during ocean floor hydrothermal metamorphism of the ophiolitic rocks of the Troodos Massif, Cyprus; Geochimica et Cosmochimica Acta, v. 41, no. 7, p. 873-890.
Spooner, E.T.C. and Fyfe, W.S.
1973: Sub-sea-floor metamorphism, heat and mass transfer; Contributions to Mineralogy and Petrology, v. 42, p. 287-304.
Suzuoki, T. and Epstein, S.
1976: Hydrogen isotope fractionation between OH-bearing minerals and water; Geochimica et Cosmochimica Acta, v. 40, no. 10, p. 1229-1240.
Williams, D.L., Von Herzen, R.P., Sclater, J.G. and Anderson, R.N.
1974: The Galapagos spreading centre: lithospheric cooling and hydrothermal circulation; Geophysical Journal of the Royal Astronomical Society, v. 38, p. 587-608.
Yeh, H.-W. and Savin, S.M.
1977: Mechanism of burial metamorphism of argillaceous sediments: 3. O-isotope evidence; Geological Society of America, Bulletin, v. 88, no. 9, p. 1321-1330.

The Basaltic Andesite-Andesite and the Andesite-Dacite Series from the ICRDG Drill Holes CY-2 and CY-2a. I. Lithology, Petrology and Geochemistry

U. BEDNARZ, G. SUNKEL AND H.-U. SCHMINCKE

Institut für Mineralogie, Ruhr-Universität Bochum, Postfach 102148, D-4630 Bochum, Federal Republic of Germany

Bednarz, U., Sunkel, G. and Schmincke, H.-U., The basaltic andesite-andesite and the andesite-dacite series from the ICRDG Drill Holes CY-2 and CY-2a. I. Lithology, petrology and geochemistry; in *Cyprus Crustal Study Project: Initial Report, Holes CY-2 and 2a, ed. P.T. Robinson, I.L. Gibson and A. Panayiotou; Geological Survey of Canada, Paper 85-29, p. 183-204, 1987.*

Abstract

Two holes were drilled into hydrothermal zones of the Troodos Ophiolite Extrusive Series (Cyprus) surrounding the Agrokipia 'A' and 'B' Fe-Cu-Zn ore bodies. One hundred and three samples were analyzed by XRF for major and trace elements and 102 thin sections were studied microscopically. Analyses of nine handpicked glasses were used to infer the approximate pre-alteration composition of the rocks by comparing concentrations of immobile elements. Sparsely olivine phyric rocks occur in the upper 25 m of CY-2 and in the upper 90 m of CY-2a, those below are aphyric to sparsely plagioclase, clinopyroxene, Fe-Ti oxide and rarely hypersthene-phyric. Silica-oversaturation is indicated by primary groundmass quartz, cristobalite and tridymite. The ratio of pillows to sheet flows in CY-2 is 1:3, intrusives are absent. In CY-2a intrusives make up about 50%, sheet flows 42%, and pillows 8%. Glassy, partly clastic rocks are interpreted as sheet lava flows brecciated during emplacement. Two arc-tholeiite magmatic series were distinguished chiefly by the Ti/Zr-ratio: A younger basaltic andesitic-andesitic (BA) group shows (Zr: 30 to 90 ppm; Ti/Zr: 80 to 110) and an andesitic-dacitic (DA) group (Zr: 50 to 110 ppm; Ti/Zr: >120, decreasing to 50 in the dacites). High volatile and relatively high LFS element concentrations and the abundance of differentiated rocks indicate a spreading environment over a subduction zone as the most plausible tectonic environment.

Résumé

Deux trous de forage ont traversé les zones hydrothermales de la série extrusive de l'ophiolite de Troodos entourant les gîtes de Fe-Cu-Zn Agrokipia 'A' et 'B'. Les éléments majeurs et en trace de 103 échantillons ont été analysés par fluorescence X et 102 lames minces ont été étudiées au microscope. Les analyses de neuf échantillons de verre triés à la main ont permis une estimation de la composition des roches avant leur altération par une comparaison des teneurs en éléments immobiles. Des roches phyriques à olivine clairsemée apparaissent dans les premiers 25 m du trou CY-2 et dans les premiers 90 m du trou CY-2a, les roches de plus grandes profondeurs sont aphyriques mais elles incluent de faibles proportions de phases phyriques à plagioclase, clinopyroxène, oxyde Fe-Ti et plus rarement à hypersthène. Le quartz, la cristobalite et la tridymite primaires dans la matrice indiquent une sursaturation en silice. Le rapport des coulées de laves en coussins et en nappes est 1:3 dans CY-2, et les roches intrusives sont absentes. Dans le trou de forage CY-2a, les roches intrusives comptent pour 50%, les coulées en nappes pour 42%, et les laves en coussins pour 8%. Des roches vitrifiées et partiellement clastiques, correspondent à des coulées de laves en nappes bréchifiées durant leur mise en place. Deux séries de tholéiites magmatiques de type d'arc ont été reconnues principalement par le rapport Ti/Zr: un groupe basaltique andésitique-andésitique (BA) plus jeune fournit (Zr: 30 à 90 ppm; Ti/Zr: 80 à 110) et un groupe andésitique-dacitique (DA) donne (Zr: 50 à 110 ppm; Ti/Zr: >120, diminuant à 50 dans les dacites). Les teneurs en éléments très volatiles et à faible force de champs ainsi que l'abondance des roches différentiées révèlent l'existence de grandes coulées de laves au-dessus d'une zone de subduction formant le milieu tectonique le plus propice.

INTRODUCTION

The Cyprus Crustal Study Project is an attempt to analyze in detail the major rock types of the Troodos ophiolite and thus to provide a firmer base for interpreting the Cyprus complex as well as to serve as a model for a comparison with sections of young ocean crust drilled in the present ocean basins and studied by geophysical methods. Three parts of the Troodos ophiolite were sampled by drilling (Figure 1): Extrusive rocks at Akaki River (CY-1; CY-1a); hydrothermally altered rocks at Agrokipia (CY-2, CY-2a), and intrusive rocks at Palekhori (CY-4). Below, we present chemical, mineralogical, and petrographic data from the two holes drilled at Agrokipia that help to evaluate the original, unaltered nature of the upper part of the Troodos extrusive rocks. A companion paper (Sunkel et al., 1987) discusses low temperature and hydrothermal alteration of these rocks. Both reports are largely descriptive.

Regional Setting

Hole CY-2 (35°02'43"N, 33°08'48"E) was drilled by the International Crustal Research Drilling Group between June 22th and July 27th, 1982 into the Troodos extrusive series near the village of Agrokipia to a depth of 226.26 m; core recovery was 91.8%. The core was divided into 14 lithological units (Figure 2; 3 pillow and 11 massive lava units, two of them dominantly glassy). It was planned to penetrate the 'Agrokipia A' ore body, but the hole was abandoned because a moderately mineralized zone was found only in the upper part.

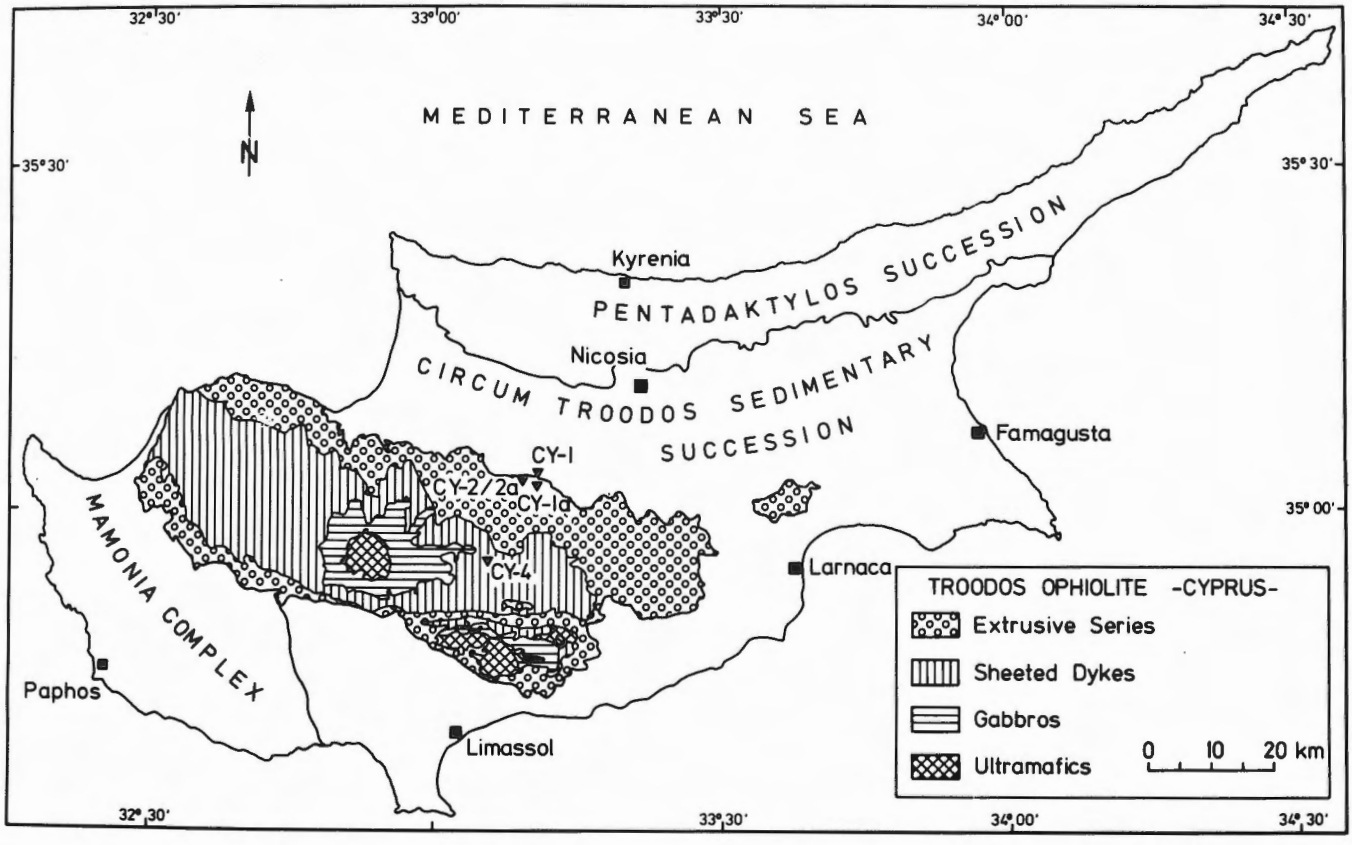

Figure 1: Simplified geologic map of the Troodos ophiolite (Cyprus - Eastern Mediterranean); after geological map compiled by the Geological Survey Department, Cyprus (1979). Sites CY-1/CY-1a: Akaki River, Sites CY-2/CY-2a: Ore bodies near Agrokipia village, Site CY-4: Palekhori village.

CY-2a (35°02′40″N, 33°08′55″E) was drilled between August 2nd and September 19th, 1982, 270 m east of CY-2 at about the same stratigraphic position into the 'Agrokipia B' ore deposit. Moderately to weakly mineralized rocks were reached at a depth of 150 m. Drilling terminated at a depth of 689.15 m. Core recovery was 93.4%. The section consists mainly of massive flows (some of them glassy) and intrusives, the latter increasing in abundance downwards to >90% (Figure 3).

The uppermost lavas drilled are about 150 m below the contact between the extrusive rocks and the overlying Upper Cretaceous to Paleogene chalks of the Lefkara and Pakhna formations.

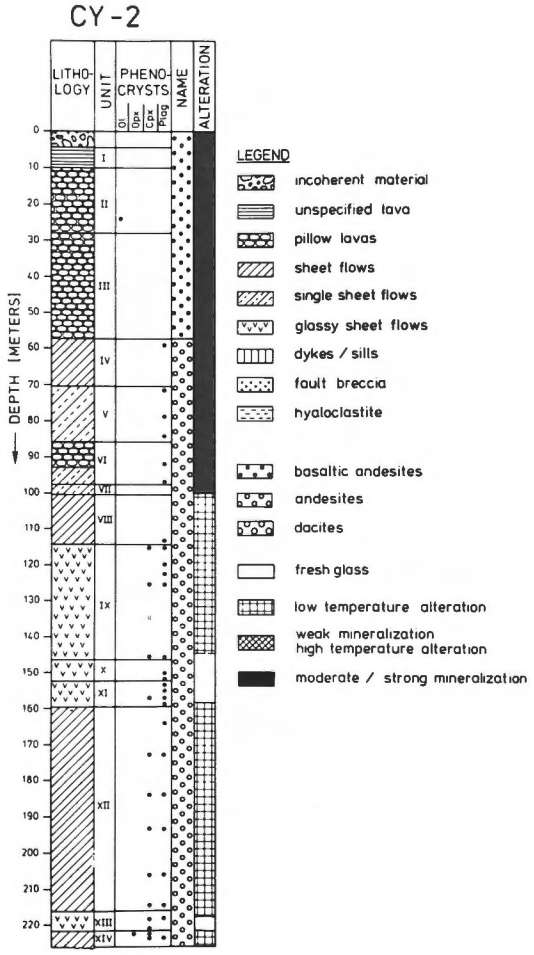

Figure 2: Columnar section of hole CY-2 showing lithology, thin section phenocryst assemblage, name, and degree of alteration of rocks. The lower boundary of the mineralization zone is not as distinct as shown, but grades into the low temperature alteration zone between 85 and 100 m depth.

ANALYTICAL METHODS

We performed bulk rock chemical analyses for 15 major and minor and 12 trace elements on 33 samples from CY-2, 71 samples from CY-2a, and 7 interlaboratory Troodos standards by X-ray fluorescence methods on glass fusion beads, using a fully automated Philips PW 1400. In addition we handpicked and analyzed 9 glass and 2 clay mineral samples from the glassy massive flows of Unit VI of CY-2a.

The fusion beads consist of rock powders (dried at 100°C overnight) and flux (lithium metaborate and dilithium tetraborate, Merck A 12) in the ratio 1:4, melted at 1000°C for 10 min. and poured into a 34 mm diameter pellet mold.

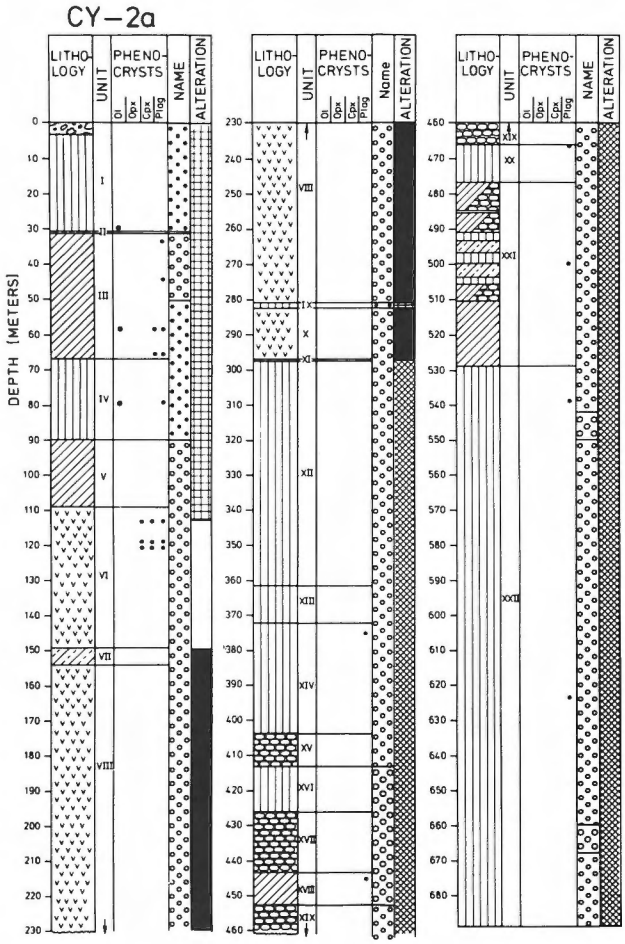

Figure 3: Columnar section of hole CY-2a showing lithology, thin section phenocryst assemblage, name, and degree of alteration of rocks. For legend see Figure 2.

Fe-(II) was determined by semi-automatic potentiometric titration of the hydrofluoric acid-silver perchlorate digested sample, with standard potassium bromide solution. As pyrite is not dissolved by hydrofluoric acid, the Fe-content of mineralized samples is only given as total FeO.

CO_2 was determined by closed-system coulometric titration of a barium perchlorate solution into which were passed the gases produced by passing oxygen over the sample roasted in a tube furnace. Sulfur in mineralized samples was analyzed by coulometric titration of a sodium sulfate solution.

H_2O+ was measured by closed-system coulometric titration of a nonaqueous Karl Fischer reagent into which was passed the carrier gas (here N_2) containing water stripped from the sample by heating in a Pt-crucible to 1300°C with an induction furnace.

Glass samples were crushed with a steel mortar. The fraction >1 mm was handpicked and cleaned repeatedly in an ultrasonic bath. Grain sizes of the samples prior to grinding ranged from 0.5 to 2 mm. 'Contamination' of the glasses by adhering alteration products ('palagonite', clay minerals) was estimated to be <10%, in many samples <5%.

Forty thin sections of CY-2 rocks and 62 thin sections of CY-2a rocks were studied for textures and modal amounts of primary and secondary phases.

DEFINITION OF TERMS

The term 'original chemical composition' is understood as the pre-alteration chemistry of the rocks as defined by a comparison of the concentrations of relatively immobile elements, especially Zr and Ti, of altered rocks with that of fresh, handpicked glasses.

LITHOLOGY

Extrusive, intrusive, and volcaniclastic rock types were distinguished in the cores of CY-2 and CY-2a. Detailed descriptions and data are given in the core descriptions (unpub. rep., Dalhousie University). A summary of the core descriptions is provided by Robinson and Gibson (1983a, 1983b).

(A) Extrusive Rocks

(1) Pillow Lavas

Pillow lavas make up 26% in CY-2 and only 7% in CY-2a (Figures 4 and 5), and decrease in abundance downwards in both holes.

In Hole CY-2, units II, III, VI, and in CY-2a units XV, XVII, XIX, and parts of XXI are interpreted as pillow lavas. The average pillow diameter could not be determined in Hole CY-2 because of poor core recovery; in CY-2a the average pillow thickness ranges from 0.63 m (unit XIX) to 1.0 m (unit XV). Three pillows from unit XXI (CY-2a) are described to be >1.5 m thick. Pillow lavas with large pillow diameters up to about 3 m - as observed in the field - are, however, difficult to distinguish from sheet flows in the core.

(2) Sheet Flows

Sheet flows are more abundant than pillow lavas in CY-2 (97% of the extrusives) and in CY-2a (85% of the extrusives; Figures 2 and 3). The average thickness of massive flows ranges from 1.25 m (CY-2, Unit VI) to 2.7 m (CY-2a, Unit V). Individual flows may, however, exceed 5 m in thickness (e.g. Unit XII, CY-2). Two thirds of the sheet-flows in CY-2a and one quarter in CY-2 are massive glassy flows. The glassy flows are of special interest because of their structure, textures and unusual abundance of fresh glass. They will, therefore, be described in more detail.

Brecciated glassy flows occur predominantly in units IX, XI, and XII of CY-2 where they have an aggregate thickness of about 18 m, and in unit VI of CY-2a with an aggregate thickness of about 15 m (ICRDG, 1984). Individual glassy zones are 0.12 m to 5.07 m thick (Robinson and Gibson, 1983b).

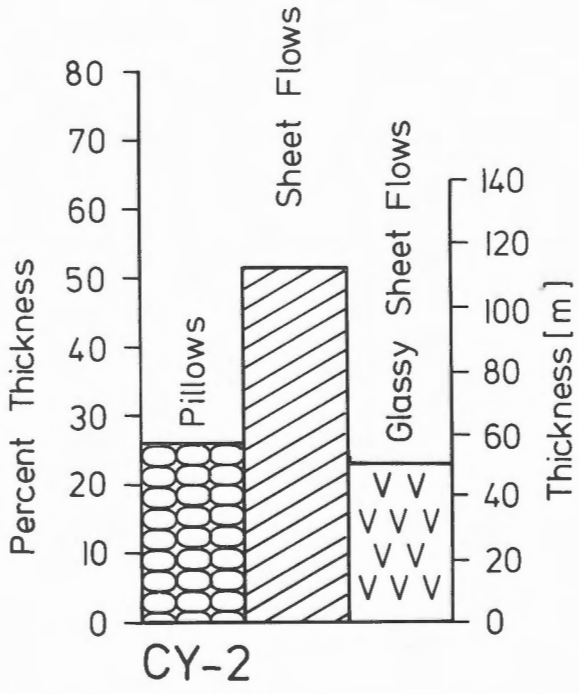

Figure 4: Relative and absolute frequency of lithologic rock types in hole CY-2.

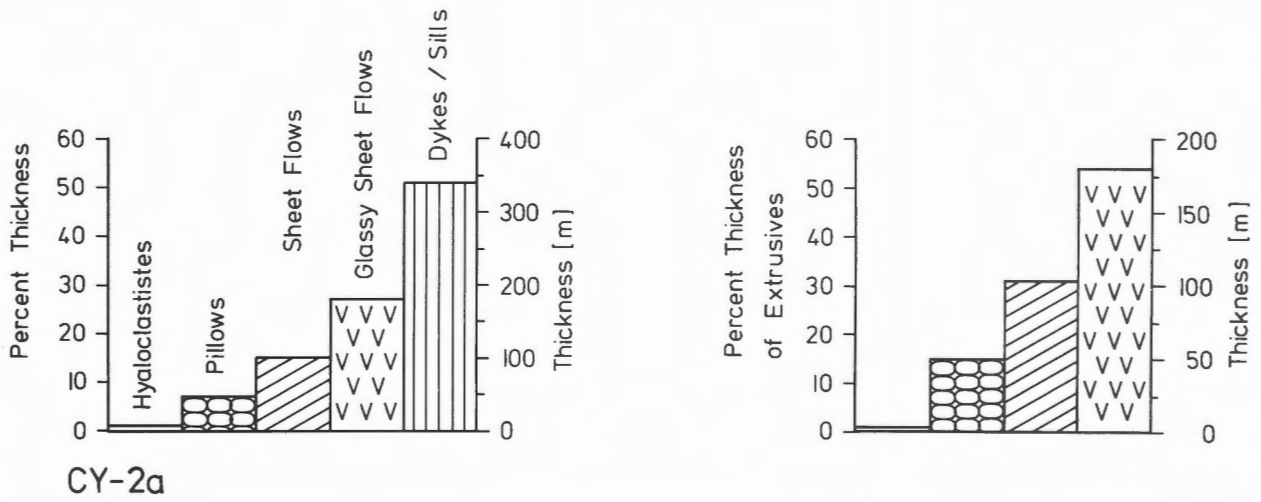

Figure 5: Relative and absolute frequency of rock types in hole CY-2a.

In the core, the glassy lava appears highly clastic and occurs as irregular mm to cm-thick layers of partly altered glass, separated by completely clay-altered portions. Detailed examination of these rocks were undertaken to determine if they represent (a) massive glassy lavas, whose brecciated appearance is due to alteration and thus only apparent, (b) slightly brecciated lava flows, or (c) hyaloclastite breccias emplaced as clastic systems.

Evidence from the examination of hand specimens and from the study of twenty thin sections clearly indicates that much of the glassy material is from a continuous lava flow as shown by unbroken rows of vesicles and common transitions from glassy through variolitic to microcrystalline zones, typical of the margins of pillow and sheet flow lavas. These rocks are quite different texturally from the bedded hyaloclastites described below.

While we can thus exclude explanation (c), we have to distinguish primary brecciation from apparent brecciation. Much of what appears to be brecciation at first sight both in the cores as well as in thin section is caused by the mechanical and optical contrast between fresh glass and glass altered to smectite. We describe the alteration textures in more detail in the companion paper (Sunkel et al., 1987).

However, all of the thin sections of glassy lavas studied by us from holes CY-2 and CY-2a contain abundant evidence for mechanical fragmentation prior to alteration. Most important is the juxtaposition of angular fragments showing contrasting orientation of aligned microlites and vesicles and, in some cases, zones differing in the degree of crystallinity (Figures 6 and 7). Several thin sections show a break in texture between what appears to be the glassy margin of a flow and adjacent spherulitic and microcrystalline zones and a brecciated zone several mm to cm thick (Figure 8). This breccia consists of larger fragments with partly broken vesicles set in a sand- to silt-sized matrix of smaller glass shards (Figure 8), some with recognizable bubble wall and bubble junction shapes, others being angular and poorly vesicular (Figure 9). Fresh glass is only preserved in the cores of lapilli-sized fragments (i.e. >2 mm in diameter).

The poor sorting, the angularity of the fragments, some very delicate, and the occurrence adjacent to glassy margins of flows strongly suggests that the clastic zones were not deposited on top of a flow but developed on its surface during flow.

The fact that we have found brecciated zones in about half of the twenty thin sections studied, comprising about 18 m of glassy lavas in CY-2 and about 13 m in CY-2a indicates that breccia zones are common.

We infer two models of origin for the clastic zones: (a) brecciation during internal shearing and (b) brecciation on the surface of a flow. The alignment of microlites and elongation of vesicles and the observation that glassy and microcrystalline bands with slight unconformity (unlike the regular zones of increasing crystallization developed inward from a glassy flow margin) indicate internal shearing of a viscous lava flow during flowage. These textures very much resemble those in dacitic to rhyolitic glassy subaerial lava flows. Some of the brecciated zones are interpreted to have formed when the viscosity of the liquid had become too high for viscous deformation resulting in fracturing of the glass.

Figure 6: Primary devitrification banding (dark streaks) in glassy lava now fragmented as shown by different orientation of bands in the three fragments. Long side of photomicrograph: 3 mm.

Figure 7: Glassy lava subdivided into fragments by cracks with marginal bands of palagonite recrystallized to smectite. Angular 'fragments' are made of fresh glass except for alteration along concentric perlitic cracks and radial dissolution tubules. Long side of photomicrograph: 3 mm.

Figure 8: Breccia zone between glassy lava flow units showing large fragments with partly broken vesicles set in a fine-grained clastic matrix. Banding due to palagonitization steps. Long side of photomicrograph: 3 mm.

Most of the breccia zones, however, appear to be associated with breakage of the quenched and frothy flow tops. The vesicularity of some fragments exceeds 50 vol.%, indicating the scoria-like nature of some flow tops.

There are several implications of these brecciated rocks. For one, such brecciated flow tops producing ash-size glass shards from vesicular glassy scoria type lava provide a ready source for winnowing out by currents of fine-grained shards that may be become deposited elsewhere and become bedded hyaloclastites (see below).

Secondly, from our field studies along the Akaki and Pediaeos river canyons, such glassy, partly brecciated lavas are unlikely to have formed continuous sheets of large lateral extent. Thus, we suspect the moderately brecciated glassy andesitic sheet flows pass laterally into highly brecciated lavas or breccia zones.

(B) Intrusives

Sills and dykes are common throughout the extrusive series. About 50% of CY-2a core was interpreted as intrusives (Figure 5), their abundance increasing downhole to >90% (Figure 3); more than one hundred individual dykes were identified (Robinson and Gibson, 1983b). Single cooling units interpreted as sills reach 27.4 m in thickness in unit I, dykes in the lower part of the hole (unit XII) range from 0.09 to 13.63 m in true thickness with an average of 1.46 m. No intrusives were identified in hole CY-2.

(C) Hyaloclastites

Only one 45-cm-thick unit of hyaloclastite was found in the core of CY-2a (Unit II - 30.72 m to 31.75 m). The hyaloclastic unit is bedded and normally graded. Maximum grain sizes range from about 5 mm to 1 mm (Figure 10). Two samples from 30.72 m and 30.82 m, studied in thin-section, are sand to silt-size, graded layers, about 3 cm thick, with maximum grain sizes of 1-2 mm at the base.

Most clasts are aphyric, angular, mostly elongate, glass shards, now completely altered to smectite. Most shards are vesicle free, but relic vesicles occur along grain boundaries. Platy shards show subparallel orientation.

Figure 9: Brecciated glassy andesite showing angular, partly unrimmed fragments set in fine-grained clastic matrix. Long side of photomicrograph: 3 mm.

Figure 10: Bedded hyaloclastite made up of uniform shards completely altered to smectite. Note polycrystalline quartz aggregate. Long side of photomicrograph: 3 mm.

Mono- and polycrystalline quartz grains make up about 2 vol.% (Figure 10). Accessory minerals are calcitized and oxidized subhedral olivine (</= 0.8 mm), clinopyroxene, plagioclase, and spinel, generally <0.5 mm. Secondary phases are mainly smectite, chlorite, zeolite, (analcite?), and recrystallized Fe-Ti - phases.

The shards are interpreted as fragments produced by spalling of the glassy crust of mafic pillows or sheet flows as discussed above. Grading and the occurrence of polycrystalline quartz clasts indicates emplacement of the hyaloclastites by mass flow. Because polycrystalline quartz occurs in CY-2a only as a secondary phase in the zone of mineralization and because olivine phenocrysts are restricted to the late basaltic rocks, we infer a time break between mineralization, erosion of mineralized basalts along fault scarps (?) and near-by deposition of the hyaloclastites.

ORIGINAL PETROGRAPHIC COMPOSITION

Two major groups of original mineral assemblages are recognized from cores of CY-2 and CY-2a representing (1) basaltic andesitic and (2) andesitic to dacitic rocks: (1) plagioclase + clinopyroxene + olivine (+ orthopyroxene?) + opaque +/- SiO_2 -phase +/- spinel (2) plagioclase + clinopyroxene +/-orthopyroxene + opaque +/- SiO_2-phase.

Assemblage (1)

Assemblage (1) is restricted to the upper part of both holes. In CY-2, it occurs from the top of the core to about 55 m, but only the uppermost part has preserved primary igneous mineralogy and hyalopilitic texture (Figure 11) while the lower part is extensively overprinted by hydrothermal alteration and the assignment to assemblage (1) is based on concentration of immobile elements. In CY-2a, assemblage (1) occurs from the top to about 30 m downhole, from about 58 m to 90 m, and in a small dyke between 280.86 m and 286.56 m (unit IX). The analyzed samples are fresher and display a well-preserved intersertal to subophitic and ophimottled texture (Figure 12) ranging in grain size from 150 µm to 400 µm.

Phenocrysts

Olivine is the typical phenocryst, but it makes up less than 5 vol.% in general. Olivine microphenocrysts varying in size about 500 µm are more common than large phenocrysts reaching up to 3.5 mm in diameter. Olivine is generally replaced by smectite, calcite or hematite/iron hydroxide but some relics occur in sample CY-2a 30.1 m. Plagioclase, up to 1.5 mm in length, occurs in some rocks (<1 vol.%) as well as microphenocrysts of clinopyroxene up to 500 µm in diameter (<1 vol.%).

Groundmass

Plagioclase is the major phase, ranging up to 60 vol.%, forming laths in the groundmass or quench crystals around irregular amygdales of smectite. Clinopyroxene is common (up to 25 vol.%). Narrow rims of smectite (10 µm) occur on some of the pyroxenes. Orthopyroxene was not definitely identified but may be present. Olivine, altered to smectite, is rare. Subhedral to euhedral crystals and skeletal quench crystals (sample CY-2 22.05 m) of opaque minerals do not exceed about 1 vol.%. Chrome-spinel is rare in the groundmass or as small inclusions in olivine. At least two SiO_2-phases occur in most samples, where they are closely associated with ophimottled textures. Quartz usually forms euhedral crystals up to 350 µm growing into the open space of irregular vesicles (Figure 13) or occur as patches with micrographic texture. Tridymite ranging up to 250 µm is identified by its typical wedge-shaped twinned crystals, cristobalite by its shrinkage cracks (Figure 14).

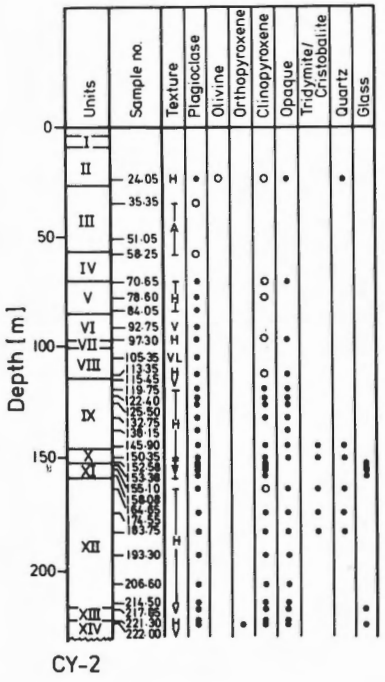

Figure 11: Distribution of primary minerals in hole CY-2. Open circle indicated replaced phases, dots indicate optically fresh occurrences. Textures: A - argillaceous, H - hyalopilitic, HT - hyalopilitic - trachytic, S - subophitic, V - vitric, VL - variolitic.

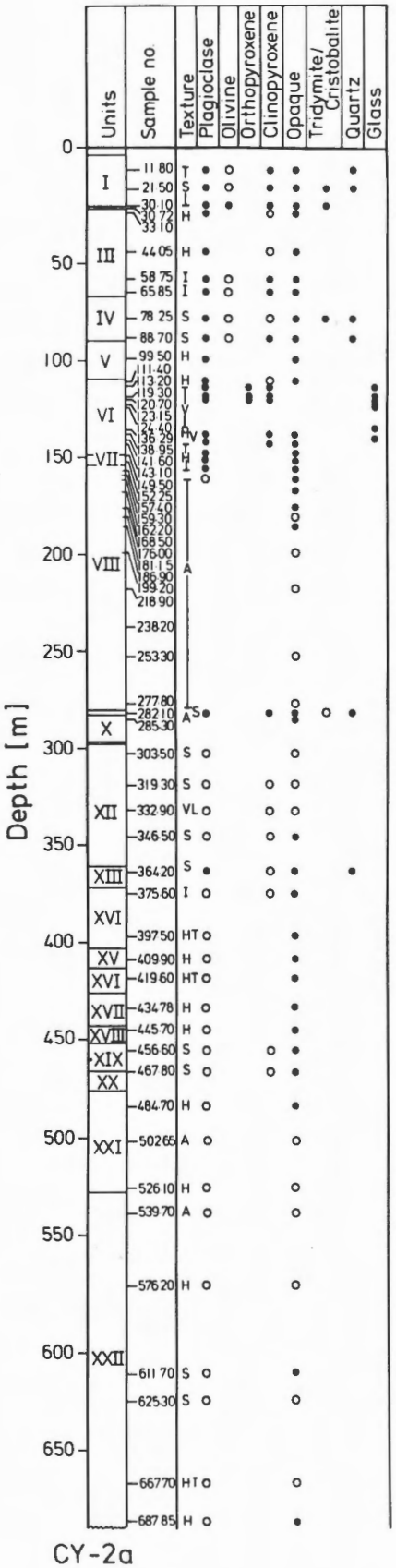

Figure 12: Distribution of primary minerals in hole CY-2a. For legend see Figure 11.

Assemblage (2)

Assemblage (2) is dominant in both cores. Igneous textures range from vitric through hyalopilitic through intersertal to subophitic and ophimottled. The rocks are slightly phyric, but glomerophyric textures are rare.

Phenocrysts

Plagioclase phenocrysts are most common but do not exceed 3-5 vol.%. Euhedral to subhedral phenocrysts, partly well zoned or with sieve-like structures characterized by glass inclusions, reach up to 1.5 mm in diameter. Clinopyroxene mostly appears in glassy rocks (about 1-3 vol.%) where it forms euhedral to subhedral crystals ranging from 350 to 700 µm in size. Clinopyroxenes commonly form glomerocrysts with magnetite and, more rarely, plagioclase. Phenocrysts in crystalline rocks are partly rimmed by smectite. Hypersthene occurs as rare phenocrysts up to 500 µm in some glassy rocks.

Groundmass

Plagioclase is the dominant phase. It occurs (a) as groundmass crystals forming laths up to 300 µm in length, (b) as quench crystals, and (c) as hairlike crystallites or spherulites in glassy rocks. Clinopyroxene reach up to 10 vol.% but usually do not exceed 5 vol.%. Opaque minerals, usually forming quench crystals in hyalopilitic rocks and subhedral to euhedral crystals up to 70 µm in diameter in more crystallized rocks, are more frequent than in assemblage (1) (up to 5 vol.%). SiO_2-phases are less abundant than in assemblage(1). As the occurrence of primary SiO_2-phases in CY-2 and CY-2a samples is restricted to thick sills, sheet flows, and dykes with additional evidence (e.g. grain size) for slow cooling rates this is most likely due to fast cooling rates of assemblage (2) rocks sufficiently fresh to have potential primary SiO_2-phases preserved.

Vesicles

In the basaltic andesitic rocks vesicles range in size from 300 µm to 3.5 mm and make up about 5 vol.%. In the andesitic to dacitic rocks, vesicles make up about 15 vol.%, maximum values extending to about 50 vol.%. Vesicles are up to 5 mm in diameter and can be very elongate, especially in the glassy lavas. In the glassy rinds of flows vesicles are spherical but become quite irregular towards the microcrystalline interiors.

Partly to totally filled segregation vesicles (Smith, 1967) are common. The segregation is characterized by hyalopilitic, quench and skeletal textures and smaller groundmass grain sizes compared to the adjacent rock. Partial fillings can form a meniscus as described by Bideau et al. (1984) or form highly irregular shapes (Figure 15 b), indicating high viscosity of the segregated liquid. Vesicularity in the segregation is often considerably higher than in the surrounding rock reaching up to about 40 vol.% (Figure 15 a), most likely due to enrichment of volatiles in the late stage melt represented by the segregated liquid.

Figure 13: Primary high temperature quartz rimming a vesicle filled by smectite. Long side of the photomicrograph: 200 µm.

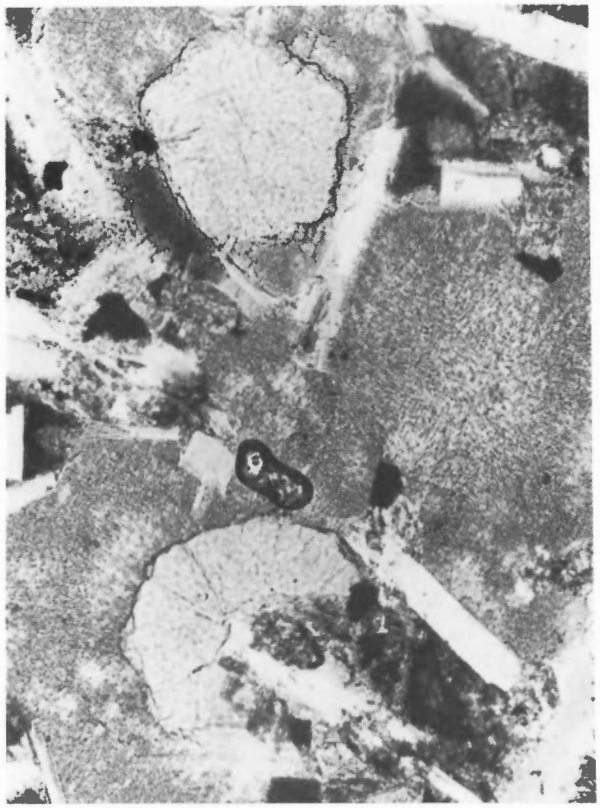

Figure 14: Cristobalite rosettes in vesicles now filled with smectite. Long side of the photomicrograph: 200 µm.

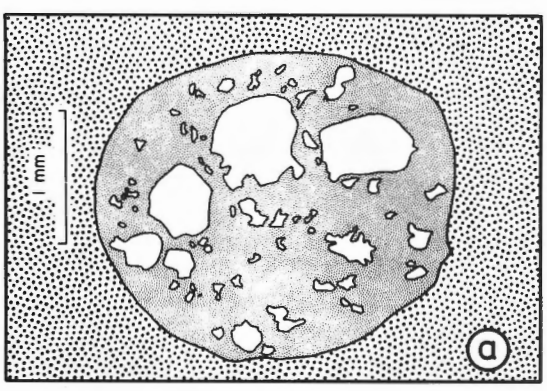

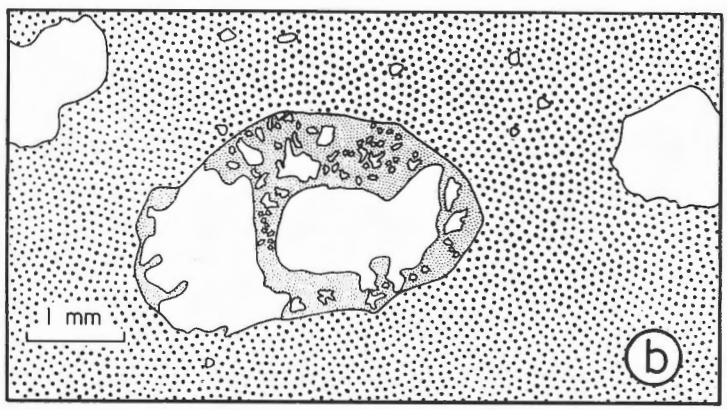

Figure 15 a, b: Sketches of segregation vesicles. Shaded area: Segregation portion; stippled area: surrounding groundmass; white area: vesicles, partly filled by secondary minerals (e.g. smectite).

Vesicles, asymmetrically and partly filled by secondary minerals can be used as paleovertical indicators in the upper part of CY-2.

The high vesicularity of the Troodos lavas is of special interest, as noted elsewhere (Schmincke et al., 1983). High vesicularity in submarine lavas can be due to high volatile contents, shallow water depth of extrusion or both (e.g. Moore and Schilling, 1973). Extrusive water depth of the Troodos lavas was around 2000 m judging from the nature of the overlying sediments (Robertson, pers. comm., 1984). Although the paleobathymetry cannot be determined precisely it must in any case have been considerably deeper than 500 m. The high vesicularity of the lavas is thus most probably due to high initial volatile concentrations. High initial volatile concentrations were also inferred from low totals of fresh glasses analyzed by microprobe (Robinson et al., 1983; Rautenschlein et al., 1985). Garcia et al. (1979) and Muenow et al. (1980) have shown that magmas from island arc settings are unusually water rich. We assume that primary H_2O concentrations of the dominating basaltic andesitic lavas were around 1.5 wt.%, based on the data in Robinson et al. (1983) and Rautenschlein et al. (1985). We further assume, that H_2O is the main vesicle-forming volatile in analogy to the relatively well-studied MORB tholeiites - although CO_2 can form a few small vesicles at great water depth because of its high partial pressure. At H_2O concentrations of about 1.5 wt.%, oversaturation and thus vesicle formation would occur at 200 to 300 bars, i.e. water depth of 2000-3000 m (MacPherson, 1984).

ORIGINAL CHEMICAL COMPOSITION

We analyzed handpicked andesitic glass fragments from Unit VI (CY-2a) in order to define the range of original magma compositions because the primary chemical composition of CY-2 and CY-2a rocks has been modified to varying degrees by alteration (Sunkel et al., 1987). The chemical composition of two mafic glasses from the Akaki River section are from Rautenschlein (unpub. data).

Among the relatively immobile elements, Zr - ranging from 30 to 110 ppm - was chosen as a fractionation index (Figures 16 and 17). We assume immobile elements to approximately resemble the initial values. In the strongly mineralized zone, however, some very low concentrations of Zr (7 and 22 ppm) and other stable elements were found and the initial composition of these rocks is thus more difficult to reconstruct.

Assuming that SiO_2 - which is commonly used to discriminate andesitic rocks (e.g. Ewart, 1982) - varies linearly between the mafic Akaki glasses and the more evolved glasses of CY-2a, we distinguish:

(I) BA-series:
- Basaltic andesites - (SiO_2: 53-56 wt.%)
  Zr: 30 to 50 ppm
  Y: 10 to 25 ppm
  P_2O_5: around 0.05 wt.%
  TiO_2: 0.4 to 0.9 wt.%
- Low-Ti andesites - (SiO_2: 56-63 wt.%)
  Zr: 50 to 90 ppm
  Y: 25 to 55 ppm
  P_2O_5: 0.05 to 0.2 wt.%
  TiO_2: 0.9 to (1.2) wt.%

(II) AD-series:
- High-Ti andesites - (SiO_2: 56-63 wt.%)
  Zr: 50 to 90 ppm
  Y: 25 to 55 ppm
  P_2O_5: 0.05 to 0.2 wt.%
  TiO_2: 1.1 to 1.6 wt.%
- Dacites - (SiO_2: $>$63 wt.%)
  Zr: $>$90 ppm
  Y: 40 to 50 ppm
  P_2O_5: around 0.15 wt.%
  TiO_2: 1.3 to 0.9 wt.%

The correlation of Zr with elements other than those listed is generally poor. The compatible elements MgO, Cr, and Ni, however, show a general trend to lower concentrations in the more evolved members of the magma series. The broader scattering of Co-values in the andesites is best explained by different initial Co-concentrations of the Low-Ti and the High-Ti andesites and fractionation of Co by olivine and Fe-Ti oxides.

Fe and V show distribution patterns similar to that of Ti: enrichment in the BA series by olivine, clinopyroxene, and plagioclase fractionation and depletion in the AD series due to titanomagnetite fractionation.

Variations of Glass Composition

The Zr concentration of the glasses ranges from 35 to 90 ppm and correlates positively with the major elements SiO_2 (54 to 66 wt.%), MnO (0.1 to 0.2 wt.%), Na_2O (1.5 to 3 wt.%), K_2O (0.05 to 0.4 wt.%), and P_2O_5 (0.04 to 0.16 wt.%). A negative correlation is observed for Al_2O_3 (16 to 14.5 wt.%), CaO (11 to 6 wt.%), and MgO (8 to 2.5 wt.%). FeO° is somewhat indifferent in the basaltic andesitic rocks and decreases in the andesites.

The trace elements Rb (3 to 22 ppm), Sr (75 to 108 ppm), and Ba (20 to 60 ppm) correlate positively with Zr, while the compatible elements Cr (270 to 10 ppm), Ni (64 to 4 ppm), and Co (36 to 20 ppm) are depleted in the andesitic rocks.

The measured H_2O concentration ranges from 2 to 3.9 wt.% in the basaltic andesitic glasses; and from 3.9 to 6.0 wt.% in the andesite glasses. CO_2 ranges from 0.08 to 0.26 wt.% in the andesitic glasses. Table 1 shows the analytical data for glasses in CY-2a.

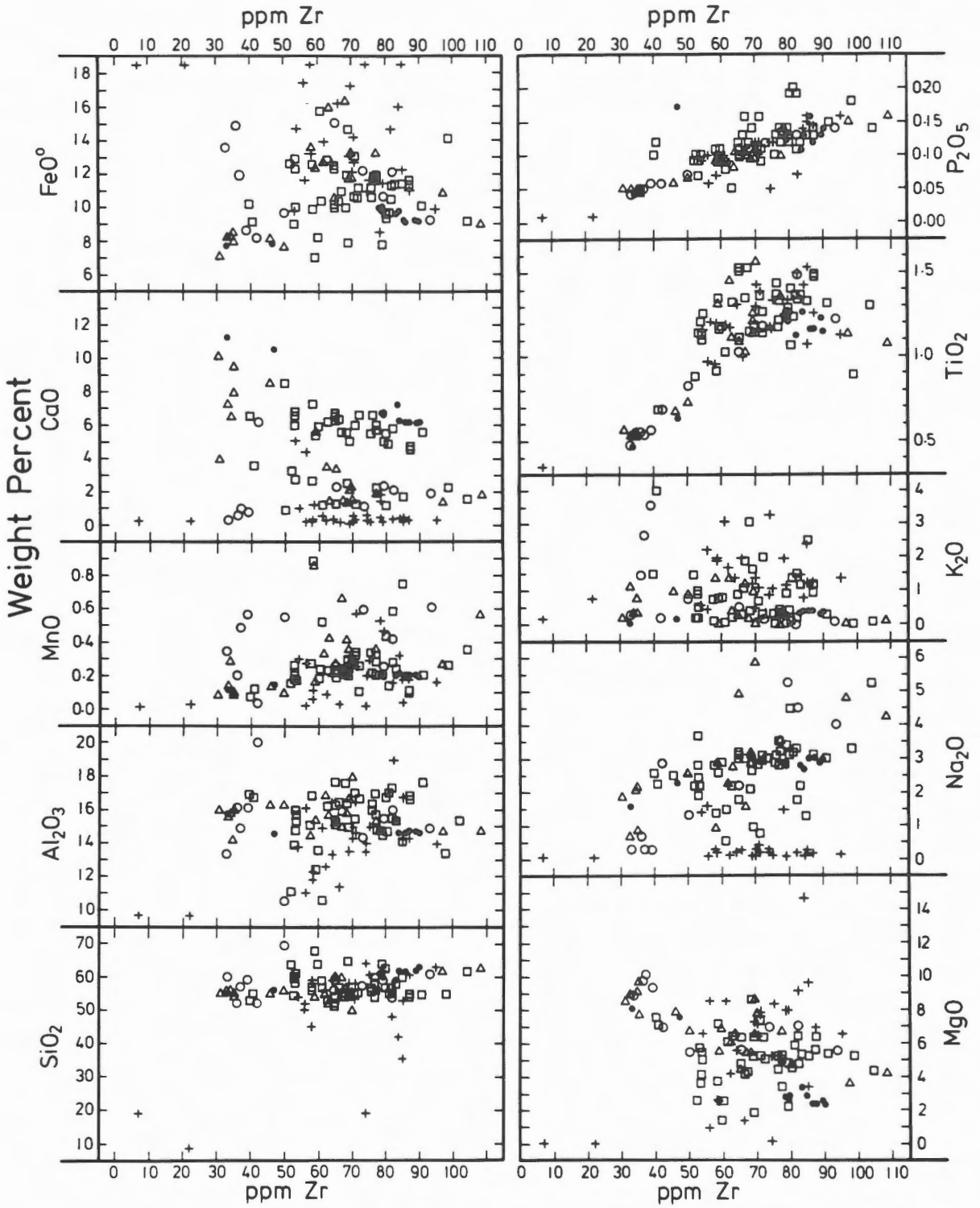

Figure 16: Zr/major element variation diagrams of CY-2 and CY-2a whole rocks and glasses. Symbols: squares - sheet flows, circles - pillows, triangles - dykes/sills, crosses - argillaceous rocks of the main sulfide mineralization zone of CY-2a, dots - glass separates. Analyses of two mafic glasses from the Akaki Canyon are from Rautenschlein (unpublished data).

Distribution in the Cores

Basaltic andesitic rocks are restricted to the uppermost part of both holes (Figures 2, 3 and 18-21). They form pillow lava units >40 m thick in CY-2 units I, II, and III. In CY-2a, basaltic andesites make up a 27.4 m thick sill (unit I) and a 42.8 m thick lava sequence in units III and IV. The upper 21.4 m belonging to unit III were interpreted as sheet flows, the lower part as sill (Robinson and Gibson, 1983b).

The discrimination between Low-Ti and High-Ti andesites in the range between 70 and 90 ppm Zr is not possible because the concentrations and ratios of all stable elements (e.g. Ti/Zr-ratio, Figure 23), including Co and V, overlap. In hole CY-2, however, a division is possible by the Ti/Zr-ratio (Figure 22), which is 90 to 105 between 55 and 130 m depth and generally >110 (up to 140) in the lower 90 m of the section. The division is uncertain only for the pillow lavas of Unit VI which compositionally fall into the range of overlap.

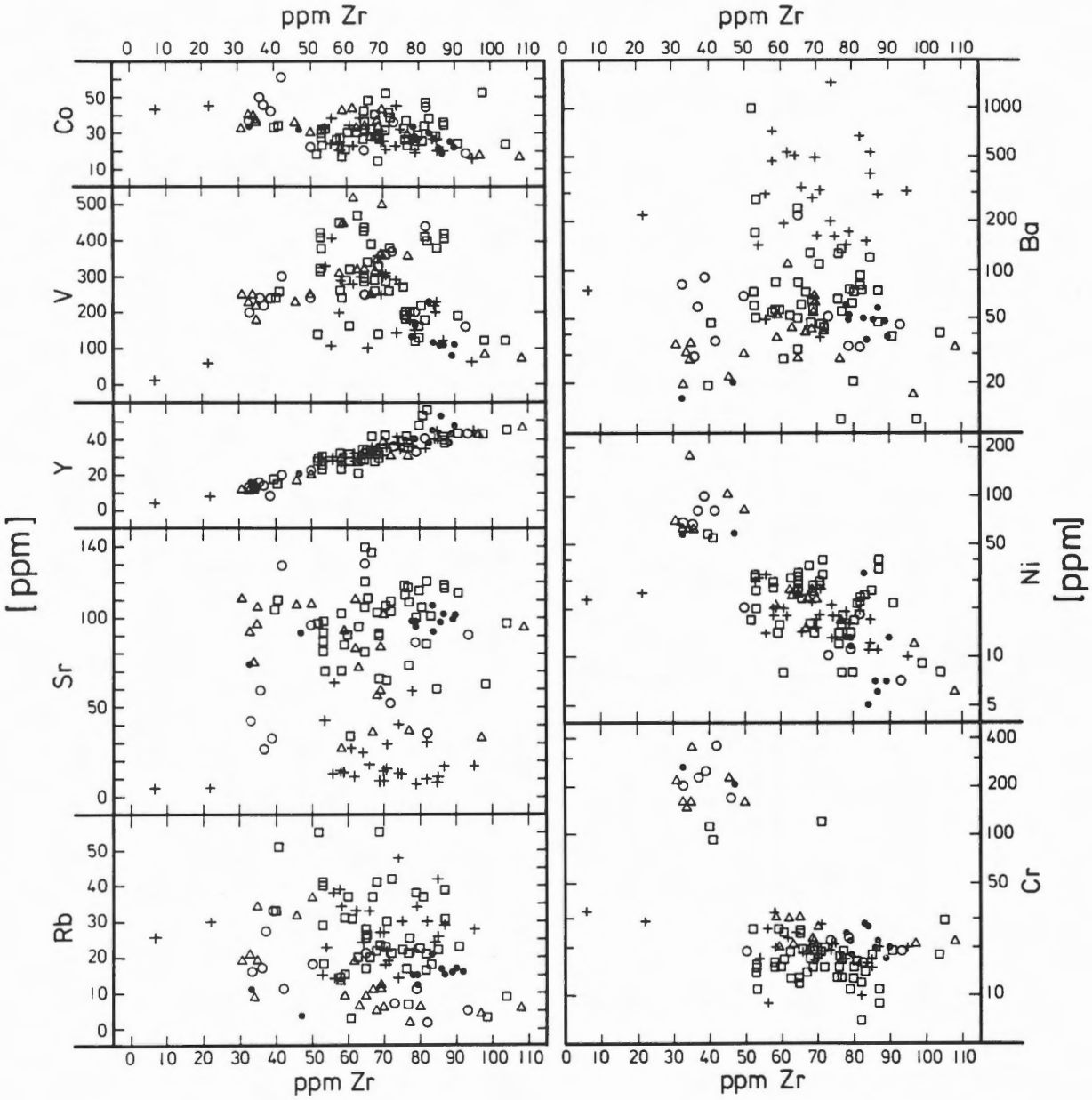

Figure 17: Zr/trace element variation diagrams for CY-2/CY-2a rocks. For explanation of symbols see Figure 16.

TABLE 1. Analyses of Glass Separates of CY-2a.

Depth	113.20 m	119.30 m	120.70 m	123.15 m	124.40 m	124.75 m	136.29 m	136.55 m	141.60 m
					Oxides as wt. %				
SiO_2	57.20	58.40	57.40	58.80	59.40	59.20	58.10	58.30	57.40
TiO_2	1.09	1.15	1.18	1.08	1.10	1.10	1.17	1.16	1.16
Al_2O_3	14.81	13.79	13.66	13.72	13.91	13.93	14.21	14.29	13.97
Fe_2O_3	2.42	2.11	2.67	1.87	2.05	1.82	2.41	2.13	2.59
FeO	7.10	6.71	6.61	6.84	6.89	7.01	7.26	7.43	7.14
MnO	0.19	0.19	0.20	0.18	0.19	0.19	0.19	0.18	0.20
MgO	3.31	2.39	2.68	2.28	2.29	2.26	2.65	2.59	2.72
CaO	7.30	5.83	5.90	5.82	6.02	5.91	6.62	6.62	6.47
Na_2O	2.68	2.68	2.48	2.81	2.83	2.89	2.75	2.78	2.63
K_2O	0.29	0.32	0.32	0.32	0.32	0.33	0.28	0.27	0.28
P_2O_5	0.11	0.12	0.12	0.13	0.15	0.11	0.13	0.12	0.11
H_2O+	4.04	5.67	5.95	5.35	5.00	4.84	4.42	3.90	5.01
CO_2	0.26	0.08	0.08	0.10	0.17	0.11	0.10	0.10	0.12
S	0.02	0.01	0.01	0.02	0.02	0.02	0.03	0.02	0.02
Cl	0.02	0.03	0.03	0.03	0.03	0.03	0.02	0.02	0.02
Total	100.84	99.48	99.29	99.35	100.37	99.75	100.34	99.91	99.84
					Trace Elements as ppm				
V	222	92	107	100	100	105	152	150	154
Cr	27	16	25	19	19	21	23	21	17
Co	29	23	24	21	20	18	33	28	25
Ni	32	7	5	12	7	6	12	12	10
Cu	307	87	60	85	279	61	64	61	61
Zn	194	145	106	120	131	106	118	105	110
Rb	21	15	15	16	16	14	14	14	11
Sr	103	93	86	95	93	97	94	91	93
Y	37	40	42	45	50	36	38	38	34
Zr	80	83	78	84	82	82	75	76	75
Nb	4	2	3	2	2	2	3	2	3
Ba	48	45	34	36	47	56	57	50	46
FeO°	9.28	8.61	9.01	8.52	8.73	8.65	9.43	9.35	9.47
Ti/Zr	81.68	83.06	90.69	77.08	80.42	80.42	93.52	91.50	92.72

FeO°: Total Fe as FeO.

NOTE:

The whole rock analyses for CY-2 and CY-2a for this paper are included at the end of this volume in 'Major Element and Trace Element Analytical Data' (under the Lab code BOC).

The grouping of Low-Ti and High-Ti andesites is much less clear in CY-2a because many analyses fall in the range of overlap and the stable element concentrations are largely altered in the main mineralization zone, especially in its upper part. We suspect, however, that all andesitic extrusives - with the possible exception of Unit III - belong to the andesitic-dacitic assemblage. Dacites, characterized by a low Ti/Zr-ratio and Zr concentrations >90 ppm occur as extrusives and intrusives in the lower half of the section.

The largest Cr and Ni variations are found in the basaltic andesitic pillows of CY-2 and and the thick sills and sheet flows of CY-2a, increasing in the former towards the top of the section, in the latter towards the base of the sills. This is probably due to settling of the olivine and clinopyroxene phenocrysts in the thick sills after emplacement, in agreement with Robinson's and Gibson's (1983b) report of 1% olivine directly at and 10 to 25% olivine about 2 m above the base of Unit I in CY-2a. The reverse trend in the pillow section at the top of CY-2 might be due to the successive tapping of a magma chamber with an increasing phenocryst content downward.

DISCUSSION

Distinction of Magmatic Series in Cores of CY-2 and CY-2a

In the Agrokipia drill holes we distinguish a basaltic-andesitic/low-Ti andesite (BA) and a high-Ti andesite/dacite (AD) magmatic series, based mainly on the Ti/Zr ratio which is 80 to 110 in the (BA)-andesites and 120 to 140 in the (DA)-andesites. Both groups belong to the low potassium tholeiitic andesite series using criteria of Irvine and Baragar (1971) and Gill (1981). The two suites correspond to the basaltic-andesitic and the andesitic-dacitic-rhyodacitic magma series proposed by Robinson et al. (1983). However, no basaltic and no rhyodacitic rocks were found among the CY-2 and CY-2a samples. We speculate that there is a compositional overlap between the two series as indicated by immobile element concentrations. The two series are unlikely related by simple fractional crystallization.

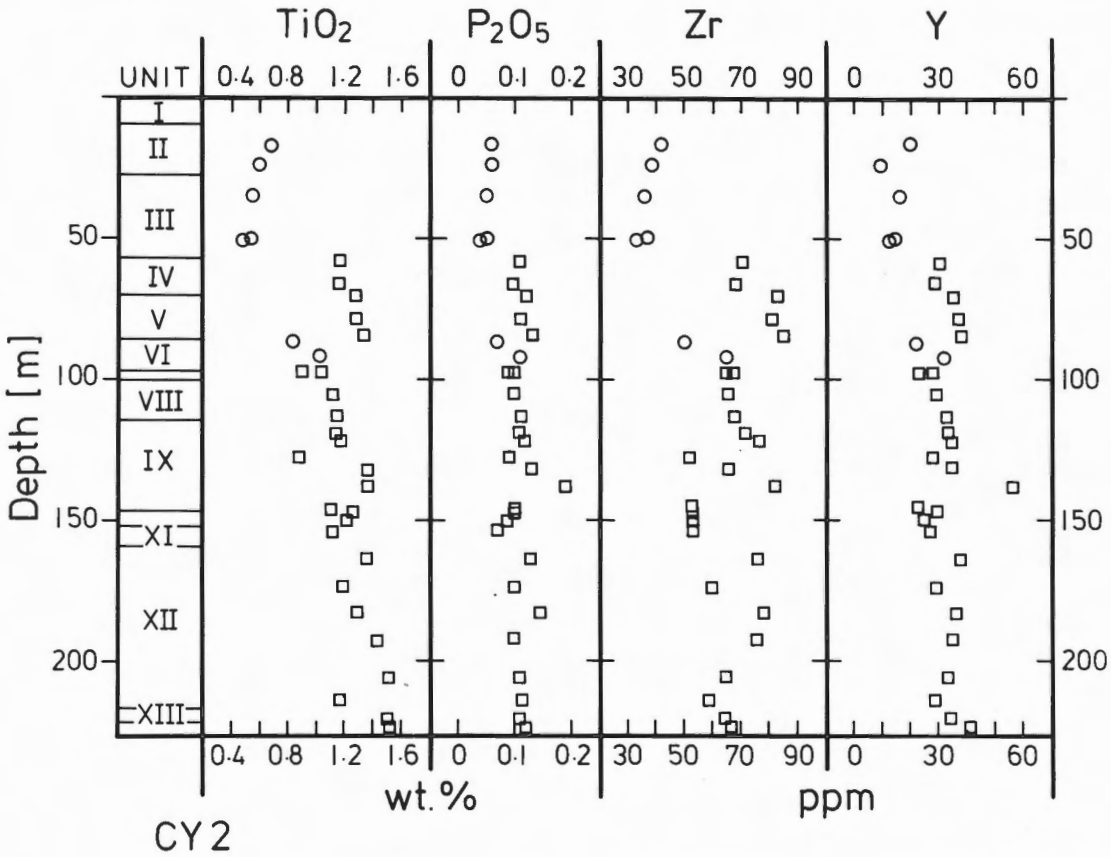

Figure 18: Variation of relatively immobile elements TiO_2, P_2O_5, Zr, and Y with depth in hole CY-2. For explanation of symbols see Figure 16.

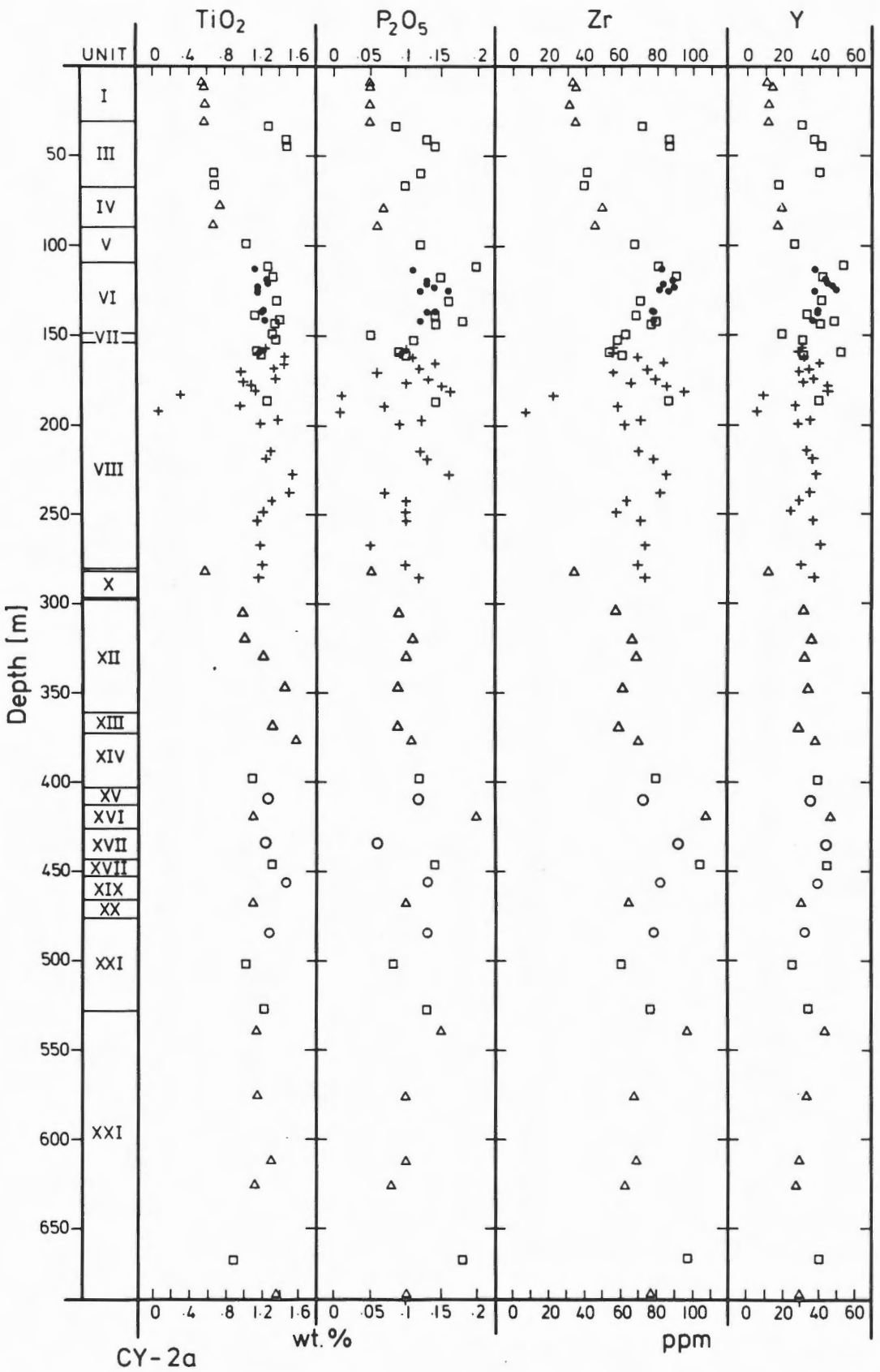

Figure 19: Variation of relatively immobile elements TiO_2, P_2O_5, Zr, and Y with depth in hole CY-2a. For explanation of symbols see Figure 16.

In hole CY-2, the ratio of basaltic andesites to andesites is about 1:3. In CY-2a the ratio basaltic andesites to andesites to dacites is about 1:8:1. The abundance of more differentiated andesitic rocks (Zr >50 ppm) is much greater than in the Akaki river section where the upper about 1000 m consist almost entirely of basaltic andesites (Schmincke et al., 1983; Rautenschlein unpub. data), even if the upper about 150 m of the extrusive section above the sites of CY-2 and CY-2a are basaltic andesites

Temporal Relationship of the Magmatic Series

The BA series appears to be younger - at least in this area - than the AD series, comparable to the stratigraphic subdivision into a lower arc tholeiite suite and an upper more mafic suite (with boninitic affinities) by Robinson et al. (1983). This two fold discrimination is, however, not compatible with the traditionally used terms of Troodos Upper and Lower Pillow Lavas (e.g. Bear, 1960).

The dykes in the lower part of hole CY-2a compositionally resemble the extrusive rocks in the upper part of the section. The only basaltic andesitic dyke recognized (Unit IX) was intruded into moderately to strongly mineralized rocks (Sunkel et al., 1987) post dating mineralization, as indicated, for instance, by the absence of sulphide minerals. Basaltic andesites occur as sills and few sheet flows (in Unit III) in the upper part of CY-2a and as pillows in the upper 50 m of CY-2. A group of dykes in the upper two-thirds of Unit XII (CY-2a) most probably belongs to the low-Ti andesites of the BA assemblage. The occurrence of smectite and the absence of sulphide minerals in some of these dykes (Sunkel et al., 1987) demonstrate that they are considerably less altered than the surrounding rocks. It seems likely that the BA group rocks intruded during the final stages partly post-dating the mineralization. Generally weakly mineralized intrusives below Unit XII belong mainly to the AD assemblage.

The extrusive rocks of the Kambia-Pediaeos area - which seem to belong dominantly to the older AD-series with a total thickness of only about 700 m (Bednarz, in preparation) - are overlain by the Perapedhi formation consisting of bentonites, umbers, and chalks, which are the oldest sediments of the circum Troodos succession (Bear, 1960). In the Akaki river, the basaltic andesites in the upper 1100 m presumably all belong to the BA-series, while AD-series rocks occur further down the section, both sections indicating that the proposed temporal relationship of the two series is of more than local significance.

Correlation of Magmatic Series between CY-2 and CY-2a

The proximity of the two holes CY-2 and CY-2a, which are about 270 m apart, provides the opportunity to test the stratigraphic correlation of compositional units and thus to evaluate effects of faulting, sea floor topography and distance of eruptive centers. The basaltic andesitic lavas extend downward to 55 m in CY-2 and 65 m in CY-2a. Assuming no offset by faulting between the drill sites, we interpret this to mean only gentle sea-floor relief prior to basaltic andesitic volcanic activity at this place. Glassy flows appear at about 110 m depth in both holes and are thus likely to represent the same unit. The chemical correlation, however, is uncertain, because the glassy flows of CY-2 partly lie in the overlap range between 70 and 90 ppm Zr and a Ti/Zr ratio between 70 and 110.

The frequency and thickness of BA-group intrusives in the upper and middle part of CY-2a might indicate that this site is closer to an eruptive center than CY-2. The same reasoning can be applied to the AD-rocks, considering the greater thickness of glassy flows in CY-2a in the same depth range. The high frequency of AD-dykes below only 530 m may be evidence for a location close to a major eruptive center. The extrusion of AD- to BA-series rocks seems to have been rather continuous as no major unconformities or intervolcanic sediments were detected. The only hyaloclastite of CY-2a occurs within the BA series, possibly being derived from a local volcanic structure (e.g. pillow volcano) or a fault scarp. In any case, this layer indicates more episodic volcanism during the late stage constructional history of the extrusive crust.

Tectonic Setting

Interpretations of the tectonic setting of the Troodos lavas based on recent major element analyses (Robinson et al., 1983), REE and isotopic studies of volcanic glasses (Rautenschlein et. al., 1985) confirmed earlier work by Miyashiro (1973), Pearce (1975) and others, that the Troodos lavas show marked differences to MORB because of their low HFS (e.g. Ti, Nb, Zr, Hf) and relatively high LFS element (e.g. K, Rb, Sr, Ba,) concentrations. High volatile concentrations (around 1.5 wt.% H_2O) in the andesites are indicated by the high vesicularity of glassy flow margins, as discussed above, and by the low totals of fresh glass analyses (Robinson et al., 1983; Rautenschlein et al., 1985).

The Troodos rocks studied by us are similar to the early arc-volcanic rocks from the island of Guam (Figure 23) except for the higher Ti/Zr ratios of these rocks (Reagan and Meijer, 1984). The Troodos BA series most closely resembles the Guam arc tholeiites

based on the stable element concentrations and ratios rather than the boninites, both, however, having fairly constant Ti/Zr-ratios over the same Zr-variation as the BA rocks.

The Troodos AD-series trend for Ti and Zr is also similar to that of basaltic to andesitic rocks from the Futuna Lavas (New Hebrides). These, however, having higher potassium concentrations, are interpreted as calc-alkaline magmatism associated with the initial stages of back arc spreading (Marcelot et al., 1983). The evolving trend, lower Ti/Zr ratio with increasing Zr content parallels that of the Guam (Meijer and Reagan, 1984) and the Tonga-Kermadec-Taupo arc (Cole, 1982) calc-alkaline series and that of the Troodos AD suite, most likely resulting from Fe-Ti oxide fractionation.

In summary, the composition of the volcanic rocks drilled in the holes CY-2 and CY-2a is most plausibly interpreted by assuming derivation of the primitive magmas from mantle material above a subduction zone. Although the composition of the lavas is most similar to island arc lavas, there are no indications such as volcaniclastic sediments for emergent island volcanoes. Oceanic crust formed in a spreading environment above a subduction zones such as postulated by Moores et al. (1984), is the most plausible scenario for formation of the Troodos lavas whether island arc volcanic edifices might have developed at this site or not.

The major difference between the Troodos lavas and those at present day oceanic crust is the abundance of differentiated volcanic rocks. We interpret this as indicating efficient fractionation in magma chambers that were more isolated and thus magmas were less frequently mixed with new batches of primitive magma. A corollary of this interpretation is the prediction that the model of a large magma chamber beneath the Troodos extrusive layer as postulated by Allen (1975) is not tenable. The extrusion of more primitive lavas during late stage volcanism may be due to late dykes bypassing rather small magma chambers.

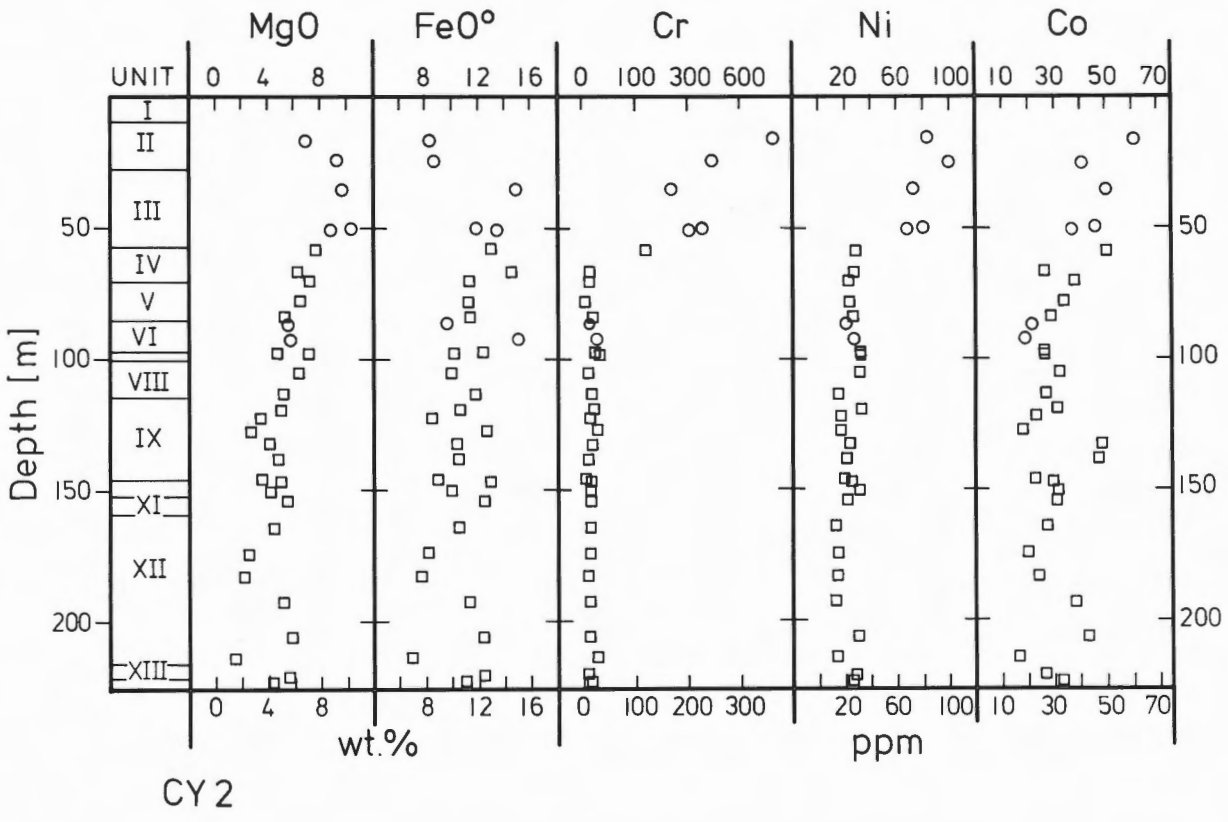

Figure 20: Variation of compatible elements MgO, FeO°, Cr, Ni, and Co with depth in hole CY-2. For explanation of symbols see Figure 16.

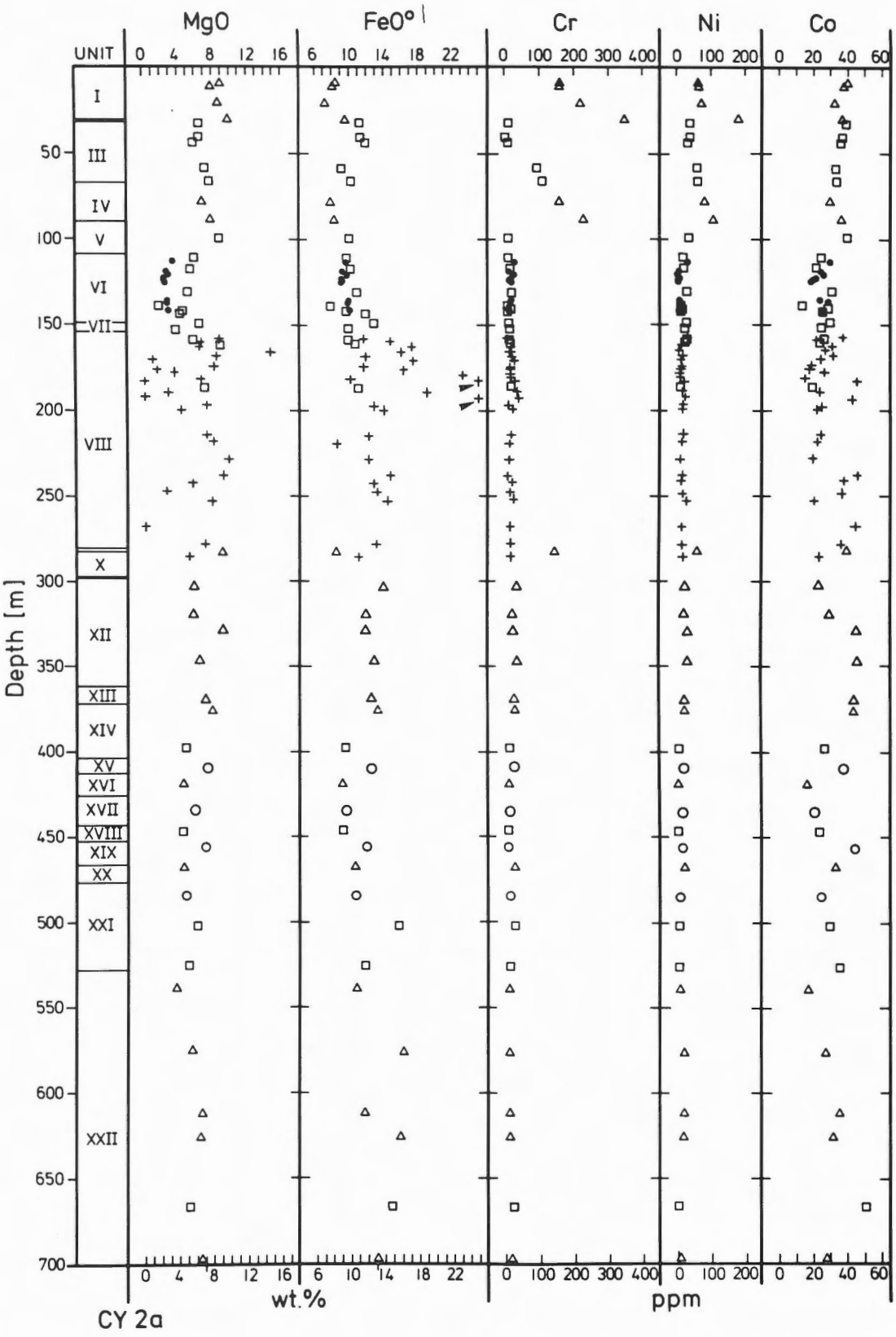

Figure 21: Variation of compatible elements MgO, FeO°, Cr, Ni, and Co with depth in hole CY-2a. For explanation of symbols see Figure 16.

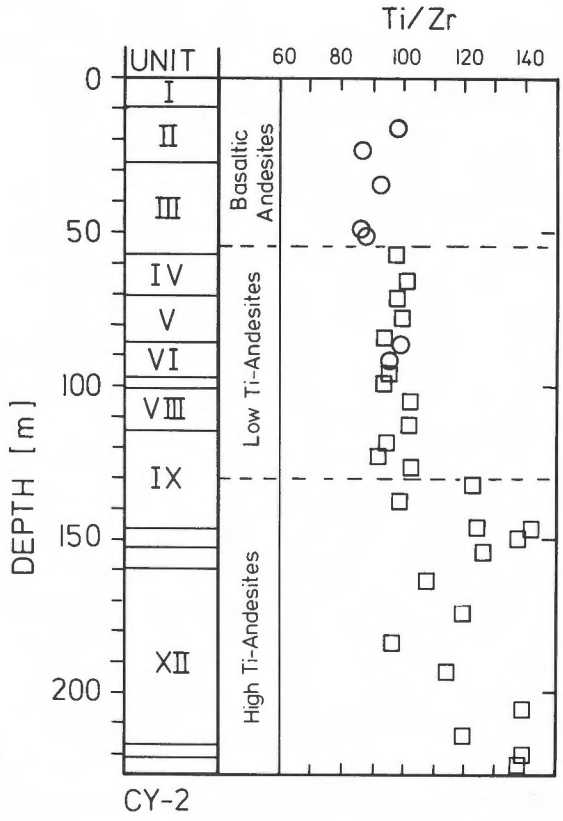

Figure 22: Variation of the Ti/Zr-ratio and basaltic andesites, low-Ti andesites, and high-Ti andesites with depth in hole CY-2. For explanation of symbols see Figure 16.

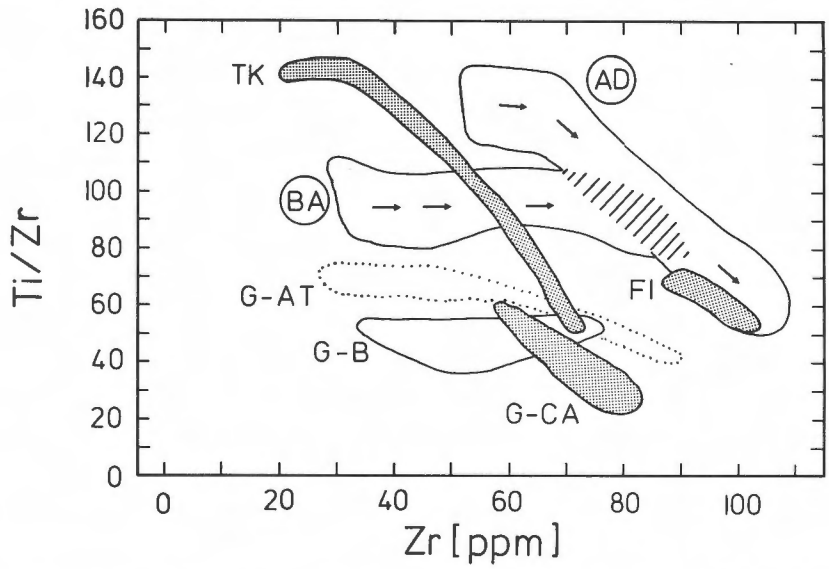

Figure 23: Zr variation diagram for the Ti/Zr-ratio, discriminating the basaltic andesite-low-Ti andesite (BA) and the high-Ti andesite-dacite (AD) series of hole CY-2 and CY-2a. The cross hatched area indicates the minimum overlap range, arrows show the differentiation trends within the series. Highly altered rocks from the main mineralization zone in CY-2a were not considered in this diagram. G-AT and G-B fields are from Guam arc tholeiitic and boninitic rocks (Reagan and Meijer, 1984). Stippled areas mark calc-alkaline trends from Guam (G-CA; Reagan and Meijer, 1984), Futuna Island (FI; Marcelot et al., 1983), and the Tonga-Kermadec-Taupo arc (TK; Cole, 1982).

ACKNOWLEDGEMENTS

Drilling costs were supported financially by VW foundation grant No. 38488. U. Bednarz was supported by European Community grant No. MSM 018 D, and G. Sunkel by the Deutsche Forschungsgemeinschaft grant No. Schm 250/29. We would like to thank M. Rautenschlein for providing unpublished chemical analyses of volcanic glasses. Figures were drawn by H. Bauszus and photographically reproduced by A. Fischer, chemical analyses were performed by H. Niephaus, and thin sections were prepared by G. Olesch. The logistic assistance by the Cyprus Geological Survey Department is gratefully acknowledged. Comments by C. Xenophontos, P. Robinson and two anonymous reviewers improved the manuscript.

REFERENCES

Allen, C.R.
1975: The petrology of a portion of the Troodos plutonic complex, Cyprus; unpublished Ph.D. thesis, Cambridge, p. 1-161.

Bear, L.M.
1960: The geology and mineral resources of the Akaki-Lythrodondha area; Cyprus Geological Survey Department, Ministry of Agriculture and Natural Resources, Memoir no. 3, p. 1-122.

Bideau, B., Prevot, M. and Lecaille, A.
1984: Segregation vesicles of ocean floor basalts. 2. Their use as paleovertical indicators; Journal of Geophysical Research, v. 89, no. B4, p. 7915-7930.

Cole, J.W.
1982: Regional distribution and character of active andesite volcanism. Tonga-Kermadec-New Zealand; *in* Andesites and Related Rocks, ed. R.S. Thorpe; John Wiley and Sons, New York-Brisbane-Toronto-Singapore, p. 25-95.

Ewart, A.
1982: Classification, petrology, and mineralogy of orogenic volcanic rocks. The mineralogy and petrology of Tertiary-recent volcanic rocks: with special reference to the andesite-basaltic compositional range; *in* Andesites and Related Rocks, ed. R.S. Thorpe; John Wiley and Sons, New York-Brisbane-Toronto-Singapore, p. 25-95.

Fisher, R.V. and Schmincke, H.-U.
1984: Pyroclastic Rocks; Springer-Verlag, Berlin-Heidelberg-New York Tokyo, p. 1-472.

Garcia, M.O., Liu, N.W.K. and Muenow, D.W.
1979: Volatiles in submarine volcanic rocks from the Mariana Island arc and trough; Geochimica et Cosmochimica Acta, v. 43, p. 305-312.

Gill, J.B.
1981: Orogenic andesites and plate tectonics. Minerals and Rocks 16; Springer-Verlag, Berlin-Heidelberg-New York, p. 1-390.

ICRDG
1984: Are Troodos deposits an East Pacific analog?; Geotimes, v. 29, no. 5, p. 12-14.

Irvine, T.N. and Baragar, W.R.
1971: A guide to the chemical classification of the common volcanic rocks; Canadian Journal of Earth Sciences, v. 8, p. 523-548.

MacPherson, G.J.
1984: A model for predicting the volumes of vesicles in submarine basalts; Journal of Geology, v. 92, p. 73-82.

Marcelot, G., Dupuy, C., Girod, M. and Maury, R.C.
1983: Petrology of Futuna island lavas (New Hebrides): an example of calc-alkaline magmatism associated with the initial stages of back-arc spreading; Chemical Geology, v. 38, p. 23-37.

Miyashiro, A.
1973: The Troodos ophiolite was probably formed in an island arc; Earth and Planetary Science Letters, v. 19, no. 2, p. 218-224.

Moore, J.G. and Schilling, J.G.
1973: Vesicles, water, and sulfur in Reykjanes Ridge basalts; Contributions to Mineralogy and Petrology, v. 41, p. 105-118.

Moores, E.M., Robinson, P.T., Malpas, J. and Xenophontos, C.
1984: Model for the origin of the Troodos massif, Cyprus, and other mideast ophiolites; Geology, v. 12, no. 8, p. 500-503.

Muenow, D.W., Liu, N.W.K., Garcia, M.O. and Saunders, A.D.
1980: Volatiles in submarine volcanic rocks from the spreading axis of the East Scotia Sea back-arc basin; Earth and Planetary Science Letters, v. 47, p. 272-278.

Pearce, J.A.
1975: Basalt geochemistry used to investigate past tectonic environments on Cyprus; Tectonophysics, v. 25, no. 1-2, p. 41-67.

Rautenschlein, M., Jenner, G.A., Kerrich, R., Hertogen, J., Hofmann, A.W., Schmincke, H.-U. and White, W.M.

1985: Isotopic and trace element composition of volcanic glass from the Akaki Canyon, Cyprus: implications for the origin of the Troodos ophiolite; Earth and Planetary Science Letters, v. 75, no. 4, p. 369-383.

Reagan, M.K. and Meijer, A.

1984: Geology and geochemistry of early arc-volcanic rocks from Guam; Geological Society of America, Bulletin no. 95, p. 701-713.

Robinson, P.T. and Gibson, I.L.

1983a: Cyprus Crustal Study Project. Hole CY-2 Lithologic Unit Summaries.

1983b: Cyprus Crustal Study Project Hole CY-2a Lithologic Unit Summaries.

Robinson, P.T., Melson, W.G., O'Hearn, T. and Schmincke, H.-U.

1983: Volcanic glass compositions of the Troodos ophiolite, Cyprus; Geology, v. 11, no. 7, p. 400-404.

Schmincke, H.-U., Rautenschlein, M., Robinson, P.T. and Mehegan, J.M.

1983: Troodos extrusive series of Cyprus: a comparison with oceanic crust; Geology, v. 11, no. 7, p. 405-409.

Smith, R.E.

1967: Segregation vesicles in basaltic lava; American Journal of Science, v. 265, p. 696-713.

Sunkel, G., Bednarz, U. and Schmincke, H.-U.

1987: The basaltic andesite-andesite and the andesite-dacite series from ICRDG drill holes CY-2 and CY-2a. II. Alteration; *in* Cyprus Crustal Study Project Initial Report Hole CY2-2a, ed. P.T. Robinson, I.L. Gibson and A. Panayiotou; Geological Survey of Canada, Paper 85-29.

The Basaltic Andesite-Andesite and the Andesite-Dacite Series from the ICRDG Drill Holes CY-2 and CY-2a. II. Alteration

G. SUNKEL, U. BEDNARZ AND H.-U. SCHMINCKE

Institut für Mineralogie, Ruhr-Universität Bochum, Postfach 102148, D-4630 Bochum, Federal Republic of Germany

Sunkel, G., Bednarz, U. and Schmincke, H.-U., The basaltic andesite-andesite and the andesite-dacite series from the ICRDG Drill Holes CY-2 and CY-2a. II. Alteration; in *Cyprus Crustal Study Project: Initial Report, Holes CY-2 and 2a, ed. P.T. Robinson, I.L. Gibson and A. Panayiotou; Geological Survey of Canada, Paper 85-29, p. 205-219, 1987.*

Abstract

Four alteration zones in the Troodos Ophiolite Extrusive Series (Cyprus) were distinguished in drill holes CY-2 and CY-2a penetrating parts of the Agrokipia Fe - Cu - Zn ore bodies: 1) Fresh glass zones restricted to intervals within the upper 150 m in CY-2a and the lower 100 m of CY-2, are characterized by fresh glass relics accompanied by smectite + celadonite + zeolites. 2) Low-temperature alteration zones in CY-2a (top to about 150 m), and in CY-2 (below 100 m) are characterized by: smectite + celadonite + zeolites +/- quartz +/- calcite. The rocks are enriched in K_2O, Rb, MgO, CO_2, and depleted in CaO. 3) A high-temperature alteration zone occurs in CY-2a below 300 m with the secondary mineral assemblage chlorite + albite + quartz + epidote + sulphide + sphene +/- calcite. These rocks are strongly enriched in Na_2O, MgO, MnO and strongly depleted in CaO, Sr, K_2O, and Rb. 4) Mineralized zones from about 150 to 300 m in CY-2a and from 0 to about 100 m in CY-2 contain chlorite + quartz + illite + sulphide as dominant secondary minerals. K_2O and chalcophile elements FeO, Cu, Zn, and S are strongly enriched, CaO, Na_2O, and Sr are depleted. Secondary mineral assemblages indicate temperatures from about 70° to about 125°C for the low-temperature zones, and minimal temperatures of about 230°C for the high-temperature and the mineralization zones. The upper part of CY-2a was most likely overprinted by 'cold' sea water weathering following low-temperature hydrothermal alteration.

Résumé

Les trous de forage CY-2 et CY-2a traversant les gîtes de Fe-Cu-Zn d'Agrokipia ont révélé que la série extrusive de l'ophiolite de Troodos (Chypre) est formée de quatre zones altération: 1) les zones de verre non altéré, apparaissant uniquement dans les 150 premiers mètres du trou de forage CY-2a et dans les 100 derniers mètres du trou de forage CY-2, sont caratérisées par des reliques de verre sain accompagnées de smectite + céladonite + zéolites. 2) Les zones d'altération de basse température dans CY-2a (du toit à 150 m), et dans CY-2 (à plus de 100 m) sont caratérisées par: smectite + céladonite + zéolites +/- quartz +/- calcite. Les roches sont enrichies en K_2O, Rb, MgO, CO_2, et appauvries en CaO. 3) Une zone d'altération de haute température apparaît dans CY-2a à 300 m et plus avec l'assemblage de minéraux secondaires chlorite + albite + quartz + épidote + sulfures + sphène +/- calcite. Ces roches sont fortement enrichies en N_2O, MgO, MnO et fortement appauvries en CaO, Sr, K_2O, et Rb. 4) Les zones minéralisées comprises entre 150 et approximativement 300 m dans CY-2a, et entre 0 et environ 100 m dans CY-2, renferment comme minéraux secondaires dominants chlorite + quartz + illite + sulfures. Elles sont considérablement enrichies en K_2O et en éléments chalcophiles FeO, Cu, Zn, et S, et appauvries en CaO, Na_2O, et Sr. Les assemblages de minéraux secondaires indiquent des températures entre 70° et environ 125°C pour les zones de basse température, et des températures supérieures à 230°C pour les zones à haute température et minéralisées. Il semble évident que postérieurement à l'altération hydrothermale de basse température la partie supérieure de CY-2a fut surimpressionnée par une altération due à de l'eau de mer froide.

INTRODUCTION

The main purpose of drilling two holes into the upper part of the extrusive series of the Troodos ophiolite at Agrokipia (CY-2: 226 m, CY-2a: 687 m) was to study hydrothermal alteration zones in which stockwork and disseminated sulphide mineralization had developed. We have discussed the primary lithology and chemical composition of the rocks drilled in a companion paper (Bednarz et al. 1987). In the present report we concentrate on the textural, mineralogical and chemical alteration features. We distinguish several types of alteration, some restricted to a specific level, others having been superimposed over each other.

An assessment of mineralogical and chemical changes is a prerequisite for defining the pre-alteration, 'primary' composition of the rocks and some of our conclusions in Bednarz et al. (1987) depend on our evaluation of secondary changes discussed below. Interpretation of the formation of the ore-forming fluids likewise must be based on a reconstruction of the pre-alteration elemental concentrations and mineralogical composition. This paper is largely descriptive. A more detailed discussion will be published elsewhere.

METHODS

Forty thin sections of CY-2 and 62 thin sections of CY-2a were optically examined. Coarse-grained assemblages were identified by X-ray powder diffraction. Methods for analyzing major and trace elements in 33 bulk rock samples of CY-2, 71 bulk rock samples of CY-2a, 9 handpicked glass-, and two clay mineral samples from glassy massive flows of unit VI of CY-2a are described by Bednarz et al. (1987).

ALTERATION ZONES

Based on concentrations and ratios of immobile elements as well as on fresh glass compositions, we have distinguished two compositional groups (1) basaltic-andesitic suite (BA), (2) andesitic-dacitic suite (AD) (Bednarz et al., 1987). These groups are in part petrographically distinct (olivine-bearing basaltic lavas and olivine-free andesites) except that andesites of both groups cannot be distinguished petrographically.

We define four types of alteration in the holes:

Fresh Glass Zones (FG)
Weakly altered lavas are characterized by the presence of volcanic glass in the form of massive flows or chilled margins of pillows. The concentrations of mobile elements (e.g. K, Rb) are close to the pre-alteration composition.

Low-Temperature Alteration (LT)
Glass is dominantly altered to smectite-group mineral phases. Mobile elements such as K and Rb are distinctly enriched.

Weakly Mineralized, High-Temperature Alteration Zone (HT)
Primary minerals are predominantly replaced by secondary minerals. Rocks show a marked depletion of Ca and Rb.

Moderately to Strongly Mineralized Hydrothermal Alteration Zone (M)
Rocks are geochemically characterized by an enrichment in chalcophile elements occuring as Fe-, Cu-, and Zn-sulfide phases. Primary igneous textures are mostly destroyed.

PETROGRAPHIC AND CHEMICAL CHARACTERISTICS OF ALTERATION ZONES

Fresh Glass Zones (FG)

The least altered rocks are thick sequences (up to 35 m) of glassy flows that occur just below the mineralization zone in CY-2 and in CY-2a just above this zone (Figures 1 and 2). Fresh light brown glass is preserved in many vitric samples of CY-2 between 145 and 160 m and around 220 m and in CY-2a between 113 and about 150 m (Bednarz et al., 1987 - Figures 11 and 12).

Igneous textures and primary mineral composition are well preserved (Bednarz et al., 1987 - Figures 11 and 12).

Glass is altered to brownish smectites (>90%) and to zeolites (<10%) principally (a) around the edges, (b) along hairline cracks, and (c) around the periphery of vesicles (Figure 3). Many vitric rocks have alteration textures that penetrate into glass fragments from the edges or from vesicle walls. We interpret these as tubular channels along which the glass was dissolved. Large glass fragments are thus subdivided into small isolated clasts of fresh glass, showing irregular round outlines and being separated by bands of alteration minerals. This has resulted in a pseudo-brecciated fabric. We emphasize, however, that this fabric has been superimposed on a rock that already had been brecciated.

Vesicles are filled with smectites (about 90 %) or zeolites (<10%), rarely by celadonite (Figures 4 and 5). Many vesicles show a concentric but homogeneous filling of brown smectite. Complex fillings of alternating green and brown smectites, zeolites and celadonite are rare. At least four types of zeolites occur.

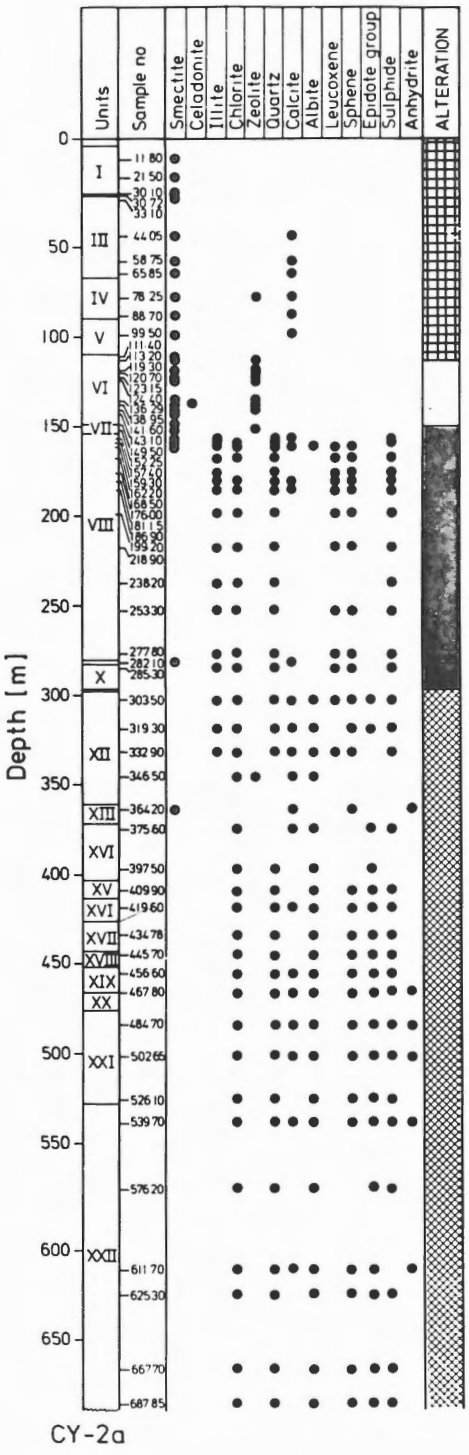

Figure 1: Downhole distribution of secondary minerals in hole CY-2a. Legend of alteration: white area - fresh glass zone, checkered - low-temperature zone, diamonds - high-temperature zone, shadowed - mineralization zone.

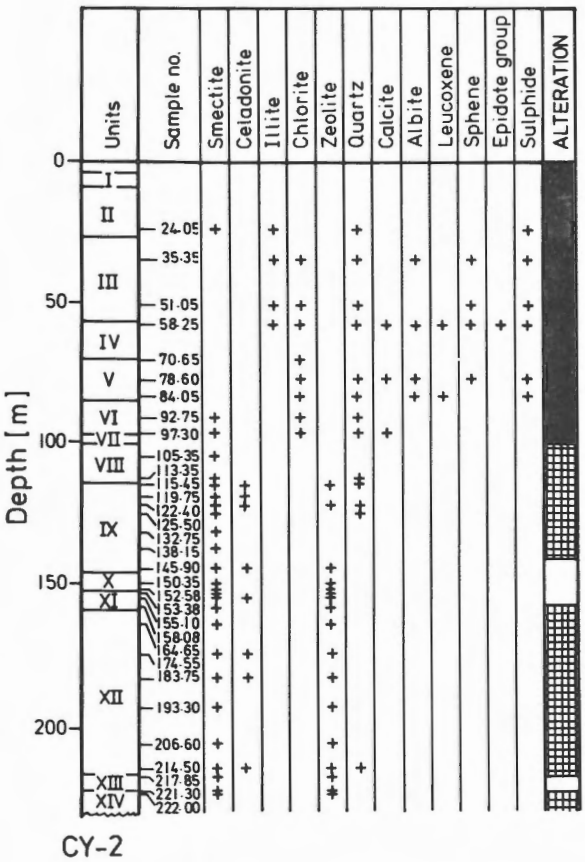

Figure 2: Downhole distribution of secondary minerals in CY-2. For explanation see Figure 1.

Differences between elemental concentrations of crystallized rocks and handpicked andesitic glass of unit VI (CY-2a) (Bednarz et al., 1987) are as follows: The whole rocks are generally enriched in Al_2O_3, MgO, Fe_2O_3, Rb, V, and slightly enriched in TiO_2, K_2O, P_2O_5, CO_2, Zn, Sr, whereas SiO_2, FeO, H_2O are depleted compared to glass samples. Concentrations of CaO, MnO, Na_2O, Cr, Co, Y, Zr, Cu, Ba are close to those of fresh glass (Figures 6-11, Table 1; Bednarz et al., 1987 - Figure 21).

Two chemical analyses of separated smectites are similar to the composition of adjacent glass (Figure 12, Table 2) indicating that smectites from low temperature alteration strongly depend on the primary chemical composition. However, compared to the glass of the same sample, the smectites are enriched in K_2O (factor of 3-4), CO_2 (factor of 1.6 to 3.5), MgO (factor of 2.3), H_2O (factor of 1.5 to 2), Rb (factor of 1.5 to 2), and MnO (factor of 1.5). Depleted oxides and elements are CaO (factor of 0.25), P_2O_5 (factor of 0.4 to 0.56), Y (factor of 0.45 to 0.5), Na_2O (factor of 0.6), Sr (factor of 0.6), Co (factor of 0.45

to 0.7). Concentrations of SiO_2, FeO° (total Fe as FeO), Al_2O_3 , TiO_2, Zr, and V are almost identical in the smectites and the glass. Elements such as Ba, Cr, Ni, Cu, and Zn are either enriched or depleted.

Low-Temperature Alteration Zones (LT)

Weakly altered rocks occur in the upper part of CY-2a from the top down to 110 m, and in CY-2 below 100 m down to the bottom of the hole including pillows, sheet flows, glassy sheet flows and sills (Figures 1 and 2; Bednarz et al., 1987 - Figures 2 and 3).

Igneous textures of crystalline rocks are well preserved, whereas vitric textures are strongly overprinted. Glass is completely replaced by alteration minerals.

Phenocrysts are fresh or occur as relics. Olivine is always extensively altered to smectite followed by calcite, except in sample CY-2a 30.1 m, where fresh olivine relics were found. Local hematite and iron hydroxide, especially in phenocrysts or microphenocrysts, indicate oxidation. Plagioclase is predominantly fresh and only partly replaced by smectites or zeolites. Most pyroxenes are slightly altered to smectite. Alteration has attacked the interior of pyroxene grains along fractures and glass inclusions or along the edges. Some phenocrysts have a thin rim of smectite. Alteration of groundmass crystals is generally more intense than that of phenocrysts.

Interstitial glass has been replaced by mixtures of smectites, celadonite, less commonly by zeolites and very rarely by calcite.

Vesicles <1 mm are commonly filled by secondary minerals. Most vesicle fillings show a consistent concentric order of filling. Smectites and celadonite are followed inward by zeolites and calcite. When present, quartz or chalcedony are usually the latest fillings. Vesicles >1 mm are predominantly open and are only rimmed by greenish or brownish smectite or celadonite. Radially shaped calcite crystals in vesicles probably indicates a replacement of early zeolites.

Chemically, zones (LT) are distinguished from the fresh glass zones by a stronger enrichment in MgO, K_2O, and Rb. CO_2 is up to about 3 wt.% (Figures 6-11, Table 1).

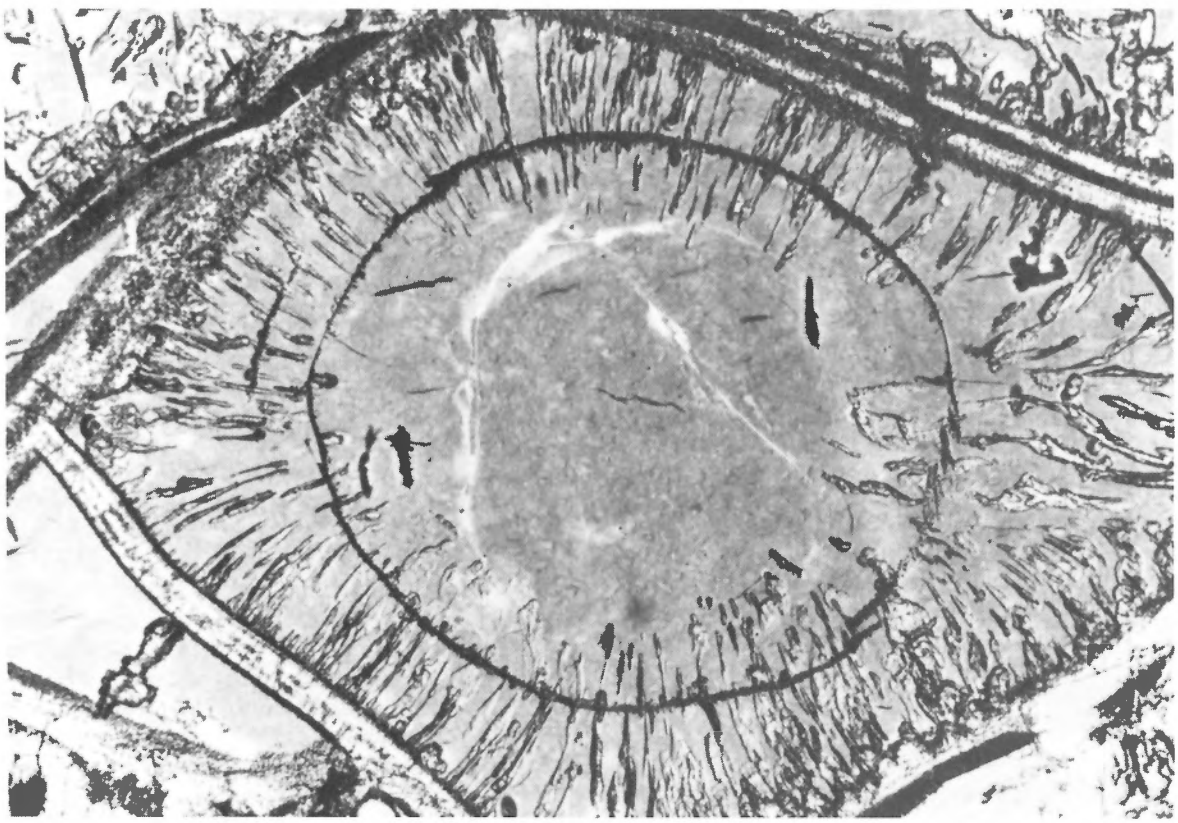

Figure 3: Radial tubular channels, interpreted as dissolution tubes, penetrate fresh glass starting from cracks and edges. Long side of the photomicrograph: 3 mm.

Weakly Mineralized, High-Temperature Alteration Zone (HT)

Hydrothermally altered rocks are characterized by complete replacement of primary minerals. They occur only in CY-2a below 300 m and affect pillow and sheet flow lavas as well as dykes (Figure 1, 2; Bednarz et al., 1987 - Figure 3).

Mineralization is restricted to veins and vesicle filling. The upper boundary is chosen somewhat arbitrarily at unit XI, which was interpreted to be a 35 cm thick fault breccia (Robinson and Gibson, 1983).

Igneous textures are largely preserved, except in strongly mineralized veins or patches.

Plagioclase phenocrysts are chiefly altered to albite. Hollow feldspars probably indicate former anorthite-rich cores. Patchy replacement of albitized feldspar by granular epidote group minerals, calcite, and anhydrite is also common.

Groundmass plagioclase is replaced by albite, calcite and epidote, whereas it is cloudy and untwinned in some slightly altered rocks. Groundmass pyroxene is altered to chlorite or replaced by calcite. Opaques have lost their euhedral shape and are partly to completely replaced by leucoxene and sphene. The degree of replacement depends on the proximity of sulphide-bearing veins where samples poor in sulphide minerals contain opaque minerals. Euhedral sulphide minerals occur in the groundmass.

Former glass is altered to chlorite, sphene, epidote group minerals, calcite, anhydrite and quartz.

Vesicles are predominantly filled by recrystallized quartz, chlorite, sulphide minerals, calcite and rare zeolite (Figure 4). The abundance of epidote group minerals and apatite increases downhole. Veins, filled with secondary minerals, are abundant.

Elemental concentrations have considerably changed compared to the inferred primary chemical composition. A general depletion in Sr (by a factor of >0.4), Rb (by a factor of >0.2), CaO (by a factor of >0.2), and K_2O is observed. MnO is enriched by a factor up to 3-4, Na_2O up to 2 times, and MgO up to 3 times (Figure 6, Table 1). All factors are related to the mean andesitic glass composition of unit VI (CY-2a) (Bednarz et al., 1987), neglecting primary compositional variations. However, these factors are considerably smaller in the andesitic to dacitic rocks of the lower part of CY-2a compared to those due to hydrothermal alteration as the enrichment and depletion factors for the relativly stable elements TiO_2, Zr, and Y vary only between 0.6 and 1.4. They are believed to be largely due to primary compositional variations.

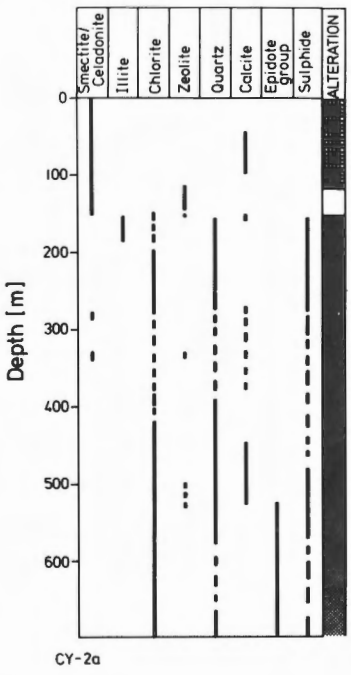

Figure 4: Downhole distribution of secondary minerals in vesicles and veins in CY-2a. For explanation of symbols see Figure 1.

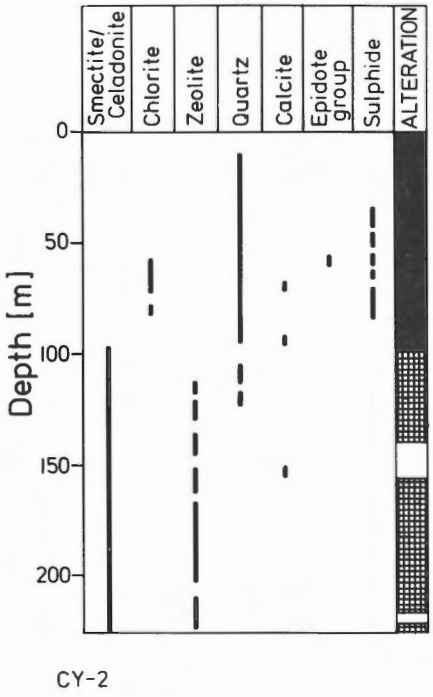

Figure 5: Downhole distribution of secondary minerals in vesicles and veins in CY-2. For explanation of symbols see Figure 1.

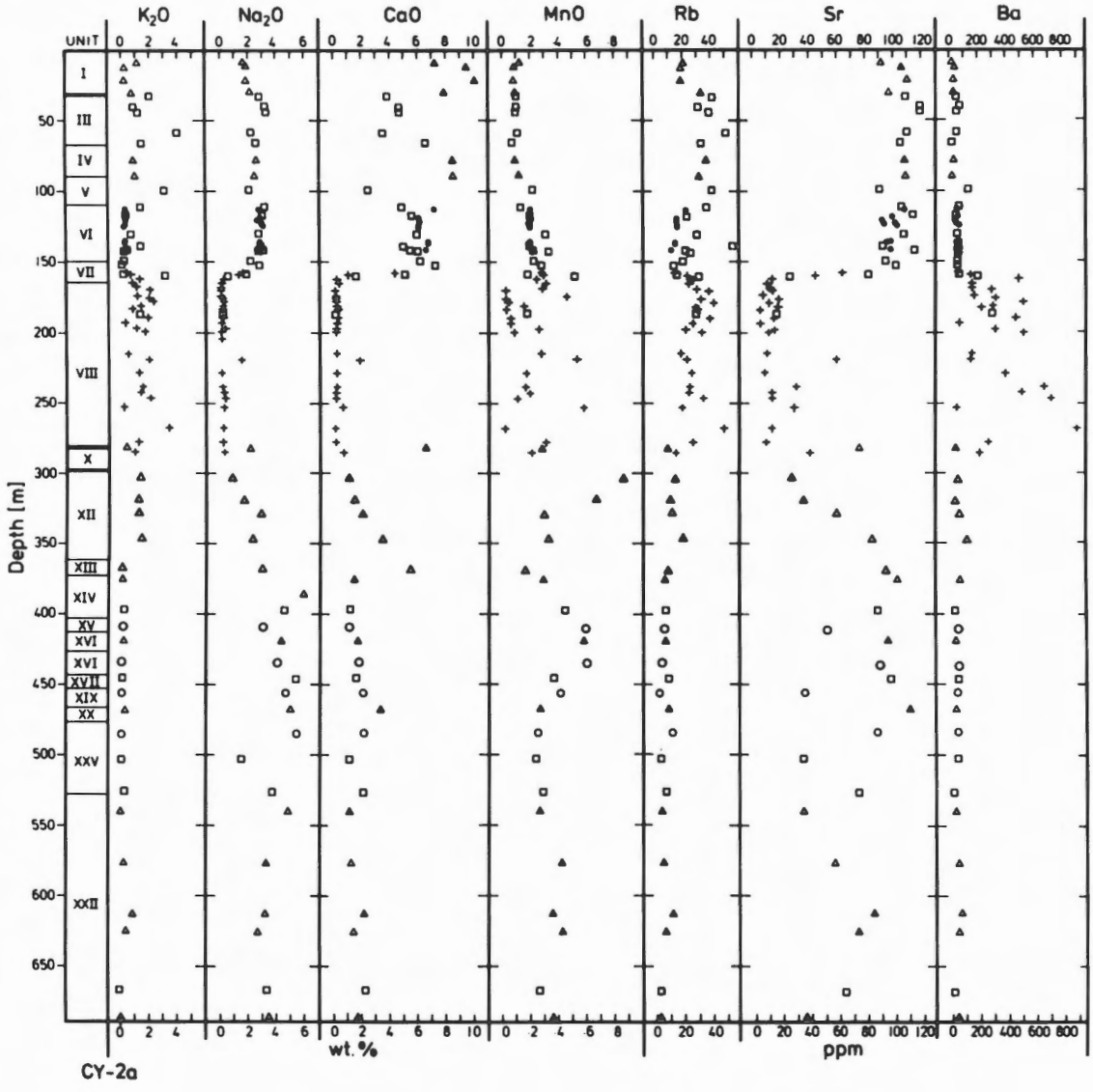

Figure 6: Variations of mobile elements K_2O, Na_2O, CaO, MnO, Rb, Sr, Ba with depth in hole CY-2a. Symbols: squares - sheet flows, circles - pillows, triangles - dykes/sills, crosses - argillaceous rocks of the main sulphide mineralization zone of CY-2a, dots - glass separates.

Mineralization in this zone is reflected by an increase of FeO° to a maximum of 16 wt.% and sulphur concentrations up to 6 wt.%. Zn concentrations - generally 150-300 ppm - reach high values of 400 to 1000 ppm in a restricted interval between 370 and 450 m. Increased Cu concentrations 250 to 500 ppm above the average value of about 100 ppm were found only in three dykes below 550 m (Figure 8).

Moderately to Strongly Mineralized Zones (M)

Moderate mineralization occurs in the upper 100 m of CY-2 where it has affected pillowed basaltic andesites and andesitic sheet flows and pillows. Moderate to strong mineralization occurs in CY-2a between 154 and 300 m and is restricted to andesitic glassy sheet flows (Figures 1 and 2; Bednarz et al., 1987 - Figures 2 and 3). Sulphide minerals occur mainly as disseminated grains and in eleven massive ore units (0.17 to 3.56 m thick).

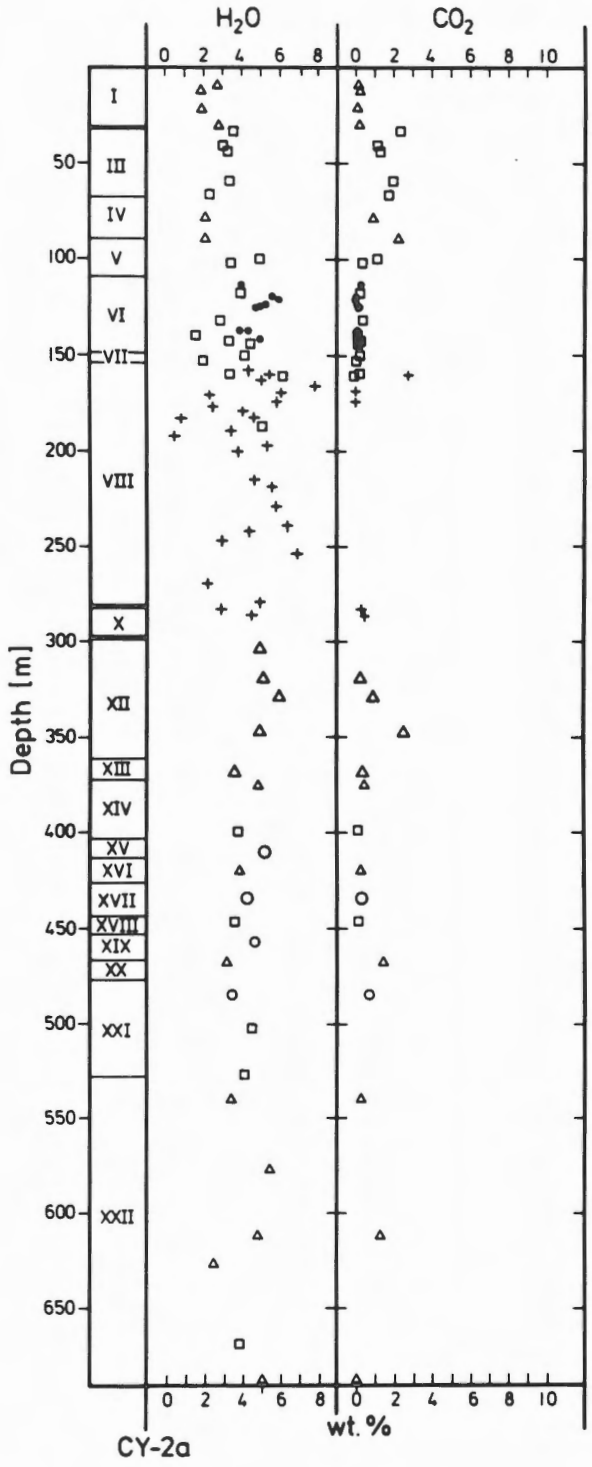

Figure 7: Variations of volatile elements H_2O, and CO_2 with depth in hole CY-2a. For explanation of symbols see Figure 6.

Primary mineralogy and textures within the strongly mineralized zone are destroyed by recrystallization. Slightly mineralized samples may preserve relics of the primary texture, recognized by replaced plagioclase crystals.

The main mineral assemblage is quartz, illite, sulphide minerals and chlorite (Figures 1 and 2). Accessory sphene appears to have replaced opaque minerals. Plagioclase is replaced by illite or, in slightly mineralized parts, by albite.

Vesicles are mostly filled by recrystallized quartz and pyrite, less commonly chlorite and illite (Figures 4 and 5). Small pyrite crystals line vesicle walls, whereas larger crystals occur in vesicle centres. Former calcite amygdales are replaced by chlorite and quartz, preserving the rhombic cleavage of the calcite.

The main mineralization zones are extremely depleted in Na_2O, CaO, and Sr - all by at least one order of magnitude. The lavas are strongly enriched in K_2O (maximum factor of >10), generally moderately enriched in MgO (maximum factor of 4), Rb (maximum factor of 3) and Ba (Figures 6 and 9, Table 1).

Maximum concentrations of chalcophile elements are about 19 wt.% FeO° (>40 wt.%) in the massive parts), 1,600 ppm Cu (in CY-2!), 20,000 ppm Zn, and about 20 wt.% S (45 wt.% in the massive ores) (Figures 8 and 11, Table 1).

TABLE 1. General Elemental Changes in the Hydrothermal Alteration Zones of Holes CY-2 and CY-2a.

	FG	LT	HT	M
SiO_2	(-)	(-)	(=)	(-)
Al_2O_3	(+)	(+)	(=)	(=)
FeO°	(=)	(+)	(+)	(++)
MnO	(=)	(=)	(+)	(+)
MgO	(+)	(+)	(+)	(+)
CaO	(-)	(-)	(- -)	(- -)
Na_2O	(=)	(+)	(+)	(- -)
K_2O	(+)	(++)	(- -)	(++)
Cu	(=)	(=)	(+)	(++)
Zn	(=)	(=)	(+)	(++)
Rb	(+)	(++)	(- -)	(+)
Sr	(+)	(+)	(- -)	(- -)
Ba	(=)	(=)	(=)	(+)

FG: Fresh glass zone, LT: Low-temperature alteration zone, HT: High-temperature alteration zone, M: Mineralization zone, FeO°: Total Fe as FeO, (+): enrichment, (++): strong enrichment, (-): depletion, (- -): strong depletion (=): changes absent or hidden in data scatter

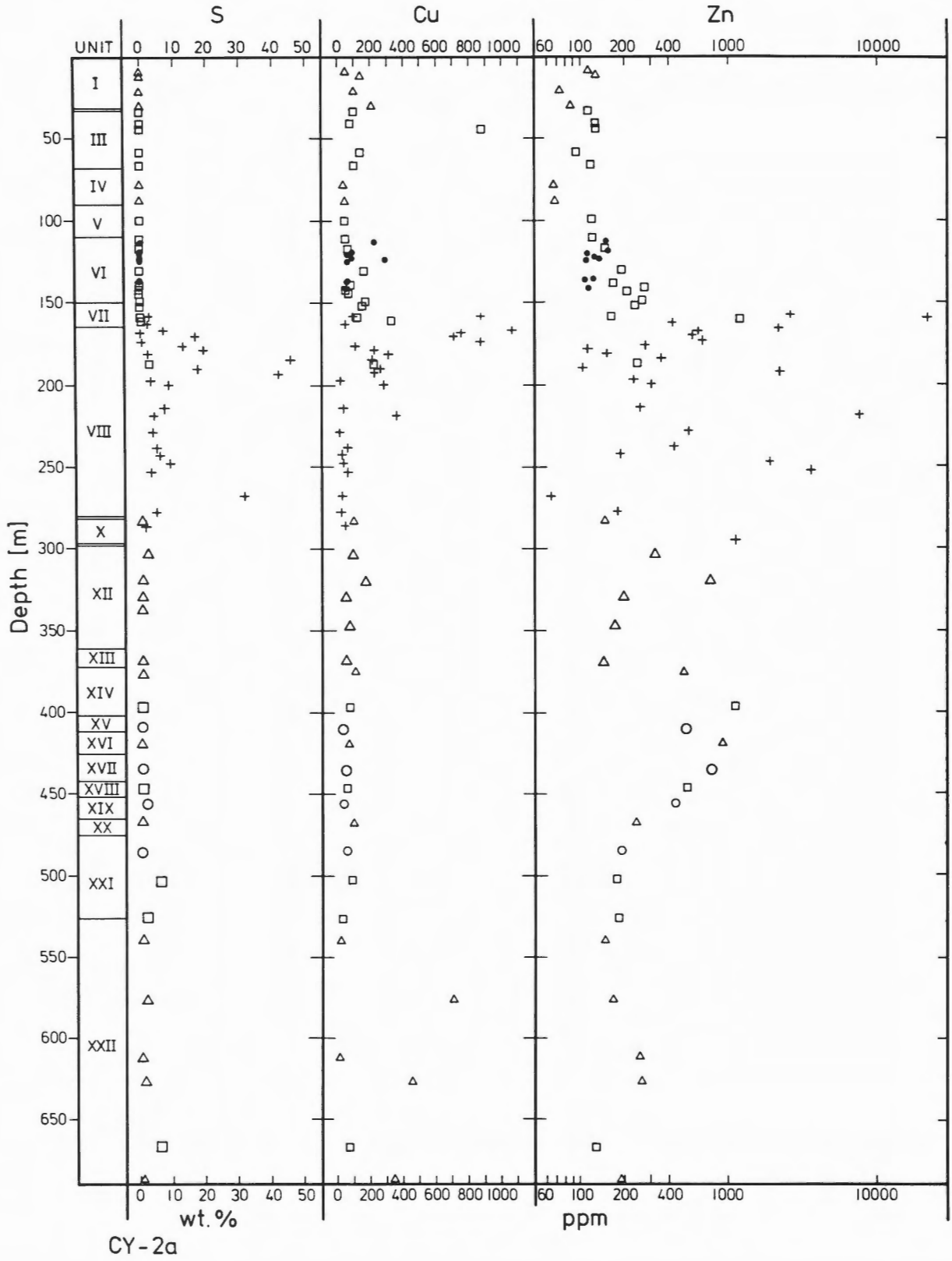

Figure 8: Variations of chalcophile elements Cu, Zn, S with depth in hole CY-2a. For explanations see Figure 6.

DISTRIBUTION OF SECONDARY MINERALS IN THE ALTERATION ZONES

Brownish and less common greenish smectites are the dominant secondary minerals in zones FG and LT, but they also occur in the marginal parts of zone M and in post-mineralization dykes within zone HT (Figures 1 and 2). Celadonite resembles smectite in its distribution but is less abundant, especially in CY-2a (Figures 1 and 2). Colourless illite occurs in varying amounts only in zone M. It is sparse in rocks of CY-2, but more common in CY-2a (Figures 1 and 2). Colourless to greenish chlorites succeed smectite as the dominant sheet-silicate in zone HT and M (Figures 1 and 2). Four zeolites are optically distinguished: heulandite, laumontite, stilbite (?) and a fibrous zeolite, probably mordenite. Most zeolites are restricted to zone FG and LT. Zeolites also occur as well in a post-mineralization dyke of zone HT (Figures 1 and 2). Secondary quartz is abundant in zone HT and M and occurs in small amounts in samples of CY-2 right below the mineralization zone (Figures 1 and 2). Calcite may be present in all zones, but is extremly rare in zone FG and M, and locally abundant in zones LT and HT. Calcite is rare in CY-2, but common in vesicles in Hole CY-2a between 44 and 100 m and in many samples below 300 m chiefly replacing plagioclase (Figures 1, 2 and 4). Albite, characteristic of zone HT, occurs as well in the marginal parts of zone M (Figures 1 and 2), but is missing in post mineralization dykes within zone HT. Microcrystalline granules of pale brown pleochroic sphene and leucoxene are common in zones HT and M (Figures 1 and 2). There is a gradual transition between leucoxene and fine-grained dusty sphene. Minerals of the epidote group are distinctive for zone HT, first appearing at 303 m (Figure 1). A single occurrence in CY-2 (58.25 m) was detected within a less mineralized part of the mineralization zone (Figure 2). Murky granular aggregates up to 50 µm of epidote group minerals grade downhole into well crystallized colourless to yellow minerals up to 400 µm. The abundance of epidote group minerals increases downhole. Sulphide minerals, predominantly pyrite and minor sphalerite and chalcopyrite are, in varying amounts, most typical for zones M and HT (Figures 1 and 2). Anhydrite occurs in small amounts in zone HT, especially below 450 m (Figure 1).

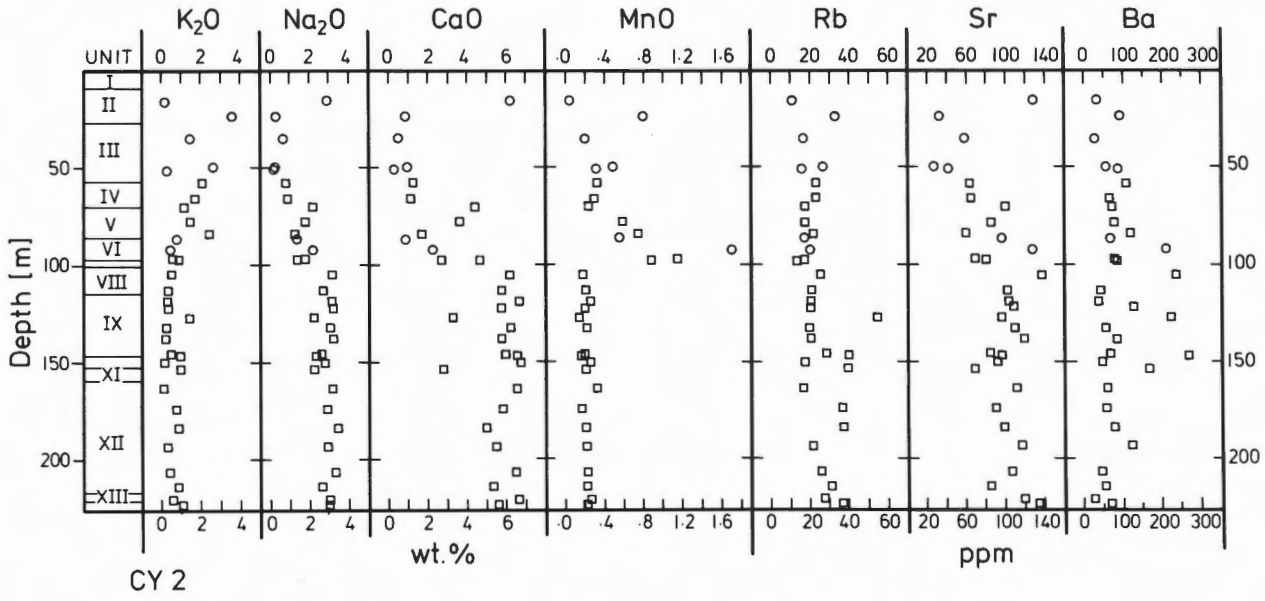

Figure 9: Variations of mobile elements K_2O, Na_2O, CaO, MnO, Rb, Sr, Ba with depth in hole CY-2. For explanation see Figure 6.

TABLE 2. XRF-Analyses of Smectite Separates of Glassy Sheet Flows in CY-2a.

Depth	124.40 m	136.55 m
Oxides as wt. %		
SiO_2	58.10	56.60
TiO_2	1.03	1.08
Al_2O_3	13.96	14.26
Fe_2O_3	9.89	10.07
FeO	0.41	0.56
MnO	0.29	0.28
MgO	5.29	5.64
CaO	1.94	2.03
Na_2O	1.69	1.62
K_2O	0.89	1.11
P_2O_5	0.08	0.05
H_2O+	7.49	8.40
CO_2	0.28	0.36
S	0.01	0.01
Cl	0.01	0.01
Total	101.36	102.08
Trace Elements as ppm		
V	85	133
Cr	22	19
Co	14	12
Ni	9	7
Cu	217	72
Zn	131	169
Rb	22	29
Sr	55	56
Y	26	17
Zr	76	69
Nb	1	2
Ba	60	17
Numbers of ions on the basis of 22 oxygens		
Si	7.68	7.55
Al(IV)	0.32	0.45
Σ	8.00	8.00
Al(VI)	1.86	1.79
Ti	0.10	0.11
Fe_3+	0.98	1.01
Fe_2+	0.05	0.06
Mn	0.03	0.03
Mg	1.04	1.12
Σ	4.06	4.12
Ca	0.27	0.29
Na	0.43	0.42
K	0.15	0.19
Σ	0.85	0.90

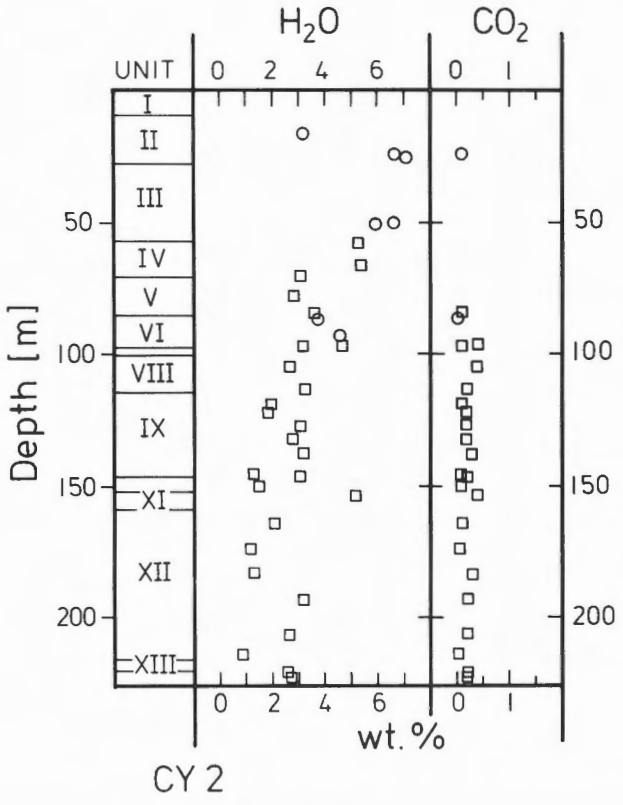

Figure 10: Variations of volatile elements H_2O, CO_2 with depth in hole CY-2. For explanations see Figure 6.

DISCUSSION

Ocean floor basalts are altered by two main processes:

1. Sea-floor weathering caused by soaking of permeable rocks by seawater in a range of temperatures not markedly exceeding the bottom temperature of ocean water. The maximum extent of cold sea water alteration may be a few hundred metres depending mainly on the sea floor morphology and time of exposure of volcanic rocks to seawater (e.g. Donnelly et al., 1979; Alt and Honnorez, 1984).
2. Hydrothermal alteration by convective fluids, which are driven by heat provided from sub sea-floor magma chambers, with a relatively cold descending branch and a hot ascending branch (e.g. Lister, 1972; Spooner and Fyfe, 1973; Mottl, 1983). The convective cells are presumed to extend at least down to the base of the sheeted dyke swarm (Spooner, 1977).

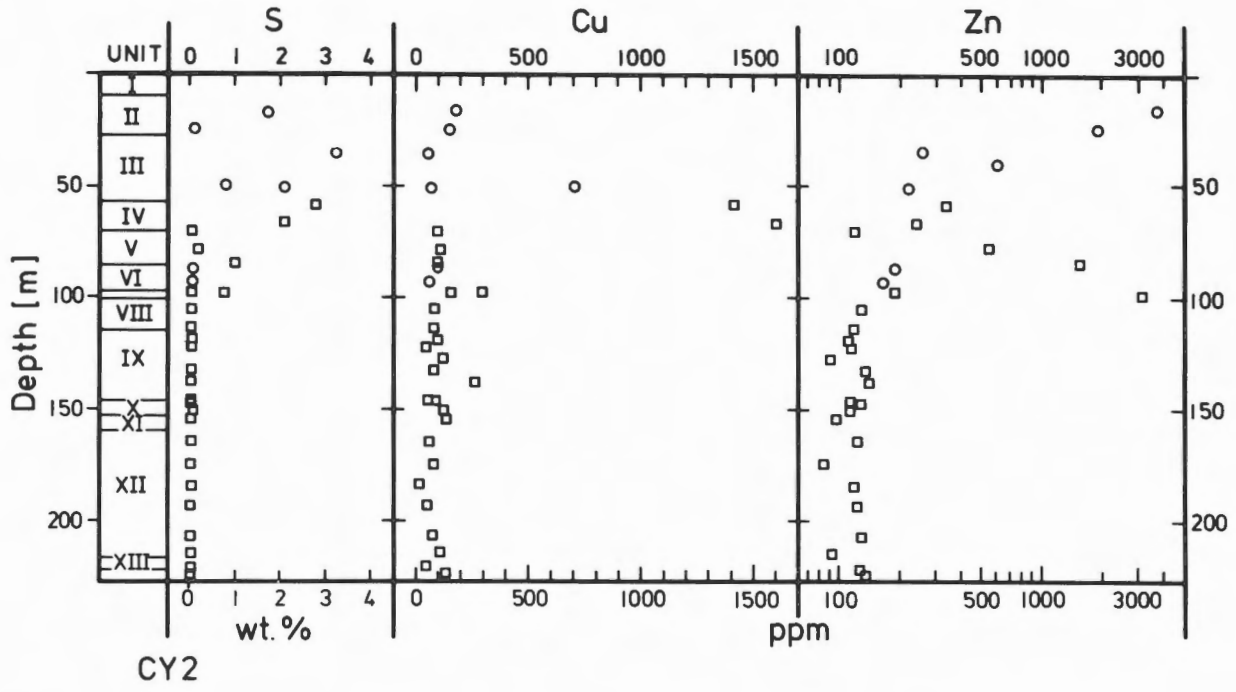

Figure 11: Variations of chalcophile elements Cu, Zn, S with depth in hole CY-2. For explanations see Figure 6.

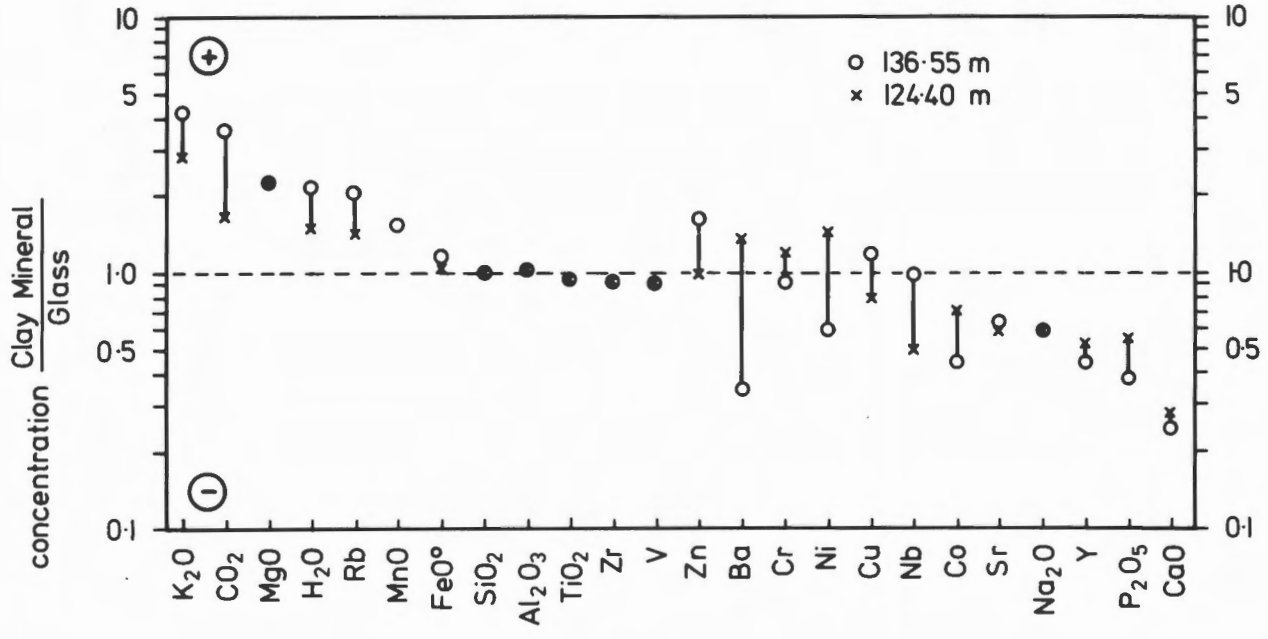

Figure 12: Chemical enrichment and depletion of separated smectites compared to adjacent glass.

In Holes CY-2 and CY-2a we distinguish four zones of hydrothermal alteration: a low-temperature zone (LT), a subtype within the low-temperature alteration zone, characterized by the presence of fresh glass (FG), a high-temperature zone (HT), and a mineralization zone (M).

(1) Temperature Ranges

Low-Temperature Zone

The characteristic secondary mineral assemblage of this zone is smectite + celadonite + zeolites (heulandite, laumontite, stilbite?, and mordenite?). Calcite and quartz are locally present.

Similar secondary mineral assemblages are known from low temperature geothermal areas in Iceland (Kristmannsdottir and Tomasson, 1978) and from the zeolite zone of the Jurassic Del Puerto ophiolite which is interpreted to have formed in a submarine hydrothermal metamorphic field (Evarts and Schiffmann, 1983). In these areas the estimated temperatures range from 50° to 125°C, as very low temperature authigenic zeolites (e.g. phillipsite and clinoptilolite) and higher temperature minerals as pumpellyite are absent (Evarts and Schiffmann, 1983), respectively from 75 to 110°C (Kristmannsdottir and Tomasson, 1978). Thus, we assume for the low temperature zone hydrothermal alteration with temperatures not exceeding 125°C. Temperatures of 70 up to 200°C are, however, indicated by stable isotope ratios smectites from the uppermost 150 m of CY-2a (Rommel and Friedrichsen, 1984).

High-Temperature Zone

In CY-2a, the mineral assemblage epidote + chlorite + albite + quartz + sphene +/- calcite indicating greenschist facies conditions as known from fossil submarine hydrothermal fields (e.g. Evarts and Schiffmann, 1983; Elthon and Stern, 1978; Alt et al., 1985) is developed first below a depth of 300 m extending to the bottom of the hole at 689 m. Epidote first appears at temperatures of 200 to 250°C (Browne, 1978; Ellis, 1979) but is not abundant below a temperature of 260°C (Palmason et al., 1979). Anderson et al. (1982) estimated an alteration temperature of at least 230°C for the parageneses chlorite + sphene + epidote + albite + quartz. The general absence of actinolite suggests, by analogy with geothermal fields, that temperatures probably did not exceed 300°C (Ellis, 1979). Thus we conclude that the temperature in the lower 389 m of hole CY-2a reached at least 230°C, but did not markedly exceed 300°C. Increasing crystallinity and concentration of epidote group minerals may be evidence for an increase in temperature downhole.

Moderate to Strong Mineralization Zone

The common secondary mineral assemblage within the mineralization zone is: chlorite + quartz + illite +/- albite + sulphide minerals and rarely epidote group minerals. Chlorite and illite, beside epidote, are indicators for minimum alteration temperatures of 200 to 230°C (Tomasson and Kristmannsdottir, 1972; Kristmannsdottir, 1976; Henley and Ellis, 1983). We therefore assume these to be minimum temperatures in the mineralization zone. This is supported by sphalerite compositions indicating formation temperatures of <250°C above 270 m depth, and >250°C below 270 m depth (Herzig, 1987).

(2) Alteration of Fresh Glass Zones.

Zones with relic fresh glass are restricted to units of glassy sheet flows, some of which are highly brecciated (Bednarz et al., 1987). These clastic zones were initially highly permeable and porous, but may have become rather impermeable following rapid initial alteration of matrix and fragment rinds to palagonite and smectite. These zones could have formed a physical barrier to large scale water circulation. It has been speculated elsewhere (ICRDG, 1984) that the glassy lavas may have formed a lid on an ascending hydrothermal plume causing, in effect, the development of the sulfide ore body at Agrokipia. We can only comment that individual sheets were probably too thin and the breccia zones too common to have formed an effective hydrological barrier initially. On the other hand, the rapid accumulation of many such flows (in a tectonic graben?) may have had the cumulate effect of being less permeable than a pillow lava pile. This, in addition to sealing resulting from rapid initial alteration may have caused a decrease in permeability although palagonitization in general is a slow diagenetic process (Fisher and Schmincke, 1984) palagonitization at higher temperatures such as in the fumarolic zone of eruptive centers (Jakobsson, 1978) can make a compact rock out of loose tephra within only a few years. Some of the colourful former palagonite bands in some glassy rocks may indeed be caused by hydrothermal solutions ascending from below the glassy lavas.

The thorough cementation of the brecciated glassy lavas prevented further circulation of pore solutions and thus led to the excellent preservation of fresh glass. The cementation is also the reason for the good preservation of these clastic rocks in the core, such material being commonly lost during drilling in the present ocean crust. Close association of abundant fresh glass and mineralization is also evident from field work in the Kambia area.

(3) Downhole and Regional Distribution of Alteration Zones

The formation and regional distribution of alteration zones as discussed in this report depend primarily on factors governed by the physical parameters of sub sea-floor magma chambers (e.g. size, depth, spatial distribution, temperature, age, life-span) as the major driving mechanism of submarine hydrothermal convection. On the other hand, important factors such as the water / rock ratio, diffusion or concentration of hydrothermal fluids are controlled by permeability (itself dependent on lithology and effectiveness of early cementation, etc.), existence of major tectonic pathways, and sea floor topography.

(a) In Hole CY-2, mineralized rocks that probably have been affected by temperatures of at least 200°C overlie rocks altered at temperatures of less than 125°C. A 30-m-thick transitional zone is indicated by a gradual decrease in Sr, Na_2O, CaO, an increase in K_2O towards the stronger mineralized rocks and an enrichment in MnO (Figure 9) compared to both zones. The low-temperature alteration zone occurs down to the bottom of the hole at 226 m.

Mineralization has affected basaltic-andesitic pillow lavas of (BA) magma group (Bednarz et al., 1987) occurring in the upper 100 m. This occurrence of mineralized rocks above a low-temperature alteration zone is most likely due to a mushrooming effect of the upwelling fluids, the drill hole being located close to the downwelling branch of a convection cell.

(b) In CY-2a low-temperature alteration occurs from the top of the hole down to a depth of about 150 m. A sharp boundary to the underlying mineralization zone is evident from an abrupt change in secondary mineral composition (Figure 1), texture and a rapid decrease in Sr, CaO, Na_2O, and a rapid increase in Ba, K_2O (Figure 6). Highly mineralized rocks were recovered in the interval between 150 and 300 m. The boundary with the high-temperature zone was chosen somewhat arbitrarily at a fault breccia (Bednarz et al., 1987) while the chemical composition indicates a gradual transition zone of at least 30 m below the fault breccia. It is marked by increasing Sr, Na_2O, and strong enrichment of MnO compared to underlying and overlying rocks (Figure 6). Rocks altered at high temperature occur below 300 m.

Mineralization is restricted to andesitic glassy sheet flows of the (AD) magma group (Bednarz et al., 1987) but has not affected the overlying basaltic andesites. Low-temperature alteration of the overlying basaltic andesitic rocks are interpreted, however, to be caused by hydrothermal processes as well. Continual and rapid increase of alteration temperatures downhole may be explained by a location near the upwelling branch of convecting hydrothermal fluids.

In CY-2a, at least the mineralizing hydrothermal activity ended during eruption of basaltic-andesitic magma, indicated by a relatively fresh post-mineralization dyke within the mineralization zone and a relatively fresh basaltic-andesitic sill at the top of the hole. Observations from active hydrothermal fields on the ocean floor indicate that black smoker activity is very short-lived (1-50 years) (Turekian and Cochran, 1981). Using general growth rates for sulphide ore bodies in the Troodos ophiolite (Mottl, 1983) the generation of the 6 million tons stockwork mineralization (ICRDG, 1984) of the 'Agrokipia B' ore body could have taken about 700 years. The mineralization zones in CY-2 and CY-2a, which belong to two distinct ore-bodies ('Agrokipia A' and 'Agrokipia B'; Adamides, 1984) are possibly not synchronous. This would support the interpretation of the existence of small, short-lived magma chambers as predicted by Moores and Vine (1971), Malpas and Langdon (1984), Bednarz et al. (1987).

Investigations on the distribution of recent hydrothermal vents at the East Pacific Rise 21°N have shown that they are located in the youngest flows - another argument for the short life-span of the systems - and that they are situated directly above the fissure which fed the flows (Ballard et al., 1981). This is in agreement with the situation of CY-2a as the high frequency of dykes in the lower part is regarded as indicating spatial proximity to a major eruptive centre (Bednarz et al., 1987).

In the Akaki river section (CY-1) which lies about 2 km to the east, the upper 300 m are notably enriched in K_2O (up to 9 wt.%), Rb (up to 70 ppm), H_2O (up to 7 wt.%), Sr (up to 150 ppm), and Fe_2O_3 (13.5 wt.%) interpreted to have resulted from 'cold' sea-floor weathering of a pillow volcano extending above the sea floor and having been exposed to sea water for an extended period of time (Rautenschlein et al., in prep.; Bednarz et al., in prep.). The enrichment of K_2O (up to 3.6 wt.%) and Rb (up to 50 ppm) in the upper part of holes CY-2 and CY-2a is significant and indicates cold sea-water alteration most likely following and overprinting hydrothermal alteration. It is most evident in CY-2a in the interval between 30 and 100 m as also indicated by calcite as vesicle filling and replacement of olivine by Fe-hydroxides. However, it is not as pronounced as in the Akaki river section at a level 150 m below the top of the extrusive rocks, most likely due to a more gentle sea floor volcanic relief at Agrokipia prior to sedimentation. This is supported by correlations of tabular lithologic units between CY-2 and CY-2a (Bednarz et al., 1987).

ACKNOWLEDGEMENTS

Drilling costs were supported financially by VW foundation grant No. I 38 488. U. Bednarz was supported by European Community grant No. MSM 018 D, and G. Sunkel by the Deutsche Forschungsgemeinschaft grant No. Schm 250/29. XRF analyses were done by H. Niephaus. Thin sections were prepared by G. Olesch, the figures were drawn by H. Bauszus and photographically reproduced by A. Fischer. The logistic assistance by the Cyprus Geological Survey Department is gratefully acknowledged. Comments by P. Robinson, C. Xenophontos, A. Morrison and one anonymous reviewers improved the manuscript.

REFERENCES

Adamides, N.G.
1984: Cyprus volcanogenic sulphide deposits in relation to their environment of formation; Unpublished Ph.D. thesis, University of Leicester, p. 1-383.

Alt, J.C. and Honnorez, J.
1984: Alteration of the upper oceanic crust, DSDP site 417: mineralogy and chemistry; Contributions to Mineralogy and Petrology, v. 87, p. 149-169.

Alt, J.C., Laverne, C. and Muehlenbachs, K.
1985: Alteration of the upper oceanic crust: mineralogy and processes in Deep Sea Drilling Project Hole 504B, Leg 83; *in* Initial Reports of the Deep Sea Drilling Project, Volume 83, ed. R.N. Anderson, J. Honnorez, K. Becker et al.; U.S. Government Printing Office, Washington D.C., v. 83, p. 217-247.

Anderson, R.N., Honnorez, J., Becker, K., Adamson, A.C., Alt, J.C., Emmermann, R., Kempton, P.D., Konoshita, H., Laverne, C., Mottl, M.J. and Newmark, R.L.
1982: DSDP hole 504B, the first reference section over 1 km through Layer 2 of the oceanic crust; Nature, v. 300, p. 589-594.

Ballard, R.D., Francheteau, J., Juteau, T., Rangan, C. and Normark, W.
1981: East Pacific Rise at 21°N: the volcanic, tectonic, and hydrothermal processes of the central axis; Earth and Planetary Science Letters, v. 55, p. 1-10.

Bednarz, U., Sunkel, G. and Schmincke, H.-U.
1987: The basaltic andesite-andesite and the andesite-dacite series from ICRDG drill holes CY-2 and CY-2a. I. Lithology, petrology, and geochemistry; *in* Cyprus Crustal Study Project Initial Report Hole CY2-2a, ed. P.T. Robinson, I.L. Gibson and A. Panayiotou; Geological Survey of Canada, Paper 85-29.

Browne, P.R.L.
1978: Hydrothermal alteration in active geothermal fields; Annual Review of Earth and Planetary Sciences, v. 6, p. 229-250.

Donnelly, T.W., Pritchard, R.G., Emmermann, R. and Puchelt, H.
1979: The aging of oceanic crust: synthesis of the mineralogical and chemical results of Deep Sea Drilling Project, Legs 51 through 53; *in* Initial Reports of the Deep Sea Drilling Project, Volume 51-53, Part 2, ed. T. Donnelly, J. Francheteau, W. Bryan, P. Robinson, M. Flower, M. Salisbury et al.; U.S. Government Printing Office, Washington, D.C., v. 51-53, p. 1563-1577.

Ellis, A.J.
1979: Explored geothermal systems; *in* Geochemistry of Hydrothermal Ore Deposits, 2nd edition, ed. H.L. Barnes; John Wiley and Sons, New York, p. 632-683.

Elthon, D. and Stern, C.
1978: Metamorphic petrology of the Sarmiento ophiolite complex, Chile; Geology, v. 6, p. 464-468.

Evarts, R.C. and Schiffmann, P.
1983: Submarine hydrothermal metamorphism on the Del Puerto ophiolite, California; American Journal of Science, v. 283, p. 289-340.

Fisher, R.V. and Schmincke, H.-U.
1984: Pyroclastic Rocks; Springer Verlag Berlin-Heidelberg-New York-Tokyo, p. 1-472.

Henley, R.W. and Ellis, A.J.
1983: Geothermal systems ancient and modern: a geochemical review; Earth Science Reviews, v. 19, p. 1-50.

Herzig, P.
1987: Sulphide mineralization, hydrothermal alteration, and chemistry in the drill core CY-2a, Agrokipia, Cyprus; *in* Cyprus Crustal Study Project Initial Report Hole CY2-2a, ed. P.T. Robinson, I.L. Gibson and A. Panayiotou; Geological Survey of Canada, Paper 85-29.

ICRDG
1984: Are Troodos deposits an East Pacific analog?; Geotimes, v. 29, no. 5, p. 12-14.

Jakobsson, S.P.
1978: Environmental factors controlling the palagonitization of the Surtsey tephra,

Iceland; Geological Society of Denmark, Bulletin, Special Issue, no. 27, p. 91-105.

Kristmannsdottir, H.
1976: Types of clay minerals in hydrothermally altered basaltic rocks; Reykjanes, Iceland, Jokull, v. 26, p. 30-39.

Kristmannsdottir, H. and Tomasson, J.
1978: Zeolite zones in geothermal areas in Iceland; *in* Natural Zeolites: Occurrence, Properties, Use, ed. L.B. Sand and F.A. Mumpton; Pergamon Press, Oxford, p. 277-284.

Lister, C.R.B.
1972: On the thermal balance of mid-ocean ridge; Geophysical Journal of the Royal Astronomical Society, v. 26, p. 515-535.

Malpas, J. and Langdon, G.
1984: Petrology of the upper pillow lava suite, Troodos ophiolite, Cyprus; *in* Ophiolites and Oceanic Lithosphere, ed. I.G. Gass, S.J. Lippard and A.W. Shelton; Geological Society of London, Special Publication, no. 13, Blackwell Scientific Publications, Oxford-London-Edinburgh-Boston-Melbourne, p. 155-167.

Moores, E.M. and Vine, F.J.
1971: The Troodos Massif, Cyprus and other ophiolites as oceanic crust: evaluation and implications; *in* A Discussion on the Petrology of Igneous and Metamorphic Rocks from the Ocean Floor; Philosophical Transactions of the Royal Society of London, Series A., v. 268, p. 443-466.

Mottl, M.J.
1983: Metabasalts, axial hot springs, and the structure of hydrothermal systems at mid-ocean ridges; Geological Society of America, Bulletin, v. 94, no. 2, p. 161-180.

Palmason, G.S., Arnorsson, I.B., Fridleifsson, H., Kristmannsdottir, K., Saemundsson, V., Stefansson, B., Steingrimsson, J., Tomasson, J. and Kristjansson, L.
1979: The Iceland crust: evidence from drill hole data on structure and processes; *in* Deep Drilling Results in the Atlantic Ocean Ocean Crust, Maurice Ewing Series, Volume 2, ed. M. Talwani, C.G. Harrison and D.E. Hayes; EOS, American Geophysical Union, Transactions, v. 2, p. 43-65.

Robinson, P.T. and Gibson I.L.
1983: Cyprus Crustal Study Project. Hole CY-2a Lithologic Unit Summaries.

Rommel, U. and Friedrichsen, H.
1984: Sauerstoff- und Wasserstoffisotopen-unter-suchungen an Basalten der Bohrung CY-2a, Troodos-Ophiolith-komplex, Zypern(Abstract); Fortschritte der Mineralogie, v. 62, p. 198-199.

Spooner, E.T.C.
1977: Hydrodynamic model for the origin of the ophiolitic cupriferous pyrite ore deposits of Cyprus; *in* Volcanic Processes in Ore Genesis; Geological Society of London, Special Publication, no. 7, p. 58-71.

Spooner, E.T.C. and Fyfe, W.S.
1973: Sub-seafloor metamorphism, heat and mass transfer; Contributions to Mineralogy and Petrology, v. 42, p. 287-304.

Tomasson, J. and Kristmannsdottir, H.
1972: High temperature alteration minerals and thermal brines, Reykjanes, Iceland; Contributions to Mineralogy and Petrology, vol. 36, p. 123-134.

Turekian, K.K. and Cochran, J.K.
1981: Growth rate of a Vesicomyid clam from the Galapagos Spreading Center; Science, vol. 214, p. 909-911.

Cyclic Geochemical Variation in the Troodos Pillow Lavas: Evidence from the CY-2a Drill Hole

FRANCOIS AUCLAIR[1] AND JOHN N. LUDDEN[2]

[1]Department of Geological Sciences, McGill University, 3450 University Street,
Frank Dawson Adams Building, Montréal, Québec, Canada, H3A 2A7
[2]Département de Géologie, Université de Montréal
Montréal, Québec, Canada, H3C 3J7

Auclair, F. and Ludden, J.N., Cyclic geochemical variation in the Troodos Pillow Lavas: evidence from the CY-2a Drill Hole; in *Cyprus Crustal Study Project: Initial Report, Holes CY-2 and 2a, ed. P.T. Robinson, I.L. Gibson and A. Panayiotou; Geological Survey of Canada, Paper 85-29, p. 221-235, 1987.*

Abstract

The volcanic rocks of the Troodos ophiolite have traditionally been divided into two units: the Upper Pillow Lavas (UPL) and the Lower Pillow Lavas (LPL). However, new information provided by samples from drill hole CY-2a of the International Crustal Research Drilling Group (ICRDG) indicates that major and trace element concentrations follow two distinct trends. The first is a cyclic evolution from tholeiitic basalts towards a more magnesian composition in four different units. The second is an evolution towards a more mafic composition from the base of the section studied to the top of the drill hole. This questions the rigid division between the UPL and LPL. It is proposed here that mafic magma slowly 'leaked' into the evolved magma chamber that fed the LPL causing the cyclic evolution observed between the units. Finally, the magma chamber was flooded by the high-MgO 'boninitic' magmas that fed the UPL. The magmas feeding the two pillow lava units are identical in trace element ratios such as La/Sm and Zr/Y and also in isotopic characteristics (Rautenschlein et al., 1985), possibly indicating that a homogeneous mantle source was sampled throughout the evolution of the Troodos ophiolite.

Résumé

La suite volcanique de l'ophiolite Troodos à Chypre a traditionnellement été divisée en deux séries distinctes: les laves en coussins supérieures (UPL) et les laves en coussin inférieures (LPL). Toutefois, des analyses d'échantillons provenant du forage CY-2a du ICRDG (International Crustal Research Drilling Group), indiquent que les concentrations en éléments majeur et trace suivent deux patrons distincts. Le premier correspond à une évolution cyclique de basaltes tholéiitiques vers des compositions plus magnésiennes et ce dans quatre unités distinctes. Le second montre une évolution vers des compositions plus mafiques de la base jusqu'au sommet de la section volcanique étudié. Cette évolution vers des compositions plus mafiques met en doute la division rigide entre les unités UPL et LPL. Il est proposé que des magmas mafiques ont suintés lentement dans la chambre magmatique plus évoluée qui 'nourrissait' les LPL causant l'évolution cyclique observé dans les quatre unités. Finalement, la chambre magmatique fut envahie par un magma boninitique riche en MgO qui 'nourrissait' les UPL. Les magmas alimentant les deux unités de laves sont similaires dans certains rapports en éléments traces, tel que La/Sm et Zr/Y et aussi dans leur rapports isotopiques (Rautenschlein et al., 1985), indiquant possiblement que la même source mantellique fut échantillonée pendant toute l'évolution de l'ophiolite Troodos.

INTRODUCTION

The volcanic rocks associated with the massive sulphide deposits of the Troodos ophiolite are affected by intense argillic alteration and silica metasomatism as a result of hydrothermal circulation through the ophiolite (Adamides, 1984; Spooner, 1977; Parmentier and Spooner, 1978). These metasomatic fluids may have affected the abundances of the major and trace elements, making identification of primary geochemical variations in the volcanic rocks problematical. However, a detailed investigation of trace element mobility in the CY-1 drill hole of the International Crustal Research Drilling Group (ICRDG) which penetrated 485 meters into the Upper Pillow lavas of the Troodos ophiolite indicated that many trace element ratios are not affected by the hydrothermal alteration. In particular, the high field strength elements (HFS) (Zr, Y, Ti, and the REE) are simply diluted by metasomatic replacement processes and the ratios of these elements are unchanged even during intense alteration (Auclair et al., in prep.; Pearce and Norry, 1979; Pearce and Cann, 1973; 1971).

While most of the papers in this volume describe the ore zone and the effects of fluids on the Agrokipia deposits, our objective has been to evaluate the primary magma composition of the lavas associated with the Agrokipia ore deposits using samples taken from the CY-2a drill hole. These data allow us to identify small scale (approximately 50 meter) cyclic geochemical variations that are superimposed on a gradual trend of increasingly more mafic lavas towards the top of the section. This gradual evolution to more mafic compositions brings into question the division of the volcanic rocks into an Upper and Lower Pillow lavas series and places important constraints on the petrogenesis of the Troodos lavas.

LITHOLOGICAL VARIATION WITHIN THE CY-2A DRILL HOLE

The CY-2a drill hole penetrated the Agrokipia 'B' ore body. In Troodos, the ore deposits are often located at the 'boundary' between the Upper Pillow Lavas and Lower Pillow Lavas (UPL and LPL). According to the ICRDG report (ICRDG, 1984) the Agrokipia 'B' deposit is situated entirely within the LPL, as defined by Bear (1960). However, our data indicate that the drill hole penetrated both the UPL and LPL type lavas. This lens and stockwork of massive sulphide ore lies 400 meters to the east and is 150 meters stratigraphically lower than the Agrokipia 'A' deposit, which is situated at the 'boundary' between the UPL and LPL. The ICRDG was able to recognize 22 lithological units throughout the 689 meters of the drill hole (ICRDG, 1984; Douma and Robinson, 1984). Three main alteration sequences have been identified:

1. Sequence 1 (3.35 to 154.23 m) comprises medium to coarse-grained massive basalts, some with cumulate olivine. Alteration in these units is limited to minor smectite in the groundmass.
2. Sequence 2 (154.23 to 297.14 m) represents an argillic zone containing pervasively altered basalts. The alteration assemblage in these units comprises illite, chlorite, pyrite, sphene and sphalerite.
3. Sequence 3 (297.14 m to base of drill hole) consists of two dyke swarms which are separated by a sequence of pillowed and massive flows. Both the flows and dykes are metamorphosed to a greenschist facies and the primary mineral phases are replaced by chlorite, epidote, quartz, albite and minor pyrite.

This study will focus on the lavas which are most closely associated with the ore zone; that is in the upper 250 m of the hole. Two lava types have been identified in this sequence:

1. light grey, vesicular and weakly mineralized lavas;
2. cream colored to light grey lavas which are highly altered.

Below 120 m many of the massive flows have glassy zones at their upper and lower boundaries. In most cases, the glass is altered to brown and green clays with some partly devitrified glass still preserved.

The samples selected for study were analyzed in different laboratories. Major elements were compiled from both XRF and AA data from Memorial University of Newfoundland and Bochum University, Germany. Trace elements (Zr, Nb, Y, Rb, Sr, Ni, Cr) and REE were analyzed by X-Ray fluorescence and by Instrumental Neutron Activation (INAA), respectively, at Université de Montréal. The glass samples were analyzed at the Lamont-Doherty Geological Observatory for the major and trace elements by Direct Current Plasma Spectrometry (DCP) (For a complete description of sample preparation and analytical techniques, see Auclair et al., in prep.; Auclair, 1986).

GEOCHEMISTRY

All the samples analyzed are basalts and/or andesites. Since most major elements are mobile as a result of hydrothermal alteration, it is often difficult to interpret primary magmatic processes in the volcanic rocks (Mottl, 1983; Humphris and Thompson, 1978a; 1978b; Mottl and Holland, 1978). However, by

TABLE 1. Major and trace element analyses of samples from the CY-2a drillhole

	4.40	9.70	11.80	19.30	21.50	25.85	30.10	33.10	40.75	42.15	44.05	58.75
SiO_2	53.80	54.20	52.30	51.90	52.30	49.20	49.80	49.70	50.60	49.40	50.20	47.90
TiO_2	.57	.52	.51	.44	.53	.40	.47	1.17	1.40	1.21	1.39	.61
Al_2O_3	14.60	15.14	14.90	14.40	14.90	12.70	12.90	15.26	15.80	14.60	15.67	15.00
Fe_2O_3	8.87	4.94	8.34	7.72	7.38	10.49	9.56	8.68	9.13	11.59	9.51	8.91
FeO	nd	3.57	nd	nd	nd	nd	nd	2.46	2.43	nd	2.36	nd
(FeO *)	7.98	8.01	7.50	6.94	6.64	9.43	8.60	10.27	10.64	10.42	10.91	8.01
MnO	.11	.13	.09	.08	.08	.09	.10	.10	.10	.09	.09	.10
MgO	7.90	8.80	8.24	9.35	8.89	10.46	10.07	5.83	5.99	5.47	5.28	6.96
CaO	4.84	7.20	8.81	8.50	9.36	8.87	7.31	6.49	5.90	5.27	6.08	5.50
Na_2O	1.69	1.63	1.84	1.73	1.81	1.78	2.21	2.67	3.14	3.12	3.04	2.31
K_2O	2.20	1.16	.26	.31	.24	.78	.76	1.87	.83	1.34	1.08	3.64
P_2O_5	.08	.05	.04	.01	nd	.03	.07	.08	.12	.08	.13	.09
TRELS	.07	.06	.08	.08	.06	.08	.08	.05	.06	.05	.05	.05
H_2O	5.66	2.77	1.86	5.58	1.91	4.42	2.84	3.58	3.11	5.86	3.34	3.44
CO_2	.07	.04	.20	.30	.07	.47	.23	2.26	1.19	1.14	1.30	1.95
S	.03	.02	.02	.03	.02	.03	.12	nd	nd	.01	nd	.04
TOTAL	100.47	100.22	97.48	100.41	97.54	99.78	96.46	100.20	99.80	99.22	99.52	96.49
						CATIONS						
Si	53.08	51.72	51.12	50.92	50.77	48.21	49.38	49.43	49.71	50.43	49.84	48.72
Ti	.42	.37	.37	.32	.39	.29	.35	.88	1.03	.93	1.04	.47
Al	16.98	17.02	17.16	16.65	17.05	14.67	15.08	17.89	18.29	17.56	18.34	17.98
Fe	6.58	6.39	6.13	5.70	5.39	7.73	7.13	8.54	8.74	8.90	9.06	6.81
Mn	.09	.11	.07	.07	.07	.07	.08	.08	.08	.08	.08	.09
Mg	11.62	12.52	12.01	13.67	12.87	15.28	14.89	8.65	8.77	8.32	7.82	10.55
Ca	5.12	7.36	9.23	8.93	9.73	9.31	7.77	6.92	6.21	5.76	6.47	5.99
Na	3.23	3.02	3.49	3.29	3.41	3.38	4.25	5.15	5.98	6.17	5.85	4.55
K	2.77	1.41	.32	.39	.30	.97	.96	2.37	1.04	1.74	1.37	4.72
P	.07	.04	.03	.01	nd	.02	.06	.07	.10	.07	.11	.08
TRELS	.05	.04	.05	.06	.04	.06	.06	.03	.04	.03	.03	.04
O -2	159.09	158.46	158.24	157.76	157.84	153.71	154.77	155.60	156.54	156.29	156.61	153.66
S	.05	.04	.04	.06	.04	.05	.23	nd	nd	.01	nd	.08
						TRACES						
Sc	nd	nd	35	36	nd	nd	nd	nd	nd	nd	nd	nd
Ti	3417	3117	3057	2638	3177	2398	2818	7014	8393	7254	8333	3657
Cr	35	148	142	201	165	205	226	10	11	8	11	103
Co	nd	nd	36	31	nd	nd	nd	nd	nd	nd	nd	nd
Ni	27	46	41	51	51	113	137	26	24	21	23	31
Cu	109	30	58	51	55	40	26	40	63	40	38	43
Zn	213	115	108	66	65	99	69	101	113	109	114	75
Rb	14	7	6	4	5	20	15	24	16	22	22	26
Sr	88	87	99	95	101	90	91	96	103	104	104	95
Y	15	10	12	10	9	14	11	29	37	34	39	16
Zr	32	27	28	26	28	23	29	62	81	75	76	35

	63.15	65.85	72.55	78.25	81.45	86.30	88.70	97.00	99.50	111.40	117.85	138.95
SiO_2	46.80	49.70	53.20	53.60	51.40	50.20	49.20	46.10	49.60	53.10	50.60	64.20
TiO_2	.64	.64	.71	.70	.57	.63	.56	1.14	1.04	1.19	1.23	.94
Al_2O_3	14.70	15.97	14.60	15.70	14.50	14.40	14.40	15.00	16.21	16.23	15.50	13.20
Fe_2O_3	8.79	7.73	7.69	5.55	7.94	7.72	8.15	9.69	7.51	7.88	10.78	8.23
FeO	nd	2.69	nd	2.39	nd	nd	nd	nd	2.48	2.21	nd	nd
(FeO *)	7.90	9.64	6.92	7.38	7.14	6.94	7.33	8.71	9.23	9.30	9.69	7.40
MnO	.11	.08	.10	.10	.10	.10	.11	.20	.20	.13	.25	.19
MgO	8.34	7.14	8.98	6.55	7.34	7.15	7.70	7.56	7.98	5.67	5.37	1.96
CaO	5.59	8.50	8.01	9.36	10.12	10.53	10.24	4.55	3.73	5.19	5.59	4.76
Na_2O	1.91	2.49	2.39	2.49	2.24	2.22	2.35	1.88	1.94	3.09	2.67	2.93
K_2O	2.19	1.42	.17	.86	.77	1.00	.90	3.04	2.86	1.32	.66	1.41
P_2O_5	.05	.09	.04	.07	.02	.02	.03	.10	.11	.19	.12	.09
TRELS	.05	.06	.07	.06	.06	.06	.07	.04	.05	.05	.06	.05
H_2O	8.47	2.34	3.00	2.07	3.00	nd	2.10	nd	5.03	3.50	3.97	1.58
CO_2	2.12	1.80	.57	.94	1.33	nd	2.22	nd	1.15	.36	.24	.10
S	.04	nd	.02	nd	.02	.02	.03	.05	nd	nd	.26	.04
TOTAL	99.78	100.65	99.54	100.44	99.41	94.05	98.05	89.32	99.89	100.11	97.17	99.66
					CATIONS							
Si	48.59	47.96	51.29	51.19	50.32	49.65	48.69	48.09	49.21	51.61	51.49	62.68
Ti	.50	.46	.51	.50	.42	.47	.42	.89	.78	.87	.94	.69
Al	17.99	18.16	16.59	17.67	16.73	16.78	16.80	18.44	18.95	18.59	18.59	15.19
Fe	6.86	7.78	5.58	5.89	5.85	5.74	6.07	7.60	7.66	7.56	8.25	6.04
Mn	.10	.07	.08	.08	.08	.08	.09	.18	.17	.11	.22	.16
Mg	12.91	10.27	12.91	9.33	10.71	10.54	11.36	11.76	11.80	8.22	8.15	2.85
Ca	6.22	8.79	8.27	9.58	10.61	11.16	10.86	5.08	3.96	5.40	6.09	4.98
Na	3.84	4.66	4.47	4.61	4.25	4.26	4.51	3.80	3.73	5.82	5.27	5.55
K	2.90	1.75	.21	1.05	.96	1.26	1.14	4.04	3.62	1.64	.86	1.76
P	.04	.07	.03	.06	.02	.02	.03	.09	.09	.16	.10	.07
TRELS	.04	.04	.05	.04	.04	.05	.05	.03	.03	.03	.04	.03
O -2	154.79	154.42	157.83	157.80	156.54	155.78	154.74	154.41	155.93	158.29	158.84	167.43
S	.08	nd	.03	nd	.04	.04	.06	.09	nd	nd	.50	.07
					TRACES							
Sc	nd	nd	nd	nd	nd	nd	nd	nd	nd	nd	29	nd
Ti	3837	3837	4256	4197	3417	3777	3357	6834	6235	7134	7374	5635
Cr	98	114	212	145	177	178	202	14	14	12	11	7
Co	nd	nd	nd	nd	nd	nd	nd	nd	nd	nd	19	nd
Ni	41	37	69	59	71	66	72	20	23	11	11	4
Cu	40	38	74	27	25	25	23	28	33	27	50	16
Zn	85	90	58	57	56	51	58	104	107	117	132	150
Rb	19	16	2	22	11	21	16	27	22	20	5	37
Sr	88	95	95	98	91	97	96	83	78	95	102	82
Y	9	18	15	20	18	18	19	29	25	54	39	35
Zr	32	37	39	42	35	30	34	11	58	70	82	64

	141.85	143.10	149.50	152.25	157.40	160.45	168.50	170.30	174.20	176.00	178.20	181.15
SiO_2	54.70	51.50	50.20	54.80	50.30	55.10	56.90	49.50	58.00	52.30	34.50	60.80
TiO_2	1.34	1.28	1.24	1.31	1.10	1.11	1.25	.87	1.26	.98	1.05	1.06
Al_2O_3	16.11	16.30	15.33	16.44	14.60	13.92	14.08	10.20	13.66	11.16	13.68	13.41
Fe_2O_3	8.19	10.59	9.87	7.48	11.84	3.41	4.93	21.69	3.67	16.72	21.91	4.38
FeO	1.84	1.90	3.16	2.91	nd	6.62	6.47	nd	7.37	.86	2.80	5.54
(FeO *)	9.21	11.42	12.04	9.64	10.65	9.69	10.90	19.51	10.67	15.90	22.50	9.48
MnO	.22	.32	.22	.27	.24	.48	.27	.02	.44	.31	.41	.15
MgO	4.38	5.05	6.01	3.70	8.92	7.97	7.88	1.04	7.48	1.41	3.41	6.29
CaO	5.56	5.98	6.16	7.12	3.99	.68	.25	.22	.24	.23	.27	.30
Na_2O	2.97	2.70	2.05	2.74	1.62	.48	.12	.24	.10	.28	.28	.17
K_2O	.37	.32	.19	.11	.45	2.93	1.05	1.84	1.11	1.96	2.30	1.36
P_2O_5	.17	.13	.05	.11	.03	.09	.11	nd	.12	.10	.15	.15
TRELS	.07	.06	.06	.07	.22	.13	.21	.17	.15	.06	.04	.05
H_2O	3.32	4.53	4.21	1.99	nd	6.18	6.10	nd	5.78	2.50	4.11	4.68
CO_2	.22	.15	.24	.04	nd	.07	.04	nd	.05	1.07	4.90	1.13
S	nd	.03	nd	.08	1.35	nd	nd	8.11	nd	nd	nd	1.09
TOTAL	99.46	100.82	98.99	99.13	93.98	99.17	99.66	89.85	99.43	89.94	89.81	100.01
						CATIONS						
Si	53.90	50.88	50.55	53.63	50.86	56.06	58.29	59.49	59.44	61.34	43.35	62.44
Ti	.99	.95	.94	.96	.84	.85	.96	.79	.97	.86	.99	.82
Al	18.71	18.98	18.19	18.96	17.40	16.69	17.00	14.45	16.50	15.43	20.26	16.23
Fe	7.59	9.44	10.13	7.89	9.00	8.24	9.34	19.60	9.14	15.59	23.65	8.14
Mn	.18	.27	.19	.22	.21	.41	.23	.02	.38	.31	.44	.13
Mg	6.43	7.44	9.02	5.40	13.44	12.09	12.04	1.86	11.43	2.47	6.39	9.63
Ca	5.87	6.33	6.65	7.46	4.32	.74	.27	.28	.26	.29	.36	.33
Na	5.67	5.17	4.00	5.20	3.18	.95	.24	.56	.20	.64	.68	.34
K	.47	.40	.24	.14	.58	3.80	1.37	2.82	1.45	2.93	3.69	1.78
P	.14	.11	.04	.09	.03	.08	.10	nd	.10	.10	.16	.13
TRELS	.04	.04	.04	.05	.16	.09	.15	.13	.11	.05	.03	.03
O -2	161.40	158.70	158.53	161.55	158.55	163.00	167.10	165.82	168.00	168.30	152.54	170.52
S	nd	.05	nd	.14	2.55	nd	nd	18.27	nd	nd	nd	2.09
						TRACES						
Sc	nd	nd	nd	nd	nd	nd	nd	29	nd	nd	nd	21
Ti	8033	7674	7434	7853	6595	6654	7494	5216	7554	5875	6295	6355
Cr	2	8	17	17	15	18	26	10	11	2	nd	13
Co	nd	nd	nd	nd	nd	nd	nd	16	nd	nd	nd	11
Ni	6	9	16	17	17	10	9	6	6	7	8	3
Cu	44	51	102	91	65	57	430	621	431	33	45	17
Zn	243	182	229	216	1487	831	1064	274	636	184	89	137
Rb	9	7	5	3	4	16	14	25	16	22	26	15
Sr	102	102	80	96	62	22	14	15	11	24	15	14
Y	46	38	17	29	29	27	32	28	34	35	45	43
Zr	73	74	46	53	48	55	61	58	73	72	91	89

	183.40	186.90	197.00	218.00	238.26	241.80
SiO_2	3.53	58.90	54.90	53.40	45.40	57.10
TiO_2	.22	1.21	1.32	1.19	1.41	1.26
Al_2O_3	.33	13.73	13.94	14.18	17.80	12.78
Fe_2O_3	54.14	4.77	5.77	2.30	7.46	7.86
FeO	.00	6.26	6.92	6.03	7.13	5.14
(FeO *)	48.69	10.55	12.11	8.10	13.84	12.21
MnO	.03	.17	.25	.50	.15	.19
MgO	.09	6.73	7.32	7.58	8.68	5.36
CaO	.34	.27	.22	1.78	.18	.20
Na_2O	.10	.15	.38	1.45	.21	.19
K_2O	.73	1.24	1.06	1.86	1.42	1.36
P_2O_5	.00	.13	.11	.12	.07	.10
TRELS	.03	.06	.05	.06	.02	.04
H_2O	nd	5.07	5.37	5.55	6.45	4.41
CO_2	nd	.04	1.21	2.92	2.03	3.08
S	7.85	nd	nd	2.31	nd	nd
TOTAL	63.47	98.73	98.82	100.07	98.41	99.07
			CATIONS			
Si	7.60	60.53	57.17	55.20	48.01	60.81
Ti	.36	.94	1.03	.93	1.12	1.01
Al	.84	16.63	17.11	17.28	22.18	16.04
Fe	87.62	9.07	10.54	7.00	12.24	10.87
Mn	.05	.15	.22	.44	.13	.17
Mg	.29	10.31	11.36	11.68	13.69	8.51
Ca	.78	.30	.25	1.97	.20	.23
Na	.42	.30	.77	2.91	.43	.39
K	2.00	1.63	1.41	2.45	1.92	1.85
P	nd	.11	.10	.11	.06	.09
TRELS	.04	.04	.03	.04	.01	.03
O -2	107.18	169.00	165.83	162.26	159.15	168.86
S	31.64	nd	nd	4.47	nd	nd
			TRACES			
Sc	5	nd	nd	28	nd	nd
Ti	1319	7254	7913	7134	8453	7554
Cr	12	5	20	13	nd	21
Co	14	nd	nd	24	nd	nd
Ni	nd	2	8	2	nd	5
Cu	12	108	17	13	nd	18
Zn	72	213	223	199	nd	173
Rb	4	12	12	4	13	13
Sr	3	15	13	5	26	9
Y	11	38	31	30	31	26
Zr	23	80	67	68	82	65

nd: non-determined, non-detected

TABLE 2. Rare earth element analyses of selected samples from the CY-2a drillhole

	11.80	19.30	117.85	170.30	181.15	183.40	218.00
La	1.40	1.20	3.00	3.20	3.50	.30	2.20
Ce	3.60	3.10	7.80	7.80	9.50	nd	6.70
Sm	1.31	1.07	3.40	2.70	3.55	.57	2.65
Eu	.45	.43	1.10	1.10	.90	.20	.60
Tb	.32	.34	.84	.54	.84	.19	.64
Ho	.56	.40	1.21	.68	1.25	.49	1.01
Yb	1.35	1.24	3.50	3.10	4.12	.75	3.27
Lu	.20	.15	.45	.40	.50	.10	.40
Hf	1.00	.90	2.20	1.50	2.50	.40	2.00
Ta	.20	.50	.10	.10	.10	nd	nd
Th	.20	.20	.30	.30	.30	.30	.30
U	.10	nd	.10	.20	.10	.10	nd

nd: non-determined, non-detected

TABLE 3. Major and trace element analyses of fresh glass collected in Pedeios Canyon

	TR-12	TR-3F	TR-3A	TR-1B
SiO_2	54.10	56.50	56.79	54.90
TiO_2	.50	1.33	1.29	1.35
Al_2O_3	15.40	14.90	14.01	14.80
(FeO *)	9.08	11.96	13.07	13.00
MnO	.15	.18	.22	.19
MgO	7.19	3.38	4.53	4.03
CaO	11.25	7.58	6.65	7.95
Na_2O	1.86	3.29	2.61	2.94
K_2O	.19	.28	.50	.33
P_2O_5	.06	.14	.12	.12
TRELS	.14	.12	.47	.14
TOTAL	99.92	99.66	100.26	99.75
		CATIONS		
Si	49.64	50.93	51.85	49.52
Ti	.34	.90	.89	.92
Al	16.65	15.83	15.07	15.73
Fe	6.97	9.01	9.98	9.81
Mn	.12	.14	.17	.15
Mg	9.83	4.54	6.17	5.42
Ca	11.06	7.32	6.50	7.68
Na	3.31	5.75	4.62	5.14
K	.22	.32	.58	.38
P	.05	.11	.09	.09
TRELS	.81	.15	.08	.16
O -2	158.40	162.01	161.87	160.84
		TRACES		
P	262	611	524	524
Sc	36	29	26	31
Ti	2998	7973	7734	8093
V	248	295	306	375
Cr	228	19	17	25
Co	31	27	37	42
Ni	58	17	17	24
Cu	93	42	57	58
Zn	70	87	84	88
Sr	86	107	141	103
Y	16	35	32	33
Zr	38	93	89	85
Ba	22	40	89	31

TABLE 4. Rare earth element analyses of fresh glasses collected in Pedeios Canyon

	TR-12	TR-3F	TR-3A	TR-1B
La	1.30	3.30	2.70	3.70
Ce	2.50	6.60	5.40	8.20
Nd	2.30	6.50	5.60	5.50
Sm	1.14	3.25	2.70	3.87
Eu	.44	1.06	.85	1.40
Gd	1.75	3.67	2.50	4.08
Tb	.34	.75	.70	.97
Dy	2.40	5.23	4.39	6.03
Ho	.57	1.24	1.17	1.54
Yb	1.33	3.32	3.01	4.10
Lu	.17	.50	.40	.60
Hf	.90	2.30	2.40	3.20
Ta	.40	nd	.20	.20
Th	.10	.10	.10	.50
U	2.30	3.30	3.30	5.10

nd: non-determined, non-detected

normalizing the molar abundances of the major elements to an immobile element, such as titanium, (Pearce, 1968), it is possible to discriminate the effects of dilution as a result of metasomatic replacement, and to define the primary geochemical variation. In Figure 1 the ratios of MgO/TiO_2 and Fe_2O_3/TiO_2 have been plotted against depth. An abrupt change in MgO and FeO content occurs around 45 m and a less well defined break around 130 m. The 45 meter break can be correlated with the presence of a significant quantity of olivine phenocrysts, and probably corresponds to the transition between the UPL and LPL (Robinson et al., 1983). For the sequence studied, a trend of decreasing Fe_2O_3/TiO_2 and increasing MgO/TiO_2 from the bottom of sequence 2 to the top of the hole is observed. These 'apparent' trends have been further evaluated using trace elements.

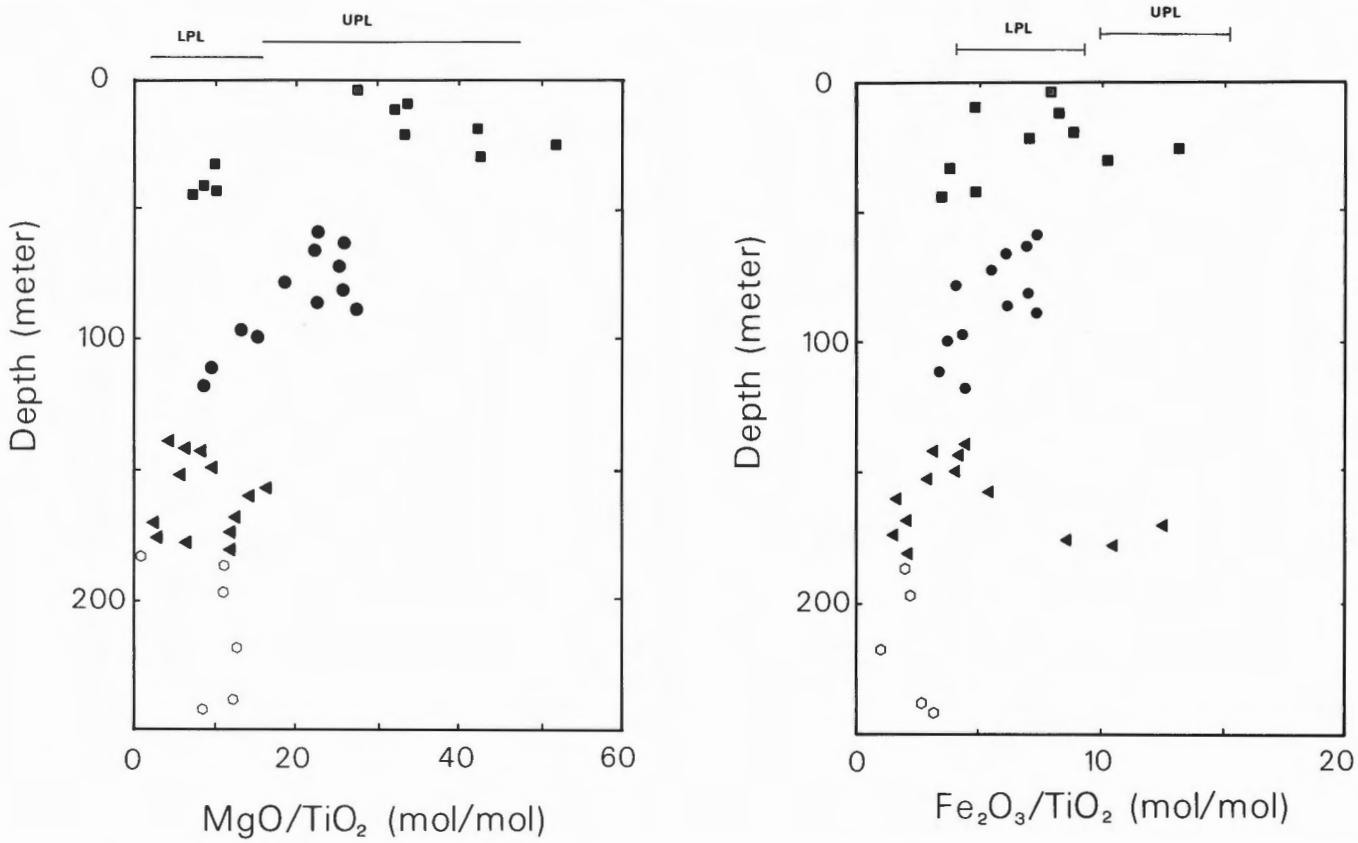

Figure 1: MgO/TiO_2 and Fe_2O_3/TiO_2 (molar concentration) versus depth. Symbols serve to define successive magma batches based on cyclic changes in geochemistry (see text). The range of MgO/TiO_2 and Fe_2O_3/TiO_2 in the fresh glasses collected by Robinson et al. (1983), are given as an indication of ranges in composition of the two volcanic units.

The HFS trace elements, such as Zr, Y and the REE have been shown to be relatively immobile under submarine hydrothermal alteration (see Ludden and Thompson, 1979; Pearce and Cann, 1973; 1971; Humphris and Thompson, 1978a). In addition, in a study of the UPL sampled in the CY-1 drill hole of the ICRDG, we have shown (Auclair et al., in prep.) that the ratio of these elements are not affected by low temperature alteration. In Figure 2, the Zr/Y ratio is plotted against Zr. The lack of fractionation of the Zr/Y ratio supports the contention that these elements were not affected by the hydrothermal alteration processes active in the Agrokipia ore deposits. In fact the range in the Zr/Y at constant Zr is most reasonably interpreted as being a result of fractionation of mineral phases having low partition coefficients for these elements. However, some of the spread in the data may be the result of metasomatic replacement during argillic alteration which would dilute Y and Zr abundances equally and produce artificially low values in the most altered samples. Furthermore, the Zr/Y ratio and Zr concentrations in

the altered samples duplicate (within analytical error) the ratio and concentration of these elements in the fresh glasses (open star for the UPL and filled stars for the LPL on the different Figures). We suspect that the abundances of trace elements in the fresh glass closely approximate true liquid composition; the fact that the trend observed in the altered rocks is similar to the trend defined by the glass analyses leads us to believe that we can make petrogenetic inferences from the geochemical data despite the extensive alteration in the lavas.

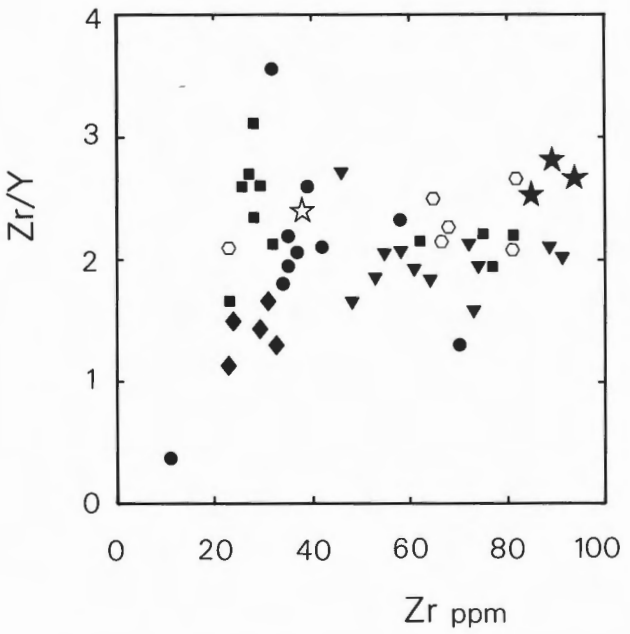

Figure 2: Zr/Y versus Zr. Insignificant fractionation of the Zr/Y ratio is observed. The analytical accuracy at the 10 ppm level for Y is in the range of 15%, at 50 ppm for Zr the accuracy is in the order of 10%. The small fluctuations in the ratio are a result of either the analytical precision, due to very low abundances of these elements, or of dilution of Y by alteration (Auclair et al., in prep.). Same symbols as in Figure 1. The filled diamonds represent CY-1 samples, the filled stars represent LPL fresh glasses and the open star represents a UPL fresh glass.

To verify this contention, we have plotted the concentration of Ni (a compatible trace element) against Zr. Nickel appears to be relatively immobile in the CY-1 drill hole section (Auclair et al., in prep.) and this is probably also the case in the CY-2a drill hole section. A series of negatively correlated trends are obtained between Ni and Zr (see Figure 3). Where it has been possible to calculate a bulk partition coefficient, values of 6 - 7 are obtained which is in fairly good agreement with bulk KD's predicted for the olivine + plagioclase assemblage (Irving, 1977). The Ni abundances in hole CY-2a are thus consistent with a model of low pressure fractionation (Robinson et al., 1983; Schmincke et al., 1983).

A range in absolute REE abundance exists within the CY-2a lavas: the most enriched samples are also the most evolved ones. This trend is comparable to the one defined by the fresh glass data for the upper and lower pillow lavas of the Troodos Complex (Figure 4). The REE data for CY-2a are plotted as La/Yb (light/heavy REE fractionation), and La/Sm (light/middle REE fractionation) versus La (degree of enrichment) in Figure 5. No relative fractionation of light REE relative to heavy REE is observed, despite the range in REE abundances. It is thus possible to identify a range in primary magmatic compositions in the drill hole.

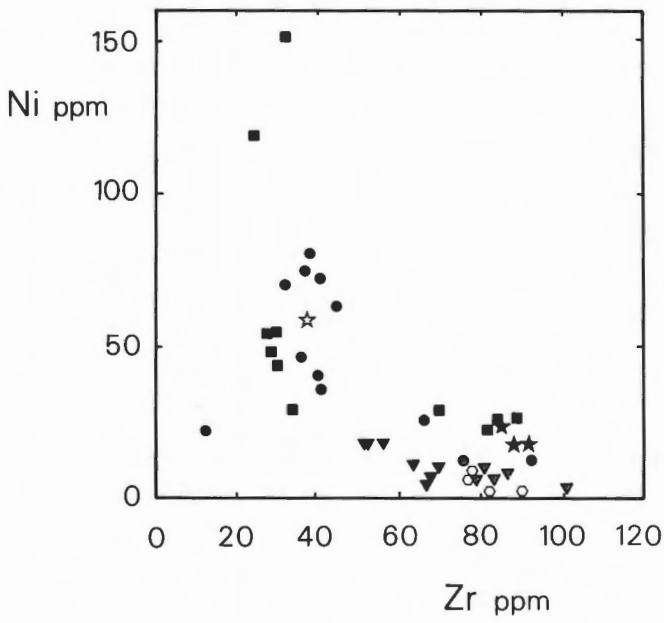

Figure 3: Ni versus Zr. This diagram indicates that a range in primary magma compositions exists within the volcanic sequence of the ophiolite. Same legend as in Figure 1. The coherent behavior of Ni attest to the immobility of this element in the CY-2a drill hole.

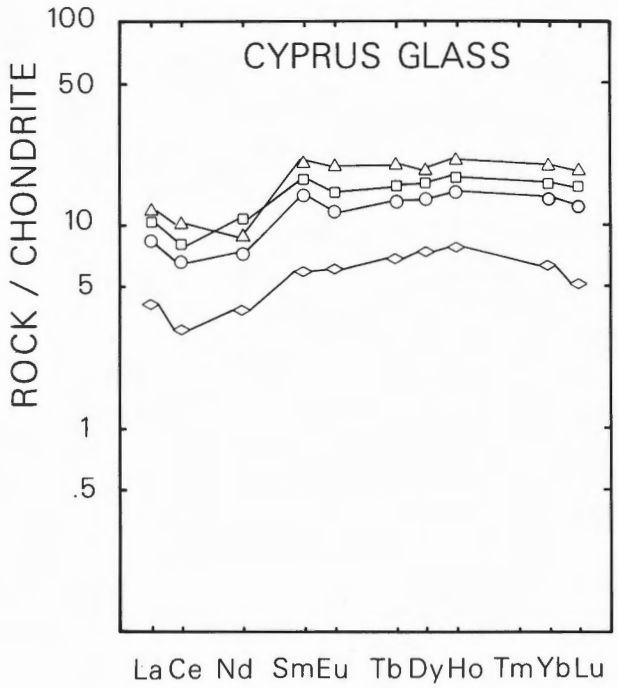

Figure 4: Rare earth element profiles for fresh glasses of the Troodos ophiolite. The diamond symbols represent UPL type lavas, and the circles, the squares and the triangles represent LPL type lavas.

In Figure 6, Zr, Y, and Ni have been plotted against depth in the drill hole. The systematic variation inferred from the major element data is confirmed and further refined. Enrichment in the incompatible elements (Zr, Y) is coupled to depletion in Ni. These variations (see later discussion) are considered to be the result of primary magmatic processes and probably represent olivine (± cpx) and plagioclase fractionation.

The geochemical changes with depth occur on two scales. Firstly, a cyclic evolution which trends towards more mafic compositions, culminating at Zr and Y minima and Ni maxima in four different units. Secondly, there is an overall evolution to more Ni rich and Zr and Y poor compositions from the base to the top of the hole. (See schematic diagram, Figure 7).

Although Robinson et al. (1983) proposed a geochemical division based on the major element chemistry of fresh glasses, our geochemical data from the CY-2a drill hole suggest that there is a gradual trend towards more mafic compositions for the lavas. Furthermore, Rautenschlein et al. (1984; 1985), have shown that there is no difference in isotope composition and incompatible trace element ratios between the UPL and LPL fresh glasses.

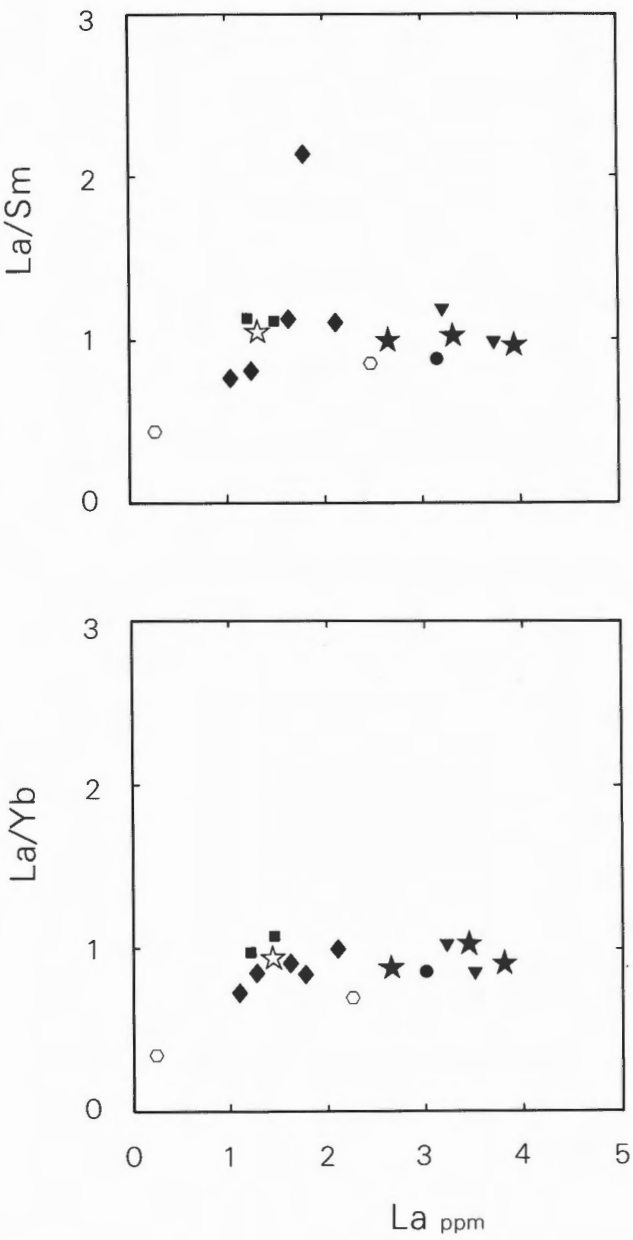

Figure 5: La/Sm and La/Yb versus La. Even more evident in this figure than in Figure 2, no fractionation is observed between the samples. Same symbols as Figure 2. One CY-1 sample shows a strong depletion in Sm, but we believe this may be the result of alteration.

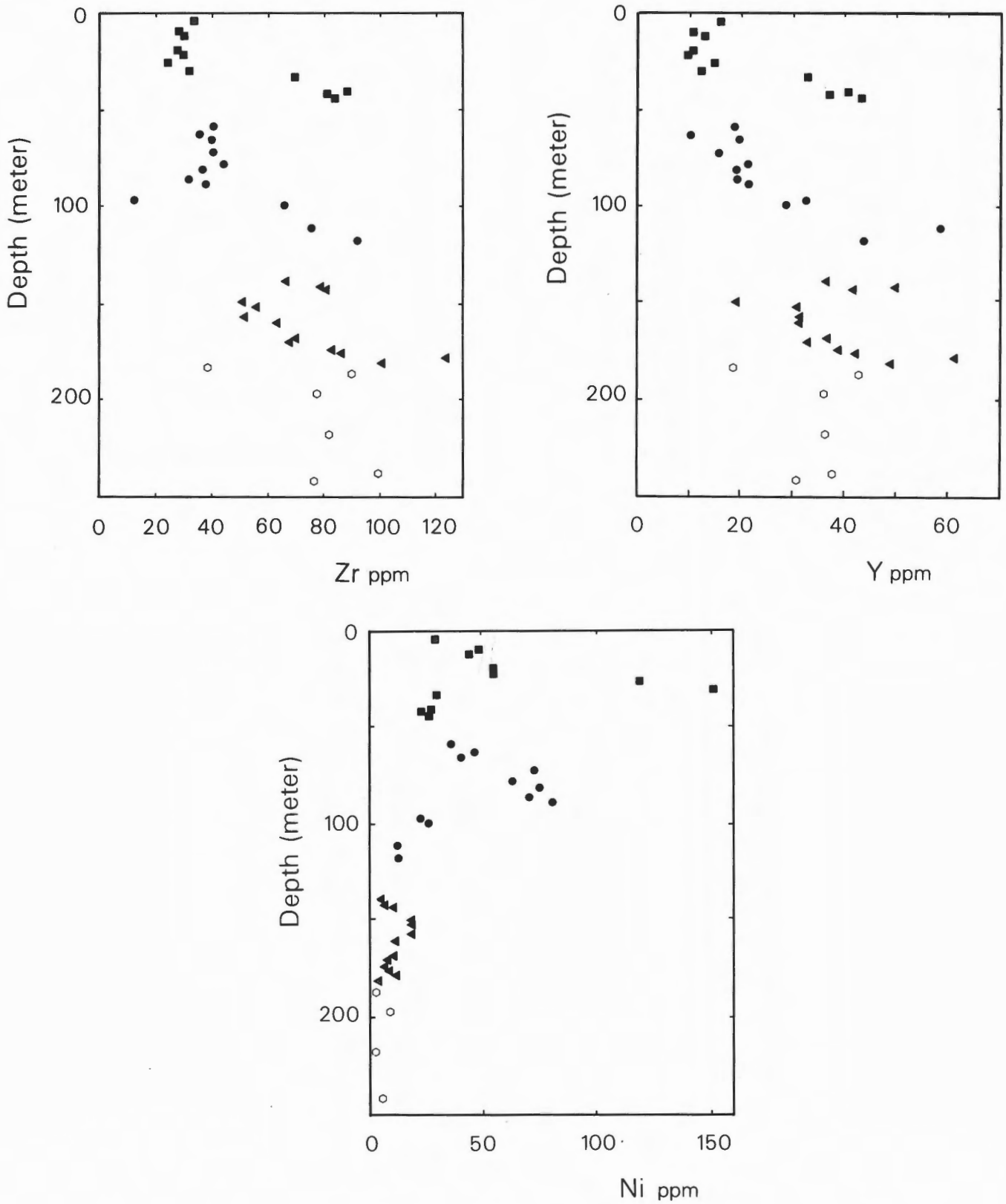

Figure 6: Zr, Y, and Ni concentration (ppm) plotted versus depth (meters). Same legend as Figure 2.

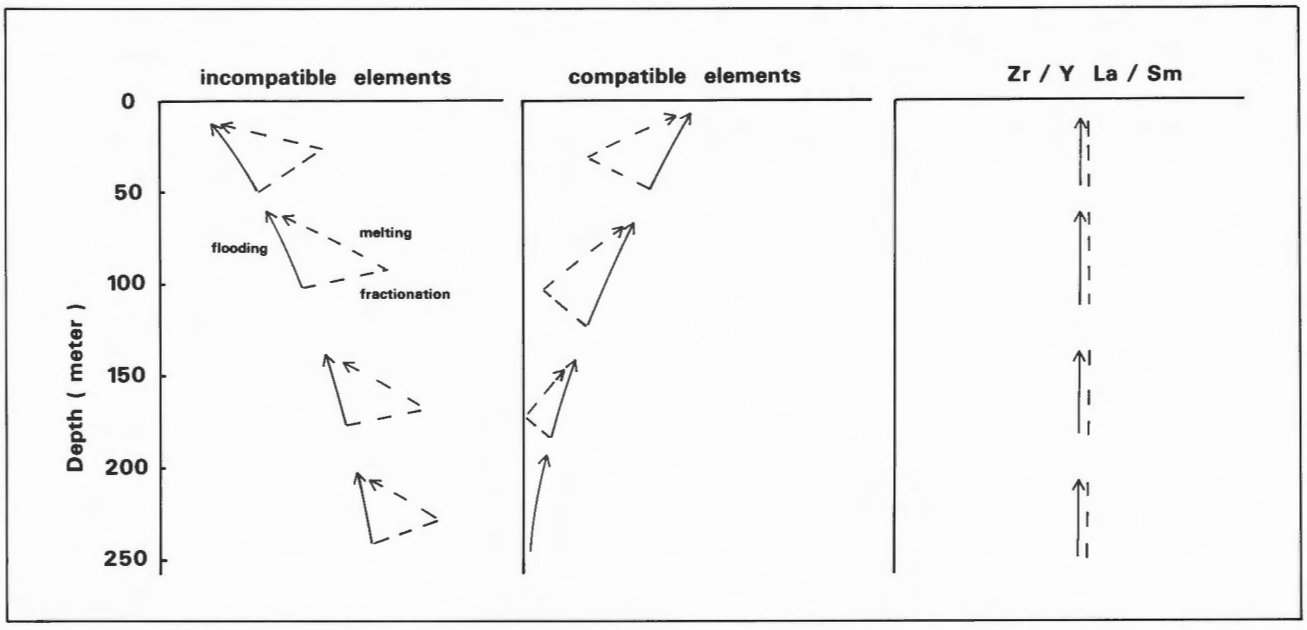

Figure 7: Schematic representation of the gradual flooding of the ophiolite magma chamber, and its relation to the behavior of trace element concentrations in the CY-2a drill hole. The continuous arrow represents gradual flooding of a low pressure magma system with a mafic magma. The dashed line represents small scale fluctuations associated with low pressure fractionation and/or progressive melting of the mantle source for individual units.

DISCUSSION

Robinson et al. (1983) and Schmincke et al. (1983) both presented arguments, based on detailed mapping and analyses of fresh glass, that the volcanic sequences in Troodos can be divided into two members; one mafic (the UPL) and one comprising more felsic lavas with affinities to arc-tholeiites (the LPL). Previous workers, including Bear, 1960; Searle and Constantinou, unpub. rep., 1968; Gass, 1968; Moores and Vine, 1971, recognized a break in the stratigraphic sequence in the field, which does not necessarily correspond to the geochemical division. The gradual evolution to more mafic compositions that we observe in the upper 250 meters of hole CY-2a leads us to propose that the division between the two pillow sequences is not as abrupt as the previous authors have proposed. The field-based division of Bear (1960) is due to differential alteration effects; the uppermost lavas are ol-rich, therefore colour due to alteration is different from that of the more evolved lavas at the base of the section. In addition, as already mentioned by Smewing et al. (1975) we note that the division between smectite-dominated alteration and hydrothermal alteration occurs approximately at the proposed UPL-LPL division. In fact, samples from the CY-1 drill hole of the ICRDG, which penetrate the UPL, show rare earth element patterns and abundances similar to those found for the fresh glasses and CY-2a samples, with no fractionation of the LREE/HREE ratio (filled diamond symbols in Figures 2.2, 2.4a and 2.4b, Auclair et al., in prep.). We therefore assume that the pattern and abundances found in the CY-2a and fresh glass samples are typical of the whole volcanic suite of the Troodos ophiolite. There appears to be no compelling arguments to invoke lithological variations to explain the cyclic variation.

The lavas in the CY-2a drill hole are massive and represent thick flows of up to 30 m. It could be suggested that the cyclic variation observed above represents sills of UPL magma emplaced in the upper sections of the LPL. However, only the uppermost unit in CY-2a is interpreted as a sill in the core descriptions. In addition, the constancy of the gradual change in individual cycles and the overall trend to higher MgO/TiO_2(mol) and lower abundances of HFS trace elements up the hole tend to discount this possibility.

The cyclic variation trend in CY-2a is interpreted

to reflect the effects of a variety of primary magmatic processes on the chemistry of the magma. The data require that magma in the conduit system feeding the CY-2a lava pile was gradually becoming more mafic (i.e., the background abundances of Ni and Zr, Y and the REE were increasing and decreasing, respectively). Superimposed upon this trend towards more mafic compositions are small scale fluctuations in the ratio of Ni relative to Zr and other incompatible elements which probably reflect an evolution from mafic (tholeiitic) to andesitic and tholeiitic-andesitic composition. These two trends are represented schematically in Figure 7.

Within the limits of the analytical precision the Zr/Y and La/Yb ratios for the CY-2a lavas and the fresh glass samples from both the UPL and LPL are indistinguishable despite a significant range in total abundances of Ni (150 to 5 ppm), Zr (125 to 15 ppm) and La (0.3 to 3.5 ppm). The processes controlling the magmatic evolution are therefore not fractionating incompatible elements and must involve mineral or fluid phases which have low KD's for these elements. This implies that the magma system was dominated by low pressure fractionation of phases such as olivine and plagioclase or that the melting process was buffered by low mineral phases with low KD's. The latter would require approximately equal melting intervals with melts being in equilibrium with an identical source mineralogy and this may be possible in situations involving extensive melting of a mantle having lost its more fertile components. This hypothesis was proposed by Duncan and Green (1980), suggesting that the pillow lavas of the Troodos ophiolite represent second stage melting of an already depleted source.

Robinson et al. (1983) and Schmincke et al. (1983) both invoke low pressure fractionation of olivine and plagioclase to explain variations in major element geochemistry and mineralogy of the two suites. However, they argued that differences between the two suites were too great to be accounted for by this process. All of the lavas plot on the low pressure cotectic defined by Walker et al. (1979). Although a contrived model involving coupled crystal fractionation and progressive partial melting can also explain the data, we prefer to interpret the observed variations to result from crystal fractionation. Both Nd (ranging from +5.5 to +7.5), and Pb isotopes show small variations (206/204: 18.597 - 18.704, 207/204: 15.553 - 15.590 and 208/204: 38.084 - 38.505) (Rautenschlein et al., 1984; 1985) in the fresh glasses, and the constant La/Yb and Zr/Y ratios discount petrogenetic models involving mixing of mantle sources, unless complete homogenization in a shallow magmatic reservoir under the ophiolite subsequently took place.

Huppert et al. (1982) and Sparks and Huppert (1984) both proposed a model where magma chambers below spreading centers were in a steady-state; the magma being supplied to the base of the magma chamber being balanced by the eruption of a more evolved magma from the top of the chamber. We propose a similar scenario for the magma chamber which fed the uppermost CY-2a lavas. The most evolved lavas of CY-2a represent the steady state situation in the low pressure magma system and their eruption was triggered by the influx of more primitive magmas. The fact that the more mafic magma becomes predominant during the eruptions towards the end of the effusive episodes in Troodos may reflect the gradual breakdown of the steady state magma chamber as a result of increasingly voluminous pulses of mafic magmas being supplied to the system. Each pulse would mix with the more evolved magma and cause the small scale fluctuations observed towards the top of the drill hole. Ultimately we must assume that a catastrophic breakdown of the low level magma chamber resulted from supply to the base that vastly exceeded the output of the system and resulted in the eruption of the olivine rich lavas of the LPL.

We suggest that all the lavas of the Troodos ophiolite are related to one, or a series of episodes of fusion, which melted an isotopically and geochemically homogeneous mantle. These magmas were filtered through a steady state low pressure magma system which gradually 'broke-down' resulting in gradual and ultimately a catastrophic evolution to more mafic lava compositions of the UPL.

However, studies of the plutonic sequence by Malpas (in prep.) suggest the presence of numerous isolated magma chambers, each with it's own evolution.

CONCLUSIONS

An evaluation of the primary geochemical variations with depth in ICRDG hole CY-2a in Cyprus has demonstrated a gradual evolution to more mafic compositions towards the top of the hole. Upon this large scale evolution are superimposed small-scale fluctuations in the abundances of incompatible and compatible trace elements. No trace element fractionation is observed between element pairs such as Zr/Y and La/Yb indicating that the variations most probably reflect low pressure fractionation of mineral phases such as olivine and plagioclase.

Both the systematic evolution to mafic compositions and the small scale geochemical fluctuations are interpreted to be a result of the gradual flooding of the low pressure magma system by mafic magmas. The stratigraphically lower lavas of the Troodos ophiolite evolved from tholeiite to andesite and dacite in a well developed low pressure magma system. This magma system was gradually

flooded by a more mafic (olivine-rich) magma. Fluxes of magma into the magma reservoir resulted in eruption of evolved lavas followed by an attempt by the magma reservoir to return to a steady state (the small scale fluctuations observed in CY-2a). Ultimately, the magma chamber was inundated by mafic magmas.

One particularly significant conclusion of this work is that, in contrast to the field evidences, the transition to mafic (olivine-rich) lavas in Troodos is gradual and can be explained by a model involving an evolving low pressure magma reservoir.

ACKNOWLEDGMENTS

This work represents part of the M.Sc. thesis of the senior author. Field and laboratory work was supported through the NSERC Operating and Collaborative Special Project programs. We would like to thank Ole Stecher and Jean Bèdard for reading the manuscript and for their constant encouragement. We acknowledge G. Gauthier and J.L. Bastien for analytical help at U. of M., and C. Langmuir for the plasma data of the fresh glasses. Critical comments by Drs P.T. Robinson, A. Panayiotou and C. Langmuir helped to greatly improve the manuscript and are acknowledged.

REFERENCES

Adamides, N.G.
1984: Cyprus volcanogenic sulfide deposits in relation to their environment of formation; unpublished Ph.D. thesis, University of Leicester, p. 1-383.

Auclair, F.
1986: Une études des variations géochimiques dans les laves de l'ophiolite Troodos, Chypre; unpublished M.Sc. thesis, Université de Montréal, p. 1-123.

Bear, L.M.
1960: The geology and mineral resources of the Akaki-Lythrodondha area; Cyprus Geological Survey Department, Ministry of Agriculture and Natural Resources, Memoir, no. 3, p. 1-122.

Douma, L. and Robinson, P.T.
1984: CY-1 Logbook; International Crustal Research Drilling Group, Center for Marine Geology, Halifax, Nova Scotia, Canada.

Duncan, R.A. and Green, D.H.
1980: Role of multistage melting in the formation of oceanic crust; Geology, v. 8, no. 1, p. 22-26.

Gass, I.G.
1968: Is the Troodos Massif of Cyprus a fragment of Mesozoic ocean floor?; Nature, v. 220, no. 5162, p. 39-42.

Humphris, S.E. and Thompson, G.
1978a: Trace element mobility during hydrothermal alteration of oceanic basalts; Geochimica et Cosmochimica Acta, v. 42, no. 1, p. 127-136.
1978b: Hydrothermal alteration of oceanic basalts by seawater; Geochimica et Cosmochimica Acta, v. 42, no. 1, p. 107-125.

Huppert, H.E., Turner, J.S. and Sparks, R.S.J.
1982: Replenished magma chambers: effects of compositional zonation and input rates; Earth and Planetary Science Letters, v. 57, no. 2, p. 345-357.

ICRDG
1984: Are Troodos deposits an East Pacific Analog?; Geotimes, v.29, no. 5, p. 12-14.

Irving, A.J.
1977: A review of experimental studies of crystal/liquid trace element partitioning; Geochimica and Cosmochimica Acta, v. 42, no. 6a, p. 743-770.

Ludden, J.N. and Thompson, G.
1979: An evaluation of the behavior of the rare earth elements during the weathering of sea-floor basalt; Earth and Planetary Science Letters, v. 43, no. 1, p. 85-92.

Moores, E.M. and Vine, F.J.
1971: The Troodos Massif, Cyprus, and other ophiolites as oceanic crust: evaluation and implications; *in* A Discussion on the Petrology of Igneous and Metamorphic Rocks from the Ocean Floor, Philosophical Transactions of the Royal Society of London, Series A, v. 268, p. 443-466.

Mottl, M.J.
1983: Metabasalts, axial hot springs, and the structure of hydrothermal systems at mid-ocean ridges; Geological Society of America, Bulletin, v. 94, no. 2, p. 161-180.

Mottl, M.J. and Holland, H.D.
1978: Chemical exchange during hydrothermal alteration of basalt by seawater. 1. Experimental results for major and minor components of seawater; Geochimica et Cosmochimica Acta, v. 42, no. 8, p. 1103-1115.

Parmentier, E.M. and Spooner, E.T.C.
1978: A theoretical study of hydrothermal convection and the origin of the ophiolitic sulphide ore deposits of Cyprus; Earth and Planetary Science Letters, v. 40, no. 1, p. 33-44.

Pearce, J.A. and Cann, J.R.
1971: Ophiolite origin investigated by discriminant analysis using Ti, Zr, and Y; Earth and Planetary Science Letters, v. 12, no. 3, p. 339-349.
1973: Tectonic setting of basic volcanic rocks determined using trace element analyses; Earth and Planetary Science Letters, v. 19, no. 1, p. 290-300.

Pearce, J.A. and Norry, M.J.
1979: Petrogenetic implications of Ti, Zr, Y, and Nb variations in volcanic rocks; Contributions to Mineralogy and Petrology, v. 69, no. 1, p. 33-47.

Pearce, T.H.
1968: A contribution to the theory of variation diagrams; Contributions to Mineralogy and Petrology, v. 19, p. 142-157.

Rautenschlein, M., Jenner, G.A., Hertogen, J., Hofmann, A.W., Kerrich, R., Schmincke, H.-U. and White, W.M.
1985: Isotopic and trace element composition of volcanic glasses from the Akaki Canyon, Cyprus: implications for the origin of the Troodos ophiolite; Earth and Planetary Science Letters, v. 75, no. 4, p. 369-383.

Rautenschlein, M., Jenner, G.A., Hofmann, A.W., White, W.M., Schmincke, H.-U. and Kerrich, R.
1984: Troodos glass chemistry - Sr, Nd, Pb, O isotopes and major and trace elements; Geological Association of Canada-Mineralogical Association of Canada (GAC-MAC), Meeting, Program with Abstracts, London, Ontario, Canada, 1984.

Robinson, P.T., Melson, W.G., O'Hearn, T. and Schmincke, H.-U.
1983: Volcanic glass compositions of the Troodos Ophiolite, Cyprus; Geology, v. 11, no. 7, p. 400-404.

Schmincke, H.-U., Rautenschlein, M., Robinson, P.T. and Mehegan, J.M.
1983: Troodos extrusive series of Cyprus: a comparison with oceanic crust; Geology, v. 11, no. 7, p. 405-409.

Smewing, J.D., Simonian, K.O. and Gass, I.G.
1975: Metabasalts from the Troodos Massif, Cyprus: genetic implication deduced from petrography and trace element geochemistry; Contributions to Mineralogy and Petrology, v. 51, p. 49-64.

Sparks, R.S.J. and Huppert, H.E.
1984: Density changes during the fractional crystallization of basaltic magmas: fluid dynamic implications; Contributions to Mineralogy and Petrology, v. 85, no. 3, p. 300-309.

Spooner, E.T.C.
1977: Hydrodynamic model for the origin of the ophiolitic cupriferous pyrite ore deposits of Cyprus; *in* Volcanic Processes in Ore Genesis; Geological Society of London, Special Publication, no. 7, p. 58-71.

Walker, D., Shibata, T. and DeLong, S.E.
1979: Abyssal tholeiites from the Oceanographer Fracture Zone. II. Phase equilibria and mixing; Contributions to Mineralogy and Petrology, v. 70, no. 2, p. 111-125.

Rock Magnetism, Oxide Petrography and Alteration State in Samples from CCSP Hole CY-2a through the Agrokipia 'B' Ore Body and Stockwork, Cyprus

JAMES M. HALL, THOMAS WARD AND BRIAN E. FISHER

Centre for Marine Geology, Dalhousie University, Halifax, N.S., Canada, B3H 3J5

Hall, J.M., Ward, T. and Fisher, B.E., Rock magnetism, oxide petrography and alteration state in samples from CCSP Hole CY-2a through the Agrokipia B Ore Body and Stockwork, Cyprus; in *Cyprus Crustal Study Project: Initial Report, Holes CY-2 and 2a, ed. P.T. Robinson, I.L. Gibson and A. Panayiotou; Geological Survey of Canada, Paper 85-29, p. 237-260, 1987.*

Abstract

A study has been made of the variation of saturation magnetization and its thermal decay in samples from Hole CY-2a through the Agrokipia 'B', Cyprus, orebody and its underlying stockwork. The ore body and its stockwork were probably formed by deposition from hot, mineralized, modified sea water, as on the present mid-ocean ridges. Alteration is assessed from the secondary mineralogy and by the state of Fe-Ti oxides. The 141-m-thick cap of unmineralized flows and glass intervals overlying the ore body shows moderate or low J_s values, depending on original lithology, and double Curie points, consistent with evidence for alteration by cold seawater. The mineralized and chloritized section from 154 to 297 m shows very low J_s, consistent with the other evidence for the nearly complete leaching of iron from primary Fe-Ti oxides. The propylitized dykes between 300 and 400 m depth are divided into an upper zone of very weak J_s, and a lower zone of variable J_s, in which leaching was followed by the formation of secondary magnetite, a feature that extends to 490 m depth into the underlying greenschist zone. From 490 to 689 m intense hydrothermal leaching of iron from oxides with corresponding very low J_s is ubiquitous. The results focus on the unusually high J_s values within the transition zone between 149 and 154 m, and suggest that the last phase of major dyke intrusion is represented by some of the dykes in the 315-490 m interval.

Résumé

Une étude a été effectuée sur la variation de l'aimantation de saturation et sur sa dégradation thermale sur des échantillons du trou de forage CY-2a traversant le gîte 'B' Agrokipia de Chypre et également le stockwerk sous-jacent. Le gîte et son stockwerk constituent possiblement un dépôt dont la précipitation provient d'une eau de mer modifiée, minéralisée, et chaude, telle que dans les crêtes médio-océaniques actuelles. Les minéraux secondaires et l'état des oxydes Fe-Ti permettent d'estimer le degré d'altération. Le gîte est recouvert par une couche formée de coulées nonminéralisées et de verres intercalés, d'une puissance de 141 m, qui fournit des valeurs de J_s, variant de faibles à modérées, dépendant de la lithologie originale, et des points Curie doubles, en accord avec les données qui attestent une altération par une eau de mer froide. Entre 154 et 297 m, les échantillons minéralisés et chloritisés sont caractérisés par des valeurs de J_s très faibles, en accord avec d'autres indices révélant un lessivage complet du fer des oxydes de Fe-Ti. Les dykes propylitisés entre 300 et 400 m de profondeur sont divisés en une zone supérieure avec des valeurs J_s très faibles, et en une zone inférieure avec des valeurs J_s variables, dans laquelle le lessivage fut suivi par la formation de magnétite secondaire, une particularité qui se continue jusqu'à 490 m de profondeur dans la zone des schistes verts sous-jacente. De 490 à 689 m, un lessivage hydrothermal intense du fer des oxydes et les valeurs correspondantes de J_s très faibles sont ubiquistes. Les résultats font ressortir des valeurs inhabituellement élevées de J_s à l'intérieur de la zone de transition, entre 149 et 154 m, et révèlent que la dernière phase d'intrusion de dykes est représentée par quelques dykes dans l'intervalle 315-490 m.

INTRODUCTION

This report describes one of a series of investigations of the variations of saturation magnetization and its temperature variation with depth in the Troodos ophiolite. In each crustal profile investigated, an attempt is made to separate, as controls on magnetic properties, the effects of variation in primary lithology and secondary alteration. This first report describes a section partly affected by high temperature fluid upwelling. Other reports describe a section of extrusives that experienced prolonged cold water drawdown and a section at the base of the Sheeted Complex where dyke rock-high temperature fluid interaction took place. Saturation magnetization and its thermal decay were measured routinely during these investigations. Oxide petrography, in conjunction with other studies of secondary alteration and mineralization, was used as the principal means of assessing alteration history.

The 689-m-deep continuously cored Cyprus Crustal Study Project Hole CY-2a was designed to sample the overlying cover, orebody and underlying stockwork zone of the Agrokipia B ore deposit, which lies within the extrusive sequence of the Troodos ophiolite, Cyprus (Bear, 1960; Constantinou, 1980; ICRDG, 1984). The rationale for the drill hole was to sample a section that was likely to show parallels in at least some important properties with the hydrothermal channelways beneath the high temperature vents, associated with sulphide ore deposition, on the present mid-ocean ridges (Oudin et al., 1981; Oudin and Constantinou, 1984). The section sampled consists of several clearly distinct primary constructional and alteration zones (L. Douma and P.T. Robinson, unpub. rep., 1983; Friedrich and Herzig, 1984):

Depth	
Drill collar:	At the boundary between Upper Pillow Lavas and Lower Pillow Lavas
000-109 m:	Massive flows, with a possible sill, in a smectite-carbonate alteration state
109-149 m:	As for 0-109, but with the addition of frequent intervals of massive glass
149-154 m:	Transition in alternating massive glass and basalt from smectite-carbonate to chloritic alteration
154-297 m:	Probably originally alternating massive lava and massive glass, now intensely altered to chlorite and mineralized with disseminated pyrite and sphalerite; locally massive ore, often associated with jasper and grey quartz; a thin, much less altered (smectite-carbonate), interval between 280 and 282 m is interpreted as a post-hydrothermal-activity dyke
297-689 m:	Largely dykes, with thin possible fault breccias in the uppermost 40 m and screens of pillowed and massive flow material in the 403 to 529 m interval; propylitic alteration, with chlorite, albite and sphene, characterizes the dykes between 297 and 403 m, whereas lower greenschist facies alteration, with epidote, chlorite, albite, sphene and calcite characterizes the 403-689 m interval

MEASUREMENTS

Measurements of saturation magnetization and Curie temperature were made using a vertical force Curie balance described in Ryall et al. (1977). Rock chips a few tens to a few hundred milligrams in weight were heated to 600-700°C at a rate of about 100°C/min in a nitrogen atmosphere while suspended from the microbalance between the pole pieces of an electromagnet. Temperature and mass were recorded continuously using an X-Y plotter. Many of the more weakly magnetic samples showed paramagnetic or weight change effects during thermal cycling that greatly exceeded the signal from any ferrimagnetic component, and, as described below, some care was needed to isolate ferrimagnetic effects. Uncertainties in well defined Curie points are typically +5°C, increasing to +10°C where Curie points are not strongly developed. Uncertainties in saturation magnetization range from +1% for high J_s samples to +10% for low J_s hydrothermally altered material.

Oxide petrographic information was obtained through the examination of polished thin sections using a Reichert Zeto-Pan Pol microscope with an oil immersion objective at a magnification of 1350 diameters.

MAGNETIC PROPERTIES

0-109 m

Largely massive basaltic flows capped by a possible sill with a thin hyaloclastite (Unit 7.01) and occasional thin glass partings.

Saturation magnetization in this interval ranges from 0.06 emu/g to 2.5 emu/g (Figure 2). Two-thirds of the values, however, fall in the 0.6 to 1.4 emu/g interval with an average value for these crystalline samples of 1.0 + 0.4 (1sd) emu/g. The three hyaloclastite and two other glassy samples all show low J_s ($0.06 < J_s < 0.13$ emu/g). The mean value for the crystalline samples is close to the value of 1.1 + 0.3 emu/g found for the massive flows among the

TABLE 1. Saturation magnetization and Curie points of samples from Cyprus Crustal Study Project Hole CY-2a.

Depth(m)	Unit, Description	J_s(emu/g)	T_c(°C)	Comments
6.85	1.01 massive basalt, probably flow, may be	1.36	345*,(485)	small wl
9.45	intrusive. Grey (carbonate) alteration	2.49	340*,510	small wl, l<h
13.65		0.96	335*,465	small wl, l>h
20.25		0.67	340*,(520)	small wl
27.65		1.01	400	small wl, l<<h
28.45		0.67	295	small wl, almost reversible
30.18		0.66	370*,530	small wl
30.75	7.01 hyaloclastite, carbonate clay	0.13	165p	large wl
30.90	alteration	0.06	435	large wl
31.02		0.08	160p	large wl
31.46	7.02 dark gray fg aphyric basalt carbonates, clay	1.35	480	large wl
33.18	8.02 aphyric basalt probably a massive	1.06	340*,530*	large wl, l<<h
35.65	flow clay-carbonate alteration	1.32	345*,505	moderate wl, l<h
38.30	9.01 fg aphyric basalt	1.32	350*,515	moderate wl, l<h
39.35	carbonate (clay)	1.39	340*,507	moderate wl, l<h
43.75	9.02 dk grey, fg, aphyric	1.81	335*,470	small wl, l=h
46.00	basalt carbonate-clay	0.09	145p,595	large wl, l=h
46.30	10.01 grey fg, aphyric,	1.38	340*,510	large wl, l<h
50.50	mod variation basalt	1.43	340*,505	small wl, l=h
54.55		1.21	520	large wl, l<<h
55.50		0.69	350,535*	large wl, l<h
57.15		0.69	340*,515	large wl, l<<h
59.85		0.81	355*,545	large wl, l<h
64.05		0.84	350*,515	large wl, l<h
64.90		0.70	530	large wl, l<<h
65.35		0.98	310*,(475)	small weight gain
68.50	15.01 greenish grey aphyric	0.87	295*,(470)	small wl
71.65	sp. vesic. massive basalt	0.74	345*,(495)	small wl
75.40	clay carbonate	0.50	555	large wl
80.30		0.91	350*,500	mod. wl, l<h
81.50		0.69	340*,540	large wl, l<h
83.68		0.22	280*,(495)	small wl
88.85		1.19	350*,555	large wl, l<h
90.05	21.01 light grey fg aphyric basalt carbonate-clay, ?soil gypsum	1.61	510	large wl, l<<h
91.75	21.02 aphyric basalt clay-carbonate	1.07	335*,505	small wl, l=h
92.50	21.03 grey to brown aphyric altered glass	0.11	175p?	large wl
94.20	21.04 light grey, fg, aphyric basalt	1.06	475	large wl, l<<h

Depth(m)	Unit, Description	J_s(emu/g)	T_c(°C)	Comments
97.00	22.01 med grey, fg, aphyric	0.91	500	large wl
97.30	basalt clay-carbonate	1.26	325*,(505)	small wl
97.60		0.79	475	large wl
97.85		0.85	495	small wl
98.10	23.01 grey, fg, aphyric basalt	0.38	475*	moderate wl, l<h
98.15		0.29	480*	large wl, l<h
100.70		1.24	525*	large wl, l<h
102.60	24.01 lt. grey fg, aphyric basalt	0.89	335*,480	small wl, l=h
103.30	carbonate-clay-zeolite	0.68	300*,485	moderate wl, l<h
105.00		0.85	490	large wl
110.55	25.01 black to greenish grey-brown, aphyric, massive, altered glass	0.07	210p	large wl
111.25	25.02 greenish grey, very fg	1.00	495	large wl
111.55	aphyric basalt, clay-carbonate	1.00	545	large wl
113.10	25.03 rubble with glass clay-zeolite	0.06	215p	large wl
113.55		0.06	220p	large wl
114.20		0.14	180p	large wl
115.50	26.01 fg aphyric massive pebbly basalt	0.91	370,435*	large wl
116.30	26.02 altered massive glass, clay	0.09	190p	large wl
116.55	26.04 highly alt aphyric massive glass clay	0.14	200p	large wl
117.50	26.05 v lg, sp. phyric, massive basalt clays	0.94	360,490	mod wl, l=h, no cooling curve
117.85		1.32	340*,(510)	small wl
118.75	27.01 highly alt aphyric glass, clays	0.07	205p	large wl
118.95	27.03 highly alt aphyric glass	0.10	195p	large wl
119.15	clay-zeolite	0.09	230p	large wl
119.80		0.28	330	large wl
121.40	27.05 highly altered massive glass, clays	0.13	230p	large wl
124.15		0.06	285p	large wl
125.70	28.01 brownish grey, very fg, aphyric, massive basalt, clay-zeolite	0.24	180p?,340	large wl, l<h
126.50	28.02 mostly glass, clay-zeolite	0.07	220p	large wl
128.00	29.01 very fg opaque basalt, clay	1.28	360*,505	moderate wl, l=h
131.20		1.43	345*,(470)	small wl
133.85	30.01 very fg aphyric massive basalt, clay	1.47	345,490	small wl, l=h
135.65	30.02 highly altered massive glass, clay	0.06	265p	large wl
136.70		0.10	240p	large wl
137.21		0.06	290p	large wl

Depth(m)	Unit, Description	J_s(emu/g)	T_c(°C)	Comments
137.85	31.01 fg-aphyric massive basalt,	1.20	350*,525	moderate wl, l<h
138.40	smectite, celadonite, (zeolite)	0.99	370*,510	moderate wl, l=h
139.05		0.74	365	large wl
139.32		1.31	350*,(465)	small weight gain
140.00		1.21	360*,485	small wl, l=h
140.30		1.13	365*,(470)	small wl
140.90		0.09	205p	large wl, glass type behaviour but not described as glass
141.45		1.54		
141.65	32.01 aphyric, highly altered, massive glass, smectite	0.10	255p	large wl
141.75	32.02 fg, aphyric basalt, smectite	0.49	485	large wl
142.58	32.03 aphyric, highly altered, massive glass, smectite	0.19	310p	large wl
142.70	32.04 aphyric massive basalt, locally	1.03	(340)*,465	small wl
143.45	aphanitic, smectite, celadonite	1.17	415*,490	moderate wl, l=h
147.50		1.53	370*,495	moderate wl, l=h
149.00-149.10	33.01 transitional from massive basalt to altered glass, now green clay	0.23	440	
149.20		0.33	465*	moderate wl, Curie point lower in cooling curve
149.30	33.02 fg aphanitic aphyric, massive basalt, clay, celadonite, chlorite vein linings	0.58	(320),465	moderate wl, l<h, intermediate Curie point in cooling curve
149.40		0.26	200p?,480	large wl, Curie temp. lower in cooling curve
149.70		1.21	360*,505	large wl, l<h
150.40		2.08	365,500*	moderate wl, l<h
151.00		1.60	355*,475	small wl, l=h
151.20		1.38	350*,490	small wl, l=h
151.40		1.29	350*,480	small wl, l=h
151.60		2.78	470	small wl, reduction J_s in moment and appearance of lower T_c or para magnetic behaviour during cooling
152.20		1.87	(375)*,415	moderate wl, l=h
152.80		0.41	520	small wl
153.40		1.88	(355)*,580	moderate wl, l<h
153.50		2.61	225*,490	small wl
153.80a		0.95	535	small wl

Depth(m)	Unit, Description	J_s(emu/g)	T_c(°C)	Comments
153.80b	33.02	1.76	490	small wl
153.95		0.08	260p	large wl
154.00		0.58	515	small wl, cooling curve also shows lower infleate, ?paramagnetism
154.20		0.71	510	small wl
154.25	35.01 brownish-grey, aphyric, altered lava, chloritic, pyrite	2.21	570	moderate wl
154.40		0.28	510	small wl, lower T_c component much stronger relatively in cooling curve
154.65		0.03	205p?,(560)	m, pt
154.75		0.05	235p	large wl, m, pt
156.05		0.04	200p,(595)	large wl, m, pt
156.60	35.02 ? altered glass, 157.40-158.70 ? originally massive flow, chloritized	0.07	215p,(625)	large wl, pt
156.91		0.007		
157.05		0.04	225p	large wl, cooling curve not recorded
157.90		1.49	635	moderate wl, l<h
158.68		0.07	160p,(580)*	large wl, m, pt
159.35	36.02 Probably originally continuous with 36.01, but more intensely altered.	0.07	225p	large wl, pt
153.37		0.002		
161.19		0.06		
161.20		0.06	200p,(605)	large wl, m, pt
161.30		0.06	230p,(635)	large wl, m, pt
164.15-164.20		0.05	(630)	large wl, m, pt
165.35	37.01 chloritized massive lava	0.05	170p	large wl, (m), pt
165.88		0.10	205p,(595)	large wl
166.65		0.16	610	large wl, m, pt
168.60-168.70	38.03 chloritized massive glass	0.13	505	large wl
169.82	38.04 chloritized massive glass with marine material	0.02	(645)	large wl, pt
170.20		0.03	(655)	large wl, pt
170.40		0.03	(660)	large wl, pt
170.70		0.02	(630)	large wl, pt
170.75		0.03	(650)	large wl, pt

Depth(m)	Unit, Description	J_s(emu/g)	T_c(°C)	Comments
171.00	39.01 chloritized massive lava	0.10	(610)	large wl, m, pt
171.20		0.07	(600)	large wl, m, pt
172.70		0.16	605	
173.66		0.14		
174.50		0.14	(615)?	large wl, m, pt
175.30	40.01 chloritized massive glass	0.08	165p,(595)	large wl, pt
175.95		0.01	200p,(660)	large wl, pt
177.00		0.10	240p,(630)	large wl, m, pt
179.00		0.05	(650)	large wl, m, pt
179.80	40.02 chloritized, no origin suggested	0.09	(600)	large wl, m, pt
181.85		0.02	(640)	large wl, (m), pt
183.50		0.002		
183.70	41.01 chloritized massive glass	0.02	(630)	large wl, pt
184.60		0.06	(620)(705)	large wl, m, pt
185.55	42.02	0.01		large wl, pt
188.60-188.70		0.02	655	
189.20		0.20		
190.20	43.01 chloritized massive glass	0.17	(610)	large wl, m, pt
192.60	43.03 chloritized massive flow	0.04	(655)	large wl, pt
193.10		0.003		
196.30-196.40	43.05 chloritized glass	0.10	(640)	large wl, m, pt
197.00	44.01 chloritized massive flow	0.08	(595)	large wl, pt
198.65	44.02 chloritized massive flow	0.01	(665)	large wl, pt
202.25		0.08	(600)	large wl, pt
204.60		0.04	(600)	large wl, pt
205.75	46.01 chloritized massive glass	0.06	(640)	large wl, m, pt
207.00		0.006		
209.75	46.02 highly mineralized material	0.03	(610)	large wl, pt
214.75	46.03 ? chloritized brecciated glass	0.08	(660)	large wl, m, pt
215.70	47.01 chloritized massive flow	0.05	(600)	large wl, pt
216.60		0.15	(555)	large wl, m, pt
218.60		0.07	(610)	large wl, m, pt
219.40	48.01 ? chloritized highly mineralized glass	0.03	(655)	large wl, pt
220.90	48.02 ?chloritized massive lava	0.14	(600)	large wl, m, pt
221.10		0.07	(595)	large wl, m, pt

Depth(m)	Unit, Description	J_s(emu/g)	T_c(°C)	Comments
222.50	48.03 ? chloritized massive glass	0.03	(635)	large wl, pt
224.60	(224.60-224.70)	0.02		large wl, pt
226.20		0.03		large wl, pt
228.75		0.05	(610)	large wl, pt
229.50	49.01 grey pyritic ore	0.005		large wl, pt
231.40	50.02 chloritized ? massive glass	0.02	(630)	large wl, pt
232.00		0.03	(645)	large wl, pt
234.00	50.05 chloritized ? massive flow	0.05	(645)	large wl, pt
234.20		0.06	645	large wl, pt
235.75	51.02 chloritized ? massive glass	0.01	(600)	large wl, pt
237.25	51.04 chloritized ? massive flow	0.07	(595)	large wl, m, pt
239.35	51.05 chloritized ? massive glass	0.15	(625)	large wl, m, pt
241.25	52.01 chloritized	0.06	(645)	large wl, m, NB: no pt
243.00	52.02 chloritized ? massive glass	0.04	(640)	large wl, pt
243.05		0.02		
244.45	53.01 chloritized ? massive glass	0.08	(635)	large wl, pt
246.85	53.05 chloritized	0.004		
247.70	53.06 chloritized	0.07		
248.05		0.09		
248.70	54.01 chloritized	0.001		
249.65	54.02 red, massive pyritic ore	0.001		
251.20	54.03 chloritized	0.03		
253.30	54.05 possible relatively less altered chloritized dyke	0.09	555	
254.00	54.06 chloritized ? massive glass	0.003		
255.10		0.003		
255.50		0.003		
256.70	55.02 chloritized	0.14		
258.00	56.01 chloritized, mineralized?, massive glass	0.07		
258.35		0.01		
258.90	56.02 chloritized ? massive flow	0.02		
260.10		0.06		
260.40		0.05	(660)	
260.82-260.90	56.03 chloritized ?massive glass	0.01		

Depth(m)	Unit, Description	J_s(emu/g)	T_c(°C)	Comments
261.50	56.04 chloritized ? massive lava	0.06		
262.20-262.25	57.02 chloritized ? massive lava	0.04		
262.60		0.08		
263.50		0.002		
265.00	57.04 chloritized ? massive lava	0.05		
265.10		0.07		
268.05	57.05 chloritized ? massive glass	0.01		
268.70		0.05		
270.00		0.06		
270.40		0.06		
270.62		0.10		
271.66		0.08		
272.10	58.01 massive ore with jasper	0.001		
272.60		0.01		
275.25	59.01 chloritized	0.12	715	
275.42	59.03 chloritized, intensely mineralized zone	0.002		
277.20	59.04 chloritized ? massive flow	0.10		
277.75		0.03		
277.85		0.07		
279.30-279.35	60.01 chloritized ? massive glass	0.03		
279.70-279.80		0.01		
282.45	60.03 basalt dyke, clay (carbonate)	1.32	495	almost exactly reversible
282.90	66.03 chloritized	0.10		
283.45	67.01 bleached, mineralized chloritic zone	0.01		
285.00	67.02 silicified, mineralized zone	0.07		
285.05		0.08		
285.60-285.70	67.04 chloritized	0.12		
286.35	67.05 chloritized	0.05		
288.50	67.06 silicified, chloritized, jasper	0.004		
289.50	68.01 chloritized	0.06		
290.30-290.40		0.002		
292.50	68.02 possibly a pre-alteration intrusion	0.11		

Depth(m)	Unit, Description	J_s(emu/g)	T_c(°C)	Comments
296.50	68.03 chloritized basalt breccia	0.06		
297.26	69.01 fault + breccia and gouge	0.15		
298.95	69.04 medium grey, medium grained, aphyric basalt, chlorite, pyrite	0.08		
299.30	69.05 chloritized	0.06	660	
301.78	69.08 greenish grey aphyric basalt,	0.09		
302.45	possibly a dyke, chlorite	0.07		
304.35	70.02 light grey, diabase basaltic indention albite-chlorite	0.09		
306.15-306.20	71.01 aphyric massive basalt, albite-chlorite	0.08		
307.76	71.03 aphyric basalt, albite-chlorite	0.07		
309.23	71.04 massive lt grey aphyric basalt,	0.08		
310.00	albite-chlorite	0.07		
310.20		1.12		
310.40		0.38		
312.18		0.08		
312.50	72.01 fg aphyric basalt, chloritic	0.08		
316.10	73.07 lt grey, highly brecciated altered basalt, clay-silica-pyrite	0.12		
316.60	73.08 lt grey, mg, altered massive phyric	0.10		
323.33	basalt albite-chlorite	0.07		
324.80	75.01 grey, fg altered basalt, chlorite, etc.	0.03		
326.00-326.05	75.03 aphanitic to mg, grey, altered aphyric basalt, albite, etc.	0.002		
329.55	76.03 grey, massive, aphyric basalt, chlorite, etc.	0.08		
331.72	77.01 lt grey massive, aphyric basalt, albite, etc.	0.07		
332.23	77.02 grey, aphanitic aphyric lava, chloritic	0.11		
332.85		0.08		
333.51	77.04 grey massive aphyric basalt, albite, etc.	0.10		
333.90		0.03		
335.55		0.07	645	
341.45	79.01 cream-grey, fg, aphyric basalt dyke, altered	0.04		

Depth(m)	Unit, Description	J_s(emu/g)	T_c(°C)	Comments
345.00		0.03		
350.45		2.45		
350.55		2.09	560*	large wl, T_c lower in cooling curve
352.58-352.60	81.02 aphanitic aphyric massive basalt, chloritic	0.09		
355.15	82.01 lt grey, fg, massive aphyric basalt, chlorite	0.17		large wl, T_c indeterm.
356.58		0.12		
359.65		1.68	565	large wl
361.55-361.65	83.02 grey fg aphyric massive basalt dyke, ?alteration	2.27	565	moderate wl
362.28	83.03 grey, f-mg, aphyric massive basalt ? chlorite-albite ? part mineralization	3.01	570	
364.59		2.87	560	
368.02		1.41	550	
369.82		2.09	565	
372.27-372.30		0.22	560,*715	
373.17		2.06	540	
375.87-376.00		0.79	535	large wl
378.43	86.03 grey green basalt, albite, etc.	0.06		
378.65		0.63		
378.95		0.77	570	moderate wl
382.44	87.02 grey f-mg aphyric basalt, albite, etc.	2.42	565	moderate wl
382.73		1.77	550	small wl
384.31-384.35	88.01 grey, fg, massive basalt, albite, etc.	3.77	535	
385.33		2.92	565	small wl, partial e type curve
386.40		1.12		
393.48	90.02 grey, fg, v.s. phyric massive basalt, chlorite ? flow or dykes	2.14	(445)*,570	small wl, partial e type curve
397.33	91.01 grey f-mg massive basalt ? flow, chlorite, etc.	0.90	570	moderate wl
403.88-403.93	92.03 grey green altered massive glass, chlorite, etc.	1.15	555	large wl
404.40		0.86	565,685	
404.50		0.07		
406.78	93.03 green grey aphyric mineralized basalt, chlorite, etc.	0.14		
406.85		0.07		
408.90	93.06 altered and mineralized glassy rock, chlorite, etc.	0.12		

Depth(m)	Unit, Description	J_s(emu/g)	T_c(°C)	Comments
409.10	93.07 grey massive basalt chlorite and epidote	0.09		
413.75	94.04 grey aphyric intrusive basalt, chlorite, etc.	1.45	560	moderate wl, suggestion of partial to type behaviour
417.25-417.30		0.08		
426.15-426.20	97.02 grey-green, fg, aphyric ? basalt altered (? chlorite)	0.09		
433.30	98.03 grey, aphyric, fg, ? basalt (? chlorite)	0.09		
436.90	99.01 grey green fg aphyric ? basalt ? pillow	0.08	615	
446.25	100.05 grey, fg, aphyric massive ? basalt, chlorite, etc.			
449.00-449.02		0.09		
450.55-450.60	101.01 greenish-grey, fg, aphyric, massive ? basalt, ? chlorite, etc.	0.09		
461.55		0.07		
463.10-463.15	104.02 ? basalt, breccia, chlorite, etc.	0.11		
469.05	104.07 grey-green, massive aphyric ? dyke, chlorite, etc.	2.93	555	
482.30-482.35	107.03 grey, fg, aphyric pillow basalt, chlorite, etc	0.44	485	large wl
482.80-482.84		2.04	560	small wl
486.00-486.10	108.03 grey, fg, aphyric massive flow, chlorite, etc.	1.38	560	small wl
503.09		0.04	630	
510.80	112.03 grey, f-mg aphyric basalt, chlorite, etc.	0.09		
514.75	113.02 grey fg aphyric massive ? basalt flow, chlorite, etc.	0.11	630	
515.70-515.75	113.03 grey, fg, aphyric massive ? basalt flow, chlorite, etc.	0.10	560	
520.20	113.04 massive aphyric, lt grey green vesic. basalt flow, chlorite, etc.	0.09	630	
526.45	115.20 grey green aphyric ? massive flow, chlorite, etc.	0.12	610	
552.47-552.49		0.09	650	

Depth(m)	Unit, Description	J_s(emu/g)	T_c(°C)	Comments
561.02- 561.04	102.02 fg, aphyric, grey ? diabase, ? dyke, chlorite, etc.	0.05	190p,675	
578.60	124.01 lt. grey, fg, aphyric, basalt dyke, chlorite, etc.	0.12	640	
581.60- 581.62	125.01 fg, aphyric, grey, ? diabase dyke, chlorite, etc.	0.02		
583.60- 583.62	125.03 probably the same as 125.01	0.03		large wl
589.78- 589.80	126.02 massive lt. grey aphyric basalt chlorite, etc.	0.08	180	large wl, pt p or e type
590.49- 590.51	127.01 grey vesicular basalt dyke, chlorite, etc.	0.11	(615)	large wl, pt
593.10 594.62- 594.64	127.03 mg vesicular dark grey basaltic dyke, chlorite, etc.	0.14 0.18	(620) 515	large wl large wl, m, pt
598.54- 598.56	127.04 lt greenish grey fg aphyric massive dyke, chlorite, etc.	0.15	(590)	large wl, pt
615.25		0.11	650	
643.90 647.00- 647.02	137.03 greenish grey fg *phyric basalt ? dyke, chlorite, etc.	0.06 0.12	660 530	 large wl, m, pt
653.68- 653.70	138.05 f-mg grey green aphyric basalt ? dyke, chlorite, etc.	0.07	(590)	large wl, m, pt
677.74	142.022 breccia, chlorite, etc.	0.07	(625)	large wl, m (pt not tested)
678.42	143.02 breccia, chlorite, etc.	0.15	565	small wl
685.65- 685.70	143.03 f-mg light grey aphyric diabase dyke, chlorite, etc.	0.09	245	pt
687.12- 687.15	144.01 grey-green mineralized basalt breccia, chlorite, etc.	0.16	585	moderate wl, m, pt
688.89- 688.94 689.10	145.01 green grey fg ? basalt, chlorite, etc.	0.11 0.07	550 (625)	large wl large wl, m, pt

wl: weight loss, l: lower Curie point component of J_s, h: higher Curie point component of J_s, Curie point in brackets: weakly developed component, p following a value in the Curie point column: broad inflexion point during assumed decay of paramagnetism, * in Curie point column: Curie point only present in heating segment of thermal cycle, m: probable magnetite produced during heating, pt: probable pyrrhotite produced during heating

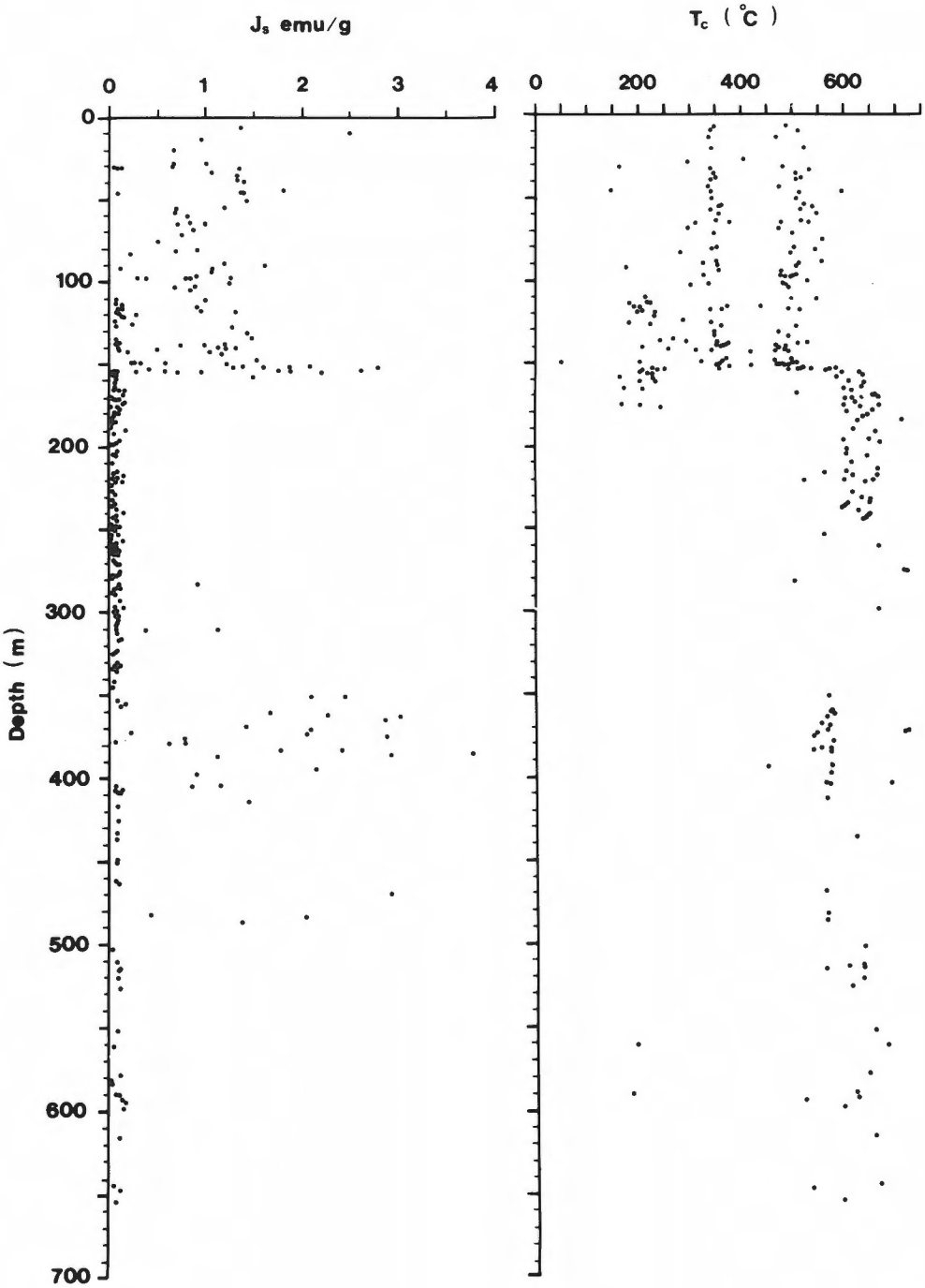

Figure 1: Profiles of J_s and Curie temperature.

Lower Pillow Lavas in the lower half of the drill hole CY-1 section and the massive flows in DSDP drill holes 319A, 417D and 418A (Wang et al., in prep.).

The thermal decay of J_s in this interval generally shows the presence of two Curie points, one usually close to 340°C and the other close to or a little over 500°C (Figures 2 and 3c). A small number of samples show either a single low or a single high Curie point. For several of the double Curie point samples, e.g. 17.20 m, 65.35 m, 83.68 m, etc. (Figure 3b), the higher Curie point phase is clearly an artifact produced by phase splitting during the heating process and this may also be the case for other high Curie point components. Cycling to 600°C results in complete phase splitting for all double Curie point samples; only a single high Curie point phase is evident during cooling. This instability during thermomagnetic cycling is typical of fairly highly cation deficient titanomagnetites both in other extrusives from Troodos and in extrusives from in-situ oceanic crust (Hall and Ryall, 1977), and is consistent with the smectite-carbonate alteration for this interval evident from the presence of single phase oxide minerals (see below). As indicated above, a smaller number of samples show either single low or high Curie points. The sample at 28.45 m (Figure 3a) is typical of the single low Curie point group with a Curie temperature of 295°C. In-situ oceanic basalt samples with Curie points of less than about 250°C generally show perfect or substantial reversibility during thermal cycling, a function of their lower degree of cation deficiency. That the occasional CY-2a samples with Curie points of up to 300°C show almost reversible J_s-T curves suggests a slightly lower ulvöspinel component in their composition than in mid-ocean ridge basalt titanomagnetites. The glass samples generally show gentle concave flexures centred on about 200°C together with very large weight loss during heating. It is thought that this concavity represents paramagnetic rather than ferrimagnetic behaviour.

109-149 m

Alternating massive basaltic flows and massive glass. Saturation magnetization in this interval is strongly bimodal in its distribution, with a sharp peak for $J_s<0.2$ emu/g and a broader peak for $0.8<J_s<1.6$ emu/g. The two peaks correspond closely to the two lithologies that alternate throughout the interval; the lower value peak to altered massive glass and the higher value peak to fine grained, aphyric, massive basalt. Two samples described as basalt fall in the lower range. Of these, the sample from 140.90 m depth (J_s: 0.09 emu/g) lies well within aphyric massive basalt unit 31.01, and no indication is given in the Core Description (L. Douma and P.T. Robinson, unpub. rep., 1983) of the presence of another lithology at this depth. The other sample in this lower interval, at 125.70 m, differs notably from typical aphyric basalt in being located within a zone of alteration with celadonite and heulandite. The thermal decay of saturation magnetization also shows two distinct styles in this interval. The aphyric massive basalt commonly shows two Curie points in the heating part of the cycle. The lower (340-380°C) values overlap but are a little higher on average than the lower peak in the 0 to 109 m interval. The higher (480-520°C) values coincide with the central part of the higher temperature range for the 0-109 m interval. In contrast, the glass or altered glass samples show a broad concave inflexion in the 200-300°C range together with large weight loss during cycling. This inflexion is interpreted as being the result of paramagnetic rather than ferrimagnetic behaviour.

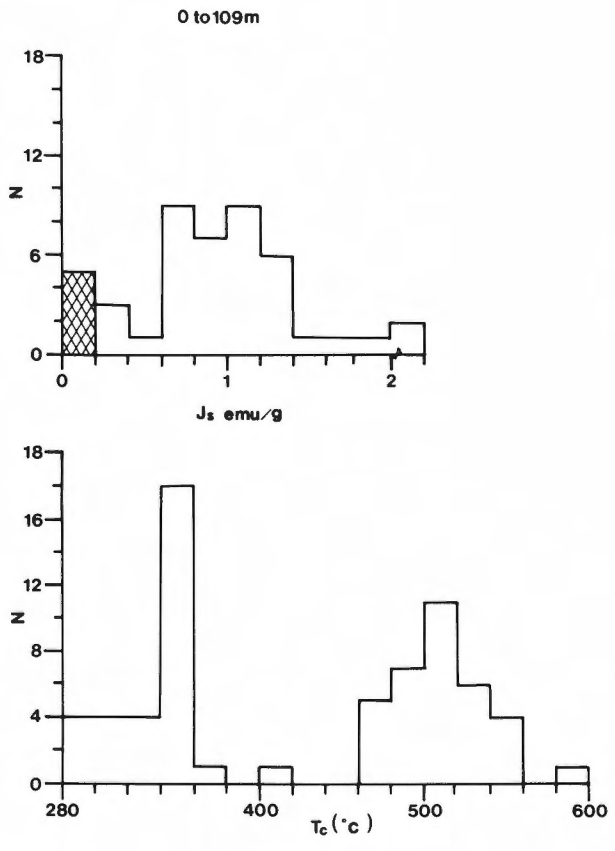

Figure 2: Distribution of J_s and Curie temperature in the 0 to 109 m interval. N is the number of samples in each J_s or T_c interval.

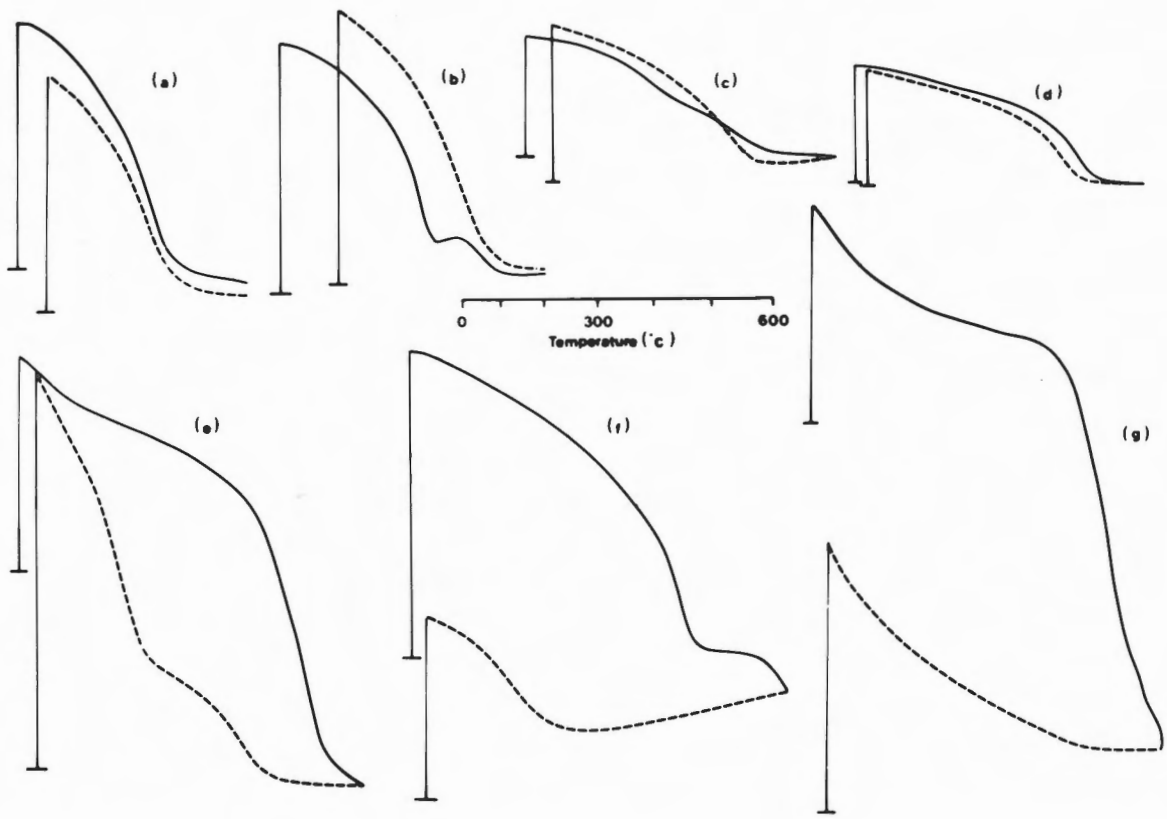

Figure 3: Variety of styles of thermal decay of J_s in the CY-2a section. Continuous Line: Heating Curve; Broken Line: Cooling Curve. Vertical scale is apparent weight with scale variable:equipment sensitivity adjusted to provide optimum signal for each sample.

(a) 28.45 m. J_s: 0.67 emu/g. T_c: 295°C. Almost reversible behaviour.

(b) 139.32 m. J_s: 1.31 emu/g. T_c: 350°C. Production of a new phase commences just above the Curie point. Experience elsewhere indicates that this is the result of the phase splitting of a highly cation deficient single phase. Phase splitting is complete before cooling commences.

(c) 50.50 m. J_s: 1.43 emu/g. T_c: 340, 510°C. The clear inflection in the heating curve is interpreted as the lower Curie point. The higher Curie point phase may be produced during heating since the lower Curie point phase is absent during cooling.

(d) 282.45 m. J_s: 0.91 emu/g. T_c: 495°C. Almost exactly reversible behaviour with negligible weight change. Postmineralization dyke.

(e) 166.65 m. J_s: 0.161 emu/g. Large weight loss in argillized mineralized massive glass. The Curie points present in the cooling curve suggest that both magnetite and pyrrhotite are produced from pyrite during thermal cycling.

(f) 350.55 m. J_s: 2.09 emu/g. T_c: 560°C. Large weight change in high J_s sample from the top of the variably magnetized interval.

(g) 593.10 m. J_s: 0.14 emu/g. Paramagnetic behaviour and large weight loss are evident during the thermal cycling of this sample.

149-154 m

Three units, two of massive glass with an intervening aphyric massive basalt, comprise this interval. The interval contains the transition from smectite-carbonate to argillic alteration. The massive basalt, unit 33.02, is notable for relatively high J_s values, typically in the 1.5 to 2.8 emu/g range, or double the average value for massive basalt intervals higher in the section. Unusually high initial susceptibility, measured on the drill core with a hand held meter, and unusually high remanent intensities (Auerbach, 1984), also characterize this unit. Two origins are possible for this high magnetization: relatively high primary oxide content, as is occasionally seen higher in the section, or the presence of additional, secondary oxide, perhaps associated with the proximity of chloritic alteration conditions. Experimentation to select between these explanations is currently under way. The Curie point distribution for the massive basalt samples closely resembles the distribution for similar material in the 109-149 m interval (Figure 4).

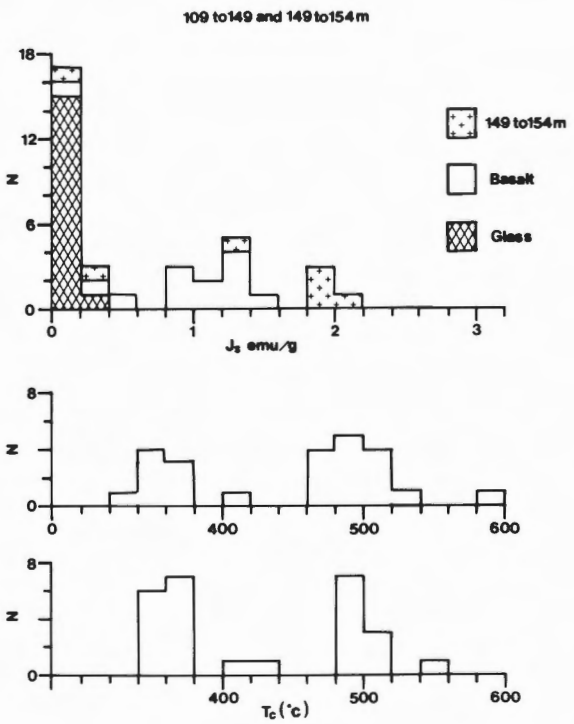

Figure 4: J_s and Curie temperature distributions for the 109 to 149 m and 149 to 154 m intervals. N is the number of samples in each J_s or T_c interval. Upper histogram: J_s distribution for 109 to 154 m interval. Lower histogram: Curie point distributions for the 109 to 149 m and 149 to 154 m intervals, respectively.

154-297 m

Argillized alternating massive basalt and massive glass comprise this interval. A thin post-mineralization dyke showing smectite-carbonate alteration occurs at 280-282 m.

Saturation magnetization in this interval is generally very low, being everywhere equal to or less than 0.2 emu/g except in the 154-158 m interval, and in the post-mineralization dyke at 280-282 m. The high J_s sample at 154.25 m is from massive basalt located almost exactly at the boundary between restricted, vein type, and pervasive, chloritic alteration. A second high J_s sample at 157.90 m is also from massive basalt, now largely chloritized. Both of these strongly magnetized samples show thermal variation of J_s that resembles less altered massive basalts from higher in the section, and it is suggested that they owe their magnetic properties to incomplete chloritization of the uppermost few metres of this interval. Within the long interval below 158 m with J_s equal to or less than 0.2 emu/g, there is a weak preference for chloritized massive basalts to have higher J_s than chloritized massive glass intervals (Figure 5). Massive ore samples are generally very weakly magnetized, with J_s usually equal to or less than 0.02.

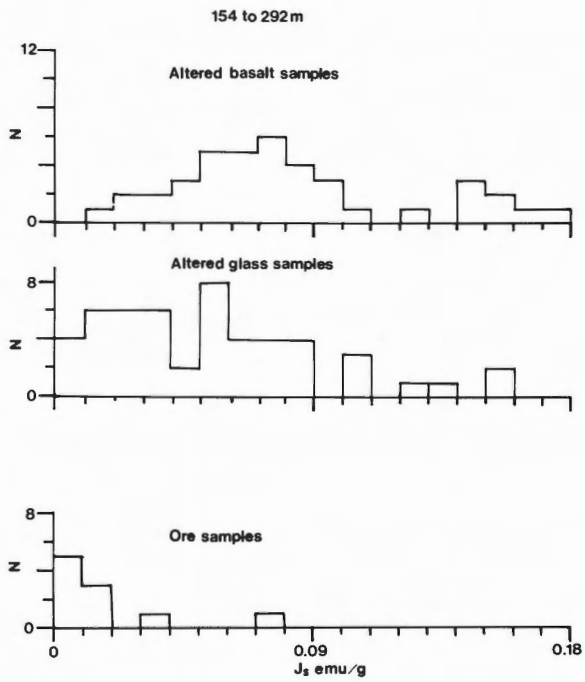

Figure 5: The distribution of J_s for chloritized massive basalt, chloritized massive glass, and ore grade material in the 154 to 292 m interval.

Large weight loss during heating is an important effect for the chloritized samples in this interval, and since the Curie balance is arranged so that the magnetic force producing an apparent weight change is in a vertical sense, the weight loss effect obscures the magnetic signal when J_s <0.1 emu/g, which is the case for most samples in this interval (Figure 3e). Careful estimation of change in weight with temperature shows that weight loss becomes important above about 500°C. Where weight loss is either not excessive or has been allowed for, a 500-600°C Curie point is evident, superimposed on the general paramagnetic behaviour of samples (Figure 6). While this figure illustrates a strong weight loss effect, it also shows that correction for weight loss leaves a residual change in base level during thermal cycling that cannot, at present, be accounted for. During cooling, many samples in this interval develop very strong magnetization. The Curie points present in the cooling curves suggest the ubiquitous production of pyrrhotite, often with a higher Curie point component, possibly corresponding to almost pure magnetite (Figure 3e).

The post-mineralization dyke at 280-282 m (Figure 3d) shows strong saturation magnetization values of 0.91 and 1.48 emu/g and an almost exactly reversible thermal cycle, with negligible weight change and a single Curie point at 495/500°C. These properties are similar to those of a number of massive basalts at depths of less than 154 m and are consistent with the observed smectite-carbonate state of alteration of the dyke.

297-689 m

(a) Propylitic Alteration Zone, 297-400 m

This interval consists of dykes, with thin possible fault breccias in the upper 40 m, now largely replaced by quartz and chlorite with some albite and pyrite, i.e. a propylitic type of alteration.

Saturation magnetization in the dykes forming the uppermost 50 m of this interval is, with two exceptions, low, i.e. less than 0.15 emu/g. This upper interval, then, is largely indistinguishable in this regard from most of the overlying interval of chloritized massive flows and glass. Saturation magnetization between 350 m and 403 m is strongly variable, with very low values alternating with values in the 0.75 <J_s<3.75 emu/g range. It is notable that intervals of high and low J_s do not always correspond to cooling units. While one thin unit (81.02) has a single low J_s value and seven units (79.04, 83.02, 86.02, 87.02, 88.01, 90.02 and 91.01) show only strong J_s values, three units (82.01, 86.03 and 92.03) show both high and very low J_s values, as does unit 94.04, located between 413 and 425 m. This pattern of J_s values suggests that the magnetic mineralogy and magnetization of the dykes in the 350-425 m interval may not be entirely of primary origin. A weak inverse relationship between J_s and weight loss (Figure 7) suggests that most, if not all, the high J_s samples have experienced at least partial hydrothermal alteration, with consequent reduction of original J_s values. Since this relationship is presently not well defined, it is perhaps most useful at this time to use the presence of weight loss as an indicator of hydrothermal alteration.

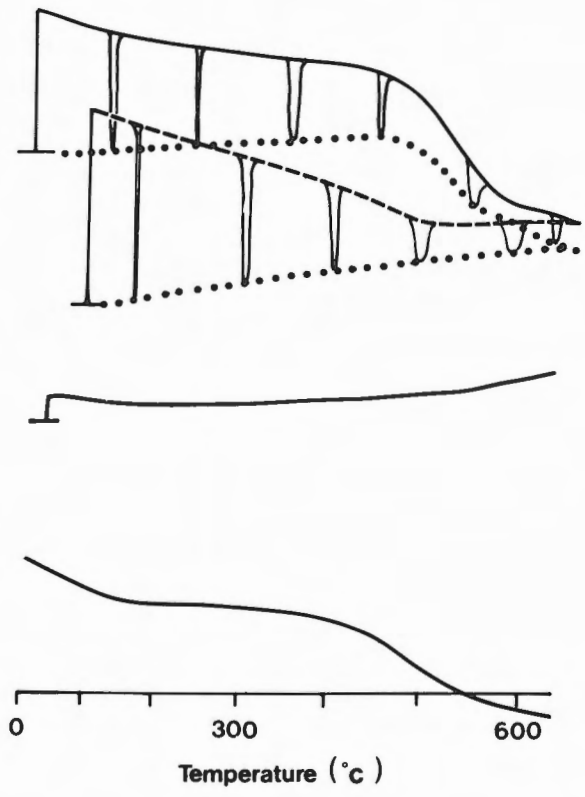

Figure 6: Weight loss behaviour during thermal cycling. Vertical scale is apparent weight for all three graphs. Upper graph: Continuous line: Heating Cycle, the narrow downwards troughs marking short time periods during which the magnetizing field was reduced to zero; Broken line: Cooling cycle; Dotted line: weight change of sample during cycling; Middle graph: apparent weight change during cycling of quartz sample holder; Lower graph: residual signal after correction for weight change of sample and sample holder.

Curie temperatures are indeterminate for the low J_s samples between 297 and 350 m. For the stronger samples between 350 and 425 m, Curie temperatures are mostly in the 535 to 570°C interval. One sample, at 393.48 m depth from Unit 90.02, has a double Curie point heating curve, the lower Curie point being at 445°C.

(b) Greenschist Alteration Zone, 400-689 m

This interval consists of dykes with screens of pillowed and massive flows to 529 m, below which only dykes occur.

Saturation magnetization below 425 m is everywhere less than 0.2 emu/g in this interval, except for the three samples between 482 and 486 m where it ranges from 0.44 to 2.04 emu/g in a sequence of pillows, perhaps with minor intrusives, underlain by a massive flow. Curie temperatures for both the stronger, lower two samples in this 4-m thick interval is 560°C, with small weight loss. A number of the low J_s samples below 600 m are sufficiently strong for a Curie point to be identified, with poorly defined values ranging from 530 to 630°C. Large weight loss is typical for these samples, as is the apparent generation of either or both pyrrhotite and magnetite during thermal cycling.

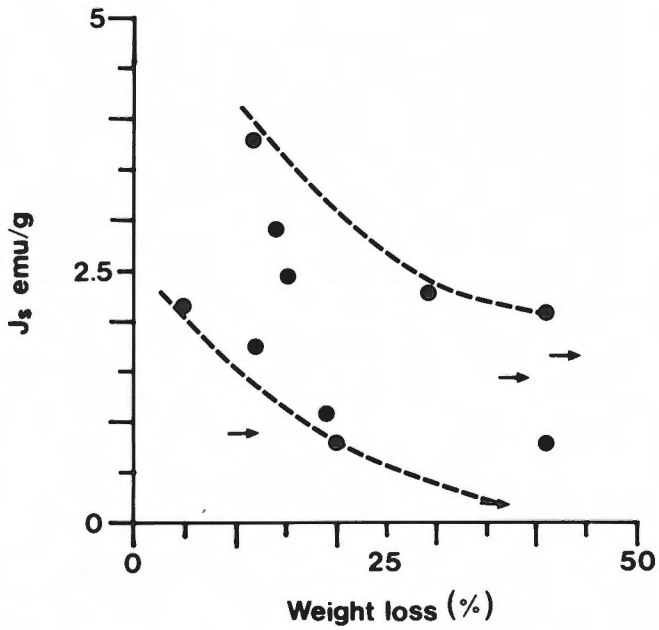

Figure 7: The relationship between J_s and weight loss in the interval of rapid property variation between 350 and 490 m. Arrows indicate minimum values of weight loss and the broken lines outline the field in which the data occurs.

OXIDE PETROGRAPHY

Twenty-one polished thin sections have been examined for the presence and state of Fe-Ti oxides to aid in the interpretation of magnetic properties. The observations suggest that the CY-2a section can be divided into four main zones that correspond in part to the alteration intervals recognized by Friedrich and Herzig (1984) and others, and to the magnetization intervals described above. Four samples from 9 to 141 m all show the characteristics of low temperature cold seawater type alteration, in particular, the curved cracking, and crack infilling that indicate a moderate cation deficient state for the Fe-Ti oxides (Figure 8a). Alteration of this type is consistent with J_s values of about 1 emu/g and double Curie point behaviour during thermal cycling. A similar combination of Fe-Ti oxide and magnetic properties is typical for in-situ oceanic crust and is also seen in the lower half of the CY-1 drill hole profile (Wang et al., 1984; in prep.). Unit 60.03/66.02, described as a post-mineralization dyke with clay-carbonate alteration, shows oxide evidence for alteration of this low temperature type.

Five samples between 182 and 336 m all show clear indications of extensive hydrothermal alteration in the almost complete removal of iron from Fe-Ti oxides, leaving anatase (TiO_2) pseudomorphs after titanomagnetite. These pseudomorphs retain the probable outline of the original Fe-Ti oxides in samples at 181.85 m and 218.60 m, suggesting that less complete reorganization of the primary phases occurred in the upper 50-100 m of the chloritized interval (Figure 8b). Both magnetization and oxides show no break in properties at the chlorite-propylite break at 300 m. Instead, a sharp change in properties occurs at close to 350 m.

Three samples between 368 and 397 m contain abundant magnetite, as does another sample at 469 m, separated from the 368-397 m group by a magnetite-free sample at 437 m. The presence of anatase pseudomorphs, granulation, sphene inclusions, recrystallization and possible secondary magnetite overgrowths (Figure 8c) indicates that this interval has experienced a complex history of high temperature, initial cooling, oxidation followed by variable hydrothermal alteration, and the formation of the largely secondary magnetite. In addition, there are areas of finely intergrown light and dark phases with a vermiform texture, sometimes alternating with the granulation texture. This additional secondary intergrowth texture may indicate a further stage of alteration. The sequence of events is similar to that already observed within the part of the Sheeted Complex comprising the uppermost 600 m of drill hole CY-4 section (Agrawal et al., 1984; in prep.). The presence of abundant secondary magnetite in the samples between 368 and 397 m is consistent with the dominance of relatively higher J_s values in this

TABLE 2. Oxide petrography of samples from Cyprus Crustal Study Project Hole CY-2a.

Sample (m)	Unit, Description	Fe-Ti	Other Opaque Phases
9.45	1.01 massive basalt, clay-carbonate alteration	Zone A Abundant light grey-brown skeletal titanomagnetite showing stages 1 to 3 low temperature alteration, i.e. curved cracking and crack infilling.	Rare, small sulphides
35.65	8.02 aphyric basalt, massive flow, clay-carbonate alteration		
111.55	25.02 aphyric massive basalt clay-carbonate alteration		
140.90	31.01 aphyric massive basalt clay-carbonate-celadonite-zeolite alteration		
181.85	40.02 chloritized massive lava	Zone B Oxides small and rare except in the post-mineralization dyke. Abundant anatase pseudomorphs after primary magnetite. The pseudomorphs are sharply defined at 189.85 and 218.60 and have euhedral to subhedral forms. Elsewhere the pseudomorphs have diffuse outline.	Abundant large sulphides
218.60	47.01 chloritized massive lava		
260.40	56.02 chloritized massive lava		
282.45	60.03/66.02 post-mineralization dyke		
299.30	69.05 chloritized/propylitized rock of uncertain origin		
335.55	77.04 propylitized dyke		
368.02	83.03 variably altered, possibly post mineralization dyke	Zone C Abundant magnetite showing moderate hydrothermal alteration. Anatase pseudomorphs, sphene inclusions and possible secondary over-growths imply several stages of alteration.	Sulphide common
373.17	85.01 propylitized basalt		
397.33	91.01 propylitized basalt		
436.90	99.01 greenschist facies pillow basalt	No Fe-Ti oxides, diffuse anatase pseudomorphs after Ti-magnetite common. Similar to Zone B or D alteration state.	Sulphides very common
469.05	104.07 greenschist facies dyke	Very common strongly granulated magnetite containing sphene inclusions. No anatase pseudomorphs. Resembles Zone C samples.	No sulphides
503.09	110.02 greenschist facies metabasalt	Zone D Magnetite rare and small. Anatase pseudomorphs of the diffuse type are common. Small hematite grains are disseminated at 689.10	Sulphides generally abundant
552.47	119.04 greenschist facies dyke		
578.60	124.01 greenschist facies		
615.25	130.01 greenschist facies dyke		
643.90	136.01		
689.10	145.01 greenschist facies metabasalt		

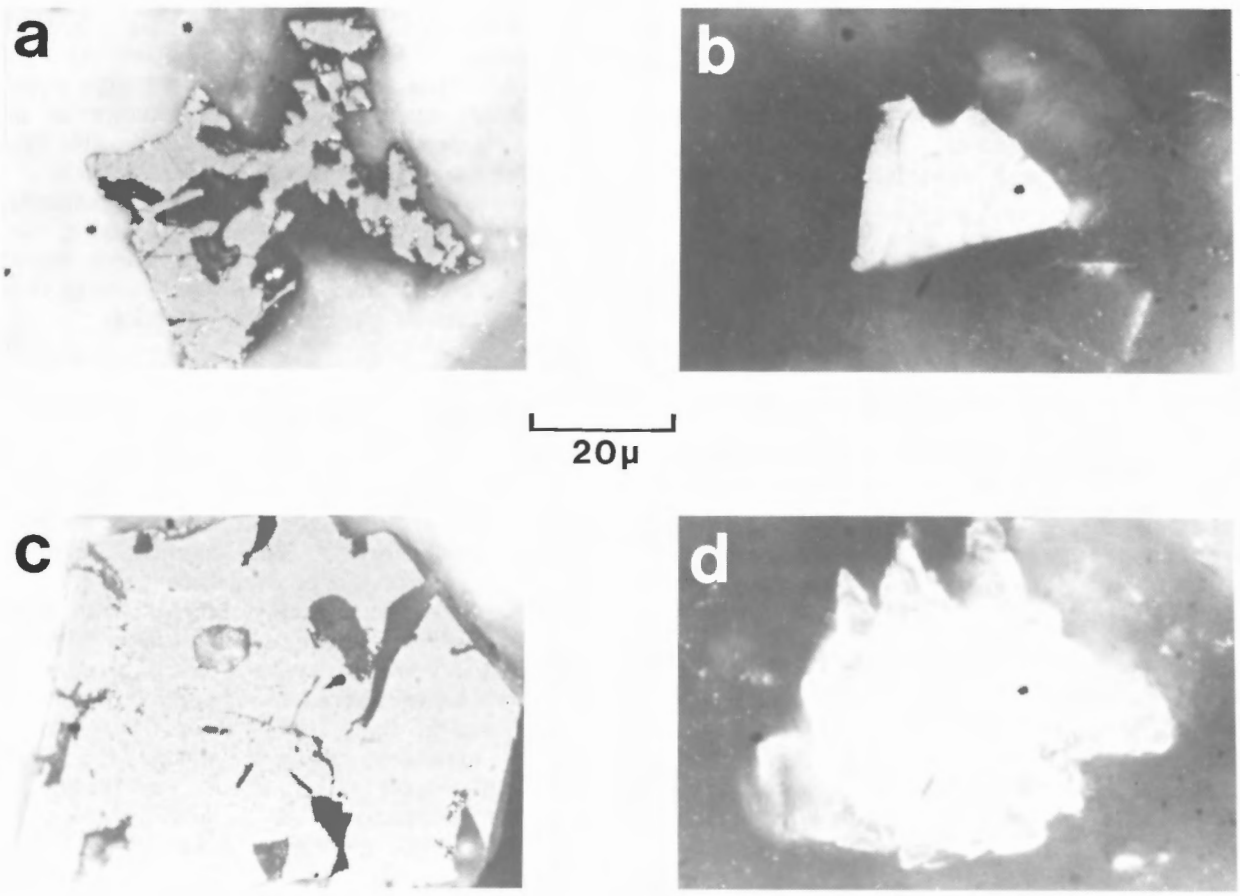

Figure 8:
(a) Cyprus, Hole Cy-2a: 140.90 m depth (grey to greenish- and brownish-grey, fine-grained to aphanitic, aphyric, massive basalt). Uniform brown skeletal titanomagnetite, with some cracking, indicating a degree of cation deficiency in a slightly red stained groundmass.

(b) Cyprus, Hole Cy-2a: 218.60 m depth (light grey, massive altered lava). This is an anatase pseudomorph after a titanomagnetite. Much of the primary texture is preserved, i.e. subhedral to euhedral form with curved cracks as the result of earlier low temperature alteration.

(c) Cyprus, Hole Cy-2a: 469.05 m depth (light grey-green, medium grained, massive, aphyric, pervasively altered dyke). This was probably a deuteric oxidation class 2 titanomagnetite in which the ilmenite lamellae were later replaced by sphene, and granulation formed where TiO_2 was still present in the magnetite as the result of hydrothermal alteration. The grain has been substantially recrystallized resulting in the breakdown of the lamellae and the aggregation and expulsion of the sphene to the grain boundaries.

(d) Cyprus, Hole Cy-2a: 615.25 m depth (light grey, medium-grained, slightly vesicular altered basalt dyke). This is an anatase pseudomorph of diffuse form after a primary titanomagnetite. None of the original structure is preserved.

interval, and with the indication, from the 535-570°C Curie points, of a low titanium content for this magnetite.

Six samples from the 503 to 689 m interval all contain anatase pseudomorphs, of diffuse form, after Fe-Ti oxides (Figure 8d), indicating an intense hydrothermal leaching history. Only rare, small grains of magnetite occur. The observations are consistent with the low J_s values found throughout the interval.

SUMMARY AND DISCUSSION

The CY-2a section shows a number of clearly defined alteration zones based on magnetic oxides some of which correspond to those defined by the distribution of secondary silicate minerals. In others, two or more zones may lie within silicate alteration mineral zones. The types of alteration present are known from other areas in Cyprus and the present oceans, and the conditions of formation, with the exceptions noted below, are reasonably well understood. The zones are:

0-149 m: Moderate J_s (about 1 emu/g) except where glass occurs, where J_s is low (<0.2 emu/g). Double Curie points are common during thermal cycling, with the irreversible lower (about 350°C) Curie point and the cracking of titanomagnetite grains, indicating a moderate to high degree of cation deficiency. All of these features are consistent with alteration by cold seawater.

149-154 m: The same as the 0-149 m interval, except that for the one massive basalt in the interval, J_s is almost double the value for similar units in the higher interval. These high values may be due either to coincidental local variation in primary nature or to alteration related to the proximity of the underlying chloritized zone. Evidence to allow a choice between these possibilities is currently being sought.

154-350 m: Weak J_s and single high Curie points, where measurable, are consistent with the petrographic evidence for intense leaching by high temperature fluids. Only the thin, post-mineralization dyke at 282 m has not been altered in this way. The top of this zone corresponds to the top of the zone of chloritic alteration, whereas the base lies near the middle of the 100-m-thick propylitic alteration zone.

350-490 m: This is a zone of rapid variation in properties with intervals of strong saturation magnetization (from 0.5 to 3.8 emu/g) alternating with intervals of weak magnetization (J_s equal to or less than 0.2 emu/g). Similar variation is seen in remanence intensity and initial susceptibility (Auerbach, 1984). Petrographic examination of the Fe-Ti oxides shows a complicated history for this interval. The low J_s samples contain only anatase pseudomorphs, indicating intense hydrothermal leaching. The high J_s samples also contain pseudomorphs with, in addition, variable amounts of secondary magnetite of a type known to postdate leaching, some of which shows the possible effects of further moderate hydrothermal alteration. Curie temperatures for high J_s samples are generally equal to or greater than 500°C. As noted above, the upper boundary of this zone is located within the zone of propylitic alteration. The lower boundary is located within the zone of greenschist alteration.

490-689 m: Intense leaching of Fe-Ti oxides, with corresponding weak magnetization, characterizes this interval.

It is evident from the above that the present magnetic and oxide characteristics reflect the alteration history. The physical conditions of alteration are reasonably well known for several of the zones. Thus, the low temperature, seawater alteration of the 0-149 m interval and of the post-mineralization dyke at 280-282 m, appears closely comparable with the well known alteration of uppermost in-situ oceanic crust seen in many studies of basaltic extrusives and minor extrusives recovered during the Deep Sea Drilling Project (e.g. Honnorez, 1981). Again, anatase pseudomorphs after Fe-Ti oxides are known from depths of more than 3 km in Icelandic crust, where it is estimated that hydrothermal alteration took place at temperatures in excess of 250°C (Hall, 1985).

An unusual feature of the CY-2a section is the close proximity of zones with very disparate alteration histories. Similar abrupt juxtaposition of zones is also seen in DSDP Hole 504B (Anderson et al., 1982; Kinoshita et al., 1985) where an 18-m-thick mineralized stockwork occurs within a thick pillow sequence. The stockwork zone is characterized by J_s, J_n and K an order of magnitude or more weaker than in the overlying pillows, whereas the underlying sequence shows rapid property variation. For example, in the CY-2a section rocks only altered by cold (about 10°C) seawater are separated from rocks that have experienced chloritic alteration (equal to or greater than 200°C) by a 6-m-thick transition zone. The proximity of zones with very different alteration histories focuses attention on two interesting intervals:

1. The transition zone from 149 to 154 m.
2. The zone of rapid property variation between 350 and 490 m.

The transition zone from 149 to 154 m shows similar Curie points to the overlying 109-149 m

interval but unusually strong J_s values for the one massive basalt in the interval. Auerbach (1984) also finds unusual properties for this interval; high J_n and K, and probable reverse polarity in a sequence that is largely normally magnetized.

The zone of rapid property variation between 350 and 490 m shows a range of unusual features. Although J_s values are comparable to values for the massive basalts in the 0 to 154 m interval, it is clear from the petrographic work that the 350-490 m interval has experienced more intense and complex alteration than the 0-154 m interval. Study of the Sheeted Complex in drill hole CY-4 (Agrawal et al., 1984; in prep.) indicates that the high J_s, secondary magnetite bearing samples in the 350-490 m interval may have experienced an alteration paragenesis along these lines:

(i) Deuteric oxidation during initial cooling leading to the subsolidus exsolution of ilmenite lamellae in titanomagnetite
(ii) Locally intense leaching of Fe-Ti oxides leading to the formation of anatase pseudomorphs
(iii) Hydrothermal alteration of remaining magnetites leading to the replacement of lamellar ilmenite by sphene and the formation of TiO_2 granules in the magnetite
(iv) Possible development of magnetite overgrowths, the result of secondary oxide deposition and partial recrystallization of the remaining primary oxides leading to the incomplete aggregation and expulsion of sphene and possibly granules

Agrawal et al. (in prep.) suggest that alteration stage (iv) is the result of thermal metamorphism following nearby dyke intrusion. Since no less-altered dykes, comparable with the dyke at 280-282 m, are preserved in the 350-490 m interval, thermal metamorphism, if it occurred, must have been followed by alteration stage (v) of the dykes responsible for the thermal pulse. It is suggested that some of the dykes in this interval were intruded towards the end of igneous and hydrothermal activity in the area, a situation that also may account for the occurrence of mixed polarity units within the interval (Auerbach, 1984). In these circumstances alteration stage (v) represents the effect of waning hydrothermal activity following the last major period of dyke intrusion at the CY-2a location.

ACKNOWLEDGMENTS

The authors acknowledge the International Crustal Research Drilling Group for the opportunity to participate in the Cyprus Crustal Study Project and in particular to take part in the investigation of the paleohydrothermal systems associated with massive sulfide ore bodies. Ulrich Bleil, Peter Herzig and Stefan Auerbach provided valuable comparative information. We also acknowledge the financial support of Dalhousie University, NSERC (Canada) through grants G0741, A4652, A9917 and A7812 and the International Development Research Centre (Ottawa) through contract 3-P-83-1021. The manuscript was typed by Jane Barrett. Lata Hall drew the figures. We are grateful for the assistance of all these colleagues. Publication No. 20, Centre for Marine Geology, Dalhousie University.

REFERENCES

Agrawal, V.D. and Hall, J.M.
1984: Cyprus drill hole CY-4: magnetization and alteration of the lower part of the Sheeted Complex of the Troodos ophiolite; Geological Association of Canada, Program with Abstracts, v. 9, p. 41.

Anderson, R.N., Honnorez, J., Becker, K., Adamson, A.C., Alt, J.C., Emmermann, R., Kempton, P.D., Kinoshita, H., Laverne, C., Mottl, M.J. and Newmark, R.L.
1982: DSDP Hole 504B, the first reference section over 1 km through Layer 2 of the oceanic crust; Nature, v. 300, p. 589-594.

Auerbach, S.T.
1984: Magnetische untersuchungen eines fossilen ozeanischen hydrothermal-systems in Troodos-Ophiolith (Zypern); unpublished thesis, Ruhr-Universität, Bochum, p. 1-179.

Bear, L.M.
1960: The geology and mineral resources of the Akaki-Lythrodondha area; Cyprus Geological Survey Department, Ministry of Agriculture and Natural Resources, Memoir, no. 3, p. 1-122.

Constantinou, G.
1980: Metallogenesis associated with the Troodos ophiolite; *in* Ophiolites: Proceedings of the International Ophiolite Symposium, Cyprus, 1979, ed. A Panayiotou, Cyprus Geological Survey Department, Ministry of Agriculture and Natural Resources, p. 663-674.

Friedrich, G.H. and Herzig, P.M.
1984: Sulfide mineralization, alteration and chemistry of a fossil hydrothermal system in the Troodos ophiolite, Cyprus; Geological Association of Canada, Program with Abstracts, v. 9, p. 64.

Hall, J.M.
1985: The Iceland Research Drilling Project crustal section: variation of magnetic properties with depth in Icelandic-type oceanic crust; Canadian Journal of Earth Sciences, v. 22, no. 1, p. 85-101.

Hall, J.M. and Ryall, P.J.C.
1977: Rock magnetism of basement rocks, Leg 37; *in* Initial Reports of the Deep Sea Drilling Project, Volume 37, ed. F. Aumento, W.G. Melson et al.; U.S. Government Printing Office, Washington, D.C., v. 37, p. 489-501.

Honnorez, J.
1981: The aging of the oceanic crust at low temperature; *in* The Sea; Ideas and Observations on Progress in the Study of the Seas, Volume 7, The Oceanic Lithosphere, ed. C. Emiliani; John Wiley and Sons, New York, N.Y., v. 7, p. 525-587.

ICRDG
1984: Are Troodos deposits an East Pacific analog?; Geotimes, v. 29, no. 5, p. 12-14.

Kinoshita, H., Furuta, T. and Kawahata, H.
1985: Magnetic properties and alteration in basalt, Hole 504B, Deep Sea Drilling Project Leg 83; *in* Initial Reports of the Deep Sea Drilling Project, Volume 83, ed. R.N. Anderson, J. Honnorez, K. Becker, et al.; U.S. Government Printing Office, Washington, D.C., v. 83, p. 331-338.

Oudin, E. and Constantinou, G.
1984: Black smoker chimney fragments in Cyprus sulphide deposits; Nature, v. 308, p. 349-353.

Oudin, E., Picot, P. and Pouit, G.
1981: Comparison of sulphide deposits from the East Pacific Rise and Cyprus; Nature, v. 291, no. 5814, p. 404-407.

Ryall, P.J.C., Hall, J.M., Clark, J. and Milligan, T.
1977: Magnetization of oceanic crustal layer 2 - results and thoughts after DSDP Leg 37; Canadian Journal of Earth Sciences, v. 14, no.4, pt. 2, p. 684-706.

Wang, B-I., Walls, C. and Hall, J.M.
1984: Cyprus drill hole CY-1: oxide petrography, magnetic properties and alteration in a section through the uppermost half kilometer of Troodos type oceanic crust; Geological Association of Canada, Program with Abstracts, v. 9, p. 114.

Magnetic Properties Variation at the Upper Boundary of the Agrokipia 'B' Ore Deposit, Troodos Ophiolite, Cyprus

GUENTHER SCHOENHARTING

Institute of General Geology, Copenhagen University, Copenhagen, Denmark

Schoenharting, G., Magnetic properties variation at the upper boundary of the Agrokipia 'B' Ore Deposit, Troodos Ophiolite, Cyprus; in *Cyprus Crustal Study Project: Initial Report, Holes CY-2 and 2a, ed. P.T. Robinson, I.L. Gibson and A. Panayiotou; Geological Survey of Canada, Paper 85-29, p. 261-265, 1987.*

Abstract

Magnetic properties of samples from drill core CY-2a change dramatically over a transitional zone several metres thick from relatively fresh to highly altered and mineralized lava flows. The change occurs within a single massive flow, which apparently capped the underlying hydrothermal circulation system. Natural remanent magnetization reaches maximum values of more than 100 A/m in the relatively fresh flow and decreases downward to values of less than 1 A/m at the top of the ore body. In the relatively fresh rocks, titanomagnetites are oxidized probably by reaction with cold seawater. The oxidation style changes rapidly with depth and close to the bottom of the massive flow a fairly stable maghemite with strong magnetization and apparent Curie point of about 590 to 610°C is present. The maghemite is recognized from thermobalance results, low field and strong field magnetic properties, and from microscopic observations. The occurrence of anomalous stable inclination values, including reverse polarities in the lower half of the massive flow may be explained by the presence of the secondary maghemite. It is not clear whether the reverse polarity was caused by maghemite formation during a reversed earth magnetic field period or by a self reversal process that may be related to magnetic fields within oxidized titanomagnetites consisting of two different compositions.

Résumé

Les propriétés magnétiques des échantillons du trou de forage CY-2a varient brusquement à l'intérieur d'une zone de transition de quelques mètres d'épaisseur marquant le passage des coulées de lave relativement fraîches à celles fortement altérées et minéralisées. Le changement apparaît au sein d'une même coulée massive laquelle apparemment coiffe le système de circulation hydrothermale sous-jacent. L'aimantation rémanente naturelle atteint des valeurs maximales dépassant 100 A/m dans la coulée relativement fraîche et les valeurs décroissent jusqu'à moins de 1 A/m au sommet du corps minéralisé. Dans les roches relativement fraîches, les titanomagnétites sont oxydées possiblement par une réaction avec l'eau de mer froide. Le style d'oxydation change rapidement selon la profondeur et se termine à la base de la coulée massive avec la présence d'une maghémite relativement stable et fortement aimantée dont le point Curie apparent est compris entre 590 et 610°C. La maghémite est identifiée par les données obtenues à la thermobalance, par les propriétés magnétiques sous champ faible et sous champ intense, et par les observations au microscope. L'apparition de valeurs stables mais anomales de l'inclinaison, incluant les polarités inverses dans la moitié inférieure de la coulé massive, peut être expliquée par la présence de maghémite secondaire. Il n'est pas évident que l'inversion de la polarité puisse résulter soit de la formation de la maghémite durant la période d'inversion du champ magnétique terrestre ou soit d'un processus d'auto-inversion qui serait relié aux champs magnétiques au sein des titanomagnétites oxydées ayant deux compositions différentes.

INTRODUCTION

Magnetic susceptibility values and remanence of igneous rock samples in the upper portion of CY-2a drill core increase gradually downhole until maximum values are reached immediately above the highly altered zone representing the Agrokipia 'B' sulfide ore deposit (Hall et al., 1987). Starting a few metres above this boundary magnetization values decrease to less than 1% of the maximum values at the top of the ore body. This paper reports some results of ongoing investigations of the magnetization in this 5-m-thick interval. This study may help to explain anomalous magnetization around sulfide deposits (e.g. Johnson et al., 1982) and assist in developing magnetic exploration methods. In addition, the changes in the magnetic signature above the ore deposit may be viewed as a compressed record of a general downward magnetic trend, caused by thermal and chemical alteration of magnetic minerals as the ore forming hydrothermal fluids brought temperatures and low oxygen pressures unusually high up in the oceanic crust. On the other hand, the processes of alteration and/or secondary formation of magnetic minerals in hydrothermal areas may differ significantly from those of seawater drawdown as sampled in drill hole CY-1 (Wang et al., 1984). Thus, this study may also contribute to the problem of vertical and lateral variation of magnetization in oceanic crust.

The investigated interval in CY-2a consists mainly of flow unit 33.02 (L. Douma and P.T. Robinson, unpub. rept., 1983), which is described as a grey to brownish-grey, fine-grained to aphanitic, aphyric massive basalt. The upper contact at 149.20 m is at the base of a layer of highly altered, aphyric glass about 0.70 m thick. The lower contact at 154.24 m is the top of unit 35.01, a brownish-grey aphyric massive flow characterized by 95% groundmass argillic alteration and pyrite and sphalerite concentrations of 2% and 1% respectively. In comparison, groundmass alteration in unit 33.02 averages about 40% and sulfides comprise less than 1%.

SAMPLING AND MEASUREMENTS

The general paleomagnetic and rock magnetic properties of CY-2a drill core have been reported by Hall et al. (1987) and Smith and Vine (1987). In order to enhance the resolution in the 5-m-thick interval above the Agrokipia 'B' ore zone, 12 samples were taken, four of them orientated with respect to up and down. Routine magnetic measurements were conducted in the laboratory comparing natural remanent magnetization (NRM), af-cleaned remanence in peak magnetic fields of up to $4.8.10^4$ A/m (600 Oe), magnetic susceptibility and remanence.

Saturation magnetization as a function of temperature from -180°C to 650°C was measured with a horizontal translation balance in air as well as in argon to determine Curie points. Eight polished sections were prepared and a ferrocolloid was used to outline strongly magnetic zones within the magnetic minerals.

RESULTS AND DISCUSSION

Paleomagnetic and rock magnetic results of the oriented samples are presented in Table 1. Two remanence directions of opposite polarities were found in all of the four samples investigated, however, only the 2 lowermost samples have end-values of reverse polarity. The uppermost sample contains only a weak reversed component, which cannot be sufficiently separated from the normal component by af cleaning. Inspection of vector plots of NRM after stepwise demagnetization indicates also a third, normal component of remanence, which is considerably less stable than the other two. This soft component of NRM with fairly strong magnetization values is mainly responsible for the very low MDF-values (Table 1). The stability of the reversed component of remanence has not been fully evaluated yet, however, its MDF-values are estimated from vector plots to be around 1.2 A/m (150 Oe).

TABLE 1. Paleomagnetic Results of 4 Samples from Flow 33.02

Depth (m)	NRM (A/m)	i_o	i stable	d_o	d stable	MDF Oe
151.60	53	53.9	44.5	63.3	74.3	65
153.20	130	40.1	22.6	179.0	173.5	75
153.80	34	49.2	-24.2	212.3	201.6	75
154.20	24	1.5	-12.2	160.5	185.4	80

i_o: inclination of NRM, d_o: arbitrary declination of NRM, MDF: Medium destructive field in $4\ 10^{-2}$ A/m

As the overwhelming majority of igneous samples of Troodos ophiolite display normal polarities, the presence of reversed samples is of great interest particularly if they have stratigraphic significance. Ore microscopic results and, particularly, saturation magnetization versus temperature curves have been used in an attempt to identify the carrier of the reverse remanence.

Curie temperatures and saturation magnetization values are presented in Table 2. Curie temperatures

for the three uppermost samples are similar to values for samples subjected to low temperature submarine weathering (Hall et al., 1987). Double Curie points are typical for these samples, the higher value being possibly a result of heating of the sample and thereby oxidizing titano-maghemite to magnetite. Below sample 151.60 Curie temperatures increase strongly, curves are more reversible and saturation magnetization somewhat higher than above. It appears that the titano-maghemite was transformed into more strongly magnetic Ti-poor magnetite by heat from the underlying hydrothermal system. For the two lowermost samples of unit 33.02, however, the magnetic phase exhibits Curie temperatures of 590°C and higher which clearly exceeds that of magnetite. The possibility of an unusual stable cation deficient maghemite, with a structure and composition relatively close to magnetite is being investigated.

TABLE 2. Some Magnetic Properties of Samples from Units 33.02 and 35.01

Unit	Depth	J_s	Tc	10^{-3}S.I.
33.02	151.00	20.0	330(450)	-
33.02	151.20	15.2	310(460)	28.2
33.02	151.60	8.3	320	24.5
33.02	152.80	35.9	490	52.2
33.02	152.89	15.8	(260)490	24.3
33.02	153.20	21.6	510	33.1
33.02	153.50	27.0	460	-
33.02	153.80	20.0	590	16.1
33.02	154.20	18.9	(330)600	18.6
35.01	155.00	1.3	-	0.8
35.01	155.50	0.6	-	0.2
35.01	157.02	0.6	-	0.2

Depth in meters, Saturation J_s magnetization in arbitrary units, Curie temperatures in °C (value in brackets, if only a minor contribution), Magnetic susceptibility

Microscopic examination of the 2 lowermost samples of unit 33.02 show 2 different phases within the boundaries of originally homogenous titanomagnetites (Figures 1a and 1b). In Figure 1a a corroded titanomagnetite grain is shown, which under high magnification can be divided into two parts having slightly different colours: a brownish colour in portion 'b' and a bluish-grey colour in portion 'a'. On the black-white reproduction this slight contrast is almost invisible, however, after covering with commercial ferrocolloid these different zones are clearly outlined and show furthermore that the brownish portion is by far the most strongly magnetic one, as the ferrocolloid is attracted to the stronger magnetic material. The bluish-grey areas are much less common in these samples than the brownish ones, however, because of their stronger magnetization they may contribute substantially to the saturation magnetization, and possibly to the remanent magnetization. The brownish colour suggests the presence of maghemite that is very close to magnetite in composition.

The preliminary results indicate that the secondary maghemite may be the carrier of the reverse magnetic component. It is not clear whether the reversed polarity is the result of maghemite formation during the presence of a reversed earth magnetic field or due to a process of self-reversal. Although self-reversal for basaltic rocks very rarely is reported in literature, the existence of two magnetic phases in a single magnetic mineral as shown in Figure 1 suggests magnetostatic interaction, resulting in reversed fields at the places where the latest phase, the maghemite, was formed. Further analysis of the magnetic components, their Curie temperatures and saturation magnetizations are needed to support a self-reversal explanation. At present such a possibility cannot be ruled out, however, a reversed earth magnetic field appears to be a more likely explanation.

If the hypothesis of magnetic field reversal is correct, it may have considerable importance as to the timing of the hydrothermal circulation, when maximum temperatures were reached in the massive flow of unit 33.02 that capped the underlying hydrothermal system.

The hydrothermal activity clearly took place during construction of the crust as indicated by the presence of post-hydrothermal dykes cutting the sequence. These dykes were found to be normally magnetized. Thus, if the hydrothermal activity occurred during a reversed earth magnetic field, reversed polarities may be found elsewhere in the extrusive section, with normal polarities on either side. From fairly elaborate paleomagnetic studies of Troodos ophiolite rocks (Moores and Vine, 1971) no consistent reversals were found. Later studies, based on interpretation of aeromagnetic anomalies (Vine et al., 1973) and on further paleomagnetic work (Schoenharting and Abrahamsen, 1982), indicated areas where reversed polarities may be found in the subsurface. However, conclusive evidence has not been given as yet and it appears worthwhile to investigate in detail areas where aeromagnetic anomalies indicate reverse polarities of exposed extrusives.

Furthermore, the detection of stable maghemite at temperatures of above 590°C deserves further investigation and may have implications for the magnetization of deeper levels of oceanic crust.

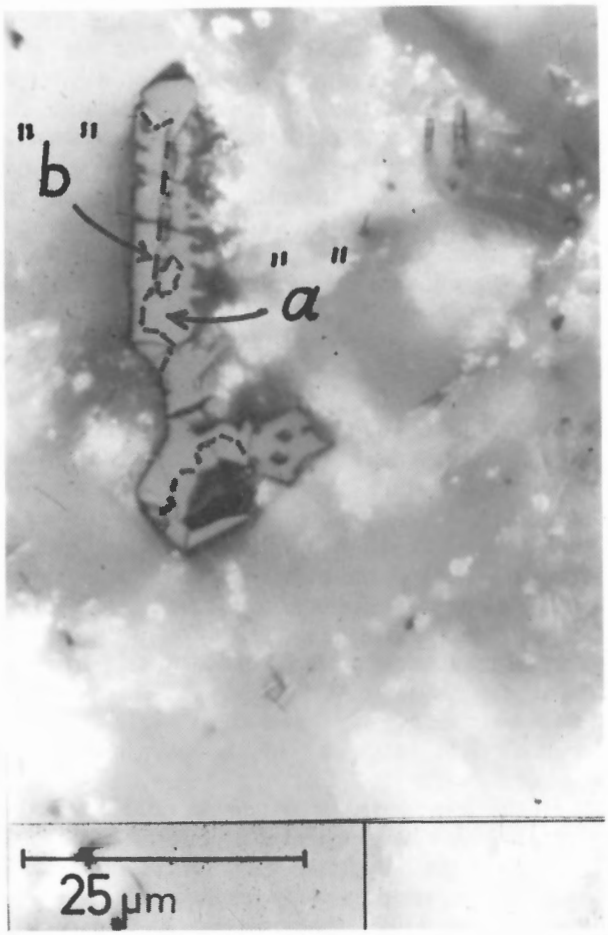

Figure 1a: Corroded titanomagnetite grains with grey-bluish 'a' portion and more brownish 'b' portion.

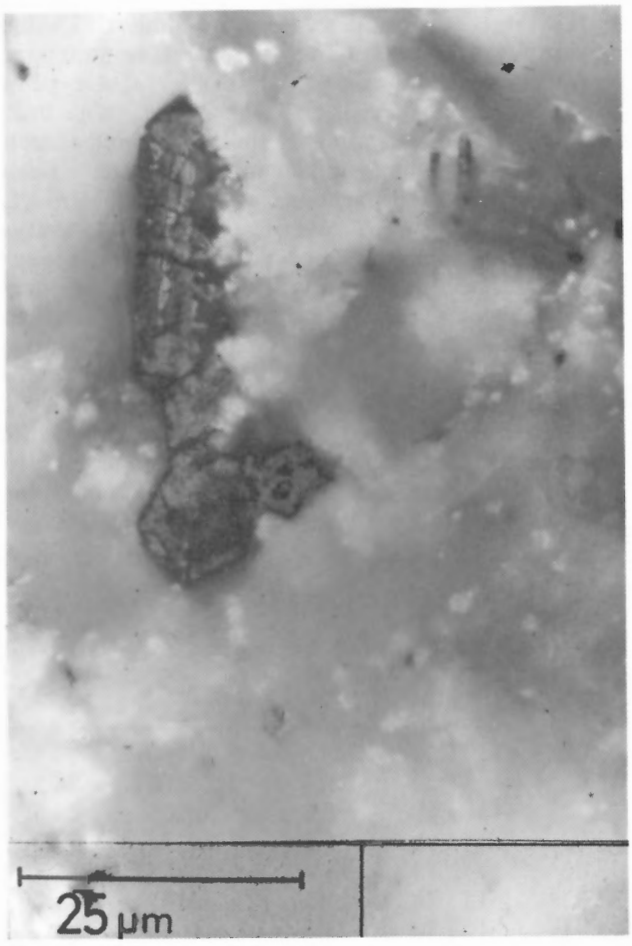

Figure 1b: Titanomagnetite grains of Figure 1a, covered with ferro colloid. 'b' areas are distinctly darker compared to 'a' areas.

ACKNOWLEDGEMENTS

The author is grateful for discussions with Dr. J.M. Hall and the support by the other paleomagnetists of the Cyprus Crustal Study Project. The Danish Natural Science Research Council (SNF) supported this study with grant J.Nr. 11-17032.

REFERENCES

Hall, J.M., Ward, T. and Fisher, B.E.
1987: Rock magnetism, oxide petrography and alteration state in samples from CCSP hole CY-2a through the Agrokipia B ore body and stockwork, Cyprus; *in* Cyprus Crustal Study Project Initial Report Hole CY2-2a, ed. P.T. Robinson, I.L. Gibson and A. Panayiotou; Geological Survey of Canada, Paper 85-29.

Johnson, H.P., Karsten, J.L., Vine, F.J., Smith, G.C. and Schoenharting, G.
1982: A low level magnetic survey over a massive sulphide orebody in the Troodos ophiolite complex, Cyprus; Marine Technology Society Journal, v. 16, no. 3, p. 76-80.

Moores, E.M. and Vine, F.J.
1971: The Troodos Massif, Cyprus, and other ophiolites as oceanic crust: evaluation and implications; *in* A Discussion on the Petrology of Igneous and Metamorphic Rocks from the Ocean Floor, Philosophical Transactions of the Royal Society of London, Series A, v. 268, p. 443-466.

Schoenharting, G. and Abrahamsen, N.
1982: Anomaleous magnetization in the extrusive section of the Troodos complex, Cyprus: indication of a reversal?; *in* Joint

European Geophysical Society/European Seismological Commission General Assembly, Abstract, Leeds, U.K., 1982; EOS, American Geophysical Union, Transactions, v. 63, no. 51, p. 1284.

Smith, G.C. and Vine, F.J.
1987: Gravity and magnetic studies of the Agrokipia sulphide ore bodies, Cyprus; *in* Cyprus Crustal Study Project Initial Report Hole CY2-2a, ed. P.T. Robinson, I.L. Gibson and A. Panayiotou; Geological Survey of Canada, Paper 85-29.

Vine, F.J., Poster, C.K. and Gass, I.G.
1973: Aeromagnetic survey of the Troodos igneous massif, Cyprus; Nature, Physical Science, v. 244, no. 133, p. 34-38.

Wang, B.-I., Walls, C. and Hall, J.M.
1984: Cyprus drill hole CY-1: oxide petrography, magnetic properties and alteration in a section through the uppermost half kilometer of Troodos type oceanic crust; Geological Association of Canada, Program with Abstracts, v. 9, p. 114.

Magnetic Study of a Fossil Oceanic Hydrothermal System in the Troodos Ophiolite (Cyprus)

S.T. AUERBACH[1] AND U. BLEIL[2]

[1]BEB Erdgas und Erdöl GmbH, Postfach 510360,
D-3000 Hannover 51, Federal Republic of Germany
[2]Fachbereich Geowissenschaften, Universität Bremen, Postfach 330440,
D-2800 Bremen 33, Federal Republic of Germany

Auerbach, S.T. and Bleil, U., Magnetic study of a fossil oceanic hydrothermal system in the Troodos Ophiolite (Cyprus); in *Cyprus Crustal Study Project: Initial Report, Holes CY-2 and 2a, ed. P.T. Robinson, I.L. Gibson and A. Panayiotou; Geological Survey of Canada, Paper 85-29, p. 267-281, 1987.*

Abstract

A Mesozoic rock series of partly mineralized pillow lavas, marine flows and dykes penetrated by the drill hole CY-2a were analyzed with respect to their paleomagnetic and rock magnetic properties. For 289 samples characteristic remanent magnetization (ChRM) directions could be determined using detailed alternating field demagnetization techniques. With a notable spread the paleolatitude of the drillsite is in close agreement with the published latitudinal position for the Troodos ophiolite complex in the Upper Cretaceous. The down-hole variation in NRM-intensity and susceptibility remarkably correlates with the lithologic stratigraphy. In mineralized zones, the primary magnetic component, titanomagnetite, is completely replaced by secondary sulphides. Compared to the unaltered parts a drastic reduction in the order of one magnitude in magnetization intensity and susceptibility is observed in these intervals. In contrast to the well-known thermomagnetic curves of basalts, the sulphide-containing rocks show a unique behaviour during the measuring cycle. Detailed investigations revealed that the presence of pyrite is responsible for these observations.

Résumé

Les roches mésozoïques pénétrées par le trou de forage CY-2a, incluant des laves en coussinets partiellement minéralisées, des coulées marines et des dykes, ont été analysées pour mesurer leurs propriétés paléomagnétiques et magnétiques. Les directions d'aimantation rémanente caractéristique (ChRM) de 289 échantillons ont pu être déterminées en utilisant les techniques détaillées de désaimantation par champ alternatif. A distance notable, la paléolatitude au site de forage s'accorde bien avec la position latitudinale pour le complex ophiolitique de Troodos dans le Crétacé supérieur. La variation vers le bas du trou de sondage de l'intensité et de la susceptibilité de l'aimantation rémanente naturelle est corrélée étroitement avec la stratigraphie lithologique. Dans les zones minéralisées, la composante magnétique primaire, titanomagnétite, est complètement remplacée des sulfures secondaires. Par comparaison avec les parties nonaltérées, on observe dans ces intervalles une diminution brusque de l'ordre d'une grandeur de magnitude dans l'intensité et la susceptibilité de l'aimantation. Contrairement aux courbes thermomagnétiques des basaltes bien connues, les roches minéralisées en sulfures présentent un comportement unique durant le cycle de mesure. Des études détaillées ont montré que la présence de pyrite est responsable de ces observations.

INTRODUCTION

At present, ophiolites are regarded as obduced oceanic crust which is created at a ridge axis. This aspect of ophiolite rock suites has been intensively investigated and has led to a much better appreciation of structural and physical processes at oceanic ridges (Coleman, 1977; Moores, 1982).

The frequently observed mineralizations in ophiolites (such as chromite, asbestos, massive sulphide ores and metalliferous muds) are of some economic value. Ophiolite belts occur world-wide and present a good opportunity to study the mechanism of metal concentration along oceanic ridges. Comparably recent hydrothermal ore formations have been found in the Red Sea and at the East Pacific Rise (Fyfe and Lonsdale, 1979).

The Troodos Massif on the island Cyprus holds a prominent place in ophiolite research. It contains a fully developed, hardly deformed, and in the upper parts, regionally mineralized oceanic rock suite. The hydrothermal sulphide ores have been exploited since ancient times, and since the middle of this century abundant geological, petrological and geophysical data have been available (Gass and Masson-Smith, 1963; Vine and Moores, 1972).

These circumstances and the possibility of analyzing a complete oceanic crustal sequence were the reasons for initiating an international, interdisciplinary drilling programme in 1980. The aim was to obtain a complete vertical cross section throughout the Troodos Massif by means of several drill holes, each of which would perforate a special section of oceanic crust.

The object of the present study is a complete paleomagnetic and rock magnetic analysis of the fossil oceanic hydrothermal system penetrated by one of these drill holes, CY-2a, in the area of the Agrokipia sulphide mine.

GEOLOGICAL SETTING

The dominant morphological structure of Cyprus is the Troodos Ophiolite which resulted from an intensive lifting in Early Tertiary (Robertson, 1977). The subsequent erosion created an oval structure with an ultrabasic core, succeeded by basic intrusive and volcanic rocks which were overlapped by pelagic sediments (Figure 1).

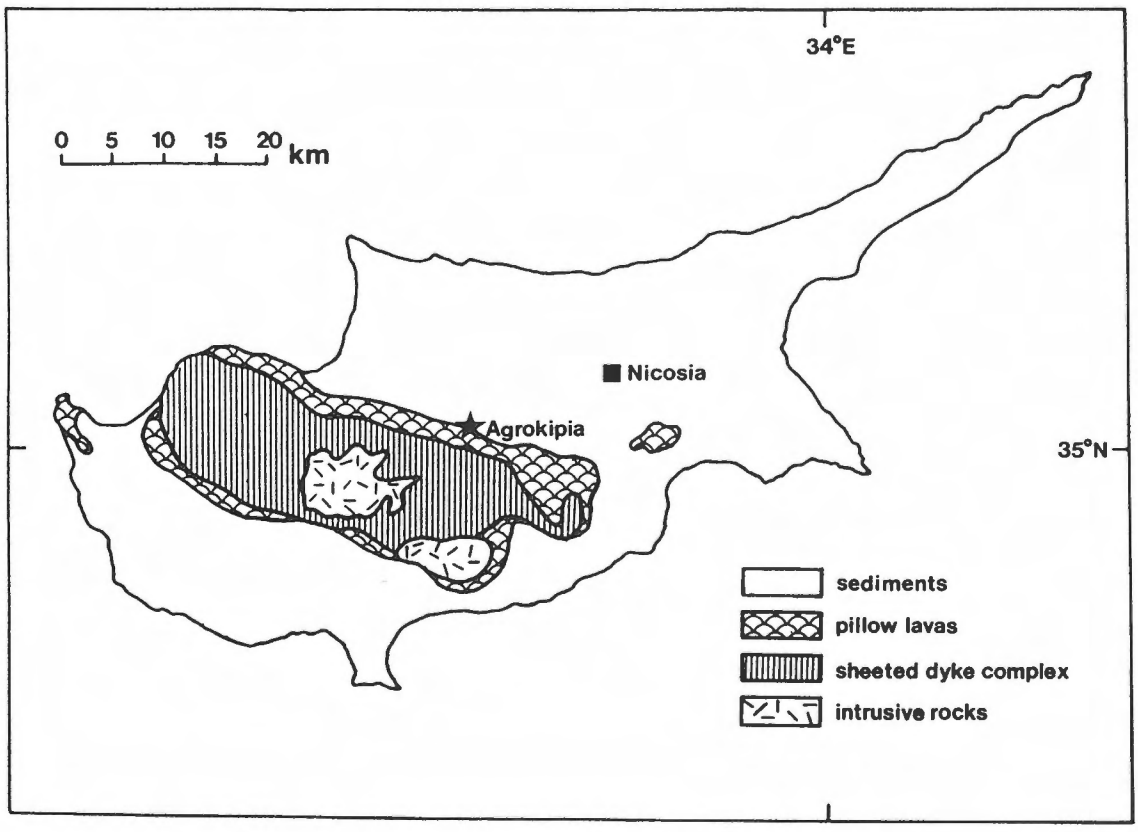

Figure 1: Geological map of Cyprus (after Constantinou and Govett, 1973).

The topography and outcrop of the mountains are an inversion of the original vertical sequence of strata. In the central part of Troodos, around the Mount Olympus, serpentinized harzburgites prevail. In the transitional zone from harzburgites to ultramafic rocks (peridotite and pyroxenite), chromite nappes are found, followed by gabbros and acid plagiogranites. The plutonic core of Troodos forms a sheeted dyke complex which is built up by several subvertical dykes. This transitional area between plutonic and extrusive rocks occupies nearly 60 p.c. of the mountain range. Wilson (1959) estimated a thickness of 1.2-1.4 km.

In several regions an intensive hydrothermal activity has led to the complete alteration of the primary mineral components. The sheeted dykes grade into pillow lavas, the characteristic forms of which are caused by rapid chilling of the magma by sea water. The basaltic pillow lava series have a total thickness of approximately 1.5 km.

Massive, cupriferous pyrite deposits, with large underlying stockwork zones, are to be found in the extrusive rocks. The uppermost parts of the ophiolitic sequence comprise consolidated deep-sea sediments of the Upper Cretaceous and the Paleogene (radiolarites and bentonites). With the help of Radiolaria stratigraphy the oldest sediments were dated back to the Campanian (Mantis, 1970). The detritus, eroded during the uplifting of the massif, was deposited in the Mesoaria Plain in front of the Kyrenia Range and south of the Troodos Mountains.

In the years 1950/56 the Hellenic Mining Company discovered several sulphide ore bodies on the northern slope of the Troodos. The drill hole CY-2a penetrated parts of the workable ore body Agrokipia 'B' and stockwork, about 20 km southwest of Nicosia (Figure 1). The core consists predominantly of basaltic rocks which were hydrothermally mineralized after emplacement and contain massive sulphide mineralization in numerous zones. Variations in the primary mineral content and the chilling margins allow the differentiation of 349 cooling units with thicknesses ranging between 27 meters and a few centimeters. These cooling units have been grouped into 22 lithological units.

MATERIAL AND ANALYTIC METHODS

For the present study small cores were taken perpendicular to the axis of the main core. As magnetic measurements require oriented cores it was impossible to sample parts of the main core which consisted merely of tiny unoriented fragments. Due to the fact that parts of the main core are not oriented both absolute and relative azimuth are absent.

A total of 289 minicores were taken from core CY-2a for this paleomagnetic study (2.5 cm in diameter, 2.5-6.0 cm long). For further analysis the cores were cut into standard-sized 2 cm long specimens, the remaining pieces were used for rock magnetic investigations.

Measurements of magnetic direction and intensity were carried out on a triaxial cryogenic magnetometer (Cryogenic Consultants Ltd., Model GM 400). For the alternating field (AF) demagnetization treatment of each specimen a Schonstedt GSD-1 single axis demagnetizer was used. Initial susceptibilities were determined by a Bison 3101 A bridge and thermomagnetic analyses were made with a horizontal Curie balance.

DEMAGNETIZATION EXPERIMENTS

In addition to the measurements of natural remanent magnetization, NRM, systematic stepwise demagnetization treatments were carried out on each sample. As commonly chosen steps of 2.5 mT were applied up to 10 mT, followed by 5 mT steps up to 30 mT and 10 mT or more beyond this stage up to 100 mT. The stable direction of the characteristic remanent magnetization, ChRM, was evaluated from graphical representations of the data (Figures 2 and 3):

1. Demagnetization curves (Figures 2a and 3a),
2. Vector diagrams (Zijderveld, 1967; Figures 2b and 3b),
3. Stereographic plots of the resultant vectors (Figures 2c and 3c),
4. Stereographic plots of the difference vectors (Hoffman and Day, 1978; Figures 2d and 3d).

The magnetization of most of the specimens possesses a stable normal component which is overlain by a weak viscous magnetization, VRM. The latter is only recognizable in the plots of the difference vectors below 10 mT and is probably the result of the sampling, transport or storage of the specimens. As an example for this, the demagnetization characteristics of sample CY-2a-272.28 are plotted in Figure 2.

A completely different kind of behaviour is exhibited by rocks with a stable inverse component which is completely overlain by a VRM. This magnetization has been overprinted by storage in the present Brunhes field. Figure 3 illustrates the typical demagnetization behaviour of these rocks. Up to 20 mT the normal component dominates, beyond 30 mT only the stable inverse one remains.

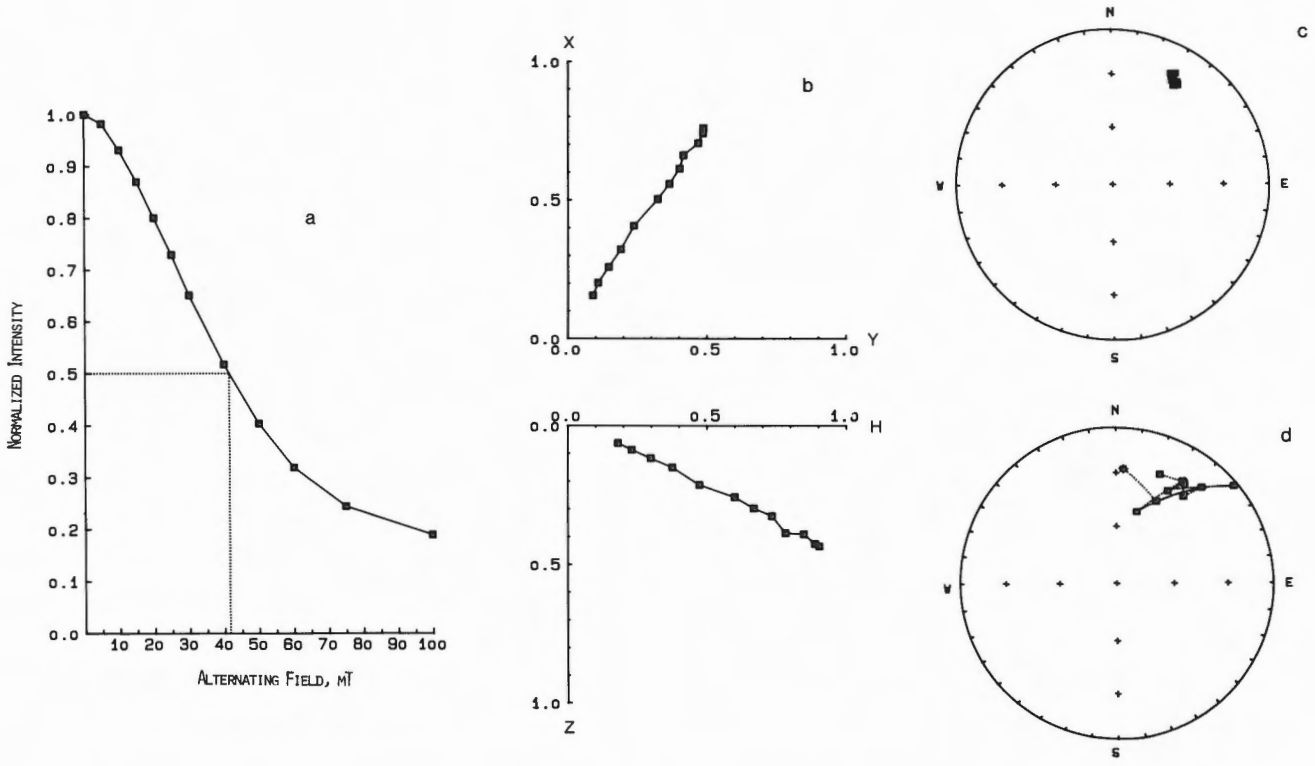

Figure 2: Demagnetization characteristics of the sample taken at 272.28 m sub-bottom.

a) Intensity of NRM-normalized remanent magnetizations as function of the applied demagnetizing alternating field. Dotted lines indicate the median destructive field, MDF.
b) Zijderveld-diagrams. Projection of the normalized remanent magnetization in (X-Y) and (H-Z)-plane.
c) Stereographic projection of the resultant vectors of magnetization. Closed symbols denote a positive, open symbols a negative inclination. The asterisk gives the NRM direction.
d) Stereographic projection of the difference vectors. Closed symbols denote a positive, open symbols a negative inclination. The asterisk gives the first demagnetization step.

CHARACTERISTIC REMANENT MAGNETIZATION

According to the results obtained by the AF treatment of the specimens, Figure 4 contains the down-hole plot of the inclination of the ChRM together with the lithostratigraphy of drill hole CY-2a and the extent of the mineralization of the rocks (Robinson and Gibson, 1983). With the exception of four zones the inclination data are positive with partly notable spreads.

At two levels, 361-372 m (unit XIII) and 466-476 m (unit XX), two-component-systems were mainly obtained (Figure 3). Both parts of the core are set up in each case by thick dykes. The upper one only intruded into the rock masses after the termination of the sulphide mineralization (Robinson and Gibson, 1983). The second dyke is also essentially fresher than the surrounding rocks but it rarely contains pyrite.

It is interesting that for the rocks of the two other zones with negative inclinations (138-154 m and 428-433 m) unequivocally stable directions with some viscous amounts are always observed. The first consists of hyaloclastic rocks, coming from the upper level of the hydrothermal mineralization, the second zone is made of sulphide-bearing pillow lavas like the surrounding material. As evident from Figure 4, several erratic variations are observable in the whole core. This could be a reflection of the regular paleosecular field variation in connection with an episodical volcanism and/or tectonic motions in the rock series. Hall and Robinson (1979) pointed out that such motions can lead to considerable tilting in the oceanic crust.

In contrast to the interpretation of the stable directions between 138 to 154 m and 428 to 433 m we assume that the behaviour of the two post-

mineralization dykes is based on more difficult field configurations. One possible explanation may be that the dykes intruded into the hydrothermal heated rock masses at a negative paleofield as found at the end of the Cretaceous quiet zone. The cooling of the dykes lasted over a very long period because the surrounding rocks had a temperature of some hundred degrees. The next magnetic field reversal occurred when the intruded material was being heated. So the dykes got a magnetic overprint from a latter positive field, a so called Paleo-VRM. This shows a very high stability against AF-demagnetization as observed in the dykes. The demagnetization curve in Figure 3a exhibits that the normal component dominates up to 20 mT and the inverse one exists only beyond 30 mT.

Assuming that fine scaling, volcano-tectonic motions prefer no distinct direction and that the penetrated rock series represent a sufficient period of time to eliminate the influences of secular variations the mean inclination of the whole drill hole meets a (dipole-) paleo-direction of the field. Table 1 summarizes the mean paleomagnetic inclinations for all rocks, fresh and mineralized rocks and dykes obtained by a special mathematical method for mean calculation (Kono, 1980).

It is noteworthy that the mean inclinations of the mineralized and non-mineralized rocks do not differ significantly. The conformity supports on the one hand the assumption that the formation of the rock series, the subsequent hydrothermal ore aggregation and the dyke intrusions took place in a short chronological sequence within an active oceanic ridge. On the other hand, the primary thermoremanent magnetization was destroyed in all rocks, in the fresh as well as in the mineralized ones, by the activity of the hydrothermal system and later substituted by a chemical remanence.

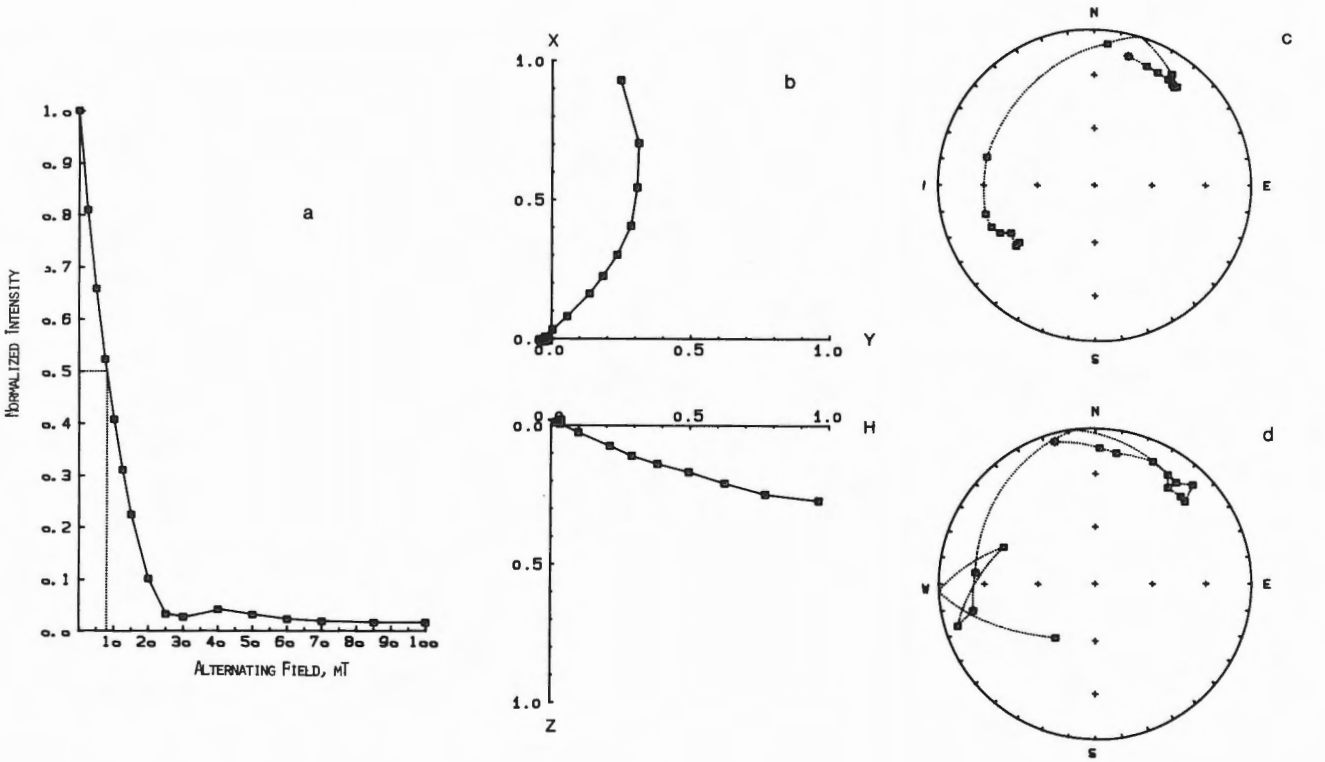

Figure 3: Demagnetization characteristics of the sample taken at 361.61 m sub-bottom. The results are characteristic for post-mineralization dykes.

a) Intensity of NRM-normalized remanent magnetizations as function of the applied demagnetizing alternating field. Dotted lines indicate the median destructive field, MDF.
b) Zijderveld-diagrams. Projection of the normalized remanent magnetization in (X-Y) and (H-Z)-plane.
c) Stereographic projection of the resultant vectors of magnetization. Closed symbols denote a positive, open symbols a negative inclination. The asterisk gives the NRM direction.
d) Stereographic projection of the difference vectors. Closed symbols denote a positive, open symbols a negative inclination. The asterisk gives the first demagnetization step.

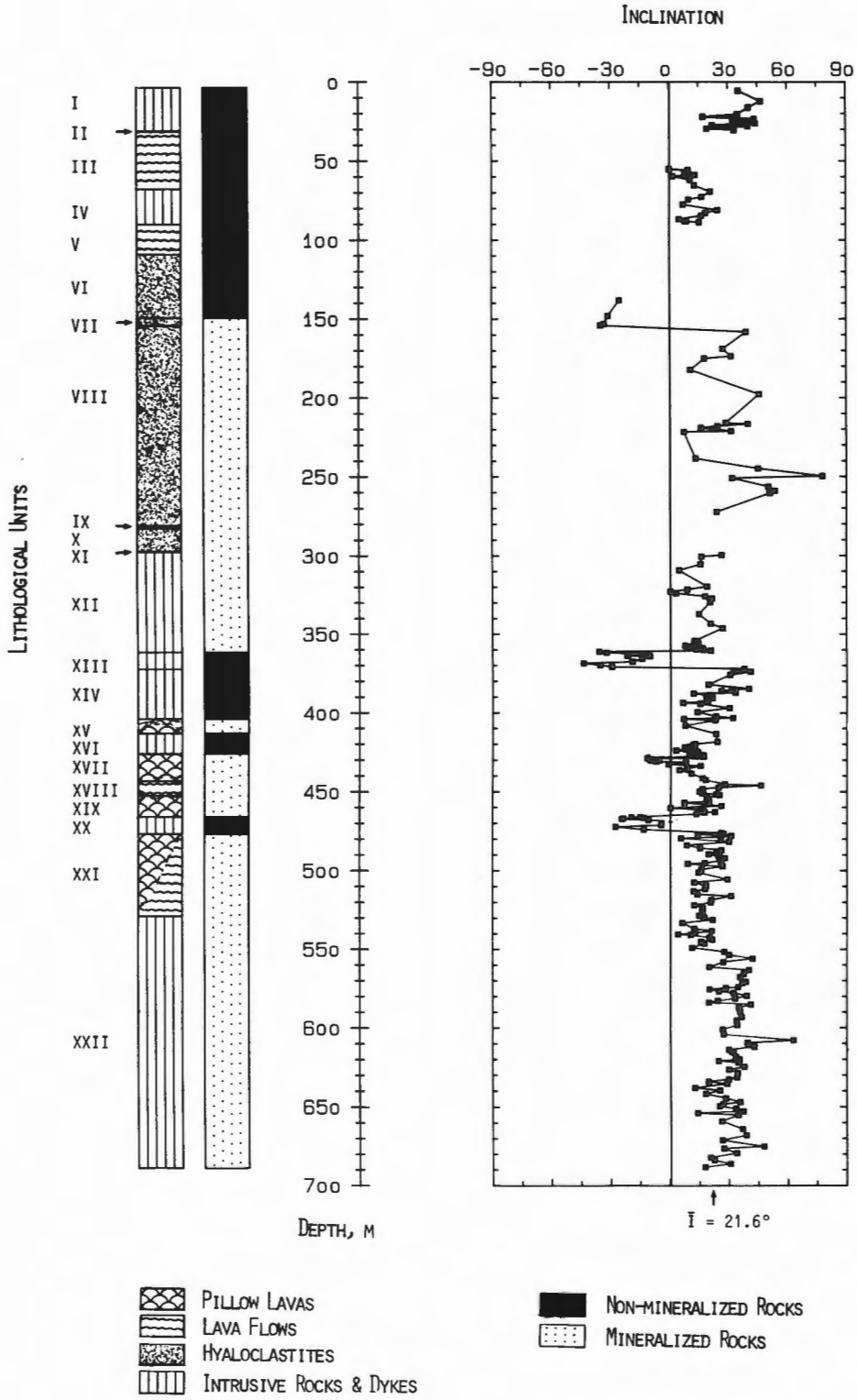

Figure 4: Down-hole plot of the inclination data of drill hole CY-2a, lithostratigraphy and extent of the mineralization.

TABLE 1. Mean Values of the Inclination Data of the Characteristic Remanent Magnetization of the Samples of Drill Hole CY-2a

	n	I	k	α_{95}
Total of samples	289	+21.6°	17	2.1°
Non-mineralized samples	91	+19.1°	13	4.3°
Mineralized samples	198	+22.8°	20	2.3°
Samples from dykes	22	-20.0°	25	6.3°

PALEOGEOGRAPHY AND AGE DETERMINATION OF TROODOS

After tectonic corrections the mean inclination results in a paleo-inclination of +32 degrees according to a geographic latitude of 18 degrees north. Paleomagnetic studies (Shelton and Gass, 1980) as well as the younger paleogeographic reconstructions of Smith et al. (1982) show a similar position for Cyprus at the time of rock-formation in the Upper Cretaceous.

This age is dated biostratigraphically (Moores and Vine, 1971) and radiometrically (Vine et al., 1973). The magnetic studies confirm this in so far that in the respective range of time long periods of normal polarity of the earth magnetic field dominated. Following the latest polarity time scale (Berggren et al., in press) the long epoch of normal field configuration from Aptian to Santonian (equivalent marine anomaly 34) terminated about 84 million years ago. Therefore, the positive magnetized rocks of drill hole CY-2a should be older. The two negative post-mineralization dykes (lithological units XIII and XX) are probably intruded in the following period of inverse polarity between the marine anomalies 33 and 34; possibly subsequently this part of oceanic crust was affected by off-axis volcanism.

ROCK MAGNETIC DATA

As well as being subject to paleomagnetic investigation the rock magnetic parameters (intensity of NRM, median destructive field, susceptibility and Koenigsberger-factor) of all 289 specimens of core CY-2a were determined.

Figure 5 shows the down-hole variation of NRM-intensity and susceptibility together with the above described lithostratigraphy (Robinson and Gibson, 1983), the extent of mineralization and a classification of the core based on the magnetic data results which will be discussed later. The massive lavas in the upper 90 m of the hole (units I-IV) show relatively consistent data. The highest values of intensity (50 A/m) and susceptibility (0.08 SI-units) are found in unit VII. In the underlying mineralized zone (units VIII-XII) remanent intensities are measured between 0.01 and 1 A/m and susceptibilities between 0.0001 and 0.001 SI-units. Below 360 m dyke intrusions (units XIII and XIV) have susceptibility and intensity values which are more than two orders of magnitude greater than those of the overlying mineralized rocks. The underlying lithologically complicated sections between 400 and 500 m depth (units XV-XXI) protrude due to the extreme, fine-scale variations in the data. The second large zone of mineralized rocks (parts of units XXI and XXII) is found at depths down to 630 m. The data in these rocks are very similar to those in the mineralized rocks higher above in the drill hole. Underneath, in the deeper sections of unit XXII, larger intensity and susceptibility values are observed in the mineralized basalts.

The linear plot in Figure 5 does not meet the measuring range because the rock magnetic parameters do not correspond to the simple Gaussian distribution. That their logarithms are normally distributed (Irving et al., 1966) is clearly illustrated by the histograms of the NRM-intensities (Figure 6). In the diagram of the data from all samples (Figure 6c), one can distinguish two relatively broad maxima which can be approximated by broad overlapping Gaussian distributions created by the separation of the rocks according to the extent of mineralization (Figure 6a, 6b). The NRM-intensities of the non-mineralized rocks (units I to IV, XIII, XIV, XVI, XX) are essentially limited to two orders of magnitude, 0.1 to 10 A/m. Just about 70 p.c. of all data (which have a geometric mean of 1.66 A/m) lie within the interval between 1 and 10 A/m. The histogram of the mineralized rocks summarizing all remaining values (Figure 6c) is obviously flattened in this part. The mean is at 0.14 A/m and is lower by a factor of ten. The measuring range is also shifted by the same factor to lower values compared to fresh rocks.

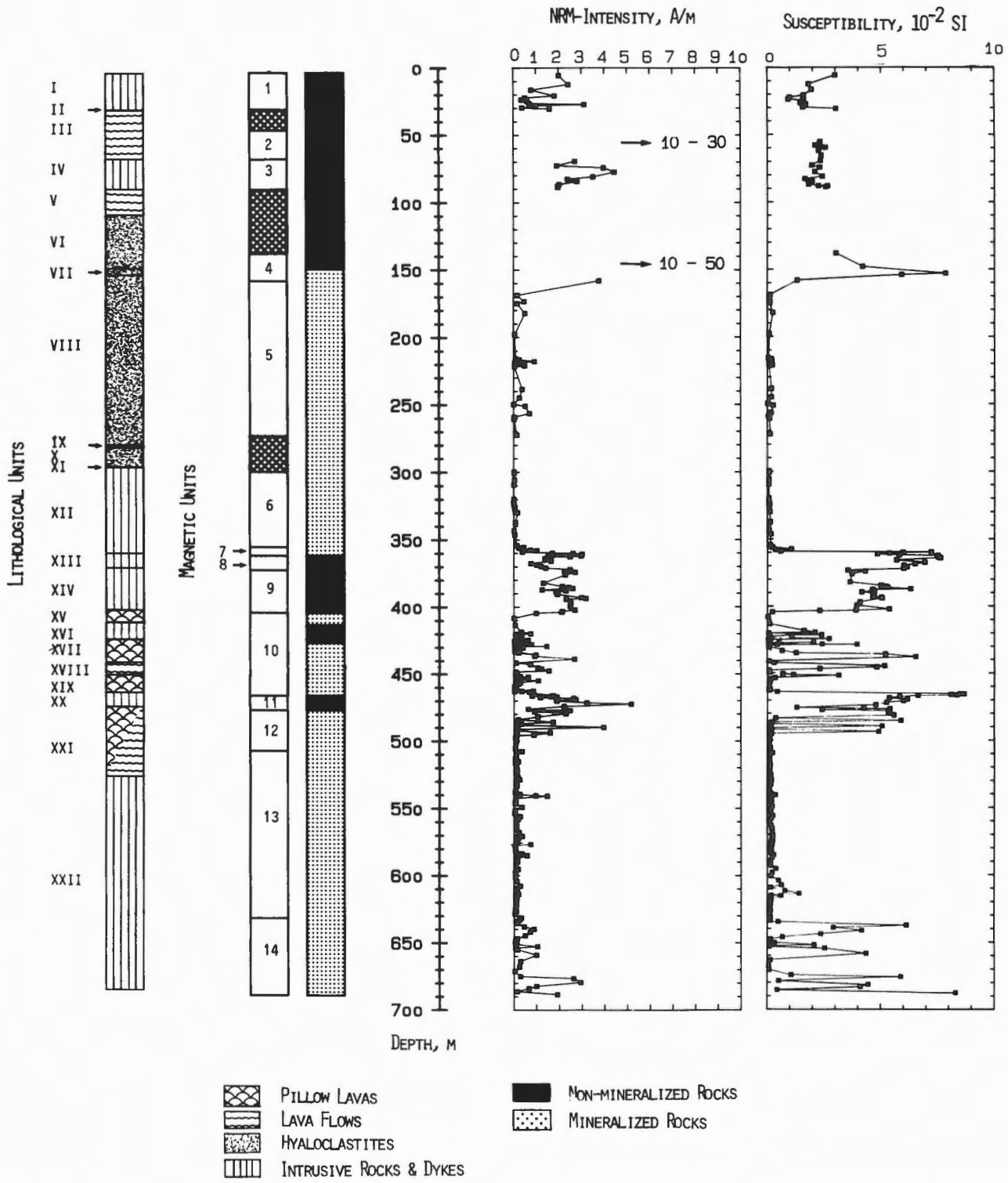

Figure 5: Down-hole plot of the NRM-intensity and susceptibility of drill hole CY-2a, extent of mineralization and the classification in lithological and magnetic units. Sampling gaps are crosshatched.

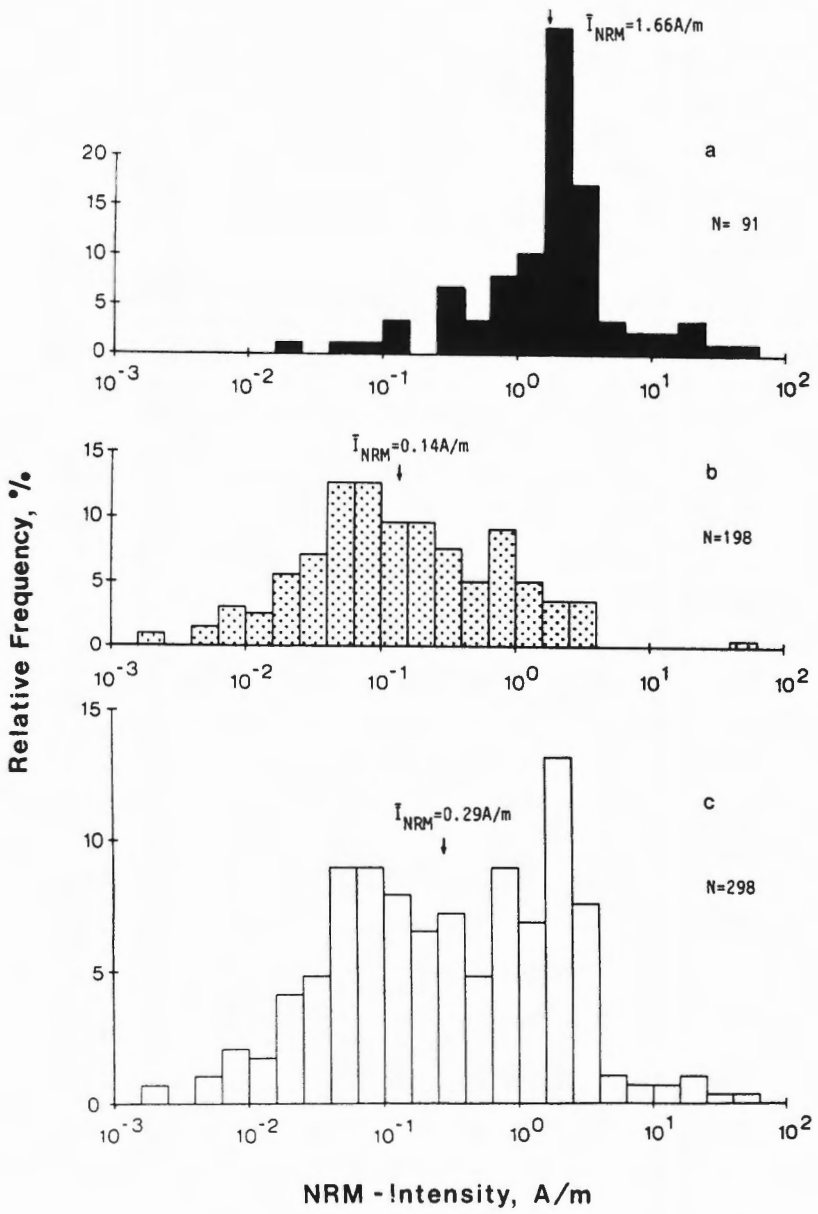

Figure 6: Histograms and mean values of the NRM-intensity for non-mineralized (a), mineralized (b) and all rocks of drill hole CY-2a (c).

The susceptibility and MDF show very similar results. The frequency distribution results from the grouping of the samples into 'fresh' and 'mineralized' rocks. The averages of the Q-factors do not differ significantly. In this respect this criterium cannot be applied as a diagnostical parameter. The geometric means and the ranges of standard deviation are compiled in Table 2 together with the equivalent data of DSDP drill holes.

Altogether, it is possible to state that the mineralized rocks are associated with considerably low NRM-intensities and susceptibilities, and that they are more stable against AF-demagnetization. This observation is independent of the primary rock type and reflects only the effects of the upwelling, high temperature fluids.

TABLE 2. Compilation of Geometric Averages and Standard Deviations for Rock Magnetic Parameters of Rocks of Drill Hole CY-2a and DSDP Drill Holes

	Non-Mineralized Rocks (CY-2a)	Mineralized Rocks (CY-2a)	DSDP Drill Holes
NRM-intensity			
mean	1.66A/m	0.14A/m	2.80A/m
s.d.	0.47 - 5.87 A/m	0.03 - 0.67 A/m	–
Susceptibility			
mean	2.65×10^{-2}	0.27×10^{-2}	1.10×10^{-2}
s.d.	$0.92 - 7.62 \times 10^{-2}$	$0.07 - 1.09 \times 10^{-2}$	–
MDF			
mean	11.8mT	19.2mT	–
s.d.	6.6 - 20.8 mT	11.1 - 32.9 mT	–
Q-factor			
mean	1.73	1.38	7.2
s.d.	0.62 - 4.68	0.46 - 4.14	–

CLASSIFICATION OF THE CORE CY-2A ON THE BASE OF ROCK MAGNETIC DATA

There is a more or less distinct correlation between the rock magnetic criteria and the extent of mineralization of the rocks. This was the reason for proposing a pattern of magnetic units in the core seen in Figure 5.

The upper 100 m of the drill hole are composed of three massive basaltic rock series. Due to the fact that they are well distinguished by the NRM-intensity, each intrusive basalt and lava flow forms a particular magnetic unit (MU 1-3).

Between 149.22 and 154.23 m the core consists of massive lavas with hydrothermal veins. Unusually high susceptibilities and remanent intensities characterize this uppermost level of hydrothermally effected rocks. The few specimens taken in that region form magnetic unit 4.

From about 165 m down to 355 m the drill hole penetrates rocks with low susceptibilities, NRM-intensities and stable magnetization directions (MU 5 and 6). Highly altered and argillized massive lava flows and massive glass dominate the upper part. It is possible to identify idiomorphic crystals of pyrite in many specimens. At several horizons porous masses of pyrite occur which contain significant amounts of silica. The sample from 249.72 m depth has the lowest susceptibility and remanent intensity values and also the highest MDF of the whole measurement. The dykes, mineralized and bleached lavas and fault breccia (unsampled between 273-299 m) are underlain by a mineralized dyke sequence. The magnetic data in MU 5 and 6 are in the same order of magnitude and were only subdivided due to a sampling gap.

One of the most spectacular zones in the core is a basaltic dyke the dark grey colour of which contrasts with the surrounding bleached rock series (361.61-372.30 m, MU 8). Petrological investigations indicate that this dyke intruded only after the termination of the hydrothermal mineralization. The high susceptibilities and NRM-intensities also suggest that the material has not been greatly mineralized. As in magnetic unit 4, there is a well documented contact zone (MU 7) at the hanging layer with continuous and systematical variations of the magnetic data. A corresponding transition zone to the underlying stratum is, however, not recognizable. There follows a thick series of dykes that differs clearly in magnetic characteristics from the post-mineralized dyke. Altogether, 12 cooling units were grouped into magnetic unit 9.

64 m of more or less mineralized rocks, pillow lavas, dykes and flows, occur down to a magnetically easily recognizable large dyke (466-476 m, MU 11). The 58 cooling units are divided into 5 lithological groups.The magnetic parameters result in an interstratification of mineralized and relatively fresh rocks that do not agree with the sequence of cooling units. Detailed investigations in that area show that hydrothermal fluids emanating from a zone of weakness intruded into the rock sequence and strongly modified the petrochemical and petrophysical properties. However, this circulation system ceased just before the whole rock series was altered. It is therefore possible to identify fresh rocks at several places. This whole section is regarded as magnetic unit 10.

In contrast magnetic unit 11, corresponding to the lithological unit XX, is homogeneous. All parameters indicate non-altered material. The variation in the data is to be explained by the grain size variability of the magnetic minerals.

Beneath lithological unit XX, the rest of the core down to 528.92 m is composed of mineralized dykes interbedded with pillow lavas and flows. Here the magnetic parameters show a relatively complex feature. Between 476 and 507 m (MU 12) the data point to an incomplete mineralization of the rocks. With increasing depth the hydrothermal stress increases and from 507 m onward altered rocks only are found (MU 13). The values of susceptibility, remanent intensity and MDF are of the same order of magnitude as between 158 and 355 m, although the sulphide mineralizations found in this upper interval are not observed.

The lowest section of the core (MU 14) is formed by 30 dykes with different thicknesses, and partly affected by hydrothermal overprint (similar to MU 10). Due to the fact that the drill hole terminates in a zone of incomplete mineralization it is impossible to decide whether the hydrothermal system ceases at this level or whether a zone similar to that between 403 and 466 m is interlaid.

THERMOMAGNETIC ANALYSIS OF ROCKS

The original mineral association of magnetic rocks is, in many cases overprinted by subsequent alteration. With regard to the primary magnetic components this occurs due to oxidation, reduction, recrystallization and exsolution. Under terrestrial conditions oxidation is the most frequently observed mechanism. Depending on the temperature, it is possible to distinguish high temperature and low temperature oxidation and hydrothermal alteration in oceanic basalts (Petersen and Bleil, 1982).

For a more detailed analysis of the magnetic mineral phases in this study the temperature dependence of the saturation magnetization and the Curie temperatures of 66 samples were determined with a magnetic balance. The results can be summarized in three types of thermomagnetic curves.

Type 1 is reversible during heating and cooling cycles and shows the presence of only one Curie point (Figure 7). Without exception Curie temperatures of about 570°C could be measured. This characterizes a nearly stoichiometric magnetite. During the measurement the slight decrease in magnetization can be explained with a partial oxidation of magnetite to hematite.

The curves of type 2 summarize all samples showing two or more Curie temperatures, and the variation of saturation magnetization during the cycle allows a further subdivision. With type 2a all irreversible curves are classified which show a few Curie temperatures and an increasing magnetization at the end of a measuring cycle (Figure 8). During the heating titanomaghemites disintegrate to paramagnetic ilmenite and an iron-rich titanomagnetite phase which has a higher magnetization than the original material. This draws attention to a narrow accessory maximum in many curves. The primary Curie temperature of type 2a is between 300 and 350°C, the secondary varies between 500 and 560°C. A lot of specimens (type 2b, Figure 9) show a weak inflection point at 390 to 440°C. The magnetization at the end of the measurement sums up to only 60-70 p.c. of the initial magnetization. In this case, the original existent titanomaghemites (extremely oxidized) disintegrate predominantly to non-detectable minerals and to a small amount to titanomagnetites with Curie temperatures of 570°C.

Although the above discussed thermomagnetic curves are well-known from studies of oceanic basalts (Ozima et al., 1974; Grommé and Mankinen, 1976; Furuta, 1983), the sulphide-containing rock samples show totally different characteristics. Type 3 (Figure 10) includes all samples which show one more or less significant Curie point around 570°C (magnetite) during the heating cycle and a second at about 310°C during the cooling. This indicates the new formation of a ferrimagnetic mineral phase. Since pyrite occurs in all samples and sulphur is lost during the cycle, it can be assumed that the newly formed ferrimagnetic phase is an iron sulphide with a lower sulphur content, pyrrhotite. The saturation magnetization increases by a factor of 10 compared to the starting point.

Various experiments which aimed at investigating the limitations of the pyrite stability field showed that the mineral becomes unstable from about 450°C onward. The originally easily recognizable gleaming crystals in the rocks are no longer macroscopically visible after thermomagnetic cycling or have a blackish overcoat. The X-ray-analysis of sample CY-2a-249.72 shows that the primary crystals of pyrite no longer exist after the measurement and corroborates the formation of pyrrhotite.

The following interpretation summarizes the results. Before the measuring cycle the highly mineralized rocks contained only a small ferrimagnetic magnetite component. Pyrite, the paramagnetic iron sulphide present becomes unstable during heating. In a non-oxidizing atmosphere a new mineral phase is created by the change of the Fe/S-ratio, a monoclinic pyrrhotite with a Curie temperature of about 315°C (Petersen and Bleil, 1982). The carriers of the remanence in type 3 rocks are magnetites. The ferrimagnetic iron sulphides are secondarily formed during the cycling and are eliminated as possible carriers of a natural remanent magnetization.

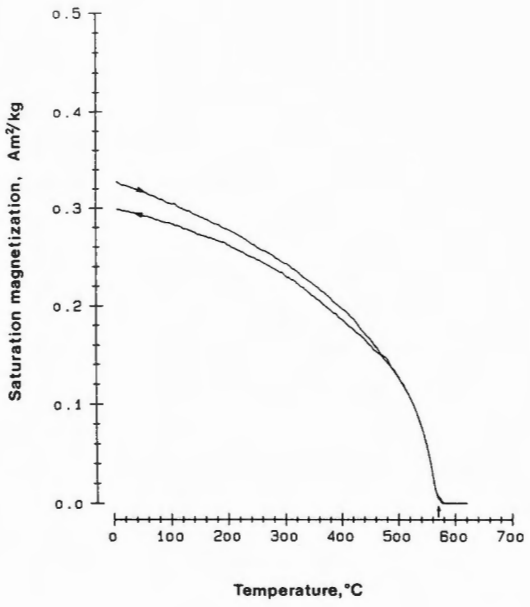

Figure 7: Thermomagnetic curve of the sample taken at 421.77 m (type 1). The Curie temperature is marked by an arrow.

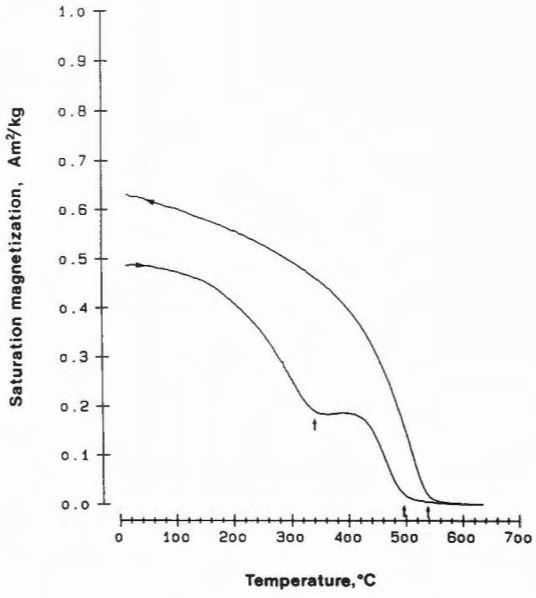

Figure 8: Thermomagnetic curve of the sample taken at 26.19 m (type 2a). The Curie temperatures are marked by arrows.

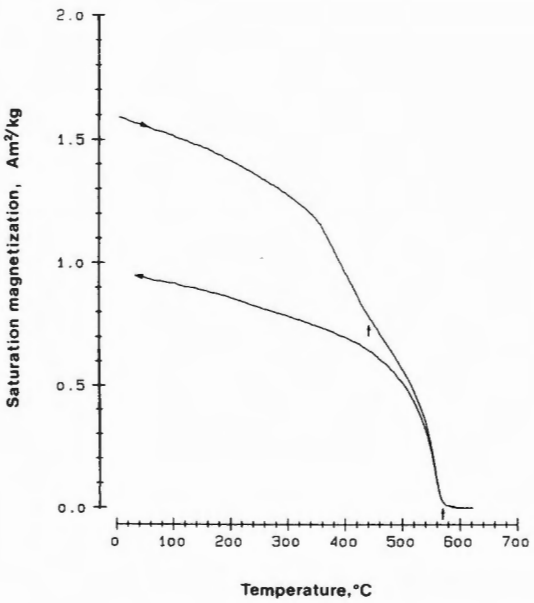

Figure 9: Thermomagnetic curve of the sample taken at 393.44 m (type 2b). The Curie temperatures are marked by arrows.

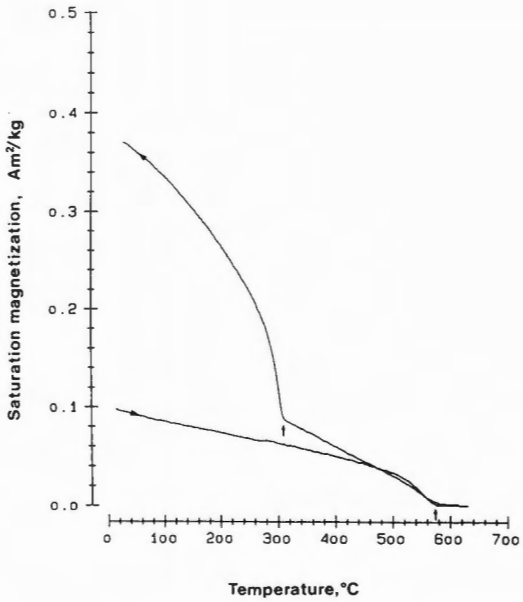

Figure 10: Thermomagnetic curve of the sample taken at 359.00 m (type 3). The Curie temperatures are marked by arrows.

SUMMARY

The magnetically analyzed drill hole CY-2a penetrated a fossil hydrothermal circulation system in the transition zone between extrusive and intrusive rock series of the oceanic crust.

A detailed paleomagnetic investigation included about 300 rock specimens. The inclinations of the characteristic remanent magnetization were determined by systematic AF demagnetization treatment. With the exception of two sections the inclination data are positive with a mean value of I = 21.6°. No significant differences were found in the inclination data of fresh and mineralized rocks. That means that the dyke intrusion and the subsequent hydrothermal ore aggregation must have happened in a relatively short chronological sequence within an active oceanic ridge. The almost uniform normal polarity confirms together with biostratigraphic and radiometric data that both, rock formation and mineralization, happened during the Santonian (about 84 million years ago) at the end of the Cretaceous quiet zone. Two inverse magnetized postmineralization dykes therefore intruded into the rock series in the Campanian age. After tectonic corrections the mean inclinations result in a primary paleogeographic latitude of 18°N for Cyprus. This result is in close agreement with older paleomagnetic studies from the Troodos massif and reconstructions of plate motions.

The rock magnetic measurements contained a distinct variation of all parameters. These reflect the primary distribution of grain size and amount of ferrimagnetic minerals as well as the effect of the subsequent hydrothermal system. The latter is shown in a clear bipartition of the histogram of the NRM-intensities. The values of non-mineralized rocks range with few exceptions between 0.5 and 10 A/m, while the mineralized ones have evidently narrower readings between 0.01 and 1 A/m. The susceptibility data in general indicate a similar trend. Compared with this the investigations have not proved significant differences with respect to the Q-factors.

Within the drill hole the rock magnetic parameter do not present any consistent depth dependence. In general a good correlation was observed between rock magnetic data and degree of mineralization. The respective subdivision of the penetrated formations shows only a limited conformity with the primary lithostratigraphy. Greater discrepancies are observed especially in those parts of the core presenting considerable distinctions of the degree of mineralization within one cooling unit. These effects make clear that hydrothermal circulation systems are limited to assumed zones of weakness in the rock formation and they influence only parts of the oceanic crust.

In all prevailing studies iron-titanium-oxides were identified as carrier of the magnetization in above oceanic basalts and ophiolitic rocks. As a result of the progressive low temperature alteration the magnetic data succumb to distinct temporal variations. Especially characteristic is an increase of the Curie temperatures from 125°C to more than 300°C. The latter data are typical for the non-mineralized rocks in CY-2a. In some cases ferrimagnetic components could not be discovered here in the mineralized rocks by thermomagnetic measurements. At the same time, however, the results of the thermic demagnetization here - as throughout the whole bottom part of the drill hole - strongly suggest nearly stoichiometric magnetite to be carrier of the remanence. The circulation of hot fluids leads to an increase of temperature and in the sequel to the disintegration of the titanomagnetites. The so created magnetite phase is intensively leached out, and substituted by iron sulphides. Above 450°C pyrite becomes instable as a result of the diminution of the Fe/S-ratio and pyrrhotite, a mineral containing more iron, is created. Because no original pyrrhotite could be detected in the rock samples the temperature could not exceed 450°C within the hydrothermal system.

The influence of hydrothermal circulation systems reduces the intensity of magnetization and susceptibility drastically. This can be of eminent consequence with regard to the modelling of marine magnetic anomalies. Especially in areas with violent hydrothermal activity or in areas which were hydrothermally overprinted in the geological past magnetization and susceptibility must be treated as a laterally highly variable parameter. Ths can lead to an important modification of the existing conceptions of modelling.

ACKNOWLEDGEMENTS

To mention but a few of the large number of colleagues and other persons who granted help and advice we would like to specially thank N.R. Nowaczyk, V. Spieβ and N. Weinreich. Partial financial support for this study was provided by the Deutsche Forschungsgemeinschaft.

REFERENCES

Berggren, W.A., Kent, D.V. and Flynn, J.J.
–: Paleogene geochronology and chronostratigraphy; *in* Geochronology and the Geological Record, ed. N.J. Snelling; Geological Society of London, Special Paper (in press).

Coleman, R.G.
1977: Ophiolites: Ancient Oceanic Lithosphere?; Springer-Verlag, Berlin; Heidelberg; New York.

Constantinou, G. and Govett, G.J.S.
1973: Geology, geochemistry and genesis of Cyprus sulfide deposits; Economic Geology, v. 68, p. 843-858.

Furuta, T.
1983: Magnetic properties of basalt samples from holes 504B and 505B on the Costa Rica Rift, Deep Sea Drilling Project Legs 69 and 70; *in* Initial Reports of the Deep Sea Drilling Project, Volume 69, ed. J.R. Cann, M.G. Langseth, J. Honnorez, R.P. Von Herzen, S.M. White, et al.; U.S. Government Printing Office, Washington, D.C., v. 69, p. 711-720.

Fyfe, W.S. and Lonsdale, P.
1979: Ocean floor hydrothermal activity; *in* The Sea; Ideas and Observations on Progress in the Study of the Seas, Volume 7, The Oceanic Lithosphere, ed. C. Emiliani; John Wiley and Sons, New York, p. 589-638.

Gass, I.G. and Masson-Smith, D.
1963: The geology and gravity anomalies of the Troodos massif, Cyprus; Philosophical Transactions of the Royal Society of London, Series A, Mathematical and Physical Sciences, v. 255, no. 1060, p. 417-467.

Grommé, S. and Mankinen, E.A.
1976: Natural remanent magnetization, magnetic properties, and oxidation of titanomagnetite in basaltic rocks from DSDP Leg 34; *in* Initial Reports of the Deep Sea Drilling Project, Volume 34, ed. R.S. Yeats, S.R. Hart, et al.; U.S. Government Printing Office, Washington, D.C., v. 34, p. 485-494.

Hall, J.M. and Robinson, P.T.
1979: Deep crustal drilling in the North Atlantic Ocean; Science, v. 204, no. 4393, p. 573-586.

Hoffman, K.A. and Day, R.
1978: Separation of multi-component NRM: a general method; Earth and Planetary Science Letters, v. 40, no. 3, p. 433-438.

Irving, E., Molyneux, L. and Runcorn, S.K.
1966: The analysis of remanent intensities and susceptibilities of rocks; Geophysical Journal of the Royal Astronomical Society, v. 10, p. 451-464.

Kono, M.
1980: Statistics of paleomagnetic inclination data; Journal of Geophysical Research, v. 85, no. B7, p. 3878-3882.

Mantis, M.
1970: Upper Cretaceous-Tertiary foraminiferal zones in Cyprus; Cyprus Research Centre, v. 3, p. 227-241.

Moores, E.M.
1982: Origin and emplacement of ophiolites; Reviews of Geophysics and Space Physics, v. 20, no. 4, p. 735-760.

Moores, E.M. and Vine, F.J.
1971: The Troodos massif, Cyprus and other ophiolites as oceanic crust: evaluation and implications; *in* A Discussion on the Petrology of Igneous and Metamorphic Rocks from the Ocean Floor; Philosophical Transactions of the Royal Society of London, Series A, v. 268, p. 443-466.

Ozima, M., Joshima, M. and Kinoshita, H.
1974: Magnetic properties of submarine basalts and the implications on the structure of the oceanic crust; Journal of Geomagnetism and Geoelectricity, v. 26, no. 3, p. 335-354.

Petersen, N. and Bleil, U.
1982: Magnetic properties of rocks; *in* Zahlenwerte und Funktionen aus Naturwissenschaften und Technik, Neue Serie, Gruppe V: Geophysik und Weltraumforschung, Band 1b, ed. G. Angenheister; Springer-Verlag, Berlin; Heidelberg; New York, v. 1b, p. 366-432.

Robertson, A.H.F.
1977: Tertiary uplift history of the Troodos massif, Cyprus; Geological Society of America, Bulletin, v. 88, p. 1763-1772.

Robinson, P.T. and Gibson, I.L.
1983: Cyprus Crustal Study Project. Hole CY-2a Lithologic Unit Summaries.

Shelton, A.W. and Gass, I.G.
1980: Rotation of the Cyprus microplate; *in* Ophiolites, Proceedings of the International Ophiolite Symposium, Cyprus, 1979, ed. A. Panayiotou; Cyprus Geological Survey Department, Ministry of Agriculture and Natural Resources, p. 61-65.

Smith, A.G., Hurley, A.M. and Briden, J.C.
1982: Paläokontinentale Weltkarten des Phanerozoikums; Enke Verlag, Stuttgart.

Vine, F.J. and Moores, E.M.
1972: A model for the gross structure, petrology and magnetic properties of oceanic crust; *in* Studies in Earth and Space Sciences, ed. R. Shagam, R.B. Hargraves, W.J. Morgan, F.B. Van Harten, C.A. Burk, H.D. Holland and L.C. Hollister; Geological Society of America, Memoir, v. 132, p. 195-205.

Vine, F.J., Poster, C.K. and Gass, I.G.
1973: Aeromagnetic survey of the Troodos

igneous massif, Cyprus; Nature, Physical Science, v. 244, no. 133, p. 34-38.

Wilson, R.A.M.
1959: The geology of the Xeros-Troodos area; Cyprus Geological Survey Department, Ministry of Agriculture and Natural Resources, Memoir, no. 1, p. 1-184.

Zijderveld, J.D.A.
1967: A.C. demagnetization of rocks: analysis of results; *in* Developments in Solid Earth Geophysics, Volume 3, Methods in Palaeomagnetism, Proceedings of the NATO Advanced Study Institute on Palaeomagnetic Methods, University of Newcastle Upon Tyne, 1964, ed. D.W. Collinson, K.M. Creer and S.K. Runcorn; Elsevier, Amsterdam; London; New York, p. 254-286.

The Effects of Hydrothermal Alteration on the Magnetic Properties of Oceanic Crust: Results from Drill Holes CY-2 and CY-2a, Cyprus Crustal Study Project

H. PAUL JOHNSON AND JANET E. PARISO

School of Oceanography, University of Washington, Seattle, Washington, U.S.A., 98195

Johnson, H.P. and Pariso, J.E., The effects of hydrothermal alteration on the magnetic properties of oceanic crust: results from drill holes CY-2 and CY-2a, Cyprus Crustal Study Project; in *Cyprus Crustal Study Project: Initial Report, Holes CY-2 and 2a, ed. P.T. Robinson, I.L. Gibson and A. Panayiotou; Geological Survey of Canada, Paper 85-29, p. 283-293, 1987.*

Abstract

Drill hole CY-2 is located on the edge of the Agrokipia 'A' massive copper-sulphide (largely removed by strip mining). Although centered on the magnetic anomaly low associated with this alteration halo, CY-2 only penetrated 100 metres of intensely altered extrusive basalt before encountering relatively fresh basalts for the remaining 116 metres. Hole CY-2a is sited directly above the subsurface Agrokipia 'B' deposit. Drilling at this site recovered about 150 m of weakly altered basalts above about 150 m of pervasively altered and mineralized extrusive rocks. This hole bottomed in a sequence of dyke swarms with pillow lava screens both of which are altered to low grade greenschist assemblages. Hydrothermal activity produced a dramatic reduction in the magnetization (NRM) of the extrusive rocks, either by oxidative alteration of the original titanomagnetite grains, or in some cases, by their replacement by non-magnetic sulphide minerals, largely pyrite. The alteration that reduced the NRM intensity did not, surprisingly, change either the weak field susceptibility or the magnetic stability as expressed by AF demagnetization. In contrast, previous studies indicated that hydrothermal alteration and oxide replacement with sulfides increases the susceptibility and decreases the magnetic stability. A large scatter in stable inclination values in CY-2/2a seems to indicate that small scale crustal deformation or rotation of rock units may have occurred on the scale of metres, thus, effectively reducing crustal magnetization.

Résumé

Le forage CY-2 est situé sur la bordure du dépôt de cuivre-sulfure massif (largement enlevé par extraction à ciel ouvert) Agrokipia 'A'. Bien que centré sur l'anomalie magnétique négative associée avec ce halo d'altération, CY-2 a penétré seulement 100 mètres de basalte extrusif intensivement altéré avant de rencontrer des basaltes relativement frais pour les autres 116 mètres. Le forage CY-2a est situé directement au-dessus du dépôt souterrain Agrokipia 'B'. Environ 150 m de basaltes faiblement altérés furent récupérés au-dessus d'environ 150 m de roches extrusives envahies par l'altération et la minéralisation. Ce forage fut arrêté dans une séquence d'essaim de dykes avec des écrans de laves en coussins, tous les deux altérés à des assemblages du faciès schistes verts de faible intensité. L'activité hydrothermale a produit une réduction dramatique dans la magnétisation (NRM) des roches extrusives, par altération oxidante des cristaux de titanomagnétite originaux, ou dans certains cas, par leurs remplacement par des minéraux sulfureux non-magnétiques, largement de la pyrite. L'altération qui a réduit l'intensité NRM n'a pas, étonnament, changé ni la susceptibilité du champ faible, ni la stabilité magnétique exprimée par démagnétisation AF. Au contraire, des études précédantes ont indiqué que l'altération hydrothermale et le remplacement d'oxides par des sulfures augmente la susceptibilité et décroît la stabilité magnétique. Une large dispersion des valeurs d'inclination stable de CY-2/2a semble indiquer que des déformation de la croûte à petite échelle ou la rotation d'unités rocheuses peut avoir survenues à l'échelle de quelques mètres, reduisant ainsi effectivement la magnétisation de la croûte.

INTRODUCTION

Drill holes CY-2 and CY-2a are located in the extrusive section of the Troodos ophiolite, within two massive sulphide deposits. The purpose of these drill holes was to examine the underlying stockwork associated with the orebody formation as an analogue for similar deposits currently found on the ocean floor (see Robinson, 1987). Samples taken from the drill core of these two holes provide an excellent opportunity to examine in the vertical dimension, the effects of hydrothermal alteration on the physical properties of the crust associated with, and adjacent to the massive sulphide deposits. The specific goal of this investigation was to determine the effects of hydrothermal alteration on the magnetic properties of oceanic crust, and to relate these properties to the geological processes of sulphide body formation.

As described in the introductory chapter of this volume, CY-2 was sited adjacent to an open pit copper mine, Agrokipia 'A', which consisted of two massive lenses of sulphide ore near the top of the Lower Pillow Lava boundary (ICRDG, 1982). Drill hole CY-2 was centered on a large (-6000 gammas) negative magnetic anomaly that surrounded the surface exposure of the Agrokipia 'A' deposit (Johnson et al., 1982). The smaller sulphide deposit that makes up Agrokipia 'B' is located 150 metres below current ground level, and was discovered by prospective drilling on a large positive gravity anomaly. This deposit is presumed to have formed through subsurface infiltration and replacement of in situ oceanic crust (ICRDG, 1982). The upper 100 m of drill core of CY-2 was characterized by intensely altered lower pillow lavas, with the lower 116 metres of drilled section being relatively unaltered basalt (see Figure 1 for a schematic diagram of CY-2 and CY-2a within the ophiolite sequence and relative degrees of alteration).

Drill hole CY-2a, which penetrated the Agrokipia 'B' deposit, is located 270 m east of CY-2, within the lower pillow lavas. The sulphide deposit at Agrokipia 'A' is currently exposed at the surface (although largely removed by strip mining), and earlier mapping by the Geological Survey of Cyprus suggested that it was an exhalative system, deposited directly on the seafloor. Agrokipia 'B' is interpreted as a replacement body, located about 150 m deeper in the section. CY-2a penetrated approximately 150 m of unaltered lower pillow lavas before encountering mineralized, altered and leached extrusives. The lower 400 m of the hole consists of two dyke swarms, separated by a 120-m-thick sequence of both pillowed and massive flows (ICRDG, 1982). The lower lithologic units of this hole are pervasively altered to greenschist mineralogy.

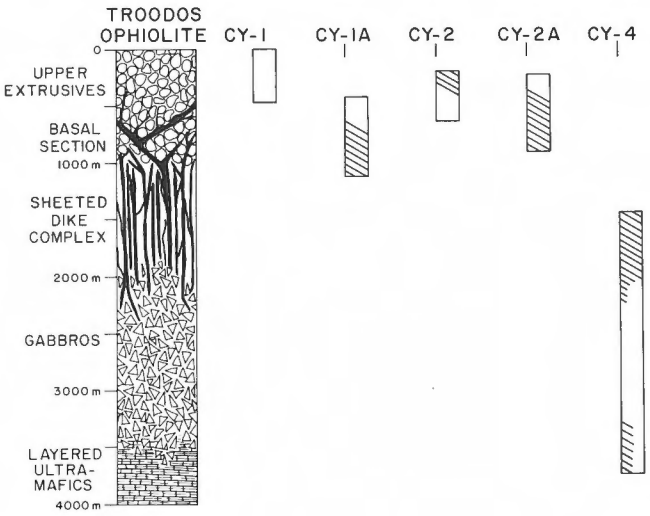

Figure 1: Schematic drawing of the depth relationship between ICRDG drill holes and a model ophiolite sequence. Hatchered areas represent heavily altered zones.

TECHNIQUES

Sample spacing for magnetic studies in both holes was somewhat uneven, but averaged 8.3 m (26 samples from 214 m) in CY-2 and 6.3 m (108 samples from 676 m). Samples for these magnetic studies were deliberately not taken from the extensive glass zones found in both holes. Natural remanent magnetization (NRM) was measured on all samples using a Schonstedt spinner magnetometer and an SCT cryogenic magnetometer. All samples were progressively step-wise demagnetized using a Schonstedt 2-axis reciprocating demagnetizer. Demagnetization intervals were 50, 100, 200, 300 oersteds and higher at 100 oe intervals until at least 50% of the original NRM was removed. Weak field susceptibility (k) measurements were made using a single-axis Schonstedt viscous magnetometer. Multiple measurements on each of the three orthogonal axes were made on each sample to check for susceptibility anisotropy, however, no detectable anisotropy was observed. Polished thin sections were made from selected samples for microscopic examination of the opaque minerals.

RESULTS

The results of magnetic properties measurements on samples from holes CY-2 and CY-2a are shown in Table 1.

TABLE 1. Results of Magnetic Properties Measurements on Drillcore Samples from CY-2 and CY-2a*

Depth (m)	Alteration	RockType	NRM	k	Q	MDF	I_s
			CY-2				
67.81	moderate	extrusive	1.27E-03	4.01E-03	0.6	155	43
71.88	moderate	extrusive	3.13E-03	5.26E-03	1.2	155	19
74.55	moderate	extrusive	7.30E-03	5.27E-03	2.8	187	—
75.85	moderate	extrusive	3.42E-03	4.29E-03	1.6	182	—
77.15	moderate	extrusive	1.22E-02	4.63E-03	5.3	39	21
101.83	moderate	extrusive	6.08E-02	2.55E-03	47.7	87	38
104.37	moderate	extrusive	2.63E-03	3.33E-03	1.6	95	-30
107.63	moderate	extrusive	3.81E-03	2.96E-03	2.6	97	34
129.48	unaltered	extrusive	4.53E-02	2.90E-03	31.2	99	21
130.25	unaltered	extrusive	1.08E-02	2.69E-03	8.0	96	19
132.24	unaltered	extrusive	5.45E-02	3.05E-03	35.7	82	28
133.00	unaltered	extrusive	2.58E-01	1.37E-03	377.7	253	24
135.42	unaltered	extrusive	3.51E-02	2.68E-03	26.2	142	36
156.29	unaltered	extrusive	2.16E-02	1.66E-03	26.0	99	-32
158.68	moderate	extrusive	3.04E-02	2.97E-03	20.5	138	25
160.70	moderate	extrusive	4.65E-03	2.84E-03	3.3	135	21
163.00	unaltered	extrusive	1.07E-02	2.26E-03	9.5	151	—
164.14	moderate	extrusive	9.39E-03	2.42E-03	7.8	188	13
184.52	unaltered	extrusive	1.40E-02	1.75E-03	16.0	147	30
185.07	moderate	extrusive	1.19E-02	2.70E-03	8.8	129	36
185.92	unaltered	extrusive	1.49E-02	2.08E-03	14.3	151	70
188.30	unaltered	extrusive	8.92E-03	2.64E-03	6.8	159	34
190.70	unaltered	extrusive	6.73E-03	2.56E-03	5.3	189	43
213.42	moderate	extrusive	1.66E-02	2.01E-03	16.6	118	-20
213.95	unaltered	extrusive	2.05E-02	3.78E-03	10.8	108	37
214.89	unaltered	extrusive	1.60E-02	3.60E-03	8.9	114	51
			CY-2a				
4.52	—	extrusive	7.94E-03	2.07E-03	7.7	71	32
5.35	—	extrusive	2.63E-04	1.70E-03	0.3	98	41
7.43	—	extrusive	6.55E-04	1.85E-03	0.7	37	—
8.75	—	extrusive	3.13E-04	1.50E-03	0.4	64	—
9.82	—	extrusive	7.08E-04	1.68E-03	0.8	81	39
10.52	—	extrusive	5.23E-04	1.23E-04	0.9	150	42
65.13	—	extrusive	1.35E-02	8.34E-04	32.4	103	—
68.80	altered	extrusive	2.51E-03	1.60E-03	3.1	175	58
69.65	altered	extrusive	8.41E-04	1.20E-03	1.4	102	16
69.99	altered	extrusive	3.39E-03	5.08E-04	13.3	193	—
70.44	altered	extrusive	8.02E-04	9.07E-04	1.8	136	—
71.52	altered	extrusive	1.97E-03	1.64E-03	2.4	162	15
98.30	altered	extrusive	8.52E-03	1.81E-03	9.4	135	56
101.38	altered	extrusive	4.40E-03	1.90E-03	4.6	130	35
157.65	altered	extrusive	8.71E-04	1.95E-03	0.9	167	18
158.20	altered	extrusive	3.09E-05	2.32E-05	2.7	287	31
160.68	altered	extrusive	1.92E-04	6.84E-05	5.6	310	—
161.75	altered	extrusive	6.94E-05	4.30E-05	3.2	343	34
164.05	altered	extrusive	5.68E-05	4.10E-05	2.8	334	-45
189.15	altered	extrusive	6.29E-04	1.68E-04	7.5	281	27
197.04	altered	extrusive	9.16E-05	5.86E-05	3.1	276	44
230.44	altered	extrusive	9.60E-04	1.69E-04	11.4	299	31

Depth (m)	Alteration	RockType	NRM	k	Q	MDF	I_s
238.48	altered	extrusive	2.99E-04	1.13E-04	5.3	261	13
262.68	altered	extrusive	1.87E-04	1.18E-04	3.2	258	27
269.00	altered	extrusive	3.63E-04	1.13E-04	6.4	179	34
269.82	altered	extrusive	7.76E-05	6.15E-05	2.5	268	34
271.68	altered	extrusive	1.57E-04	5.99E-05	5.2	276	-29
305.22	altered	extrusive	2.72E-05	5.17E-05	1.1	228	19
306.75	altered	extrusive	3.34E-05	4.49E-05	1.5	238	24
307.00	altered	extrusive	4.94E-05	3.87E-05	2.6	235	21
308.44	altered	extrusive	3.55E-05	4.58E-05	1.5	234	18
309.98	altered	extrusive	1.92E-05	6.51E-05	0.6	232	23
311.52	altered	extrusive	1.30E-05	4.70E-05	0.6	239	6
311.90	altered	extrusive	8.28E-06	4.29E-05	0.4	295	—
335.05	altered	extrusive	7.77E-06	5.85E-05	0.3	209	—
336.50	altered	extrusive	1.38E-05	6.83E-05	0.4	180	22
337.60	altered	extrusive	1.06E-04	8.23E-05	2.6	167	14
339.30	altered	extrusive	8.06E-06	5.22E-05	0.3	205	21
340.40	altered	extrusive	4.47E-05	6.19E-05	1.4	177	20
343.20	altered	extrusive	1.53E-05	4.63E-05	0.7	275	25
370.10	altered	extrusive	1.06E-03	4.05E-03	0.5	54	24
371.35	altered	extrusive	1.29E-03	4.85E-03	0.5	73	—
372.75	altered	extrusive	2.62E-03	2.61E-03	2.0	155	—
373.04	altered	extrusive	1.83E-03	2.52E-03	1.5	154	-33
374.04	altered	extrusive	1.83E-03	2.25E-03	1.6	165	48
375.40	altered	extrusive	1.87E-02	3.29E-03	11.4	181	27
400.30	altered	extrusive	4.84E-03	2.83E-03	3.4	188	—
402.05	altered	extrusive	4.16E-03	4.54E-03	1.8	195	20
402.70	altered	extrusive	1.86E-03	2.52E-03	1.5	150	31
403.70	altered	extrusive	5.92E-05	4.96E-05	2.4	330	—
405.46	altered	extrusive	4.28E-05	6.55E-05	1.3	335	—
406.60	altered	extrusive	3.51E-04	7.83E-05	9.0	316	—
408.80	altered	extrusive	1.27E-04	5.06E-05	5.0	349	—
435.40	altered	extrusive	7.76E-04	4.71E-04	3.3	347	—
436.90	altered	extrusive	1.49E-06	5.89E-05	0.1	—	—
439.10	altered	extrusive	1.04E-03	3.31E-03	0.6	138	14
440.00	altered	extrusive	1.16E-03	3.09E-03	0.8	286	27
441.70	altered	extrusive	4.94E-04	2.02E-04	4.9	357	—
442.10	altered	extrusive	1.15E-03	3.15E-04	7.3	358	13
444.00	altered	extrusive	2.43E-05	2.50E-05	1.9	361	—
445.15	altered	extrusive	3.57E-04	1.26E-03	0.6	137	—
473.82	altered	extrusive	1.17E-03	2.46E-03	1.0	102	27
475.33	altered	extrusive	8.28E-05	9.59E-05	1.7	207	21
478.08	altered	extrusive	2.00E-03	3.75E-03	1.1	183	—
478.28	altered	extrusive	5.89E-04	1.49E-03	0.8	127	27
479.31	altered	extrusive	9.28E-04	1.82E-03	1.0	207	14
481.72	altered	extrusive	1.40E-03	3.06E-03	0.9	130	29
482.75	altered	extrusive	6.12E-03	3.75E-03	3.3	99	-12
513.07	altered	extrusive	2.29E-05	2.98E-04	0.2	208	17
514.71	altered	extrusive	2.51E-05	7.38E-05	0.7	—	28
515.52	altered	extrusive	2.57E-05	7.94E-05	0.6	195	—
516.75	altered	extrusive	1.31E-04	9.44E-05	2.8	243	—
518.17	altered	extrusive	7.11E-05	1.16E-04	1.2	231	10
519.75	altered	extrusive	1.01E-04	1.16E-04	1.7	217	17
521.38	altered	extrusive	6.28E-04	1.59E-04	7.9	359	—
522.35	altered	extrusive	3.79E-04	1.06E-04	7.2	295	13

Depth (m)	Alteration	RockType	NRM	k	Q	MDF	I_s
552.23	altered	extrusive	7.59E-05	1.87E-04	0.8	139	26
553.84	altered	dyke	3.39E-05	1.07E-04	0.6	189	24
554.96	altered	dyke	2.03E-04	6.05E-05	6.7	211	24
556.32	altered	dyke	3.11E-03	1.20E-03	5.2	39	32
558.05	altered	dyke	1.72E-04	2.10E-04	1.6	212	30
559.40	altered	dyke	1.99E-04	1.64E-04	2.4	226	35
560.58	altered	dyke	2.92E-04	9.87E-05	5.9	231	20
561.98	altered	dyke	4.79E-05	9.23E-05	1.0	210	21
590.25	altered	dyke	5.88E-05	1.19E-04	1.0	178	29
592.24	altered	dyke	9.98E-05	1.51E-04	1.3	42	—
593.40	altered	dyke	2.41E-05	1.42E-04	0.3	281	31
594.35	altered	dyke	1.29E-04	4.17E-03	0.1	145	32
595.97	altered	dyke	5.74E-05	1.01E-04	1.1	244	31
597.14	altered	dyke	2.63E-05	6.64E-05	0.8	220	40
598.74	altered	dyke	5.03E-05	1.52E-04	0.7	177	38
599.97	altered	dyke	6.89E-05	1.16E-04	1.2	53	37
628.68	altered	dyke	1.15E-05	6.36E-05	0.4	153	34
629.99	altered	dyke	3.19E-05	7.02E-05	0.9	171	32
631.75	altered	dyke	2.56E-04	8.43E-05	6.1	240	30
631.92	altered	dyke	3.77E-04	9.00E-05	8.4	—	35
633.78	altered	dyke	2.08E-04	8.26E-05	5.0	262	—
634.96	altered	dyke	3.15E-04	5.56E-04	1.1	38	37
636.52	altered	dyke	8.18E-03	3.15E-03	5.2	35	—
637.45	altered	dyke	3.20E-04	4.63E-03	0.1	113	—
666.03	altered	breccia	8.66E-05	4.27E-05	4.1	248	29
667.48	altered	breccia	1.10E-04	5.26E-05	4.2	289	33
668.81	altered	breccia	5.26E-04	2.29E-04	4.6	347	27
670.27	altered	breccia	4.06E-04	1.43E-04	5.7	309	29
672.35	altered	extrusive	2.65E-03	4.66E-03	1.1	115	42
673.21	altered	extrusive	1.74E-03	3.70E-03	0.9	151	49
674.95	altered	extrusive	3.73E-04	1.11E-03	0.7	154	39
676.09	altered	breccia	2.36E-03	5.45E-03	0.9	154	34

*All units are cgs.

Drill Hole CY-2

Figure 2 shows the values of NRM and the Koenigsberger (Q) as a function of depth for CY-2. The parameter Q is a measure of the magnetization induced in the present magnetic field, and is defined as NRM/kH, where H is 0.5 oersted. This parameter is commonly used to determine the relative contribution of the remanent magnetization (vs. the induced component) to the magnetic anomaly observed at sea level. Although the data are scattered, the effects of hydrothermal alteration in reducing the magnetization of the upper 100 metres of extrusives are clearly evident. In the transition zone between the upper altered and the lower, relatively unaltered extrusives at 100 metres depth, both high values of 0.061 emu/cc and low values of 0.0026 emu/cc are observed. Similar scatter is observed in the values for Q. Below the transition zone at 100 metres, NRM values range from extremely high (relative to average MORB values) of 0.050 emu/cc to more typical values of 0.001-0.0015 emu/cc. The data are too sparse to indicate if the general decrease in NRM with depth is a convincing trend. Values of Q for the entire section below the transition are above 5 (dimensionless units), and in some cases above 30, well above the necessary value of 2 or 3 required to be a significant contributor to marine magnetic anomalies (Swift and Johnson, 1984). The low values of NRM associated with the alteration of the extrusive rocks in the immediate vicinity of the sulphide deposit compared with unaltered rocks below the alteration zone are almost certainly the source of the overlying magnetic anomaly low which was observed in a near-surface magnetic survey over the region surrounding the sulphide deposit (Johnson et al., 1982).

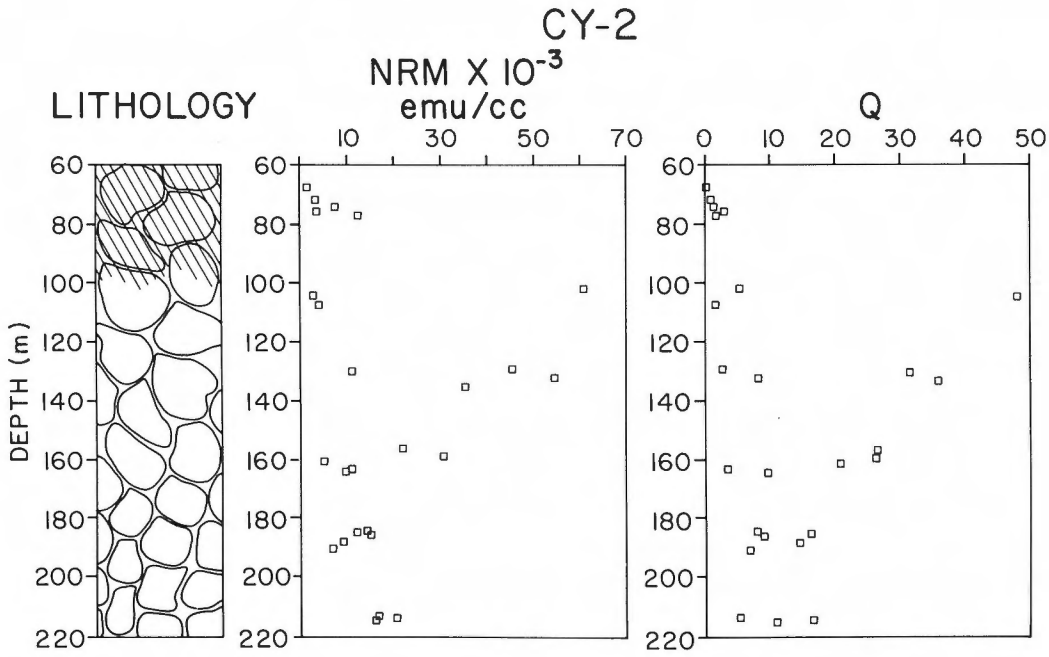

Figure 2: NRM values in emu/cc (1 emu/cc = 1000 Amps/m) and Q ratios plotted versus depth for drill hole CY-2.

Figure 3 shows the variation in weak field susceptibility as a function of depth for Hole CY-2. These data show a relatively high susceptibility associated with the alteration zone, and below that, a relatively constant value of k, comparable to other submarine basalts (e.g. DSDP Hole 504B, Furuta and Levi, 1983). The k values shown in Figure 3 do not show the large scatter in susceptibility that was observed using a hand-held meter applied to the core log (ICRDG, 1982). The obvious difference in these two data sets is likely to be the type and number of measurements; the hand-held measurements took data from the entire drill core, including the massive glassy units, whereas the discrete sample measurements reported here were only done on intact samples composed of less altered rock.

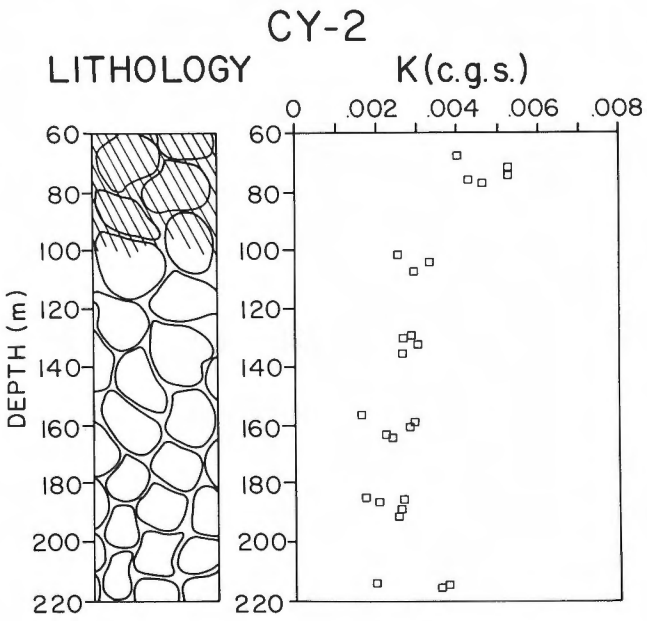

Figure 3: Magnetic susceptibility in cgs units (1 cgs = 12.56 SI units) plotted versus depth in drill hole CY-2.

The median demagnetizing field (MDF) is the value of the AF demagnetizing field that caused the sample magnetization to be decreased to one half the original NRM value, and was graphically determined from demagnetization curves. MDF values are plotted against depth in Figure 4 and show little difference in the stability of the magnetization for the upper, altered section compared to the lower, unaltered samples. This lack of change is surprising because the altered samples have a substantial amount of the original magnetic minerals (presumably magnetite or titanomagnetite) replaced with sulphide minerals. The number of samples with MDF values for which this conclusion is reached is small, and the agreement between the altered and unaltered sections may be fortuitous.

The right-hand diagram in Figure 4 shows the values for stable magnetic inclination as a function of depth. Previous work has determined an age of crustal formation for the Troodos ophiolite of approximately 85 million years during the normally magnetized Cretaceous Quiet Epoch, and a paleomagnetic latitude of 21°N (Moores and Vine, 1971). Given these assumptions, the expected stable inclination for tectonically undisturbed crustal sections for the Troodos ophiolite would be approximately +38 degrees. Four of the 5 samples from the altered zone show a clustering of inclination values near 15 degrees and one sample shows a value near +40 degrees. Generally the data from the unaltered zone below 100 metres show scattered values averaging +23 degrees, substantially lower than the value for the undisturbed ophiolite. However, surface mapping of the section near the drill sites has shown that previously horizontal layering is now dipping at over 20 degrees from the horizontal. Since it is not possible to relate these mapped tectonic crustal disturbances to the horizontally unoriented core, the conclusions that can be drawn from this figure are limited. The three reversely magnetized samples shown as crosses in Figure 4 are assumed to be an artifact of incorrect sampling.

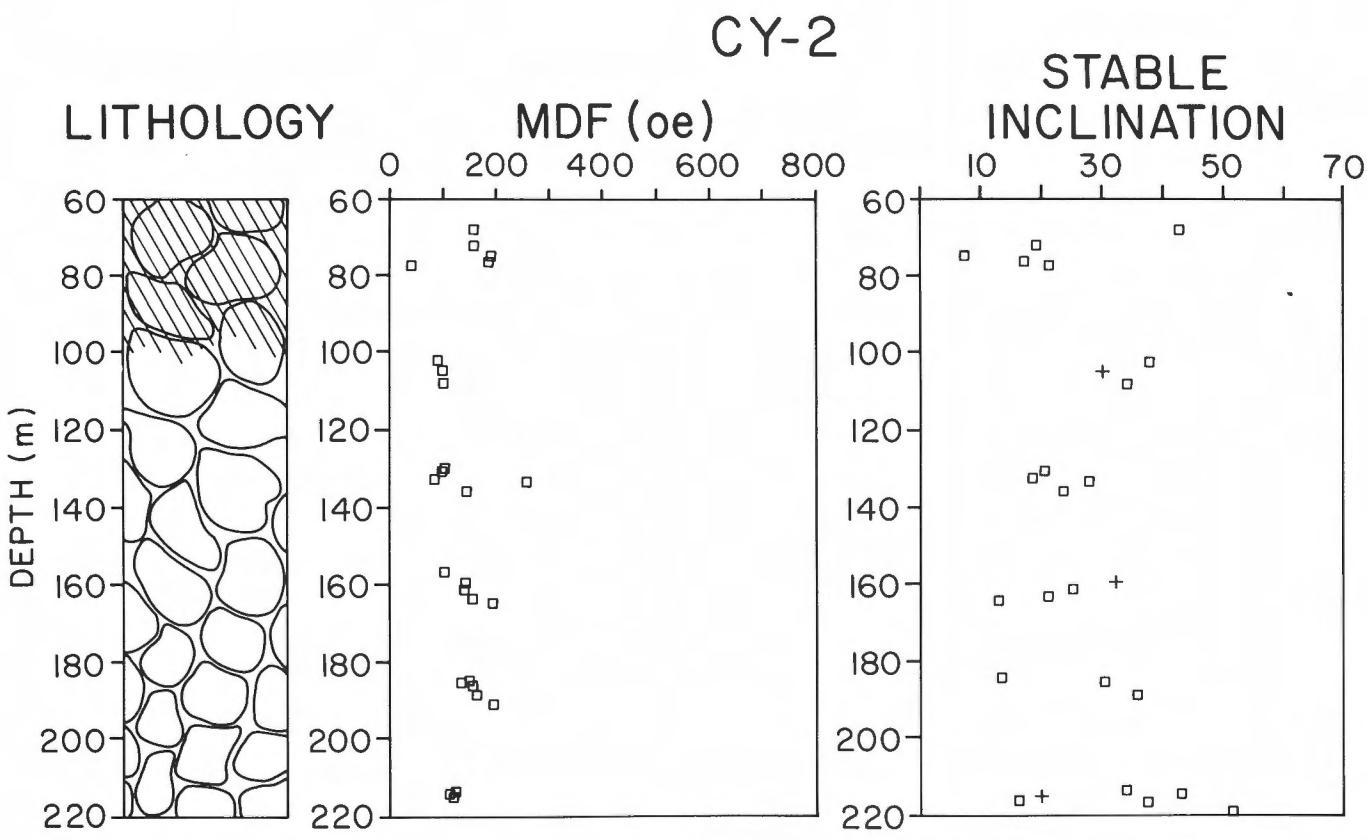

Figure 4: Mean demagnetizing field (MDF) and stable inclination plotted versus depth for drill hole CY-2. Units are in oersteds and degrees, respectively.

Drill Hole CY-2a

Figure 5 shows the distribution of magnetic intensities (NRM) as a function of depth. The large scale on the horizontal axis was chosen in order to compare the measured values with those of the rest of the Troodos samples and data from normal oceanic crust. Two geological processes are in evidence here; low temperature oxidation of the upper 150 metres of rock presumably after emplacement and exposure of the ophiolite, and hydrothermal alteration in the lower part, resulting in a dramatic decrease in magnetic intensity. After emplacement and erosion of the ophiolite, the newly exposed crust was subjected to 'surface weathering' to the depth of about 100 m. This exposure apparently reactivated low-temperature oxidation of the extrusive basalts, with a subsequent reduction in NRM intensity that has been observed in other environments (Irving et al., 1970; Johnson and Atwater, 1977). This low temperature weathering is evident in the reduced NRM values for the unaltered extrusives from all the Cyprus drill holes, including CY-2. Figure 5 shows the non-hydrothermally altered rocks from the upper crustal section with reduced NRM values (for Troodos extrusives) of 5-10 emu/cc. Below the transition zone from weakly altered to severely hydrothermally altered rocks at approximately 150 metres, NRM values fall an order of magnitude, from 0.005 to 0.0001 emu/cc. The pervasive greenschist alteration in the lower parts of CY-2a has clearly reduced the original magnetization, often by replacement of the original titanomagnetite grains with sulphide mineral phases. Also in Figure 5, Q values are plotted as a function of depth. Both the processes of low-temperature oxidation and hydrothermal alteration have the effect of reducing Q values substantially from that expected for unaltered extrusive crust (Figure 2, below 100 metres). Figure 6 shows that this reduction in Q values for CY-2a is due to the reduction in NRM, not a change in weak field susceptibility, which remains relatively unchanged except for a low region between 200 and 375 metres. Although Figure 6 seems to show a bimodal distribution of k values ('normal' extrusive k values scattered around 3 x 10^{E-3} cgs units, and values an order of magnitude lower), the average values for susceptibility do not differ dramatically from unaltered extrusives. Comparison of these data with the core log data (ICRDG, 1982) shows general agreement, probably reflecting the larger number of samples in the CY-2a discrete sample data set.

Figure 7 shows the variation of MDF and stable inclination values as a function of depth for CY-2a. The upper 100 metres of 'surface weathered' extrusives show a substantially reduced magnetic stability, with MDF values less than 150 oe. Below 150 metres, however, the MDF values rise again to above 200 oe, a result consistent for that previously observed for the altered zone of CY-2. The observation that the complete or partial replacement of the original magnetic oxide minerals with sulphides does not affect the magnetic stability should warrant further rock magnetic studies.

Stable magnetic inclination values as a function of depth are shown on the right hand side of Figure 7. Because this drill hole is only displaced 300 metres from the side of CY-2, the previous assumptions regarding expected stable inclinations also apply here. The near-surface stable inclinations show a clustering near the current dipole inclination of 52 degrees, arguing that these samples, exposed to the highest degree of surface weathering, have been at least partially remagnetized in the direction of the current magnetic field. Deeper in the crustal section, from 150 metres to approximately 550 metres, the stable inclination values cluster (with much scatter) below the expected paleo-inclination of 38 degrees. Between 550 metres and the bottom of the section near 650 metres, within the area dominated by dyke swarms, the stable inclination values cluster around higher (but closer to the expected paleoinclination) values of 35 to 40 degrees.

Three possible explanations could account for these higher inclination values deeper in the section. First, the dyke section could have had the same initial stable magnetic direction as the rocks higher in crustal section, and have been rotated with respect to the upper extrusives. This would require that the dykes would have been injected, cooled and magnetized, tectonically rotated, and then covered by the extrusive units, a scenario that we find complicated. A second explanation is that the dykes were injected after the crustal section represented by the Troodos ophiolite had moved northward to a higher latitude with a steeper magnetic inclination. This argument requires volcanic activity over many millions of years and the agreement in magnetic polarity between the dykes and the extrusives would be attributed to chance, a possible but not completely plausible explanation. A final possible explanation is that the hydrothermal alteration has made the dyke units (but not the extrusive basalts!) more susceptible to acquisition of a component of viscous magnetization in the direction of the present field. In this explanation, there are no coherently rotated rock units within the entire crustal section. The upper section has been remagnetized by (subaerial) surface weathering, the lower section of hydrothermally altered dykes has acquired a strong (and stable) component of viscous magnetization, which is parallel to the present field, and the middle altered extrusives (150 to 550 m depth) retain their original stable directions.

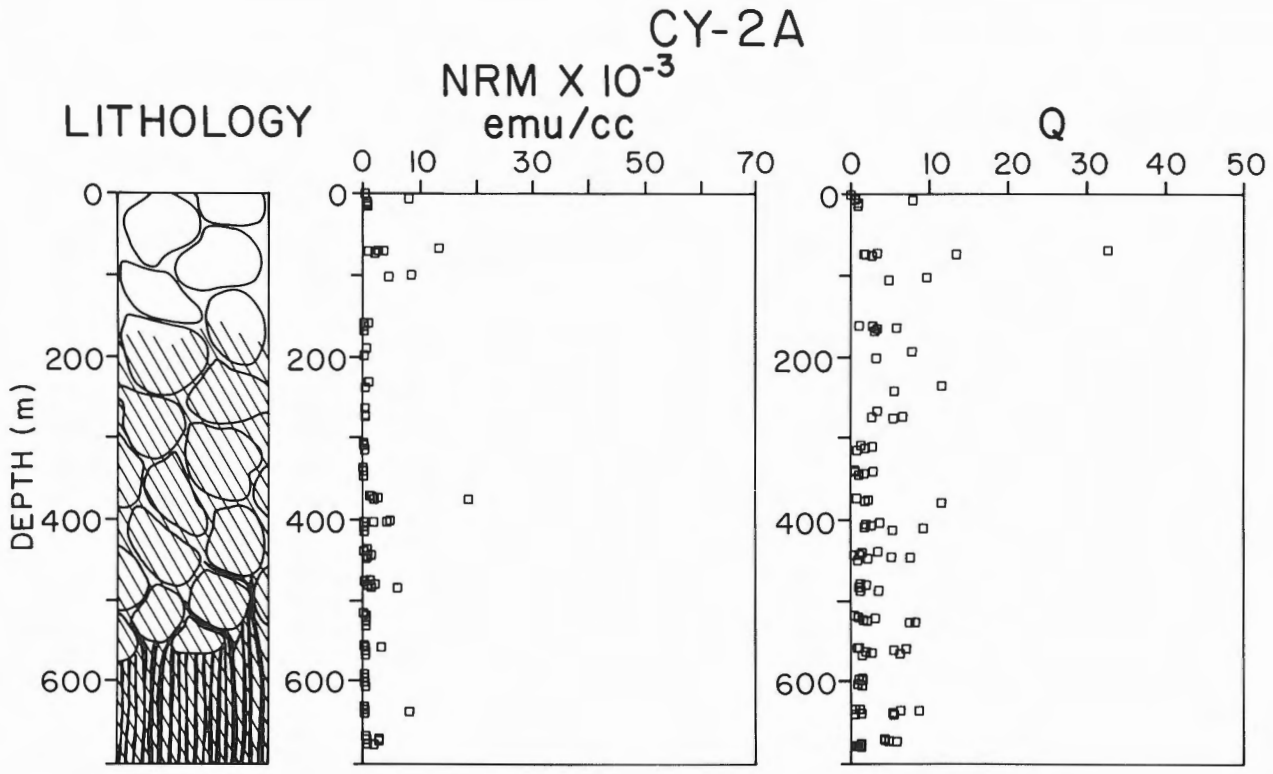

Figure 5: NRM values in emu/cc (1 emu/cc = 1000 Amps/m) and Q ratios plotted versus depth for drill hole CY-2a.

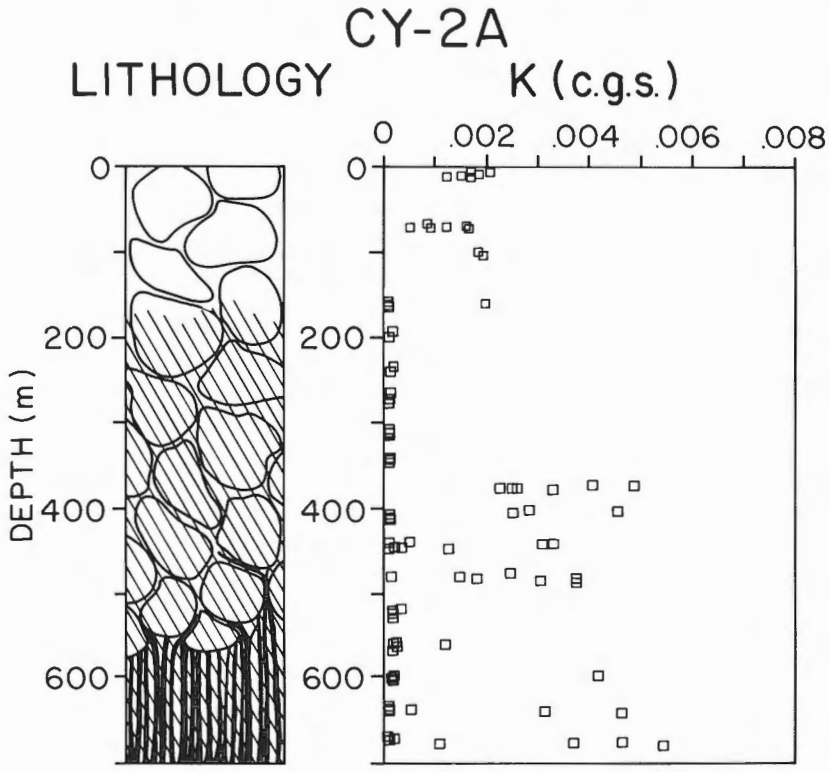

Figure 6: Magnetic susceptibility in cgs units (1 cgs = 12.56 SI units) plotted versus depth for drill hole CY-2a.

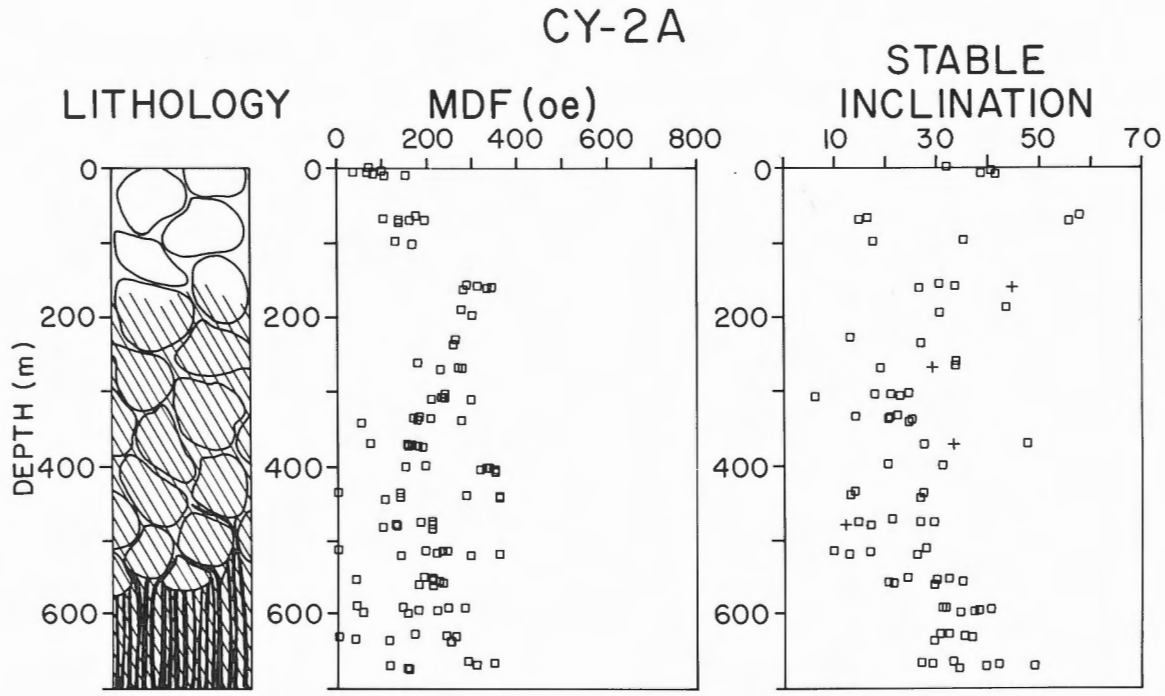

Figure 7: Mean demagnetizing field and stable inclination plotted versus depth for drill hole CY-2a. Units are oersteds and degrees, respectively.

CONCLUSIONS AND DISCUSSION

Although the interpretation is not yet complete, the data from this study allow some preliminary conclusions. First, hydrothermal activity causes a dramatic reduction in NRM intensity of the extrusive rocks, perhaps through the replacement of the original titanomagnetite grains with sulphides. This reduction in intensity can manifest itself as a spatially coherent feature that can be observed in the near-bottom magnetic anomalies that overlie the crust (Johnson et al., 1982). Surprisingly, this alteration affects the magnetic intensity but does not substantially affect either the weak field susceptibility or the magnetic stability as expressed by the MDF. However, both the low temperature alteration associated with surface weathering, and viscous magnetization in the altered dyke section can apparently cause stable (against AF demagnetization) partial remagnetization in the direction of the current earth's field. Finally, and this conclusion is only inferred from the large scatter in the stable inclination values from the extrusives that cannot be attributed to either paleolatitude changes or remagnetization, it would appear that small-scale (on the order of metres or individual rock units) crustal deformation or tectonic rotation has been important. If this observation is correct, the main effect of such deformation is a net lowering of the effective magnetization of any given crustal section.

ACKNOWLEDGEMENTS

We gratefully acknowledge the support of NSF grant EAR-8311776 to this project. In addition, we would like to thank Jim Hall, Paul Robinson, and the scientific field party of the ICRDG for assistance in providing the samples on which this study is based. Brian Halbert of the University of Washington provided substantial assistance during the measurement phase of this study.

REFERENCES

Furuta, T. and Levi S.
1983: Basement paleomagnetism of Hole 504B; *in* Initial Reports of the Deep Sea Drilling Project, Volume 69, ed. J.R. Cann, M.G. Langseth, J. Honnorez, R.P. Von Herzen, S.M. White et al.; U.S. Government Printing Office, Washington, D.C., v. 69, p. 697-703.

ICRDG and Cyprus Geological Survey Department
1982: Hydrothermal circulation in a spreading environment: evidence from research drilling of the Agrokipia massive sulphide deposits, Cyprus.

Irving, E., Robertson, W.A. and Aumento, F.
1970: The Mid-Atlantic Ridge near 45°N. VI.

Remanent intensity, susceptibility, and iron content of dredged samples; Canadian Journal of Earth Sciences, v. 7, no. 2, part 1, p. 226-238.

Johnson, H.P. and Atwater, T.
1977: Magnetic study of basalts from the Mid-Atlantic Ridge lat 37°N; Geological Society of America, Bulletin, v. 88, p. 637-647.

Johnson, H.P., Karsten, J.L., Vine, F.J., Smith, G.C. and Schoenharting, G.
1982: A low level magnetic survey over a massive sulphide orebody in the Troodos ophiolite Complex, Cyprus; Marine Technology Society Journal, v. 16, no. 3, p. 76-80.

Moores, E.M. and Vine, F.J.
1971: The Troodos Massif, Cyprus, and other ophiolites as oceanic crust: evaluation and implications; *in* A Discussion on the Petrology of Igneous and Metamorphic Rocks from the Ocean Floor; Philosophical Transactions of the Royal Society of London, Series A, v. 268, p. 443-466.

Robinson, P.T.
1987: An introduction to the Cyprus Crustal Study Project Hole CY2-2a; *in* Cyprus Crustal Study Project Initial Report Hole CY2-2a, ed. P.T. Robinson, I.L. Gibson and A. Panayiotou; Geological Survey of Canada, Paper 85-29,

Swift, B.A. and Johnson, H.P.
1984: Magnetic properties of the Bay of Islands Ophiolite Suite and implications for the magnetization of oceanic crust; Journal of Geophysical Research, v. 89, no B5, p. 3291-3308.

Seismic Velocities in Basalts from CCSP Drill Holes CY-2 and CY-2a at Agrokipia Mines, Cyprus

G.C. SMITH AND F.J. VINE

School of Environmental Sciences, University of East Anglia, Norwich, U.K., NR4 7TJ

Smith, G.C. and Vine, F.J., Seismic velocities in basalts from C.C.S.P. Drill Holes CY-2 and CY-2a at Agrokipia Mines, Cyprus; in *Cyprus Crustal Study Project: Initial Report, Holes CY-2 and 2a, ed. P.T. Robinson, I.L. Gibson and A. Panayiotou; Geological Survey of Canada, Paper 85-29, p. 295-306, 1987.*

Abstract

Compressional and shear-wave velocities (V_p and V_s) have been measured to a confining pressure of 0.1 GPa at laboratory temperature for seawater saturated basalt samples from C.C.S.P. drill holes CY-2 and CY-2a. Velocities range from V_p = 2.77 to 6.07 km s^{-1} and V_s = 1.50 to 3.53 km s^{-1} at 0.05 GPa reflecting the varied lithology of the samples. Empirical relationships derived for velocities as a function of density (ρ) and porosity (η) show that the generally low velocities are associated with anomalously high porosities and low grain densities. A comparison of the Troodos velocities with those measured on samples from DSDP cores suggests that the extrusive section on Troodos is a poor analogue of oceanic crust. Because there is no definitive velocity contrast between the mineralized and unaltered basalts, it is considered unlikely that seismic techniques will be of value in the search for hydrothermal orebodies on the Troodos.

Résumé

Les vitesses des ondes de compression et de cisaillement (V_p et V_s) ont été mesurées à une pression de confinement de 0,1 GPa à la température ambiante du laboratoire sur des échantillons de basalte saturés en eau de mer prélevés dans les trous de forage CY-2 et CY-2a du projet C.C.S.P. A 0,05 GPa, les vitesses varient pour V_p de 2,77 à 6,07 km s^{-1} et pour V_s de 1,50 à 3,53 km s^{-1}, conformément à la nature lithologique des échantillons. Les relations empiriques dérivées pour les vitesses en fonction de la densité (ρ) et de la porosité (η) révèlent que les faibles vitesses généralement sont associées à des porosités anomalement élevées et aux densités faibles des grains. La comparaison des vitesses du Troodos avec celles mesurées sur les échantillons de carottes du projet DSDP indique que la coupe extrusive du Troodos ne forme avec la croûte océanique qu'une pauvre analogie. Vu l'absence d'un contraste de vitesse évident entre les basaltes minéralisés et frais, il est considéré que les techniques sismiques n'offrent qu'un faible potentiel pour la prospection de gîtes hydrothermaux dans le Troodos.

INTRODUCTION

Drill holes CY-2 and CY-2a are located within the Agrokipia Mining area on the northern flank of the Troodos ophiolite. Drill hole CY-2, drilled into the stockwork of the Agrokipia 'A' orebody, penetrated about 70 metres of hydrothermally altered lavas and then passed into relatively fresh glassy lava flows to a depth of 226 metres. Drill hole CY-2a, drilled to a depth of 689 metres into the Agrokipia 'B' orebody penetrated 154 metres of relatively fresh lava flows and intrusives overlying 150 metres of intensely hydrothermally altered and mineralized massive and pillowed lavas. Below this zone is a sequence of dykes with pillow lava screens which exhibit greenschist facies metamorphism and weak mineralization and alteration along fractures. A detailed account of the lithology of the drilled material is given by Robinson and Gibson (1983a, b). In this study variations in the seismic velocities in samples from the drilled material are identified and explained as a function of depth, density, porosity and degree of alteration and mineralization. The viability of using seismic prospecting techniques in the search for sulphide orebodies on Cyprus and on the ocean floor is then assessed.

Density (ρ) and porosity (η) measurements were made on 42 samples from CY-2 and 123 from CY-2a. Velocity measurements were made on a subset of these representing the range of lithologies, densities, porosities and depths. However, problems arise when trying to select a representative set of samples from what is both a laterally and vertically heterogeneous suite of rocks. Firstly, it is probable that more highly fractured, brecciated and glassy zones are under-represented in the sample set. Secondly, the presence of veins and vugs on a scale of millimeters may lead to the laboratory velocities, densities and porosities being unrepresentative of the true in situ values. Thirdly, major open fractures, i.e. on a scale of centimeters, will clearly not be represented in the laboratory samples. In general, therefore, laboratory velocities will be higher than in situ velocities.

METHOD

The measured samples are cylinders 2.43 to 2.52 cm in diameter and 1.71 to 2.33 cm in length after being cut and lapped to give smooth ends. Measurements of seismic velocity employed the pulse-transmission method of Birch (1960). P and S waves were transmitted and received at 1 MHz by lead zirconate titanate S-wave transducers (which give a P-wave forerunner) housed in steel holders at the ends of the rock cylinders (Evans, 1980; Vine, 1981).

Each sample was saturated with filtered seawater under vacuum and the transducers and sample enclosed in a PTFE sleeve to prevent contamination of the pore-water by the confining pressure medium ('Plexol' oil). The pore-water pressure was kept at atmospheric pressure for all measurements. Samples were pressure cycled to 0.05 GPa initially with measurements made on the rising and falling cycle, and subsequently to 0.1 GPa. The cycle was repeated until observations on the increasing and decreasing cycles differed by less than the estimated experimental error. This reduced the possibility of errors arising from transient effects as the sample responds to changes in confining pressure. As a further check, changes in the electrical conductivity of the sample were monitored after each change in pressure to ensure that the sample had reached equilibrium. The variation in electrical conductivity can also give an indication of the state of saturation of the sample. An initial increase in conductivity with the application of pressure would suggest that the sample is not fully saturated. This would lead to an anomalously low velocity. However, for these samples the conductivity typically decreases with increasing pressure (Smith and Vine, 1987a) so that undersaturation is not thought to be a problem. Correction factors were taken into account at each pressure for the effect of changes in the sample length. The velocities are estimated to be accurate to better than $\pm 1\%$ above 0.02 GPa but only to $\pm 3\%$ below 0.02 GPa due to attenuation of the seismic signal. These estimates are based on consideration of the errors involved in measuring the travel time of the seismic pulse and the sample dimensions.

RESULTS

Velocities as a function of pressure and bulk densities and porosities at atmospheric pressure are tabulated in Table 1. Histograms of the densities and porosities and of velocities and Poisson's ratio at 0.05 GPa are shown in Figure 1. For some samples at low pressures it was not possible to obtain a satisfactory signal. Other samples fractured at higher pressures. Figure 2 shows the effect of increasing confining pressure on V_p, V_s and Poisson's Ratio (σ). Poisson's ratio, defined as:

$$\sigma = \frac{r^2-2}{2(r^2-1)} \quad \text{where} \quad r = \frac{V_p}{V_s}$$

is a particularly useful parameter in summarizing the elastic properties of rocks since it is highly sensitive to variations in the velocity ratio 'r' which is in turn highly dependent upon the mineral composition and porosity of the rock.

A number of elastic parameters can be calculated from V_p, V_s and ρ. These include the bulk

TABLE 1. Velocities, Densities, Porosities

Lithology	Depth (m)	Density (g cm^{-3})	Porosity (%)	Mode	Compressional (P) and Shear (S) Wave Velocities (km/s) at varying pressures (GPa) 0.001	0.005	0.01	0.02	0.03	0.05	0.07	0.10
Hole CY-2												
Altered Pillowed (?) Lava	25.30	2.346	17.5	P	–	2.53	2.60	2.71	2.75	2.77	2.82	–
				S	–	1.35	1.40	1.44	1.47	1.50	1.51	–
Highly Altered Pillowed (?) Lava	50.55	2.446	12.7	P	2.98	3.10	3.17	3.18	3.23	3.27	3.32	3.41
				S	1.63	1.73	1.74	1.74	1.76	1.77	1.77	1.79
Altered Massive Flow	67.85	2.320	24.1	P	2.91	3.02	3.03	3.05	3.09	3.15	–	–
Massive (?) Flow	79.92	2.434	7.2	P	–	–	4.61	4.76	4.88	4.86	–	–
				S	–	–	2.48	2.50	2.50	2.51	–	–
Massive (?) Flow	97.61	2.391	8.8	P	3.65	3.65	3.70	3.73	3.78	3.83	–	–
				S	1.93	1.96	1.97	1.98	2.00	2.01	–	–
Massive Flow	111.97	2.405	4.8	P	–	3.50	3.63	3.79	3.82	3.82	–	–
				S	–	2.14	2.19	2.22	2.24	2.24	–	–
Altered Massive Flow	132.10	2.070	28.2	P	2.68	2.65	2.73	2.85	2.89	2.93	3.01	3.15
				S	1.21	1.34	1.35	1.42	1.45	1.49	1.50	1.51
Massive Flow	163.98	2.384	1.9	P	–	3.96	3.97	3.97	3.99	4.02	–	–
				S	–	2.31	2.32	2.36	2.39	2.42	–	–
Massive Flow	179.25	2.283	7.8	P	–	3.30	3.36	3.46	3.53	3.57	–	–
				S	–	2.09	2.10	2.12	2.15	2.15	–	–
Massive Flow	209.29	2.462	16.8	P	3.84	3.89	3.91	3.97	4.02	4.06	–	–
				S	2.13	2.15	2.17	2.19	2.20	2.22	–	–
Massive Flow	225.10	2.458	10.1	P	4.32	4.43	4.51	4.56	4.67	4.74	–	–
				S	2.11	2.15	2.23	2.26	2.28	2.29	–	–
Hole CY-2a												
Basalt sill (?)	10.17	2.483	8.3	P	4.16	–	4.19	4.25	4.33	4.35	4.48	–
				S	2.24	–	2.26	2.28	2.33	2.34	2.43	–
Massive Basalt Flow	40.43	2.279	19.5	P	3.14	3.15	3.20	3.21	3.21	3.21	–	–
				S	–	1.64	1.64	1.64	1.65	1.66	–	–
Intrusive Massive Basalt	74.53	2.382	12.1	P	–	4.51	4.52	4.53	4.54	4.59	4.61	–
				S	–	2.32	2.33	2.33	2.33	2.33	2.34	–
Massive Basalt Flow	104.80	2.213	27.7	P	2.94	2.96	2.98	3.00	3.04	3.04	3.08	–
Massive Crystalline Basalt	138.11	2.360	11.5	P	–	4.16	4.29	4.32	4.34	4.44	–	–
				S	–	2.40	2.41	2.42	2.42	2.42	–	–

Lithology	Depth (m)	Density (g cm^{-3})	Porosity (%)	Mode	Compressional (P) and Shear (S) Wave Velocities (km/s) at varying pressures (GPa) 0.001	0.005	0.01	0.02	0.03	0.05	0.07	0.10
Massive Hydrothermally Altered Lavas	153.03	2.226	20.6	P	–	3.65	3.67	3.69	3.70	3.72	3.74	–
				S	–	1.93	1.95	1.96	1.97	2.02	2.04	–
Highly Altered and Argillized Massive Lava	187.14	2.521	9.1	P	3.97	4.01	4.07	4.14	4.14	4.15	4.26	4.28
				S	2.23	2.25	2.27	2.29	2.31	2.31	2.32	2.32
Highly Altered and Argillized Massive Lava	230.53	2.404	23.5	P	3.11	3.37	3.42	3.68	3.68	3.72	3.76	3.83
				S	1.62	1.78	1.82	1.87	1.89	1.91	1.95	1.98
Highly Altered and Argillized Massive Lava	261.30	2.474	22.1	P	3.24	3.54	3.74	3.75	3.81	3.93	3.95	4.05
				S	1.88	1.96	2.00	2.09	2.12	2.16	2.18	2.21
Jasper/Pyrite	272.40	2.416	2.4	P	–	5.76	5.85	5.94	6.00	6.07	–	–
				S	–	3.47	3.49	3.51	3.53	3.53	–	–
Highly Altered and Bleached Lava	292.50	2.619	5.6	P	4.41	4.47	4.51	4.52	4.52	4.57	4.63	4.64
				S	2.34	2.36	2.38	2.39	2.40	2.42	2.45	2.47
Altered Dike	340.25	2.538	3.1	P	3.83	4.16	4.22	4.26	4.31	4.39	4.55	4.80
Basalt Dike	366.63	2.546	3.3	P	4.41	4.48	4.62	4.68	4.71	4.78	–	4.80
				S	2.21	2.21	2.24	2.27	2.28	2.28	–	2.29
Massive Basalt Dike	390.49	2.502	11.8	P	4.43	4.61	4.64	4.68	4.72	4.75	4.96	4.98
				S	2.39	2.42	2.48	2.51	2.52	2.54	2.57	2.58
Altered Pillow Lava	438.05	2.423	18.4	P	–	3.46	3.54	3.67	3.78	4.00	4.21	4.31
				S	–	2.05	2.09	2.13	2.14	2.16	2.18	2.20
Altered Basalt Dike (?)	492.00	2.559	13.6	P	4.43	4.46	4.55	4.64	4.73	4.80	4.82	4.83
				S	2.39	2.45	2.51	2.51	2.54	2.56	2.60	2.61
Altered Basalt Dike	551.95	2.575	14.3	P	–	–	3.85	4.09	4.14	4.20	4.29	4.34
				S	–	1.96	2.01	2.04	2.06	2.08	2.09	2.10
Altered Basalt Dike	611.17	2.636	8.4	P	4.81	4.88	4.97	5.02	5.10	5.17	5.20	5.23
				S	2.53	2.63	2.76	2.78	2.81	2.84	–	–
Altered Basalt Dike	681.28	2.677	9.4	P	–	–	4.21	4.22	4.28	4.34	4.42	4.43
				S	–	–	2.19	2.20	2.21	2.23	2.34	2.26

modulus (K), the seismic parameter (ϕ) defined as K/ρ, compressibility (β), shear modulus (μ), Youngs modulus (E) and Lame's constant (λ). Table 2 gives these parameters calculated at 0.05 GPa assuming that the density at 0.05 GPa is not significantly different from that measured at atmospheric pressure.

DEPTH VARIATIONS IN VELOCITIES, DENSITY AND POROSITY

Figures 3a and 3b show depth logs of V_p, V_s, density and porosity for CY-2 and CY-2a, respectively. Schematic geological logs are shown for comparison. Variations in the primary and secondary mineralogy, the type of unit (massive flow, pillow lava, etc.) and the degree and style of alteration, will modify velocities, densities and porosities and explain the variability of the observed values of these physical properties.

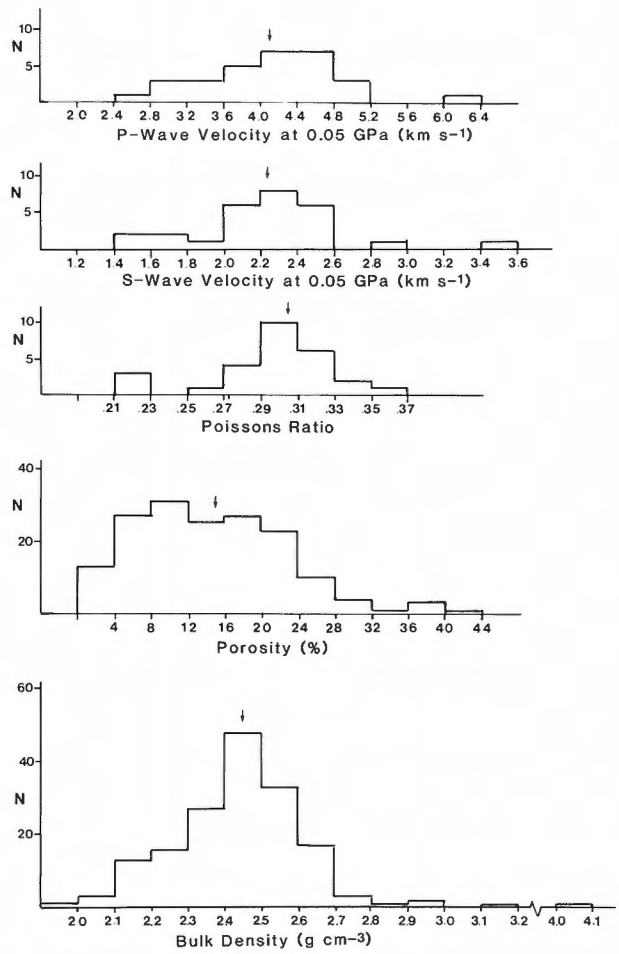

Figure 1: Histograms of physical properties. Average values (Arithmetic means) are arrowed.

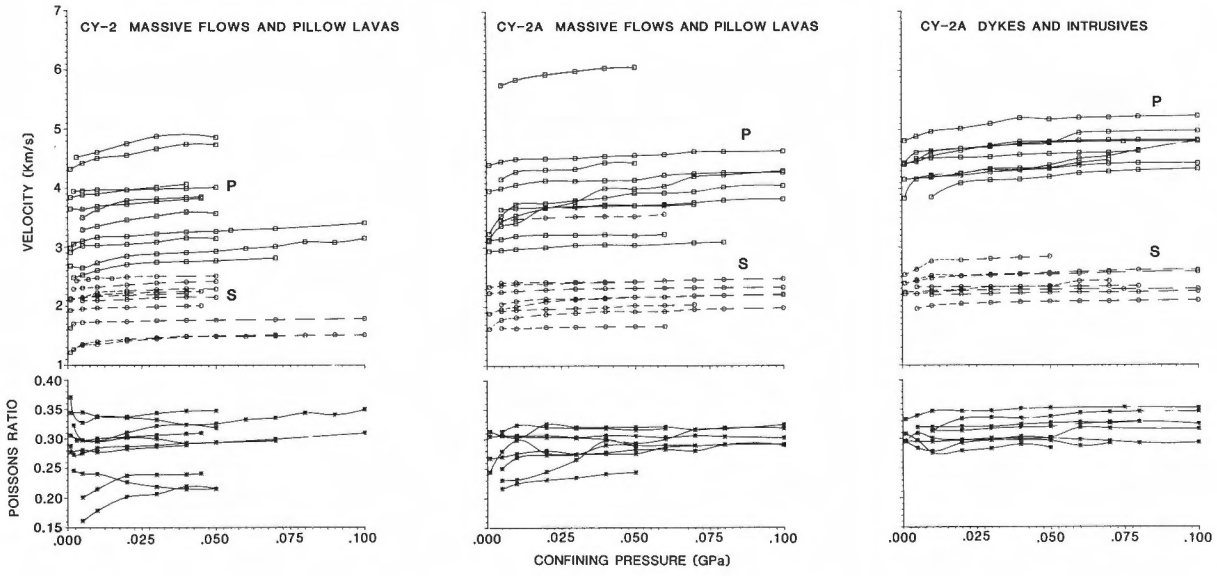

Figure 2: The variation in velocities and Poisson's Ratio with confining pressure. P-wave velocities are shown as solid lines with squares, S-wave velocities are shown as dashed lines with circles.

TABLE 2. Elastic Constants Calculated from V_p, V_s and ρ at 0.05 GPa

Hole	Depth (m)	V_p (km/s)	V_s (km/s)	η (%)	ρ (g/cm^{-3})	σ	V_p/V_s	ϕ (km/s)^2	K (Mb)	β (Mb^{-1})	μ (Mb)	E (Mb)	λ (Mb)
CY-2	25.30	2.77	1.50	17.5	2.35	0.29	1.85	4.7	0.11	9.12	0.05	0.14	0.07
	50.55	3.27	1.77	12.7	2.45	0.29	1.85	6.5	0.16	6.27	0.08	0.20	0.11
	79.92	4.86	2.51	7.2	2.45	0.32	1.94	15.2	0.37	2.70	0.15	0.40	0.27
	97.61	3.83	2.01	8.8	2.39	0.31	1.91	9.3	0.22	4.51	0.10	0.25	0.16
	111.97	3.82	2.24	4.8	2.40	0.24	1.71	7.9	0.19	5.26	0.12	0.30	0.11
	132.10	2.93	1.49	28.2	2.07	0.33	1.97	5.6	0.12	8.59	0.05	0.12	0.09
	163.98	4.02	2.42	1.9	2.38	0.22	1.66	8.4	0.20	5.02	0.14	0.34	0.11
	179.25	3.57	2.15	7.8	2.28	0.22	1.66	6.6	0.15	6.66	0.11	0.26	0.08
	209.29	4.06	2.22	16.8	2.46	0.29	1.83	9.9	0.24	4.10	0.12	0.31	0.16
	225.10	4.74	2.29	10.1	2.46	0.35	2.07	15.5	0.38	2.63	0.13	0.35	0.29
CY-2a	10.17	4.35	2.34	8.3	2.48	0.30	1.86	11.6	0.29	3.47	0.14	0.35	0.20
	40.43	3.20	1.66	19.5	2.28	0.32	1.93	6.6	0.15	6.68	0.06	0.17	0.11
	74.53	4.59	2.33	12.1	2.38	0.33	1.97	13.8	0.33	3.04	0.13	0.34	0.24
	138.11	4.44	2.42	11.5	2.36	0.29	1.83	11.9	0.28	3.56	0.14	0.36	0.19
	153.03	3.72	2.02	20.6	2.23	0.29	1.84	8.4	0.19	5.35	0.09	0.23	0.13
	187.14	4.15	2.31	9.1	2.52	0.28	1.80	10.1	0.25	3.92	0.13	0.34	0.17
	230.53	3.72	1.91	23.5	2.40	0.32	1.95	9.0	0.22	4.64	0.09	0.23	0.16
	261.30	3.93	2.16	22.1	2.47	0.28	1.82	9.2	0.23	4.38	0.12	0.30	0.15
	272.40	6.07	3.53	2.4	2.56	0.24	1.72	20.2	0.52	1.93	0.32	0.79	0.31
	292.50	4.57	2.42	5.6	2.62	0.31	1.89	13.1	0.34	2.92	0.15	0.40	0.24
	366.63	4.78	2.28	3.3	2.55	0.35	2.10	15.9	0.41	2.47	0.13	0.36	0.32
	390.49	4.75	2.54	11.8	2.50	0.30	1.87	14.0	0.35	2.86	0.16	0.42	0.24
	438.05	4.00	2.16	18.4	2.42	0.29	1.85	9.8	0.24	4.22	0.11	0.29	0.16
	492.00	4.80	2.56	13.6	2.56	0.30	1.87	14.3	0.37	2.73	0.17	0.44	0.25
	551.95	4.20	2.08	14.3	2.58	0.34	2.02	11.9	0.31	3.27	0.11	0.30	0.23
	611.17	5.17	2.83	8.4	2.64	0.29	1.83	16.1	0.42	2.36	0.21	0.54	0.28
	681.28	4.34	2.23	9.4	2.68	0.32	1.95	12.2	0.33	3.06	0.13	0.35	0.24

A clear distinction can be drawn between the low velocity, high porosity altered samples and higher velocity, lower porosity, relatively fresh samples from CY-2 (Figure 3a). For the fresh material velocities range from V_p = 3.57 to 4.86 and V_s = 2.0l to 2.51 whereas for altered material velocities are in the ranges V_p = 2.77 to 3.27; V_s = 1.49 to 1.77 km s^{-1}. There is a tendency for velocity to increase with depth although this is not statistically conclusive.

Velocities of samples from CY-2a are generally higher than for CY-2 (Figure 3a and 3b). CY-2 samples are, with the exception of two pillow lava samples (from 25.30 m and 50.55 m) all massive flows whereas CY-2a has intrusives, dykes, massive flows and pillow lavas in various states of alteration and mineralisation. Altered pillow lavas from CY-2a have higher velocities than the altered flows and lavas from CY-2 indicating that a different style of alteration is prevalent with a greater degree of mineralisation in CY-2a.

Two intrusives in the top 150 m of CY-2a (0-30.72 m and 67.50-89.95 m) are characterized by higher velocities, lower porosities and higher densities than the massive lavas into which they are intruded. In the mineralized zone below 149.11 m, anomalously high densities result from pyrite and are associated with porosities up to 40%, with correspondingly lower velocities. The exception is the sample from a depth of 272.40 m which consists entirely of jasper and pyrite. This sample has a porosity of 2.4% and anomalously high P and S-wave velocities of 6.07 km s^{-1} and 3.53 km s^{-1}, respectively.

Below the orebody fresh to altered dykes have velocities ranging from V_p = 4.20 to 5.17 km s^{-1} and V_s = 2.28 to 2.56 km s^{-1}. Fresh and altered dykes are indistinguishable from each other on the basis of their seismic velocities (Figure 3b), although both petrologically and magnetically (Smith and Vine, 1987b) they have contrasting properties.

Regression analysis shows no convincing relationship of increase in velocity with depth such as that deduced by Whitmarsh (1978) and others from oceanic refraction data. This is, perhaps, to be expected when the variability of lithologies is taken into account.

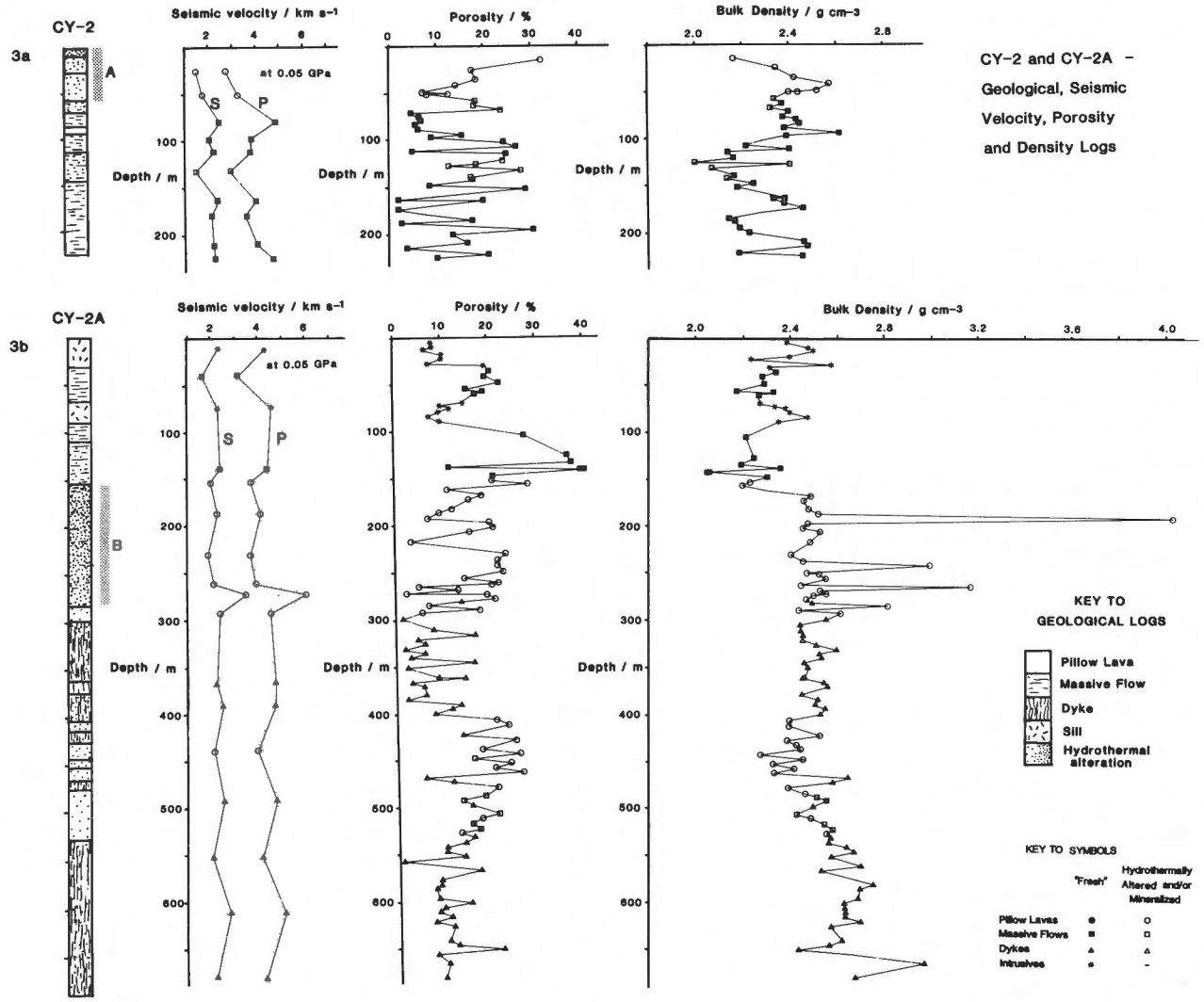

Figure 3: Depth logs of geology, seismic velocities, density and porosity for: a) CY-2, and b) CY-2a. Vertical bars on geology logs indicate the extent of highly altered zones associated with the orebodies Agrokipia 'A' and 'B'.

VELOCITY-DENSITY-POROSITY-POISSON'S RATIO RELATIONSHIPS

Correlations between compressional and shear wave velocities and density have been presented by a number of authors for oceanic basalts as well as for more comprehensive data sets (Birch, 1960; Simmons, 1964; Christensen and Shaw, 1970; Ludwig, et al. 1970; Christensen and Salisbury, 1975; Hyndman and Drury, 1976). Typically, however, the basalts in these data sets have porosities less than 5% and rarely exceeding 10%. They vary from fresh to strongly seafloor weathered samples (Christensen and Salisbury, 1972). Few measurements of seismic velocity have been presented on relatively highly hydrothermally altered porous basalt such as much of that recovered from drill holes CY-2 and CY-2a.

Figures 4, 5, 6 and 7 show the relationship between density and porosity, velocity and density, velocity and porosity and Poisson's ratio and porosity, respectively. Linear regression equations for velocities versus density, velocities versus porosity and density versus porosity, and multiple regression equations for velocities as a function of density and porosity are

given in Table 3. Generally, the level of correlation between these parameters is less than that observed by other investigators.

The density-velocity relationship (Figure 5) is typically considered to approximate a linear relationship. However, for the samples from this study there is considerable scatter reflecting the variable mineralogy and porosity of the samples. This is illustrated well by the density-porosity plot (Figure 4) which shows samples to have projected grain densities varying from 2.22 to 4.26 g cm^{-3} with a correspondingly poor correlation between these variables.

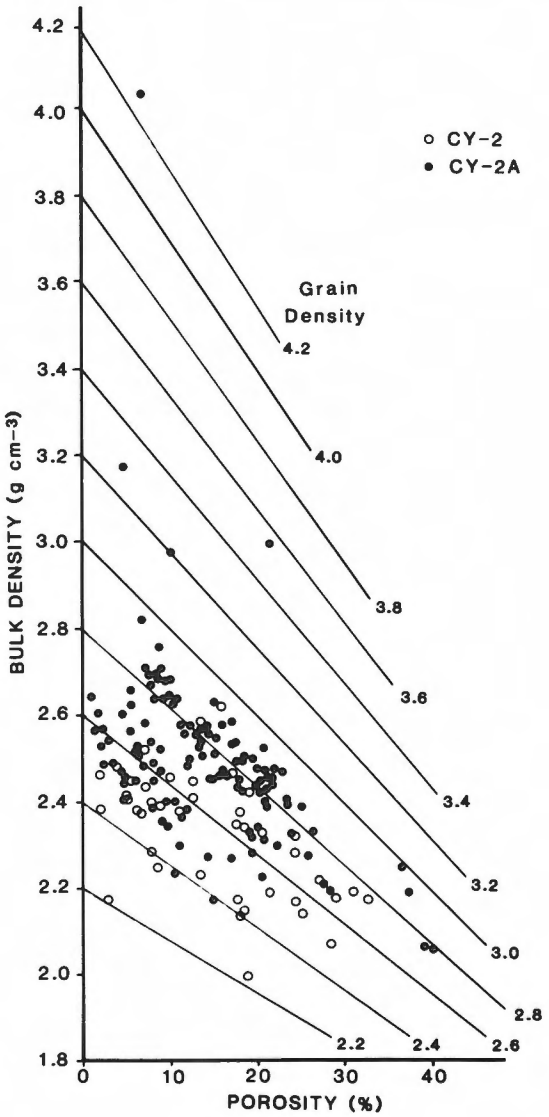

Figure 4: The relationship between bulk density and porosity showing lines of constant grain density.

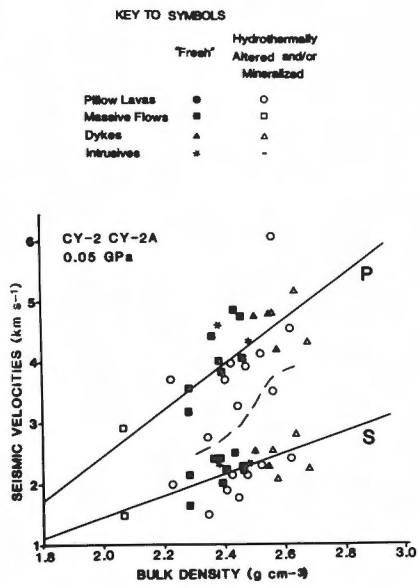

Figure 5: The relationship between velocities and bulk density.

The best fit to the velocity-porosity plot for these samples (Figure 6) was found to be a relationship of the form $1/V_{OBS} = A + B\phi$ as proposed by Pickett (1963) where V_{OBS} = observed velocity, ϕ = fractional porosity and A and B are constants. The Wyllie Time-Average equation (Wyllie et al., 1958):

$$\frac{1}{V_{OBS}} = \frac{\phi}{V_w} + \frac{1-\phi}{V_m}$$

and simple Area-Average equation:

$$V_{OBS} = V_w\phi + V_m(1-\phi)$$

(where V_w = pore fluid velocity and V_m = matrix velocity) describe an envelope within which P-velocity versus porosity points will lie for a particular matrix velocity, the actual velocity depending upon pore shape and orientation as well as matrix velocity and porosity. Pickett's function can be applied to give the best empirical fit to the data within these limits. In addition, it provides a non-linear fit to the S-wave data for which Wyllie's equation fails since V_w becomes zero.

The Poisson's ratio-porosity curve (Figure 7) has been calculated from the empirical velocity-porosity functions. An increase in Poisson's ratio with porosity is anticipated from Pickett's function but is not evident from these data.

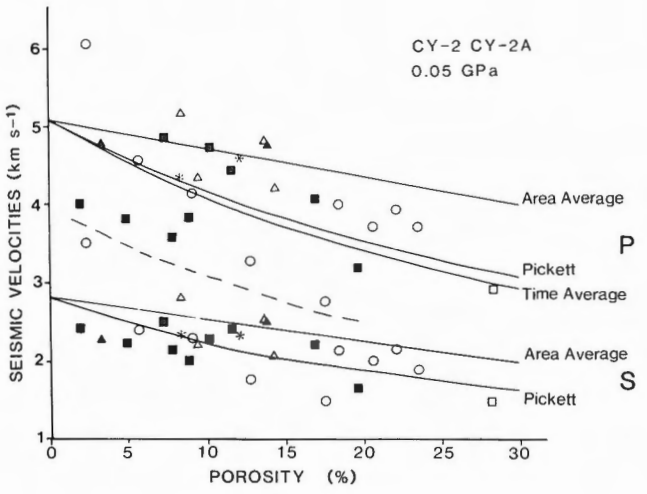

Figure 6: The relationship between velocities and porosity showing the fit of Pickett's equation to the data. Area and time-average curves are shown for comparison for the same projected matrix velocity. The key to the symbols is as for Figure 5.

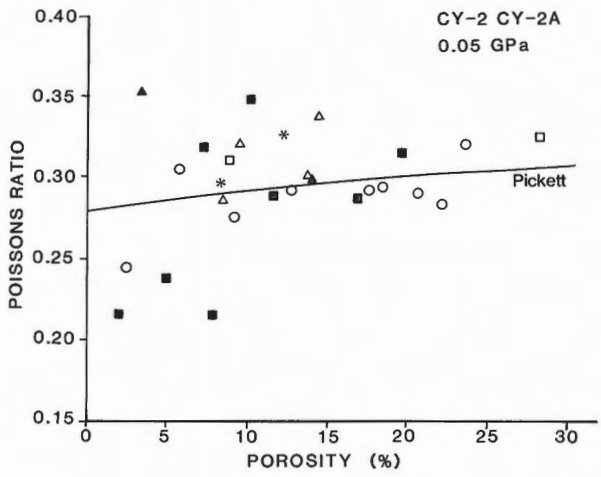

Figure 7: The relationship between Poisson's Ratio and porosity showing the best fit to the data derived from Pickett's equation of Figure 6. The key to the symbols is as for Figure 5.

TABLE 3. Linear and Multiple Regression Equations for V_p and V_s versus ρ and ϕ* at 0.05 GPa

Sample set			r	r^2 (%)	n
CY-2	V_p	$= 3.607\rho - 4.793$	0.599	35.9	11
	V_s	$= 1.737\rho - 2.058$	0.587	34.5	10
	ρ	$= -0.925\phi + 2.460$	-0.558	31.1	42
	$1/V_p$	$= 0.416\phi + 0.223$	0.675	45.6	11
	$1/V_s$	$= 1.06\phi + 0.379$	0.807	65.1	10
	V_p	$= -3.43\phi + 2.13\rho + 0.88$	0.684	46.8	11
	V_s	$= -3.29\phi + 0.458\rho + 1.36$	0.797	63.2	10
CY-2a	V_p	$= 3.451\rho - 4.207$	0.678	46.0	19
	V_s	$= 1.619\rho - 1.682$	0.498	24.8	17
	ρ	$= -1.339\phi + 2.692$	-0.491	24.1	123
	$1/V_p$	$= 0.436\phi + 0.180$	0.825	68.1	19
	$1/V_s$	$= 0.799\phi + 0.340$	0.718	51.5	17
	V_p	$= -5.87\phi + 1.16\rho + 2.21$	0.805	65.3	19
	V_s	$= -3.99\phi + 0.323\rho + 2.04$	0.695	48.3	17
CY-2 + CY-2a	V_p	$= 3.798\rho - 5.131$	0.706	49.9	30
	V_s	$= 1.800\rho - 2.158$	0.592	35.0	27
	$1/V_p$	$= 0.425\phi + 0.197$	0.683	46.6	30
	$1/V_s$	$= 0.864\phi + 0.356$	0.680	46.2	27
	V_p	$= -3.59\phi + 2.59\rho - 1.73$	0.764	58.4	30
	V_s	$= -2.84\phi + 1.04\rho + 0.04$	0.712	50.7	27

*ϕ is the fractional porosity: $\phi = \eta/100$

DISCUSSION AND CONCLUSIONS

The contrast between laboratory and in situ velocities can be illustrated by comparing the preliminary results of a downhole seismic experiment in CY-2a with laboratory velocities for the upper 150 metres of CY-2a. P-wave velocities were determined for the upper 150 metres of the lava pile in the vicinity of CY-2a from blasts at 50, 100 and 150 metres down the hole. Observed in situ velocities range from 2.62 to 3.13 km s^{-1} while laboratory measurements on samples from this depth interval range from 2.94 to 4.51 km s^{-1}. The discrepancy is thought to be due to the presence of 'large scale' fractures, glassy zones and brecciated zones not represented in the sample set. Further comparisons of laboratory and in situ velocities derived by a number of techniques are shown in Table 4. With the exception of the anomalous sample from 272.40 m, velocities from C.C.S.P. samples (Table 4) vary from V_p = 2.72 to 5.17 km s^{-1} and V_s = 1.29 to 2.56 km s^{-1} at 0.05 GPa. These values are considerably lower than laboratory velocities measured on samples from the extrusive sections of other ophiolites such as the Bay of Islands (for which V_p = 5.61 to 6.36 km s^{-1} and V_s = 3.07 to 3.39 km s^{-1}) and the Oman (for which V_p = 4.79 to 5.94 km s^{-1} and V_s = 2.43 to 3.36 km s^{-1}) which are more highly metamorphosed.

A comparison of the Troodos velocities with velocities for oceanic layer 2 (Table 4) suggests that the Troodos is a poor seismic analogue of oceanic crust. The lower velocities observed for the Troodos reflect the fact that the Troodos extrusive section is anomalously porous and that the upper part of the extrusive section has been affected by intensive seafloor weathering reducing grain densities.

TABLE 4. Compressional and Shear Wave Velocities for Various Studies on Troodos, on other Ophiolites and in the Oceans

V_p (km s^{-1})	V_s (km s^{-1})	Location/Sample Set	Technique	Reference
2.9-3.7	–	Troodos, Pillow Lavas	Outcrop Velocities	Matthews et al. (1971)
3.25	–	Troodos, Pillow Lavas	Seismic Refraction	Khan et al. (1972)
4.07-4.55	–	Troodos, Pillow Lavas	Laboratory Measurements*	Poster (1973)
2.72-4.37	1.29-2.28	Troodos, CY-1	Laboratory Measurements*	Smith and Vine (1984)
2.77-5.17	1.50-2.56	Troodos, CY-2 and CY-2a	Laboratory Measurements*	This Study
2.62-3.13	–	Troodos, CY-2a	In-hole Seismic Experiment	
5.61-6.36	3.07-3.39	Bay of Islands, Metabasalts	Laboratory Measurements+	Salisbury and Christensen (1978)
4.79-5.94	2.43-3.36	Oman, Pillow Lavas	Laboratory Measurements+	Christensen and Smewing (1981)
4.7	2.2±0.3	Nootka fault zone (off Western Canada)	Seismic Refraction	Au and Clowes (1984)
4.5	2.2	Guadalupe	Seismic Refraction	Spudich and Orcutt (1980)
3.5-6.6	1.8-3.7	Oceanic Layer 2 Basalts	Laboratory Measurements*	Christensen and Salisbury (1975)
3.33-4.12	–	Oceanic Layer 2A Basalts	Sonobuoy	Houtz and Ewing (1976)
4.80-5.63	–	Oceanic Layer 2B Basalts	Sonobuoy	Houtz and Ewing (1976)

*at 0.05 GPa, +at confining pressures appropriate to the seafloor, 0.03-0.11 GPa

The mineralized lavas and dykes of the Agrokipia Mining area are not seismically distinguishable from the unmineralized lavas and dykes occurring elsewhere on the Troodos. It is therefore considered unlikely that seismic surveys will be of value in the location or evaluation of ore bodies on Troodos. This may not, however, be the case in other ophiolites or on the ocean floor where existing data suggest incompatibility with the Troodos extrusive section. Definitive velocity contrasts between mineralized and unmineralized lavas may well exist therefore in these environments.

ACKNOWLEDGMENTS

We wish to thank Sotiris Kramvis of the Cyprus Geological Survey Department for co-ordinating the in-hole seismic experiment at CY-2a. John Toussaint-Jackson assisted in the collection of the laboratory seismic data. This research was supported by the U.K. Natural Environment Research Council grant number GR3/4473.

REFERENCES

Au, D. and Clowes R.M.
1984: Shear-wave velocity structure of the oceanic lithosphere from ocean bottom seismometer studies; Geophysical Journal of the Royal Astronomical Society, v. 77, no. 1, p. 105-123.

Birch, F.
1960: The velocity of compressional waves in rocks to 10 kilobars, Part 1; Journal of Geophysical Research, v. 65, no. 4, p. 1083-1102.

Christensen, N.I. and Salisbury, M.H.
1972: Sea floor spreading, progressive alteration of layer 2 basalts, and associated changes in seismic velocities; Earth and Planetary Science Letters, v. 15, no. 4, p. 367-375.
1975: Structure and constitution of the lower oceanic crust; Reviews of Geophysics and Space Physics, v. 13, no. 1, p. 57-86.

Christensen, N.I. and Shaw, G.H.
1970: Elasticity of mafic rocks from the Mid-Atlantic Ridge; Geophysical Journal of the Royal Astronomical Society, v. 20, p. 271-284.

Christensen, N.I. and Smewing, J.D.
1981: Geology and seismic structure of the northern section of the Oman ophiolite; Journal of Geophysical Research, v. 86, no. B4, p. 2545-2555.

Evans, C.J.
1980: The seismic and electrical properties of crystalline rocks under simulated crustal conditions; unpublished Ph.D. thesis, University of East Anglia, Norwich, U.K.

Houtz, R. and Ewing, J.
1976: Upper crustal structure as a function of plate age; Journal of Geophysical Research, v. 81, no. 14, p. 2490-2498.

Hyndman, R.D. and Drury, M.J.
1976: The physical properties of oceanic basement rocks from deep drilling on the Mid-Atlantic Ridge; Journal of Geophysical Research, v. 81, no. 23, p. 4042-4052.

Khan, M.A., Summers, C., Bamford, S.A.D., Chroston, P.N., Poster, C.K. and Vine, F.J.
1972: Reversed seismic refraction line on the Troodos Massif, Cyprus; Nature, Physical Science, v. 238, no. 87, p. 134-136.

Ludwig, W.J., Nafe, J.E. and Drake, C.L.
1970: Seismic refraction; *in* The Sea, Ideas and Observations on Progress in the Study of the Seas, Volume 4, New Concepts of Sea Floor Evolution, Part I: Regional Observations, Concepts, ed. A.E. Maxwell; John Wiley and Sons, New York, v. 4, p. 53-84.

Matthews, D.H., Lort, J., Vertue, T., Poster, C.K. and Gass, I.G.
1971: Seismic velocities at the Cyprus outcrop; Nature, Physical Science, v. 231, no. 26, p. 200-201.

Pickett, G.R.
1963: Acoustic character logs and their applications in formation evaluation; Journal of Petroleum Technology, June, p. 659-667.

Poster, C.K.
1973: Ultrasonic velocities in rocks from the Troodos Massif, Cyprus; Nature, Physical Science, v. 243, no. 123, p. 2-3.

Raitt, R.W.
1963: The crustal rocks; *in* The Sea, Ideas and Observations on Progress in the Study of the Seas, Volume 3, The Earth beneath the Sea, ed. M.N. Hill; John Wiley and Sons, New York, v. 3, p. 85-102.

Robinson, P.T. and Gibson, I.L.
1983a: Cyprus Crustal Study Project. Hole CY-2 Lithologic Unit Summaries.
1983b: Cyprus Crustal Study Project. Hole CY-2a Lithologic Unit Summaries.

Salisbury, M.H. and Christensen, N.I.
1978: The seismic velocity structure of a traverse through the Bay of Islands ophiolite complex, Newfoundland: an

exposure of oceanic crust and upper mantle; Journal of Geophysical Research, v. 83, no. B2, p. 805-817.

Simmons, G.
1964: Velocity of shear waves in rocks to 10 kilobars, Part 1; Journal of Geophysical Research, v. 69, no. 6, p. 1123-1130.

Smith, G.C. and Vine, F.J.
1984: Physical property data from ICRDG drill hole CY-1, Akaki Canyon, Cyprus; Geophysical Journal of the Royal Astronomical Society, v. 77, no. 1, p. 298.
1987a: Electrical conductivity of basalts from C.C.S.P. drill holes CY-2 and CY-2a at Agrokipia Mines, Cyprus; *in* Cyprus Crustal Study Project Initial Report Hole CY2-2a, ed. P.T. Robinson, I.L. Gibson and A. Panayiotou; Geological Survey of Canada, Paper 85-29.
1987b: Gravity and magnetic studies of the Agrokipia sulphide ore bodies, Cyprus; *in* Cyprus Crustal Study Project Initial Report Hole CY2-2a, ed. P.T. Robinson, I.L. Gibson and A. Panayiotou; Geological Survey of Canada, Paper 85-29.

Spudich, P.K. and Orcutt, J.
1980: Petrology and porosity of an oceanic crustal site: results from wave form modelling of seismic refraction data; Journal of Geophysical Research, v. 85, no. B3, p. 1409-1433.

Vine, F.J.
1981: Introduction: physical properties of rocks; *in* Progress in Experimental Petrology; Fifth Progress Report of Research Supported by N.E.R.C., The Natural Environment Research Council Publications, Series D, no. 18, p. 261-263.

Whitmarsh, R.B.
1978: Seismic refraction studies of the upper igneous crust in the North Atlantic and porosity estimates for layer 2; Earth and Planetary Science Letters, v. 37, no. 3, p. 451-464.

Wyllie, M.R.J., Gregory, A.R. and Gardner, G.H.F.
1958: An experimental investigation of factors affecting elastic wave velocities in porous media; Geophysics, v. 23, p. 459-493.

Seismic Properties of Samples from the Volcanic Section of the Troodos Ophiolite, Hole CY-2a

NIKOLAS I. CHRISTENSEN[1], WILLIAM W. WEPFER[1] AND MATTHEW H. SALISBURY[2]

[1]Department of Earth and Atmospheric Sciences, Purdue University,
West Lafayette, Indiana, U.S.A.
[2]Centre for Marine Geology, Dalhousie University, Halifax, Nova Scotia, Canada

Christensen, N.I., Wepfer, W.W. and Salisbury, M.H., Seismic properties of samples from the volcanic section of the Troodos Ophiolite, Hole CY-2a; in *Cyprus Crustal Study Project: Initial Report, Holes CY-2 and 2a, ed. P.T. Robinson, I.L. Gibson and A. Panayiotou; Geological Survey of Canada, Paper 85-29, p. 307-315, 1987.*

Abstract

Compressional and shear wave velocities are reported to confining pressures of 600 MPa for 17 altered igneous samples from ICRDG Hole CY-2a in the Troodos Ophiolite. Velocities increase with increasing depth and correlate well with bulk density and porosity. The compressional wave velocity gradient (dV_p/dZ) is approximately 2.1/s in good agreement with a Layer 2 velocity gradient of 1.9/s reported in the Pacific at DSDP Site 504B by Stephen and Harding (1983). Since pillow basalts are uncommon in the section and the intensity and grade of metamorphism increase with depth, our results suggest that positive velocity gradients similar to those observed in oceanic Layer 2 can be produced by changes in microporosity and metamorphic grade.

Résumé

Les vitesses des ondes de compression et de cisaillement à des pressions de confinement de 600 MPa ont été déterminées pour 17 échantillons de roches ignées altérées du trou de forage CY-2a, ICRDG, dans l'ophiolite de Troodos. Les vitesses augmentent avec l'accroissement de la profondeur et la corrélation est excellente avec la densité apparente et la porosité. Le gradient de la vitesse des ondes de compressions (dV_p/dZ) est approximativement 2,1/s, en accord le gradient de vitesse de 1,9/s pour la Couche 2 dans le Pacifique obtenu au site 504B du projet DSDP par Stephen et Harding (1983). Vu que les basaltes en coussinets sont peu abondants dans la section et que l'intensité et le degré du métamorphisme croissent avec la profondeur, nos résultats révèlent que les gradients de vitesse positifs similaires à ceux observés dans la Couche 2 océanique peuvent être dus à des changements de microporosité et de degré de métamorphisme.

INTRODUCTION

During the past two decades our knowledge of Layer 2 of the oceanic crust has increased considerably. While early oceanic seismic refraction studies (e.g. Raitt, 1963) only provided average compressional wave velocities for Layer 2, more detailed sonobuoy techniques enabled Houtz and Ewing (1976) to subdivide Layer 2 into three units: an upper unit (2A) with velocities below 4 km/s, an intermediate unit (2B) with velocities between 4.8 and 5.7 km/s, and a lower unit (2C) with velocities in excess of 6.0 km/s. More recent studies using amplitude as well as travel time analysis have shown that the velocity structure of Layer 2 consists of gradients (Helmberger and Morris, 1969) and velocity logs obtained to a sub-basement depth of 1030 m in DSDP Hole 504B substantiate these models (Salisbury et al., 1985). Upper Layer 2 compressional wave velocities corresponding to Layer 2A are 4.0 km/s or less. Velocities generally increase with depth to 1 km, where they reach 6.0 km/s.

Worldwide recovery by DSDP of samples from the basement demonstrates that basalt is the most common rock type forming the upper portion of Layer 2. Since laboratory measurements of velocities in DSDP basaltic rocks at appropriate confining pressures and conditions of water saturation are generally much higher than 4.0 km/s (Christensen and Salisbury, 1975), it is generally concluded that the velocities in Layer 2A are lowered by the presence of porosity in the form of large scale fractures and rubble zones (Hyndman and Drury, 1976) and that the observed gradients reflect decreasing crack porosity with depth. Compressional wave velocities in basalt samples collected from the Bay of Islands and Samail ophiolites are also higher than the Layer 2 velocities determined by seismic refraction and logging (Salisbury and Christensen, 1978; Christensen and Smewing, 1981), supporting the crack porosity model.

Between 1983 and 1985, the International Crustal Research Drilling Group (ICRDG) drilled an array of holes through different stratigraphic levels of the Troodos Ophiolite in an attempt to reconstruct the petrology, geochemistry and geophysical properties of the complex as a function of depth for comparison with the results of drilling and geophysical studies at sea. While many of the results are consistent with those observed at sea (the volcanic section grades downward from pillow basalts at the sediment/basement contact through sheeted dykes at depth and the metamorphic grade increases markedly with depth), some features are quite different (the volcanic section is composed of andesites and basaltic andesites rather than tholeiites and contains a high proportion of massive sheet flows), leading the ICRDG investigators to characterize the complex as oceanic with island arc affinities.

In this paper, we present laboratory velocity data for 17 samples obtained from various depths in Hole CY-2a which was spudded near the village of Agrokipia in the vicinity of the pillow basalt/sheet flow transition about 200 m below the sediment/basement contact and penetrated a mineralized stockwork zone. As can be seen in Table 1, the hole was drilled through a 689 m section of dykes, sills, sheet flows and minor pillows of predominantly andesitic composition. Importantly, the core shows a marked increase in the intensity and grade of metamorphic alteration with depth: from 0-149 m (Units I-VI), the section shows evidence of variable low temperature alteration (halmyrolysis); glass is locally preserved but is often partially replaced, along with the groundmass, by smectite and minor calcite. From 149-297 m (Units VII-X), the section has undergone pervasive hydrothermal alteration: the rocks are cream-coloured, pyrite is abundant (up to 10%), and the groundmass has been almost completely replaced by chlorite and illite plus minor calcite, quartz and zeolites. Between 297-689 m, the section has undergone pervasive greenschist facies alteration, with the groundmass being completely replaced by chlorite, epidote, quartz and albite plus minor calcite and pyrite. Although the section drilled cannot be regarded as strictly equivalent to oceanic Layer 2, the data from this interval suggests an alternate origin for velocity gradients such as those observed in Layer 2.

EXPERIMENTAL TECHNIQUE AND DATA

Compressional and shear wave velocity measurements were made on the samples at elevated pressures using the pulse transmission method summarized by Birch (1960) and described in detail by Christensen (1985). Minicores were taken perpendicular to the drill core (i.e. horizontal relative to the surface) using a diamond drill. The ends of the samples were then cut with a diamond cut-off saw to form a right circular cylinder and hand polished on a lap wheel until flat and parallel to within 0.008 cm. Typical dimensions for the samples after cutting and polishing were 2.54 cm in diameter and 4.00 cm in length. After the dry bulk densities had been determined from the mass and dimensions of each sample, the cores were saturated by placing them in distilled water and pulling a moderate vacuum. The wet bulk densities and effective porosities presented in Table 2 were then determined by re-weighing the samples.

Each sample was surrounded with a fine mesh copper screen and jacketed in copper foil. The screen allowed for the migration of fluid from the pores while the sample was under pressure to prevent

excessive pore pressure build up. Brass shim discs were spot soldered on each end of the copper jackets to provide an electrical ground for the transducers.

Appropriately oriented lead zirconate titanate (PZT) transducers of nominal 1 MHz resonant frequency were used both in the compressional measurements and as the receiving transducers in the shear wave velocity determinations. AC cut quartz crystals were the sending transducers for the shear wave measurements. Each transducer was mounted on a brass electrode through which the electrical connection was made. A transducer was placed on each end of the core in contact with the brass shim disc and gum rubber tubing was fitted over the interface to exclude the pressure medium.

The sample assembly was then placed in the hydraulic press described by Christensen (1985) and velocities were measured to 600 MPa (6 kbar) using a calibrated mercury delay line. The values obtained, together with bulk modulus (K), shear modulus (μ), Poisson's ratio (σ) and V_p/V_s values calculated from the velocities and densities at selected pressures, are given in Table 2. The velocities and densities used in the calculations were corrected for length and volume changes at elevated pressures using an iterative routine and dynamically determined compressibilities.

TABLE 1. Lithology, Petrology and Nature of Alteration vs. Depth in Hole CY-2a*

Depth (m)	Unit	Lithology	Petrology	Alteration
3.35-30.72	I	Dikes/Sills	Basaltic Andesite	
31.15-67.50	III	Sheet Flows	Andesite and Basaltic Andesite	Variable, low temperature alteration. Groundmass fresh to strongly replaced by dark green clay plus minor calcite, zeolites.
67.50-89.90	IV	Dikes/Sills	Basaltic Andesite	
89.90-109.00	V	Sheet Flows	Andesite	
109.00-297.14	VI-X	Glassy Sheet Flows	Andesite	Variable, low temperature alteration to smectite; glass locally preserved. Pervasive hydrothermal alteration. Groundmass replaced by chlorite, illite, plus minor calcite, smectite, quartz, celadonite. Pyrite abundant.
297.49-403.80	XII-XIV	Dikes/Sills	Andesites	
403.80-528.90	XV-XXI	Pillows/Screens	Andesite & Dacite	Pervasive high temperature alteration. Groundmass replaced by chlorite, epidote, quartz, albite.
528.90-689.15	XXII	Dikes/Sills	Andesite	

*(after Robinson and Gibson, 1983; Bednarz et al., 1987)

TABLE 2. Compressional (V_p) and Shear (V_s) Wave Velocities, Densities (ρ), Porosities (ϕ), Poisson's Ratios (σ), Bulk Moduli (K), and Shear Moduli (μ) of CY-2a Rocks

Sample Depth	P (MPa)	V_p (km/s)	V_s (km/s)	V_p/V_s	σ	K (MPa x 10^5)	μ (MPa x 10^5)
10.25 m	20	3.39	2.05	1.65	0.21	0.14	0.10
ρ = 2.37 g cm^{-3}	40	3.43	2.08	1.65	0.21	0.14	0.10
ϕ = 16.8%	60	3.48	2.11	1.65	0.21	0.15	0.11
	80	3.53	2.18	1.62	0.19	0.15	0.11
	100	3.59	2.20	1.63	0.20	0.15	0.12
	200	3.83	2.27	1.69	0.23	0.19	0.12
	400	4.25	2.37	1.79	0.27	0.25	0.13
	600	4.44	2.42	1.83	0.29	0.28	0.14
84.31 m	20	4.22	2.34	1.80	0.28	0.27	0.14
ρ = 2.57 g cm^{-3}	40	4.32	2.37	1.82	0.28	0.29	0.14
ϕ = 6.2%	60	4.34	2.39	1.82	0.28	0.29	0.15
	80	4.39	2.40	1.83	0.29	0.30	0.15
	100	4.42	2.41	1.83	0.29	0.30	0.15
	200	4.54	2.46	1.85	0.29	0.32	0.16
	400	4.67	2.48	1.88	0.30	0.35	0.16
	600	4.74	2.50	1.90	0.31	0.37	0.16
138.35 m	20	4.30	2.39	1.80	0.28	0.27	0.14
ρ = 2.46 g cm^{-3}	40	4.33	2.44	1.77	0.27	0.27	0.15
ϕ = 8.9%	60	4.35	2.48	1.75	0.26	0.26	0.15
	80	4.36	2.50	1.74	0.26	0.26	0.15
	100	4.37	2.52	1.73	0.25	0.26	0.16
	200	4.41	2.58	1.71	0.24	0.26	0.16
	400	4.48	2.62	1.71	0.24	0.27	0.17
	600	4.54	2.64	1.72	0.24	0.28	0.17
217.90 m	20	3.93	2.00	1.97	0.33	0.25	0.10
ρ = 2.41 g cm^{-3}	40	3.97	2.06	1.93	0.32	0.24	0.10
ϕ = 14.0%	60	3.99	2.10	1.91	0.31	0.24	0.11
	80	4.02	2.13	1.89	0.31	0.24	0.11
	100	4.03	2.15	1.88	0.30	0.25	0.11
	200	4.11	2.22	1.85	0.29	0.25	0.12
	400	4.24	2.28	1.86	0.30	0.27	0.13
	600	4.43	2.32	1.91	0.31	0.30	0.13
258.83 m	20	3.93	2.02	1.94	0.32	0.24	0.10
ρ = 2.36 g cm^{-3}	40	3.96	2.06	1.92	0.31	0.24	0.10
ϕ = 12.9%	60	3.99	2.10	1.90	0.31	0.24	0.10
	80	4.01	2.12	1.89	0.31	0.24	0.11
	100	4.03	2.14	1.88	0.30	0.24	0.11
	200	4.11	2.21	1.86	0.30	0.24	0.12
	400	4.23	2.28	1.86	0.30	0.26	0.12
	600	4.34	2.33	1.87	0.30	0.28	0.13

Sample Depth	P (MPa)	V_p (km/s)	V_s (km/s)	V_p/V_s	σ	K (MPa x 10^5)	μ (MPa x 10^5)
260.28 m	20	4.53	2.30	1.97	0.33	0.34	0.13
ρ = 2.49 g cm^{-3}	40	4.55	2.36	1.93	0.32	0.33	0.14
ϕ = 10.2%	60	4.57	2.39	1.91	0.31	0.33	0.14
	80	4.59	2.42	1.90	0.31	0.33	0.15
	100	4.60	2.44	1.89	0.30	0.33	0.15
	200	4.67	2.51	1.86	0.30	0.33	0.16
	400	4.78	2.58	1.85	0.30	0.35	0.17
	600	4.89	2.64	1.85	0.29	0.37	0.17
278.59 m	20	3.88	2.07	1.87	0.30	0.22	0.10
ρ = 2.37 g cm^{-3}	40	3.92	2.13	1.84	0.29	0.22	0.11
ϕ = 12.8%	60	3.95	2.15	1.84	0.29	0.22	0.11
	80	3.98	2.17	1.83	0.29	0.23	0.11
	100	4.01	2.19	1.83	0.29	0.23	0.11
	200	4.12	2.28	1.81	0.28	0.24	0.12
	400	4.30	2.40	1.79	0.27	0.26	0.14
	600	4.46	2.49	1.79	0.27	0.28	0.15
320.01 m	20	4.48	2.46	1.82	0.28	0.31	0.15
ρ = 2.55 g cm^{-3}	40	4.51	2.50	1.81	0.28	0.31	0.16
ϕ = 5.2%	60	4.53	2.53	1.79	0.27	0.31	0.16
	80	4.51	2.56	1.76	0.26	0.30	0.17
	100	4.57	2.58	1.77	0.27	0.31	0.17
	200	4.63	2.66	1.74	0.25	0.31	0.18
	400	4.69	2.72	1.72	0.25	0.31	0.19
364.31 m	20	4.70	2.61	1.80	0.28	0.34	0.18
ρ = 2.59 g cm^{-3}	40	4.72	2.64	1.79	0.27	0.34	0.18
ϕ = 3.9%	60	4.74	2.66	1.78	0.27	0.34	0.18
	80	4.76	2.75	1.73	0.25	0.33	0.20
	100	4.80	2.70	1.78	0.27	0.34	0.19
	200	4.88	2.76	1.77	0.26	0.35	0.20
	400	4.98	2.83	1.76	0.26	0.37	0.21
385.01 m	20	4.75	2.65	1.80	0.28	0.34	0.18
ρ = 2.54 g cm^{-3}	40	4.78	2.67	1.79	0.27	0.34	0.18
ϕ = 4.5%	60	4.80	2.69	1.78	0.27	0.34	0.18
	80	4.82	2.71	1.78	0.27	0.34	0.19
	100	4.83	2.72	1.77	0.27	0.34	0.19
	200	4.87	2.77	1.76	0.26	0.34	0.20
	400	4.94	2.83	1.75	0.26	0.35	0.20
402.50 m	20	4.64	2.45	1.89	0.31	0.35	0.16
ρ = 2.58 g cm^{-3}	40	4.68	2.53	1.85	0.29	0.35	0.16
ϕ = 6.8%	60	4.71	2.58	1.83	0.29	0.35	0.17
	80	4.73	2.61	1.81	0.28	0.34	0.18
	100	4.75	2.64	1.80	0.28	0.34	0.18
	200	4.81	2.73	1.76	0.26	0.34	0.19
	400	4.92	2.83	1.74	0.25	0.35	0.21

Sample Depth	P (MPa)	V_p (km/s)	V_s (km/s)	V_p/V_s	σ	K (MPa x 10^5)	μ (MPa x 10^5)
426.35 m	20	4.20	2.39	1.76	0.26	0.25	0.14
ρ = 2.48 g cm^{-3}	40	4.22	2.42	1.75	0.26	0.25	0.14
ϕ = 15.2%	60	4.24	2.43	1.75	0.26	0.25	0.15
	80	4.26	2.45	1.74	0.25	0.25	0.15
	100	4.27	2.45	1.74	0.25	0.25	0.15
	200	4.34	2.48	1.75	0.26	0.26	0.15
	400	4.45	2.50	1.78	0.27	0.29	0.16
476.30 m	20	4.62	2.43	1.90	0.31	0.34	0.15
ρ = 2.50 g cm^{-3}	40	4.65	2.48	1.88	0.30	0.34	0.15
ϕ = 10.3%	60	4.68	2.52	1.86	0.30	0.34	0.16
	80	4.69	2.55	1.84	0.29	0.33	0.16
	100	4.70	2.57	1.83	0.29	0.33	0.17
	200	4.73	2.63	1.80	0.28	0.33	0.17
	400	4.81	2.70	1.78	0.27	0.34	0.18
529.6 m	20	4.45	2.35	1.90	0.31	0.31	0.14
ρ = 2.51 g cm^{-3}	40	4.49	2.43	1.85	0.29	0.31	0.15
ϕ = 10.5%	60	4.52	2.48	1.82	0.29	0.31	0.15
	80	4.58	2.51	1.82	0.29	0.32	0.16
	100	4.56	2.54	1.80	0.28	0.31	0.16
	200	4.64	2.63	1.76	0.26	0.31	0.17
	400	4.77	2.70	1.77	0.26	0.33	0.18
569.40 m	20	4.65	2.25	2.07	0.35	0.38	0.13
ρ = 2.55 g cm^{-3}	40	4.74	2.31	2.05	0.34	0.39	0.14
ϕ = 8.9%	60	4.71	2.36	2.00	0.33	0.38	0.14
	80	4.73	2.40	1.97	0.33	0.37	0.15
	100	4.74	2.43	1.95	0.32	0.37	0.15
	200	4.80	2.51	1.91	0.31	0.37	0.16
	400	4.92	2.58	1.91	0.31	0.39	0.17
624.4 m	20	4.93	2.54	1.94	0.32	0.42	0.17
ρ = 2.67 g cm^{-3}	40	5.02	2.60	1.93	0.32	0.43	0.18
ϕ = 5.1%	60	5.07	2.66	1.91	0.31	0.43	0.19
	80	5.10	2.70	1.89	0.30	0.43	0.19
	100	5.13	2.80	1.83	0.29	0.42	0.21
	200	5.20	2.85	1.82	0.28	0.43	0.22
	400	5.29	2.91	1.82	0.28	0.45	0.23
672.4 m	20	5.53	3.11	1.78	0.27	0.48	0.26
ρ = 2.71 g cm^{-3}	40	5.59	3.13	1.78	0.27	0.49	0.27
ϕ = 1.4%	60	5.63	3.16	1.78	0.27	0.50	0.27
	80	5.65	3.17	1.78	0.27	0.50	0.27
	100	5.67	3.18	1.78	0.27	0.51	0.27
	200	5.72	3.21	1.78	0.27	0.52	0.28
	400	5.78	3.23	1.79	0.27	0.53	0.28

DISCUSSION

In Figure 1, velocities at 40 MPa are plotted versus sample depths in Hole CY-2a. Compressional wave velocities are extremely low in the upper part of the hole but are seen to increase rapidly with depth from approximately 3.7 km/s at the top of CY-2a to 5.2 km/s at the base while shear wave velocities increase from 2.1 km/s to 2.7 km/s over an equivalent depth range. Calculated gradients from least squares solutions to the data in Figure 1 are 2.1/s and 0.9/s for compressional and shear wave velocities, respectively. Poisson's ratios derived from the least squares velocity-depth solutions vary from 0.27 at the surface to 0.31 at total depth. Regression parameters are given in Table 3. A multiple linear regression of compressional velocity on porosity and depth determined by R. Carlson (pers. comm.) using the same data gives $V_p = 4.6 - 6.9\phi + 1.32z$ with r = 0.92 and an rms error of 0.14 km/s. This is an improvement over the regressions given in Table 3 and suggests that the observed velocity-depth profiles are influenced by several factors.

Since the section drilled in Hole CY-2a consists almost entirely of rocks of andesitic composition and these are relatively massive throughout most of the hole, the observed increases in velocity with depth are apparently related in large part to changes in mineralogy, although decreasing microporosity (grain boundary porosity) and glass content are responsible in part for the observed velocity gradients. In Figure 2, velocities at 40 MPa are plotted versus wet bulk densities. Figure 3, in which velocities are shown versus porosities, clearly shows that the lower velocities and densities correlate with high porosities. This figure also shows that the intrinsic (zero-porosity) velocity of the samples (5.3 km/s) is lower than that of andesite (6.0 km/s) or basalt (6.4 km/s). This can only be due to alteration. In particular, we attribute the low velocities in the top of the section to the presence of clay and glass, the low velocities at intermediate depths to the presence of chlorite and illite and the increase in velocity at greater depths to the disappearance of illite and the appearance of epidote.

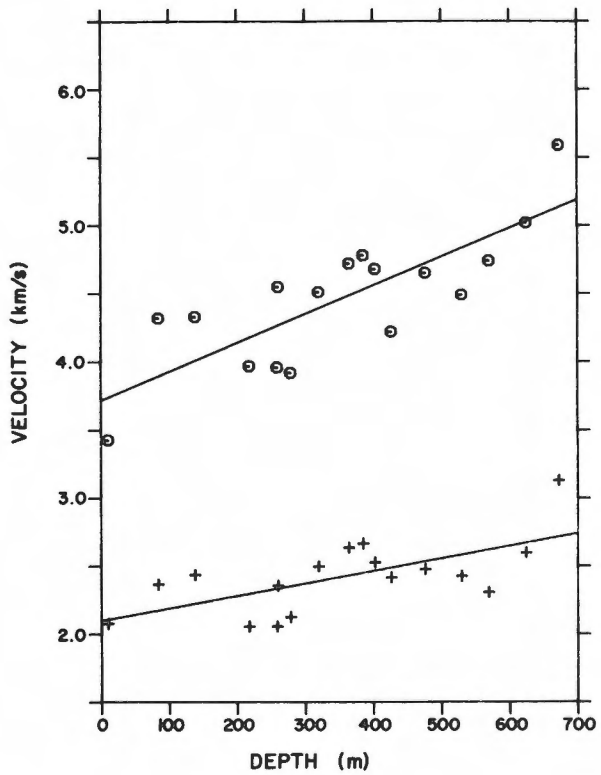

Figure 1: Compressional (0) and shear (+) wave velocities versus depth at 40 MPa confining pressure.

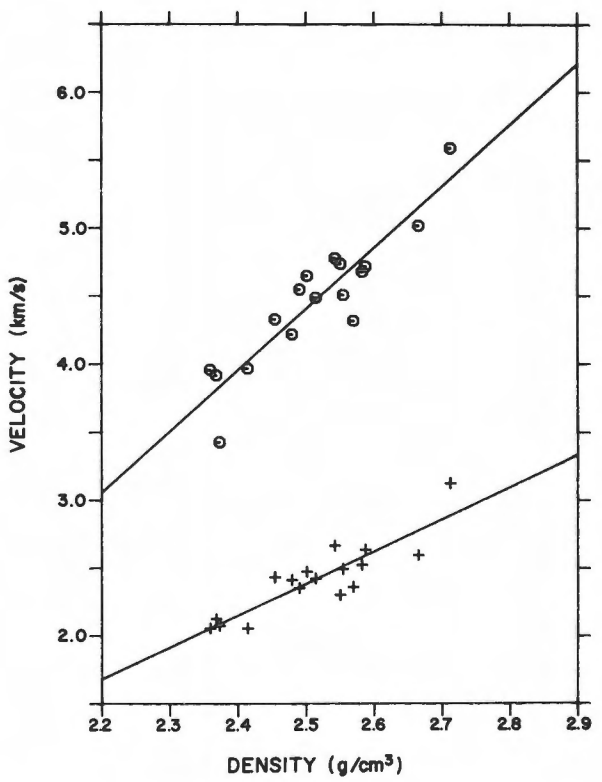

Figure 2: Compressional (0) and shear (+) wave velocities versus wet bulk densities at 40 MPa confining pressure.

TABLE 3. Regression Line Parameters

Equation	Slope	Intercept	r
$V_p = mz + b$ (km)	2.1 l/s	3.7 km/s	0.80
$V_s = mz + b$ (km)	0.9 l/s	2.1 km/s	0.64
$V_p = m\rho + b$ (g/cm^3)	4.5 $\frac{\text{km/s}}{\text{g/cm}^3}$	-6.9 km/s	0.91
$V_s = m\rho + b$ (g/cm^3)	2.4 $\frac{\text{km/s}}{\text{g/cm}^3}$	-3.5 km/s	0.88
$V_p = m\phi + b$ (%)	-0.096 km/s	5.3 km/s	-0.86
$V_s = m\phi + b$ (%)	-0.051 km/s	2.9 km/s	-0.84

z: depth, ρ: density, ϕ: porosity, r: correlation coefficient

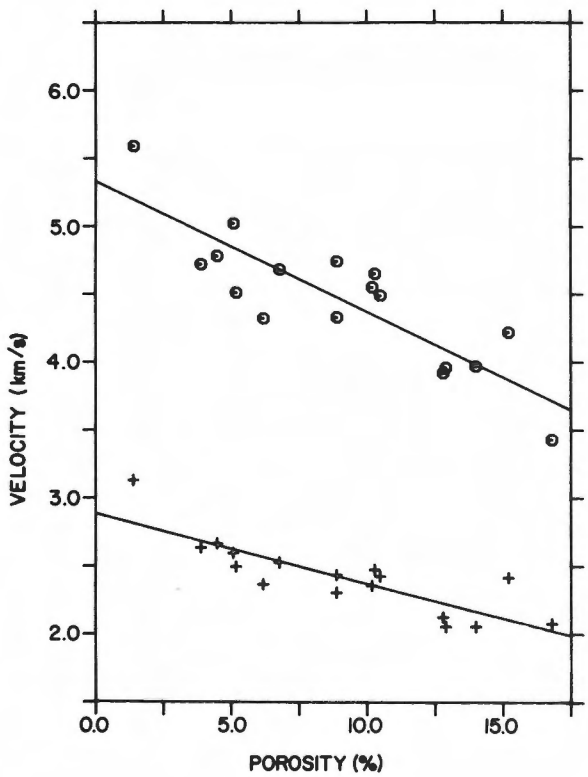

Figure 3: Compressional (0) and shear (+) wave velocities versus porosity at 40 MPa confining pressure.

Low seismic velocities in the upper portion of Layer 2 are commonly attributed to the presence of fractures (Hyndman and Drury, 1976). As was discussed earlier, strong support for this explanation is found in many oceanic regions where laboratory measurements of DSDP cores give significantly higher velocities than those determined by refraction and borehole techniques. In Hole 504B, for example, where sample velocities range narrowly between 5.7 and 6.3 km/s, the compressional wave formation velocities measured both by logging (Salisbury et al., 1985) and by refraction (Stephen and Harding, 1983) increase steadily from 4.0 to 6.0 km/s in response to crack closure in the uppermost kilometre of the volcanics. While the velocity gradient measured in samples from Hole CY-2a is nearly identical to that in Hole 504B, our measurements in the Cyprus volcanics suggest that such gradients may also originate from changes in mineralogy and microporosity. Thus, the positive velocity gradient within Layer 2 may locally originate from decreasing microporosity and increasing metamorphic grade with depth rather than decreasing cracks and fractures.

ACKNOWLEDGEMENTS

This study was supported by NSF Grant No. 8311776AZ, ONR contract N00014-84-K-0207, and NSERC Grant No. IRP-8403.

REFERENCES

Bednarz, U., Sunkel, G. and Schmincke, H.-U.
1987: The basaltic andesite-andesite and the andesite-dacite series from ICRDG drill holes CY-2 and CY-2a. I. Lithology, petrology and geochemistry; *in* Cyprus Crustal Study Project Initial Report Hole CY2-2a, ed. P.T. Robinson, I.L. Gibson and A. Panayiotou; Geological Survey of Canada, Paper 85-29.

Birch, F.
1960: The velocity of compressional waves in rocks to 10 kilobars, Part 1; Journal of Geophysical Research, v. 65, no. 4, p. 1083-1102.

Christensen, N.I.
1985: Measurements of dynamic properties of rock at elevated temperatures and pressures; *in* Measurement of Rock Properties at Elevated Pressures and Temperatures, American Society for Testing and Materials, Special Technical Publication 869, ed. H.J. Pincus and E.R. Hoskins; American Society for Testing and Materials, Philadelphia, no. 869, p. 93-107.

Christensen, N.I. and Salisbury, M.H.
1975: Structure and constitution of the lower oceanic crust; Reviews of Geophysics and Space Physics, v. 13, no. 1, p. 57-86.

Christensen, N.I. and Smewing, J.D.
1981: Geology and seismic structure of the northern section of the Oman ophiolite; Journal of Geophysical Research, v. 86, no. B4, p. 2545-2555.

Helmberger, D.V. and Morris, G.B.
1969: A travel time and amplitude interpretation of a marine refraction profile: primary waves; Journal of Geophysical Research, v. 74, no. 2, p. 483-494.

Houtz, R. and Ewing, J.
1976: Upper crustal structure as a function of plate age; Journal of Geophysical Research, v. 81, no. 14, p. 2490-2498.

Hyndman, R.D. and Drury, M.J.
1976: The physical properties of oceanic basement rocks from deep drilling on the Mid-Atlantic Ridge; Journal of Geophysical Research, v. 81, no. 23, p. 4042-4052.

Raitt, R.W.
1963: The crustal rocks; *in* The Sea, Ideas and Observations on Progress in the Study of the Seas, Volume 3, The Earth beneath the Sea, ed. M.N. Hill; John Wiley and Sons, New York, v. 3, p. 85-102.

Robinson, P.T. and Gibson, I.L.
1983: Cyprus Crustal Study Project. Hole CY-2a Lithologic Unit Summaries.

Salisbury, M.H. and Christensen, N.I.
1978: The seismic velocity structure of a traverse through the Bay of Islands ophiolite complex, Newfoundland: an exposure of oceanic crust and upper mantle; Journal of Geophysical Research, v. 83, no. B2, p. 805-817.

Salisbury, M.H., Christensen, N.I., Becker, K. and Moos, D.
1985: The velocity structure of Layer 2 at Deep Sea Drilling Project Site 504 from logging and laboratory experiments; *in* Initial Reports of the Deep Sea Drilling Project, Volume 83, ed. R.N. Anderson, J. Honnorez, K. Becker, et al.; U.S. Government Printing Office, Washington, D.C., v. 83, p. 529-539.

Stephen, R.A. and Harding, A.J.
1983: Travel time analysis of borehole seismic data; Journal of Geophysical Research, v. 88, no. B10, p. 8289-8298.

A Seismic Survey at the Agrokipia Mine, Cyprus: The Velocity Structure of a Hydrothermally Altered Extrusive Section of the Troodos Ophiolite

SERGHIS ELEFTHERIOU[1] AND GUENTHER SCHOENHARTING[2]

[1]Geological Survey Department, Nicosia, Cyprus
[2]Copenhagen University, Copenhagen, Denmark

Eleftheriou, S. and Schoenharting, G., A seismic survey at the Agrokipia Mine, Cyprus: the velocity structure of a hydrothermally altered extrusive section of the Troodos Ophiolite; in *Cyprus Crustal Study Project: Initial Report, Holes CY-2 and 2a, ed. P.T. Robinson, I.L. Gibson and A. Panayiotou; Geological Survey of Canada, Paper 85-29, p. 317-326, 1987.*

Abstract

During the Agrokipia mine seismic survey, 11 shots in the vicinity of Cyprus Crustal Study Project Holes CY-2 and CY-2a were fired into a 3-segment spread and recorded digitally with a 24-channel seismic unit. Velocities of both P and S waves were determined for the uppermost 100 to 200 m using arrivals from diving waves. Below this depth velocities were modelled to fit traveltime-distance observations from critically refracted/reflected waves for spreads offset farther to the east and southeast. 1-D modelling was performed for each shotpoint and a 2-D raytracing model was established for a W-E profile, which includes Holes CY-2 and CY-2a. Comparison with velocity data measured on drill core samples revealed generally systematic differences towards lower velocities from our study. This feature is believed to reflect the different sampling scales and possible bias in drillcore sampling. The local velocity structure around the Agrokipia 'A' and 'B' deposits departs considerably from the average extrusive section outside. The Agrokipia 'B' ore deposit is characterized by a low velocity body surrounded by a high velocity zone that parallels the alteration zone of highly silicified rocks at the top of the stockwork. The average velocity gradient for the upper 300 m at Agrokipia is about 5 s^{-1}. For the 300 to 800 m interval the gradient is about 2 s^{-1}, which falls into the range of oceanic layer 2 values.

Résumé

Dans le levé sismique effectué sur la mine Agrokipia, 11 coups ont été tirés à proximité des trous de forage CY-2 et CY-2a du Cyprus Crustal Study Project, ils couvraient trois segments d'une aire et les données furent recueillies par un sismographe à enregistrement numérique à 24 canaux. Les temps d'arrivées des ondes plongeantes ont été utilisés pour mesurer les vitesses des ondes P et S des premiers 100 à 200 m sous la surface. Pour une plus grande profondeur, on a élaboré un modèle d'harmonisation des vitesses avec les observations faites sur les temps de propagation-distances des ondes critiquement réfractées/réfléchies résultant du décalage entre des aires explorées plus à l'est et au sud-est. Une modélisation à 1-D a été réalisée pour chaque point de tir et un modèle à 2-D du traçage de la trajectoire des rayons fut établi pour un profil ouest-est incluant les trous CY-2 et CY-2a. Une comparaison avec les vitesses mesurées sur les échantillons des carottes des trous de forage révèlent en général des différences de vitesse systématiquement plus faibles que dans notre étude. Ce phénomène résulte possiblement des différences dans les échelles d'échantillonnage et de la déviation du trou d'échantillonnage. La structure de vitesse locale autour des gîtes Agrokipia 'A' et 'B' diffère considérablement de celle dans la coupe volcanique externe. Le gîte Agrokipia 'B' est un corps caractérisé par une vitesse faible et il est entouré d'une bande à vitesse élevée parallèle à la zone d'altération constituée des roches profondément silicifiées au toit du stockwerk. Le gradient moyen de vitesse pour les premiers 300 m sous la surface à Agrokipia est environ 5 s^{-1}. Pour l'intervalle de 300 à 800 m le gradient est environ 2 s^{-1}, lequel correspond à la gamme des valeurs vavoisinant 2 dans la couche océanique.

INTRODUCTION

As part of the geophysical studies associated with the Cyprus Crustal Study Project carried out by the International Crustal Research Drilling Group (ICRDG) on the Troodos ophiolite, seismic surveys were carried out in the vicinity of Holes CY-2 and CY-2a in order to better define the structure and stratigraphic setting of the Agrokipia ore deposits. Furthermore, the surveys were designed to compare the velocity structure of the ophiolite with that of the oceanic crust. There are now clear geochemical and geologic indications that the Troodos ophiolite was formed by supra-subduction zone spreading (Moores et al., 1984; Schmincke et al., 1983; Robinson et al., 1983). However, certain characteristics such as the sheeted dyke complex, grabens associated with listric faulting (Verosub and Moores, 1981) and ore deposits similar to modern day East Pacific Rise deposits (Oudin et al., 1981; Malahoff, 1982) indicate also similarities with oceanic crust formed at mid-oceanic ridges.

Previous seismic studies on Troodos (Matthews et al., 1971; Khan et al., 1972; Lort and Matthews, 1972; Eleftheriou, 1983) indicated rather low seismic velocities compared with those of in-situ oceanic crust (Spudich and Orcutt, 1980a).

In this paper the results of the seismic survey around the Agrokipia mine are presented. This survey forms part of a larger experiment, conducted in 1983 and 1984, aiming at mapping the seismic velocity structure of the extrusive section in the triangle between the villages of Agrokipia, Aredhiou and Klirou (Figure 1).

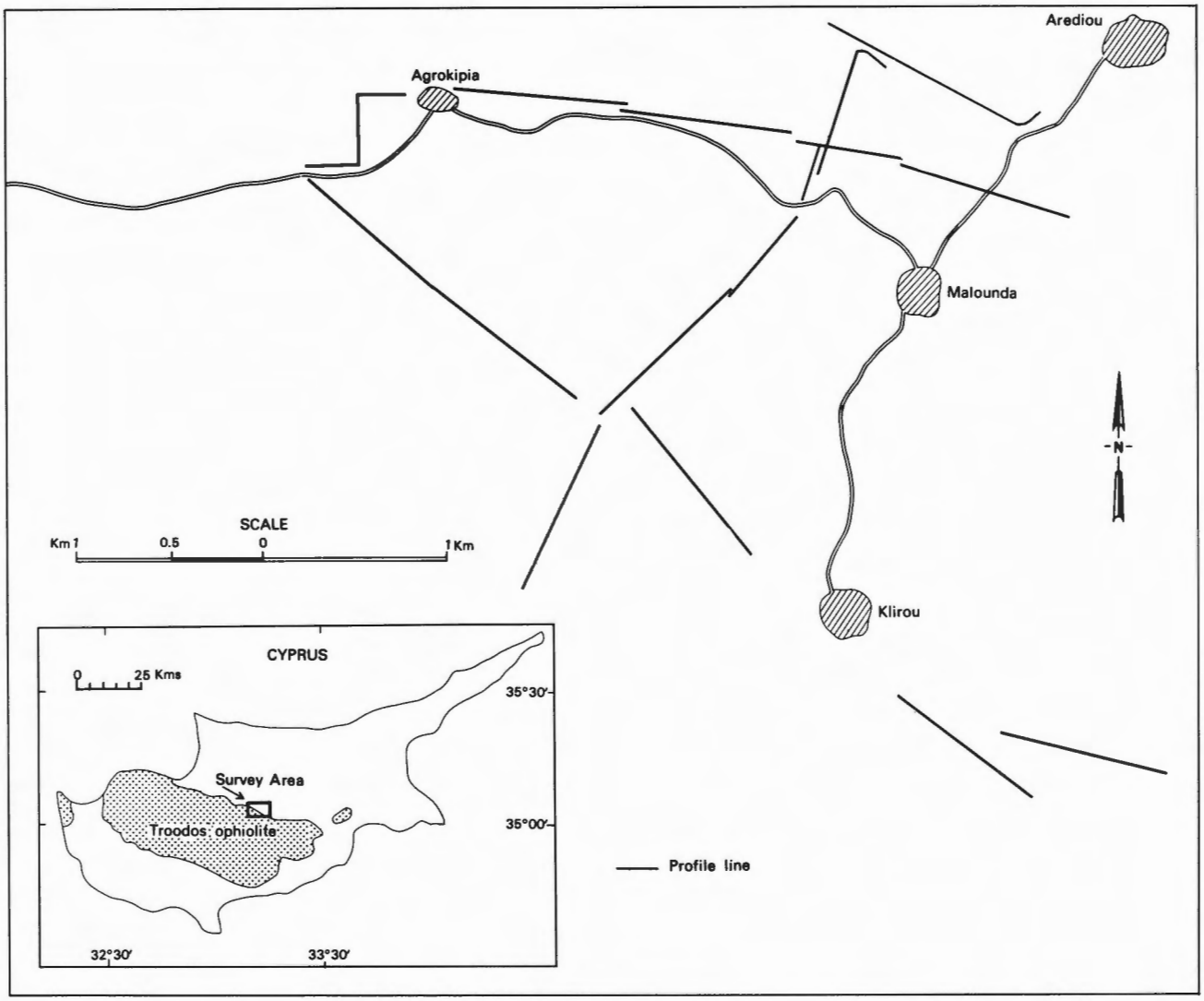

Figure 1: Location of seismic surveys carried out in Cyprus 1983-1984.

FIELD METHODS

A 24-channel digital seismic unit (Terraloc, ABEM Co.) was employed throughout the survey. The geophone spread was laid out in a pattern of three adjacent segments, perpendicular to each other (Figure 2). This pattern was chosen to detect the azimuth of dips of reflectors and/or refractors present. Furthermore, by shooting from several shotholes around and within the spread, stacking of reflection signals corresponding to about the same reflection point (CMP) could be attempted. Finally, the rugged topography of the mine tailings presented severe constraints as regards the shape of the spread. The overall length of the spread was one kilometre. Twelve channels were connected with hexagonal, geophone settings, each consisting of six vertical component geophones with a cut-off frequency of 6 Hz. The side of the hexagon was 6 m long. The remaining twelve channels were occupied by single vertical component geophones with a cut-off frequency of around 3 Hz. It was hoped that the hexagonal setting would more clearly indicate reflection signals as compared with the rest of the geophone settings. The results, however, were not up to the expectations due to inhomogeneities of the underground; reflections were observed only for offsets close to and beyond the critical distances.

Charge sizes up to 3 kgs were electrically detonated. Some charges were detonated in the Agrokipia mine pit lake in order to ensure good coupling of energy with the ground. Other charges were detonated in exploratory boreholes (up to 40 m depth) kindly offered by the Hellenic Mining Co., as well as in 3-feet-deep holes dug in the ground. Shot instants were transmitted by radio. Records were stored on magnetic tape and play back seismograms were obtained in the field using various filter settings of the Terraloc to check for data quality.

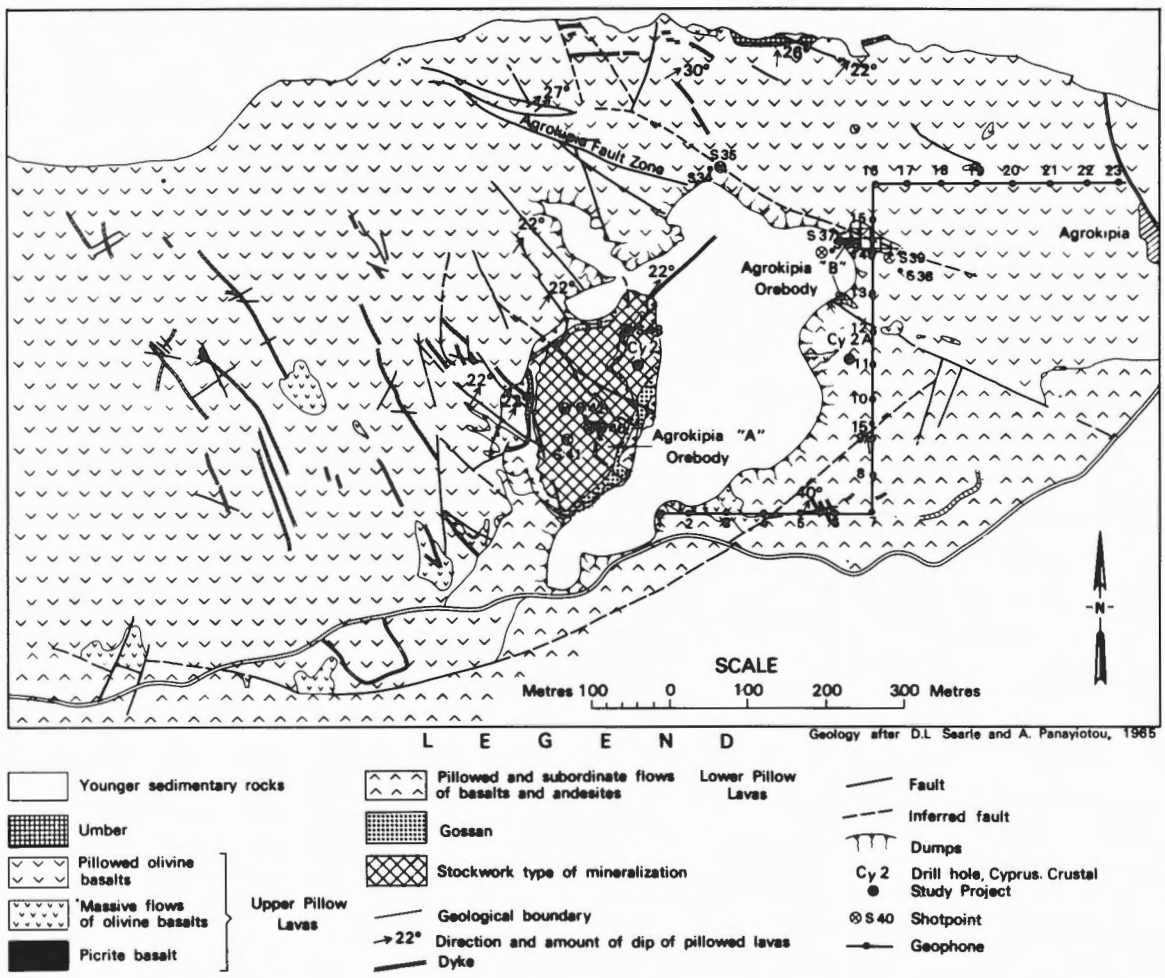

Figure 2: Locations of shotpoints and seismic lines in the Agrokipia mine area. Geology after D.L. Searle and A. Panayiotou (unpub. rep., 1965).

RESULTS

Velocity Analysis

Apparent velocities of first and later arrivals have been determined from filtered play back records and velocity-depth functions have been obtained by 1-D modelling. In Table 1, average velocities for P and S waves, the ratio Vp/Vs and Poisson's ratio are given. It can be clearly seen that velocities for the shots from the mine pit (shots 40 to 43) are distinctly higher for similar depth intervals when compared with the remainder of the shots. This partly reflects the deeper stratigraphic level of shots 40 to 43, with the shot 43 location possibly being the shallowest.

On the other hand, strong local variations in the alteration of rocks in the vicinity of ore bodies 'A' and 'B' partly mask the primary trends in velocities which were observed outside the mine area (G. Schoenharting and S. Eleftheriou, in prep.). In most cases, S wave arrivals could be picked against surface waves, or P waves from the water table, on the grounds of frequency and relative delay times. The accuracy of Vs velocity determinations is, however, somewhat less than that for P waves. Values of Vp/Vs and Poisson's ratio fall well within the range obtained from measurements on rock samples (Smith and Vine, 1987) and oceanic crust (e.g. White, 1984). Synthetic seismograms were obtained from 1-D modelling which helped in the interpretation of reflected and/or refracted waves close to the critical distances. Altogether, only one reflection/refraction event from deeper levels could be identified with certainty. This event stems from a steep gradient zone/discontinuity which, for the wavelengths used, appears as a discontinuity beneath the ore bodies. However, it continues at somewhat deeper levels eastward from Agrokipia where it appears to be a gradient zone.

Typical examples of velocity functions, as derived from modelling, together with calculated and observed traveltimes are shown in Figures 3, 4 and 5. For comparison, arrival times using velocity functions from sample measurements (Smith and Vine, 1987) are shown in the same figures. Velocities of thoroughly saturated rock samples were determined at a pressure of 0.1 GPa while pore pressures were kept at atmospheric pressure (Smith and Vine, 1987). Velocities obtained from modelling field observations are consistently lower compared to those from sample measurements of CY-2a drill core. This holds for both the interval from surface down to the upper boundary of orebody 'B' as well as within the orebody from 155 to 270 m. For the latter case, the first appearance of a critically refracted wave at a high velocity marker below the massive ore zone has been used to define the extent and amount of the low velocity zone shown in Figures 3 and 4. The differences in velocities noted above suggest a bias in the sampling of the drill core, particularly for those intervals in which breccia, glass and other unconsolidated material is present. In addition, the different scales of sampling should be emphasized. The seismic P waves of the field experiment attain wavelengths of 30 to 60 m. Open fractures at that scale will affect the average velocities of the seismic experiment, but not those of the core measurements.

TABLE 1. Average velocities for P and S waves and Poisson's ratio for the uppermost 100 to 200 m, Agrokipia mine seismic survey

Record/ shot	Recording distance (km)	Approx. depth (m)	Geological setting	Vp (km/s)	Vs (km/s)	Vp/Vs	σ
43	0.22-0.39	40-90	LPL,STWK	2.9	1.6	1.81	0.28
43	0.32-0.65	80-150	LPL, STWK, UPL	3.0	1.9	1.62	0.19
42	0.17-0.40	30-80	LPL	3.3	2.0	1.66	0.22
42	0.38-0.74	80-150	STWK, LPL	3.5	1.8	1.94	0.32
41	0.14-0.39	30-90	STWK, LPL	3.3	1.8	1.85	0.29
41	0.41-0.76	90-180	STWK, LPL, UPL	3.1	1.7	1.83	0.29
40	0.13-0.37	20-70	STWK, LPL	3.5	2.0	1.78	0.27
40	0.39-0.74	70-180	STWK, LPL, UPL	3.1	1.9	1.65	0.21
39	0.04-0.30	10-90	UPL	2.7	-	-	-
38	0.05-0.30	10-90	UPL	2.7	1.4	1.87	0.30
38	0.30-0.41	90-120	LPL	3.3	1.6	2.04	0.34
37	0.17-0.37	30-80	UPL, LPL, STWK	2.8	-	-	-
35	0.12-0.30	20-70	UPL	2.7	1.4	1.86	0.30
35	0.30-0.44	70-110	UPL	3.1	1.7	1.82	0.28

LPL: lower pillow lavas, UPL: upper pillow lavas, STWK: stockwork

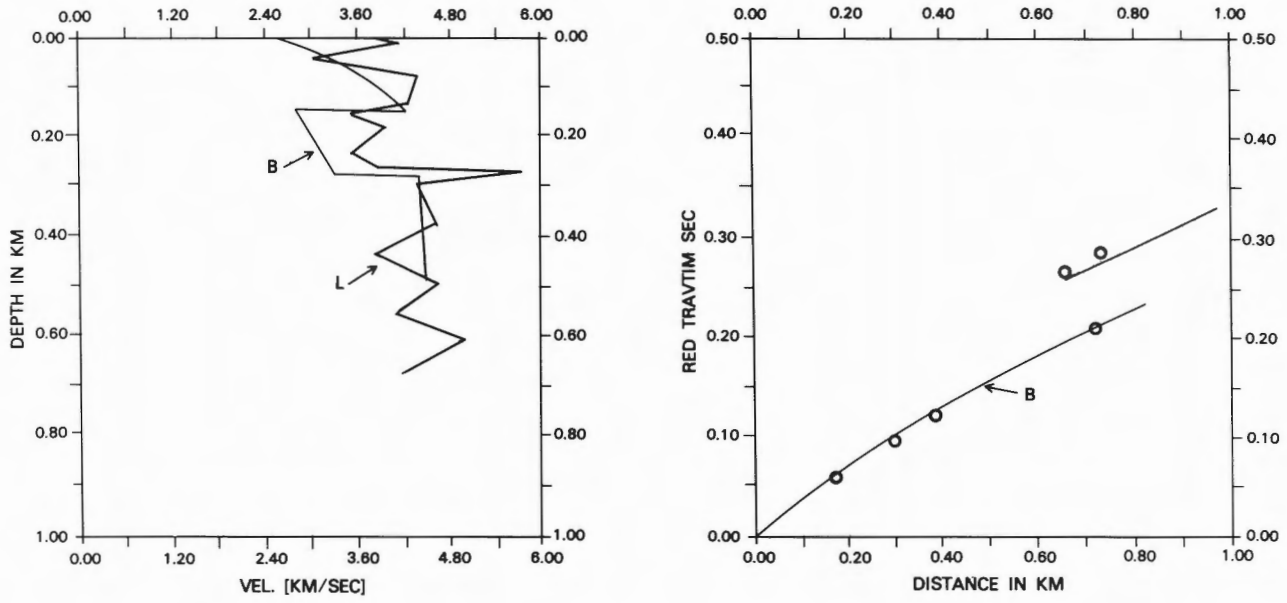

Figure 3: 1-D velocity-depth function and traveltime-distance curve for shot 42. Circles represent observed traveltimes. B: Velocities and traveltimes from 1-D modelling using shot 42. L: Velocities measured on CY-2a samples (Smith and Vine, 1987).

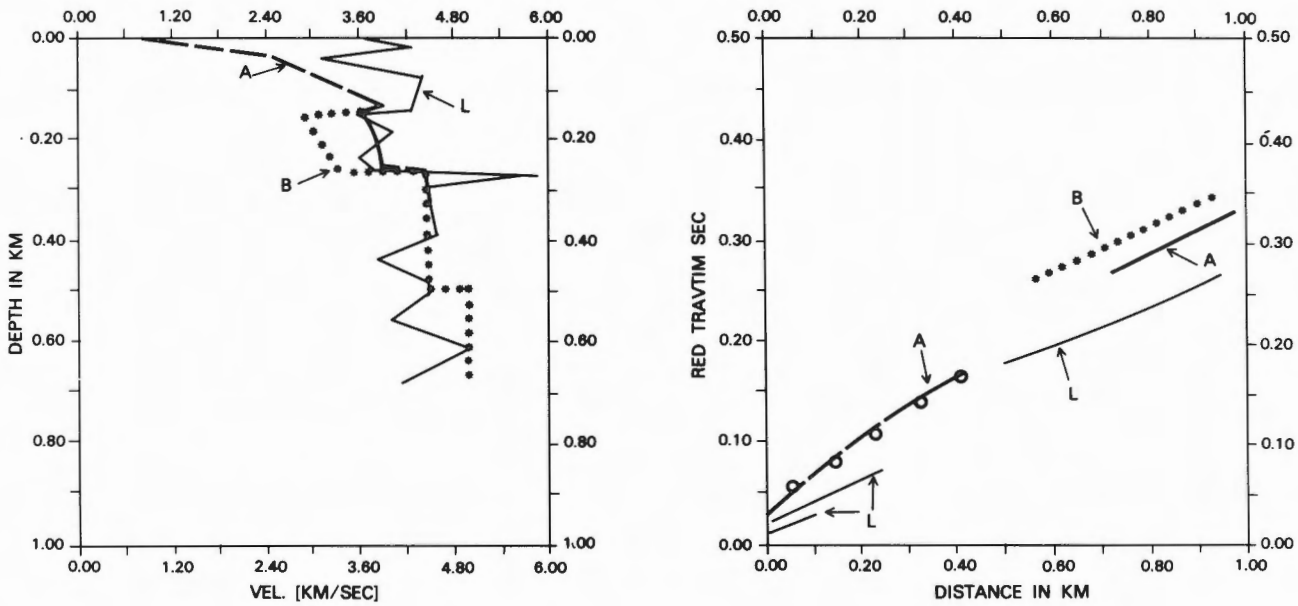

Figure 4: 1-D velocity-depth function and traveltime-distance curve for shot 39. A: Velocities and traveltimes from 1-D modelling using shot 39. B: Modified velocities and traveltime modelling using shot 39. L: Velocities measured on CY-2a samples (Smith and Vine, 1987).

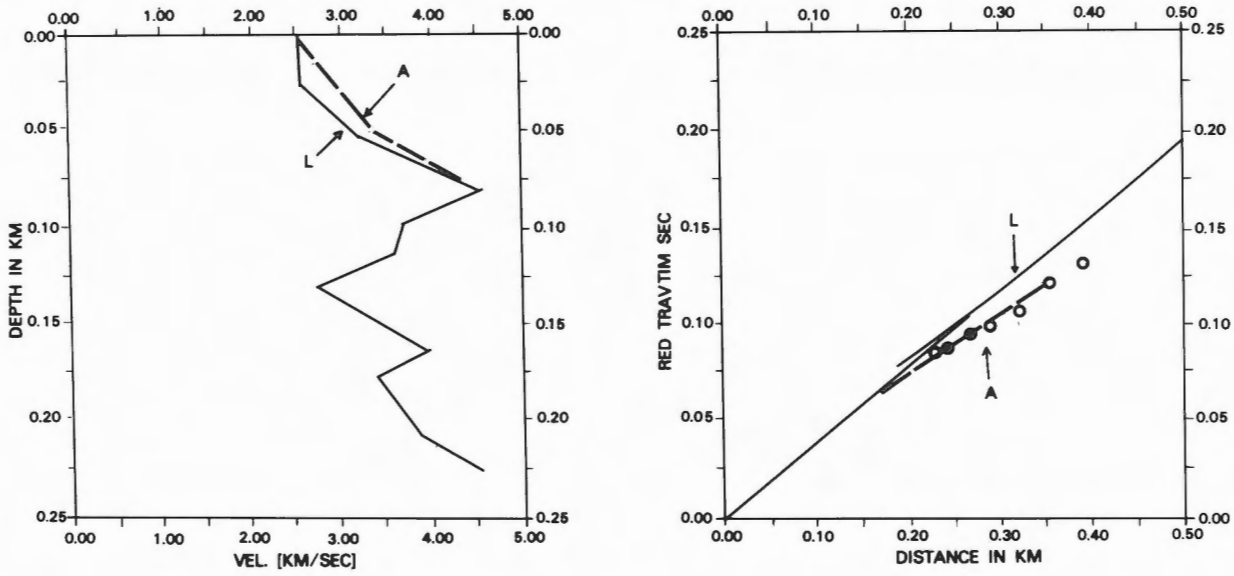

Figure 5: 1-D velocity-depth function and traveltime-distance curve for shot 43. A: Velocities and traveltimes from 1-D modelling using shot 43. L: CY-2 sample velocities (Smith and Vine, 1987).

In Hole CY-2, however, sample velocities for the upper 60 m are lower than those obtained from the seismic survey (Figure 5). In this case the seismic cable was located a considerable distance from the drill hole (Figure 2) and the survey velocities are presumably more typical of the average mineralized zone of Agrokipia 'A' than of the drill core located close to the eastern boundary of 'A'.

From both sample measurements and from our modelling results, the velocity structure of and around an orebody is significantly different from that outside. In spite of the high velocities of massive ore, the extremely low velocities of the rock matrix, in which the massive ore is embedded, renders the zone of massive ore and transitional mineralization as a low velocity zone. On the other hand, silicification of the country rock and part of the stockwork zone below the orebody causes a reduction of porosity and consequently a high velocity zone which partly surrounds the orebody.

In order to obtain a more realistic, although schematic, model of the seismic structure of the Agrokipia mine area, 2-D ray tracing models have been employed and traveltimes compared with the results from the Agrokipia mine seismic spread as well as the next spread to the east (Figures 1 and 6). The starting model for the ray tracing outside the Agrokipia mine area was again a 1-D derived model (Figure 6) which satisfies the first appearance of two critically refracted events with velocities of about 4.0 and 5.0 km/s, respectively.

Agrokipia E-W 2-D Model

Ray tracing after a programme of McMechan and Mooney (1980) with determination of traveltimes and synthetic seismograms has been carried out at the RECKU - university computer centre in Copenhagen. With the limited amount of observed seismic information available, only 5 layers were modelled. Each layer boundary contained 11 points at which velocities on either side of the boundary were assigned. The programme calculates a polynomial velocity function for each boundary and thereafter, by linear interpolation between the boundaries, the x,z variation of velocity. Thus, it was possible to accommodate the 'exotic' features of low velocity zones associated with the Agrokipia 'A' and 'B' deposits rather easily. This velocity structure is shown in the form of isovelocity contours (Figure 8). This figure should be compared with figure 7, the diagram of the model boundaries, ray paths and corresponding traveltimes. It is emphasized that this rather simplistic model is sufficient to explain the observed P wave traveltimes in and adjacent to the Agrokipia area, and that the range of other possible models has not been investigated. Analysis of synthetic seismograms has not as yet been completed and the Vp/Vs ratio variation has not been taken into account for the interpretation of structural versus rock-property changes (Salisbury and Christensen, 1978; Spudich and Orcutt, 1980a).

The main elements in the model (Figures 7 and 8) are:

1. Two mineralized zones (Agrokipia 'A' and 'B') with steep velocity gradients at their lower boundaries.
2. A minor fault between the Agrokipia 'A' and 'B' bodies.
3. A fault about 100 m east of CY-2a, with a downthrow of approximately 100 m to the east.
4. A high velocity feature close to the surface at the eastern end of the model representing a sheet-like gabbroic intrusion which crops out at the surface.

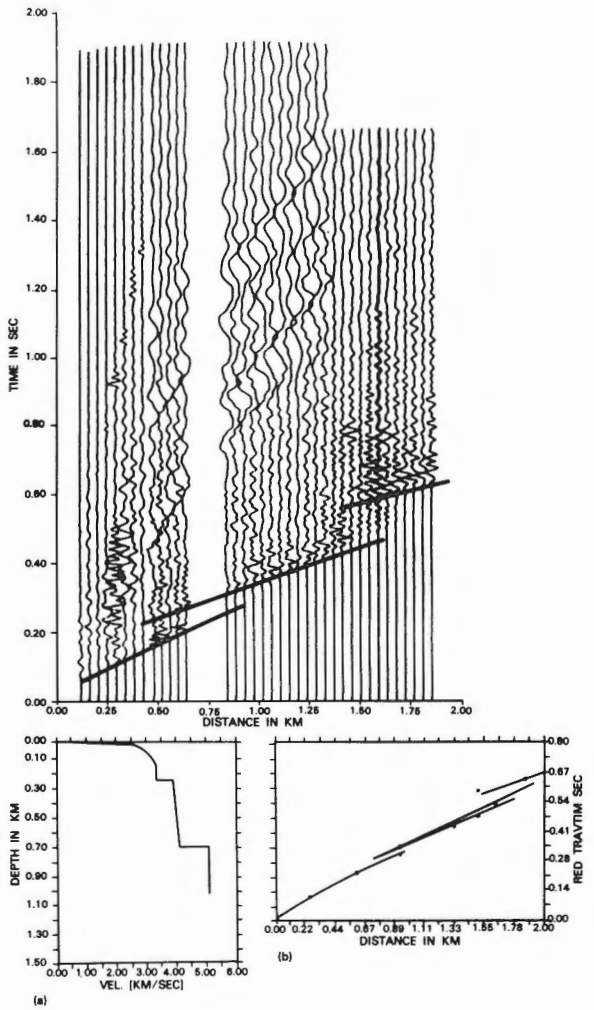

Figure 6: Seismic record in the vicinity of the Agrokipia mine and eastwards: (a) 1-D velocity-depth function and (b) traveltime-distance curve with circles representing observed traveltimes.

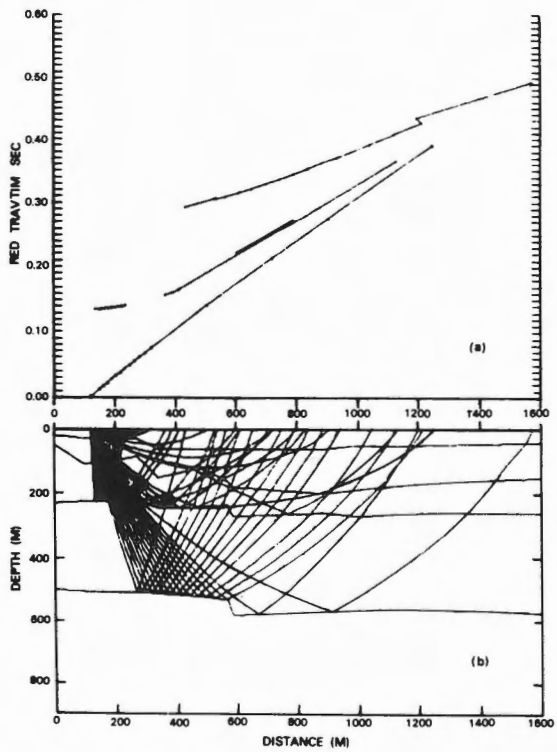

Figure 7: 2-D seismic model in the vicinity of the Agrokipia mine and eastwards. Above: Traveltimes for the model depicted in (b). Below: 2-D ray tracing model showing layer boundaries and rays for shot 42.

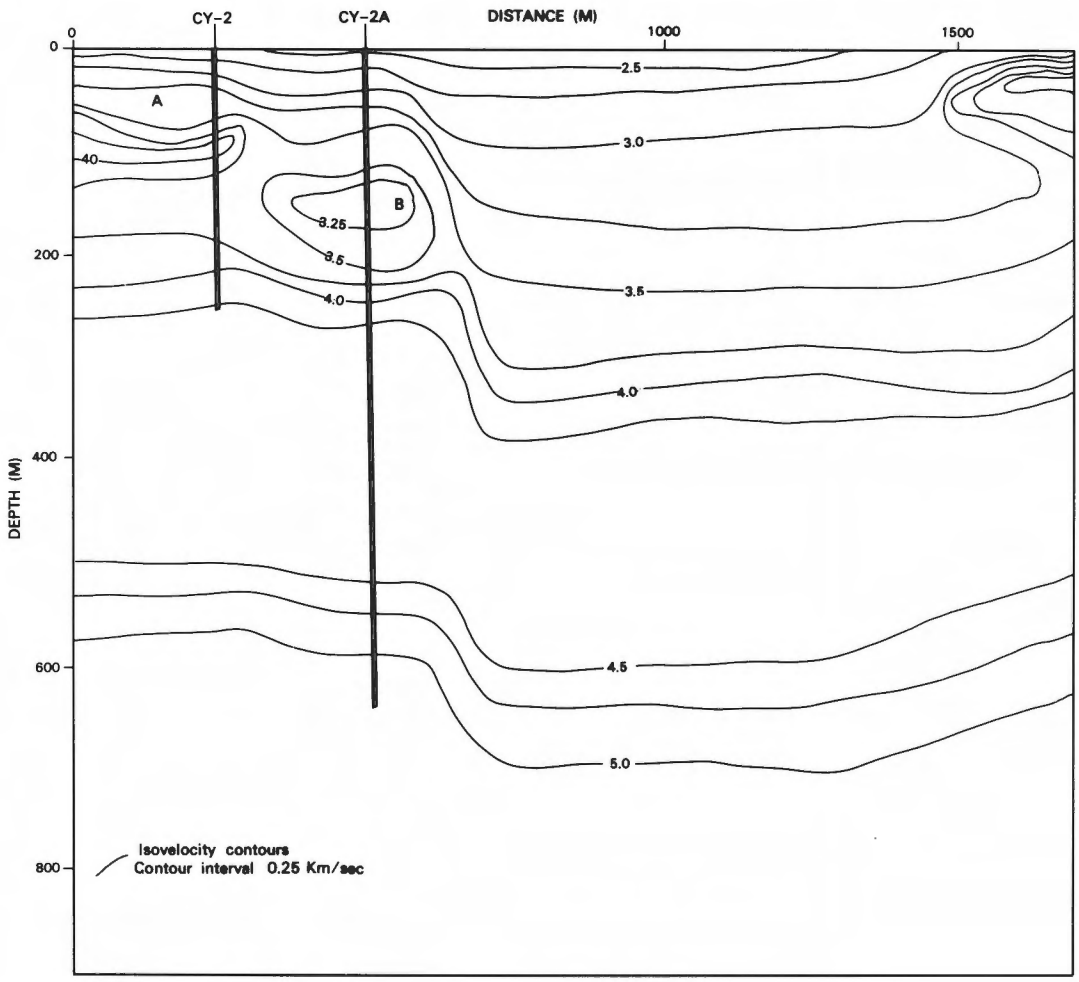

Figure 8: Velocity-depth section of the 2-D seismic model used for ray tracing. Agrokipia A and B deposits are shown together with the locations of holes CY-2 and CY-2a.

DISCUSSION AND CONCLUSIONS

The 2-D velocity depth model depicts various zones where velocity gradients change rather abruptly. The average gradient for the upper 800 m (excluding the uppermost weathered layer) is about 3.5 s^{-1}. This is almost twice the typical value for oceanic layer 2 (e.g. White, 1984) and presumably reflects a high porosity in the extrusives, the presence of open fractures and a low lithostatic pressure. In addition, a large amount of hyaloclastites within the upper extrusives of the area (Schmincke et al., 1983) may add to the high average gradient which really is an expression of low velocities in the uppermost 300 m. In the interval between 300 and 800 m, the average velocity gradient is about 2 s^{-1} which is in better agreement with layer 2 values (Spudich and Orcutt, 1980b; White, 1984).

Two discontinuities or gradient zones with steep gradients are distinguished. One of them lies between 250 and 300 m depth and is approximately marked by the 4 km/s velocity contour, whereas the other one, at

a depth of 550 to 650 m, is shown by the velocity contours of about 4.75 to 5.0 km/s. The latter zone is tentatively correlated with the top of the Basal Group Unit, that is where dykes exceed 90% of the section, with only minor screens of extrusives between dykes. The upper one, however, is more difficult to explain. In the vicinity of hole CY-2a, it appears to be a discontinuity, with corresponding reflections on the seismogram, related to the silicified, less porous zone below the orebody 'B'. Outside the zone the gradient appears to be less steep and may be due to other causes. It may be related to a change in secondary minerals within the zeolite facies of the extrusive section at the UPL/LPL boundary. Gass and Smewing (1973), suggest that at this level chalcedonic silica and albite appear which should give a reduction in porosity - possibly distributed over a zone which is broader than that below the orebodies. Gillis and Robinson (1985), however, dispute the existence of the UPL/LPL boundary based on secondary mineralogy. Alternatively, the increase of velocity may be attributed to an increase in dyke frequency and/or a decrease in the frequency of low velocity breccia zones. Further analysis should allow better definition of the amount and nature of the steeper gradients because of the relatively small wavelengths of our seismic experiments compared to those from studies of in-situ oceanic crust.

A distinct difference exists in the velocity distribution of the upper 300 m between the area of the Agrokipia 'A' and 'B' and the more normal section further east, with the latter area exhibiting a more regular increase of velocity with depth (Figures 7 and 8). If a similar velocity distribution is typical of other orebodies, it may be possible to detect orebodies by seismic methods. In such a case, one would look for limited zones of velocity inversions, with high velocity markers below, close to major fault lines which presumably acted as channelways for ascending thermal fluids. Further work is necessary, however, in order to substantiate these ideas. Also reprocessing of the field data should assist in picking other reflection events hidden in the source reverberations and surface waves. Finally, a detailed comparison of observed seismograms with synthetic ones is needed to further reduce the ambiguities of the interpretation.

ACKNOWLEDGEMENTS

We thank Dr. G. Constantinou, Director of the Geological Survey Department, Nicosia, for manpower support and transportation during the survey. The organizational help and geological advice of Dr. A. Panayiotou and Dr. C. Xenophontos of G.S.D. is especially acknowledged. The Hellenic Mining Company and Dr. Maliotis provided accommodations and made available boreholes for shooting. Thanks are also extended to Mr. G. Smith and Dr. F. Vine for permission to use their data on drill core samples for comparison with our results. We also thank the Danish UN-contingent, Cyprus for transport of equipment. The Danish Research Council (SNF) supported this study with grant J. Nr. 11-17032.

REFERENCES

Eleftheriou, S.
1983: The Malounda damsite seismic survey; Report for the Geological Survey Department, Ministry of Agriculture and Natural Resources, Cyprus.

Gass, I.G. and Smewing, J.D.
1973: Intrusion, extrusion and metamorphism at constructive margins: evidence from the Troodos massif, Cyprus; Nature, v. 242, p. 26-29.

Gillis, K.M. and Robinson, P.T.
1985: Low-temperature alteration of the extrusive sequence, Troodos Ophiolite, Cyprus; Canadian Mineralogist, v. 23, p. 431-441.

Khan, M.A., Summers, C., Bamford, S.A.D., Chroston, P.N., Poster, C.K. and Vine, F.J.
1972: Reversed seismic refraction line on the Troodos Massif, Cyprus; Nature, Physical Science, v. 238, no. 87, p. 134-136.

Lort, J.M. and Matthews, D.H.
1972: Seismic velocities measured in rocks of the Troodos igneous complex; Geophysical Journal of the Royal Astronomical Society, v. 27, p. 383-392.

Malahoff, A.
1982: A comparison of the massive submarine poly-metallic sulphides of the Galapagos rift with some continental deposits; Marine Technology Society, Journal, v. 16, no. 3.

Matthews, D.H., Lort, J., Vertue, T., Poster, C.K. and Gass, I.G.
1971: Seismic velocities at the Cyprus outcrop; Nature, Physical Science, v. 231, no. 26, p. 200-201.

McMechan, G.A. and Mooney, W.D.
1980: Asymptotic ray theory and synthetic seismograms for laterally varying structure: theory and application to the Imperial valley, California; Seismological Society of America, Bulletin, no. 70, p. 2021-2036.

Moores, E.M., Robinson, P.T., Malpas, J. and Xenophontos, C.
1984: Model for the origin of the Troodos massif, Cyprus, and other mideast

ophiolites; Geology, v. 12, no. 8, p. 500-503.

Oudin, E., Picot, P. and Pouit, G.
1981: Comparison of sulphide deposits from the East Pacific Rise and Cyprus; Nature, v. 291, no. 5814, p. 404-407.

Robinson, P.T., Melson, W.G., O'Hearn, T. and Schmincke, H.-U.
1983: Volcanic glass compositions of the Troodos Ophiolite, Cyprus; Geology, v.11, no. 7, p. 400-404.

Salisbury, M.H. and Christensen, N.I.
1978: The seismic velocity structure of a traverse through the Bay of Islands ophiolite complex, Newfoundland: an exposure of oceanic crust and upper mantle; Journal of Geophysical Research, v. 83, no. B2, p. 805-817.

Schmincke, H.-U., Rautenschlein, M., Robinson, P.T. and Mehegan, J.M.
1983: Troodos extrusive series of Cyprus: a comparison with oceanic crust; Geology, v. 11, no. 7, p. 405-409.

Smith, G.C. and Vine, F.J.
1987: Seismic velocities in basalts from ICRDG drill holes CY-2 and CY-2a at Agrokipia mines, Cyprus; *in* Cyprus Crustal Study Project Initial Report Hole CY2-2a, ed. P.T. Robinson, I.L. Gibson and A. Panayiotou; Geological Survey of Canada, Paper 85-29.

Spudich, P. and Orcutt, J.
1980a: A new look at the seismic velocity structure of the oceanic crust; Reviews of Geophysics and Space Physics, v. 18, p. 627-645.
1980b: Petrology and porosity of an oceanic crustal site: results from waveform modelling of seismic refraction data; Journal of Geophysical Research, v. 85, no. B3, p. 1409-1433.

Verosub, K.L. and Moores, E.M.
1981: Tectonic rotations in extensional regimes and their palaeomagnetic consequences for oceanic basalts; Journal of Geophysical Research, v. 86, no. B7, p. 6335-6349.

White, R.S.
1984: Atlantic oceanic crust: seismic structure of a slow spreading ridge; *in* Ophiolites and Oceanic Lithosphere, ed. I.G. Gass, S.J. Lippard and A.W. Shelton; Geological Society of London, Special Publication, no. 13, p. 101-112.

Gravity and Magnetic Studies of the Agrokipia Sulphide Orebodies, Cyprus

G.C. SMITH AND F.J. VINE

School of Environmental Sciences, University of East Anglia, Norwich, U.K., NR4 7TJ

Smith, G.C. and Vine, F.J., Gravity and magnetic studies of the Agrokipia Sulphide Orebodies, Cyprus; in *Cyprus Crustal Study Project: Initial Report, Holes CY-2 and 2a, ed. P.T. Robinson, I.L. Gibson and A. Panayiotou; Geological Survey of Canada, Paper 85-29, p. 327-337, 1987.*

Abstract

A ground magnetic survey has been carried out over partially worked massive sulphide orebodies in the extrusive section of the Troodos ophiolite complex. A pronounced magnetic 'low' is observed over the shallow Agrokipia 'A' orebody with a weaker and poorly defined magnetic 'low' over the deeper but related Agrokipia 'B' orebody. Measurements of the magnetic properties of samples from drill holes CY-2 and CY-2a (at Agrokipia 'A' and 'B' respectively) show the lavas to be very weakly magnetized in the highly mineralized and altered zone while enhanced values of magnetic susceptibility are observed on the periphery. Koenigsberger ratios range typically from 5 to 50. The natural remanent component of magnetization therefore dominates the induced component. Measurements of densities are highly variable reflecting the effects of alteration and mineralization. Density contrasts are noted between Upper Pillow Lavas, Lower Pillow Lavas, mineralized lavas and the Basal Group. Modelling shows that the gravity and magnetic anomalies define the structural setting of the orebodies, supporting the interpretation that the mineralization occurs within an uplifted fault bounded block. A combination of gravity and magnetic surveys may be of value in delineating the likely extent and degree of mineralization in known or suspected orebodies elsewhere on the Troodos or in other ophiolites. It is considered unlikely, however, that either technique would be useful in the search for hydrothermal orebodies on the ocean floor.

Résumé

Un levé magnétique a été exécuté sur des gisements de sulfures massifs partiellement exploités dans la coupe extrusive du complexe ophiolitique du Troodos. Un 'creux' magnétique très prononcé est observé au-dessus du gîte 'A' de faible profondeur d'Agrokipia, lequel est accompagné d'un autre 'creux' plus faible et moins bien défini au-dessus du gîte 'B' de plus grande profondeur, ce dernier appartient également au massif d'Agrokipia. Les mesures des propriétés magnétiques des échantillons prélevés dans les trous de forage CY-2 et CY-2a (à Agrokipia 'A' et 'B', respectivement) révèlent que les laves ne sont que très faiblement aimantées dans la zone altérée et fortement minéralisée, tandis qu'en bordure les valeurs de susceptibilité magnétique deviennent plus élevées. Les rapports de Koenigsberger varient typiquement de 5 à 50. La composante de rémanence naturelle d'aimantation domine par conséquent la composante induite. Les valeurs mesurées des densités sont très variables et reflètent les effets de l'altération et de la minéralisation. Des changements brusques des densités sont observés entre la couche supérieure de laves en coussinet, la couche inférieure de laves en coussinet, les laves minéralisées et le groupe Basal. La modélisation montre que les anomalies gravimétriques et magnétiques définissent le contexte structural des corps minéralisés et elle appuie l'interprétation que la minéralisation apparaît dans un bloc de failles soulevé. La combinaison des levés gravimétriques et magnétiques peut être utile pour délimiter l'étendue probable et le degré de minéralisation dans des massifs de minerai connus ou potentiels ailleurs dans le Troodos ou dans d'autres ophiolites. Cependant, il est peu probable que ces deux méthodes puissent être profitables à la prospection de gîtes hydrothermaux de plancher océanique.

INTRODUCTION

Recent discoveries of massive sulphides produced by the circulation of hydrothermal fluids during the formation of oceanic crust (Francheteau et al., 1979; Hekinian et al., 1983) have renewed interest in the study of the sulphide orebodies found in some ophiolites.

In April 1982 the I.C.R.D.G. (International Crustal Research Drilling Group) started drilling on Cyprus to complement and extend the results of drilling into the oceanic crust at sea. Part of this Cyprus Crustal Study Project (C.C.S.P.) included the location of two drill holes in the vicinity of the Agrokipia massive sulphide orebodies (Figures 1 and 2).

Here we present the results of laboratory studies of the magnetic properties and densities of the drilled material and correlate these with existing gravity data and a recently completed magnetic survey over the Agrokipia orebodies in an attempt to assess the suitability of these methods for the location and definition of massive sulphide deposits both in ophiolites and on the seafloor.

Figure 2a shows the geological situation of the Agrokipia orebodies near to the Upper Pillow Lava (UPL) - Lower Pillow Lava (LPL) contact. The Agrokipia 'A' orebody is a pyrite bearing body which has been mined as an open pit. The deeper, but genetically related Agrokipia 'B' orebody is a pyrite and sphalerite bearing orebody and has been mined to a limited extent underground.

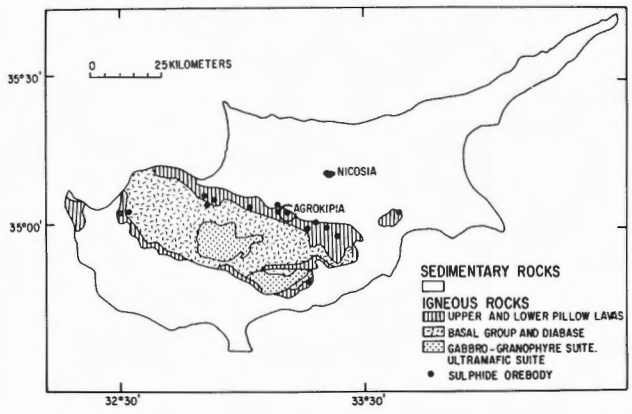

Figure 1: Schematic geological map of Cyprus showing the general location of the Troodos Massif and the sulphide bodies.

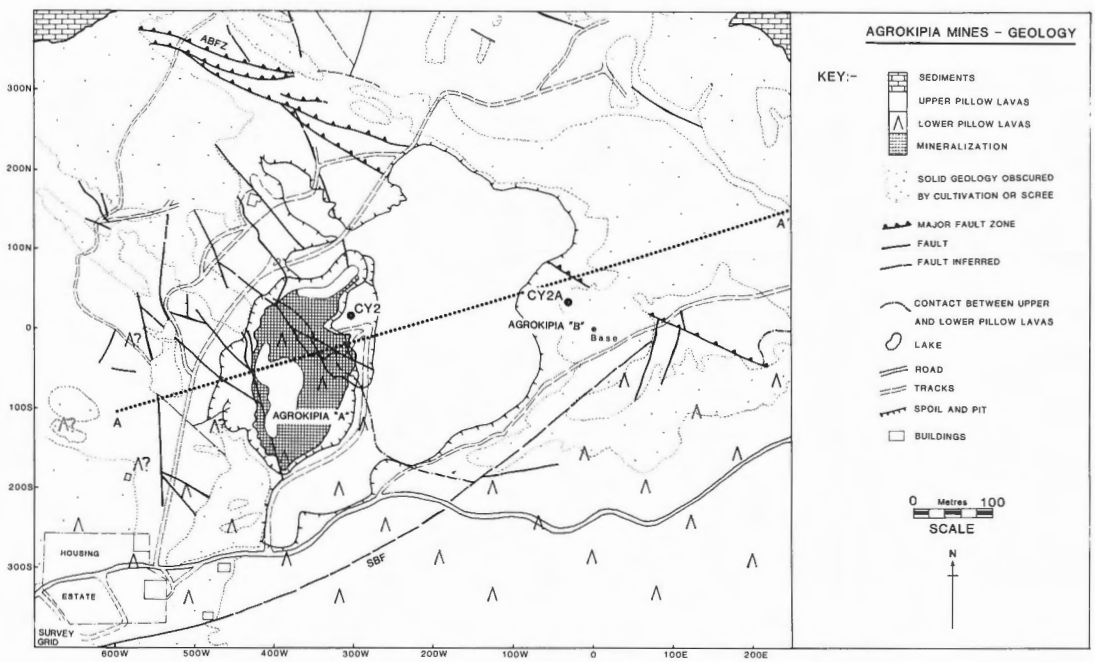

Figure 2a: The geological situation of the Agrokipia orebodies, after Searle (1978).

CY-2 and CY-2a are the locations of the two C.C.S.P. drill holes, into Agrokipia 'A' and 'B', respectively, from which samples have been taken for laboratory studies. In addition samples from drill hole CY-1 which lies about 4 km to the east and penetrates 475 metres into an unmineralized lava sequence from the lava-sediment contact, provide data for comparison with values determined for the hydrothermally altered and mineralized material from CY-2 and CY-2a.

GEOPHYSICAL SURVEYS

A vertical component magnetic survey over the Agrokipia area was carried out in April 1982 (Johnson et al., 1982) and extended and revised by the present authors in August 1982. In theory, the intense hydrothermal alteration which occurs during the formation of sulphide deposits should produce a characteristic signature. In the mineralized zone the replacement of Fe-Ti oxides with non-magnetic pyrite and sphene should give a magnetic low relative to the surrounding areas. The subsequent sub-aerial oxidation of the peripheral zones of pyrite mineralization to magnetite should then give a magnetic high around the central low. This signature has been used to define porphyry copper orebodies (Jerome, 1966) but has not been identified in submarine hydrothermal deposits now exposed in ophiolites. One of the aims of this survey was to ascertain if such an anomaly pattern is associated with the Agrokipia deposits.

Due to the steep magnetic gradients encountered in preliminary surveys, an ABEM 'Minimag' was chosen as the most suitable instrument for the survey. The 'Minimag' is a vertical field compensation instrument capable of measuring the vertical component of the magnetic field over a range of $\pm 10{,}000$ nT to an accuracy of ± 100 nT.

The contoured results of the survey are shown in Figure 2b after filtering by two-dimensional upward continuation to a height of 10 metres and matching of values at cross-over points. The map shows clearly a magnetic low (amplitude approx. 4,000 nT) associated with the Agrokipia 'A' orebody. Due to logistic difficulties around the pit, the west side of the magnetic low is poorly defined. A broad and poorly defined magnetic low can be seen over the deeper Agrokipia 'B' orebody (amplitude approx. 2,000 nT).

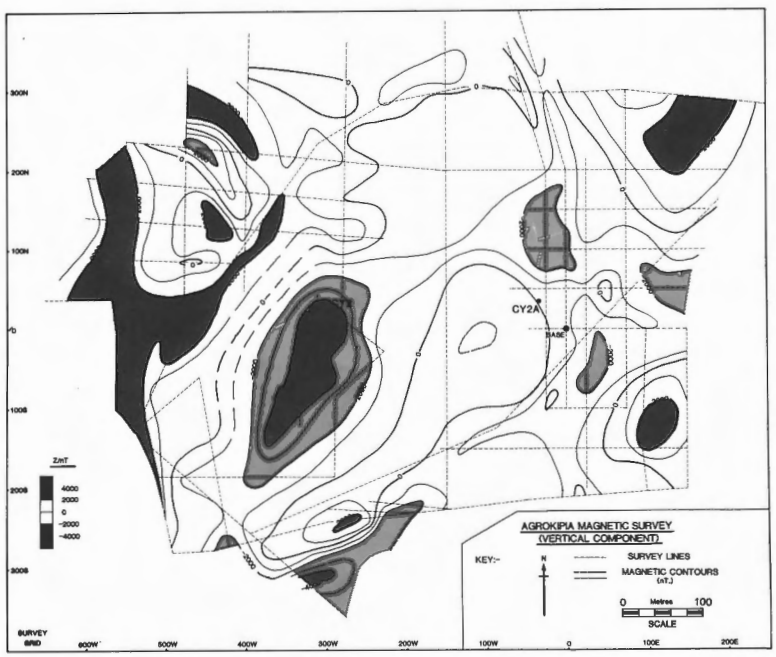

Figure 2b: The Agrokipia magnetic survey (vertical component). Dashed contours are drawn in areas of limited survey coverage, notably to the north-west of the Agrokipia 'A' negative anomaly.

To the west a major fault trending N-S is clearly defined by a ridge of magnetic high, indicating that more strongly magnetized rocks lie to the west. A second inferred fault (the Southern Boundary Fault, SBF, Figure 2a) striking SW-NE through Agrokipia 'B' is poorly defined by a discontinuous trough of magnetic low indicating that more strongly magnetized rocks occur to the southeast. Over the mining spoil to the east of Agrokipia 'A' the magnetic signal is attenuated and the survey coverage less detailed. The magnetic signature associated with the 'Agrokipia Boundary Fault Zone' (ABFZ, Figure 2a) which trends NW-SE through Agrokipia 'B' is seen in the northwest of the survey area where it is defined by a trough of magnetic low with a parallel ridge of magnetic high to the southwest. Simple modelling shows this signature to be in agreement with the interpretation that the altered and mineralized rocks to the southwest have been uplifted relative to the unaltered Upper Pillow Lavas to the north of the fault zone (Maliotis and Khan, 1980). In the region immediately to the northwest of the Agrokipia 'A' pit it is difficult to correlate the magnetic anomalies with mapped geological information. The area is geologically complex and the survey grid too coarse to allow a detailed interpretation. The general trend of faulting, i.e. NW-SE is, however, reflected to some extent in the observed magnetic anomalies. The narrow ridge of magnetic high which skirts the north and western margins of the pit is thought to be a topographic effect. We find no conclusive evidence from the survey for the existence of a 'ring of magnetic high' around the orebodies. It is possible that the effect is small and has been disrupted by anomalies arising from structural and topographic features.

The gravity survey shown in Figure 2c was completed in 1951 by the Hellenic Mining Company before mining began. In theory, the high densities associated with pyrite, 4,950 to 5,030 kg m^{-3} (Deer et al., 1969), should give rise to observable gravity anomalies. However, on a number of occasions anomalies thought to be indicative of the presence of an ore deposit have been shown, on drilling, to result from relatively high density intrusives at shallow depths in the extrusive section (G. Maliotis, pers. comm.). Indeed, although it is true that the higher densities associated with mineralized lavas should result in observable gravity anomalies, gravity techniques have yet to find an ore deposit on Cyprus. This may, in part, reflect observations that both massive ores and mineralized lavas often have relatively high porosities giving lower densities than expected (Constantinou, 1972).

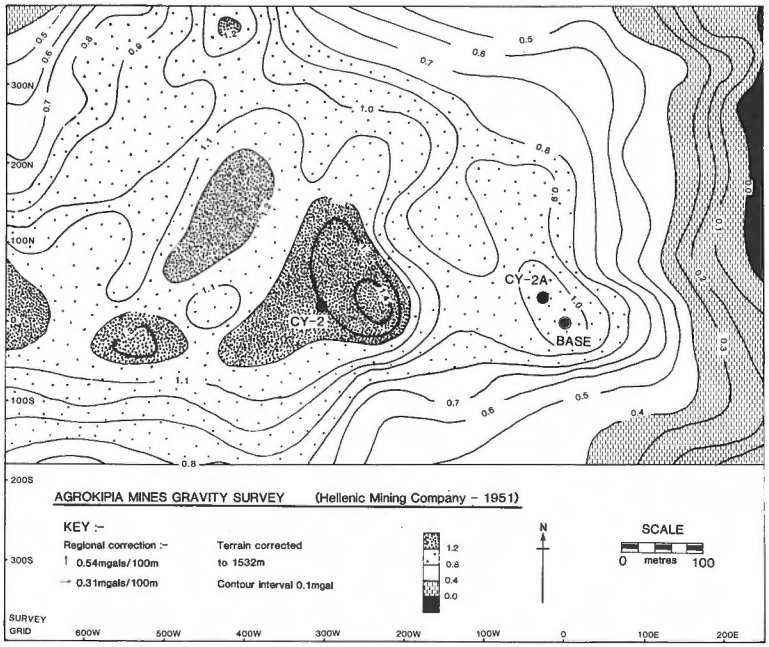

Figure 2c: The Agrokipia gravity survey, modified from Hellenic Mining Company data.

At Agrokipia, the gravity stations were located on a 100 metre grid with additional intermediate stations where considered necessary. The gravity data were fully reduced assuming a Bouguer density of 2,000 kg m^{-3}.

A small (approx. 0.2 mGal) local positive anomaly is seen offset to the east of Agrokipia 'A' with a second smaller positive anomaly over Agrokipia 'B'. The latter is thought to be due to the presence of intrusive material close to the surface. Steep gradients to the northeast, east and southeast of the orebodies define faults bounding the mineralized zone including the Agrokipia Boundary Fault Zone and the Southern Bounding Fault (SBF) also indicated by the magnetic survey. There is no evidence from the gravity for the N-S trending fault to the west of the orebodies which is so clearly defined by the magnetic survey.

MAGNETIC PROPERTIES

In this section we present and discuss the results of laboratory measurements of susceptibility and NRM intensity and calculated values of the Koenigsburger ratios (Q_n) for samples from drill holes CY-1, CY-2 and CY-2a. Samples were taken, where possible, at 5 metre intervals. Generalized geological logs are shown (Figure 3) for comparison with the magnetic and density logs. Susceptibilities were measured on 25.4 mm right cylindrical mini-core samples with a Bison susceptibility meter and are estimated to be accurate to $\pm 5\%$. NRM intensities were measured on a 'Digico' spinner magnetometer and are also accurate to $\pm 5\%$.

Measurements of magnetic susceptibility provide a useful indication of the extent of 'sulphurization', i.e. the conversion of Fe-Ti oxides to pyrite and sphene, or of the extent of greenschist facies metamorphism. The susceptibility log for drill hole CY-1 (Figure 4a), a 474.88 m sequence through pillow lavas and massive flows, shows low values in the top 200 metres (typically 10-15 x 10^{-3} S.I.) and higher values below 200 metres (typically 15-30 x 10^{-3} S.I., but may be as high as 38 x 10^{-3} S.I.). In the upper 200 metres the lavas have been altered by pervasive sea-floor weathering with alteration of olivine phenocrysts to clays and filling of veins and vesicles with clay and carbonate. Below 200 metres the lavas are progressively less altered and there is a higher and increasing proportion of massive flows and intrusives.

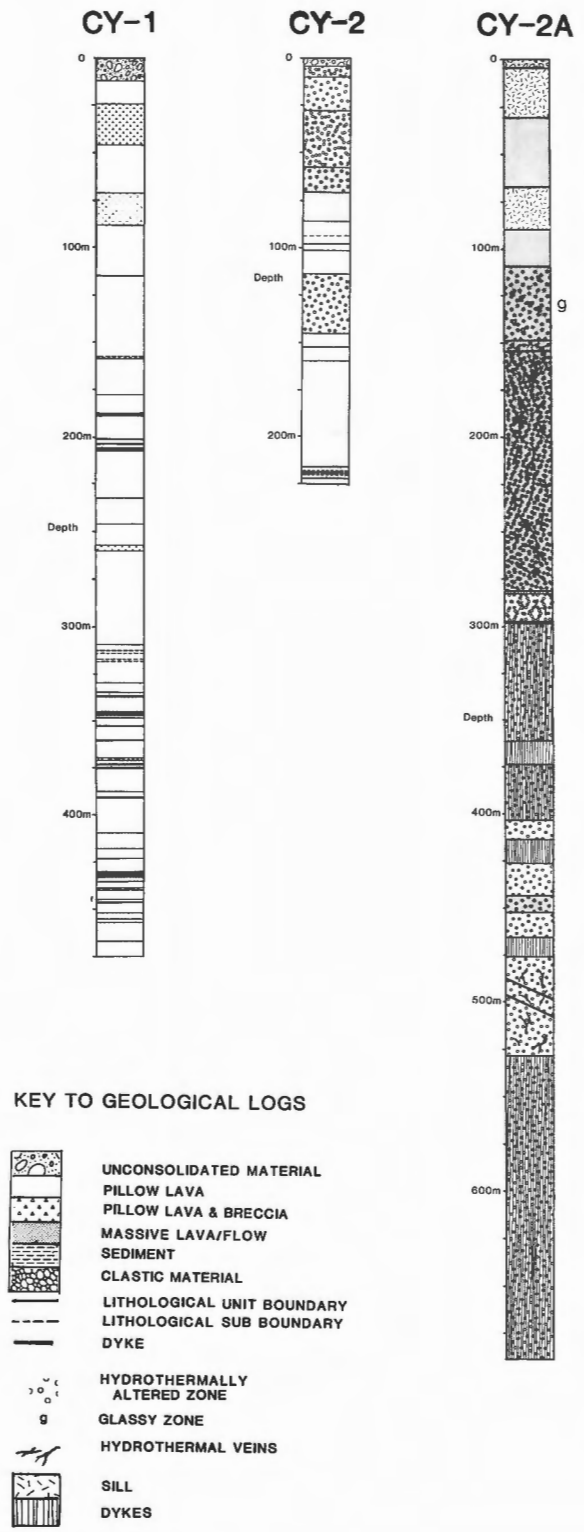

Figure 3: C.C.S.P. drill holes - geological logs (after Robinson and Gibson, 1983a, b, c).

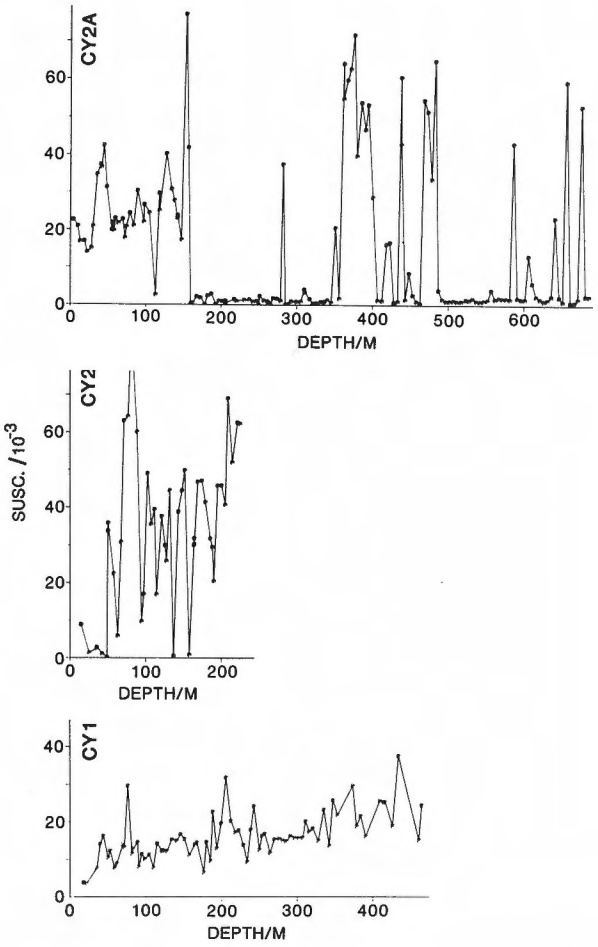

Figure 4a: C.C.S.P. drill holes - susceptibility logs (S.I. Units).

Samples from the top 70 metres of drill hole CY-2, through the stockwork of the Agrokipia 'A' ore deposit are from mineralized and variably altered pillowed and massive flows with susceptibilities in the upper 50 metres typically less than 10 x 10^{-3} S.I. From 50 to 100 metres very high susceptibilities, up to 80 x 10^{-3} S.I., were observed. These high values may result from oxidation on the periphery of the mineralized zone. Below 100 metres values vary from <1 x 10^{-3} to 70 x 10^{-3} S.I. The underlying trend is, however, of increasing susceptibility with depth. Between 120 and 140 metres, a second altered zone contains jasper and celadonite but no sulphides. There is, surprisingly, no obvious contrast in susceptibility values between this altered zone and the unaltered material above and below. Stratigraphically, most of the CY-2 core is at a lower level than the base of CY-1. Thus in the fresh material the trend of increase in susceptibility with depth is seen to continue as the proportion of massive flows increases.

The susceptibility log for drill hole CY-2a, through the pyrite and sphalerite bearing Agrokipia 'B' orebody, shows clearly the onset of mineralization at 150 metres with a reduction in susceptibility values by a factor of 20. In the interval above the mineralized zone there are two intrusives (15-25 x 10^{-3} S.I.) in a sequence of massive flows (20-40 x 10^{-3} S.I.). Immediately above the mineralized zone is a sequence of alternating layers of altered massive basalt and massive glass. In the lower part of this sequence, on the periphery of the mineralized zone, high susceptibility values, up to 75 x 10^{-3} S.I., were measured. From 150 to 280 metres susceptibility values are very low, typically <1 x 10^{-3} S.I. This is a zone of mineralized and argillized flows with abundant pyrite, quartz, red jasper and clays. From 280-530 metres there is a sequence of altered dykes, pillow lavas and pillow breccias with less altered material and post-mineralization dykes giving higher values (up to 70 x 10^{-3} S.I.) of susceptibility. For the altered material, susceptibilities are typically 1-2 x 10^{-3} S.I. At 530 metres, the 'contact' between the Lower Pillow Lavas and the Basal Group is drawn, as it is in the field, on the basis of the increasing percentage of dykes in the sequence. Susceptibility values are lower than one would expect for unmineralized Basal Group rocks, i.e. 20-25 x 10^{-3} S.I. (Vine and Moores, 1972). This, together with the continued presence of disseminated pyrite and the products of greenschist alteration, e.g. chlorite, and abundant quartz suggests that the drill hole is still within the stockwork of the hydrothermal system.

Figure 4b shows logs of NRM intensity. NRM intensity values characteristically show a greater contrast than susceptibility values, varying by a factor of more than 5,000 (from <0.01 to 50 A m^{-1}) compared with a factor of 400 (from <0.2 x 10^{-3} to 80 x 10^{-3} S.I) for susceptibility. There are, of course, marked similarities between the NRM and susceptibility logs. Thus, the log for CY-1 shows lower values in the upper 200 metres than below 200 metres due to seafloor weathering. However the contrast in values of NRM between these two zones is more marked and therefore more diagnostic than the contrast in susceptibilities.

The NRM log for CY-2 is similar to the susceptibility log except that in the zone from 50 to 100 metres there is no increase in intensity as might be expected from the susceptibility log.

The most striking contrast between the NRM intensity and susceptibility logs for CY-2a is the relative absence of high values of NRM below 280 metres. Apart from several high intensities associated with post-mineralization dykes (up to 60 A m^{-1}) values are typically below 1 A m^{-1}. Above the mineralized zone, from 0-150 metres, the two intrusives give lower NRM values than the massive flows and pillowed flows. As in the case of CY-2,

high susceptibility values on the edge of the mineralized zone are not matched by high NRM intensities .

For the interpretation of the magnetic survey it is necessary to assess the relative contributions of the remanent and induced components of magnetization to the magnetic field (or, in this case, vertical component of the field) at the surface. Figure 4c shows the measured remanent magnetizations plotted against values of induced magnetization calculated from measured susceptibilities. The ratio of the remanent and induced magnetizations, expressed as Q_n, the Koenigsburger ratio is, for fresh material, typically in the range 5-50. It is the distribution of remanent magnetization which is, therefore, of prime importance in determining the observed magnetic anomaly pattern at the surface. Mineralized and intrusive samples tend to give lower values of Q_n but through a reduction of NRM rather than an increase in susceptibility. It is, therefore, reasonable to propose models to simulate the observed anomalies which use NRM values and ignore the minor component due to induced magnetization.

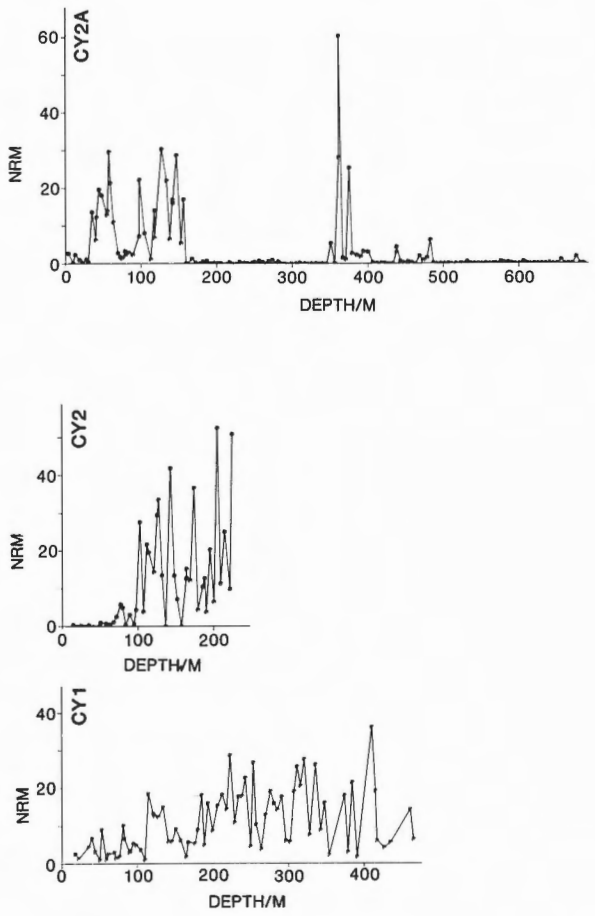

Figure 4b: C.C.S.P. drill holes - NRM intensity logs (Intensities in $A.m^{-1}$).

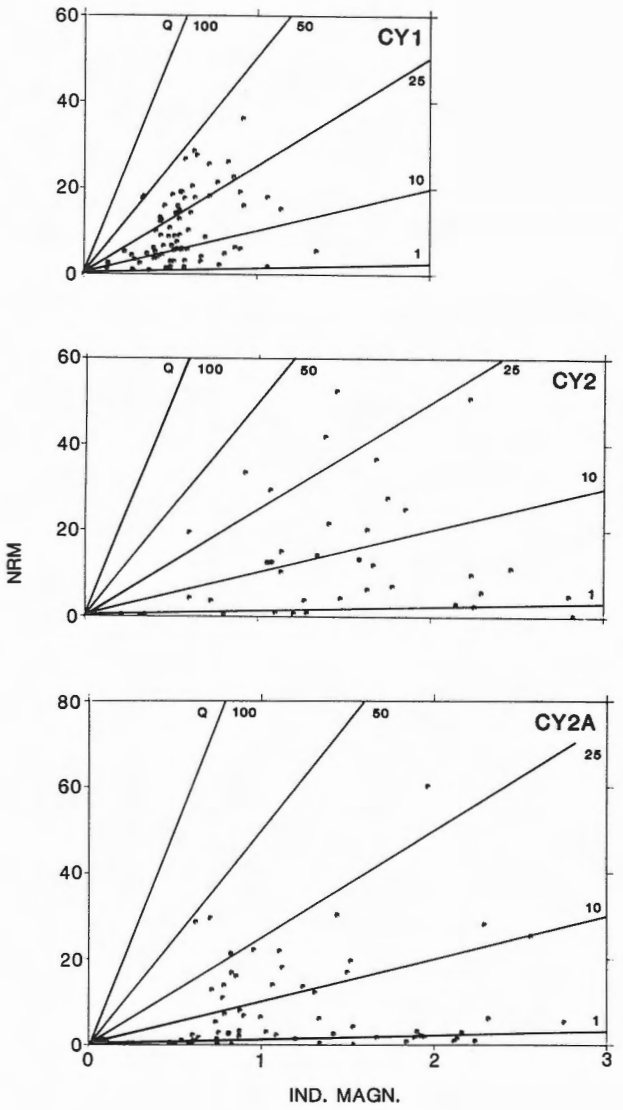

Figure 4c: C.C.S.P. drill holes - NRM intensity vs. induced magnetization (in $A.m^{-1}$) showing the range of values of Koenigsberger ratios (Q_n). The induced magnetization is calculated from susceptibility for the present magnetic field at the site.

DENSITIES

The density logs (Figure 5) show values of saturated bulk densities determined as follows: 25.4 mm diameter cylindrical cores were cut to the required length, the ends faced off and lengths and diameters measured to ± 0.02 mm with Vernier calipers. The dry weight was determined after heating for more than 10 hours at 80°C in a vacuum of 10^{-4} Torr. This procedure was repeated and then the vacuum chamber was flooded with saturating fluid (filtered seawater) while still under partial vacuum after heating. The saturated sample weight was then determined after leaving the sample for several days to ensure complete saturation. Thus the dry and saturated bulk densities, porosities and grain or matrix densities could be determined. The values of saturated bulk density are estimated to be accurate to better than ± 50 kg m^{-3}. In the discussion below 'density' refers to the saturated bulk density, unless otherwise stated.

The density log for drill hole CY-1 shows an increase in density with depth. The high degree of variability of values reflects the presence of differing lithologies (pillow lavas, pillow breccias, massive flows and intrusives), variations in porosity within cooling units and variations in vesicle and vein infillings. Averaging of values over the upper 200 metres gives a density of 2,225 kg m^{-3} while for samples below 250 metres the average density is 2,360 kg m^{-3}, reflecting an increasing proportion of massive flows and intrusives which are less altered than the higher flows and breccias.

The log for CY-2 shows relatively high densities in the upper 100 metres of altered and mineralized lavas and flows. The overall effect is, therefore, of the increase in density due to mineralization exceeding the reduction due to alteration. The average density here is 2,410 kg m^{-3}. In the second altered zone, from 120 to 140 metres, the effect of intense alteration without mineralization is to cause a significant reduction in density to 2,150 kg m^{-3}. Below 140 metres values rise again and are comparable to those observed in the lower part of CY-1.

The two intrusives in the upper part of CY-2a have relatively high densities (2,300 to 2,500 kg m^{-3}), particularly the intrusive near the surface and this probably explains the small positive gravity anomaly observed in the vicinity of CY-2a. Just above the mineralized zone, densities as low as 2,100 kg m^{-3} are observed due to partial alteration, the occurrence of massive fractured glass and, below 149.22 m, the first evidence of hydrothermal alteration. At about 160 metres there is a sharp increase in density to 2,500 kg m^{-3} with several samples, those consisting almost entirely of quartz (or jasper) and pyrite, having considerably higher densities.

Below 280 metres, high densities persist in the altered pillow lavas, dykes and massive flows due to the presence of disseminated pyrite. At 530 metres there is a further increase in density to 2,650 kg m^{-3} in the Basal Group. This value is thought to be rather high for the Basal Group and is due, again, to the presence of disseminated pyrite and also to epidote.

GRAVITY AND MAGNETIC MODELLING

The observed gravity and magnetic profiles along line AA' (indicated on Figure 2a) over the 'A' and 'B' bodies have been modelled with a 2-dimensional computer modelling program using the polygon method of Talwani et al. (1959) and Talwani and Heirtzler (1964).

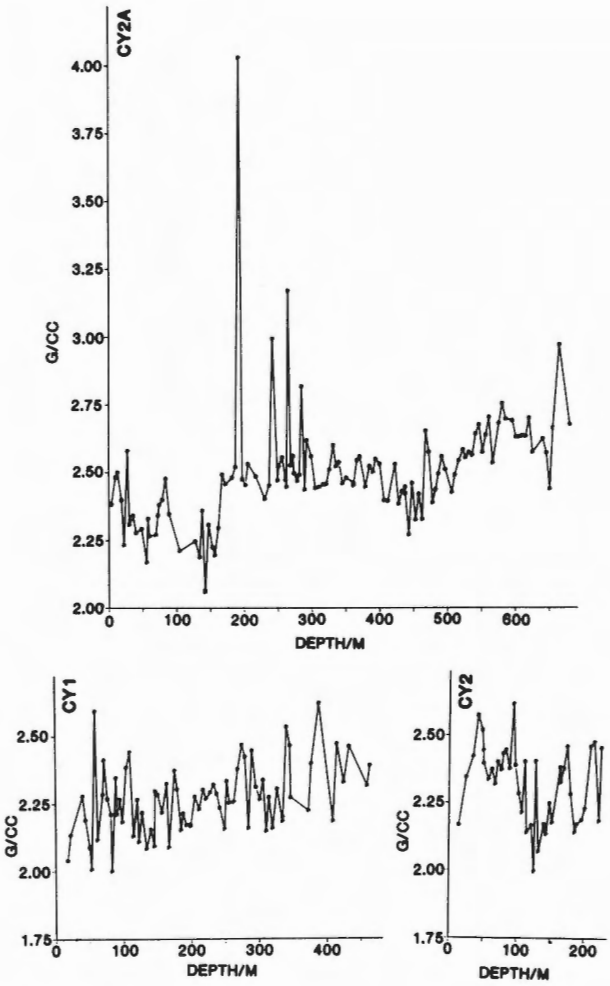

Figure 5: C.C.S.P. drill holes - saturated bulk density logs.

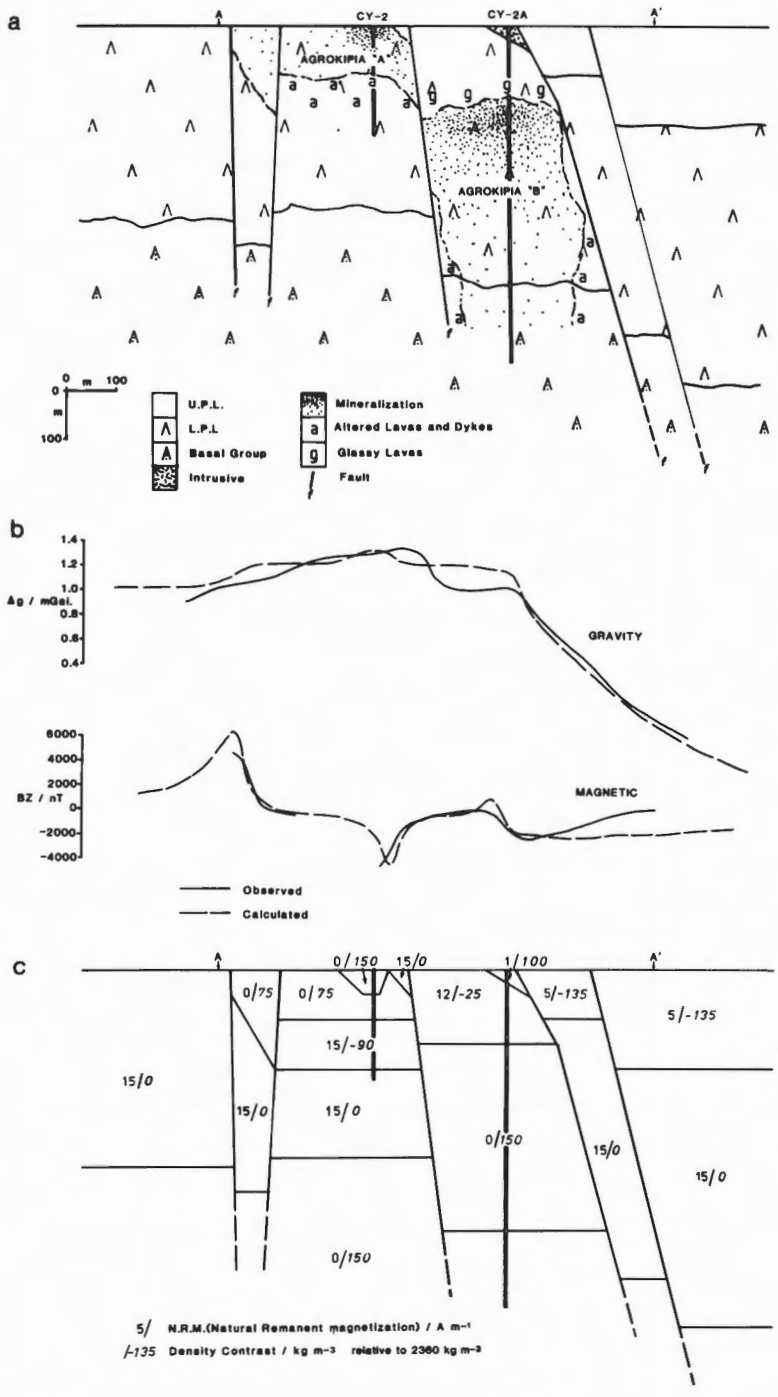

Figure 6: (a) A schematic geological section along the profile A - A′ shown in Figure 2a. The section is based on Hellenic Mining Company borehole data and the geophysical models shown below. Drill holes CY-2 and CY-2a are projected onto the profile A - A′ and provide further geological control. (b) Observed and calculated gravity and magnetic profiles along A - A′. (c) The 2D geophysical models from which the gravity and magnetic profiles were calculated. NRM and density contrasts are shown in non-italic and italic numerals respectively. The direction of remanent magnetization is assumed to be: inclination = 25°, declination = 275°.

The sections shown in Figures 6a and 6c are compiled from geological sections based on percussion drilling by the Hellenic Mining Company, from existing geological maps, and from geological (Robinson and Gibson, 1982a, b, c) and geophysical data (this paper) from the C.C.S.P drill holes. The gravity and magnetic models (Figure 6c) represent a simplification of the geological section which has been assumed (Figure 6a). Gravity and magnetic profiles calculated from the models compare fairly well with the observed data (Figure 6b) bearing in mind the potential errors in the 2-dimensional interpretation of what is a 3-dimensional problem.

The magnetic low observed over Agrokipia 'A' is reproduced in shape and amplitude by the model. The poorly defined low over Agrokipia 'B' appears to arise from the weakly magnetized intrusive which was penetrated at CY-2a. Magnetic modelling shows that variations in the magnetization of rocks below about 100 metres appear to have virtually no observable magnetic effect. For example, the anomaly due to the mineralized zone of Agrokipia 'B' is relatively small and is overwritten by edge effects and anomalies dūe to the overlying UPL's, LPL's and intrusives.

Conversely, gravity modelling shows that the anomalies arising from variations in density at depth represent a major component of the observed gravity anomaly. The most significant feature on the gravity profile, i.e. the strong gradient to the east of Agrokipia 'B', reflects variations in the depths to the UPL-LPL and LPL-Basal Group contacts combined with the density contrast between the mineralized LPL's of Agrokipia 'B' and the unmineralized LPL's to the east. The small positive gravity anomaly over Agrokipia 'A' is poorly reproduced by the model although the amplitude of the calculated anomaly is close to that observed. The small high over Agrokipia 'B' arises from the high density intrusive at the surface. Given the ambiguous nature of gravity interpretation, the spacing of survey data, and the small amplitude of the local anomalies, the value of more detailed modelling of these data is debatable.

DISCUSSION AND CONCLUSIONS

Rona (1978a, b, 1980) described anomalous gravity values and lows in residual magnetic intensity as two features characteristic of hydrothermal deposits in oceanic crust and in ophiolites. Magnetic lows have been observed associated with the discharge zones of a number of high-intensity hydrothermal systems on the sea floor such as the TAG hydrothermal field at 26°N on the Mid-Atlantic Ridge and the Atlantis II Deep of the Red Sea. These hydrothermal systems and their associated magnetic lows extend, typically, over several kilometres and so are not strictly comparable to smaller black-smoker type hydrothermal deposits such as Agrokipia 'A' and 'B'. It is highly unlikely that a deposit of the size of those at Agrokipia could be located on the seafloor by a magnetic survey. Relatively shallow burial of the orebody beneath fresh lavas would reduce the observed magnetic anomaly considerably. It seems quite feasible, however, that detailed magnetic surveys of known or suspected hydrothermal deposits in ophiolites, or deep-towed magnetic surveys on the ocean floor could be of value in determining the extent and degree of hydrothermal alteration.

On Cyprus anomalous gravity values may reflect density contrasts between mineralized and unmineralized lavas, between upper and lower pillow lavas, between the lower pillow lavas and the Basal Group or a combination of these. Interpretation of the gravity data is therefore ambiguous. A positive gravity anomaly is not necessarily due to mineralization. However, gravity surveys may be of value in combination with magnetic surveys because the coincidence of a magnetic low attributed to hydrothermal alteration and a gravity high is likely to indicate a mineralized zone.

ACKNOWLEDGMENTS

The assistance of Paul Johnson, Jill Karsten, Guenther Schoenharting and C.C.S.P. trainees in the collection and synthesis of magnetic survey data is gratefully acknowledged. We wish to thank the Hellenic Mining Company, particularly George Maliotis and Nikos Adamides for the provision of gravity survey data and geological sections. Andreas Panayiotou provided additional geological and geophysical data. This research was supported by the U.K. Natural Environment Research Council grant number GR3/4473.

REFERENCES

Constantinou, G.
1972: The geology and genesis of the sulphide ores of Cyprus; unpublished Ph.D. thesis, University of London.

Deer, W.A., Howie, R.A. and Zussman, J.
1969: An Introduction to the Rock Forming Minerals; John Wiley, New York.

Francheteau, J., Needham, H.D., Choukroune, P., Juteau, T., Séguret, M., Ballard, R.D., Fox, P.J., Normark, W., Carranza, A., Cordoba, D., Guerrero, J., Rangin, C., Bougault, H., Cambon, P. and Hekinian, R.
1979: Massive deep-sea sulphide ore deposits discovered on the East Pacific Rise; Nature, v. 277, p. 523-528.

Hekinian, R., Fevrier, M., Avedik, F., Cambon, P.,

Charlou, J.L., Needham, H.D., Raillard, J., Boulegue, J., Merlivat, L., Moinet, A., Manganini, S. and Lange, J.
1983: East Pacific Rise near 13°N: Geology of new hydrothermal fields; Science, v. 219, p. 1321-1324.
Jerome, S.E.
1966: Some features pertinent in exploration of porphyry copper deposits; *in* Geology of the Porphyry Copper Deposits, ed. S.R. Tithey and C.L. Hicks; University of Arizona Press, Tuson, Arizona.
Johnson, H.P., Karsten, J.L., Vine, F.J., Smith, G.C. and Schoenharting G.
1982: A low level magnetic survey over a massive sulphide orebody in the Troodos ophiolite complex, Cyprus; Marine Technology Society Journal, v. 16, no.3, p. 76-80.
Maliotis, G. and Khan, M.A.
1980: The applicability of the induced polarization method of geophysical exploration in the search for sulphide mineralization within the Troodos ophiolite complex of Cyprus; *in* Ophiolites: Proceedings of the International Ophiolite Symposium, Cyprus, 1979, ed. A. Panayiotou; Cyprus Geological Survey Department, Ministry of Agriculture and Natural Resources, p. 129-138.
Robinson, P.T. and Gibson I.L.
1983a: Cyprus Crustal Study Project. Hole CY-1 Lithologic Unit Summaries.
1983b: Cyprus Crustal Study Project. Hole CY-2 Lithologic Unit Summaries.
1983c: Cyprus Crustal Study Project. Hole CY-2a Lithologic Unit Summaries.
Rona, P.A.
1978a: Criteria for recognition of hydrothermal mineral deposits in oceanic crust; Economic Geology, v. 73, no. 2, p. 135-160.
1978b: Magnetic signatures of hydrothermal alteration and volcanogenic mineral deposits in oceanic crust; Journal of Volcanology and Geothermal Research, v. 3, p. 219-225.
1980: TAG hydrothermal field: Mid-Atlantic Ridge crest at latitude 26°N; Geological Society of London, Journal, v. 137, pt. 4, p. 385-402.
Searle, D.L.
1978: Geological Map of the Agrokipia Area, United Nations Special Fund Project, Survey of Ground Water and Mineral Resources; Cyprus Geological Survey Department, Ministry of Agriculture and Natural Resources.
Talwani, M. and Heirtzler, J.R.
1964: Computation of magnetic anomalies caused by two dimensional structures of arbitrary shape; *in* Computers in the Mineral Industries, Part 1; Stanford University Publications, Geological Sciences, v. 9, no. 1, pt. 1, p. 464-480.
Talwani, M., Worzel J.L. and Landisman M.
1959: Rapid gravity computations for two-dimensional bodies with application to the Mendocino submarine fracture zone; Journal of Geophysical Research, v. 64, no. 1, p. 49-59.
Vine, F.J. and Moores, E.M.
1972: A model for the gross structure, petrology and magnetic properties of oceanic crust; *in* Studies in Earth and Space Sciences, ed. R. Shagam, R.B. Hargraves, W.J. Morgan, F.B. Van Harten, C.A. Burk, H.D. Holland, L.C. Hollister; Geological Society of America, Memoir, v. 132, p. 195-205.

Electrical Conductivity of Basalts from CCSP Drill Holes CY-2 and CY-2a at Agrokipia Mines, Cyprus

G.C. SMITH AND F.J. VINE

School of Environmental Sciences, University of East Anglia, Norwich, U.K., NR4 7TJ

Smith, G.C. and Vine, F.J., Electrical conductivity of basalts from C.C.S.P. Drill Holes CY-2 and CY-2a at Agrokipia Mines, Cyprus; in *Cyprus Crustal Study Project: Initial Report, Holes CY-2 and 2a, ed. P.T. Robinson, I.L. Gibson and A. Panayiotou; Geological Survey of Canada, Paper 85-29, p. 339-346, 1987.*

Abstract

Laboratory measurements of electrical conductivity (σ) have been made to a confining pressure of 0.1 GPa at room temperature for seawater saturated basalt samples from C.C.S.P. drill holes CY-2 and CY-2a. Conductivities vary from 0.0069 to 0.302 S m^{-1} at 0.05 GPa (geometric mean = 0.052 S m^{-1}). The interconnected porosity (η) ranges from 1.9 to 40.2% and the exponent (m) in Archie's Law from 1.08 to 2.98 with a strong positive correlation between m and η. Conductivity is largely a function of porosity since pore-fluid conduction is the dominant conduction mechanism. Conductivity surveys are unlikely to be of value, therefore, in the search for hydrothermal orebodies on Cyprus as there is little or no porosity contrast between mineralized and unaltered lavas. However, because the Troodos extrusive section is anomalously porous, this may not be so for hydrothermal deposits on the ocean floor.

Résumé

Les mesures en laboratoire de la conductivité électrique (σ) ont été effectuées à une pression de confinement de 0,1 GPa à la température ambiante sur des échantillons de basalte saturés en eau de mer prélevés dans les trous de forage CY-2 et CY-2a du projet C.C.S.P. A 0,05 GPa, les conductivités varient de 0,0069 à 0,302 S m^{-1} (moyenne géométrique = 0,052 S m^{-1}). La porosité ouverte (η) varie de 1,9 à 40,2% et l'exposant (m) dans la loi d'Archie de 1,08 à 2,98; il existe une forte corrélation positive entre m et η. La conductivité est principalement une fonction da la porosité car la conduction par le fluide des pores forme le mécanisme dominant de conduction. Les études de conductivité pour la prospection de gîtes hydrothermaux sur l'île de Chypre n'offrent qu'un faible potentiel à cause de l'absence ou du peu de contraste de porosité entre les laves minéralisées et fraîches. Cependant, la coupe extrusive du Troodos exhibe une porosité anomale, par conséquent il peut en être autrement pour les gîtes hydrothermaux de plancher océanique.

INTRODUCTION

The C.C.S.P. (Cyprus Crustal Study Project) Drill holes CY-2 and CY-2a are situated within the Agrokipia Mining Area on the northern flank of the Troodos ophiolite. The drill holes penetrate the genetically related Agrokipia 'A' and 'B' orebodies. Drill hole CY-2, into the 'A' orebody penetrates 70 meters of hydro-thermally altered lavas and flows and passes into a sequence of relatively fresh flows to a depth of 226 meters. Drill hole CY-2a penetrates 154 meters of fresh lava flows and high-level intrusives overlying about 150 metres of hydrothermally altered and mineralized massive and pillowed flows; the Agrokipia 'B' orebody. Below this zone is a sequence of greenschist facies dykes and pillow lava screens with weak mineralization and alteration along fractures. A detailed account of the lithology of the drilled material is given by Robinson and Gibson (1983a, b).

In this study the variation in electrical conductivity of samples of the drilled material at appropriate confining pressures is explained as a function of porosity and the degree of alteration and mineralization. In particular the Archie-type relationship between conductivity and porosity is investigated. The implications for the use of electrical prospecting techniques in the search for sulphide orebodies on Cyprus and on the ocean-floor is assessed.

Conductivities were measured simultaneously with seismic velocities to a confining pressure of 0.1 GPa, as described by Smith and Vine (1987), using an a.c. transformer bridge (1592 Hz) and with the steel transducer holders acting as electrodes. All the measurements were made on seawater saturated samples with the pore fluid pressure equal to atmospheric pressure. A PTFE (Teflon) sleeve isolates the sample and pore fluid from the pressure transmitting medium - in this case, oil. The conductivities are estimated to be accurate to 5% from consideration of errors involved in measuring the conductance and the sample dimensions.

RESULTS

The results of all the measurements and their mean values are given in Tables 1 and 2, respectively. Histograms of conductivity (σ), porosity (η) and Archie's Exponent (m) are given in Figure 1. The value for m is calculated from conductivity and porosity as explained below.

Conductivities range from 0.0069 to 0.302 S m^{-1} with sample porosities ranging from 1.9% to 40.2%. The geometric mean conductivity is 0.052 S m^{-1}, significantly higher than that observed by other authors for oceanic basalts (see Table 2).

Figure 2 shows the observed variation in conductivity with pressure for all the samples measured. With the application of confining pressure and the resulting closure of cracks, a reduction in conductivity is anticipated as the available conductive paths are reduced in number. However, in several cases an initial increase in conductivity is observed. This is thought to be because the sample is not fully saturated initially. In an undersaturated sample, incompletely saturated cracks become continuous conductive pathways as the pressure is increased and as the cracks start to close. There is, therefore, an initial increase in conductivity. With the further increase in pressure the conductivity will start to decrease. A similar effect has been observed by Brace and Orange (1968) and Chroston et al. (1978). Little change is seen in conductivity above 0.025 GPa. All the conductivities tabulated here are measured at 0.05 GPa. This guarantees that initial effects such as undersaturation, the possibility of developing a contact resistance between the sample and the electrodes or conduction between the PTFE sleeve and the sample are no longer significant.

On the sea-floor it is likely that the pore fluid pressure will be hydrostatic and not zero as assumed in these measurements. The assumption is valid as electrical conductivity tends to obey a simple 'effective' pressure law (Lee et al., 1983) and for these samples is not strongly pressure dependent. The effect of increasing the pore fluid pressure on the measured conductivity is, therefore, predictable and in this case negligible.

THE CONDUCTIVITY-POROSITY RELATIONSHIP

The relationship between conductivity and porosity for rocks where conduction through fluid-filled pores is the dominant mechanism is given by Archie's Law (Archie, 1942):

$$\sigma = a\sigma_f\phi^m \qquad (1)$$

where σ_f is the conductivity of the pore fluid (here seawater σ_f = 4.54 S m^{-1}), ϕ (= $\eta/100$) is the interconnected porosity expressed as a fraction of the rock's volume, and 'a' and 'm' are constants. The value for 'a' is typically close to and frequently taken as 1 (Brace et al., 1965; Shankland and Waff, 1974), although values ranging from 0.6 to 1.3 have been determined for marine sedimentary rocks (Keller, 1967). For samples where conduction is through narrow fluid-filled cracks, the value of m is 1 whereas for conduction through spherical, randomly connected pores, the expected value is 2. These values are based on modelling of porosity changes using arrays of resistors (Shankland and Waff, 1974). Figure 3 shows

TABLE 1. Electrical Conductivities, Porosities and Archie's Exponents

Sample	Lithology	Depth (m)	Porosity at Atmospheric Pressure (%)	Electrical Conductivity at 0.05 GPa (S m^{-1})	Archie's Exponent 'm'*
CY-2-2	Altered Pillowed (?) Lava	25.30	17.5	0.132	2.035
CY-2-7	Highly Altered Pillowed (?) Lava	50.55	12.7	0.0760	1.990
CY-2-11	Altered Massive Flow	67.85	24.1	0.123	2.514
CY-2-14	Massive (?) Flow	79.92	7.2	0.0359	1.852
CY-2-18	Massive (?) Flow	97.61	8.8	0.101	1.570
CY-2-21	Massive Flow	111.97	4.8	0.0173	1.840
CY-2-33	Massive Flow	163.98	1.9	0.00689	1.647
CY-2-38	Massive Flow	179.25	7.8	0.0182	2.162
CY-2-45	Massive Flow	209.29	16.8	0.0803	2.265
CY-2-48	Massive Flow	225.10	10.1	0.0372	2.077
CY-2a-2	Basalt Sill (?)	10.17	8.3	0.0573	1.755
CY-2a-9	Massive Basalt Flow	40.43	19.5	0.139	2.132
CY-2a-20	Intrusive Massive Basalt	74.53	12.1	0.0725	1.958
CY-2a-27	Massive Basalt Flow	104.80	27.7	0.221	2.356
CY-2a-33	Massive Crystalline Basalt	138.11	11.5	0.0315	2.299
CY-2a-35	Massive Crystalline Basalt	142.10	40.2	0.302	2.977
CY-2a-37	Massive Hydrothermally Alt. Lava	153.03	20.6	0.110	2.353
CY-2a-53	Altered, Argillized Massive Lava	230.53	23.5	0.0778	2.779
CY-2a-60	Altered, Argillized Massive Lava	261.30	22.1	0.0699	2.761
CY-2a-64	Jasper/Pyrite	272.40	2.4	0.0773	1.089
CY-2a-70	Highly Altered and Bleached Lava	292.50	5.6	0.0318	1.727
CY-2a-81	Altered Dyke	340.25	3.1	0.0156	1.633
CY-2a-87	Basalt Dyke	366.63	3.3	0.0374	1.402
CY-2a-103	Altered Pillow Lava	438.05	18.4	0.0671	2.488
CY-2a-114	Altered Basalt Dyke (?)	492.00	13.6	0.0267	2.577
CY-2a-126	Altered Basalt Dyke	551.95	14.3	0.0411	2.420
CY-2a-152	Altered Basalt Dyke	681.28	9.4	0.0136	2.459

* m is calculated from $\sigma = 4.54\phi^m$

TABLE 2. Mean Values of Electrical Conductivity and Porosity

	Saturated Rock Conductivity (Geometric mean) (S m^{-1})	Porosity at Atmospheric Pressure (Arithmetic mean) (%)
CY-2 and CY-2a (this study, CY-2a-64 omitted)	0.052* n = 26	14.51 n = 165
[a]DSDP Basalts (Legs 2-14, 26, 34 and 37)	0.0053+ n = 153	7.04 n = 137
[b]DSDP Legs 51, 52 and 53	0.0083+ n = 48	8.4 n = 104
[c]DSDP 504B	0.022+ n = 56	4.1 n = 64

[a]Drury and Hyndman (1979), [b]Hamano (1979), [c]Karato (1983), *at 0.05 GPa, +at Atmospheric Pressure

TABLE 3. Regression Equations for CY-2 and CY-2a
(CY-2a-64 is omitted)

	r	r^2	n
Log σ = -2.36 + 1.02 Log ϕ	0.826	68.3	26
m = 1.047 + 1.054 Log ϕ	0.821	67.4	26

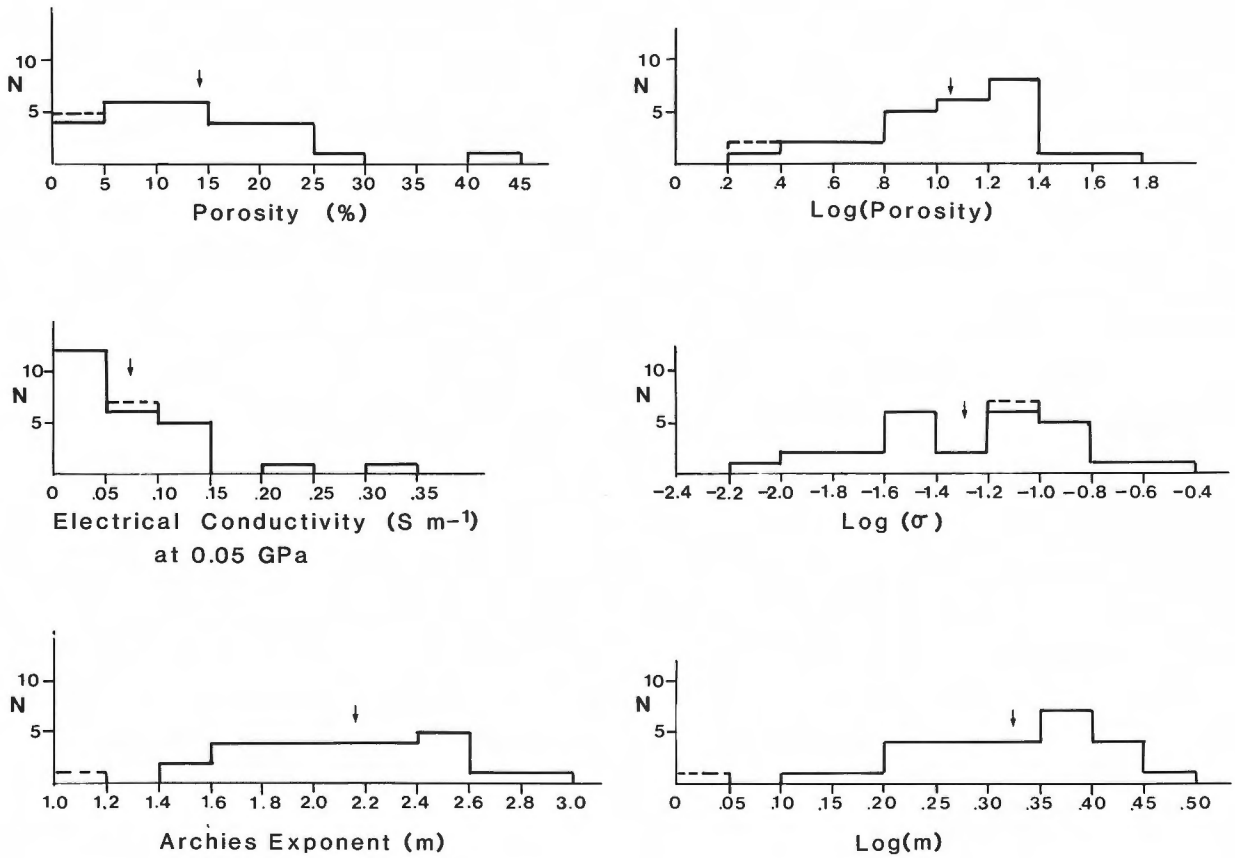

Figure 1: Histograms of porosity, conductivity and Archie's exponent. Arithmetic and geometric means are arrowed. Sample CY-2a-64 is excluded from the calculations and is shown dashed. Conductivity and porosity are log-normally distributed.

the fit of the CY-2 and CY-2a data to Archie's relationship for various values of m.

Assuming a = 1 and σ_f = 4.54 S m^{-1}, then re-arranging Archie's equation gives:

$$m = \frac{\text{Log}(\sigma/4.54)}{\text{Log } \phi} \qquad (2)$$

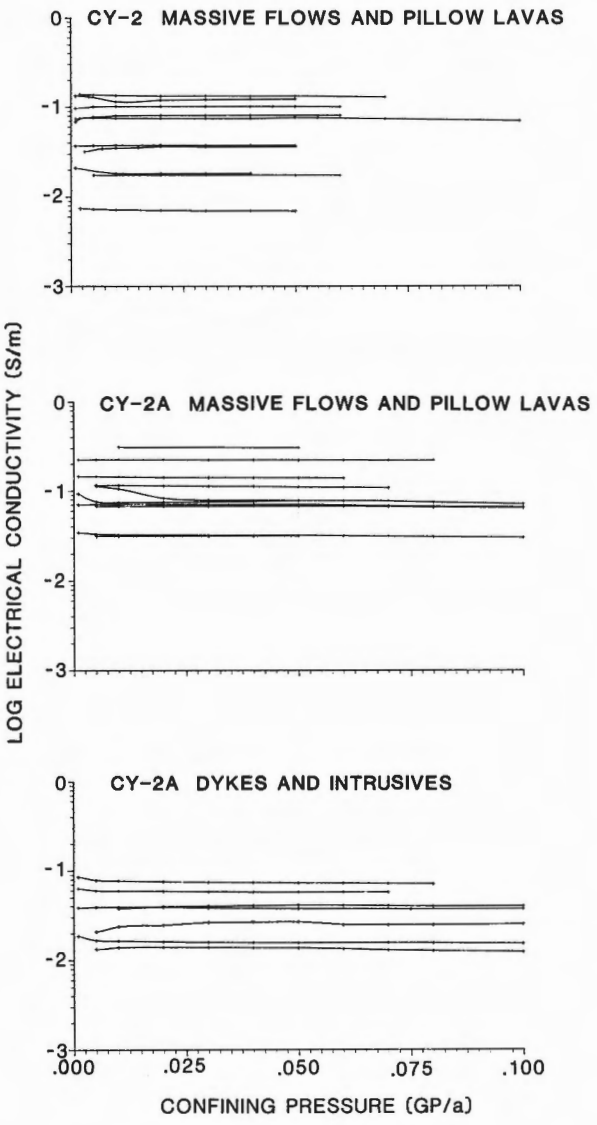

Figure 2: The variation of electrical conductivity with confining pressure.

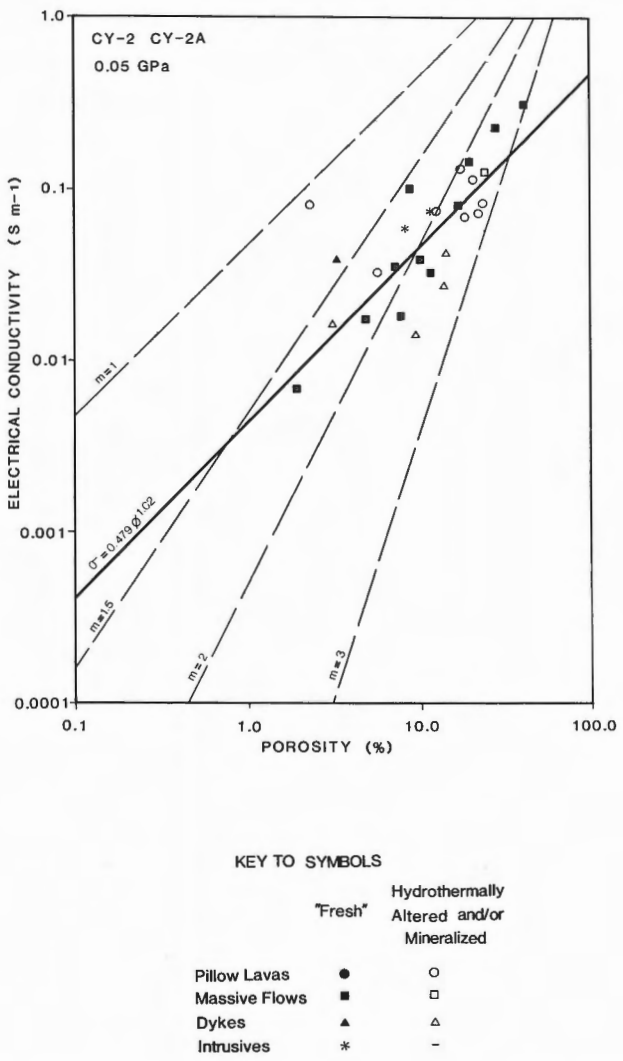

Figure 3: The relationship between conductivity and porosity. Dashed lines are Archie's fit for seawater saturated samples for exponents of 1.0, 1.5, 2.0 and 3.0. The solid line is the best-fit regression line to the data (excluding sample CY-2a-64).

'Observed' values of m range from 1.09 to 2.98. The anomalously high values imply that the conductivity is lower than expected for rocks of this porosity. Higher values, as Figure 4 shows, correlate with higher porosities. Values of m approaching 3.0 are not unprecedented. Cann and Von Herzen (1983) explained high m values determined from resistivity and neutron (porosity) logging of Deep Sea Drilling Project drill hole 504B by a reduction in the degree of connectedness of pores by hydrothermal alteration. Drury and Hyndman's laboratory data (1979) suggest values of m up to 3.0 assuming σ_f = 4.54 S m^{-1} (seawater). In both of these studies 'a' is assumed to be 1.

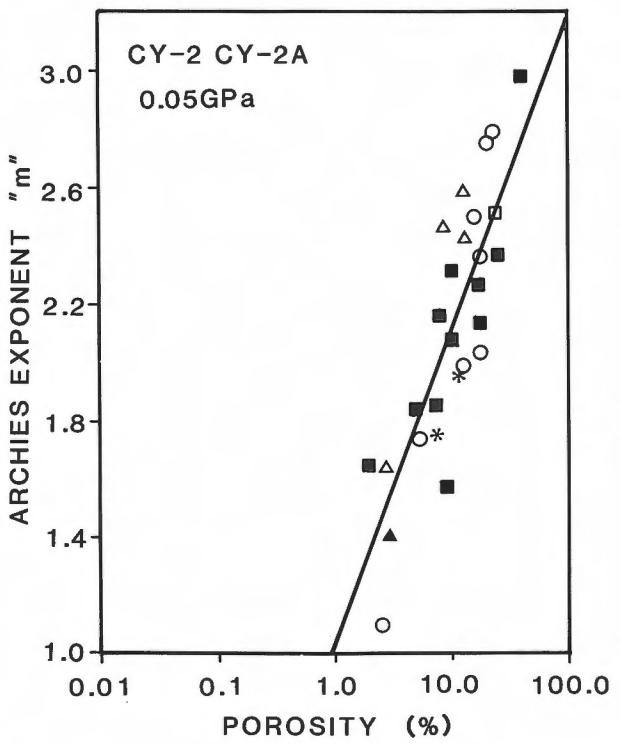

Figure 4: The relationship between Archie's exponent and porosity showing the best-fit regression to the data. Sample CY-2a-64 is excluded from the calculation. The key to the symbols is as for Figure 3.

Because Archie's Law assumes that pore fluid conduction is the dominant conduction mechanism, it will give anomalous results if other major conductive paths exist. For high porosity samples this is unlikely to be the case. However, for lower porosity samples conduction through clays lining pores and the presence of disseminated and vein pyrite may give anomalously high conductivities and correspondingly lower values of m. Sample CY-2a-64, consisting largely of jasper and pyrite with a porosity of 2.37% has the lowest value of m (1.09) with a conductivity 25 times higher than would be predicted from pore fluid conduction alone assuming a value of 2 for m (Table 1). The conductivity of pyrite ranges from 10 to 10^5 S m^{-1}, with a typical average value of 10^2 S m^{-1}, much greater than basalt mineral conductivities and significantly greater than sea water. A small amount of pyrite infilling fractures could lead to highly anomalous observed conductivities. Similarly the presence of clay minerals lining pores can give enhanced conductivities, both by conduction through clays and by effecting an increase in the pore fluid conductivity (Toussaint-Jackson, 1984). Although the conductivities observed in some of the lower porosity samples are anomalously high, they are not so high as to allow us to differentiate between higher porosity unaltered lavas and lower porosity altered and mineralized lavas on the basis of conductivity measurements alone.

The relationship between conductivity and porosity for these samples is therefore more complex than a simple Archie relationship, depending not only on interconnected porosity and pore-shape but also on alteration, specifically the presence of clay minerals and of pyrite.

The empirical equation relating conductivity and porosity for these samples:

$$\sigma = 0.479\ \phi^{1.02} \qquad (3)$$

suggests that a pore fluid conductivity of 0.479 S m^{-1} and a value for m of 1.02 are appropriate. This deceptive result arises from the fact that it assumes m to be constant. Nevertheless, the equation may be useful for the prediction of conductivity from porosity (or vice versa) for similarly mineralized and altered lavas and dykes.

DISCUSSION

Because electrical conductivity is largely a function of porosity, the potential of resistivity surveys in locating and delineating mineralized zones in ophiolites and on the sea-floor will depend on the contrast in porosity and pore fluid conductivity between mineralized and unmineralized lavas.

Resistivity surveys carried out in Cyprus since the 1930's have shown no definitive contrast in the lavas in which most of the economic deposits occur (Maliotis and Khan, 1980), despite the variable modes of occurrence of sulphide mineralization in the Troodos ophiolite. Major deposits such as Skouriotissa and Kalavasos were formed when the mineralizing fluids reached the surface and were unconformably overlain by the Upper Pillow Lavas. The ore consists of hard blocks of pyrite and chalcopyrite in a soft friable pyrite matrix. The porosity of this ore ranges from 10% to 90% (Constantinou, 1972).

In other deposits on the ophiolite, massive concentrations of sulphides occur in highly brecciated zones or associated with faults which may or may not reach the surface. An example is the Kambia mineralized fault. In the south the mineralization is shallow (about 10 meters deep) but concealed and confined to a very narrow zone (about 20 meters wide). Although there is a distinct I.P. anomaly which can be traced for 2 kilometers to the north as the depth to the mineralization increases, the resistivity anomaly is small and only observable where the depth of burial is very shallow (Maliotis and

Khan, 1980). The positive resistivity anomaly suggests that the porosity of the mineralized lavas is lower than that of the surrounding unmineralized lavas.

Similarly, at Agrokipia 'B', resistivity surveys show the top of the mineralized zone to be of lower conductivity than the surrounding unmineralized lavas. It is suggested that this is due to the silicification which accompanies the mineralization. However, drilling at CY-2a found not only highly silicified zones but also zones of soft friable pyrite in the Agrokipia 'B' orebody which are not represented in the samples studied here (Robinson and Gibson, 1983b). In addition the laboratory samples cannot illustrate the effect of large scale fractures or brecciated or glassy zones within the orebody. These would lead to the field conductivities being higher than those observed in the laboratory. A comparison of the laboratory data and the field results of Maliotis and Khan (1980, Figure 6) for Agrokipia shows the laboratory conductivities to range from <0.01 to 0.3 S m^{-1} while field values range from approximately 0.03 to 0.2 S m^{-1}. Since the field values are subject to an averaging effect the true range will be greater, giving an even better agreement between the two sets of data. However, this comparison assumes that the in situ pore fluid conductivities are comparable to that of the seawater used to saturate the laboratory samples, and that the in situ rocks are similarly saturated. If the in situ pore fluid conductivity is lower than that of seawater, the comparable laboratory and field conductivities imply that the in situ porosity is greater than that assumed from laboratory measurements, the excess porosity being accommodated in major fractures and brecciated zones not represented in the laboratory samples.

CONCLUSIONS

What are the implications of this study for the use of conductivity surveys, on the sea-floor and in ophiolites? Firstly, since porosity is undoubtedly the major influence on conductivity, the success of surveys will depend upon the existence of a porosity contrast between the mineralized and unmineralized lavas. Secondly, the altered and mineralized lavas found on Cyprus may be either more or less porous than the surrounding lavas, although the contrast is typically small. For example at Agrokipia 'B' there is some evidence of a reduction in the porosity of the mineralized lavas due to silicification whereas the altered material from Agrokipia 'A' is arguably more porous than the surrounding lavas, the porosity having been increased by solution. Where porosity contrasts are small the effect of relatively shallow burial of the mineralization by porous and conductive lavas will be to severely limit the potential of conductivity surveys. Thirdly, unless the porosity is low, the effect of conduction in clays lining pore spaces and in pyrite will not be significant. Where porosities are low, anomalously low values of Archie's exponent 'm' might indicate the presence of pyrite or clays thus identifying mineralized or hydrothermally altered zones. This observation could be of value in the interpretation of geophysical logging where both conductivities and porosities are available. Where only conductivities are available it will not be possible to discriminate between high conductivities due to pore fluid conduction in porous lavas and those arising from conduction in sulphides and clays in lower porosity mineralized and altered lavas. Thus, conductivity surveys are unlikely to be of value in the search for hydrothermal orebodies on Cyprus. However, the Troodos extrusive section is anomalously porous so this conclusion may not be valid for hydrothermal deposits on the ocean floor. Here there may be a definitive contrast in porosity, and hence in conductivity, between the mineralized and unaltered lavas. Alternatively, the enhanced conductivity provided by clays and sulphides in the mineralized and altered zones in these generally lower porosity terrains may give rise to conductivity anomalies.

ACKNOWLEDGMENTS

This research was supported by the U.K. Natural Environment Research Council grant number GR3/4473.

REFERENCES

Archie, G.E.
1942: The electrical resistivity log as an aid in determining some reservoir characteristics; American Institute of Mining, Metallurgical, and Petroleum Engineers, Transactions, Petroleum Division, v. 146, p. 54-67.

Brace, W.F. and Orange, A.S.
1968: Further studies of the effects of pressure on electrical resistivity of rocks; Journal of Geophysical Research, v. 73, no. 16, p. 5407-5420.

Brace, W.F., Orange, A.S. and Madden, T.R.
1965: The effect of pressure on the electrical resistivity of water-saturated crystalline rocks; Journal of Geophysical Research, v. 70, no. 22, p. 5669-5678.

Cann, J.R. and Von Herzen, R.P.
1983: Downhole logging at Deep Sea Drilling Project sites 501, 504 and 505, near the Costa Rica Rift; *in* Initial Reports of the Deep Sea Drilling Project, Volume 69, ed. J.R. Cann, M.G. Langseth, J.

Honnorez, R.P. Von Herzen, S.M. White, et al.; U.S. Government Printing Office, Washington, D.C., v. 69, p. 281-299.

Chroston, P.N., Evans, C.J. and Lee, C.
1978: Laboratory measurements of compressional wave velocities and electrical resistivity of basalts from Deep Sea Drilling Project Leg 49; *in* Initial Reports of the Deep Sea Drilling Project, Volume 49, ed. B.P. Luyendyk, J.R. Cann, et al.; U.S. Government Printing Office, Washington, D.C., v. 49, p. 761-763.

Constantinou, G.
1972: The geology and genesis of the sulphide ores of Cyprus; unpublished Ph.D. thesis, University of London.

Drury, M.J. and Hyndman, R.D.
1979: The electrical resistivity of oceanic basalts; Journal of Geophysical Research, v. 84, no. B9, p. 4537-4545.

Hamano, Y.
1979: Physical properties of basalts from holes 417D and 418A; *in* Initial Reports of the Deep Sea Drilling Project, Volumes 51-53, Part 2, ed. T. Donnelly, J. Francheteau, W. Bryan, P. Robinson, M. Flower, M. Salisbury, et al.; U.S. Government Printing Office, Washington, D.C., v. 51-53, pt. 2, p. 1457-1466.

Karato, S.
1983: Physical properties of basalts from Deep Sea Drilling Project hole 504B, Costa Rica Rift; *in* Initial Reports of the Deep Sea Drilling Project, Volume 69, ed. J.R. Cann, M.G. Langseth, J. Honnorez, R.P. Von Herzen, S.M. White, et al.; U.S. Government Printing Office, Washington, D.C., v. 69, p. 687-695.

Keller, G.V.
1967: Supplementary guide to the literature on electrical properties of rocks and minerals; *in* Electrical Properties of Rocks, E.I. Parkhomenko, ed./trans. G.V. Keller; Monographs in Geoscience, Plenum Press, New York, p. 277.

Lee, C.D., Vine, F.J. and Ross, R.G.
1983: Electrical conductivity models for the continental crust based on laboratory measurements on high-grade metamorphic rocks; Geophysical Journal of the Royal Astronomical Society, v. 72, no. 2, p. 353-371.

Maliotis, G. and Khan, M.A.
1980: The applicability of the induced polarization method of geophysical exploration in the search for sulphide mineralization within the Troodos ophiolite complex of Cyprus; *in* Ophiolites: Proceedings of the International Ophiolite Symposium, Cyprus, 1979, ed. A. Panayiotou; Cyprus Geological Survey Department, Ministry of Agriculture and Natural Resources, p. 129-138.

Robinson, P.T. and Gibson, I.L.
1983a: Cyprus Crustal Study Project. Hole CY-2 Lithologic Unit Summaries.
1983b: Cyprus Crustal Study Project. Hole CY-2a Lithologic Unit Summaries.

Shankland, T.J. and Waff, H.S.
1974: Conductivity in fluid-bearing rocks; Journal of Geophysical Research, v. 79, no. 32, p. 4863-4868.

Smith, G.C. and Vine, F.J.
1987: Seismic velocities in basalts from C.C.S.P. drill holes CY-2 and CY-2a at Agrokipia Mines, Cyprus; *in* Cyprus Crustal Study Project Initial Report Hole CY2-2a, ed. P.T. Robinson, I.L. Gibson and A. Panayiotou; Geological Survey of Canada, Paper 85-29.

Toussaint-Jackson, J.E.
1984: Laboratory and theoretical studies of electrical conduction in crystalline rocks; unpublished Ph.D. thesis, University of East Anglia, Norwich, U.K.

Geology and Geophysics of the CY-2 and CY-2a Boreholes, Cyprus Crustal Study Project: Summary

PAUL T. ROBINSON[1] AND JOHN MALPAS[2]

[1]Centre for Marine Geology, Dalhousie University,
Halifax, Nova Scotia, Canada, B3H 3J5
[2]Department of Earth Sciences, Memorial University,
St. John's, Newfoundland, Canada, A1B 3X5

Robinson, P.T. and Malpas, J., Geology and geophysics of the CY-2 and CY-2a Boreholes, Cyprus Crustal Study Project: summary; in *Cyprus Crustal Study Project: Initial Report, Holes CY-2 and 2a, ed. P.T. Robinson, I.L. Gibson and A. Panayiotou; Geological Survey of Canada, Paper 85-29, p. 347-352, 1987.*

Abstract

A model for the formation of the Agrokipia ore bodies of the Troodos ophiolite has been formulated from research drilling and study of surface exposures and percussion drilling records. The deposits are thought to lie atop a small volcanic pile which focussed the hydrothermal activity. The Agrokipia 'A' ore body is an exhalative deposit formed at the sea floor whereas Agrokipia 'B' formed by replacement of massive, probably originally glassy, lavas. The massive flows probably formed by ponding in a small topographic depression associated with the volcanic edifice. Many similarities between the Cyprus ore bodies and those of active spreading ridges suggest formation by analogous processes.

Résumé

Un modèle pour la formation des dépôts de minerai d'Agrokipia de l'ophiolite de Troodos a été formulé d'après des forages de recherche et l'étude des surfaces exposées et les rapports de forage à percussion. On pense que les dépôts reposent au-dessus d'une petit édifice volcanique qui a concentré l'activité hydrothermale. Le dépôt de minerai Agrokipia 'A' est un dépôt exhalatif formé sur le plancher océanique tandis que Agrokipia 'B' fut formé par remplacement de lave massives, probablement originellement vitreuses. Les coulées massives se sont probablement formées par stagnation dans une petite dépression topographique associée à l'édifice volcanique. Plusieurs similarités entre les dépôts de minerai de Cyprus et ceux des rides d'extension en activité suggèrent une formation par des processus analogues.

INTRODUCTION

The discovery of active hydrothermal vents on the seafloor provided an opportunity to study hydrothermal solutions and the ore deposits formed from them. However, little has yet been learned about the stockwork zones underlying such systems, in particular, the paths of fluid flow, the ways in which the fluids interact with the wallrock, and how they evolve with time.

One of the principal goals of the Cyprus Crustal Study Project was to investigate in three dimensions a fossil hydrothermal system in the Troodos ophiolite. Although it was understood that the Troodos ophiolite was formed in a suprasubduction zone rather than at a normal mid-ocean ridge, it was thought that the fossil hydrothermal systems of Troodos provided reasonable analogues for modern systems. Fluid inclusion and strontium isotope studies of the Troodos deposits had confirmed that seawater was the main ore-bearing fluid (Spooner and Bray, 1977; Spooner et al., 1977) and textural and mineralogical comparisons with black smoker deposits of the East Pacific Rise (Oudin and Constantinou, 1984) suggested a similar mode of formation.

The massive sulphide ore bodies of the Troodos ophiolite typically occur in clusters in the extrusive section. Individual ore bodies range in size from about 50,000 to 20,000,000 tonnes and have average copper contents between 0.5 and 4.5 percent (Constantinou, 1980). They are commonly lenticular in cross section and are sometimes overlain by thin layers of ochre, probably formed by seafloor weathering of the deposits. Formation during crustal construction is indicated by overlying lava flows and by post-mineralization dykes.

Most of the massive ores have a conglomeratic texture consisting of irregularly-shaped blocks in a matrix of sandy sulphide (Constantinou, 1980). Pyrite, chalcopyrite, marcasite and sphalerite are the most common ore minerals and the bodies consist chiefly of sulphur, iron, and copper with minor amounts of zinc and nickel. These massive ores are believed to be exhalative deposits formed around hydrothermal units on the seafloor.

Beneath the massive ores are stockwork zones consisting of mineralized and hydrothermally altered breccias, pillowed and massive lava flows and dykes. Mineralization in these zones is chiefly in the form of quartz-sulphide veins. These stockwork zones are believed to be the conduits through which the hydrothermal fluids reached the seafloor.

The original plan was to drill a single deep (1000 m or more) hole vertically through such a stockwork zone in order to determine spatial and temporal variations in the composition of the hydrothermal fluids, and the nature of alteration. Two holes were actually drilled into and beneath the Agrokipia ore deposits, with a total penetration of 915 m.

Study of the recovered drill core, outcrop samples and percussion drilling records, has provided a relatively clear three-dimensional picture of the Agrokipia fossil hydrothermal system.

GEOLOGIC SETTING

The Agrokipia ore deposits lie about 1 km west of Agrokipia village in the Tamassos mining district on the northern flank of the Troodos ophiolite. In this area northward-dipping upper Cretaceous and Tertiary sedimentary rocks overlie a sequence of olivine-phyric pillow lavas, which in turn overlies a sequence of aphyric, locally glassy lavas. The two lava sequences correspond approximately to the earlier defined upper and lower pillow lavas (Bear, 1960) (See Malpas, 1987 (this volume)).

Two district ore bodies occur in the Agrokipia area. Agrokipia 'A' consisted of two lens-shaped bodies near the top of the aphyric lavas. The ore has been removed by open pit mining. Reserves were estimated to be about 700,000 tonnes. Agrokipia 'B' lies about 300 m east and 150 m deeper in the section. The 'B' orebody does not crop out at the surface and was discovered by Hellenic Mining Company through percussion drilling on a gravity anomaly. The main body has a pyramidal shape with a vertical extent of about 150 m. Two smaller bodies appear to be downthrown segments north of the Agrokipia Fault. Ore reserves are estimated at about 5-6 million tonnes.

DRILLING RESULTS

Hole CY-2 was spudded on the eastern margin of the pit from which the Agrokipia 'A' ore body had been removed. The hole was terminated at 226 m after it had clearly passed out of the stockwork into a sequence of relatively fresh lavas. Hole CY-2a was spudded 270 m to the east, directly over the Agrokipia 'B' ore deposit. This hole penetrated 689 m and passed through the Agrokipia 'B' ore deposit and into the underlying stockwork zone.

Hole CY-2 penetrated variably altered pillowed and massive lavas. Fourteen lithologic units, ranging from 3 to 57 m thick, were identified on the basis of lithology, mineralogy, structure and degree of alteration. The upper 86 m consists of hydrothermally altered and weakly mineralized extrusives. The degree of alteration and mineralization decreases down the hole until fresh volcanic glass appears at a depth of 114 m. The lower half of the core consists of relatively fresh lavas that contain many layers of volcanic glass.

Hole CY-2a penetrated a sequence of lavas and

dykes, which has been divided into 22 lithologic units ranging from 0.4 to 160 m thick. Three major divisions of the core are recognizable on the basis of alteration. The upper 154 m consist of massive and pillowed lavas that have undergone varying degrees of low temperature alteration. Massive layers of fresh volcanic glass first appear at 109 m and then alternate with massive crystalline flows to a depth of 154 m. At 154 m, the core is cut by narrow veins of laumontite, the first indication of higher temperature, hydrothermal alteration. This alteration increases rapidly downhole and the rocks are completely bleached and altered at 158 m. The highly bleached and altered zone extends to 297 m where it is truncated by a minor fault. From 297 m to the bottom of the hole the sequence consists chiefly of altered dykes with a zone of pillowed and massive lavas between about 400 and 500 m. This entire lower sequence has been altered to a subgreenschist facies mineral assemblage.

ORIGINAL LAVA COMPOSITIONS

Two major compositional units have been recognized in the extrusive rocks on the northern flank of Troodos. A lower andesite-dacite-rhyodacite series and an upper basaltic andesite series with local picritic units (Robinson et al., 1983; Schmincke et al., 1983). Rocks of the lower sequence are sparsely phyric with plagioclase, clinopyroxene and Fe-Ti oxides as liquidus minerals, whereas those of the upper unit typically have variable amounts of olivine, clinopyroxene, orthopyroxene and spinel phenocrysts. Geochemically, the lower sequence is significantly more enriched than the upper one and has markedly higher total iron and TiO_2 at equivalent MgO.

Study of the CY-2 and CY-2a drill core indicates that the holes were spudded near the boundary between the upper and lower units. Basaltic andesites of the upper sequence are found only in the uppermost parts of both holes (Bednarz et al., 1987). They occur as pillow lavas in the upper 40 m (units I, II, and III) of CY-2 and as sills or massive flows in the upper 70 m of CY-2a. Below these depths all of the fresh and altered lavas appear to belong to the andesite-dacite-rhyodacite assemblage.

The glassy lavas penetrated in both holes are only partially altered and some fresh material is still preserved. The fresh glasses are all andesites which range from about 57 to 61 wt.% SiO_2 (Gibson et al., 1987). They contain microphenocrysts of plagioclase, clinopyroxene and orthopyroxene and clearly belong to the lower, enriched lava series.

ALTERATION

Three types or styles of alteration have been recognized in holes CY-2 and CY-2a: (a) low grade seawater rock interaction, (b) pervasive hydrothermal argillic or propylitic alteration and mineralization, and (c) subgreenschist facies hydrothermal alteration.

The low grade background alteration is characterized by smectite or celadonite accompanied by lesser amounts of heulandite, cristobalite and rare calcite. It is patchily developed and fresh glass is locally preserved in these zones. Variations in the degree of alteration appear to be controlled largely by permeability. Celadonite appears to have formed in the most permeable zones where fresh seawater gained access to the rocks. Temperatures for this type of alteration are estimated to have been between about 30-100°C (Sunkel et al., 1987; Gillis, 1986).

The low grade background alteration is preserved only in the lower half of CY-2 and the upper 154 m of CY-2a; elsewhere in the core it has been obliterated by later hydrothermal activity.

Argillic or propylitic alteration occurs in the upper half of hole CY-2 and between 154-297 m in hole CY-2a. The boundary of this zone with the overlying zone of background alteration is gradational. The argillic zone is characterized by intense bleaching and pervasive development of chlorite and sericite. Sulphide mineralization is variable ranging from lenses of massive pyrite and jasper ore to thin veins of pyrite and sphalerite. Small amounts of sphalerite occur locally in the core. This assemblage probably formed at temperatures somewhat lower than the subgreenschist facies which contains abundant epidote. The paucity of epidote in the argillic zone suggests temperatures between about 200 and 250°C. Below 297 m in CY-2a, the rocks have been pervasively altered to a subgreenschist facies assemblage of chlorite + epidote + albite + quartz + sphene. Based on the abundance of epidote and the absence of actinolite, temperatures in this zone probably ranged from about 230-300°C. This sequence is separated from the overlying zone of argillic alteration by a small fault. A thin zone of surface oxidation is superimposed on the argillic type alteration in the upper part of hole CY-2. It is recognized by the presence of such minerals as cuprite, goethite, delafossite, and parabutlerite (Kurnosov et al., 1987).

GEOCHEMISTRY OF ALTERED ROCKS

Major Elements

When normalized with respect to Al or Ti (Pearce and Cann, 1973) the following elemental variations are noted in hole CY-2a.

Potassium shows a decrease going downhole from

the upper pillow lava sequence, through the argillic or propylitic rocks into the subgreenschist facies rocks at the base of the hole. The mineralized zone is enriched in potassium. Potassium is released from feldspars and the glassy mesostasis during alteration and fixed in sericite-illite or in zeolites and celadonite.

The argillic or propylitic and subgreenschist facies rocks deeper in the hole are depleted in calcium. However, Na is enriched. This complementary behaviour results in the transformation of Ca plagioclase to oligoclase-albite. This release of calcium also balances the precipitation of Mg from seawater. The mineralized zone between 154-297 m is strongly depleted in both Ca and Na as a result of the complete breakdown of primary minerals.

Mg values are highest in the argillic or propylitic and subgreenschist facies zones where Mg-chlorite is the dominant mineral. Iron contents are closely related to the zones of extensive sulphide mineralization. Silica is enriched in the pervasively mineralized zone as indicated by quartz-jasper-sulphide assemblages and the highest SiO_2 values occur at the top and bottom of the main ore zone.

Trace Elements

The mineralized zone in hole CY-2a (154-297 m) is characterized by enrichment in Zn, Cu, Ba, As and general depletion in Ni, Co, Sr, and Rb compared with the unmineralized uppermost lavas. The mineralized zone is characterized by higher Zn than Cu and the Cu/Zn ratio decreases upwards in the zone indicating a decreasing temperature gradient. However, no distinct zonation from Cu-rich base to Zn-rich top typical of other volcanogenic sulphide deposits has been detected.

A strong positive correlation is shown between mineralization and Ba content. Barium was presumably mobilized by breakdown of plagioclase lower in the sequence and was redeposited in the mineralized zones, probably in the K-bearing sericite/illite.

Isotope data produced during this study include measurements of oxygen, hydrogen and strontium isotopes. Oxygen and hydrogen data suggest alteration temperatures of up to 150°C for the zone of low temperature alteration in hole CY-2a and up to 485°C for the subgreenschist facies (Rommel and Friedrichsen, 1987). These temperatures are somewhat higher than those estimated from the mineral assemblages. Strontium isotope data suggest that alteration took place under high water/rock ratios. The isotope data, however, do not confirm categorically that the Agrokipia 'B' deposit was either exhalative or replacement in origin.

COMPARISON WITH ACTIVE BLACK-SMOKER DEPOSITS

Sulphide deposits are forming at the present time on the ocean floor on the East Pacific Rise, the Galapagos Ridge and the Juan de Fuca Ridge. It is, therefore, natural to compare the massive sulphide deposits of the Troodos ophiolite, themselves formed in a marine environment, with their contemporary examples.

Oudin and Constantinou (1984) have noted similarities in mineral associations, textures and zonations between the Cyprus ore bodies, including the Agrokipia example, and black smokers on the ocean ridge system.

Typical vent fragment morphologies, including chimney and mound samples, have been sampled in both occurrences. The most common type of Cyprus ore, the massive pyritiferous, colloform variety, has been repeatedly sampled on the Galapagos Ridge. However, the Cyprus ores are marked by the absence of unstable phases, dissolved during aging of the ore body, and additional silicification which occurred during secondary alteration. This alteration of the Cyprus vent fragments indicates that they lay on the seafloor prior to being embedded in and replaced by a matrix of fine-grained pyrite and silica.

Both ridge-crest sulphide bodies and Cyprus ore deposits are characterized by similar primary mineral associations, mineral habits and intergrowths and the presence of rare mineral species (e.g. jordanite $Pb_{14}As_6S_{26}$, Oudin and Constantinou, 1984)

Young, active smoker chimneys from EPR at 21°N have zoned walls. The outside wall consists primarily of anhydrite but when hydrothermal activity ceases, this is dissolved and replaced by sulphides. It is not surprising then, that the anhydrite zone is not found in the old, inactive Cyprus deposits. The inner walls of the EPR chimneys are formed of an aggregate of crystalline sulphides. Variations in grain-size and the chemical composition of these minerals (e.g. Fe-content of chalcopyrite) give rise to a further primary zonation. Secondary zonation arises initially as a result of high-temperature oxidation of active chimneys. In EPR 21°N samples from inactive zones, sulphides are commonly replaced by sulphates.

The fossil chimney wall fragments from the Cyprus ore bodies preserve a zonation in grain size in the porous aggregates of embedded chalcopyrite. Re-equilibration during aging, removes the primary chemical zonation and dissolves phases such as anhydrite. Goethite is a common oxidation product of EPR samples at relatively high temperature and is found as discontinuous asymmetric rims on the Cyprus examples. The asymmetrical nature of the rims in Cyprus, however, suggests that the oxidation here might be due to late supergene enrichment events rather than high temperature oxidation (or at

least to a combination of the two).

Other types of vent deposit, including layered dendritic pyritiferous ores and mound fragments also occur in Cyprus. The mound fragments are characteristically altered zinc sulphides (to covellite) and contain rounded inclusions of galena and jordanite, similar to those found in some Juan de Fuca samples. Inclusions of zinc sulphide and secondary pyrite are also common and chalcopyrite and gypsum are found lining cavities. In addition, worm tubes and other organic remains, common in Galapagos examples, have been tentatively identified in Cyprus ores (Oudin and Constantinou, 1984).

GRAVITY AND MAGNETIC PROFILES

Both Agrokipia 'A' and 'B' deposits are characterized by aerially limited gravity highs and magnetic lows. The gravity highs are not entirely the result of the sulphide ores since a gravity high persists at Agrokipia 'A' even though the ore has been removed. Rather, they appear to be due to a combination of factors such as juxtaposition of different lava types across fault zones, intrusion of dykes, and mineralization.

Gravity modelling shows that variations in density at depth contribute significantly to the overall anomalies. The gravity high over Agrokipia 'B' may therefore be due in part to the high density dyke swarm that underlies the deposit

On the basis of magnetic susceptibility studies made on the core with a hand held meter, and subsequent lab studies, strong contrasts occur between massive glass and massive basalt in intervals where smectite alteration occurs and between the zones of smectite alteration and intervals of pervasive argillic or propylitic and subgreenschist facies alteration. The very low magnetic susceptibility found in massive glass, zones of argillic alteration and in parts of the subgreenschist zone results from leaching of iron from primary titanomagnetites.

Magnetic susceptibility is higher in non-glassy zones of the extrusive series and in post-mineralization dykes. There are potential compensating factors in the overall magnetic picture. In addition, the peripheral regions of the mineralized zones show high susceptibilities as a result of oxidation.

There is a contrast in values for NRM intensity and magnetic susceptibility in CY-2a below 280 m. High NRMS here are apparently associated only with post-mineralization dykes.

It is clear that the distribution of remanent magnetization, rather than induced magnetization, is the most important factor in determining the magnetic anomaly pattern observed at the surface. Therefore, rocks with low remanent magnetism generally have a low surface anomaly. Thus, modelling the magnetic low over the Agrokipia 'B' ore body suggests that it results from the weakly magnetized intrusive in the upper part of hole CY-2a. Below 100 m depth, variations in magnetization of rocks appear to have no effect on the surface anomaly. Any magnetic low that might result from the altered and mineralized zone of Agrokipia 'B' is obliterated by edge (oxidation) effects and anomalies in the overlying pillow lavas sequence.

FORMATION OF THE AGROKIPIA ORE BODIES

The geochemical stratigraphy recorded in holes CY-2 and CY-2a indicates that the Agrokipia deposits lie on a thick accumulation of differentiated lavas (lower andesite-dacite-rhyodacite series). This thick sequence of lavas may mark the presence of a volcanic centre which served to localize the hydrothermal circulation. This interpretation is strengthened by the presence of a dyke swarm at relatively shallow levels in hole CY-2a (Gibson et al., 1987).

The considerable thickness of massive flows, including layers of massive glass, penetrated in holes CY-2 and CY-2a, is possibly due to ponding of the lavas in a topographic depression. Such depressions are commonly associated with small seamounts on the East Pacific Rise.

The thermal anomaly associated with such a volcanic edifice may have driven the hydrothermal system at Agrokipia leading to copper sulphide mineralization. Based on its form and texture, the Agrokipia 'A' ore body is interpreted as an exhalative deposit formed on the seafloor. The Agrokipia 'B' deposit was probably formed by replacement of pre-existing lavas during hydrothermal alteration. The contact between the mineralized zone and the overlying massive lavas in hole CY-2a is gradational and there is no evidence that this part of the system ever vented onto the seafloor. The ores in Agrokipia 'B' occur in lenses and pods interlayered with altered lavas rather than as massive bodies of pure ore. Perhaps the thick section of massive lavas overlying the Agrokipia 'B' deposit inhibited upward flow of the hydrothermal fluids, causing alteration and mineralization within the lava pile.

REFERENCES

Bear, L.M.

1960: The geology and mineral resources of the Akaki-Lythrodondha area; Cyprus Geological Survey Department, Ministry of Agriculture and Natural Resources, Memoir, no. 3, p. 1-122.

Bednarz, U., Sunkel, G. and Schmincke, H.-U.

1987: The basaltic andesite-andesite and the andesite-dacite series from the ICRDG drill holes CY-2 and CY-2a. I. Lithology, petrology and geochemistry; *in* Cyprus Crustal Study Project Initial Report Hole CY2-2a, ed. P.T. Robinson, I.L. Gibson and A. Panayiotou; Geological Survey of Canada, Paper 85-29.

Constantinou, G.
1980: Metallogenesis associated with the Troodos ophiolite; *in* Ophiolites: Proceedings of the International Ophiolite Symposium, Cyprus, 1979, ed. A. Panayiotou; Cyprus Geological Survey Department, Ministry of Agriculture and Natural Resources, p. 663-674.

Gibson, I.L., McGill, G.C. and Robinson, P.T.
1987: The geochemistry and nature of unusual glassy lavas from CCSP holes CY-2 and CY-2a, Troodos Ophiolite, Cyprus; *in* Cyprus Crustal Study Project Initial Report Hole CY2-2a, ed. P.T. Robinson, I.L. Gibson and A. Panayiotou; Geological Survey of Canada, Paper 85-29.

Gillis, K.M.
1986: Multistage alteration of the extrusive sequence, Troodos ophiolite, Cyprus; unpublished Ph.D. thesis, Dalhousie University, Halifax, Nova Scotia, Canada, p. 1-387.

Kurnosov, V.B., Robinson, P.T., Chudaev, O.V., Kholodkevich, I.V. and Petrachenko, E.D.
1987: Secondary minerals in the CCSP drill holes CY-2 and CY-2a, Agrokipia, Cyprus; *in* Cyprus Crustal Study Project Initial Report Hole CY2-2a, ed. P.T. Robinson, I.L. Gibson and A. Panayiotou; Geological Survey of Canada, Paper 85-29.

Malpas, J.
1987: The geology and geophysics of the area surrounding the CY-2 and CY-2a drill holes of the Cyprus Crustal Study Project; *in* Cyprus Crustal Study Project Initial Report Hole CY2-2a, ed. P.T. Robinson, I.L. Gibson and A. Panayiotou; Geological Survey of Canada, Paper 85-29.

Oudin, E. and Constantinou, G.
1984: Black smoker chimney fragments in Cyprus sulphide deposits; Nature, v. 308, p. 349-353.

Pearce, J.A. and Cann, J.R.
1973: Tectonic setting of basic volcanic rocks determined using trace element analyses; Earth and Planetary Science Letters, v. 19, no. 1, p. 290-300.

Robinson, P.T., Melson, W.G., O'Hearn, T. and Schmincke, H.-U.
1983: Volcanic glass compositions of the Troodos ophiolite, Cyprus; Geology, v. 11, no. 7, p. 400-404.

Rommel, U. and Friedrichsen, H.
1987: The alteration chemistry of CCSP hole CY-2a: a stable and radiogenic isotope study; *in* Cyprus Crustal Study Project Initial Report Hole CY2-2a, ed. P.T. Robinson, I.L. Gibson and A. Panayiotou; Geological Survey of Canada, Paper 85-29.

Schmincke, H.-U., Rautenschlein, M., Robinson, P.T. and Mehegan, J.M.
1983: Troodos extrusive series of Cyprus; a comparison with oceanic crust; Geology, v. 11, no. 7, p. 405-409.

Spooner, E.T.C. and Bray, C.J.
1977: Hydrothermal fluids of seawater salinity in ophiolitic sulphide ore deposits in Cyprus; Nature, v. 266, no. 5605, p. 808-812.

Spooner, E.T.C., Chapman, H.J. and Smewing, J.D.
1977: Strontium isotopic contamination and oxidation during ocean floor hydrothermal metamorphism of the ophiolitic rocks of the Troodos Massif, Cyprus; Geochimica et Cosmochimica Acta, v. 41, no. 7, p. 873-890.

Sunkel, G., Bednarz, U. and Schmincke, H.-U.
1987: The basaltic andesite-andesite and the andesite-dacite series from the ICRDG drill holes CY-2 and CY-2a. II. Alteration; *in* Cyprus Crustal Study Project Initial Report Hole CY2-2a, ed. P.T. Robinson, I.L. Gibson and A. Panayiotou; Geological Survey of Canada, Paper 85-29.

Major Element and Trace Element Analytical Data: Cyprus Crustal Study Project Hole CY2-2a

U. BEDNARZ[1], T. BRACE[2], J.R. CANN[3], P. HERZIG[4], H.E. JAMIESON[5], J.W. LYDON[6] AND J. MALPAS[2]

[1]Institut für Mineralogie, Ruhr-Universität Bochum, Postfach 102148, D-4630 Bochum, Federal Republic of Germany
[2]Department of Earth Sciences, Memorial University of Newfoundland, St. John's, Newfoundland, Canada, A1B 3X5
[3]Department of Geology, The University of Newcastle Upon Tyne, Newcastle Upon Tyne, England, NE1 7RU
[4]Institut für Mineralogie und Lagerstättenlehre, Rheinisch-Westfälische Technische Hochschule Aachen, D-5100 Aachen, Federal Republic of Germany
[5]Department of Geological Sciences, Queen's University, Kingston, Ontario, Canada, K7L 3N6
[6]Geological Survey of Canada, 601 Booth Street, Ottawa, Ontario, Canada, K1A 0E8

Bednarz, U., Brace, T., Cann, J.R., Herzig, P., Jamieson, H.E., Lydon, J.W. and Malpas, J., Major element and trace element analytical data: Cyprus Crustal Study Project Hole CY2-2a; in *Cyprus Crustal Study Project: Initial Report, Holes CY-2 and 2a, ed. P.T. Robinson, I.L. Gibson and A. Panayiotou; Geological Survey of Canada, Paper 85-29, p. 353-381, 1987.*

Abstract

Major element data (SiO_2, Al_2O_3, Fe_2O_3, FeO, MgO, CaO, Na_2O, K_2O, TiO_2, P_2O_5, MnO, H_2O+, CO_2) is presented for 217 samples from Hole CY-2 and 504 samples from Hole CY-2a. Data are arranged according to sample depth, and, in addition to the analytical data, the responsible laboratory is also indicated. Comparable information, usually for splits from the same samples, is provided for the trace elements (Sr, Ba, Ga, La, Ce, Zr, Nb, Y, Co, Cr, Ni, V, Pb, Cu, Zn), the data tables listing results for 217 samples from CY-2 and 503 samples from CY-2a. Some data on the analytical methods, accuracy and precision are also given.

Résumé

Des données sur les éléments majeurs (SiO_2, Al_2O_3, Fe_2O_3, FeO, MgO, CaO, Na_2O, K_2O, TiO_2, P_2O_5, MnO, H_2O+, CO_2) sont présentées pour 217 échantillons du forage CY-2 et pour 504 échantillons du forage CY-2a. Les données sont arrangées selon la profondeur échantillonée, et en plus de la donnée analytique, le laboratoire responsable est aussi indiqué. De l'information comparable, habituellement pour des parties des mêmes échantillons, est fournie pour les éléments traces (Sr, Ba, Ga, La, Ce, Zr, Nb, Y, Co, Cr, Ni, V, Pb, Cu, Zn), les tables de données énumérant les résultats de 217 échantillons de CY-2 et 503 échantillons de CY-2a. Quelques données sur les méthodes analytiques, l'exactitude et la précision sont aussi fournies.

Major Element Data

Depth	SiO_2	Al_2O_3	Fe_2O_3	FeO	MgO	CaO	Na_2O	K_2O	TiO_2	P_2O_5	MnO	H_2O+	CO_2	Lab
						CY-2								
1.00	44.12	22.11	10.80	–	1.07	0.07	1.17	2.40	0.43	0.06	0.01	18.46	–	AAC
2.90	51.60	26.00	3.11	0.18	1.43	0.20	0.10	2.46	0.57	0.03	0.02	12.29	–	NEW
6.80	47.54	26.16	2.87	–	1.69	0.12	0.41	2.63	0.50	0.04	0.02	18.60	–	AAC
9.20	48.30	24.80	–	2.98	1.81	0.27	0.09	2.66	0.49	0.01	0.03	17.86	–	MUN
10.01	46.80	20.33	9.18	–	3.25	0.53	0.42	1.19	0.54	0.04	0.03	17.77	–	AAC
12.90	47.65	16.61	7.85	–	6.49	4.65	1.21	0.67	0.58	0.04	0.05	12.56	–	AAC
13.90	47.13	16.02	8.69	–	7.83	5.02	1.23	0.51	0.57	0.04	0.05	11.05	–	AAC
16.75	49.80	19.10	6.67	1.82	6.61	5.92	2.74	0.18	0.66	0.06	0.04	3.12	0.20	BOC
16.75	48.20	18.30	–	8.27	6.79	5.43	2.60	0.18	0.67	–	0.04	8.88	–	MUN
20.00	46.07	14.88	9.26	–	12.05	4.65	1.25	0.37	0.52	0.05	0.10	12.63	–	AAC
22.50	48.81	15.00	9.80	–	12.26	0.99	0.60	2.11	0.54	0.05	0.25	9.30	–	AAC
22.65	49.60	14.50	–	8.35	12.64	1.35	0.73	1.62	0.54	0.02	0.26	9.65	–	MUN
24.05	54.10	14.30	–	8.49	9.36	0.92	0.38	3.20	0.44	0.02	0.66	8.85	–	MUN
24.05	54.60	15.00	4.31	4.14	8.70	0.92	0.32	3.33	0.53	0.06	0.74	6.71	0.08	BOC
24.05	55.50	15.40	3.66	4.69	8.51	0.99	0.44	3.23	0.59	0.06	0.73	7.13	–	NEW
25.55	50.26	12.72	18.28	–	8.24	0.20	0.46	0.54	0.50	0.05	0.31	8.52	–	AAC
29.00	51.11	15.53	15.21	–	11.11	0.15	0.46	0.37	0.53	0.05	0.16	7.09	–	AAC
35.35	48.60	14.90	6.35	8.02	9.09	0.51	0.64	1.41	0.52	0.05	0.19	7.12	0.03	BOC
35.35	49.50	14.40	–	14.88	9.82	0.46	0.56	1.37	0.31	–	0.18	8.15	–	MUN
38.05	53.80	13.20	–	16.56	6.57	0.23	0.43	0.41	0.51	–	0.17	8.01	–	MUN
38.40	51.44	12.73	19.74	–	7.72	0.10	0.46	0.21	0.46	0.05	0.20	7.79	–	AAC
46.10	50.62	14.27	19.02	–	9.13	0.12	0.47	0.12	0.53	0.05	0.24	6.69	–	AAC
46.30	52.14	13.48	19.61	–	8.28	0.12	0.47	0.09	0.51	0.05	0.21	6.24	–	AAC
47.95	50.96	13.73	16.60	–	8.96	0.16	0.46	0.72	0.50	0.05	0.58	7.53	–	AAC
48.30	47.85	13.05	20.86	–	5.58	0.19	0.44	1.17	0.48	0.04	0.20	11.06	–	AAC
50.10	51.70	13.40	–	11.56	10.34	0.86	0.32	2.60	0.48	0.04	0.40	6.85	–	MUN
50.10	52.50	13.70	4.38	7.02	9.38	0.91	0.24	2.53	0.50	0.05	0.45	6.56	0.17	BOC
50.10	53.30	14.20	–	10.98	9.23	0.94	0.32	2.51	0.55	0.04	0.44	7.11	–	NEW
51.05	56.60	12.50	5.03	8.07	8.31	0.28	0.22	0.30	0.45	0.04	0.30	5.93	1.27	BOC
51.05	56.50	11.90	–	13.66	9.01	0.24	0.27	0.30	0.19	0.02	0.28	6.32	–	MUN
53.45	42.31	16.34	20.03	–	10.23	0.23	0.45	0.41	0.58	0.05	0.17	9.66	–	AAC
54.30	55.51	13.94	13.47	–	7.23	1.45	1.38	0.26	1.32	0.08	0.22	6.38	–	AAC
55.65	52.33	15.15	14.26	–	7.40	1.87	1.35	0.56	1.38	0.08	0.20	6.36	–	AAC
58.25	51.90	14.60	5.51	7.25	6.91	1.23	0.70	1.94	1.10	0.10	0.30	5.27	1.72	BOC
58.25	51.60	14.20	–	13.48	7.47	1.19	0.84	1.83	0.40	–	0.27	6.38	–	MUN
64.70	56.07	14.62	13.09	–	7.36	1.43	0.75	2.41	1.19	0.08	0.40	4.47	–	AAC
66.50	52.60	14.10	7.39	7.14	5.96	1.16	0.88	1.63	1.11	0.09	0.28	5.39	0.05	BOC
66.50	54.30	14.50	–	13.95	5.92	1.25	0.97	1.65	1.18	0.08	0.28	5.35	–	NEW
66.50	53.30	13.90	–	12.92	6.51	1.06	0.93	1.67	0.88	0.05	0.27	5.42	–	MUN
70.65	54.60	14.50	5.13	6.10	5.00	5.64	2.03	1.12	1.29	0.11	0.23	3.11	1.13	BOC
70.65	53.40	13.90	–	11.78	5.23	5.17	2.06	1.15	1.17	0.10	0.23	4.50	–	MUN
73.80	55.50	14.52	11.65	–	5.32	5.29	2.29	1.15	1.33	0.11	0.31	3.69	–	AAC
75.00	54.50	14.32	11.21	–	5.16	5.24	2.39	1.24	1.30	0.09	0.30	4.14	–	AAC
75.62	54.40	14.00	–	11.14	5.16	5.11	2.35	1.13	1.20	0.09	0.26	5.10	–	MUN
75.65	54.45	14.19	11.38	–	5.59	4.00	2.34	1.41	1.27	0.09	0.34	4.52	–	AAC
76.45	56.00	14.90	4.30	6.39	5.46	4.32	2.23	1.39	1.35	0.10	0.38	3.80	–	NEW
76.45	54.90	14.40	–	11.40	5.94	4.04	2.11	1.36	1.36	0.10	0.36	4.41	–	MUN
78.60	54.40	14.80	5.64	5.77	6.22	3.75	1.77	1.43	1.31	0.11	0.57	3.92	0.19	BOC
78.60	54.30	14.00	–	11.46	6.61	3.51	1.76	1.40	1.19	0.07	0.53	4.65	–	MUN
79.87	54.40	14.20	–	11.33	5.06	4.43	2.41	1.18	1.20	0.10	0.32	4.30	–	MUN
80.10	55.07	14.29	11.40	–	5.22	3.90	2.25	1.29	1.27	0.09	0.39	4.89	–	AAC
80.25	54.01	14.05	11.94	–	5.70	3.59	2.10	1.31	1.25	0.09	0.39	5.13	–	AAC

Depth	SiO_2	Al_2O_3	Fe_2O_3	FeO	MgO	CaO	Na_2O	K_2O	TiO_2	P_2O_5	MnO	H_2O+	CO_2	Lab
83.40	53.80	14.00	.	10.97	5.15	5.07	2.37	1.06	1.19	0.06	0.29	5.28	.	MUN
83.40	54.70	14.90	6.10	4.60	4.77	5.45	2.49	1.03	1.40	0.10	0.31	3.48	.	NEW
83.55	53.33	14.36	11.68	.	4.75	5.12	2.41	1.07	1.27	0.09	0.43	5.11	.	AAC
84.05	57.90	13.00	.	12.16	5.50	1.71	1.40	2.30	0.97	0.07	0.66	4.37	.	MUN
84.50	57.00	13.40	5.03	6.26	5.05	1.70	1.27	2.33	1.27	0.12	0.71	3.62	0.07	BOC
85.60	59.24	13.73	10.82	.	4.04	2.44	1.29	2.95	1.35	0.13	0.78	2.75	.	AAC
86.70	66.30	9.64	.	9.85	5.64	0.88	1.33	0.78	0.80	.	0.48	3.65	.	MUN
86.70	66.60	10.10	3.88	5.91	5.25	0.95	1.26	0.79	0.80	0.07	0.53	3.75	0.07	BOC
88.50	52.17	14.61	11.45	.	5.27	5.55	1.94	2.43	1.22	0.09	0.40	4.98	.	AAC
90.25	57.18	13.94	11.19	.	4.34	5.27	2.73	0.70	1.42	0.10	0.35	4.40	.	AAC
90.80	52.40	14.50	.	14.90	5.24	3.97	2.13	0.71	1.31	0.23	0.88	3.66	.	MUN
90.80	53.30	15.00	8.60	5.93	4.73	4.18	2.16	0.67	1.48	0.16	0.92	3.35	.	NEW
92.75	51.30	14.20	8.81	5.91	5.26	2.14	1.99	0.45	0.95	0.10	1.57	4.62	0.04	BOC
92.75	52.10	14.00	.	15.12	5.70	2.01	2.24	0.49	0.86	0.15	1.52	4.71	.	MUN
93.90	56.00	14.20	.	10.84	5.37	5.00	2.12	0.90	1.04	0.06	0.49	3.96	.	MUN
94.40	55.29	14.21	11.91	.	5.49	4.21	1.85	0.76	1.00	0.08	0.69	5.28	.	AAC
94.75	55.95	14.49	11.52	.	4.91	5.86	1.98	0.83	1.03	0.08	0.80	3.84	.	AAC
95.60	53.72	15.14	11.29	.	6.01	5.08	3.32	0.10	1.18	0.09	0.34	3.68	.	AAC
96.75	50.80	14.60	.	13.20	11.60	0.15	0.14	0.26	0.54	0.04	0.51	7.59	.	NEW
96.75	50.50	13.80	.	14.01	12.88	0.20	0.15	0.28	0.40	.	0.46	7.13	.	MUN
97.30	56.40	14.30	.	10.14	5.02	4.62	1.89	0.86	0.91	0.08	1.06	3.62	.	MUN
97.30	57.00	14.50	4.68	5.58	4.64	5.01	1.77	0.85	1.00	0.10	1.10	3.16	0.40	BOC
97.35	54.10	13.60	.	11.88	7.21	2.55	1.30	0.74	0.72	0.04	0.76	5.64	.	MUN
97.35	53.30	14.20	5.43	6.88	6.77	2.65	1.36	0.72	0.86	0.08	0.83	4.72	0.08	BOC
100.90	55.95	14.15	11.34	.	4.99	3.69	1.57	1.12	1.00	0.08	1.02	5.94	.	AAC
103.83	53.24	17.29	9.14	.	3.63	6.64	3.29	0.83	1.09	0.12	0.24	4.52	.	AAC
103.85	50.60	16.40	.	10.23	6.13	6.67	2.92	0.47	0.94	0.05	0.21	5.69	.	MUN
103.85	52.10	17.40	7.60	2.79	5.81	7.27	3.15	0.44	1.07	0.11	0.23	2.67	.	NEW
105.35	51.70	17.10	7.90	2.49	6.19	6.45	3.01	0.54	1.07	0.10	0.18	2.66	0.39	BOC
105.35	50.70	16.20	.	10.25	6.48	5.92	3.41	0.52	1.01	0.21	0.17	5.17	.	MUN
105.65	48.19	15.80	10.19	.	7.13	6.84	2.82	0.09	1.00	0.08	0.24	7.12	.	AAC
107.00	49.80	16.20	.	10.40	6.37	6.39	3.00	0.43	0.97	0.12	0.21	6.10	.	MUN
109.00	47.98	15.71	11.06	.	6.48	6.54	2.94	0.26	1.01	0.09	0.17	7.99	.	AAC
110.40	50.89	15.45	10.23	.	3.52	6.21	3.01	0.34	1.23	0.11	0.15	6.87	.	AAC
110.75	56.60	16.40	7.70	2.59	3.49	6.02	3.35	0.38	1.22	0.13	0.22	2.40	.	NEW
110.75	54.80	15.60	.	10.17	3.52	5.63	3.27	0.37	1.18	0.09	0.20	4.77	.	MUN
113.30	50.16	14.15	11.85	.	4.67	5.14	2.39	0.70	1.02	0.10	0.17	9.32	.	AAC
113.35	52.90	15.80	10.10	2.42	5.01	5.83	2.64	0.37	1.11	0.11	0.20	3.30	0.22	BOC
113.35	49.80	14.70	.	12.00	5.18	5.25	2.66	0.39	0.97	0.12	0.19	7.98	.	MUN
115.35	50.69	12.23	9.38	.	4.03	2.65	2.35	0.67	0.93	0.07	0.16	16.83	.	AAC
117.45	62.55	10.38	10.57	.	2.52	3.41	2.05	2.40	0.76	0.09	0.12	5.33	.	AAC
117.45	53.20	14.90	.	10.21	3.75	4.52	3.25	1.24	1.05	0.10	0.14	7.21	.	MUN
118.70	55.00	16.80	7.50	2.88	4.52	6.47	3.53	0.34	1.24	0.13	0.24	2.28	.	NEW
118.70	53.10	16.00	.	10.46	4.73	6.04	3.26	0.26	1.30	0.10	0.22	4.83	.	MUN
119.35	53.50	16.32	8.43	2.73	4.97	6.71	2.98	0.34	1.11	0.11	0.25	2.03	0.11	BOC
119.65	64.91	13.92	7.12	.	1.54	5.35	3.08	1.22	1.09	0.11	0.17	1.54	.	AAC
119.75	51.80	15.50	.	11.04	5.16	6.16	2.94	0.34	1.03	0.08	0.23	5.34	.	MUN
119.95	60.24	15.38	7.76	.	2.93	6.14	2.87	0.65	1.08	0.13	0.14	2.53	.	AAC
119.95	57.60	15.40	.	7.97	3.14	6.09	3.12	0.55	1.05	0.08	0.14	2.98	.	MUN
120.00	59.21	15.71	7.55	.	3.05	6.52	3.28	0.56	1.10	0.11	0.19	2.22	.	AAC
121.65	48.55	15.54	11.41	.	5.29	5.58	2.88	0.32	1.21	0.11	0.22	8.81	.	AAC
122.10	55.30	14.90	9.00	3.00	5.03	5.25	2.87	0.70	1.15	0.14	0.21	2.93	.	NEW
122.10	52.20	13.30	.	11.45	5.16	4.60	2.63	0.65	0.99	0.05	0.17	8.69	.	MUN
122.40	59.00	15.41	6.41	2.52	3.41	5.92	3.10	0.40	1.15	0.12	0.20	1.92	0.17	BOC
122.40	57.00	15.10	.	8.83	3.40	5.15	3.53	0.33	1.14	0.08	0.18	3.95	.	MUN

Depth	SiO_2	Al_2O_3	Fe_2O_3	FeO	MgO	CaO	Na_2O	K_2O	TiO_2	P_2O_5	MnO	H_2O+	CO_2	Lab
124.50	49.28	14.64	11.68	.	5.38	5.05	3.12	0.20	1.14	0.11	0.24	10.17	.	AAC
124.70	57.00	14.90	.	8.71	3.36	5.14	3.48	0.34	1.12	0.09	0.18	3.99	.	MUN
125.55	65.80	13.70	.	6.86	1.57	5.25	3.07	0.65	0.95	.	0.18	2.00	.	MUN
125.55	65.30	14.40	4.24	2.56	1.51	5.66	3.19	0.65	1.02	0.13	0.20	1.70	.	NEW
126.80	53.02	16.12	9.28	.	3.36	5.39	3.62	0.31	1.26	0.17	0.21	7.31	.	AAC
127.55	59.40	10.20	.	13.30	2.76	3.25	2.21	1.42	0.78	0.10	0.13	5.72	.	MUN
127.55	61.50	10.66	11.77	1.84	2.63	3.43	2.10	1.46	0.86	0.09	0.15	3.06	0.18	BOC
129.15	66.96	10.47	10.74	.	1.35	4.12	2.41	1.01	0.83	0.09	0.12	2.99	.	AAC
130.05	49.60	16.10	.	10.47	6.43	6.55	3.10	0.42	0.97	0.15	0.24	5.70	.	MUN
130.90	54.60	15.50	8.80	3.06	4.63	5.30	2.97	0.44	1.25	0.10	0.17	3.30	.	NEW
131.95	50.57	13.44	12.79	.	4.63	4.96	2.42	0.53	1.12	0.07	0.18	8.69	.	AAC
132.65	48.68	15.21	12.48	.	5.13	6.43	2.93	0.09	1.25	0.11	0.25	7.84	.	AAC
132.75	52.70	14.90	.	10.37	4.21	5.81	2.93	0.27	1.18	0.10	0.18	6.33	.	MUN
133.75	54.80	15.88	8.41	2.38	4.07	6.37	2.87	0.25	1.30	0.13	0.21	2.82	0.21	BOC
135.00	53.70	13.50	.	10.32	3.55	4.53	2.91	0.70	1.04	0.15	0.20	8.35	.	MUN
135.15	50.00	16.70	.	9.74	6.34	9.97	2.17	0.12	0.65	0.04	0.19	4.38	.	MUN
135.15	51.10	17.40	5.90	3.97	5.74	10.60	2.42	0.08	0.76	0.06	0.20	1.82	.	NEW
135.45	64.02	9.93	4.56	.	0.70	3.15	2.55	0.97	0.79	0.09	0.11	13.01	.	AAC
137.35	49.22	14.42	11.24	.	4.61	5.24	2.74	0.28	1.14	0.12	0.23	10.61	.	AAC
137.40	60.19	9.58	11.44	.	2.52	2.95	1.81	1.49	0.65	0.09	0.11	9.17	.	AAC
137.84	47.45	14.17	12.09	.	5.45	5.85	2.53	0.14	1.12	0.10	0.28	10.30	.	AAC
138.15	53.30	16.80	8.94	2.10	4.65	5.99	3.19	0.18	1.31	0.18	0.27	3.25	0.28	BOC
138.15	50.80	15.70	.	10.42	4.83	5.43	3.10	0.22	1.16	0.12	0.24	7.70	.	MUN
140.32	49.84	15.29	11.52	.	5.21	6.20	2.68	0.18	1.19	0.07	0.22	8.22	.	AAC
140.93	49.94	16.32	11.08	.	5.30	6.74	2.70	0.09	1.21	0.11	0.32	7.33	.	AAC
142.20	50.40	15.20	.	11.14	6.22	5.72	2.90	0.16	1.10	0.06	0.20	6.91	.	MUN
143.25	51.20	14.30	.	12.46	5.60	5.41	2.49	0.63	0.98	0.07	0.17	6.28	.	MUN
143.25	53.40	15.30	9.40	3.27	5.06	5.82	2.69	0.59	1.10	0.07	0.19	3.88	.	NEW
143.90	59.18	14.22	8.87	.	3.10	6.16	2.82	0.62	1.06	0.10	0.15	3.69	.	AAC
144.70	59.80	14.17	10.10	.	2.94	5.99	2.66	1.18	1.03	0.07	0.15	3.12	.	AAC
145.90	58.10	14.00	.	9.50	3.79	6.18	2.69	0.57	1.05	0.08	0.19	2.36	.	MUN
145.90	59.80	14.58	6.25	3.12	3.62	6.61	2.56	0.52	1.08	0.10	0.21	1.28	0.09	BOC
146.65	49.60	13.80	.	13.14	4.95	5.46	2.41	0.91	1.06	0.13	0.16	7.22	.	MUN
146.65	52.10	15.07	10.98	2.48	4.82	6.01	2.32	0.93	1.21	0.10	0.16	3.11	0.19	BOC
147.40	60.22	13.82	10.30	.	2.12	5.52	2.40	1.68	1.12	0.09	0.13	2.50	.	AAC
150.05	56.29	14.62	10.53	.	3.71	6.54	2.60	0.19	1.20	0.08	0.27	3.90	.	AAC
150.35	57.50	15.03	7.03	3.45	4.09	6.80	2.75	0.17	1.20	0.09	0.26	1.49	0.12	BOC
150.35	57.80	15.30	5.50	4.80	4.16	6.64	2.96	0.18	1.27	0.10	0.26	1.40	.	NEW
150.35	55.70	14.60	.	10.47	4.28	6.29	2.81	0.19	1.14	0.10	0.25	2.98	.	MUN
151.90	49.16	14.89	12.52	.	5.23	5.88	2.76	0.55	1.17	0.08	0.21	6.95	.	AAC
152.92	49.51	12.08	12.17	.	5.02	3.94	2.24	0.36	1.08	0.04	0.23	13.24	.	AAC
154.00	56.60	13.15	10.35	2.28	5.25	3.17	2.04	0.97	1.07	0.07	0.20	5.24	0.40	BOC
154.00	51.50	11.50	.	11.52	5.09	2.70	1.93	0.83	0.91	0.04	0.18	13.41	.	MUN
155.85	50.39	14.65	11.75	.	4.82	5.96	2.66	0.48	1.15	0.08	0.19	7.37	.	AAC
156.30	57.19	14.16	10.46	.	3.23	6.64	2.46	0.55	1.08	0.08	0.23	4.12	.	AAC
158.65	55.40	14.36	9.24	.	2.77	5.49	3.15	0.37	1.22	0.14	0.23	7.09	.	AAC
158.80	57.30	13.70	.	8.40	2.54	4.66	3.06	0.48	1.08	0.11	0.16	7.33	.	MUN
160.10	64.00	13.74	7.18	.	1.57	5.07	3.53	0.52	1.15	0.14	0.18	3.66	.	AAC
163.25	53.60	15.00	.	10.06	3.69	6.06	2.97	0.28	1.26	0.10	0.24	5.14	.	MUN
163.25	56.20	16.30	7.50	2.98	3.62	6.54	3.32	0.24	1.42	0.13	0.25	2.87	.	NEW
163.75	63.88	13.76	8.00	.	1.95	6.11	3.38	0.46	1.16	0.11	0.17	2.92	.	AAC
164.65	52.70	15.00	.	10.78	4.60	6.03	2.92	0.09	1.25	0.11	0.28	5.75	.	MUN
164.65	54.70	16.14	8.40	2.81	4.42	6.67	3.05	0.07	1.34	0.13	0.32	2.13	0.13	BOC
165.05	67.90	12.90	6.23	.	1.06	5.09	3.27	0.81	1.13	0.12	0.17	1.92	.	AAC
167.80	58.19	14.70	9.92	.	3.63	7.07	2.98	0.12	1.25	0.10	0.29	3.32	.	AAC

Depth	SiO_2	Al_2O_3	Fe_2O_3	FeO	MgO	CaO	Na_2O	K_2O	TiO_2	P_2O_5	MnO	H_2O+	CO_2	Lab
169.05	57.80	14.60	.	9.56	3.64	6.33	2.88	0.22	1.25	0.08	0.22	2.69	.	MUN
169.45	56.00	14.70	.	10.58	4.32	6.10	2.91	0.20	1.13	0.06	0.24	3.12	.	MUN
169.45	56.70	15.80	6.90	3.60	4.16	6.56	3.26	0.18	1.36	0.10	0.25	1.84	.	NEW
170.10	61.88	12.80	10.48	.	2.74	5.43	2.45	1.53	1.13	0.09	0.17	2.13	.	AAC
171.05	65.48	12.61	8.01	.	1.92	5.42	2.76	0.73	1.11	0.09	0.18	2.59	.	AAC
174.55	63.50	12.90	.	8.87	2.72	5.54	2.91	0.82	1.11	0.08	0.16	2.06	.	MUN
174.55	63.30	13.54	5.70	3.12	2.62	5.94	2.85	0.80	1.18	0.11	0.18	1.18	0.06	BOC
175.00	60.64	12.01	10.19	.	2.72	5.71	2.82	1.33	1.05	0.08	0.16	3.23	.	AAC
176.80	59.56	14.79	7.05	.	1.63	5.57	3.41	0.15	1.32	0.13	0.24	7.29	.	AAC
178.60	62.88	14.59	8.41	.	2.01	5.26	3.78	0.42	1.23	0.14	0.25	2.76	.	AAC
179.55	56.90	15.10	.	8.21	2.79	5.36	3.42	0.14	1.20	0.13	0.25	4.76	.	MUN
180.05	56.62	14.58	9.64	.	2.59	6.15	3.08	0.41	1.23	0.11	0.28	5.45	.	AAC
180.55	57.70	15.50	.	8.23	2.34	5.71	3.80	0.10	1.22	0.15	0.30	3.26	.	MUN
180.55	59.50	16.70	5.29	2.92	2.38	6.08	4.10	0.10	1.36	0.15	0.34	2.14	.	NEW
181.95	53.91	15.54	9.22	.	3.35	4.99	3.66	0.30	1.38	0.13	0.15	8.83	.	AAC
183.75	62.30	14.24	5.88	2.39	2.28	5.23	3.31	0.87	1.26	0.14	0.21	1.31	0.30	BOC
183.75	58.90	13.90	.	8.27	2.39	4.84	3.42	0.89	1.16	0.17	0.20	2.23	.	MUN
184.40	54.85	14.61	10.70	.	3.71	5.22	3.34	0.52	1.32	0.12	0.20	5.30	.	AAC
186.00	59.68	14.56	9.47	.	2.61	5.52	3.32	0.32	1.30	0.12	0.20	4.74	.	AAC
188.20	63.30	13.90	.	8.57	1.93	5.22	3.51	0.73	1.24	0.10	0.25	1.23	.	MUN
189.40	56.40	16.80	7.62	1.97	3.41	5.00	3.94	0.28	1.33	0.20	0.17	3.90	.	NEW
189.40	52.90	15.70	.	9.14	3.51	4.70	3.54	0.26	1.29	0.18	0.16	7.51	.	MUN
191.15	56.41	14.09	7.99	.	2.89	4.62	3.05	0.36	1.13	0.18	0.15	7.54	.	AAC
193.30	50.40	14.20	.	11.50	5.25	5.03	2.77	0.30	1.26	0.09	0.19	8.39	.	MUN
193.30	53.90	15.41	8.71	3.13	5.12	5.65	2.83	0.31	1.39	0.10	0.20	3.25	0.23	BOC
195.40	63.81	13.08	8.76	.	2.35	5.28	2.81	1.23	1.15	0.12	0.18	2.19	.	AAC
196.15	61.54	12.75	8.53	.	2.55	5.23	2.95	1.24	1.12	0.11	0.18	2.15	.	AAC
196.50	61.50	13.50	.	8.33	2.35	5.32	2.96	1.12	1.15	0.12	0.19	1.73	.	MUN
198.75	51.31	15.14	12.15	.	4.10	6.60	2.79	0.61	1.35	0.10	0.24	6.50	.	AAC
200.65	50.94	14.62	13.24	.	4.53	6.24	2.60	1.24	1.32	0.09	0.25	5.76	.	AAC
201.05	51.80	14.30	.	12.49	5.40	6.08	2.98	0.83	1.25	0.07	0.25	4.41	.	MUN
201.05	53.60	15.40	8.10	4.17	5.12	6.46	3.18	0.80	1.52	0.11	0.27	1.95	.	NEW
201.85	49.59	14.80	12.68	.	5.81	5.86	2.68	0.68	1.38	0.11	0.19	7.74	.	AAC
202.70	48.89	15.47	12.62	.	5.12	6.85	3.13	0.37	1.46	0.07	0.22	6.49	.	AAC
206.60	49.40	14.70	.	12.91	6.03	6.14	2.99	0.42	1.27	0.12	0.19	5.92	.	MUN
206.60	50.80	15.83	9.33	3.66	5.69	6.56	3.06	0.41	1.46	0.11	0.21	2.56	0.19	BOC
207.15	48.71	15.17	12.83	.	5.37	6.53	2.84	0.50	1.39	0.01	0.22	7.05	.	AAC
211.00	50.00	14.20	.	12.81	6.38	5.86	3.07	0.44	1.31	0.09	0.14	5.65	.	MUN
211.00	49.65	14.81	13.01	.	5.92	6.16	3.01	0.41	1.37	0.09	0.16	6.96	.	AAC
213.65	68.89	12.35	6.78	.	1.25	5.06	2.48	0.70	1.18	0.10	0.19	2.87	.	AAC
214.10	61.90	13.50	.	8.61	2.46	5.51	2.87	0.68	1.18	0.12	0.20	2.14	.	MUN
214.10	63.10	14.10	4.80	3.33	2.48	5.75	2.97	0.62	1.28	0.12	0.22	1.35	.	NEW
214.40	65.25	12.25	7.40	.	1.85	5.15	2.69	0.87	1.16	0.10	0.18	3.58	.	AAC
214.50	67.70	12.10	.	7.46	1.54	5.12	2.66	0.84	1.10	0.11	0.20	0.84	.	MUN
214.50	67.10	12.20	4.45	2.98	1.45	5.42	2.57	0.83	1.16	0.11	0.22	0.85	0.07	BOC
218.15	56.59	13.44	9.94	.	2.87	4.46	3.58	0.27	0.80	0.19	0.20	8.86	.	AAC
218.90	54.72	13.50	11.78	.	3.55	4.85	2.68	2.14	1.26	0.11	0.13	5.46	.	AAC
221.30	50.60	15.76	8.92	3.96	5.41	6.75	2.90	0.55	1.46	0.12	0.25	2.62	0.23	BOC
221.30	49.40	14.90	.	12.97	5.77	6.42	2.97	0.54	1.26	0.12	0.23	5.40	.	MUN
223.80	53.60	15.33	8.36	3.07	4.14	5.63	2.88	1.10	1.47	0.16	0.21	2.78	0.21	BOC
223.80	54.20	15.90	7.70	3.69	4.35	5.69	3.16	1.09	1.61	0.17	0.22	3.20	.	NEW
223.80	52.90	14.80	.	11.56	4.39	5.39	3.05	1.09	1.42	0.12	0.21	4.70	.	MUN
223.85	49.19	15.31	12.66	.	5.49	5.75	3.02	0.77	1.48	0.15	0.28	7.21	.	AAC
226.15	48.79	15.19	13.11	.	5.49	6.40	2.93	0.61	1.44	0.09	0.19	6.27	.	AAC

Depth	SiO_2	Al_2O_3	Fe_2O_3	FeO	MgO	CaO	Na_2O	K_2O	TiO_2	P_2O_5	MnO	H_2O+	CO_2	Lab
						CY-2a								
4.40	53.80	14.60	.	8.87	7.90	4.84	1.69	2.20	0.57	0.08	0.11	5.94	.	MUN
4.40	55.30	15.50	4.87	3.96	8.58	5.14	1.94	2.31	0.57	0.05	0.10	2.68	.	NEW
7.60	51.42	14.54	9.96	.	9.11	6.01	1.89	1.85	0.54	0.05	0.19	3.43	.	AAC
8.35	53.86	13.94	8.43	.	8.92	3.97	1.41	4.62	0.55	0.05	0.16	3.02	.	AAC
9.70	52.30	14.20	.	8.36	9.20	6.52	1.70	1.14	0.51	0.04	0.12	6.06	.	MUN
9.70	54.20	15.14	4.94	3.57	8.80	7.20	1.63	1.16	0.52	0.05	0.13	2.77	0.04	BOC
11.05	53.31	16.94	9.29	.	7.61	8.98	2.64	0.39	0.67	0.05	0.09	1.66	.	AAC
11.80	52.30	14.90	.	8.34	8.24	8.81	1.84	0.26	0.51	0.04	0.09	4.30	.	MUN
11.80	54.10	15.74	4.97	3.32	7.68	9.57	1.86	0.25	0.55	0.05	0.09	1.86	0.20	BOC
12.95	54.47	15.62	8.69	.	8.25	9.60	1.91	0.24	0.54	0.05	0.09	1.80	.	AAC
15.00	54.24	15.62	8.11	.	8.78	9.98	1.92	0.23	0.51	0.05	0.09	1.77	.	AAC
17.35	51.96	14.11	11.00	.	7.63	8.95	1.79	1.35	0.49	0.05	0.11	2.75	.	AAC
19.30	51.90	14.40	.	7.72	9.35	8.50	1.73	0.31	0.44	0.01	0.08	4.78	.	MUN
19.30	55.20	15.40	4.18	3.58	7.09	9.03	1.94	0.31	0.51	0.04	0.08	1.95	.	NEW
19.65	53.57	15.75	8.12	.	9.07	9.82	2.11	0.32	0.53	0.05	0.08	1.95	.	AAC
21.00	54.34	15.28	8.40	.	8.55	9.66	2.07	0.36	0.55	0.05	0.10	1.66	.	AAC
21.50	52.30	14.90	.	7.38	8.89	9.36	1.81	0.24	0.53	.	0.08	3.83	.	MUN
21.50	53.00	15.51	4.09	3.20	8.32	9.90	1.82	0.23	0.55	0.05	0.09	1.91	0.07	BOC
22.80	55.17	15.84	7.38	.	8.39	9.78	2.14	0.32	0.58	0.05	0.09	1.83	.	AAC
24.38	52.50	14.46	9.94	.	8.50	9.20	2.08	0.76	0.52	0.05	0.09	2.43	.	AAC
25.85	49.20	12.70	.	10.49	10.46	8.87	1.78	0.78	0.40	0.03	0.09	5.92	.	MUN
28.66	49.27	11.76	8.60	.	15.50	7.66	1.52	0.20	0.42	0.05	0.13	3.76	.	AAC
30.10	49.80	12.90	.	9.56	10.07	7.31	2.21	0.76	0.47	0.07	0.10	5.89	.	MUN
30.10	52.00	13.69	7.50	2.36	9.46	7.89	2.15	0.75	0.55	0.05	0.10	2.84	0.23	BOC
30.10	53.00	14.20	7.06	2.60	9.56	7.74	2.44	0.77	0.56	0.05	0.10	2.80	.	NEW
30.55	48.86	13.64	8.89	.	5.17	10.68	1.25	3.51	0.51	0.05	0.21	7.03	.	AAC
31.18	52.38	14.83	9.33	.	9.61	7.52	2.44	1.19	0.51	0.05	0.13	2.78	.	AAC
31.45	50.74	15.57	11.49	.	6.17	5.12	2.87	1.94	1.16	0.08	0.09	3.96	.	AAC
33.10	49.70	15.26	8.68	2.46	5.83	6.49	2.67	1.87	1.17	0.08	0.10	3.58	2.26	BOC
33.10	48.00	14.40	.	10.73	5.96	5.79	2.66	1.88	1.06	0.08	0.09	9.27	.	MUN
33.40	40.40	8.81	9.74	.	7.15	15.28	0.96	2.07	0.31	0.04	0.38	14.99	.	AAC
35.80	49.89	15.06	12.35	.	4.50	6.29	3.23	3.15	1.32	0.13	0.14	2.54	.	AAC
40.75	50.60	15.80	9.13	2.43	5.99	5.90	3.14	0.83	1.40	0.12	0.10	3.11	1.19	BOC
40.75	49.00	14.80	.	11.20	6.18	5.34	3.08	0.80	1.28	0.10	0.09	8.34	.	MUN
42.15	49.40	14.60	.	11.59	5.47	5.27	3.12	1.34	1.21	0.08	0.09	7.02	.	MUN
42.15	51.90	15.60	8.50	3.08	5.27	5.57	3.33	1.36	1.32	0.13	0.10	2.91	.	NEW
44.05	50.20	15.67	9.51	2.36	5.28	6.08	3.04	1.08	1.39	0.13	0.09	3.34	1.30	BOC
44.05	48.20	14.80	.	11.48	5.44	5.55	3.04	1.03	1.21	0.14	0.08	8.53	.	MUN
44.45	51.40	15.41	12.13	.	4.94	6.34	1.95	1.29	1.37	0.11	0.10	4.72	.	AAC
49.45	51.37	16.21	13.07	.	5.71	4.94	4.00	1.59	1.40	0.12	0.10	3.05	.	AAC
49.55	48.60	14.70	.	11.58	5.84	4.89	3.02	1.95	1.21	0.16	0.10	8.36	.	MUN
53.80	51.77	16.02	12.55	.	6.50	4.45	1.59	1.83	1.46	0.12	0.11	3.91	.	AAC
54.70	49.99	16.80	9.88	.	8.57	4.15	1.02	2.78	0.68	0.09	0.18	5.61	.	AAC
55.45	51.10	16.20	6.38	2.70	7.32	4.77	2.11	3.54	0.64	0.10	0.12	4.16	.	NEW
55.45	48.30	15.20	.	9.05	7.63	4.48	2.03	3.54	0.64	0.10	0.11	9.38	.	MUN
57.50	50.50	15.97	9.54	.	7.83	5.09	1.20	2.36	0.63	0.05	0.10	8.02	.	AAC
58.75	47.90	15.00	.	8.91	6.96	5.50	2.31	3.64	0.61	0.09	0.10	8.18	.	MUN
58.75	50.70	15.45	6.69	2.34	6.55	5.82	2.07	3.69	0.63	0.11	0.11	3.44	1.95	BOC
59.30	51.50	12.50	.	14.98	6.88	0.96	1.07	0.54	1.10	.	0.28	7.39	.	MUN
59.40	47.90	15.54	8.93	.	7.91	9.32	2.27	1.69	0.62	0.05	0.16	6.62	.	AAC
61.65	47.20	14.23	9.44	.	7.21	7.50	1.09	3.83	0.59	0.13	0.16	7.13	.	AAC
63.15	46.80	14.70	.	8.79	8.34	5.59	1.91	2.19	0.64	0.05	0.11	10.66	.	MUN
65.10	51.50	15.20	6.46	2.48	6.76	10.10	2.65	1.35	0.64	0.06	0.13	2.73	.	NEW

Depth	SiO_2	Al_2O_3	Fe_2O_3	FeO	MgO	CaO	Na_2O	K_2O	TiO_2	P_2O_5	MnO	H_2O+	CO_2	Lab
65.10	49.30	14.20	.	8.75	7.12	9.26	2.47	1.37	0.59	0.05	0.12	5.88	.	MUN
65.85	49.70	15.97	7.73	2.69	7.14	8.50	2.49	1.42	0.64	0.09	0.08	2.34	1.80	BOC
65.85	48.70	15.30	.	8.89	7.68	8.09	2.61	1.44	0.60	0.08	0.08	6.63	.	MUN
69.05	50.47	15.26	8.92	.	6.40	12.13	1.41	1.29	0.61	0.05	0.12	4.83	.	AAC
70.35	52.46	14.76	6.81	.	8.35	9.74	2.52	0.53	0.61	0.05	0.13	2.84	.	AAC
72.55	53.20	14.60	.	7.69	8.98	8.01	2.39	0.17	0.71	0.04	0.10	4.35	.	MUN
73.35	50.88	16.25	8.51	.	9.06	9.07	2.47	0.20	0.67	0.05	0.10	2.15	.	AAC
74.35	55.24	15.93	8.09	.	7.68	8.51	2.70	0.23	0.70	0.05	0.10	1.53	.	AAC
75.80	52.70	14.90	5.30	2.57	6.65	10.50	2.53	1.06	0.70	0.06	0.11	2.76	.	NEW
75.80	50.00	14.10	.	7.74	7.01	9.57	2.52	1.06	0.55	0.08	0.11	4.53	.	MUN
75.95	52.28	14.85	8.25	.	6.46	10.43	2.49	1.13	0.61	0.05	0.13	1.53	.	AAC
78.25	53.60	15.70	5.55	2.39	6.55	9.36	2.49	0.86	0.70	0.07	0.10	2.07	0.94	BOC
78.25	52.70	15.00	.	8.00	7.11	8.95	2.68	0.84	0.82	0.07	0.10	4.00	.	MUN
78.50	52.61	13.91	8.98	.	6.76	9.86	2.40	1.14	0.55	0.05	0.10	2.96	.	AAC
80.25	53.47	14.94	8.11	.	7.92	9.74	2.49	0.30	0.61	0.05	0.13	2.32	.	AAC
81.15	51.56	14.64	7.92	.	6.64	10.36	2.31	1.05	0.58	0.05	0.11	2.96	.	AAC
81.45	51.40	14.50	.	7.94	7.34	10.12	2.24	0.77	0.57	0.02	0.10	4.36	.	MUN
84.30	51.30	14.44	8.42	.	6.83	10.74	2.45	0.82	0.58	0.05	0.11	2.83	.	AAC
86.30	50.20	14.40	.	7.72	7.15	10.53	2.22	1.00	0.63	0.02	0.10	4.74	.	MUN
86.30	52.80	15.10	5.21	2.53	6.72	11.00	2.45	0.99	0.66	0.06	0.10	2.50	.	NEW
87.20	51.42	14.88	8.12	.	7.13	11.75	2.70	0.74	0.60	0.05	0.12	1.35	.	AAC
88.70	49.20	14.40	.	8.15	7.70	10.24	2.35	0.90	0.56	0.03	0.11	5.10	.	MUN
88.70	50.10	15.06	5.69	2.37	7.26	10.76	2.30	0.90	0.62	0.06	0.12	2.10	2.22	BOC
90.10	47.78	15.68	8.34	.	5.66	12.41	1.50	1.07	0.66	0.07	0.18	6.51	.	AAC
97.00	46.10	15.00	.	9.69	7.56	4.55	1.88	3.04	1.14	0.10	0.20	11.17	.	MUN
99.05	52.14	17.19	10.62	.	8.43	2.61	1.24	2.65	1.06	0.10	0.16	4.84	.	AAC
99.50	49.60	16.21	7.51	2.48	7.98	3.73	1.94	2.86	1.04	0.11	0.20	5.03	1.15	BOC
99.50	49.80	16.20	7.50	2.57	7.86	3.77	2.13	2.76	1.05	0.10	0.20	6.60	.	NEW
99.50	47.50	15.00	.	9.60	8.30	3.36	2.03	2.76	0.98	0.09	0.18	11.00	.	MUN
103.70	48.80	16.70	.	9.14	7.69	3.80	2.50	1.25	1.11	0.10	0.17	9.41	.	MUN
111.40	53.10	16.23	7.88	2.21	5.67	5.19	3.09	1.32	1.19	0.19	0.13	3.50	0.36	BOC
111.40	51.20	15.00	.	9.64	5.82	4.77	3.09	1.24	1.13	0.16	0.12	8.18	.	MUN
111.95	53.21	17.14	10.99	.	7.00	6.04	1.83	0.38	1.21	0.12	0.19	2.98	.	AAC
117.85	50.60	15.50	.	10.78	5.37	5.59	2.67	0.66	1.23	0.12	0.25	7.25	.	MUN
117.85	52.60	16.84	8.61	1.84	5.11	5.68	2.88	0.30	1.26	0.14	0.19	3.97	0.24	BOC
121.00	57.31	13.79	10.03	.	5.33	2.04	0.82	1.00	1.10	0.05	0.21	7.64	.	AAC
130.60	52.40	16.29	9.02	2.14	4.99	6.24	2.67	0.64	1.30	0.15	0.30	2.88	0.43	BOC
130.60	52.20	16.80	8.20	2.84	5.04	6.05	2.92	0.65	1.37	0.14	0.27	3.43	.	NEW
138.75	59.84	13.49	10.14	.	2.88	5.02	2.89	1.45	1.07	0.11	0.27	1.62	.	AAC
138.95	64.20	13.20	.	8.23	1.96	4.76	2.93	1.41	0.94	0.09	0.19	1.70	.	MUN
138.95	64.20	13.47	5.87	2.45	1.82	5.10	2.86	1.40	1.10	0.14	0.20	1.58	0.10	BOC
141.85	54.70	16.11	8.19	1.84	4.38	5.56	2.97	0.37	1.34	0.17	0.22	3.32	0.22	BOC
141.85	52.60	15.00	.	9.82	4.57	5.15	2.99	0.35	1.19	0.15	0.20	7.40	.	MUN
143.10	49.00	15.00	.	12.08	5.20	5.33	2.54	0.34	1.12	0.09	0.28	8.16	.	MUN
143.10	51.50	16.30	10.59	1.90	5.05	5.98	2.70	0.32	1.28	0.13	0.32	4.53	0.15	BOC
143.10	52.40	16.20	9.80	2.65	5.02	5.73	2.85	0.31	1.29	0.16	0.30	4.49	.	NEW
143.15	81.61	3.05	6.29	.	2.28	0.49	0.48	2.27	0.06	0.05	0.05	3.57	.	AAC
143.20	55.31	15.77	9.73	.	3.58	6.19	3.08	0.32	1.25	0.10	0.23	2.74	.	AAC
145.40	62.51	16.53	7.02	.	1.66	6.39	3.39	0.91	1.27	0.14	0.18	1.04	.	AAC
149.50	50.20	15.33	9.87	3.16	6.01	6.16	2.05	0.19	1.24	0.05	0.22	4.21	0.24	BOC
149.50	48.40	14.00	.	12.40	6.32	5.72	1.99	0.17	1.12	0.07	0.20	9.71	.	MUN
152.25	53.90	15.70	.	10.48	4.06	6.74	2.74	0.13	1.20	0.09	0.24	4.07	.	MUN
152.25	54.80	16.44	7.48	2.91	3.70	7.12	2.74	0.11	1.31	0.11	0.27	1.99	0.04	BOC
153.60	57.29	14.80	11.69	.	4.69	5.64	2.94	0.15	1.22	0.07	0.17	2.84	.	AAC
154.40	53.30	15.26	11.95	.	5.12	4.44	2.98	0.32	1.18	0.06	0.28	3.38	.	AAC

Depth	SiO_2	Al_2O_3	Fe_2O_3	FeO	MgO	CaO	Na_2O	K_2O	TiO_2	P_2O_5	MnO	H_2O+	CO_2	Lab
156.65	50.46	16.59	10.80	.	9.67	5.09	2.65	0.14	1.20	0.05	0.13	3.54	.	AAC
157.40	50.30	14.60	.	11.84	8.92	3.99	1.62	0.45	1.10	0.03	0.24	7.37	.	MUN
157.40	51.20	15.50	.	10.90	8.15	4.09	1.68	0.42	1.25	0.12	0.26	5.12	.	NEW
157.40	50.10	15.32	.	11.09	8.27	4.21	1.54	0.42	1.16	0.10	0.27	4.35	.	BOC
157.84	54.47	16.32	10.03	.	6.38	4.92	2.17	0.40	1.17	0.07	0.23	3.65	.	AAC
157.90	54.50	14.50	.	9.92	5.89	4.83	1.83	0.17	0.98	0.09	0.10	5.86	.	MUN
158.90	57.10	15.54	6.55	3.63	5.62	5.16	1.80	0.18	1.10	0.09	0.17	3.36	0.19	BOC
159.66	61.74	3.03	12.12	.	0.61	0.30	2.80	0.55	0.24	0.05	0.03	9.27	.	AAC
160.45	55.10	13.92	3.41	6.62	7.97	0.68	0.48	2.93	1.11	0.09	0.48	6.18	0.07	BOC
160.45	56.20	14.00	.	9.90	7.82	0.72	0.54	2.83	1.06	0.09	0.46	6.54	.	NEW
160.45	54.20	13.30	.	9.39	8.64	0.68	0.51	2.94	1.14	0.07	0.45	7.34	.	MUN
161.00	54.65	14.41	12.84	.	5.95	1.74	1.80	1.29	1.25	0.10	0.37	5.66	.	AAC
162.20	53.10	13.80	.	9.15	8.47	1.71	1.42	1.85	1.13	.	0.47	7.32	.	MUN
162.20	50.50	13.60	.	15.66	5.87	0.19	0.25	1.27	1.30	0.10	0.23	4.95	.	BOC
163.05	50.99	15.82	11.42	.	8.64	2.00	2.39	1.31	1.38	0.11	0.46	5.54	.	AAC
165.40	41.30	15.30	.	15.40	13.10	0.35	0.18	0.71	1.36	0.11	0.29	8.28	.	NEW
165.40	39.10	14.50	.	17.13	14.89	0.41	0.18	0.67	1.27	.	0.27	11.46	.	MUN
165.40	38.80	15.15	.	14.69	13.44	0.37	0.09	0.70	1.31	0.13	0.29	7.80	.	BOC
166.42	66.17	3.43	17.48	.	1.89	0.22	0.46	0.22	0.29	0.13	0.08	8.83	.	AAC
167.75	49.84	13.22	19.40	.	6.64	0.26	0.45	1.20	1.20	0.07	0.18	9.41	.	AAC
168.50	56.90	14.08	4.93	6.47	7.88	0.25	0.12	1.05	1.25	0.11	0.27	6.10	0.04	BOC
168.50	55.80	13.60	.	11.80	8.83	0.28	0.22	1.05	1.11	.	0.26	6.54	.	MUN
168.72	51.28	15.31	14.00	.	9.29	0.26	0.46	1.25	1.33	0.08	0.20	7.51	.	AAC
170.30	49.50	10.20	.	21.69	1.04	0.22	0.24	1.83	0.87	.	0.02	13.40	.	MUN
171.05	69.26	2.54	15.46	.	0.38	0.27	0.65	0.40	0.24	0.05	0.02	9.45	.	AAC
174.20	58.00	13.66	3.67	7.37	7.48	0.24	0.10	1.11	1.26	0.12	0.44	5.78	0.05	BOC
174.20	59.00	13.70	.	10.50	7.32	0.26	0.12	1.12	1.38	0.10	0.42	6.09	.	NEW
174.20	57.20	12.90	.	11.64	8.15	0.31	0.14	1.09	1.04	.	0.41	5.69	.	MUN
174.60	57.53	13.44	12.27	.	7.17	0.27	0.47	0.85	1.27	0.09	0.29	5.57	.	AAC
174.75	59.66	13.82	12.52	.	6.87	0.27	0.47	1.11	1.27	0.10	0.32	5.24	.	AAC
175.50	47.05	14.50	15.44	.	10.22	0.17	0.45	0.67	1.38	0.06	0.17	9.70	.	AAC
176.00	52.30	11.16	16.72	0.86	1.41	0.23	0.28	1.96	0.98	0.10	0.03	2.50	11.07	BOC
176.00	53.60	11.10	.	18.73	1.62	0.27	0.36	2.02	0.89	.	0.03	11.24	.	MUN
177.30	59.85	12.97	12.27	.	5.40	0.25	1.24	1.55	1.05	0.13	0.10	7.05	.	AAC
178.20	34.60	13.20	.	28.08	3.87	0.29	0.28	2.36	0.98	.	0.05	16.73	.	MUN
178.30	34.50	13.68	21.91	2.80	3.41	0.27	0.28	2.30	1.05	0.15	0.04	4.11	14.90	BOC
180.06	34.73	15.38	26.97	.	3.70	0.41	0.53	2.73	1.20	0.19	0.05	15.69	.	AAC
180.55	62.19	13.86	10.35	.	6.17	0.29	0.47	1.56	1.10	0.14	0.20	5.51	.	AAC
181.15	59.40	12.80	.	10.36	6.69	0.34	0.23	1.34	0.65	.	0.14	5.90	.	MUN
181.15	60.80	13.41	4.38	5.54	6.29	0.30	0.17	1.36	1.06	0.15	0.15	4.68	1.13	BOC
181.15	62.20	13.50	.	9.54	6.26	0.28	0.23	1.34	1.07	0.17	0.15	5.24	.	NEW
182.25	60.74	12.75	11.15	.	6.22	0.25	0.05	1.32	1.17	0.07	0.10	7.50	.	AAC
183.40	6.75	3.51	.	57.20	0.06	0.36	0.10	0.72	0.31	.	0.03	29.96	.	MUN
183.40	8.00	3.19	.	37.34	0.07	0.31	0.06	0.70	0.29	0.01	0.03	0.94	.	BOC
185.50	4.27	0.83	58.82	.	0.10	1.62	0.33	0.15	0.07	0.03	0.19	33.30	.	AAC
185.70	3.74	0.74	60.22	.	0.10	0.91	0.32	0.16	0.03	0.03	0.10	35.39	.	AAC
186.25	11.19	5.00	52.07	.	1.66	0.20	0.35	0.75	0.46	0.04	0.04	29.69	.	AAC
186.30	40.48	13.94	21.53	.	3.37	0.28	0.41	2.30	1.25	0.12	0.04	17.62	.	AAC
186.90	58.90	13.73	4.77	6.26	6.73	0.27	0.15	1.24	1.21	0.13	0.17	5.07	0.04	BOC
186.90	57.00	13.20	.	11.66	7.40	0.34	0.25	1.21	1.03	.	0.16	6.20	.	MUN
189.85	44.40	11.90	.	22.10	2.82	0.40	0.25	1.92	1.07	0.07	0.07	4.16	.	NEW
189.85	41.77	14.67	29.94	.	3.52	0.90	0.47	2.49	1.20	0.06	0.11	6.76	.	AAC
189.85	42.30	11.22	.	18.05	2.68	0.41	0.18	1.85	0.91	0.07	0.06	3.46	.	BOC
189.90	43.70	10.80	.	23.96	2.96	0.51	0.28	1.91	0.89	.	0.07	14.87	.	MUN
191.90	27.73	0.53	44.17	.	0.11	1.34	0.37	0.07	0.04	0.04	0.01	26.61	.	AAC

Depth	SiO_2	Al_2O_3	Fe_2O_3	FeO	MgO	CaO	Na_2O	K_2O	TiO_2	P_2O_5	MnO	H_2O+	CO_2	Lab
192.30	53.62	14.42	12.95	.	7.55	0.23	0.46	1.49	1.34	0.08	0.13	8.31	.	AAC
192.95	28.96	2.50	43.10	.	0.11	0.06	0.37	0.57	0.23	0.04	0.01	25.06	.	AAC
192.95	17.60	0.82	.	51.80	0.00	0.30	0.05	0.21	0.00	0.01	0.03	27.65	.	MUN
192.95	18.30	1.05	.	35.46	0.06	0.33	0.10	0.19	0.08	0.01	0.02	0.57	.	BOC
194.25	28.31	12.56	34.66	.	2.92	0.45	0.41	2.19	1.20	0.07	0.06	18.81	.	AAC
197.00	54.90	13.94	5.77	6.92	7.32	0.22	0.38	1.06	1.32	0.11	0.25	5.37	1.21	BOC
197.00	53.90	13.30	.	13.25	8.15	0.29	0.22	1.01	1.14	.	0.24	6.76	.	MUN
199.20	56.30	12.50	.	14.90	4.21	0.18	0.21	1.65	1.24	0.09	0.10	4.35	.	NEW
199.20	56.80	11.70	.	16.56	4.51	0.26	0.22	1.63	1.25	.	0.09	9.24	.	MUN
199.20	53.50	11.91	.	13.13	4.04	0.18	0.11	1.63	1.12	0.09	0.09	3.78	.	BOC
200.90	53.54	10.34	21.00	.	2.10	0.15	0.45	1.85	0.97	0.05	0.04	10.93	.	AAC
202.70	52.86	14.48	15.39	.	8.32	0.27	0.46	1.02	1.39	0.09	0.21	7.31	.	AAC
212.70	54.16	4.36	24.32	.	0.14	0.14	0.42	1.00	0.42	0.04	0.01	15.05	.	AAC
214.70	50.20	13.20	.	18.08	6.33	0.33	0.21	1.17	1.25	.	0.20	8.87	.	MUN
214.70	53.30	13.61	.	11.52	6.90	0.27	0.10	0.45	1.24	0.11	0.27	4.73	.	BOC
215.50	46.44	11.61	26.91	.	2.30	0.15	0.45	2.02	1.07	0.05	0.07	10.75	.	AAC
216.33	53.21	14.84	14.74	.	5.56	0.25	0.46	1.94	1.39	0.11	0.11	8.65	.	AAC
218.00	54.30	13.20	.	13.29	7.77	0.34	0.09	0.43	0.86	.	0.24	7.90	.	MUN
218.00	53.40	14.18	2.30	6.03	7.58	1.78	1.45	1.86	1.19	0.12	0.50	5.55	2.92	BOC
219.40	43.90	10.90	.	23.80	1.75	0.16	0.24	1.97	1.11	0.04	0.05	2.83	.	NEW
219.40	42.80	10.30	.	26.44	1.70	0.17	0.24	1.96	0.84	.	0.04	14.88	.	MUN
220.30	55.61	13.89	13.26	.	6.68	0.23	0.47	1.25	1.30	0.10	0.21	6.56	.	AAC
221.00	57.70	13.60	.	12.91	6.26	0.39	0.23	1.30	1.25	.	0.15	6.70	.	MUN
223.10	52.28	9.17	21.52	.	2.95	0.07	0.44	1.26	0.86	0.04	0.07	12.96	.	AAC
223.90	38.80	14.20	.	26.22	0.22	0.26	0.34	3.34	1.36	.	0.01	15.32	.	MUN
228.70	50.60	15.94	5.65	6.55	9.20	0.24	0.11	1.19	1.45	0.15	0.17	5.93	2.34	BOC
228.70	51.20	15.70	.	11.90	9.12	0.28	0.17	1.16	1.47	0.14	0.17	6.57	.	NEW
228.70	50.70	15.40	.	13.05	10.21	0.36	0.16	1.15	1.38	.	0.15	7.89	.	MUN
229.40	16.58	1.51	52.32	.	0.11	0.04	0.35	0.39	0.14	0.04	0.01	29.67	.	AAC
234.30	52.00	11.00	.	20.14	3.43	0.22	0.27	1.29	0.85	.	0.13	10.23	.	MUN
237.00	52.50	13.00	.	14.21	7.84	0.21	0.18	0.99	1.16	.	0.25	7.56	.	MUN
238.26	45.40	17.80	7.46	7.13	8.68	0.18	0.21	1.42	1.41	0.07	0.15	6.45	2.03	BOC
238.26	46.60	17.70	.	14.00	8.65	0.26	0.30	1.38	1.53	0.06	0.15	7.69	.	NEW
238.26	45.70	17.30	.	14.77	9.52	0.30	0.26	1.37	1.27	.	0.14	8.66	.	MUN
241.80	57.10	12.78	7.86	5.14	5.36	0.20	0.19	1.36	1.26	0.10	0.19	4.41	3.08	BOC
241.80	56.10	12.40	.	13.46	5.92	0.30	0.15	1.32	1.15	.	0.17	7.54	.	MUN
241.83	58.91	13.33	11.95	.	4.47	0.20	0.46	1.85	1.32	0.09	0.15	7.17	.	AAC
243.00	48.70	14.70	.	18.28	4.19	0.28	0.30	2.28	1.23	.	0.07	10.55	.	MUN
243.50	55.11	14.05	13.17	.	7.88	0.23	0.47	1.07	1.07	0.05	0.18	6.66	.	AAC
245.80	33.70	18.80	.	21.30	7.19	0.22	0.28	2.40	1.55	0.11	0.14	6.62	.	NEW
245.80	32.50	17.90	.	23.17	7.82	0.32	0.28	2.39	1.42	.	0.13	13.73	.	MUN
246.00	59.41	12.04	13.31	.	4.30	0.29	0.46	1.68	1.04	0.12	0.14	7.54	.	AAC
247.60	57.30	11.80	.	15.03	2.82	0.22	0.24	1.79	1.11	.	0.11	8.75	.	MUN
247.60	57.00	11.94	11.10	2.76	2.53	0.19	0.32	1.91	1.16	0.10	0.11	2.96	7.14	BOC
247.70	52.08	14.21	14.65	.	6.28	0.24	0.47	1.52	1.37	0.08	0.29	6.82	.	AAC
250.50	53.30	12.90	.	14.54	6.71	0.34	0.14	1.24	1.30	.	0.30	7.84	.	MUN
252.90	57.30	12.10	.	14.00	3.90	0.20	0.16	1.71	1.23	0.11	0.20	4.44	.	NEW
252.90	56.10	11.50	.	14.88	4.20	0.30	0.17	1.73	1.16	.	0.19	8.58	.	MUN
253.30	50.50	14.20	.	14.48	7.93	0.72	0.24	0.16	1.02	.	0.49	8.34	.	MUN
253.30	48.20	14.55	.	12.58	7.01	0.66	0.20	0.15	1.02	0.09	0.51	6.85	.	BOC
254.00	61.50	11.50	.	11.39	5.37	0.40	0.13	1.14	0.36	.	0.18	6.09	.	MUN
255.10	4.92	0.16	61.34	.	0.10	0.01	0.33	0.07	0.01	0.03	0.01	34.21	.	AAC
258.20	60.11	12.14	13.07	.	4.91	0.33	0.47	1.29	1.20	0.09	0.23	6.87	.	AAC
259.85	63.88	13.02	9.51	.	4.29	0.35	0.47	1.88	1.04	0.12	0.18	6.05	.	AAC
259.90	62.34	13.47	11.04	.	4.66	0.36	0.47	1.72	1.08	0.11	0.22	5.93	.	AAC

Depth	SiO_2	Al_2O_3	Fe_2O_3	FeO	MgO	CaO	Na_2O	K_2O	TiO_2	P_2O_5	MnO	H_2O+	CO_2	Lab
261.20	49.74	11.68	20.64	.	3.10	0.33	0.44	1.79	1.00	0.07	0.14	12.44	.	AAC
262.40	58.90	12.70	.	13.10	3.86	0.31	0.20	1.77	1.12	0.12	0.14	4.24	.	NEW
262.40	57.20	12.10	.	14.14	4.19	0.28	0.22	1.68	0.93	.	0.14	7.56	.	MUN
262.50	58.17	13.17	13.99	.	3.74	0.28	0.46	2.03	1.15	0.12	0.16	8.44	.	AAC
262.62	58.28	12.41	14.25	.	4.29	0.23	0.46	1.51	1.09	0.09	0.17	8.03	.	AAC
263.50	1.82	0.12	59.70	.	0.09	0.02	0.31	0.06	0.01	0.03	0.01	38.94	.	AAC
268.00	20.20	13.20	.	39.09	0.26	0.24	0.33	3.25	1.23	.	0.01	22.55	.	MUN
268.00	17.70	12.79	.	28.48	0.21	0.14	0.19	3.08	1.12	0.05	0.02	2.31	.	BOC
268.24	1.13	0.63	59.88	.	0.09	0.06	0.31	0.16	0.04	0.03	0.01	38.73	.	AAC
268.50	52.16	15.21	13.69	.	6.63	0.39	0.46	1.50	1.31	0.13	0.13	8.41	.	AAC
269.44	53.93	14.14	15.16	.	6.61	0.26	0.46	1.47	1.22	0.09	0.21	8.15	.	AAC
270.20	25.60	16.30	.	30.55	4.13	0.28	0.30	2.86	1.40	.	0.06	17.64	.	MUN
272.30	71.49	0.18	15.86	.	0.14	0.07	0.45	0.09	0.02	0.05	0.02	9.78	.	AAC
273.65	56.20	13.30	.	12.33	7.09	0.31	0.14	1.13	0.51	.	0.22	6.96	.	MUN
273.65	57.90	13.90	.	12.00	6.34	0.25	0.12	1.10	1.18	0.13	0.22	5.52	.	NEW
273.90	61.08	12.86	12.14	.	5.60	0.26	0.47	1.34	0.97	0.10	0.20	6.62	.	AAC
276.20	42.47	8.98	29.35	.	2.26	0.37	0.42	1.39	0.81	0.07	0.09	15.74	.	AAC
277.01	36.79	7.87	34.15	.	2.78	0.16	0.44	1.15	0.76	0.04	0.11	17.52	.	AAC
277.80	55.30	12.40	.	13.69	7.59	0.24	0.13	1.11	0.84	.	0.27	7.13	.	MUN
277.80	56.30	13.09	.	12.59	7.02	0.20	0.13	1.14	1.17	0.10	0.30	5.00	.	BOC
278.00	54.00	13.50	14.29	.	7.36	0.26	0.46	1.04	1.23	0.07	0.30	7.16	.	AAC
278.50	57.74	12.80	14.20	.	6.51	0.22	0.46	1.23	1.12	0.07	0.25	7.05	.	AAC
281.65	56.17	14.74	9.61	.	8.97	6.05	1.63	0.47	0.53	0.05	0.26	3.26	.	AAC
282.10	54.80	15.38	4.54	3.94	8.80	6.69	2.04	0.32	0.53	0.05	0.28	2.90	0.32	BOC
282.74	54.14	13.29	15.51	.	6.34	0.34	0.46	1.26	1.12	0.10	0.23	7.80	.	AAC
283.50	21.80	7.66	.	43.78	0.67	0.27	0.22	1.49	0.68	.	0.03	22.90	.	MUN
285.30	59.50	12.90	.	10.60	4.97	1.30	0.28	0.86	1.02	0.11	0.19	4.94	.	NEW
285.30	58.00	12.76	6.55	4.07	4.86	1.28	0.30	0.81	1.06	0.11	0.18	4.52	0.50	BOC
285.70	59.98	13.16	11.96	.	4.83	1.92	0.47	0.36	1.15	0.08	0.25	6.56	.	AAC
288.75	51.98	11.96	17.63	.	6.51	0.20	0.56	1.09	1.15	0.06	0.21	9.75	.	AAC
291.20	53.40	13.40	.	13.50	7.90	0.24	0.16	0.92	1.20	0.10	0.32	5.68	.	NEW
291.20	53.30	12.90	.	14.21	8.67	0.30	0.18	0.88	1.04	.	0.31	7.94	.	MUN
293.00	53.75	14.73	12.93	.	8.96	0.52	0.46	0.91	1.18	0.07	0.74	7.61	.	AAC
297.90	57.23	13.97	13.51	.	5.65	1.63	0.87	1.22	0.94	0.07	0.52	5.75	.	AAC
299.57	64.14	13.13	10.41	.	2.61	2.82	1.77	0.72	0.85	0.11	0.70	4.44	.	AAC
299.75	61.70	12.80	.	11.10	3.02	1.43	1.53	0.84	0.89	0.11	0.74	4.40	.	NEW
301.18	62.25	13.15	10.74	.	2.47	2.66	1.15	0.88	0.82	0.12	0.67	4.03	.	AAC
302.55	57.14	13.79	14.47	.	5.64	1.21	0.97	1.29	0.96	0.08	0.88	5.19	.	AAC
303.50	55.00	13.10	.	13.91	5.77	1.12	1.07	1.30	0.94	.	0.78	6.30	.	MUN
303.50	54.70	13.55	.	12.73	5.30	1.12	0.88	1.33	0.92	0.08	0.82	4.85	.	BOC
305.35	57.61	12.56	14.01	.	3.38	3.36	2.30	0.56	0.80	0.11	0.34	6.58	.	AAC
307.45	63.85	13.44	10.51	.	3.19	2.43	2.16	0.88	0.87	0.12	0.39	4.09	.	AAC
308.60	62.10	13.30	.	9.54	3.71	2.22	2.14	0.63	0.89	0.12	0.37	4.18	.	NEW
308.60	62.90	12.70	.	10.42	3.91	2.11	2.12	0.63	0.81	.	0.33	4.79	.	MUN
311.30	63.74	13.49	9.78	.	3.63	2.20	2.51	0.63	0.87	0.13	0.33	3.62	.	AAC
313.27	54.92	14.00	13.68	.	6.87	1.11	1.87	0.71	0.98	0.06	0.46	5.31	.	AAC
313.50	56.62	14.33	13.21	.	7.18	1.04	1.90	0.68	0.95	0.06	0.48	5.21	.	AAC
315.40	56.80	13.80	.	11.30	6.85	1.29	1.35	1.06	1.02	0.08	0.60	6.25	.	NEW
315.50	55.26	14.48	14.58	.	6.61	0.89	2.09	0.47	1.02	0.07	0.47	5.46	.	AAC
319.20	54.93	14.88	14.61	.	4.92	1.14	0.80	1.55	1.03	0.07	0.42	6.10	.	AAC
319.30	56.50	14.01	6.25	5.39	5.15	1.64	1.53	1.13	0.96	0.10	0.63	4.99	0.15	BOC
323.20	63.52	13.51	9.39	.	3.85	0.57	1.48	0.89	0.87	0.10	0.30	4.15	.	AAC
325.00	66.31	15.03	5.58	.	1.16	2.58	4.55	1.10	1.10	0.06	0.04	4.02	.	AAC
326.00	62.60	13.00	.	7.86	4.17	2.41	3.14	0.22	0.89	0.19	0.22	3.30	.	NEW
327.00	50.40	16.46	13.54	.	8.12	1.92	1.92	0.82	1.28	0.07	0.32	4.82	.	AAC

Depth	SiO_2	Al_2O_3	Fe_2O_3	FeO	MgO	CaO	Na_2O	K_2O	TiO_2	P_2O_5	MnO	H_2O+	CO_2	Lab
328.90	50.40	15.41	2.61	8.37	8.02	2.93	2.67	1.09	1.13	0.09	0.28	5.81	0.81	BOC
330.30	51.11	14.69	11.74	.	7.64	2.93	2.38	0.85	1.24	0.08	0.25	5.73	.	AAC
331.20	62.96	12.98	9.75	.	4.57	1.80	3.13	0.48	0.93	0.08	0.22	3.50	.	AAC
338.25	50.34	13.70	11.84	.	7.27	3.87	1.84	0.41	1.12	0.06	0.34	7.32	.	AAC
339.45	50.87	14.34	11.72	.	7.97	3.39	1.96	0.42	1.12	0.08	0.45	6.60	.	AAC
341.75	56.11	15.05	12.24	.	5.79	0.86	4.66	0.13	1.12	0.08	0.30	5.00	.	AAC
341.85	58.90	14.40	.	8.93	5.32	1.49	4.52	0.22	1.09	0.22	0.28	4.39	.	NEW
343.80	62.91	13.27	9.22	.	3.93	1.67	3.63	0.80	0.89	0.11	0.30	4.12	.	AAC
344.75	59.18	17.03	8.79	.	2.52	1.43	6.17	1.16	1.59	0.07	0.15	3.15	.	AAC
346.50	49.40	14.90	.	11.10	5.52	5.88	2.23	1.27	1.31	0.09	0.28	6.09	.	NEW
346.50	48.60	15.02	4.21	7.48	5.40	5.96	2.08	1.28	1.29	0.08	0.29	4.79	2.26	BOC
347.50	48.14	15.68	13.75	.	7.98	3.82	2.01	1.02	1.42	0.06	0.24	7.17	.	AAC
351.18	61.07	13.76	8.93	.	4.88	2.41	3.29	0.44	0.93	0.10	0.16	4.61	.	AAC
351.99	55.61	12.07	13.60	.	3.63	3.95	2.35	0.59	0.79	0.08	0.32	6.10	.	AAC
352.60	48.26	19.14	11.98	.	6.61	1.33	5.55	0.32	1.69	0.10	0.38	4.47	.	AAC
357.35	57.25	13.31	12.94	.	6.05	0.58	2.37	0.41	1.22	0.10	0.37	4.81	.	AAC
359.40	55.63	14.22	12.68	.	6.05	1.79	3.36	0.50	1.29	0.11	0.35	4.28	.	AAC
360.00	56.00	13.80	.	12.80	5.40	0.88	3.01	0.58	1.28	0.13	0.36	4.83	.	NEW
363.00	52.78	14.20	11.98	.	4.96	6.50	2.86	0.37	1.27	0.08	0.19	5.85	.	AAC
363.85	51.43	14.78	12.79	.	5.78	6.18	1.84	0.21	1.28	0.07	0.25	5.27	.	AAC
367.40	53.59	14.51	12.60	.	5.64	5.68	2.82	0.10	1.30	0.07	0.21	4.64	.	AAC
368.20	52.70	14.74	9.16	3.53	6.64	5.51	2.83	0.03	1.28	0.09	0.16	3.46	0.22	BOC
369.25	52.55	14.71	12.70	.	5.98	6.04	2.49	0.10	1.31	0.07	0.21	4.84	.	AAC
370.50	53.20	14.70	.	10.70	5.29	6.54	2.00	0.06	1.30	0.07	0.37	4.50	.	GSC
372.95	51.85	14.25	11.41	.	6.33	4.15	3.65	0.53	1.16	0.08	0.23	6.06	.	AAC
373.70	55.81	16.19	11.22	.	5.80	2.01	4.62	0.69	1.16	0.08	0.20	3.71	.	AAC
374.40	53.25	14.94	12.68	.	6.22	2.41	3.32	0.65	1.14	0.08	0.22	6.05	.	AAC
375.60	48.00	17.00	.	12.60	7.36	1.98	5.54	0.08	1.62	0.11	0.26	5.56	.	NEW
375.60	47.60	16.95	6.08	6.99	7.41	1.82	5.57	0.05	1.48	0.10	0.27	4.77	0.30	BOC
376.10	43.39	16.81	16.07	.	10.24	1.45	4.17	0.09	1.20	0.08	0.34	6.70	.	AAC
377.10	53.31	15.11	11.68	.	7.02	2.48	3.96	0.45	1.10	0.08	0.21	4.76	.	AAC
378.82	55.61	15.89	11.04	.	7.01	1.44	3.13	0.17	1.17	0.08	0.20	4.32	.	AAC
380.10	49.90	17.18	12.56	.	8.09	1.67	5.61	0.33	1.23	0.10	0.24	4.56	.	AAC
382.45	53.82	15.06	11.05	.	6.26	4.06	3.56	0.50	1.05	0.07	0.25	5.39	.	AAC
384.20	59.37	14.81	10.48	.	5.25	1.34	5.13	0.19	1.02	0.08	0.40	3.37	.	AAC
386.45	57.49	14.52	10.90	.	5.25	1.41	4.48	0.19	1.03	0.08	0.40	3.79	.	AAC
387.80	61.84	14.38	10.12	.	4.45	1.36	4.87	0.27	1.01	0.09	0.41	3.04	.	AAC
389.60	61.92	14.26	9.71	.	4.26	1.63	5.13	0.42	0.95	0.11	0.33	3.08	.	AAC
392.15	57.62	13.39	10.86	.	4.59	1.36	4.47	0.31	0.92	0.09	0.52	4.00	.	AAC
393.64	61.28	14.09	10.37	.	4.85	1.23	4.45	0.23	1.02	0.11	0.32	3.59	.	AAC
394.00	60.30	14.60	.	9.27	4.72	1.29	4.92	0.14	1.13	0.18	0.32	3.42	.	NEW
397.21	60.13	13.52	12.40	.	3.75	0.88	3.36	0.55	1.01	0.09	0.35	3.83	.	AAC
397.50	61.10	14.26	3.01	6.42	4.55	1.21	4.40	0.15	1.04	0.12	0.43	3.75	0.02	BOC
398.50	63.10	13.90	.	8.10	4.39	1.38	4.10	0.19	1.02	0.12	0.38	3.60	.	GSC
400.70	61.87	13.75	12.25	.	3.32	1.39	4.01	0.38	1.05	0.11	0.38	3.13	.	AAC
401.40	47.78	18.35	14.78	.	5.92	1.33	6.10	0.10	1.40	0.10	0.58	5.28	.	AAC
404.58	55.74	14.25	12.78	.	5.99	1.41	4.01	0.10	1.29	0.08	0.45	5.53	.	AAC
405.66	56.84	13.15	14.35	.	7.20	0.41	2.35	0.11	1.19	0.08	0.59	5.18	.	AAC
406.30	53.60	13.20	.	11.80	6.77	0.38	1.70	0.26	1.18	0.09	0.39	7.10	.	GSC
407.92	57.57	13.07	12.42	.	6.01	0.44	3.10	0.14	1.24	0.08	0.83	5.69	.	AAC
409.90	54.20	13.60	.	11.65	6.72	1.13	2.82	0.15	1.22	0.11	0.57	4.92	.	BOC
411.07	50.39	15.73	13.91	.	8.61	1.42	3.19	0.10	1.44	0.09	0.84	5.35	.	AAC
414.00	58.60	14.50	.	9.90	5.30	1.69	4.15	0.16	1.26	0.19	0.36	4.13	.	NEW
414.90	60.31	13.47	10.62	.	4.53	1.48	3.59	0.18	1.04	0.12	0.40	4.01	.	AAC
416.42	61.94	13.10	12.14	.	3.42	0.64	2.95	0.81	1.01	0.12	0.32	4.92	.	AAC

Depth	SiO_2	Al_2O_3	Fe_2O_3	FeO	MgO	CaO	Na_2O	K_2O	TiO_2	P_2O_5	MnO	H_2O+	CO_2	Lab
419.60	60.10	14.04	1.95	6.84	4.10	1.95	4.06	0.13	1.04	0.15	0.55	3.82	0.20	BOC
419.78	60.12	14.38	9.75	.	4.51	1.61	3.15	0.20	1.07	0.14	0.59	2.61	.	AAC
421.90	61.80	14.30	.	8.43	4.16	1.98	4.34	0.14	1.09	0.16	0.30	3.85	.	NEW
424.57	54.12	15.90	10.84	.	5.25	1.59	5.29	0.10	1.24	0.12	0.61	3.79	.	AAC
424.62	57.73	14.02	12.22	.	6.79	1.41	3.39	0.10	1.23	0.09	0.62	3.89	.	AAC
426.00	49.00	12.80	.	13.00	5.52	1.49	2.70	0.09	1.11	0.07	0.55	7.10	.	GSC
427.12	53.99	15.07	11.69	.	6.34	1.90	4.20	0.10	1.29	0.08	0.77	4.43	.	AAC
431.25	52.87	14.34	12.07	.	6.24	1.66	3.66	0.10	1.25	0.08	1.06	4.74	.	AAC
432.79	45.48	10.40	20.02	.	5.27	2.03	2.35	0.09	0.97	0.05	0.99	9.53	.	AAC
434.50	46.50	13.60	.	10.90	6.52	1.50	2.20	0.07	1.16	0.10	1.02	6.90	.	GSC
434.50	57.00	15.20	.	9.20	5.61	1.88	3.40	0.13	1.29	0.13	0.79	5.00	.	GSC
434.78	58.70	14.30	.	8.97	5.43	1.96	4.10	0.10	1.22	0.14	0.56	4.35	.	NEW
434.78	57.70	14.00	2.46	6.42	5.23	1.88	3.87	0.08	1.16	0.13	0.57	4.09	0.06	BOC
435.65	58.31	14.31	10.06	.	5.15	1.68	4.80	0.11	1.23	0.10	0.40	3.37	.	AAC
441.63	65.49	13.17	8.72	.	3.99	1.39	4.79	0.10	1.19	0.09	0.20	2.33	.	AAC
445.20	59.69	14.89	9.96	.	4.70	1.51	5.44	0.10	1.32	0.12	0.35	2.79	.	AAC
445.70	59.80	15.00	.	9.09	4.37	1.63	5.17	0.10	1.34	0.13	0.34	3.47	.	NEW
445.70	59.70	14.87	3.53	5.78	4.26	1.58	5.13	0.07	1.27	0.14	0.35	3.63	0.05	BOC
449.90	63.09	12.89	9.02	.	3.98	2.10	4.75	0.10	1.12	0.12	0.18	4.07	.	AAC
452.10	57.35	14.72	9.90	.	5.59	2.08	4.80	0.10	1.26	0.12	0.21	3.92	.	AAC
455.90	48.60	15.30	.	13.20	8.24	1.63	2.30	0.02	1.45	0.07	0.76	7.00	.	GSC
456.60	50.60	15.15	.	11.28	6.66	2.01	4.34	0.01	1.38	0.12	0.40	4.56	.	BOC
456.95	54.84	12.76	12.24	.	2.13	3.35	5.89	0.09	1.20	0.09	0.15	7.05	.	AAC
458.35	60.64	7.70	17.32	.	2.75	1.30	2.45	0.09	0.68	0.05	0.21	7.81	.	AAC
460.10	57.00	14.90	.	10.20	5.64	1.81	4.77	0.04	1.54	0.11	0.32	4.06	.	NEW
462.00	48.60	10.60	.	14.30	3.84	2.23	2.70	0.06	1.00	0.09	0.19	7.80	.	GSC
462.05	47.88	5.47	22.83	.	1.47	5.70	2.05	0.09	0.55	0.05	0.12	12.01	.	AAC
462.80	45.33	16.13	14.30	.	8.39	3.24	4.24	0.09	1.46	0.08	0.44	5.53	.	AAC
467.20	54.86	14.22	12.03	.	4.56	3.75	4.71	0.16	1.09	0.08	0.25	4.11	.	AAC
467.80	54.40	14.40	.	9.81	4.22	4.98	4.48	0.26	1.05	0.11	0.24	3.49	.	NEW
467.80	54.90	14.24	4.03	6.19	4.14	5.03	4.53	0.25	1.02	0.09	0.25	3.17	1.45	BOC
469.51	56.13	14.18	10.53	.	3.87	4.44	5.02	0.16	1.07	0.07	0.28	3.99	.	AAC
471.80	54.42	14.38	14.09	.	5.72	2.13	3.00	0.30	1.04	0.09	0.41	4.38	.	AAC
472.45	55.39	14.77	11.26	.	5.44	3.06	4.63	0.10	1.04	0.06	0.31	3.78	.	AAC
474.90	56.10	12.50	.	10.30	3.77	2.24	2.60	0.14	1.01	0.12	0.29	5.50	.	GSC
475.00	55.80	12.70	.	11.40	3.63	2.34	2.70	0.16	0.97	0.11	0.27	6.00	.	GSC
475.73	52.21	11.65	18.80	.	3.30	1.91	3.41	0.12	1.00	0.11	0.24	8.57	.	AAC
476.85	57.46	12.65	13.31	.	4.49	1.52	3.55	0.10	1.07	0.08	0.29	4.94	.	AAC
478.80	62.00	14.30	.	8.82	3.82	1.67	5.03	0.04	1.16	0.21	0.22	3.13	.	NEW
479.39	57.63	12.98	11.53	.	4.01	2.09	4.26	0.10	0.96	0.13	0.24	4.64	.	AAC
481.66	52.96	13.76	13.70	.	6.39	1.23	4.15	0.10	1.22	0.10	0.35	4.48	.	AAC
483.80	52.80	15.60	.	11.00	6.13	1.39	4.10	0.03	1.31	0.12	0.31	5.00	.	GSC
484.70	55.70	14.63	3.91	6.43	4.59	2.90	5.04	0.06	1.19	0.12	0.24	3.48	0.66	BOC
486.01	64.18	12.73	9.65	.	3.81	2.12	4.49	0.10	1.12	0.09	0.21	1.95	.	AAC
487.88	51.17	10.87	21.03	.	4.24	3.30	2.82	0.09	0.99	0.08	0.22	5.22	.	AAC
489.20	56.90	14.00	.	11.10	6.43	1.66	3.78	0.08	1.21	0.15	0.28	4.63	.	NEW
490.90	39.09	16.23	21.54	.	8.57	1.45	3.24	0.09	1.18	0.08	0.32	9.47	.	AAC
491.48	37.36	9.96	29.44	.	3.72	2.97	1.94	0.09	0.86	0.06	0.17	14.48	.	AAC
494.69	47.84	12.51	20.35	.	6.20	1.62	2.22	0.29	1.07	0.07	0.27	8.83	.	AAC
495.20	46.60	12.60	.	19.60	5.48	2.02	2.36	0.26	1.01	0.10	0.24	4.82	.	NEW
497.40	41.20	8.90	.	22.50	2.63	2.16	1.60	0.16	0.90	0.07	0.17	2.40	.	GSC
500.60	60.26	14.59	10.35	.	4.42	2.01	4.50	0.14	1.22	0.10	0.23	3.93	.	AAC
501.33	51.15	14.76	16.21	.	5.56	1.65	4.14	0.19	1.24	0.09	0.24	6.51	.	AAC
502.65	55.20	10.24	.	15.20	5.88	1.10	1.41	0.04	0.98	0.08	0.23	4.51	.	BOC
503.40	49.60	14.10	.	12.90	6.84	1.91	2.50	0.10	1.40	0.10	0.34	7.40	.	GSC

Depth	SiO_2	Al_2O_3	Fe_2O_3	FeO	MgO	CaO	Na_2O	K_2O	TiO_2	P_2O_5	MnO	H_2O+	CO_2	Lab
504.52	53.90	14.85	13.76	.	5.29	2.89	4.39	0.11	1.27	0.08	0.31	3.00	.	AAC
508.09	56.48	13.03	14.50	.	4.76	1.97	3.40	0.23	1.27	0.09	0.29	5.40	.	AAC
510.80	58.53	13.43	12.43	.	4.95	1.75	3.79	0.11	1.15	0.10	0.32	4.36	.	AAC
511.60	57.70	14.30	.	11.00	5.01	1.53	3.82	0.26	1.19	0.12	0.30	4.38	.	NEW
515.70	55.40	13.70	.	11.20	4.83	1.63	2.80	0.10	1.18	0.10	0.28	5.40	.	GSC
516.09	57.84	14.44	12.97	.	5.26	1.83	3.82	0.10	1.23	0.09	0.28	3.71	.	AAC
518.06	53.49	13.48	15.37	.	5.02	2.33	3.55	0.11	1.15	0.08	0.29	6.22	.	AAC
518.79	57.79	13.24	14.34	.	4.52	1.86	2.88	0.22	1.15	0.08	0.30	4.76	.	AAC
521.53	37.95	12.15	29.10	.	5.89	1.11	2.04	0.09	1.03	0.05	0.27	11.92	.	AAC
522.60	57.40	13.90	.	11.20	5.34	2.02	3.10	0.20	1.16	0.11	0.28	4.43	.	NEW
526.10	55.60	14.30	.	11.36	4.89	2.11	3.44	0.32	1.18	0.12	0.28	4.09	.	BOC
526.45	48.20	11.12	23.08	.	4.31	1.21	2.62	0.13	1.11	0.07	0.22	9.36	.	AAC
528.30	50.40	11.70	.	15.30	3.99	1.62	2.20	0.10	1.11	0.10	0.22	8.30	.	GSC
528.85	40.66	16.49	22.54	.	7.20	1.86	2.95	0.13	1.44	0.10	0.36	7.69	.	AAC
529.37	58.16	14.42	13.17	.	3.86	1.84	3.99	0.23	1.23	0.11	0.28	4.08	.	AAC
530.93	47.09	12.03	23.10	.	4.43	1.83	1.93	0.34	0.96	0.08	0.23	9.88	.	AAC
534.60	56.93	14.96	13.15	.	5.05	1.54	4.07	0.14	1.26	0.10	0.29	4.19	.	AAC
535.60	49.07	11.46	21.56	.	3.94	1.54	2.84	0.14	1.01	0.09	0.22	9.20	.	AAC
539.40	43.50	13.70	.	16.10	4.56	1.55	3.00	0.34	1.19	0.12	0.25	8.60	.	GSC
539.55	54.90	12.55	15.07	.	3.93	1.70	4.16	0.09	1.18	0.06	0.19	6.74	.	AAC
539.70	60.00	14.40	.	10.80	3.61	1.42	4.67	0.02	1.18	0.16	0.26	3.86	.	NEW
539.70	60.10	14.37	2.81	8.07	3.56	1.36	4.65	0.01	1.11	0.15	0.26	3.44	0.16	BOC
541.15	50.10	11.95	18.30	.	3.12	2.56	3.22	0.43	1.01	0.07	0.18	9.50	.	AAC
544.00	51.80	13.10	.	13.60	5.15	1.49	2.50	0.26	1.12	0.12	0.25	7.50	.	GSC
545.40	54.09	15.08	13.77	.	5.05	1.71	4.51	0.10	1.27	0.10	0.31	4.82	.	AAC
548.76	47.05	11.12	22.68	.	3.89	1.56	2.47	0.32	0.83	0.09	0.21	10.26	.	AAC
550.70	54.20	14.10	.	14.20	5.12	1.42	3.58	0.02	1.12	0.09	0.24	4.81	.	NEW
551.57	57.39	13.89	12.99	.	4.27	1.87	4.05	0.15	1.21	0.09	0.20	4.87	.	AAC
553.50	54.80	13.10	.	11.70	4.96	1.51	2.70	0.23	1.13	0.08	0.21	6.20	.	GSC
554.20	35.33	7.39	33.64	.	3.54	1.19	1.38	0.17	0.65	0.04	0.12	17.12	.	AAC
556.29	50.68	14.33	11.47	.	5.76	7.40	1.88	0.42	1.05	0.06	0.19	6.91	.	AAC
558.87	50.85	14.13	18.61	.	5.03	1.49	2.85	0.19	1.00	0.06	0.38	5.93	.	AAC
561.03	34.84	7.63	32.15	.	2.91	1.90	2.14	0.08	0.75	0.04	0.11	18.05	.	AAC
562.40	52.75	14.28	16.74	.	4.40	1.93	3.93	0.09	1.37	0.09	0.34	5.60	.	AAC
563.41	30.14	5.33	37.10	.	2.08	2.34	1.24	0.08	0.54	0.04	0.11	21.22	.	AAC
567.86	41.57	16.19	21.19	.	5.88	3.06	2.80	0.50	1.16	0.07	0.56	6.62	.	AAC
569.87	41.60	15.89	21.24	.	5.77	3.61	2.79	0.35	1.08	0.07	0.55	6.79	.	AAC
570.20	53.00	15.50	.	12.70	5.60	1.83	3.83	0.22	1.21	0.11	0.42	5.35	.	NEW
572.63	51.42	14.17	17.09	.	4.87	1.27	3.06	0.36	1.06	0.09	0.40	5.23	.	AAC
576.20	51.00	15.00	.	15.39	5.19	1.22	2.99	0.19	1.08	0.09	0.40	5.37	.	BOC
576.50	50.90	8.50	.	17.90	3.51	1.55	1.30	0.07	0.86	0.06	0.22	3.50	.	GSC
576.59	48.47	10.69	22.57	.	4.29	1.47	2.33	0.10	1.05	0.07	0.26	10.08	.	AAC
577.47	42.51	18.23	20.45	.	6.22	1.47	2.54	0.10	1.29	0.08	0.55	5.46	.	AAC
580.02	46.29	8.59	33.67	.	3.17	1.48	2.27	0.10	0.88	0.05	0.17	4.94	.	AAC
581.58	50.91	12.07	19.63	.	5.08	1.45	2.62	0.09	1.14	0.08	0.33	7.41	.	AAC
583.20	49.90	15.00	.	16.90	5.23	1.24	3.33	0.14	1.11	0.10	0.36	5.79	.	NEW
583.60	19.59	5.64	43.74	.	2.55	2.17	1.11	0.08	0.55	0.04	0.15	22.58	.	AAC
585.24	40.21	15.95	18.43	.	5.38	1.33	3.15	0.17	1.15	0.08	0.48	15.19	.	AAC
586.30	55.75	13.59	15.53	.	4.05	1.52	3.79	0.09	1.34	0.10	0.32	5.06	.	AAC
587.60	55.20	13.30	.	11.50	4.14	1.54	3.10	0.13	1.26	0.09	0.34	5.90	.	GSC
589.85	50.89	11.88	19.36	.	5.43	1.71	2.48	0.09	1.22	0.08	0.29	8.12	.	AAC
591.85	20.66	11.87	41.15	.	6.35	1.46	1.02	0.08	0.99	0.08	0.44	16.47	.	AAC
593.50	51.60	13.30	.	15.80	4.77	1.58	3.01	0.14	1.12	0.14	0.26	4.90	.	NEW
594.28	55.67	13.63	16.12	.	5.38	1.43	2.93	0.10	1.30	0.09	0.41	4.76	.	AAC
595.79	49.10	15.01	18.17	.	5.88	1.37	1.97	0.13	1.13	0.07	0.47	5.58	.	AAC

Depth	SiO_2	Al_2O_3	Fe_2O_3	FeO	MgO	CaO	Na_2O	K_2O	TiO_2	P_2O_5	MnO	H_2O+	CO_2	Lab
600.30	51.60	15.40	.	13.40	6.10	1.58	3.80	0.04	1.24	0.13	0.48	4.73	.	NEW
600.45	52.82	15.73	13.93	.	6.22	1.45	4.12	0.10	1.13	0.06	0.46	4.25	.	AAC
603.30	49.29	14.76	18.81	.	5.48	1.56	3.30	0.10	1.09	0.06	0.49	4.76	.	AAC
605.97	45.22	16.20	20.01	.	5.66	1.30	3.26	0.10	1.21	0.10	0.56	4.79	.	AAC
606.90	48.14	15.30	19.00	.	5.71	1.36	3.34	0.09	1.14	0.07	0.48	5.38	.	AAC
610.59	48.28	15.17	18.53	.	5.56	1.40	3.13	0.09	1.18	0.09	0.53	5.08	.	AAC
610.70	51.60	15.30	.	13.80	5.60	1.55	2.80	0.07	1.14	0.09	0.52	6.00	.	GSC
611.70	51.60	15.27	1.98	8.96	6.17	4.41	2.90	0.90	1.16	0.09	0.33	4.74	1.15	BOC
613.38	51.04	15.34	17.13	.	5.79	1.48	3.35	0.10	1.16	0.09	0.49	4.44	.	AAC
614.30	53.47	15.34	12.81	.	6.55	1.37	3.76	0.10	1.09	0.08	0.41	3.87	.	AAC
616.90	51.20	14.80	.	15.10	5.64	1.71	3.08	0.70	1.12	0.18	0.40	5.41	.	NEW
618.60	46.18	15.13	19.94	.	6.06	1.30	2.74	0.09	1.12	0.07	0.54	5.64	.	AAC
622.27	47.31	15.18	18.96	.	5.84	1.76	2.25	0.21	1.13	0.08	0.54	5.62	.	AAC
623.56	47.39	14.51	18.91	.	5.77	1.69	2.25	0.21	1.13	0.06	0.52	5.52	.	AAC
624.00	53.90	15.60	.	11.00	6.92	1.90	2.00	0.85	1.18	0.08	0.44	5.10	.	GSC
625.30	50.70	14.91	.	15.11	6.19	1.46	2.69	0.42	1.05	0.08	0.41	2.35	.	BOC
627.72	51.13	14.83	15.07	.	6.42	1.43	3.21	0.10	1.04	0.06	0.47	4.94	.	AAC
628.85	46.65	15.20	19.00	.	6.56	1.36	2.25	0.09	1.14	0.08	0.51	5.47	.	AAC
631.20	55.63	11.01	15.08	.	4.47	1.92	2.17	0.09	1.00	0.06	0.28	6.29	.	AAC
632.70	58.60	13.10	.	10.70	4.86	1.66	3.36	0.24	1.08	0.16	0.22	3.98	.	NEW
633.82	64.54	9.70	10.80	.	3.58	1.51	2.61	0.10	0.81	0.08	0.17	4.79	.	AAC
635.10	54.40	13.40	.	13.10	4.22	2.12	2.00	0.91	1.06	0.06	0.40	5.00	.	GSC
636.65	54.97	13.35	14.62	.	4.69	1.68	2.46	0.56	1.03	0.08	0.39	4.43	.	AAC
639.55	51.78	14.00	17.00	.	4.98	2.00	4.30	0.93	1.06	0.10	0.40	4.71	.	AAC
641.60	54.60	13.90	.	14.00	4.40	1.61	3.21	0.67	1.14	0.12	0.36	4.17	.	NEW
643.89	34.44	12.58	27.08	.	6.08	2.37	2.49	0.09	1.23	0.10	0.30	12.47	.	AAC
646.10	54.31	13.08	13.22	.	4.82	1.48	4.88	0.09	1.30	0.09	0.29	5.40	.	AAC
647.60	46.10	13.50	.	14.80	7.26	1.59	2.60	0.03	1.33	0.08	0.39	8.70	.	GSC
647.70	37.92	10.73	26.02	.	5.80	3.13	1.95	0.09	1.09	0.06	0.32	11.95	.	AAC
649.22	52.51	13.73	14.22	.	6.42	3.58	2.65	0.10	1.22	0.05	0.34	4.09	.	AAC
650.10	47.90	10.90	.	16.30	3.84	2.17	2.70	0.03	1.15	0.11	0.23	3.20	.	GSC
650.58	51.74	13.53	14.01	.	6.32	3.53	2.61	0.09	1.20	0.05	0.33	5.49	.	AAC
653.85	51.91	13.60	14.85	.	5.81	2.76	4.29	0.09	1.16	0.08	0.30	5.89	.	AAC
656.37	56.05	13.76	13.98	.	3.72	1.90	4.30	0.10	1.26	0.11	0.28	3.30	.	AAC
656.60	56.50	14.00	.	13.30	3.80	1.97	4.26	0.02	1.28	0.11	0.28	3.61	.	NEW
658.10	54.50	12.40	.	10.40	4.26	2.16	3.00	0.15	1.12	0.08	0.28	5.70	.	GSC
658.80	31.99	7.77	32.68	.	3.86	2.14	1.71	0.10	0.72	0.07	0.19	17.52	.	AAC
659.95	50.53	13.53	15.61	.	7.55	2.04	2.72	0.09	1.26	0.08	0.40	5.61	.	AAC
661.19	21.17	7.49	40.83	.	5.52	1.48	0.94	0.08	0.78	0.04	0.25	20.76	.	AAC
662.17	42.76	8.28	24.98	.	3.81	3.15	1.42	0.09	0.81	0.05	0.22	13.27	.	AAC
665.35	49.71	10.10	23.79	.	5.19	1.30	2.53	0.10	0.97	0.06	0.23	4.93	.	AAC
666.49	40.87	11.23	19.81	.	6.97	1.79	2.06	0.08	1.06	0.07	0.30	15.41	.	AAC
667.00	50.10	12.50	.	13.20	5.09	3.17	2.50	0.02	1.01	0.09	0.26	7.40	.	GSC
667.00	52.00	13.10	.	11.90	5.57	1.43	3.30	0.02	1.24	0.06	0.27	6.50	.	GSC
667.70	53.30	13.00	.	14.50	5.27	2.28	3.40	0.02	0.80	0.12	0.26	4.13	.	NEW
667.70	53.40	12.88	.	13.76	5.21	2.28	3.27	0.01	0.87	0.18	0.26	3.77	.	BOC
668.68	42.72	17.19	16.87	.	6.77	1.89	5.14	0.09	1.33	0.09	0.44	6.02	.	AAC
670.00	53.40	14.40	.	9.00	1.82	10.30	1.00	0.02	0.85	0.14	0.26	3.60	.	GSC
670.00	61.30	14.60	.	7.40	3.62	1.59	4.50	0.04	1.14	0.20	0.24	3.60	.	GSC
670.99	59.27	12.02	10.97	.	5.71	2.25	2.93	0.10	1.26	0.11	0.28	4.13	.	AAC
673.00	51.30	15.40	.	11.00	5.22	5.73	2.20	0.82	1.32	0.11	0.36	4.20	.	GSC
677.40	62.05	13.46	8.48	.	2.68	4.12	3.95	0.10	0.83	0.19	0.23	2.98	.	AAC
677.92	41.28	16.70	18.33	.	9.40	2.10	3.89	0.09	1.93	0.15	0.54	5.45	.	AAC
678.10	54.10	15.00	.	12.20	6.97	1.35	3.68	0.02	1.27	0.11	0.38	5.37	.	NEW
680.10	55.80	13.30	.	8.40	1.80	10.50	0.90	0.04	0.74	0.19	0.24	4.70	.	GSC

Depth	SiO_2	Al_2O_3	Fe_2O_3	FeO	MgO	CaO	Na_2O	K_2O	TiO_2	P_2O_5	MnO	H_2O+	CO_2	Lab
680.10	63.60	12.30	.	6.60	2.79	3.18	3.50	0.03	0.88	0.19	0.20	3.70	.	GSC
681.05	46.92	13.36	17.14	.	8.17	2.00	2.56	0.09	1.39	0.09	0.39	6.79	.	AAC
684.56	50.26	12.71	17.31	.	6.42	1.93	2.65	0.09	1.35	0.10	0.32	6.85	.	AAC
684.80	56.10	12.50	.	11.50	4.89	1.87	2.40	0.02	1.26	0.09	0.30	5.60	.	GSC
685.80	52.40	13.60	.	12.20	6.63	2.81	2.10	0.05	1.24	0.07	0.37	4.20	.	GSC
686.44	46.22	11.99	17.96	.	6.67	5.35	1.64	0.09	1.14	0.06	0.32	7.72	.	AAC
687.60	41.30	14.80	.	10.50	3.77	14.30	0.00	0.05	1.03	0.07	0.34	7.20	.	GSC
687.85	53.40	14.60	.	13.00	6.49	1.94	3.62	0.02	1.47	0.10	0.34	5.04	.	NEW
687.85	53.20	14.63	6.16	7.04	6.49	1.90	3.46	0.02	1.31	0.10	0.34	4.99	0.05	BOC
688.29	56.45	14.13	12.86	.	4.91	1.91	3.90	0.37	1.37	0.10	0.27	2.88	.	AAC
688.88	52.10	14.83	13.47	.	6.09	3.05	5.25	0.10	1.34	0.10	0.35	4.77	.	AAC

MAJOR ELEMENT ANALYTICAL METHODS

Technische Hochschule Aachen (AAC)

Major element chemical analyses were carried out using a Philips PW1400 X-ray fluorescence spectrometer with an on-line Philips PM851 computer. Prior to analysis, samples were ignited at 1,000°C for two hours to oxidize sulfide sulfur, and the loss on ignition was determined. Glass beads incorporating lithium tetra- and metaborate (rock to flux ratio 1:10) were prepared from the ignited samples. The major element analyses have been recalculated, using the LOI, to a 110°C basis. The analytical programs for the major element analyses were calibrated against a series of twenty international standard rock samples. For analytical quality control the internal ICRDG standards TRS 1-7 were analyzed.

Ruhr-Universität Bochum (BOC)

A Philips PW1400 X-ray spectrometer was utilized for the determination of the major elements, measurements being made on fused glass beads incorporating lithium tetra- and meta-borate. Analysis for ferrous iron was by digestion of samples in hydrofluoric acid and silver perchlorate, and the potentiometric titration of excess perchlorate with standard potassium bromide solution. H_2O+ was determined by ignition in a dry inert gas atmosphere, followed by colorimetric titration of the carrier gas in Karl Fischer reagent. CO_2 was determined by igniting samples in a tube furnace in oxygen followed by colorimetric titration of the effluent gas in barium perchlorate solution.

Geological Survey of Canada (GSC)

The major elements, except for H_2O, CO_2, and FeO, were determined by X-ray fluorescence spectrometry on fused discs. Matrix effects were corrected using alpha coefficients. The accuracy of the procedure is shown in the following table:

	Calibration Range wt.%	Max. error	Relative error %	s.d.
SiO_2	0-100	0.40	1	0.53
TiO_2	0-3	0.02	1	0.02
Al_2O_3	0-60	0.40	1	0.40
Fe_2O_3	0-90	0.10	1	0.10
FeO	0-30	0.03	2	—
MnO	0-1	0.01	2	0.01
MgO	0-50	0.10	1	0.14
CaO	0-35	0.10	1	0.15
Na_2O	0-10	0.50	1	0.50
K_2O	0-15	0.05	1	0.16
P_2O_5	0-1	0.02	1	0.02
H_2O+	0-5	0.05	5	—

In all cases, the detection limit is approximately the same as the maximum absolute error in weight percent.

Memorial University of Newfoundland (MUN)

Bulk rock analyses: all elements and oxides, except FeO, have been determined by X-ray fluorescence spectrometry (Philips PW1450). Major elemental analyses were performed on glass beads (except Na, which was analyzed on pressed powder pellets). Twenty international standard values were used for calibrations. Combined analytical error involved in sample preparation and instrumental variation was monitored on ten glass discs from one sample. Each monitor was run 10 times. Ferrous iron was determined titrimetrically employing the potassium dichromate method.

Newcastle University (NEW)

Samples were analyzed H_2O-free after drying at 110°C, using atomic absorption spectroscopy for all elements except for P, determined colorimetrically, and H_2O+, determined using a modified Penfield tube method.

Trace Element Data

Depth	Sr	Ba	Ga	La	Ce	Zr	Nb	Y	Co	Cr	Ni	V	Pb	Cu	Zn	Lab
								CY-2								
1.00	23	31	15	–	–	33	–	10	20	–	20	–	52	1684	55	AAC
2.90	–	–	–	–	–	–	–	–	16	334	24	300	10	1010	96	NEW
4.40	80	76	13	10	16	34	2	18	–	18	19	290	0	116	176	MUN
6.80	35	30	13	–	–	36	–	10	20	–	20	–	10	995	96	AAC
9.20	36	109	12	11	14	27	2	0	–	338	14	415	0	798	85	MUN
10.01	16	30	20	–	–	38	–	10	23	–	20	–	10	1659	315	AAC
12.90	60	30	17	–	–	42	–	10	48	–	67	–	10	18000	1111	AAC
13.90	70	30	16	–	–	40	–	11	48	–	60	–	10	18000	992	AAC
16.75	123	34	–	–	–	40	2	19	58	345	78	283	–	165	3513	BOC
16.75	107	48	12	8	–	38	0	19	–	335	45	345	53	108	–	MUN
20.00	64	30	15	–	–	38	–	12	49	–	82	–	10	90	1403	AAC
22.50	24	30	15	–	–	39	–	12	37	–	46	–	43	89	1317	AAC
22.65	33	81	13	5	6	29	2	16	–	292	60	323	38	91	1306	MUN
24.05	24	128	12	4	0	30	2	8	–	212	62	290	0	57	1271	MUN
24.05	30	84	–	–	–	36	2	8	38	229	93	220	–	143	1771	BOC
24.05	–	–	–	–	–	–	–	–	42	191	66	230	3	100	1660	NEW
25.55	18	87	16	–	–	37	–	13	47	–	57	–	20	254	5978	AAC
29.00	36	86	20	–	–	38	–	11	32	–	52	–	10	20	128	AAC
35.35	55	27	–	–	–	33	3	15	46	158	61	224	–	51	237	BOC
35.35	50	54	12	4	–	32	3	15	–	189	34	325	4	0	–	MUN
38.05	49	171	9	12	–	38	2	5	–	198	45	314	13	197	–	MUN
38.40	11	86	17	–	–	36	–	11	30	–	40	–	10	91	238	AAC
46.10	14	46	16	–	–	39	–	13	31	–	45	–	10	23	334	AAC
46.30	10	30	16	–	–	37	–	11	19	–	44	–	10	91	501	AAC
47.95	31	171	20	–	–	38	–	11	33	–	47	–	10	20	300	AAC
48.30	45	261	19	–	–	36	–	12	48	–	41	–	10	73	179	AAC
50.10	20	90	14	3	2	28	1	17	–	215	45	286	5	323	465	MUN
50.10	24	54	–	–	–	34	2	13	42	211	74	205	–	657	558	BOC
50.10	–	–	–	–	–	–	–	–	41	190	53	210	3	660	500	NEW
51.05	39	76	–	–	–	31	2	12	35	190	64	190	–	67	209	BOC
51.05	36	132	11	0	–	27	2	12	–	208	28	293	5	26	–	MUN
53.45	63	117	31	–	–	44	–	12	42	–	31	–	10	20	196	AAC
54.30	112	30	18	–	–	81	–	29	28	–	20	–	10	20	326	AAC
55.65	102	30	23	–	–	84	–	31	26	–	20	–	10	20	286	AAC
58.25	51	132	17	21	25	62	3	35	–	0	4	447	1	724	292	MUN
58.25	61	99	–	–	–	67	3	29	49	110	26	338	–	1331	323	BOC
64.70	41	38	19	–	–	73	–	23	28	–	20	–	10	442	280	AAC
66.50	62	61	–	–	–	65	2	27	25	18	26	312	–	1507	230	BOC
66.50	–	–	–	–	–	–	–	–	27	6	18	310	3	1230	200	NEW
66.50	52	79	14	7	–	61	3	33	–	0	6	438	10	687	–	MUN
70.65	83	86	15	13	18	70	3	37	–	0	7	410	0	55	84	MUN
70.65	95	69	–	–	–	78	2	33	36	13	23	376	–	92	113	BOC
73.80	95	30	20	–	–	91	–	31	29	–	20	–	10	68	107	AAC
75.00	97	30	19	–	–	87	–	30	32	–	20	–	10	82	90	AAC
75.62	87	106	14	12	22	73	1	39	–	0	1	420	0	45	77	MUN
75.65	84	30	20	–	–	85	–	30	28	–	20	–	10	66	118	AAC
76.45	77	98	17	9	20	74	2	41	–	0	6	425	3	66	106	MUN
76.45	–	–	–	–	–	–	–	–	30	6	11	330	7	89	135	NEW
78.60	72	111	14	9	27	71	1	38	–	0	7	472	0	66	390	MUN
78.60	81	76	–	–	–	79	2	35	33	7	22	394	–	103	505	BOC
79.87	88	103	13	12	20	71	4	38	–	0	10	458	0	51	76	MUN
80.10	91	35	21	–	–	83	–	30	33	–	20	–	10	87	101	AAC

Depth	Sr	Ba	Ga	La	Ce	Zr	Nb	Y	Co	Cr	Ni	V	Pb	Cu	Zn	Lab
80.25	88	36	19	–	–	82	–	30	30	–	20	–	10	66	128	AAC
83.40	87	103	18	13	26	71	2	39	–	0	10	420	0	57	73	MUN
83.40	–	–	–	–	–	–	–	–	30	7	11	340	3	74	101	NEW
83.55	91	40	20	–	–	84	–	30	29	–	20	–	10	79	97	AAC
84.05	52	110	13	5	–	74	2	42	–	0	7	446	28	43	–	MUN
84.50	57	113	–	–	–	81	3	36	27	17	25	341	–	99	1463	BOC
85.60	58	84	18	–	–	80	–	30	22	–	20	–	13	22	656	AAC
86.70	84	144	11	4	9	41	–	23	–	0	5	333	1	7	156	MUN
86.70	93	65	–	–	–	48	2	21	21	18	19	232	–	95	184	BOC
88.50	81	97	18	–	–	71	–	27	28	–	20	–	10	32	98	AAC
90.25	112	45	18	–	–	86	–	32	25	–	20	–	10	21	106	AAC
90.80	76	109	13	6	22	72	2	37	–	0	7	470	3	43	189	MUN
90.80	–	–	–	–	–	–	–	–	24	15	13	370	14	81	230	NEW
92.75	112	258	16	4	5	59	2	35	–	0	13	352	0	20	120	MUN
92.75	119	196	–	–	–	60	3	29	18	23	24	231	–	58	152	BOC
93.90	76	164	15	6	14	53	3	34	–	4	10	360	3	40	98	MUN
94.40	67	52	18	–	–	64	–	27	27	–	20	–	13	58	145	AAC
94.75	78	65	17	–	–	67	–	27	28	–	20	–	10	49	124	AAC
95.60	65	74	18	–	–	70	–	24	24	–	20	–	10	49	525	AAC
96.75	–	–	–	–	–	–	–	–	33	176	55	210	3	15	280	NEW
96.75	11	98	9	0	–	30	4	18	–	216	51	343	13	0	–	MUN
97.30	69	123	16	13	5	55	3	31	–	0	9	347	1	21	141	MUN
97.30	78	80	–	–	–	62	3	27	25	23	32	281	–	287	180	BOC
97.35	58	112	15	6	12	54	2	28	–	0	4	327	3	58	2070	MUN
97.35	66	79	–	–	–	55	2	22	25	17	27	246	–	153	3053	BOC
100.90	113	30	18	–	–	79	–	27	30	–	20	–	16	85	161	AAC
103.83	124	30	21	–	–	71	–	32	20	–	20	–	10	22	110	AAC
103.85	116	79	15	13	14	54	–	29	–	0	13	341	0	38	81	MUN
103.85	–	–	–	–	–	–	–	–	27	13	19	260	7	46	99	NEW
105.35	134	229	–	–	–	63	3	28	31	13	30	281	–	82	125	BOC
105.35	119	141	14	4	–	59	1	34	–	0	15	334	12	36	–	MUN
105.65	116	30	20	–	–	69	–	22	32	–	20	–	10	95	110	AAC
107.00	117	96	12	10	18	58	3	34	–	0	12	343	3	44	86	MUN
109.00	116	106	20	–	–	68	–	29	34	–	20	–	10	101	135	AAC
110.40	104	30	21	–	–	87	–	39	25	–	20	–	10	52	116	AAC
110.75	–	–	–	–	–	–	–	–	23	14	5	210	7	36	125	NEW
110.75	95	40	14	11	–	73	2	46	–	0	0	300	6	19	–	MUN
113.30	92	30	20	–	–	67	–	29	20	–	20	–	10	67	122	AAC
113.35	87	62	15	8	21	61	3	41	–	0	–	277	0	53	85	MUN
113.35	99	45	–	–	–	65	2	32	26	16	15	246	–	77	115	BOC
115.35	56	30	15	–	–	71	–	24	20	–	20	–	10	37	87	AAC
117.45	72	30	15	–	–	63	–	26	20	–	20	–	10	20	77	AAC
117.45	103	43	16	8	–	76	3	39	–	0	5	223	9	16	–	MUN
118.70	100	74	17	10	15	78	3	43	–	0	3	261	4	43	97	MUN
118.70	–	–	–	–	–	–	–	–	34	14	11	200	3	52	117	NEW
119.35	101	42	–	–	–	70	2	33	40	19	31	254	–	97	109	BOC
119.65	84	30	17	–	–	79	–	28	20	–	20	–	10	21	95	AAC
119.75	92	102	14	4	9	64	1	40	–	1	12	305	1	52	80	MUN
119.95	89	30	20	–	–	74	–	31	20	–	20	–	10	28	91	AAC
119.95	90	34	13	5	–	65	2	39	–	3	9	328	0	18	–	MUN
120.00	92	30	20	–	–	76	–	30	20	–	20	–	10	20	104	AAC
121.65	102	30	21	–	–	84	–	37	31	–	20	–	10	59	123	AAC
122.10	–	–	–	–	–	–	–	–	26	14	13	210	3	45	102	NEW
122.10	87	35	12	2	–	69	3	46	–	0	7	239	7	23	–	MUN
122.40	106	131	–	–	–	75	2	34	22	17	18	190	–	47	116	BOC

Depth	Sr	Ba	Ga	La	Ce	Zr	Nb	Y	Co	Cr	Ni	V	Pb	Cu	Zn	Lab
122.40	96	43	14	5	–	88	3	46	–	0	0	141	3	22	–	MUN
124.50	101	30	19	–	–	94	–	33	25	–	20	–	10	42	88	AAC
124.70	97	46	16	6	–	85	0	47	–	0	1	140	7	21	–	MUN
125.55	80	78	17	10	16	68	–	40	–	0	4	179	2	22	85	MUN
125.55	–	–	–	–	–	–	–	–	15	14	10	160	7	22	102	NEW
126.80	112	30	24	–	–	97	–	51	20	–	20	–	10	51	134	AAC
127.55	79	787	11	7	8	47	3	31	–	0	5	165	0	45	73	MUN
127.55	94	990	–	–	–	50	3	27	17	25	16	137	–	120	88	BOC
129.15	79	256	14	–	–	56	–	27	20	–	20	–	10	20	65	AAC
130.05	112	107	14	8	19	56	2	36	–	0	17	348	0	52	82	MUN
130.90	–	–	–	–	–	–	–	–	27	9	10	340	3	78	106	NEW
131.95	104	624	18	–	–	65	–	25	27	–	20	–	10	67	112	AAC
132.65	97	30	21	–	–	70	–	30	25	–	20	–	10	116	109	AAC
132.75	39	30	14	2	–	57	0	39	–	0	5	398	4	49	–	MUN
133.75	107	58	–	–	–	64	2	34	46	18	22	329	–	84	133	BOC
135.00	98	156	11	5	–	65	2	46	–	0	0	180	10	26	–	MUN
135.15	81	65	16	8	17	36	–	19	–	34	31	320	0	38	67	MUN
135.15	–	–	–	–	–	–	–	–	36	87	38	410	3	46	80	NEW
135.45	82	30	15	–	–	62	–	15	20	–	20	–	10	20	56	AAC
137.35	97	30	18	–	–	85	–	32	21	–	20	–	10	51	110	AAC
137.40	81	80	16	–	–	53	–	25	20	–	20	–	10	35	78	AAC
137.84	89	30	19	–	–	75	–	31	20	–	20	–	10	65	76	AAC
138.15	116	87	–	–	–	79	2	54	45	12	21	177	–	256	138	BOC
138.15	99	36	13	0	–	75	2	59	–	0	2	207	3	32	–	MUN
140.32	95	93	20	–	–	71	–	27	26	–	20	–	10	90	108	AAC
140.93	99	30	20	–	–	71	–	28	28	–	20	–	10	134	118	AAC
142.20	95	48	10	3	–	64	1	38	–	0	3	346	5	50	–	MUN
143.25	82	77	14	7	13	48	3	28	–	0	8	398	0	63	85	MUN
143.25	–	–	–	–	–	–	–	–	28	9	15	330	3	73	101	NEW
143.90	83	30	18	–	–	59	–	24	26	–	20	–	10	51	103	AAC
144.70	81	30	17	–	–	57	–	20	22	–	20	–	10	25	88	AAC
145.90	79	89	15	3	17	50	1	31	–	0	6	345	3	20	80	MUN
145.90	86	72	–	–	–	52	2	23	23	11	20	316	–	62	111	BOC
146.65	84	173	15	12	20	50	1	39	–	0	9	470	4	54	93	MUN
146.65	94	258	–	–	–	51	1	29	29	14	25	399	–	90	123	BOC
147.40	77	30	18	–	–	57	–	25	23	–	20	–	10	55	86	AAC
150.05	84	30	19	–	–	61	–	22	28	–	20	–	10	111	98	AAC
150.35	83	83	17	5	9	49	3	34	–	0	16	455	0	96	80	MUN
150.35	90	50	–	–	–	52	2	25	30	15	30	401	–	120	114	BOC
150.35	–	–	–	–	–	–	–	–	31	9	16	370	3	111	106	NEW
151.90	118	30	22	–	–	64	–	33	29	–	20	–	10	59	125	AAC
152.92	65	30	13	–	–	58	–	15	27	–	20	–	10	94	77	AAC
154.00	52	180	11	9	14	41	2	27	–	0	6	345	2	46	62	MUN
154.00	66	164	–	–	–	50	2	26	29	15	21	294	–	134	92	BOC
155.85	91	30	20	–	–	62	–	28	26	–	20	–	10	71	107	AAC
156.30	83	30	19	–	–	60	–	25	31	–	20	–	10	40	97	AAC
158.65	101	30	20	–	–	85	–	40	20	–	20	–	10	33	105	AAC
158.80	97	23	13	0	–	71	2	47	–	0	0	142	0	20	–	MUN
160.10	91	30	18	–	–	80	–	31	20	–	20	–	10	31	90	AAC
163.25	99	87	18	12	21	71	3	49	–	0	–	225	0	37	93	MUN
163.25	–	–	–	–	–	–	–	–	22	9	7	210	7	44	115	NEW
163.75	91	30	17	–	–	74	–	31	20	–	20	–	10	21	85	AAC
164.65	98	70	17	13	23	68	2	43	–	0	0	218	0	42	86	MUN
164.65	110	64	–	–	–	74	3	38	26	15	14	189	–	64	122	BOC
165.05	82	30	17	–	–	71	–	29	20	–	20	–	10	20	85	AAC

Depth	Sr	Ba	Ga	La	Ce	Zr	Nb	Y	Co	Cr	Ni	V	Pb	Cu	Zn	Lab
167.80	91	30	19	–	–	66	–	25	26	–	20	–	10	135	114	AAC
169.05	85	86	15	6	17	62	2	36	–	0	2	381	0	66	98	MUN
169.45	86	101	18	10	15	57	0	33	–	0	3	376	0	47	78	MUN
169.45	–	–	–	–	–	–	–	–	29	7	11	310	3	62	106	NEW
170.10	77	30	17	–	–	61	–	22	20	–	20	–	10	31	77	AAC
171.05	79	30	16	–	–	63	–	24	20	–	20	–	10	20	88	AAC
174.55	82	73	13	9	15	57	4	33	–	0	0	301	4	13	57	MUN
174.55	89	56	–	–	–	60	3	29	20	15	16	283	–	75	84	BOC
175.00	80	30	15	–	–	61	–	25	20	–	20	–	10	20	63	AAC
176.80	101	30	18	–	–	92	–	39	20	–	20	–	10	30	115	AAC
178.60	94	30	20	–	–	93	–	34	20	–	20	–	10	37	103	AAC
179.55	102	75	16	1	17	81	2	50	–	0	–	101	0	27	87	MUN
180.05	108	32	19	–	–	90	–	40	20	–	20	–	10	55	112	AAC
180.55	100	87	18	6	24	87	4	51	–	0	0	90	2	32	88	MUN
180.55	–	–	–	–	–	–	–	–	12	4	3	80	3	28	117	NEW
181.95	106	30	21	–	–	92	–	36	20	–	20	–	10	28	110	AAC
183.75	85	92	15	12	12	71	2	40	–	0	0	128	3	16	79	MUN
183.75	98	75	–	–	–	77	2	35	22	11	14	114	–	19	115	BOC
184.40	98	30	21	–	–	87	–	34	24	–	20	–	10	26	113	AAC
186.00	96	30	19	–	–	85	–	35	20	–	20	–	10	25	109	AAC
188.20	84	69	15	12	21	71	1	45	–	0	0	138	0	11	76	MUN
189.40	103	96	20	11	19	95	2	55	–	0	0	51	0	26	91	MUN
189.40	–	–	–	–	–	–	–	–	14	4	10	70	3	36	114	NEW
191.15	102	30	20	–	–	100	–	45	20	–	20	–	10	23	107	AAC
193.30	100	109	15	7	15	66	1	36	–	0	0	303	0	33	92	MUN
193.30	114	121	–	–	–	73	2	34	31	13	12	263	–	50	120	BOC
195.40	100	30	20	–	–	77	–	33	30	–	20	–	10	76	122	AAC
196.15	83	30	17	–	–	70	–	29	20	–	20	–	10	26	86	AAC
196.50	80	74	16	14	16	61	1	36	–	0	0	283	0	22	76	MUN
198.75	99	30	20	–	–	75	–	32	28	–	20	–	10	50	99	AAC
200.65	94	69	21	–	–	66	–	217	39	–	20	–	10	108	98	AAC
201.05	86	102	14	8	18	62	2	38	–	0	17	453	0	54	93	MUN
201.05	–	–	–	–	–	–	–	–	49	8	20	370	3	74	119	NEW
201.85	92	30	21	–	–	70	–	33	40	–	20	–	10	123	124	AAC
202.70	100	30	21	–	–	73	–	31	38	–	20	–	10	102	114	AAC
206.60	89	85	19	15	19	57	2	34	–	0	10	487	0	54	94	MUN
206.60	103	48	–	–	–	63	3	32	41	18	29	419	–	78	126	BOC
207.15	94	30	21	–	–	70	–	28	36	–	20	–	10	98	107	AAC
211.00	89	65	15	9	25	61	3	38	–	0	8	488	1	52	89	MUN
211.00	91	30	19	–	–	68	–	30	38	–	20	–	10	75	109	AAC
213.65	79	30	16	–	–	63	–	26	20	–	20	–	10	20	82	AAC
214.10	82	91	17	12	11	54	1	34	–	0	0	325	0	34	79	MUN
214.10	–	–	–	–	–	–	–	–	19	11	7	270	3	34	100	NEW
214.40	81	30	18	–	–	64	–	26	20	–	20	–	10	20	83	AAC
214.50	74	74	13	11	17	56	1	34	–	0	0	246	0	16	63	MUN
214.50	84	54	–	–	–	58	2	29	17	26	14	238	–	107	92	BOC
218.15	95	30	19	–	–	128	–	51	20	–	20	–	10	20	107	AAC
218.90	175	30	19	–	–	65	–	29	24	–	20	–	10	72	96	AAC
221.30	116	31	–	–	–	63	3	33	36	12	28	417	–	48	123	BOC
221.30	111	28	15	5	–	65	3	41	–	0	12	485	0	26	–	MUN
223.80	117	99	15	8	19	64	1	46	–	0	6	418	0	36	102	MUN
223.80	131	69	–	–	–	64	3	39	31	13	23	377	–	85	130	BOC
223.80	–	–	–	–	–	–	–	–	26	9	10	440	3	46	125	NEW
223.85	102	30	22	–	–	75	–	30	34	–	20	–	10	65	134	AAC
226.15	99	30	21	–	–	73	–	29	30	–	20	–	10	60	119	AAC

Depth	Sr	Ba	Ga	La	Ce	Zr	Nb	Y	Co	Cr	Ni	V	Pb	Cu	Zn	Lab
								CY-2a								
4.40	–	–	–	–	–	–	–	–	38	32	25	250	3	183	202	NEW
4.40	80	76	13	10	–	34	2	18	–	18	19	290	0	116	–	MUN
7.60	80	32	14	–	–	40	–	13	55	–	41	–	10	27	156	AAC
8.35	71	39	14	–	–	40	–	14	38	–	33	–	10	29	94	AAC
9.70	83	76	9	12	12	32	3	17	–	105	40	275	6	23	88	MUN
9.70	90	19	–	–	–	32	2	11	39	152	61	227	–	45	110	BOC
11.05	101	30	16	–	–	47	–	18	43	–	32	–	10	126	105	AAC
11.80	90	68	15	14	7	31	0	13	–	72	39	272	0	69	93	MUN
11.80	104	34	–	–	–	34	1	14	36	154	62	218	–	137	127	BOC
12.95	90	30	15	–	–	38	–	12	38	–	42	–	10	116	91	AAC
15.00	88	30	14	–	–	37	–	12	35	–	49	–	10	71	74	AAC
17.35	82	30	14	–	–	35	–	13	39	–	47	–	10	20	98	AAC
19.30	88	73	15	2	14	30	1	13	–	124	46	294	–	66	54	MUN
19.30	–	–	–	–	–	–	–	–	36	241	51	250	3	82	74	NEW
19.65	92	30	14	–	–	40	–	12	37	–	53	–	10	68	68	AAC
21.00	92	30	14	–	–	39	–	12	35	–	46	–	10	53	70	AAC
21.50	95	72	12	5	3	29	3	12	–	109	45	310	1	62	52	MUN
21.50	106	33	–	–	–	30	2	12	31	213	68	245	–	99	72	BOC
22.80	93	30	14	–	–	39	–	13	33	–	48	–	10	70	62	AAC
24.38	90	30	14	–	–	37	–	12	35	–	56	–	10	20	74	AAC
25.85	84	74	10	8	9	26	2	18	–	163	107	214	0	41	79	MUN
28.66	65	30	11	–	–	32	–	11	52	–	325	–	10	54	59	AAC
30.10	81	76	11	12	13	33	1	13	–	180	137	166	0	17	58	MUN
30.10	93	27	–	–	–	34	2	12	36	337	173	176	–	204	86	BOC
30.10	–	–	–	–	–	–	–	–	38	181	128	210	3	23	79	NEW
30.55	74	30	14	–	–	38	–	18	25	–	55	–	10	20	69	AAC
31.18	82	30	14	–	–	37	–	13	45	–	47	–	10	72	203	AAC
31.45	93	30	17	–	–	74	–	28	38	–	23	–	10	42	94	AAC
33.10	100	38	–	–	–	66	2	28	36	14	37	343	–	98	103	BOC
33.10	88	43	13	9	–	57	1	29	–	0	17	384	11	26	–	MUN
33.40	60	30	10	–	–	26	–	15	39	–	198	–	10	32	206	AAC
35.80	90	30	20	–	–	86	–	32	32	–	20	–	10	23	86	AAC
40.75	111	69	–	–	–	82	3	36	35	8	38	395	–	76	123	BOC
40.75	97	46	16	12	–	75	1	43	–	0	21	462	0	46	–	MUN
42.15	98	107	17	17	22	76	2	42	–	0	20	420	0	39	94	MUN
42.15	–	–	–	–	–	–	–	–	30	4	20	440	3	47	115	NEW
44.05	111	44	–	–	–	81	3	38	34	10	33	381	–	824	121	BOC
44.05	98	38	14	12	–	74	4	46	–	0	15	452	7	18	–	MUN
44.45	100	30	20	–	–	87	–	38	32	–	24	–	10	42	109	AAC
49.45	95	30	20	–	–	90	–	35	41	–	23	–	10	36	105	AAC
49.55	85	45	15	4	–	74	2	43	–	0	14	426	0	21	–	MUN
53.80	86	30	20	–	–	92	–	36	40	–	26	–	10	40	117	AAC
54.70	83	62	16	–	–	44	–	23	34	–	42	–	10	33	85	AAC
55.45	–	–	–	–	–	–	–	–	31	101	38	240	3	38	92	NEW
57.50	77	30	15	–	–	43	–	10	37	–	45	–	10	48	82	AAC
58.75	89	92	14	14	8	33	–	18	–	77	26	272	0	46	62	MUN
58.75	101	43	–	–	–	38	2	14	31	86	52	234	–	123	87	BOC
59.40	87	30	15	–	–	41	–	16	34	–	45	–	10	69	82	AAC
61.65	88	52	16	–	–	40	–	23	30	–	30	–	10	50	72	AAC
63.15	82	89	10	11	12	37	2	15	–	75	39	280	0	43	72	MUN
65.10	81	54	12	9	8	37	2	22	–	113	52	208	0	12	41	MUN
65.10	–	–	–	–	–	–	–	–	31	262	61	190	3	14	58	NEW
65.85	92	78	15	15	5	36	3	18	–	71	30	253	2	33	72	MUN

Depth	Sr	Ba	Ga	La	Ce	Zr	Nb	Y	Co	Cr	Ni	V	Pb	Cu	Zn	Lab
65.85	99	18	–	–	–	38	2	17	32	106	55	229	–	97	113	BOC
69.05	87	30	14	–	–	47	–	19	29	–	55	–	10	20	61	AAC
70.35	88	30	15	–	–	48	–	18	33	–	79	–	10	267	55	AAC
72.55	94	64	14	9	11	41	3	18	–	160	63	247	0	79	48	MUN
73.35	91	30	15	–	–	52	–	21	39	–	63	–	10	84	58	AAC
74.35	91	30	17	–	–	53	–	15	31	–	66	–	10	71	60	AAC
75.80	86	55	14	9	9	38	3	19	–	128	56	216	0	23	41	MUN
75.80	–	–	–	–	–	–	–	–	31	236	66	200	3	26	51	NEW
75.95	88	30	15	–	–	48	–	16	31	–	61	–	10	26	46	AAC
78.25	91	76	13	14	12	45	2	21	–	96	43	258	0	23	44	MUN
78.25	104	29	–	–	–	48	3	19	29	158	79	240	–	30	65	BOC
78.50	82	30	14	–	–	46	–	17	32	–	64	–	10	21	53	AAC
80.25	88	35	15	–	–	46	–	17	33	–	65	–	10	74	60	AAC
81.15	85	30	15	–	–	46	–	18	33	–	65	–	10	29	61	AAC
81.45	89	63	14	16	13	40	3	19	–	125	63	221	2	24	46	MUN
84.30	87	30	15	–	–	47	–	17	33	–	67	–	10	20	52	AAC
86.30	88	87	12	14	10	44	2	20	–	127	60	216	0	25	47	MUN
86.30	–	–	–	–	–	–	–	–	31	260	67	240	3	31	51	NEW
87.20	88	30	15	–	–	44	–	18	32	–	61	–	10	23	53	AAC
88.70	88	82	12	21	14	40	4	23	–	138	60	226	0	20	46	MUN
88.70	100	20	–	–	–	43	3	17	33	215	96	215	–	45	72	BOC
90.10	90	30	16	–	–	46	–	28	26	–	44	–	10	37	69	AAC
97.00	76	139	13	13	15	54	0	33	–	0	17	279	4	29	85	MUN
99.05	71	64	18	–	–	68	–	24	39	–	22	–	10	28	101	AAC
99.50	83	118	–	–	–	63	3	25	37	14	35	264	–	46	113	BOC
99.50	–	–	–	–	–	–	–	–	34	13	16	280	3	35	105	NEW
99.50	72	106	11	10	–	57	3	32	–	0	14	299	1	23	–	MUN
103.70	88	112	17	12	18	60	1	33	–	3	20	384	3	63	98	MUN
111.40	102	69	–	–	–	78	3	52	24	15	21	211	–	46	119	BOC
111.40	86	14	16	5	–	69	1	58	–	0	4	234	6	14	–	MUN
111.95	93	30	20	–	–	80	–	43	36	–	20	–	10	43	134	AAC
117.85	88	92	18	19	19	64	3	45	–	0	11	314	0	57	136	MUN
117.85	108	36	–	–	–	87	3	40	4	18	21	177	–	66	142	BOC
121.00	56	30	19	–	–	79	–	18	20	–	20	–	10	30	111	AAC
130.60	102	44	–	–	–	68	2	40	30	18	28	274	–	153	187	BOC
130.60	–	–	–	–	–	–	–	–	30	14	11	240	3	67	164	NEW
138.75	84	30	17	–	–	74	–	34	23	–	20	–	10	35	136	AAC
138.95	77	88	17	17	18	63	2	39	–	0	0	160	0	15	127	MUN
138.95	90	56	–	–	–	68	4	33	14	15	14	135	–	83	169	BOC
141.85	110	58	–	–	–	77	2	46	28	12	16	158	–	57	272	BOC
141.85	92	31	16	5	–	70	3	54	–	0	2	185	10	35	–	MUN
143.10	95	77	13	5	23	72	2	44	–	0	4	219	0	48	151	MUN
143.10	111	54	–	–	–	74	2	39	25	12	15	188	–	62	202	BOC
143.10	–	–	–	–	–	–	–	–	27	8	5	180	4	54	185	NEW
143.15	61	30	12	–	–	34	–	13	20	–	20	–	10	20	90	AAC
143.20	98	30	21	–	–	81	–	33	26	–	20	–	10	44	199	AAC
145.40	94	30	19	–	–	82	–	37	20	–	20	–	10	33	235	AAC
149.50	89	49	–	–	–	59	3	19	28	12	29	446	–	163	252	BOC
149.50	72	36	10	4	–	50	2	20	–	0	7	523	21	97	–	MUN
152.25	86	81	15	12	16	51	3	33	–	0	11	516	1	91	191	MUN
152.25	99	52	–	–	–	56	3	30	25	16	26	439	–	150	235	BOC
153.60	109	254	17	–	–	61	–	29	44	–	412	–	55	74	339	AAC
154.40	130	912	16	–	–	57	–	28	39	–	20	–	260	134	2832	AAC
156.65	87	162	19	–	–	56	–	27	34	–	20	–	74	45	282	AAC
157.40	61	47	–	–	–	53	2	29	36	9	31	387	–	95	2548	BOC

Depth	Sr	Ba	Ga	La	Ce	Zr	Nb	Y	Co	Cr	Ni	V	Pb	Cu	Zn	Lab
157.40	58	97	16	5	23	48	2	36	–	0	6	511	76	70	1510	MUN
157.40	–	–	–	–	–	–	–	–	35	8	15	390	100	114	2360	NEW
157.84	65	30	19	–	–	60	–	26	30	–	21	–	221	226	5445	AAC
157.90	68	39	22	8	–	47	3	32	–	0	12	476	16	63	–	MUN
158.90	78	58	–	–	–	51	3	28	25	14	29	369	–	111	160	BOC
159.30	38	173	22	8	–	50	3	30	–	0	5	450	43	189	–	MUN
159.66	20	30	10	–	–	21	–	10	24	–	36	–	10	2605	10000	AAC
160.45	21	237	14	6	18	48	1	29	–	0	6	412	21	68	743	MUN
160.45	25	176	–	–	–	57	2	29	32	16	19	300	–	297	1128	BOC
160.45	–	–	–	–	–	–	–	–	28	12	7	400	29	100	940	NEW
161.00	57	30	19	–	–	76	–	32	24	–	20	–	57	204	5140	AAC
162.20	13	447	–	–	–	64	3	28	28	19	14	271	–	42	386	BOC
162.20	47	119	14	0	–	66	3	41	–	0	0	227	93	103	–	MUN
163.05	79	64	20	–	–	85	–	36	26	–	20	–	53	607	4407	AAC
165.40	9	138	–	–	–	77	2	37	25	15	10	199	–	975	2071	BOC
165.40	–	–	–	–	–	–	–	–	25	5	1	240	54	1390	1880	NEW
165.40	45	140	21	6	–	74	5	45	–	0	0	290	68	778	–	MUN
166.42	10	30	10	–	–	24	–	11	26	–	20	–	10	15000	8540	AAC
167.75	10	163	23	–	–	66	–	26	30	–	20	–	46	696	1364	AAC
168.50	11	147	–	–	–	70	2	32	30	20	17	257	–	699	589	BOC
168.50	8	170	12	7	–	56	1	39	–	5	1	367	7	300	–	MUN
168.72	10	131	25	–	–	79	–	33	25	–	20	–	11	114	421	AAC
170.30	9	436	18	19	20	59	3	33	–	0	0	145	19	839	320	MUN
171.05	20	30	10	–	–	22	–	10	20	–	20	–	125	574	17000	AAC
174.20	7	157	–	–	–	74	2	34	18	17	15	138	–	806	648	BOC
174.20	–	–	–	–	–	–	–	–	20	14	1	140	3	900	610	NEW
174.20	6	171	14	2	–	67	3	40	–	0	0	197	12	480	–	MUN
174.60	20	133	19	–	–	82	–	35	20	–	20	–	10	278	325	AAC
174.75	11	143	19	–	–	76	–	33	23	–	20	–	10	437	345	AAC
175.50	10	121	27	–	–	84	–	37	20	–	20	–	10	27	358	AAC
176.00	18	311	–	–	–	65	3	30	18	19	14	98	–	105	271	BOC
176.00	17	404	13	3	–	68	4	40	–	0	2	136	19	21	–	MUN
177.30	13	241	18	–	–	86	–	34	20	–	20	–	10	109	450	AAC
178.00	12	628	10	8	–	85	6	53	–	0	2	231	8	25	–	MUN
178.30	11	502	–	–	–	83	3	43	26	15	12	190	–	222	112	BOC
180.06	15	991	28	–	–	115	–	52	30	–	20	–	24	27	1467	AAC
180.55	12	196	19	–	–	95	–	42	20	–	20	–	10	34	218	AAC
181.15	13	402	19	16	21	84	2	47	–	0	0	69	1	14	104	MUN
181.15	16	286	–	–	–	91	3	43	15	19	10	54	–	292	146	BOC
181.15	–	–	–	–	–	–	–	–	13	15	1	70	3	26	122	NEW
182.25	10	238	18	–	–	74	–	31	21	–	20	–	10	20	105	AAC
183.40	5	205	–	–	–	20	3	8	42	27	23	48	–	192	343	BOC
183.40	7	423	0	25	11	33	5	1	–	16	0	94	44	12	271	MUN
185.50	10	201	10	–	–	20	–	10	47	–	26	–	72	83	374	AAC
185.70	10	74	10	–	–	20	–	10	50	–	31	–	86	89	550	AAC
186.25	10	530	10	–	–	49	–	13	53	–	34	–	69	138	176	AAC
186.30	19	746	27	–	–	98	–	41	22	–	20	–	17	32	118	AAC
186.90	16	279	–	–	–	83	3	38	19	19	11	119	–	216	238	BOC
186.90	14	370	16	0	–	74	4	44	–	0	0	163	4	111	–	MUN
189.85	13	436	–	–	–	55	2	26	23	31	19	188	–	241	101	BOC
189.85	–	–	–	–	–	–	–	–	25	27	5	210	3	30	83	NEW
189.85	17	833	22	–	–	74	–	33	38	–	24	–	12	121	105	AAC
189.95	11	678	14	4	–	57	2	35	–	11	0	260	10	10	–	MUN
191.90	10	33	10	–	–	20	–	10	39	–	30	–	50	225	4576	AAC
192.30	11	322	21	–	–	70	–	29	22	–	20	–	10	20	120	AAC

Depth	Sr	Ba	Ga	La	Ce	Zr	Nb	Y	Co	Cr	Ni	V	Pb	Cu	Zn	Lab
192.95	5	72	–	–	–	7	1	5	41	33	22	11	–	216	2191	BOC
192.95	1	187	0	15	0	12	9	0	–	11	0	30	6	196	1800	MUN
192.95	10	392	10	–	–	25	–	10	35	–	28	–	55	144	3866	AAC
194.25	15	1442	29	–	–	73	–	32	48	–	20	–	11	45	311	AAC
197.00	15	289	–	–	–	68	2	32	24	18	17	294	–	20	216	BOC
197.00	12	432	18	5	–	61	2	38	–	0	2	427	1	4	–	MUN
199.20	10	493	–	–	–	59	3	27	22	22	17	261	–	272	293	BOC
199.20	–	–	–	–	–	–	–	–	26	12	7	290	3	58	260	NEW
199.20	10	700	17	2	–	59	4	33	–	1	1	365	14	28	–	MUN
200.90	13	808	20	–	–	58	–	24	33	–	20	–	26	46	320	AAC
202.70	11	276	22	–	–	68	–	30	26	–	20	–	10	20	255	AAC
212.70	10	439	10	–	–	30	–	10	27	–	20	–	65	116	720	AAC
214.70	9	149	–	–	–	67	2	31	24	16	11	236	–	37	240	BOC
214.70	14	645	16	8	–	69	1	32	–	0	0	405	12	7	–	MUN
215.50	13	1124	16	–	–	60	–	27	38	–	20	–	12	463	2651	AAC
216.33	15	674	19	–	–	76	–	30	22	–	20	–	14	24	107	AAC
218.00	6	237	19	16	22	64	3	3	–	0	1	332	3	14	211	MUN
218.00	56	130	–	–	–	74	3	34	21	16	18	170	–	346	7467	BOC
219.40	12	1005	13	23	23	60	8	33	–	0	6	272	13	62	574	MUN
219.40	–	–	–	–	–	–	–	–	38	8	2	240	3	46	490	NEW
220.30	17	425	19	–	–	78	–	31	20	–	20	–	10	20	245	AAC
221.00	20	708	16	4	–	69	1	35	–	0	0	304	10	3	–	MUN
223.10	10	634	16	–	–	55	–	20	25	–	20	–	10	265	295	AAC
223.90	16	1288	34	6	–	71	2	40	–	0	7	303	13	51	–	MUN
228.70	8	367	–	–	–	81	3	37	19	16	12	222	–	18	518	BOC
228.70	–	–	–	–	–	–	–	–	22	5	1	230	3	20	460	NEW
228.70	8	483	14	3	–	73	3	44	–	0	0	299	10	3	–	MUN
229.40	10	375	10	–	–	20	–	10	109	–	32	–	19	111	1181	AAC
237.00	9	513	20	23	23	58	–	31	–	0	0	448	1	49	963	MUN
238.26	28	620	–	–	–	77	2	33	43	9	18	383	–	55	407	BOC
238.26	–	–	–	–	–	–	–	–	45	7	7	360	3	38	420	NEW
238.26	27	819	11	3	–	72	3	40	–	0	0	512	13	14	–	MUN
241.80	12	478	–	–	–	62	3	28	37	24	11	291	–	26	179	BOC
241.80	8	682	15	8	–	58	1	33	–	8	0	431	0	5	–	MUN
241.83	12	576	17	–	–	66	–	29	21	–	20	–	10	20	129	AAC
243.00	18	1109	22	11	–	68	5	38	–	0	0	515	6	0	–	MUN
243.50	10	271	20	–	–	61	–	24	27	–	20	–	10	20	372	AAC
245.80	–	–	–	–	–	–	–	–	27	4	1	300	3	43	460	NEW
245.80	18	1256	18	11	–	90	5	47	–	0	1	403	4	19	–	MUN
246.00	12	597	17	–	–	70	–	29	20	–	20	–	10	20	623	AAC
247.60	11	1026	14	15	15	52	–	28	–	0	0	390	3	22	1407	MUN
247.60	13	688	–	–	–	56	2	24	36	19	17	280	–	35	1912	BOC
247.70	11	573	21	–	–	69	–	29	24	–	20	–	10	20	266	AAC
250.50	7	680	14	10	–	63	0	34	–	0	0	504	5	9	–	MUN
252.90	–	–	–	–	–	–	–	–	20	6	7	190	3	38	1730	NEW
252.90	10	770	11	1	–	66	2	37	–	0	2	267	8	6	–	MUN
253.30	26	34	–	–	–	63	2	33	19	25	27	271	–	57	3231	BOC
253.30	23	31	17	7	–	63	2	37	–	0	10	436	3	4	–	MUN
254.00	11	420	16	10	13	88	1	44	–	0	0	121	0	18	956	MUN
255.10	10	144	10	–	–	20	–	10	74	–	33	–	10	66	100	AAC
258.20	13	387	19	–	–	77	–	31	20	–	20	–	10	166	133	AAC
259.85	13	525	16	–	–	93	–	38	21	–	20	–	10	20	104	AAC
259.90	17	425	17	–	–	95	–	38	20	–	20	–	10	20	241	AAC
261.20	22	927	18	–	–	82	–	34	40	–	20	–	10	20	305	AAC
262.40	12	950	13	17	24	79	3	44	–	0	0	217	0	16	153	MUN

Depth	Sr	Ba	Ga	La	Ce	Zr	Nb	Y	Co	Cr	Ni	V	Pb	Cu	Zn	Lab
262.40	–	–	–	–	–	–	–	–	20	12	2	180	3	13	160	NEW
262.50	16	803	18	–	–	95	–	37	20	–	20	–	10	20	82	AAC
262.62	16	594	16	–	–	88	–	35	25	–	20	–	10	111	693	AAC
263.50	10	30	10	–	–	20	–	10	59	–	40	–	18	128	2746	AAC
268.00	12	1337	–	–	–	70	2	39	43	18	20	273	–	29	61	BOC
268.00	19	2105	11	16	–	88	2	49	–	0	0	375	12	0	–	MUN
268.24	10	183	10	–	–	20	–	10	114	–	31	–	10	75	174	AAC
268.50	23	482	16	–	–	88	–	37	20	–	20	–	10	20	76	AAC
269.44	16	590	19	–	–	84	–	34	24	–	20	–	10	20	139	AAC
270.20	15	1504	6	16	–	85	3	57	–	0	0	409	6	0	–	MUN
272.30	10	136	10	–	–	20	–	10	30	–	20	–	10	667	21000	AAC
273.65	11	430	18	7	16	83	3	45	–	0	4	248	0	28	856	MUN
273.65	–	–	–	–	–	–	–	–	23	8	5	240	3	28	1060	NEW
273.90	14	308	17	–	–	83	–	35	20	–	20	–	10	20	128	AAC
276.20	20	1077	12	–	–	53	–	19	54	–	22	–	16	20	74	AAC
277.01	12	958	14	–	–	56	–	30	56	–	20	–	10	20	111	AAC
277.80	9	262	–	–	–	67	1	29	35	16	21	344	–	18	176	BOC
277.80	3	415	21	17	20	61	–	33	–	0	10	475	0	14	151	MUN
278.00	15	270	18	–	–	75	–	29	22	–	20	–	10	20	150	AAC
278.50	11	324	21	–	–	69	–	27	21	–	20	–	10	20	178	AAC
281.65	64	30	12	–	–	35	–	13	35	–	40	–	10	58	108	AAC
282.10	73	30	–	–	–	33	2	11	39	146	61	247	–	98	144	BOC
282.74	20	487	19	–	–	83	–	33	20	–	20	–	10	20	269	AAC
283.50	8	1054	7	21	14	52	4	21	–	0	1	277	2	49	1245	MUN
285.30	36	182	–	–	–	67	1	34	21	19	12	132	–	47	1656	BOC
285.30	–	–	–	–	–	–	–	–	22	4	4	166	7	51	1730	NEW
285.70	41	58	17	–	–	74	–	32	20	–	20	–	10	35	1711	AAC
288.75	14	440	18	–	–	85	–	29	26	–	20	–	10	20	138	AAC
291.20	–	–	–	–	–	–	–	–	42	9	12	404	7	11	177	NEW
291.20	17	291	12	4	–	67	1	38	–	0	0	496	10	0	–	MUN
293.00	12	31	18	–	–	70	–	26	31	–	20	–	10	515	407	AAC
297.90	33	51	16	–	–	60	–	28	20	–	20	–	10	86	113	AAC
299.57	44	30	16	–	–	85	–	37	20	–	20	–	10	77	103	AAC
299.75	–	–	–	–	–	–	–	–	21	7	4	108	19	846	195	NEW
301.18	40	30	17	–	–	89	–	36	20	–	20	–	10	129	121	AAC
302.55	18	30	17	–	–	58	–	28	20	–	20	–	10	20	299	AAC
303.50	25	50	–	–	–	54	2	29	21	29	19	292	–	96	301	BOC
303.50	20	47	12	47	–	45	2	30	–	0	1	406	0	44	–	MUN
305.35	49	30	18	–	–	90	–	40	22	–	20	–	10	21	179	AAC
307.45	46	41	15	–	–	88	–	36	20	–	20	–	10	91	224	AAC
308.60	43	69	16	7	18	77	1	48	–	0	0	107	6	119	165	MUN
308.60	–	–	–	–	–	–	–	–	18	7	2	90	3	184	193	NEW
311.30	49	30	16	–	–	90	–	38	20	–	20	–	10	41	221	AAC
313.27	29	30	17	–	–	54	–	25	24	–	20	–	10	635	286	AAC
313.50	27	30	16	–	–	53	–	25	23	–	20	–	10	945	293	AAC
315.40	–	–	–	–	–	–	–	–	29	12	15	373	7	270	1110	NEW
315.50	30	30	18	–	–	60	–	21	21	–	20	–	10	186	240	AAC
319.20	27	46	19	–	–	69	–	32	20	–	20	–	10	20	164	AAC
319.30	34	38	–	–	–	63	2	34	26	18	14	231	–	167	748	BOC
323.20	35	30	19	–	–	90	–	41	20	–	20	–	10	27	127	AAC
325.00	97	30	13	–	–	64	–	23	20	–	20	–	10	20	23	AAC
326.00	–	–	–	–	–	–	–	–	19	6	5	105	15	86	500	NEW
327.00	48	30	20	–	–	71	–	28	43	–	20	–	10	43	204	AAC
328.90	54	64	–	–	–	64	2	29	41	21	23	335	–	55	186	BOC
330.30	41	30	18	–	–	72	–	33	35	–	20	–	10	39	163	AAC

Depth	Sr	Ba	Ga	La	Ce	Zr	Nb	Y	Co	Cr	Ni	V	Pb	Cu	Zn	Lab
331.20	52	30	14	–	–	75	–	33	20	–	20	–	10	58	825	AAC
338.25	42	30	18	–	–	63	–	27	32	–	20	–	10	35	111	AAC
339.45	44	30	18	–	–	68	–	28	30	–	20	–	10	30	205	AAC
341.75	57	30	18	–	–	73	–	27	22	–	20	–	10	340	675	AAC
341.85	–	–	–	–	–	–	–	–	25	5	4	200	25	31	610	NEW
343.80	60	30	16	–	–	79	–	33	20	–	20	–	11	41	646	AAC
344.75	91	36	17	–	–	73	–	25	39	–	20	–	10	33	114	AAC
346.50	74	95	–	–	–	55	1	29	39	27	23	466	–	70	154	BOC
346.50	–	–	–	–	–	–	–	–	37	14	15	520	7	57	149	NEW
347.50	55	53	19	–	–	62	–	31	44	–	20	–	10	60	128	AAC
351.18	67	30	16	–	–	83	–	35	22	–	20	–	10	39	161	AAC
351.99	55	30	16	–	–	76	–	46	20	–	20	–	18	500	717	AAC
352.60	89	30	22	–	–	79	–	27	27	–	20	–	12	52	263	AAC
357.35	31	30	18	–	–	82	–	31	20	–	20	–	10	267	288	AAC
359.40	59	30	17	–	–	85	–	37	27	–	20	–	10	68	385	AAC
360.00	–	–	–	–	–	–	–	–	32	7	9	326	14	196	280	NEW
363.00	73	32	16	–	–	61	–	26	37	–	20	–	10	53	88	AAC
363.85	70	30	20	–	–	64	–	29	40	–	20	–	10	51	97	AAC
367.40	87	30	18	–	–	63	–	27	39	–	20	–	10	50	160	AAC
368.20	90	37	–	–	–	57	2	27	41	19	20	439	–	53	144	BOC
369.25	87	30	17	–	–	61	–	26	42	–	20	–	10	40	167	AAC
370.50	88	65	–	–	–	60	–	–	–	4	–	–	7	48	106	GSC
372.95	70	30	18	–	–	70	–	33	34	–	20	–	10	70	186	AAC
373.70	70	30	17	–	–	65	–	28	32	–	20	–	10	44	178	AAC
374.40	60	30	17	–	–	70	–	32	31	–	20	–	10	64	291	AAC
375.60	96	60	–	–	–	66	1	36	41	25	23	469	–	99	480	BOC
375.60	–	–	–	–	–	–	–	–	37	15	15	514	17	81	440	NEW
376.10	65	30	25	–	–	74	–	32	42	–	20	–	10	149	499	AAC
377.10	68	30	18	–	–	67	–	27	34	–	20	–	10	55	297	AAC
378.82	77	30	17	–	–	71	–	30	35	–	20	–	10	59	229	AAC
380.10	85	30	20	–	–	75	–	32	32	–	20	–	10	54	217	AAC
382.45	63	30	17	–	–	64	–	27	33	–	20	–	10	44	109	AAC
384.20	81	30	16	–	–	70	–	28	24	–	20	–	10	32	474	AAC
386.45	76	30	18	–	–	74	–	32	24	–	20	–	10	25	654	AAC
387.80	78	30	16	–	–	77	–	34	20	–	20	–	10	20	499	AAC
389.60	76	30	18	–	–	81	–	36	23	–	20	–	10	36	375	AAC
392.15	69	30	17	–	–	82	–	36	22	–	20	–	24	173	2525	AAC
393.64	68	30	16	–	–	78	–	33	23	–	20	–	10	315	284	AAC
394.00	–	–	–	–	–	–	–	–	21	3	5	179	15	34	460	NEW
397.21	62	30	19	–	–	81	–	34	20	–	20	–	10	1140	461	AAC
397.50	84	19	–	–	–	78	1	39	26	15	8	129	–	76	1098	BOC
398.50	74	30	–	–	–	80	–	–	–	4	–	–	3	11	552	GSC
400.70	66	30	18	–	–	80	–	36	20	–	20	–	10	1062	600	AAC
401.40	82	30	23	–	–	92	–	40	24	–	20	–	10	512	1193	AAC
404.58	52	30	17	–	–	71	–	26	26	–	20	–	10	109	1310	AAC
405.66	27	30	21	–	–	67	–	26	25	–	20	–	10	450	806	AAC
406.30	34	40	–	–	–	60	–	–	–	4	–	–	5	52	480	GSC
407.92	40	30	16	–	–	68	–	20	33	–	20	–	18	47	424	AAC
409.90	50	49	–	–	–	70	1	34	34	21	10	357	–	37	513	BOC
411.07	51	30	21	–	–	89	–	41	30	–	20	–	10	20	595	AAC
414.00	–	–	–	–	–	–	–	–	23	2	4	203	17	102	620	NEW
414.90	67	30	18	–	–	101	–	41	20	–	20	–	10	131	1579	AAC
416.42	41	53	18	–	–	99	–	42	20	–	20	–	27	20	770	AAC
419.60	90	31	–	–	–	103	1	45	16	21	6	67	–	71	866	BOC
419.78	78	30	18	–	–	109	–	43	20	–	20	–	10	20	509	AAC

Depth	Sr	Ba	Ga	La	Ce	Zr	Nb	Y	Co	Cr	Ni	V	Pb	Cu	Zn	Lab
421.90	–	–	–	–	–	–	–	–	16	2	2	100	37	19	250	NEW
424.57	95	30	17	–	–	90	–	39	21	–	20	–	12	41	1713	AAC
424.62	60	30	17	–	–	74	–	30	28	–	20	–	64	60	569	AAC
426.00	42	30	–	–	–	60	–	–	–	4	–	–	73	94	558	GSC
427.12	94	30	17	–	–	75	–	29	29	–	20	–	60	38	437	AAC
431.25	77	30	10	–	–	82	–	34	27	–	20	–	1095	108	1656	AAC
432.79	47	30	18	–	–	61	–	29	43	–	20	–	154	813	18000	AAC
434.50	66	35	–	–	–	80	–	–	–	8	–	–	6570	1291	760	GSC
434.50	76	20	–	–	–	80	–	–	–	7	–	–	338	38	610	GSC
434.78	85	42	–	–	–	88	1	41	18	18	7	153	–	53	744	BOC
434.78	–	–	–	–	–	–	–	–	22	2	4	194	130	54	730	NEW
435.65	85	30	17	–	–	93	–	36	21	–	20	–	47	41	463	AAC
441.63	78	30	15	–	–	86	–	32	20	–	20	–	10	20	159	AAC
445.20	54	30	18	–	–	100	–	39	20	–	20	–	10	52	362	AAC
445.70	94	39	–	–	–	101	2	44	23	17	8	115	–	53	505	BOC
445.70	–	–	–	–	–	–	–	–	19	4	4	149	15	48	500	NEW
449.90	69	30	15	–	–	86	–	32	27	–	20	–	23	20	144	AAC
452.10	75	30	17	–	–	98	–	34	23	–	20	–	10	20	155	AAC
455.90	70	59	14	9	9	30	0	25	–	220	60	251	0	51	74	MUN
455.90	46	35	–	–	–	70	–	–	–	6	–	–	13	45	620	GSC
456.60	33	31	–	–	–	77	2	38	42	15	18	420	–	38	418	BOC
456.95	77	30	10	–	–	74	–	29	37	–	20	–	47	40	154	AAC
458.35	37	30	10	–	–	48	–	19	27	–	20	–	329	81	950	AAC
460.10	–	–	–	–	–	–	–	–	25	4	4	273	15	19	320	NEW
462.00	48	45	–	–	–	40	–	–	–	8	–	–	58	35	236	GSC
462.05	52	30	10	–	–	39	–	25	40	–	20	–	132	58	163	AAC
462.80	46	30	23	–	–	83	–	32	36	–	20	–	10	20	444	AAC
467.20	89	30	17	–	–	59	–	27	33	–	20	–	10	28	563	AAC
467.80	102	26	–	–	–	60	2	29	31	29	23	293	–	91	223	BOC
467.80	–	–	–	–	–	–	–	–	29	22	15	381	15	72	218	NEW
469.51	93	30	17	–	–	64	–	28	30	–	20	–	10	68	196	AAC
471.80	72	30	19	–	–	65	–	29	32	–	20	–	10	150	383	AAC
472.45	88	30	16	–	–	66	–	26	34	–	20	–	10	55	261	AAC
474.90	56	35	–	–	–	70	–	–	–	4	–	–	9	8	217	GSC
475.00	56	30	–	–	–	50	–	–	–	4	–	–	8	7	206	GSC
475.73	71	30	17	–	–	83	–	33	27	–	20	–	10	20	255	AAC
476.85	64	30	18	–	–	71	–	30	25	–	20	–	10	20	205	AAC
478.80	–	–	–	–	–	–	–	–	16	3	4	143	7	13	195	NEW
479.39	70	30	16	–	–	103	–	41	23	–	20	–	10	20	191	AAC
481.66	56	24	18	–	–	79	–	31	43	–	20	–	10	60	279	AAC
483.80	42	30	–	–	–	80	–	–	–	4	–	–	7	4	210	GSC
484.70	81	31	–	–	–	75	1	31	24	22	10	192	–	56	182	BOC
486.01	69	30	15	–	–	76	–	27	23	–	20	–	10	20	151	AAC
487.88	80	30	16	–	–	80	–	33	39	–	20	–	10	20	189	AAC
489.20	–	–	–	–	–	–	–	–	33	5	15	395	4	230	240	NEW
490.90	63	30	22	–	–	70	–	35	38	–	20	–	10	20	230	AAC
491.48	77	34	18	–	–	55	–	26	37	–	20	–	11	36	255	AAC
494.69	59	30	17	–	–	64	–	27	48	–	20	–	10	20	237	AAC
495.20	–	–	–	–	–	–	–	–	61	5	10	330	9	13	170	NEW
497.40	42	25	–	–	–	30	–	–	–	6	–	–	8	8	128	GSC
500.60	86	30	17	–	–	77	–	31	26	–	20	–	10	20	144	AAC
501.33	76	30	19	–	–	80	–	31	39	–	20	–	10	20	177	AAC
502.65	33	27	–	–	–	59	2	26	29	24	8	159	–	83	160	BOC
503.40	56	20	–	–	–	70	–	–	–	6	–	–	4	6	208	GSC
504.52	73	30	18	–	–	74	–	32	32	–	20	–	10	497	191	AAC

Depth	Sr	Ba	Ga	La	Ce	Zr	Nb	Y	Co	Cr	Ni	V	Pb	Cu	Zn	Lab
508.09	69	30	17	–	–	78	–	29	26	–	20	–	10	20	203	AAC
510.80	68	30	17	–	–	74	–	31	25	–	20	–	10	26	212	AAC
511.60	–	–	–	–	–	–	–	–	33	3	2	226	4	8	191	NEW
515.70	48	25	–	–	–	70	–	–	–	4	–	–	5	5	146	GSC
516.09	54	30	19	–	–	77	–	29	27	–	20	–	10	20	160	AAC
518.06	76	30	17	–	–	74	–	30	32	–	20	–	10	20	195	AAC
518.79	64	30	16	–	–	74	–	31	24	–	20	–	10	20	164	AAC
521.53	41	30	21	–	–	70	–	29	41	–	20	–	10	25	189	AAC
522.60	–	–	–	–	–	–	–	–	22	2	2	229	4	4	164	NEW
526.10	70	10	–	–	–	74	1	34	35	18	8	176	–	30	165	BOC
526.45	54	30	16	–	–	68	–	27	50	–	20	–	10	20	166	AAC
528.30	32	25	–	–	–	50	–	–	–	4	–	–	4	5	127	GSC
528.85	58	30	25	–	–	91	–	38	34	–	20	–	10	20	251	AAC
529.37	72	30	17	–	–	88	–	35	21	–	20	–	10	20	142	AAC
530.93	44	30	17	–	–	75	–	28	38	–	20	–	10	20	166	AAC
534.60	69	30	19	–	–	78	–	32	20	–	20	–	10	20	158	AAC
535.60	60	30	17	–	–	69	–	27	53	–	20	–	10	26	195	AAC
539.40	40	35	–	–	–	40	–	–	–	5	–	–	10	8	145	GSC
539.55	57	30	18	–	–	63	–	22	43	–	20	–	10	20	126	AAC
539.70	33	16	–	–	–	94	3	42	17	20	12	84	–	20	145	BOC
539.70	–	–	–	–	–	–	–	–	13	4	2	114	4	23	147	NEW
541.15	64	30	14	–	–	76	–	29	35	–	20	–	10	20	104	AAC
544.00	40	25	–	–	–	50	–	–	–	4	–	–	6	4	130	GSC
545.40	40	30	22	–	–	88	–	34	20	–	20	–	10	20	193	AAC
548.76	38	30	17	–	–	83	–	31	44	–	20	–	10	51	128	AAC
550.70	–	–	–	–	–	–	–	–	32	6	16	406	7	650	136	NEW
551.57	66	30	16	–	–	70	–	26	29	–	20	–	10	20	100	AAC
553.50	42	25	–	–	–	70	–	–	–	4	–	–	6	7	105	GSC
554.20	38	30	13	–	–	47	–	19	196	–	21	–	10	31	113	AAC
556.29	68	30	17	–	–	56	–	24	42	–	20	–	10	20	82	AAC
558.87	61	30	18	–	–	58	–	25	35	–	20	–	10	20	163	AAC
561.03	45	30	12	–	–	55	–	20	61	–	20	–	10	30	124	AAC
562.40	25	30	22	–	–	84	–	33	30	–	20	–	10	952	147	AAC
563.41	37	30	10	–	–	42	–	16	193	–	20	–	10	22	106	AAC
567.86	23	51	22	–	–	66	–	28	38	–	20	–	10	20	207	AAC
569.87	38	30	21	–	–	64	–	27	27	–	20	–	10	23	197	AAC
570.20	–	–	–	–	–	–	–	–	28	10	11	363	4	85	206	NEW
572.63	56	49	17	–	–	63	–	25	29	–	20	–	10	267	150	AAC
576.20	53	40	–	–	–	64	1	31	26	19	22	303	–	671	159	BOC
576.50	30	20	–	–	–	40	–	–	–	4	–	–	7	243	128	GSC
576.59	49	30	15	–	–	69	–	26	45	–	20	–	10	49	139	AAC
577.47	52	30	23	–	–	76	–	27	32	–	20	–	10	20	196	AAC
580.02	40	30	23	–	–	73	–	16	24	–	20	–	10	2310	170	AAC
581.58	35	30	18	–	–	76	–	19	36	–	20	–	10	217	167	AAC
583.20	–	–	–	–	–	–	–	–	26	9	15	375	7	867	142	NEW
583.60	30	30	15	–	–	52	–	12	100	–	23	–	10	210	159	AAC
585.24	44	30	12	–	–	59	–	21	108	–	20	–	10	2603	105	AAC
586.30	55	30	17	–	–	93	–	31	30	–	20	–	10	318	130	AAC
587.60	48	30	–	–	–	60	–	–	–	4	–	–	6	82	142	GSC
589.85	44	30	19	–	–	84	–	28	52	–	20	–	10	109	144	AAC
591.85	17	30	29	–	–	69	–	23	193	–	26	–	10	571	248	AAC
593.50	–	–	–	–	–	–	–	–	44	5	5	329	4	31	114	NEW
594.28	44	30	17	–	–	81	–	29	20	–	20	–	10	164	170	AAC
595.79	62	30	19	–	–	67	–	26	31	–	20	–	10	217	261	AAC
600.30	–	–	–	–	–	–	–	–	33	12	15	365	4	151	360	NEW

Depth	Sr	Ba	Ga	La	Ce	Zr	Nb	Y	Co	Cr	Ni	V	Pb	Cu	Zn	Lab
600.45	68	30	19	–	–	69	–	25	21	–	20	–	10	52	364	AAC
603.30	51	30	19	–	–	69	–	26	25	–	20	–	10	151	220	AAC
605.97	44	30	22	–	–	74	–	28	25	–	20	–	10	746	236	AAC
606.90	61	30	19	–	–	67	–	28	34	–	20	–	10	427	222	AAC
610.59	68	30	18	–	–	74	–	28	24	–	20	–	10	587	276	AAC
610.70	48	15	–	–	–	30	–	–	–	8	–	–	5	285	251	GSC
611.70	77	50	–	–	–	63	1	27	33	20	24	322	–	10	231	BOC
613.38	68	30	18	–	–	68	–	27	26	–	20	–	10	289	415	AAC
614.30	64	30	16	–	–	65	–	23	27	–	20	–	10	20	408	AAC
616.90	–	–	–	–	–	–	–	–	29	12	16	376	4	263	290	NEW
618.60	56	30	20	–	–	68	–	30	29	–	20	–	10	107	331	AAC
622.27	71	30	18	–	–	77	–	30	23	–	20	–	10	160	304	AAC
623.56	70	30	18	–	–	64	–	24	31	–	20	–	10	294	307	AAC
624.00	64	20	–	–	–	70	–	–	–	7	–	–	5	100	382	GSC
625.30	68	41	–	–	–	60	2	26	30	20	23	308	–	428	251	BOC
627.72	69	30	18	–	–	63	–	25	21	–	20	–	10	262	288	AAC
628.85	48	30	19	–	–	68	–	27	28	–	20	–	10	21	232	AAC
631.20	53	30	14	–	–	69	–	25	20	–	20	–	10	34	180	AAC
632.70	–	–	–	–	–	–	–	–	30	6	2	259	11	10	147	NEW
633.82	65	30	13	–	–	60	–	22	20	–	20	–	10	37	106	AAC
635.10	46	25	–	–	–	40	–	–	–	6	–	–	7	179	158	GSC
636.65	69	30	16	–	–	62	–	26	27	–	20	–	10	320	185	AAC
639.55	70	31	16	–	–	60	–	26	28	–	20	–	10	415	186	AAC
641.60	–	–	–	–	–	–	–	–	27	11	11	393	22	209	160	NEW
643.89	73	30	22	–	–	91	–	34	65	–	20	–	10	38	180	AAC
646.10	42	30	16	–	–	79	–	30	20	–	20	–	10	20	163	AAC
647.60	20	55	–	–	–	50	–	–	–	8	–	–	15	9	206	GSC
647.70	65	30	24	–	–	62	–	26	30	–	20	–	10	45	223	AAC
649.22	52	30	16	–	–	84	–	33	21	–	20	–	10	20	161	AAC
650.10	30	30	–	–	–	60	–	–	–	4	–	–	4	9	113	GSC
650.58	85	30	20	–	–	62	–	25	24	–	20	–	10	21	185	AAC
653.85	75	30	19	–	–	54	–	23	20	–	20	–	10	20	197	AAC
656.37	57	30	17	–	–	83	–	32	20	–	20	–	10	93	183	AAC
656.60	–	–	–	–	–	–	–	–	28	5	2	284	11	189	185	NEW
658.10	56	30	–	–	–	50	–	–	–	4	–	–	5	6	150	GSC
658.80	53	30	14	–	–	60	–	20	76	–	20	–	10	433	197	AAC
659.95	36	30	20	–	–	59	–	23	33	–	20	–	10	20	241	AAC
661.19	26	30	21	–	–	53	–	19	143	–	20	–	10	102	277	AAC
662.17	73	30	14	–	–	48	–	21	87	–	20	–	10	31	153	AAC
665.35	29	30	18	–	–	55	–	23	30	–	20	–	10	20	194	AAC
666.49	44	30	21	–	–	67	–	29	37	–	20	–	10	28	288	AAC
667.00	38	20	–	–	–	40	–	–	–	12	–	–	9	16	118	GSC
667.00	10	25	–	–	–	50	–	–	–	10	–	–	8	11	138	GSC
667.70	62	11	–	–	–	96	2	41	51	26	9	119	–	69	130	BOC
667.70	–	–	–	–	–	–	–	–	48	6	2	144	15	72	131	NEW
668.68	54	30	24	–	–	76	–	32	20	–	20	–	10	20	198	AAC
670.00	244	45	–	–	–	80	–	–	–	7	–	–	11	5	56	GSC
670.00	22	20	–	–	–	110	–	–	–	9	–	–	8	159	95	GSC
670.99	53	30	15	–	–	69	–	26	20	–	20	–	10	124	130	AAC
673.00	76	55	–	–	–	60	–	–	–	9	–	–	4	19	131	GSC
677.40	104	30	18	–	–	115	–	41	20	–	20	–	10	40	72	AAC
677.92	16	30	22	–	–	106	–	40	34	–	20	–	10	20	208	AAC
678.10	–	–	–	–	–	–	–	–	26	6	9	310	7	13	167	NEW
680.10	258	65	–	–	–	90	–	–	–	6	–	–	9	30	41	GSC
680.10	56	30	–	–	–	130	–	–	–	8	–	–	8	13	56	GSC

Depth	Sr	Ba	Ga	La	Ce	Zr	Nb	Y	Co	Cr	Ni	V	Pb	Cu	Zn	Lab
681.05	51	30	20	–	–	86	–	35	37	–	20	–	10	258	171	AAC
684.56	35	30	18	–	–	88	–	32	30	–	20	–	10	53	149	AAC
684.80	22	20	–	–	–	60	–	–	–	8	–	–	9	33	112	GSC
685.80	34	20	–	–	–	50	–	–	–	8	–	–	7	37	122	GSC
686.44	102	30	20	–	–	62	–	24	35	–	20	–	10	153	149	AAC
687.60	300	50	–	–	–	60	–	–	–	8	–	–	12	25	87	GSC
687.85	35	27	–	–	–	73	1	29	28	16	16	342	–	332	179	BOC
687.85	–	–	–	–	–	–	–	–	29	5	4	409	4	291	161	NEW
688.29	72	30	14	–	–	78	–	28	20	–	20	–	10	20	127	AAC
688.88	69	30	18	–	–	78	–	33	33	–	20	–	10	238	141	AAC

TRACE ELEMENT ANALYTICAL METHODS

Technische Hochschule Aachen (AAC)

Trace element determinations on bulk rock samples were carried out using a Philips PW1400 X-ray fluorescence spectrometer with an on-line Philips PM851 computer. Determinations were done on pressed powder pellets of the original samples. The analytical programs for the trace element analyses were calibrated against a series of twenty international standard rock samples. For analytical quality control the internal ICRDG standards TRS 1-7 were analyzed.

Ruhr-Universität Bochum (BOC)

A Philips X-ray spectrometer was utilized for the determination of the trace elements, measurements being made on pressed powder pellets.

Geological Survey of Canada (GSC)

The trace elements Pb, Sr and Zr were analyzed by energy dispersive XRF techniques. The estimated validity of the results is ±10% of the concentration. Ba, Cr, and Cu, were determined using an optical emission spectrograph and results for these elements are estimated to be accurate to within ±15% of the value reported.

Memorial University of Newfoundland (MUN)

All trace elements were analyzed on pressed powder pellets, using X-ray fluorescence methods and a Philips PW1450 spectrometer.

Newcastle University (NEW)

Samples were analyzed for Co, Cr, Ni, V, Pb, Cu and Zn using atomic absorption spectroscopy.

Energy, Mines and Resources Canada
Énergie, Mines et Ressources Canada